DEVELOPMENT OF THE β-PRESSURE DERIVATIVE

A Thesis

by

NIMA HOSSEINPOUR-ZONOOZI

Submitted to the Office of Graduate Studies of
Texas A&M University
in partial fulfillment of the requirements for the degree of

MASTER OF SCIENCE

December 2006

Major Subject: Petroleum Engineering

DEVELOPMENT OF THE β-PRESSURE DERIVATIVE

A Thesis

by

NIMA HOSSEINPOUR-ZONOOZI

Submitted to the Office of Graduate Studies of
Texas A&M University
in partial fulfillment of the requirements for the degree of

MASTER OF SCIENCE

Approved by:

Chair of Committee,	Thomas A. Blasingame
Committee Members,	Peter P. Valko
	Ali Beskok
Head of Department,	Stephen A. Holditch

December 2006

Major Subject: Petroleum Engineering

ABSTRACT

Development of the β-Pressure Derivative. (December 2006)
Nima Hosseinpour-Zonoozi,
B.S., Petroleum University of Technology
Chair of Advisory Committee: Dr. Thomas A. Blasingame

The proposed work provides a new definition of the pressure derivative function [that is the β-derivative function, $\Delta p_{\beta d}(t)$], which is defined as the derivative of the logarithm of pressure drop data with respect to the logarithm of time

This formulation is based on the "power-law" concept. This is not a trivial definition, but rather a definition that provides a unique characterization of "power-law" flow regimes which are uniquely defined by the $\Delta p_{\beta d}(t)$ function [that is a constant $\Delta p_{\beta d}(t)$ behavior].

The $\Delta p_{\beta d}(t)$ function represents a new application of the traditional pressure derivative function, the "power-law" differentiation method (that is computing the $d\ln(\Delta p)/d\ln(t)$ derivative) provides an accurate and consistent mechanism for computing the primary pressure derivative (that is the Cartesian derivative, $d\Delta p/dt$) as well as the "Bourdet" well testing derivative [that is the "semilog" derivative, $\Delta p_d(t)=d\Delta p/d\ln(t)$]. The Cartesian and semilog derivatives can be extracted directly from the power-law derivative (and vice-versa) using the definition given above.

Have no fear of perfection — you'll never reach it

Salvador Dali (1904 - 1989)

ACKNOWLEDGEMENTS

I want to express my gratitude and appreciation to:

Dr. Tom Blasingame for his knowledge and energy — and his friendship that shall last forever.

Dr. Peter Valko for his support and guidance during this research.

Dr. Ali Beskok for serving as a member of my advisory committee.

TABLE OF CONTENTS

Page

Page

LIST OF FIGURES

FIGURE Page

LIST OF TABLES

CHAPTER I

INTRODUCTION

1.1 Introduction

In this work we present the definition and application of a new pressure derivative function to be used for well test analysis. The genesis of this work is the need to diagnose the characteristic power-law pressure signal [*i.e.*, $\Delta p=\alpha t^{\beta}$ and $\Delta p_{\beta d}=d\ln(\Delta p)/d\ln(t)$] — as opposed to the semi-log behavior, (*i.e.* $\Delta p_d=d\Delta p/d\ln(t)$, which is the Bourdet well testing derivative function). We also provide "type curve" solutions (graphical renderings of various solutions) as a mechanism for graphical well test analysis.

1.2 Objectives

The following objectives are proposed for this work:

- To develop the analytical solutions in dimensionless form as well as graphical presentations (type curves) of the β-derivative functions for the following cases:
  - — Wellbore storage domination.
  - — Reservoir boundaries (homogeneous reservoirs).
  - — Unfractured wells (homogeneous and dual porosity reservoirs).
  - — Fractured wells (homogeneous and dual porosity reservoirs).
  - — Horizontal wells (homogeneous reservoirs).
- To demonstrate the new β-derivative functions using type curves applied to field data cases for pressure drawdown/buildup and injection/falloff test data.

1.3 Statement of the Problem

The "Bourdet" well testing pressure derivative function [ref. 1, Bourdet *et al*] $\Delta p_d(t)$, is known to be a powerful mechanism for well test interpretation — this is perhaps the most significant single development in the history of well test analysis. The $\Delta p_d(t)$ function as defined by Bourdet *et al* [*i.e.*, $\Delta p_d(t)=d\Delta p/d\ln(t)$] provides a *constant value* for the case of a well producing at a constant rate in an infinite-acting homogeneous reservoir. That is, $\Delta p_d(t)$ = *constant* during *infinite-acting radial flow behavior*.

This single observation has made the Bourdet derivative [$\Delta p_d(t)$] the most popular diagnostic tool for pressure transient analysis — but what about cases where the reservoir model is *not* infinite-acting radial flow? Of what value then is the $\Delta p_d(t)$ function? The answer is complicated in light of the fact that the Bourdet derivative function has almost certainly been generated for every reservoir model in existence.

This thesis follows the style and format of the *SPE Journal*.

Reservoir engineers have come to use the characteristic shapes in the Bourdet derivative for the diagnosis and analysis of wellbore storage, boundary effects, fractured wells, horizontal wells, and heterogeneous reservoirs. For this work we prepare the β-derivative for all of those cases — however, for heterogeneous reservoirs, we consider only the case of a dual porosity reservoir with pseudosteady-state interporosity flow.

The challenge in terms of diagnostics is to actually define a flow regime with a *particular* plotting function. For example, a derivative-based plotting function that could classify a fractured well by a unique signature would be of significant value — as would be such functions which could be used for wellbore storage, boundary effects, horizontal wells, and heterogeneous reservoir systems.

The purpose of this work is to demonstrate that the "power-law" β-derivative formulation does just that — it provides a single plotting function which can be used (in isolation) as a mechanism to interpret the pressure performance behavior for systems with wellbore storage, boundary effects, fractured wells, horizontal wells.

The power-law derivative formulation (*i.e.*, the β-pressure derivative) is given by:

$$\Delta p_{\beta d}(t) = \frac{d\ln(\Delta p)}{d\ln(t)} = \frac{1}{\Delta p} t \frac{d\Delta p}{dt} = \frac{\Delta p_d(t)}{\Delta p} \quad \text{.....(1.1)}$$

where $\Delta p_d(t)$ is the "Bourdet" well testing derivative.

The origin of the β-derivative [$\Delta p_{\beta d}(t)$] was an effort [ref. 2, Sowers] to demonstrate that this formulation would provide *a consistently better estimate* of the Bourdet derivative function [$\Delta p_d(t)$] than either of the existing "Cartesian" or "semilog" formulations. For orientation, we present the definition of each derivative formulation below:

The "Cartesian" pressure derivative (taken with respect to time) is defined as:

$$\Delta p_{Pd}(t) = \frac{d\Delta p}{dt} \quad \text{.....(1.2)}$$

where $\Delta p_{Pd}(t)$ is also known as the "primary pressure derivative" [ref. 3, Mattar].

The "semilog" or "Bourdet" pressure derivative is defined as:

$$\Delta p_d(t) = t\frac{d\Delta p}{dt} = \frac{d\Delta p}{d\ln(t)} \quad \text{.....(1.3)}$$

Solving Eq. 1.1 for the "Cartesian" or "primary pressure derivative," we obtain:

$$\frac{d\Delta p}{dt} = \frac{\Delta p}{t}\Delta p_{\beta d}(t) \quad \text{.....(1.4)}$$

Solving Eq. 1.1 for the "semilog" or "Bourdet" pressure derivative yields

$$\Delta p_d(t) = \Delta p \, \Delta p_{\beta d}(t) \quad \text{.....(1.5)}$$

Now the discussion turns to the calculation of these derivatives — what approach is best? Our options are:

1. A simple finite-difference estimate of the "Cartesian" (or "primary") pressure derivative function [$\Delta p_{Pd}(t) = d\Delta p/dt$].
2. A simple finite-difference estimate of the "semilog" (or "Bourdet") pressure derivative function [$\Delta p_d(t) = d\Delta p/d\ln(t)$].
3. Some type of weighted finite-difference or central difference estimate of either the "Cartesian" or the "semilog" pressure derivative functions. This approach of [ref. 1, Bourdet *et al* and ref. 4, Clark and van Golf-Racht] is by far the most popular technique used to compute pressure derivative functions for the purpose of pressure transient analysis, and will be presented in detail later in this thesis.
4. Other more elegant and statistical sophisticated algorithms (such as moving regression functions, spline approximation, etc.) have been proposed for use in pressure transient (or well test) analysis, but the Bourdet *et al.* algorithm (and its variations) continue to be the most popular approach — most likely due to the simplicity and consistency of this algorithm. To be certain, *the Bourdet et al. algorithm does not provide the most accurate estimates of the various derivative functions*. However; the predictability of the algorithm is very good, and the purpose of the derivative function is as a diagnostic mechanism — it is not used to provide a highly accurate estimate for the computation of other parameters.

1.4 Inventory of Type Curves

To demonstrate the effectiveness of the β-derivative function, we provide type curve solutions for a variety of reservoir systems, (**Appendices A** to **E**):

- Unfractured well in an infinite-acting homogeneous reservoir. (**Appendix A**)
- Unfractured well in a bounded homogeneous reservoir. (**Appendix A**)
- Unfractured well in a homogeneous reservoir, various sealing fault configurations. (**Appendix A**)
- Fractured well in an infinite-acting homogeneous reservoir. (**Appendix B**)
- Unfractured well in an infinite-acting naturally fractured (dual porosity) reservoir. (**Appendix C**)
- Fractured well in an infinite-acting naturally fractured (dual porosity) reservoir. (**Appendix D**)
- Horizontal well in a homogeneous reservoir. (**Appendix E**)

For each case we generated dimensionless solutions with and without wellbore storage effects. In addition to the β-derivative type curves, we also generated pressure and Bourdet pressure derivative type curves to develop a complementary suite of diagnostic functions to identify as many specific flow regimes as possible.

We applied our β-derivative type curve solutions to several field cases obtained from the literature (**Chapter IV**) — comparison of our new technique with "conventional" pressure/pressure derivative type curve analysis lead us to conclude that our new approach has the following advantages :

- The β-derivative introduces a straightforward way to diagnose *wellbore storage effects, boundary domination flow effects, linear flow and bilinear flow regimes* — the β-derivative is a good diagnostic toll for confirming the power-law characteristic behavior of the measured pressure data.
- The β-derivative match is fixed along vertical axis (*i.e.*, this match is independent of permeability). This characteristic should yield an improved matching process for pressure transient test data, in addition to the diagnostic advantages of the β-pressure derivative function.

We would like to mention that the advent of the β-derivative function as proposed in this work is not expected to replace the Bourdet derivative (nor should this happen). The β-derivative function is proposed simply to serve as a better interpretation device for certain flow regimes — in particular, those flow regimes which are represented by "power-law" functions (*e.g.*, wellbore storage domination, closed boundary effects, fractured wells, horizontal wells, etc.).

1.5 Organization of the Thesis

The outline of the proposed research thesis is as follows:

- Chapter I — Introduction
  - Introduction
  - Objectives
  - Statement of the Problem
  - Inventory of Type Curves
- Chapter II — Development of the β-Derivative Formulation
  - Literature review
  - Calculation of the β-Derivative Function
  - Discussion of Power-Law Derivative
  - Diagnostic Values of Pressure β-Derivative Function
- Chapter III — Development of New β-Derivative Type Curves
  - Unfractured Wells — Infinite-Acting Homogeneous Reservoirs
  - Unfractured Wells — Boundary Effects
  - Fractured Wells — Infinite-Acting Homogeneous Reservoirs
  - Unfractured Wells — Dual Porosity/Naturally Fractured Reservoir System
  - Fractured Wells — Dual Porosity/Naturally Fractured Reservoir System
  - Horizontal Wells — Infinite-Acting Homogeneous Reservoirs
  - Application Procedure for the β-Derivative Type Curves

CHAPTER II

DEVELOPMENT OF THE β-DERIVATIVE FORMULATION

2.1 Literature Review

As mentioned earlier, the Bourdet algorithm is the standard method for taking the pressure derivative — and. at present, all of the pressure transient analysis software utilize the Bourdet weighted finite-difference method. Clark and Van Golf-Racht [ref. 4] as well as Sowers [ref. 2] introduced modifications for computing the pressure derivative using a weighted finite-difference approach — where such algorithms are favored due to simplicity (these methods will be discussed in detail later in this chapter).

A sampling of the other pressure derivative algorithms used in the industry are summarized below:

- Moving polynomial or another type of moving regression function — this is generally referred to as a "window" approach (or "windowing").
- A smoothing spline approximation [Lane *et al,* ref. 5] is a powerful approach, but as pointed out in a general assessment of the computation of the pressure derivative [Escobar *et al,* ref. 6], the spline approximation requires considerable user input to obtain the "best fit" of the data. For that reason, the spline and other functional approximation methods are less desirable than the traditional, weighted finite-difference formulation [Bourdet *et al,* ref. 1].
- A combination of power-law and logarithmic functions has also been proposed to represent the characteristic pressure signal [Gonzalez *et al,* ref. 7], and regression was used to tune these functions to the data over a specified window.
- The fast Fourier transform and frequency-domain constraints have also been proposed to improve the performance of the original Bourdet algorithm by optimizing the size of search window [Cheng *et al,* ref. 8]. A Gaussian filter was also used to denoise the pressure derivative data, which resulted in an adaptive smoothing procedure that uses recursive differentiation and integration.

2.2 Calculation of the β-Derivative Function

To minimize the effect of truncation error, Bourdet *et al* [ref. 1] introduced a weighted central-difference derivative formula which is given as: (this is the so-called "semilog" formulation)

$$\Delta p_d(t) = \frac{d\Delta p}{d[\ln(\Delta t)]} = \frac{\Delta T_R}{\Delta T_L + \Delta T_R}\frac{\Delta P_L}{\Delta T_L} + \frac{\Delta T_L}{\Delta T_L + \Delta T_R}\frac{\Delta P_R}{\Delta T_R} \quad \text{..... (2.1.a)}$$

where:

$\Delta p(t) = a + b \ln(t)$ (base Δp relation, where Δp_d yields a constant value for this model) ..... (2.1.b)

$\Delta T_L = \ln(\Delta t_{calc}) - \ln(\Delta t_{left})$ ..... (2.1.c)

$\Delta T_R = \ln(\Delta t_{right}) - \ln(\Delta t_{calc})$ ..... (2.1.d)

$\Delta P_L = \Delta p_{calc} - \Delta p_{left}$ ..... (2.1.e)

$\Delta P_R = \Delta p_{right} - \Delta p_{calc}$ ..... (2.1.f)

The left- and right-hand subscripts represent the "left" and "right" neighbor points located at a specified distance (L) from the objective point. The *calc* subscript represents the point of interest at which the derivative is to be computed (**Fig. 2.1**). As for the L-value, Bourdet *et al* [ref. 1] give only general guidance as to its selection, but we have long used a formulation where L is the fractional proportion of a log-cycle ($\log_{10}$ base). Therefore, L=0.2 would translate into a "search window" of 20 percent of a log-cycle from the point in question.

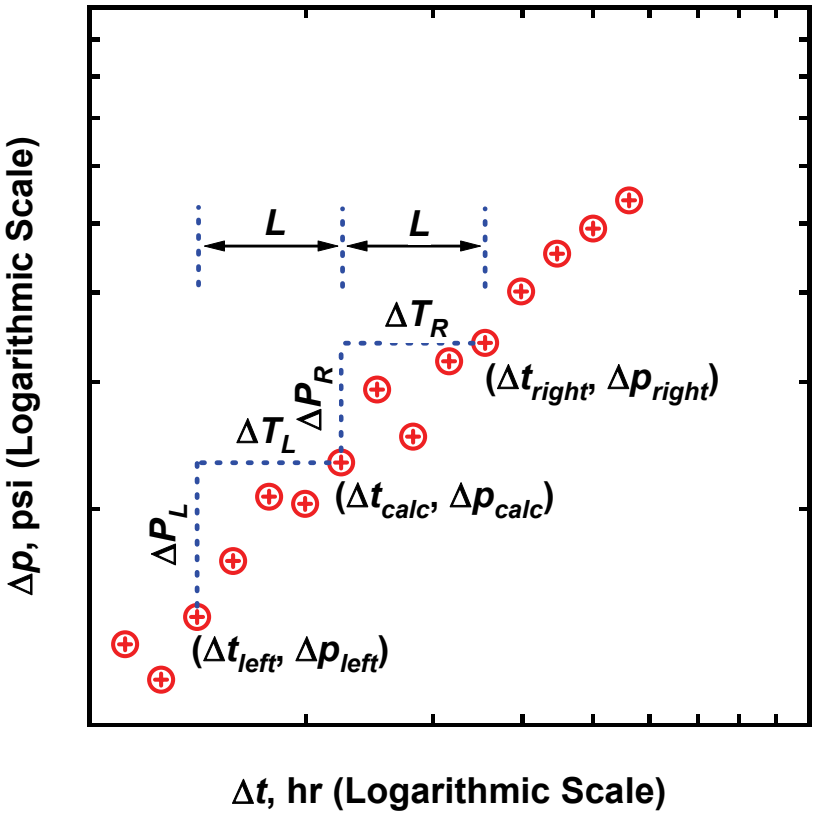

Figure 2.1 — Schematic of the role of search criterion L in the derivative calculation.

This search window approach (*i.e.*, L) helps to reduce the influence of data noise on the derivative calculation. However, choosing a "small" L-value will cause Eq. 2.1.a to revert to a simple central-difference between a point and its nearest neighbors — and data noise will be amplified. On the contrary, choosing a "large" L-value will cause Eq. 2.1.a to yield a central-difference derivative computed over a very great distance — which will yield a poor estimate for the derivative, and this "large" L-value will tend to "smooth" the derivative response (perhaps over-smoothing the derivative). The common range for the search window is between 10 and 50 percent of a log-cycle ($0.1 < L < 0.5$) — where we prefer a starting L-value of 0.2 [20 percent of a log-cycle (recall that log is the $\log_{10}$ function)].

Sowers [ref. 2] proposed the "*power-law*" formulation of the weighted central difference as a method that he believed would provide a better representation of the pressure derivative than the original Bourdet formulation. In particular, Sowers [ref. 2] provides the following definition of the power-law (or "β") derivative formulation:

$$\Delta p_{\beta d}(t) = \frac{d\left[\ln(\Delta p)\right]}{d\left[\ln(\Delta t)\right]} = \frac{\Delta T_R}{\Delta T_L + \Delta T_R}\frac{\Delta P_L}{\Delta T_L} + \frac{\Delta T_L}{\Delta T_L + \Delta T_R}\frac{\Delta P_R}{\Delta T_R} \quad \text{.....(2.2.a)}$$

where:

$\Delta p(t) = \alpha\, t^{\beta}$ (base Δp relation, where Δp_d yields a constant value for this model).....(2.2.b)

$\Delta T_L = \ln(\Delta t_{calc}) - \ln(\Delta t_{left})$.....(2.2.c)

$\Delta T_R = \ln(\Delta t_{right}) - \ln(\Delta t_{calc})$.....(2.2.d)

$\Delta P_L = \Delta p_{calc} - \Delta p_{left}$.....(2.2.e)

$\Delta P_R = \Delta p_{right} - \Delta p_{calc}$.....(2.2.f)

Multiplying the right-hand-side of Eq. 2.2a by Δp_{calc} (recall that Δp_{calc} is the pressure drop at the point of interest), will yield the "well-testing pressure derivative" function [*i.e.*, the typical "Bourdet" derivative definition ($\Delta p_d(t)$)]. Sowers [ref. 2] provides an exhaustive evaluation of the "power-law" derivative formulation using various levels of noise in the Δp function and he found that the power-law (or β) derivative formulation always showed improved accuracy of the well testing pressure derivative [*i.e.*, the Bourdet derivative function, $\Delta p_d(t)$].

In addition, Sowers found that the β-derivative formulation was less sensitive to the L-value than the original Bourdet formulation — which is a product of how well the power-law relation represents the pressure drop over a specific period. Sowers [ref. 2] *did not* pursue the specific application of the β-derivative function [$\Delta p_{\beta d}(t) = d\ln(\Delta p)/d\ln(t)$] as a diagnostic plotting function, as we propose in this work.

2.3 Discussion of Power-Law Pressure Derivative

In the previous section we noted that, after exhaustive testing of the power-law derivative using synthetic data, Sowers [ref. 2] made the following conclusions:

- The power-law derivative formulation always yields a more accurate pressure derivative estimate as compared to the Bourdet (semilog) derivative formulation.
- The power-law derivative formulation is less sensitive to the L-value than the original Bourdet formulation — which should ensure consistent performance of the power-law algorithm.

To support these observations we need to consider the basic models for which each derivative calculation is defined (*i.e.* Eqs. 2.1.b and 2.2.b). The semilog model (Eq. 2.1.b) is the base model for the Bourdet derivative function [$\Delta p_d(t)$] and yields a unique, *constant* behavior for transient radial flow behavior. In contrast, the power law model (Eq. 2.2.b) is the characteristic model for the following flow regimes:

- Wellbore storage
- Bounded reservoir
- 2-parallel faults
- 3-perpendicular faults
- Linear flow regime (formation linear flow — infinite conductivity fracture or horizontal well)
- Bilinear flow regime (bilinear flow — finite conductivity fracture)

The uniqueness of the power-law model for the flow regimes listed above provides us with a basis (and a motivation) for application of this derivative formulation. In the next section we identify the specific characteristic behavior of the power-law (or β-derivative) formulation [$\Delta p_{\beta d}(t)$ (or $p_{D\beta d}$ in dimensionless form)] — that is, we provide the specific values of β for each of the flow regimes listed above (**Table 2.1**).

2.4 Diagnostic Values of Pressure β-Derivative Function

Recalling the definition of pressure β-derivative, we have:

$$\Delta p_{\beta d}(t) = \frac{d\ln(\Delta p)}{d\ln(t)} = \frac{1}{\Delta p} t \frac{d\Delta p}{dt} = \frac{\Delta p_d(t)}{\Delta p} \quad \text{.....(1.1)}$$

where $\Delta p_d(t)$ is the "Bourdet" well testing derivative.

$\Delta p_{\beta d}(t)$ will yield a constant value when Δp behaves as a power-law function (*i.e.* $\Delta p(t) = \alpha t^{\beta}$). In **Fig. 2.2** we present a schematic plot created for illustrative purposes to represent the character of the β-derivative for several distinctly different cases. We present the β-derivative profiles (in schematic (*i.e.*, dimensionless) form) for an unfractured well (infinite-acting radial flow), 2 fractured well cases, and a horizontal well case. We note immediately the strong character of the fractured well responses ($p_{D\beta d}$ = 1/2 for the infinite conductivity fracture case and 1/4 for the finite conductivity fracture case). Interestingly, the

horizontal well case shows a p_{Dd} slope of approximately 1/2, but the $p_{D\beta d}$ function never achieves the expected 1/2 value, perhaps due to the "thin" reservoir configuration that was specified for this particular horizontal well case. We also note that, for all cases of boundary-dominated flow, the $p_{D\beta d}$ function yields a constant value of unity, as expected. This observation suggests that the $p_{D\beta d}$ function (or an auxiliary function based on the $p_{D\beta d}$ form) may be of value for the analysis of production data.

Table 2.1 — Characteristic values of the β-derivative for various flow regimes.

Case	$\Delta p_{\beta d}(t)$
● Wellbore storage domination:	1
● Reservoir boundaries:	
— Closed reservoir (circle, rectangle, etc.).	1
— 2-Parallel faults (large time).	1/2
— 3-Perpendicular faults (large time).	1/2
● Fractured wells:	
— Infinite conductivity vertical fracture.	1/2
— Finite conductivity vertical fracture.	1/4
● Horizontal wells:	
— Formation linear flow.	1/2

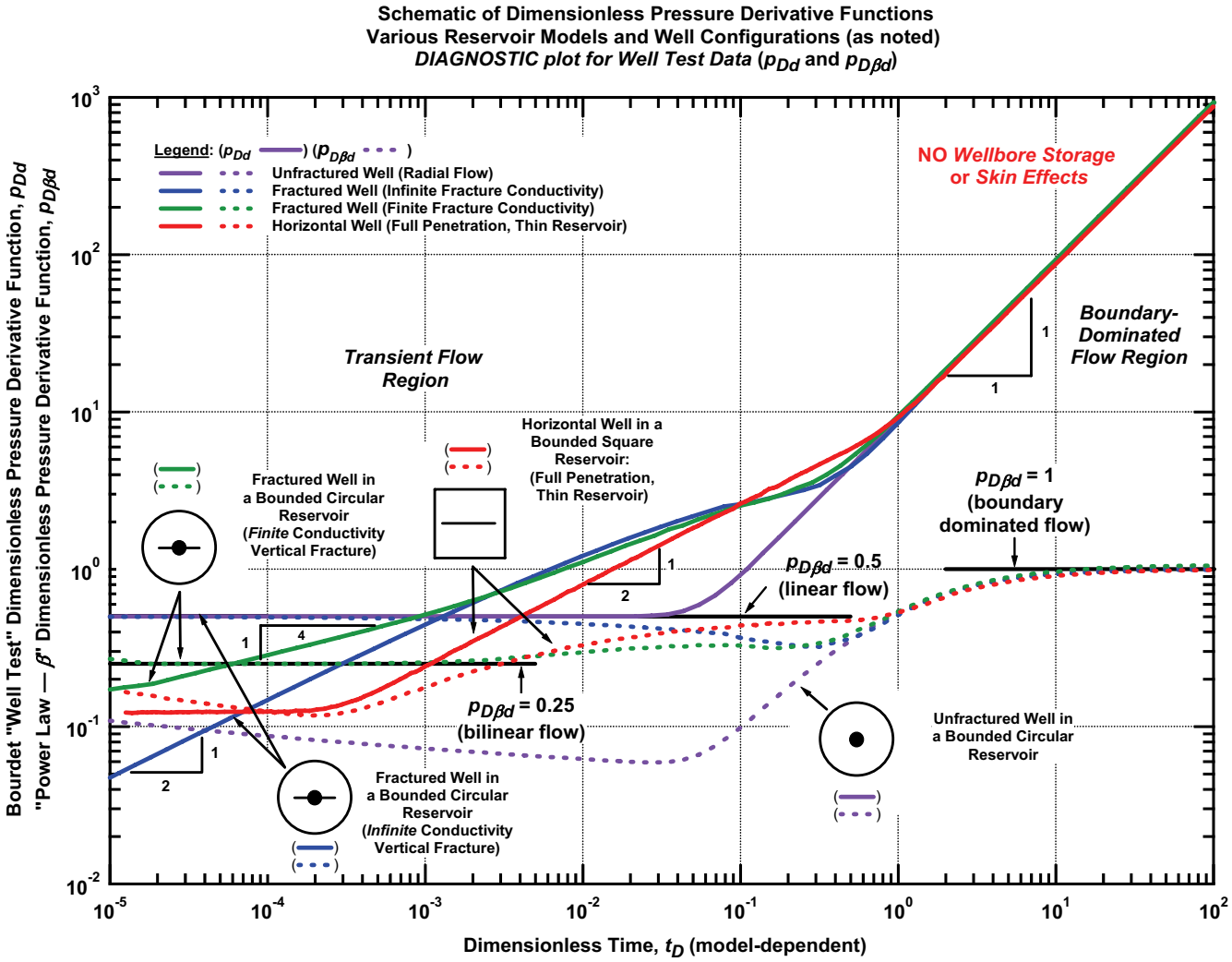

Figure 2.2 — Schematic of p_{Dd} and $p_{D\beta d}$ vs. t_D — various reservoir models and well configurations (no wellbore storage or skin effects).

CHAPTER III

DEVELOPMENT OF THE NEW β-DERIVATIVE TYPE CURVES

3.1 Background

Without question, the Bourdet definition of the pressure derivative function is the standard for all well test analysis applications — from hand methods to sophisticated interpretation/analysis/modeling software.

In the development of the models and type curves for the β-derivative function, we reviewed numerous literature articles which proposed plotting functions based on the Bourdet pressure derivative or related functions (*e.g.*, the primary pressure derivative [ref. 3, Mattar]). In the late 1980's the "pressure derivative ratio" was proposed [ref. 9, Onur and Reynolds; and ref. 10, Doung], where this function was defined as the pressure derivative divided by the pressure drop (or $2\Delta p$ in radial flow applications)) — this ratio was (obviously) a dimensionless quantity. In particular, the pressure derivative ratio was applied as an interpretation device — as it is a dimensionless quantity, the type curve match consisted of a vertical axis overlay (which is fixed) and a floating horizontal axis (which is typically used to find the end of wellbore storage distortion effects). The pressure derivative ratio has found most utility in such interpretations.

The primary utility of the β-derivative is the resolution that this function provides for cases where the pressure drop can be represented by a power law function — again, fractured wells, horizontal wells, and boundary-influenced (faults) and boundary-dominated (closed boundaries) are all good candidate for identification/interpretation using the β-derivative. Infinite-acting radial flow — the "utility" case for the Bourdet (semilog) derivative function is not a good candidate for interpretation using the β-derivative as the radial flow regime is represented by a logarithmic approximation which can not be represented by a power-law model.

3.2 Unfractured Wells — Infinite-Acting Homogeneous Reservoirs

The β-derivative function for a single well producing at a constant flowrate in an infinite-acting homogeneous reservoir was computed using the cylindrical source solution (Laplace domain solution) [ref. 11, van Everdingen and Hurst]:

$$\bar{p}_D(s) = \frac{1}{s}\frac{K_0(\sqrt{s})}{\sqrt{s}K_1(\sqrt{s})} \qquad \text{.....(3.1)}$$

Recalling the definition of β-pressure derivative:

$$p_{D\beta d}(t_D) = \frac{d\ln(p_D(t_D))}{d\ln(t_D)} = \frac{t_D}{p_D(t_D)}\frac{dp_D(t_D)}{dt_D} = \frac{p_{Dd}(t_D)}{p_D(t_D)} \qquad \text{.....(3.2)}$$

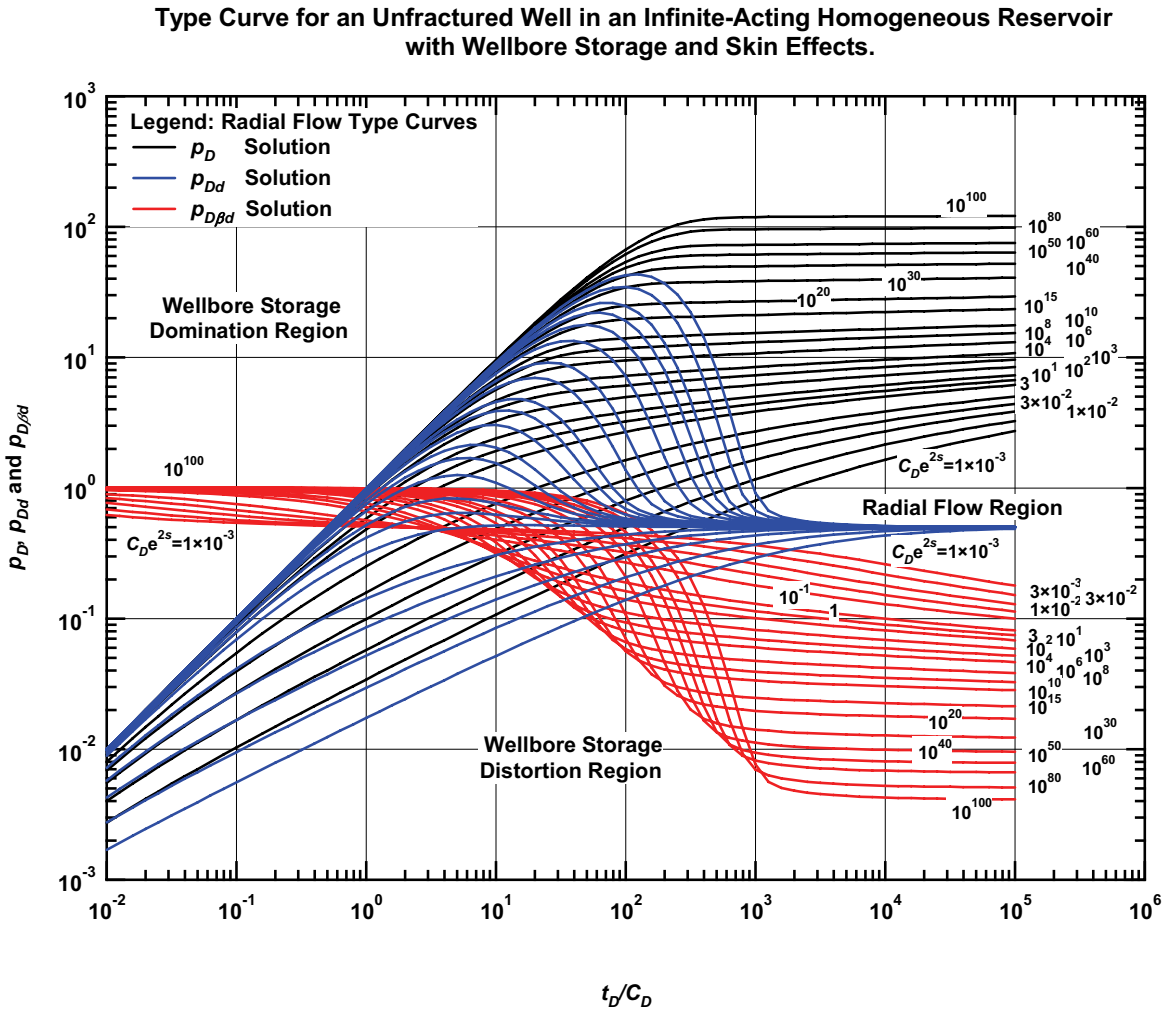

Figure 3.1 — p_D, p_{Dd}, and $p_{D\beta d}$ vs. t_D/C_D — solutions for an unfractured well in an infinite-acting homogeneous reservoir — wellbore storage and skin effects included (various C_D values).

Recalling, the Laplace transform of the time-dependent derivative is given by:

$$\mathcal{L}\{f'(t)\} = s\mathcal{L}\{f(t)\} - f(0) \quad \text{.....(3.3)}$$

Therefore,

$$\mathcal{L}\left\{\frac{dp_D(t_D)}{dt_D}\right\} = \frac{K_0(\sqrt{s})}{\sqrt{s}K_1(\sqrt{s})} \quad \text{.....(3.4)}$$

Combining Eqs. 3.1, 3.2, and 3.4 we obtain the β-derivative formulation for this case:

$$p_D\beta d(t_D) = t_D\frac{\dfrac{dp_D(t_D)}{dt_D}}{p_D(t_D)} = t_D\frac{\mathcal{L}^{-1}\left\{\dfrac{K_0(\sqrt{s})}{\sqrt{s}K_1(\sqrt{s})}\right\}}{\mathcal{L}^{-1}\left\{\dfrac{1}{s}\dfrac{K_0(\sqrt{s})}{\sqrt{s}K_1(\sqrt{s})}\right\}} \quad \text{.....(3.5)}$$

The direct, analytical inversion of the cylindrical source solution from the Laplace domain to the time domain is not available — nor are most of the solutions relevant for petroleum engineering applications. As such, we must use numerical techniques for Laplace transform inversion [ref. 12, Stehfest; ref. 13, Valko and Abate].

In **Fig. 3.1** we present the β-derivative solution with wellbore storage and skin effects for the case of a single well producing at a constant (surface) rate in an infinite-acting homogenous reservoir. This is the typical configuration used as the starting point for interpretation and analysis of pressure transient data. We apply the following identity to account for wellbore storage effects:

$$[\bar{p}_D(s)]_{WBS} = \frac{1}{\dfrac{1}{[\bar{p}_D(s)]_{noWBS}} + s^2C_D} \quad \text{.....(3.6)}$$

Where we note that in Eq. 3.6, the *WBS* subscript implies the inclusion of wellbore storage effects. As mentioned earlier, the β-derivative function does not demonstrate a constant behavior for the radial flow case [however it appears on **Fig. 3.1** as a mirror image of the pressure function since it is a product of pressure derivative (constant at radial flow p_{Dd}=0.5) solution divided by pressure solution]. We also note that the β-derivative function for the wellbore storage domination flow regime yields $p_{D\beta d}$ = 1. The time domain dimensionless pressure solutions (line source solutions) for radial flow and wellbore storage are presented in Appendix A.

3.3 Unfractured Wells — Boundary Effects

The p_{Dd}-format (Bourdet) type curves for cases of a single well producing at a constant flow rate in an infinite-acting homogeneous reservoir with single, double, and triple-sealing faults oriented some distance n

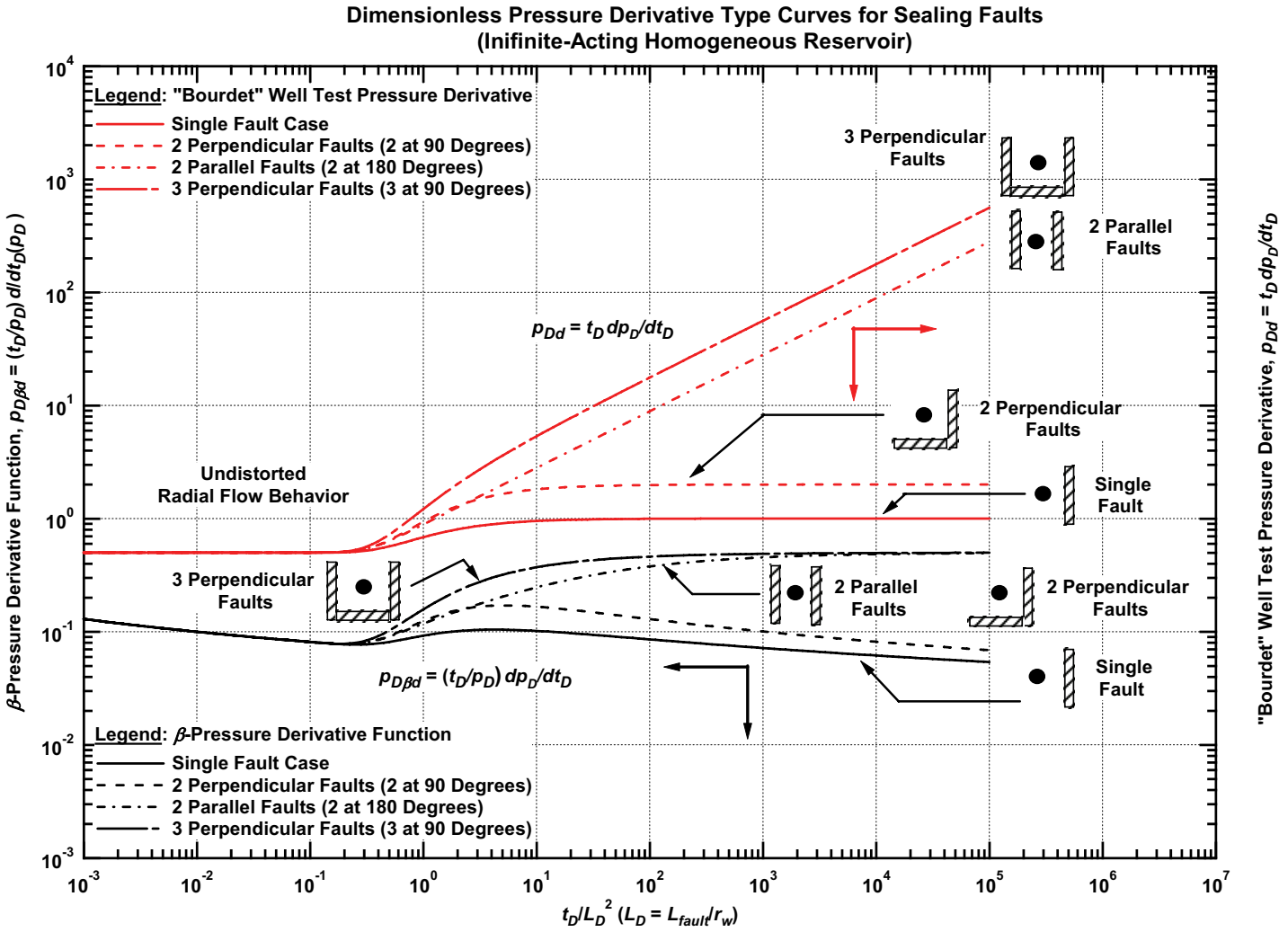

Figure 3.2 — p_{Dd} and $p_{D\beta d}$ vs. t_D/L_D^2 — various sealing faults configurations (no wellbore storage or skin effects).

from the well were originally proposed by Stewart *et al* [ref. 14]. This case provides an opportunity to illustrate the performance of the β-derivative function where the $p_{D\beta d}$ functions yield diagnostic value in general, but specifically illustrate that the 2-parallel sealing faults and 3-perpendicular fault cases achieve $p_{D\beta d} = 1/2$ at very long times (see **Fig. 3.2** and Appendix A).

We generate constant production rate well in a homogenous reservoir surrounded by a circular no flow boundary at $r_{eD} = 100$ (well located in the center of the circle) to show the close boundary effect. Cylindrical source solution is also applied here:

$$\bar{p}_D(s) = \frac{1}{s}\frac{K_0(\sqrt{s})I_1(\sqrt{s}r_{eD}) + K_1(\sqrt{s}r_{eD})I_0(\sqrt{s})}{\sqrt{s}K_1(\sqrt{s})I_1(\sqrt{s}r_{eD}) - \sqrt{s}I_1(\sqrt{s})K_1(\sqrt{s}r_{eD})} \quad \text{.....(3.7)}$$

The β-derivative formulation for this case is:

$$p_{D\beta d}(t_D) = t_D \frac{\dfrac{dp_D(t_D)}{dt_D}}{p_D(t_D)} = t_D \frac{\mathcal{L}^{-1}\left\{\dfrac{K_0(\sqrt{s})I_1(\sqrt{s}r_{eD}) + K_1(\sqrt{s}r_{eD})I_0(\sqrt{s})}{\sqrt{s}K_1(\sqrt{s})I_1(\sqrt{s}r_{eD}) - \sqrt{s}I_1(\sqrt{s})K_1(\sqrt{s}r_{eD})}\right\}}{\mathcal{L}^{-1}\left\{\dfrac{1}{s}\dfrac{K_0(\sqrt{s})I_1(\sqrt{s}r_{eD}) + K_1(\sqrt{s}r_{eD})I_0(\sqrt{s})}{\sqrt{s}K_1(\sqrt{s})I_1(\sqrt{s}r_{eD}) - \sqrt{s}I_1(\sqrt{s})K_1(\sqrt{s}r_{eD})}\right\}} \quad \text{.....(3.8)}$$

In **Fig. 3.3** we present the case of wellbore storage combined with closed circular boundary effects as a means to demonstrate that these two influences have the same effect (*i.e.*, $p_{D\beta d} = 1$). For more detail regarding the $p_{D\beta d}$ function, we present the line source solutions for this case in Appendix A.

Another aspect of this particular case is that we show the plausibility of using the β-derivative for the analysis of the boundary-dominated flow regime — *i.e.*, the β-derivative (or another auxiliary form) may be a good diagnostic for the analysis of production data. In particular, the β-derivative may be less influenced by data errors that lead to artifacts in the conventional pressure derivative function (*i.e.*, the Bourdet (or "semilog") form of the pressure derivative).

3.4 Fractured Wells — Infinite-Acting Homogeneous Reservoirs

In this section we consider the case of a well with a *finite* conductivity vertical fracture where the β-derivative type curves were generated using the solution provided by Cinco and Meng [ref. 15]:

$$\bar{p}_D(s) = \frac{1}{2}\int_0^1 \bar{q}_{fD}(x',s)\left[K_0\left(\left|x_D - x'\right|\sqrt{s}\right) + K_0\left(\left|x_D + x'\right|\sqrt{s}\right)\right]dx' - \frac{\pi}{C_{fD}}\int_0^{x_D}\int_0^{x'} \bar{q}_{fD}(x',s)dx''dx' + \frac{\pi x_D}{sC_{fD}}$$

.....(3.9)

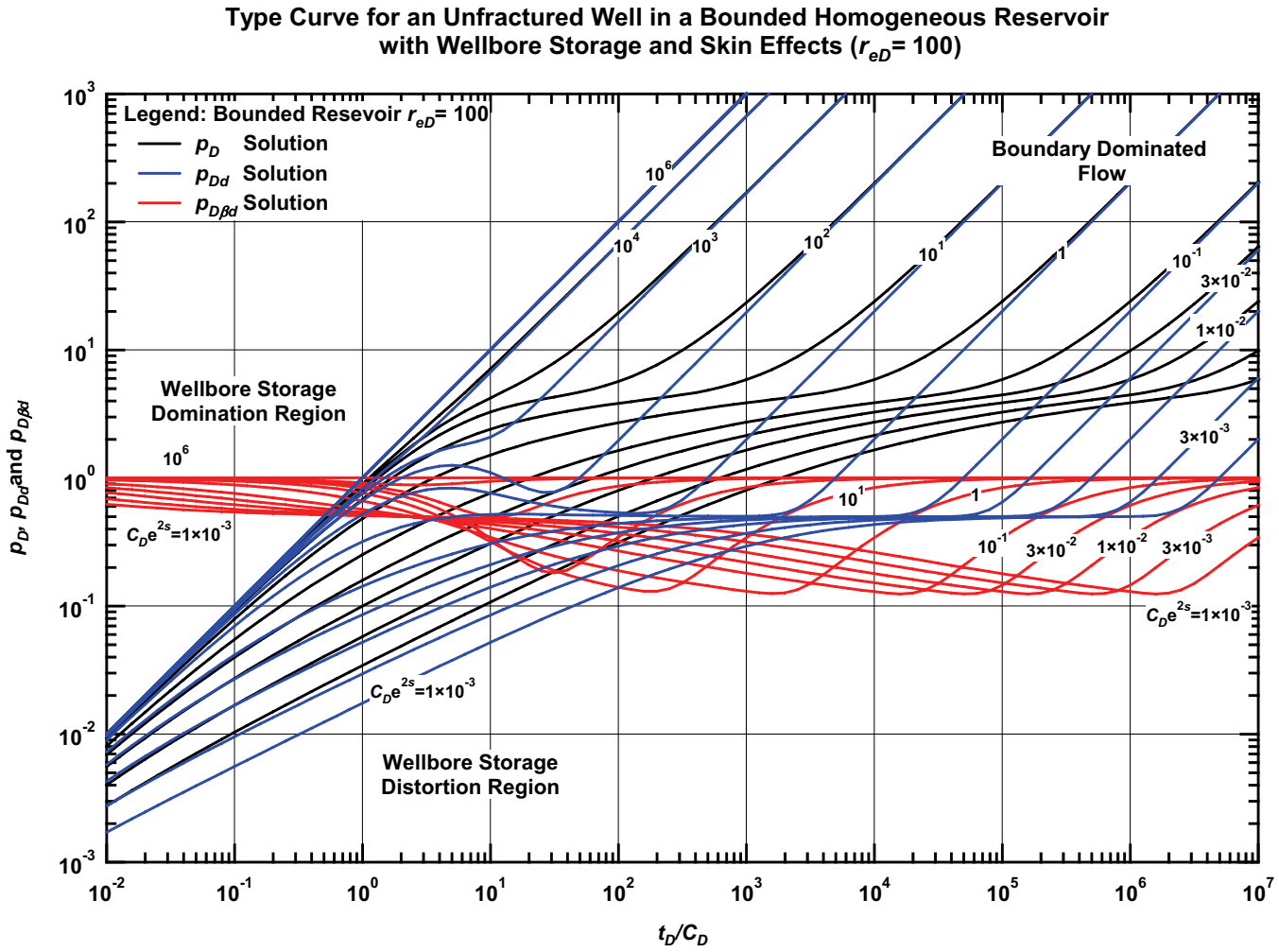

Figure 3.3 — p_D and $p_{D\beta d}$ vs. t_D/C_D — r_{eD} =100, bounded circular reservoir case — includes wellbore storage and skin effects. This graph illustrates combined influence of wellbore storage and boundary effects.

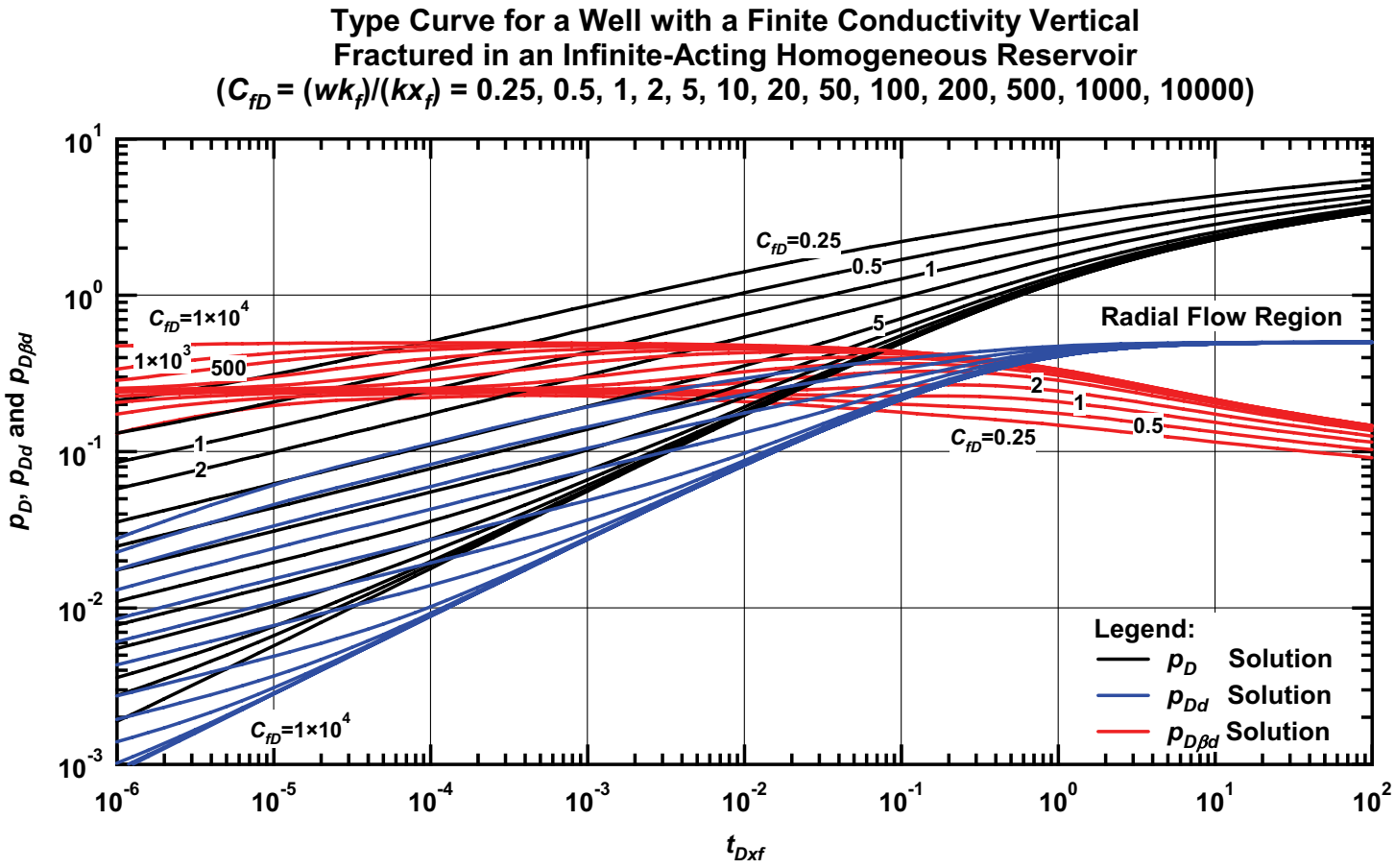

Figure 3.4 — p_D, p_{Dd}, and $p_{D\beta d}$ vs. t_{Dxf} — solutions for a fractured well in an infinite-acting homogeneous reservoir — no wellbore storage or skin effects (various C_{fD} values).

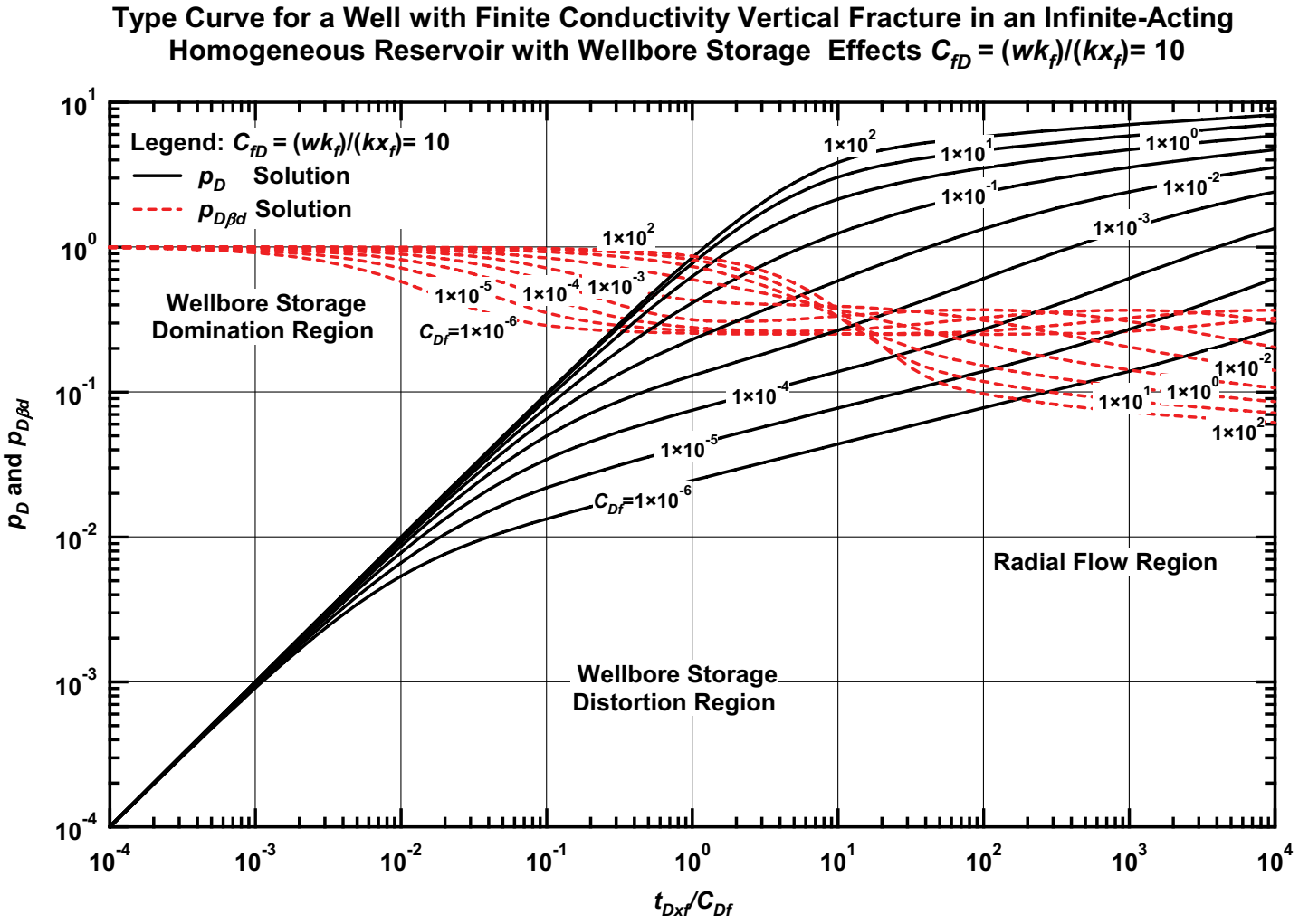

Figure 3.5 — p_D and $p_{D\beta d}$ vs. t_{Dxf}/C_{Df}—C_{fD} = 10 (fractured well case — includes wellbore storage effects).

Equation 3.9 describes the fracture as n consecutive blocks of the same dimension and with time-dependent flux — since the flux term is implicit we need to form an $n \times n$ system of equations to solve for the pressure at each block that will lead us to wellbore block pressure.

$$p_{D\beta d}(t_{Dxf}) = t_{Dxf}\frac{\dfrac{dp_D(t_{Dxf})}{dt_{Dxf}}}{p_D(t_{Dxf})} = t_{Dxf}\frac{\mathcal{L}^{-1}\left\{\begin{array}{l}\dfrac{s}{2}\int_0^1 \bar{q}_{fD}(x',s)\left[K_0(|x_D - x'|\sqrt{s}) + K_0(|x_D + x'|\sqrt{s})\right]dx' \\ -\dfrac{s\pi}{C_{fD}}\int_0^{x_D}\int_0^{x'}\bar{q}_{fD}(x',s)\,dx''dx' + \dfrac{\pi x_D}{C_{fD}}\end{array}\right\}}{\mathcal{L}^{-1}\left\{\begin{array}{l}\dfrac{1}{2}\int_0^1 \bar{q}_{fD}(x',s)\left[K_0(|x_D - x'|\sqrt{s}) + K_0(|x_D + x'|\sqrt{s})\right]dx' \\ -\dfrac{\pi}{C_{fD}}\int_0^{x_D}\int_0^{x'}\bar{q}_{fD}(x',s)\,dx''dx' + \dfrac{\pi x_D}{sC_{fD}}\end{array}\right\}}$$

.....(3.10)

To produce our type curves we divided the fracture into 30 segments and used a variety of fracture conductivity values (see Appendix B) with and without wellbore storage effects (to ensure accuracy, we compared the 30-segment results with 50 and 70-segment results, and we note that the difference in these solutions was less that 0.01 percent). In **Figs**. **3.4** and **3.5** the linear and bilinear flow regimes are seen in the β-derivative function as horizontal lines with half (1/2) and quarter (1/4) values, respectively (recall that these are characteristic values for high and low fracture conductivities, respectively). We believe that the $p_{D\beta d}$ function (*i.e.*, the β-derivative) will substantially improve the diagnosis of flow regimes for hydraulically fractured wells.

As a check, we used the line source solution (integral of continuous point sources) given in ref. 16 [ref. 16, Ozkan] as a means to model the case of a well with an *infinite conductivity* vertical fracture.

$$\bar{p}_D(s) = \frac{1}{2s}\frac{1}{\sqrt{s}}\left[\int_0^{(1-x_D)\sqrt{s}} K_0(z)\,dz + \int_0^{(1+x_D)\sqrt{s}} K_0(z)\,dz\right]$$

[Uniform-flux (x_D=0) or infinite conductivity (x_D=0.732)].....(3.11)

$$p_{D\beta d}(t_{Dxf}) = t_{Dxf}\frac{\dfrac{dp_D(t_{Dxf})}{dt_{Dxf}}}{p_D(t_{Dxf})} = t_{Dxf}\frac{\mathcal{L}^{-1}\left\{\dfrac{1}{2}\dfrac{1}{\sqrt{s}}\left[\int_0^{(1-x_D)\sqrt{s}} K_0(z)dz + \int_0^{(1+x_D)\sqrt{s}} K_0(z)dz\right]\right\}}{\mathcal{L}^{-1}\left\{\dfrac{1}{2s}\dfrac{1}{\sqrt{s}}\left[\int_0^{(1-x_D)\sqrt{s}} K_0(z)dz + \int_0^{(1+x_D)\sqrt{s}} K_0(z)dz\right]\right\}}$$

[Uniform-flux (x_D=0) or infinite conductivity (x_D=0.732)].....(3.12)

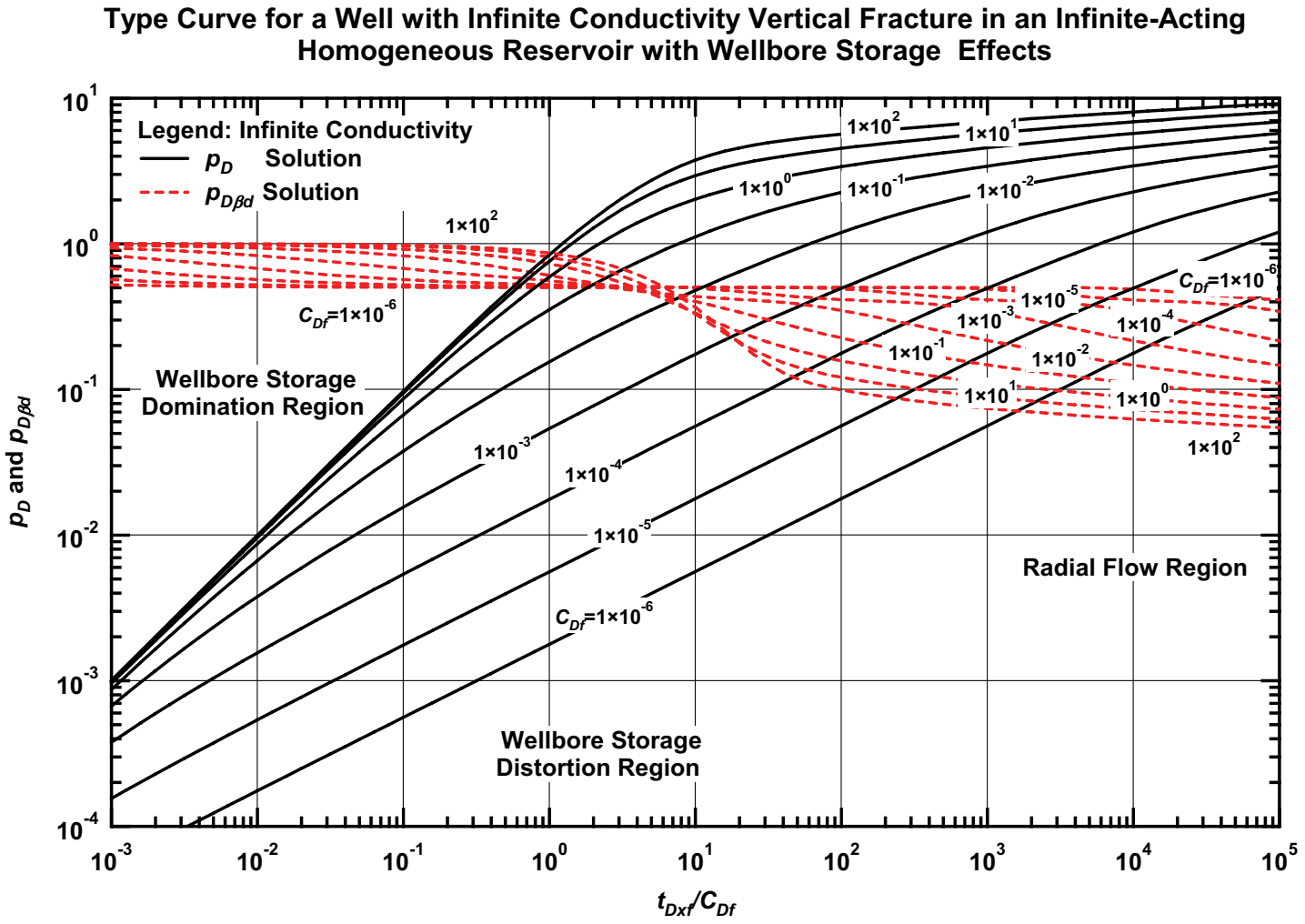

Figure 3.6 — p_D and $p_{D\beta d}$ vs. t_{Dxf}/C_{Df} — $C_{fD} = \infty$ (fractured well case — includes wellbore storage effects).

For the case of an infinite conductivity vertical fracture in an infinite-acting homogeneous reservoir, we note that the linear flow regime (characteristic of a very high fracture conductivity) is clearly seen in the β-derivative function (*i.e.,* $p_{D\beta d}(t_{Dxf})$=0.5), as shown in **Fig. 3.6**.

3.5 Unfractured Wells — Dual Porosity/Naturally Fractured Reservoir System

We used the pseudosteady-state interporosity flow model [ref. 17, Warren. and Root] to produce the β-derivative type curves for a single well in an infinite-acting, dual porosity reservoir with or without wellbore storage and skin effects. We selected the pseudosteady-state interporosity flow model because it is the most "extreme" (largest contrast in performance) of the dual porosity/naturally fractured reservoir models. The cylindrical source solution (in the Laplace domain) for the case of a well producing at a constant (surface) rate in a homogeneous infinite-acting reservoir is given as:

$$\bar{p}_D(s) = \frac{1}{s}\frac{K_0(\sqrt{sf(s)})}{\sqrt{sf(s)}K_1(\sqrt{sf(s)})} \quad \text{.....(3.13)}$$

Where $f(s)$ is the natural fracture system model and defined as:

$$f(s) = \frac{\lambda + \omega(1-\omega)s}{\lambda + (1-\omega)s} \quad \text{.....(3.14)}$$

The β-derivative formulation for this case is given by:

$$p_{D\beta d}(t_D) = t_D \frac{\dfrac{dp_D(t_D)}{dt_D}}{p_D(t_D)} = t_D \frac{\mathcal{L}^{-1}\left\{\dfrac{K_0(\sqrt{sf(s)})}{\sqrt{sf(s)}K_1(\sqrt{sf(s)})}\right\}}{\mathcal{L}^{-1}\left\{\dfrac{1}{s}\dfrac{K_0(\sqrt{sf(s)})}{\sqrt{sf(s)}K_1(\sqrt{sf(s)})}\right\}} \quad \text{.....(3.15)}$$

We chose to present our cases (which include wellbore storage) using the type curve format of ref. 18 [ref. 18, Angel], where the family parameters for the type curves are the ω and α-parameters ($\alpha = \lambda C_D$).

In **Fig. 3.7** we present a general set of cases ($\omega = 1\times10^{-1}$, 1×10^{-2}, and 1×10^{-3} and $\lambda = 5\times10^{-9}$, 5×10^{-6}, and 5×10^{-3}) *with no wellbore storage or skin effects*. **Fig. 3.7** shows the unique signature of the $p_{D\beta d}$ functions for this case, but we can also argue that, since this model is tied to infinite-acting radial flow, the $p_{D\beta d}$ functions can (at best) be used as a diagnostic to view idealized behavior.

In **Fig. 3.8** we present cases where $\omega = 1\times10^{-1}$ and $\alpha = \lambda C_D = 1\times10^{-4}$ for $1\times10^{-4} < C_D < 1\times10^{100}$. As with the results for the p_{Dd} functions shown by Angel [ref. 18], these $p_{D\beta d}$ functions do provide some insight into the form and character of the behavior for the case of a well producing at infinite-acting flow conditions in a dual porosity/naturally fractured reservoir system. In Appendix C we present the pressure, pressure derivative and β-pressure derivative solution for different values of omega (ω) and alpha (α).

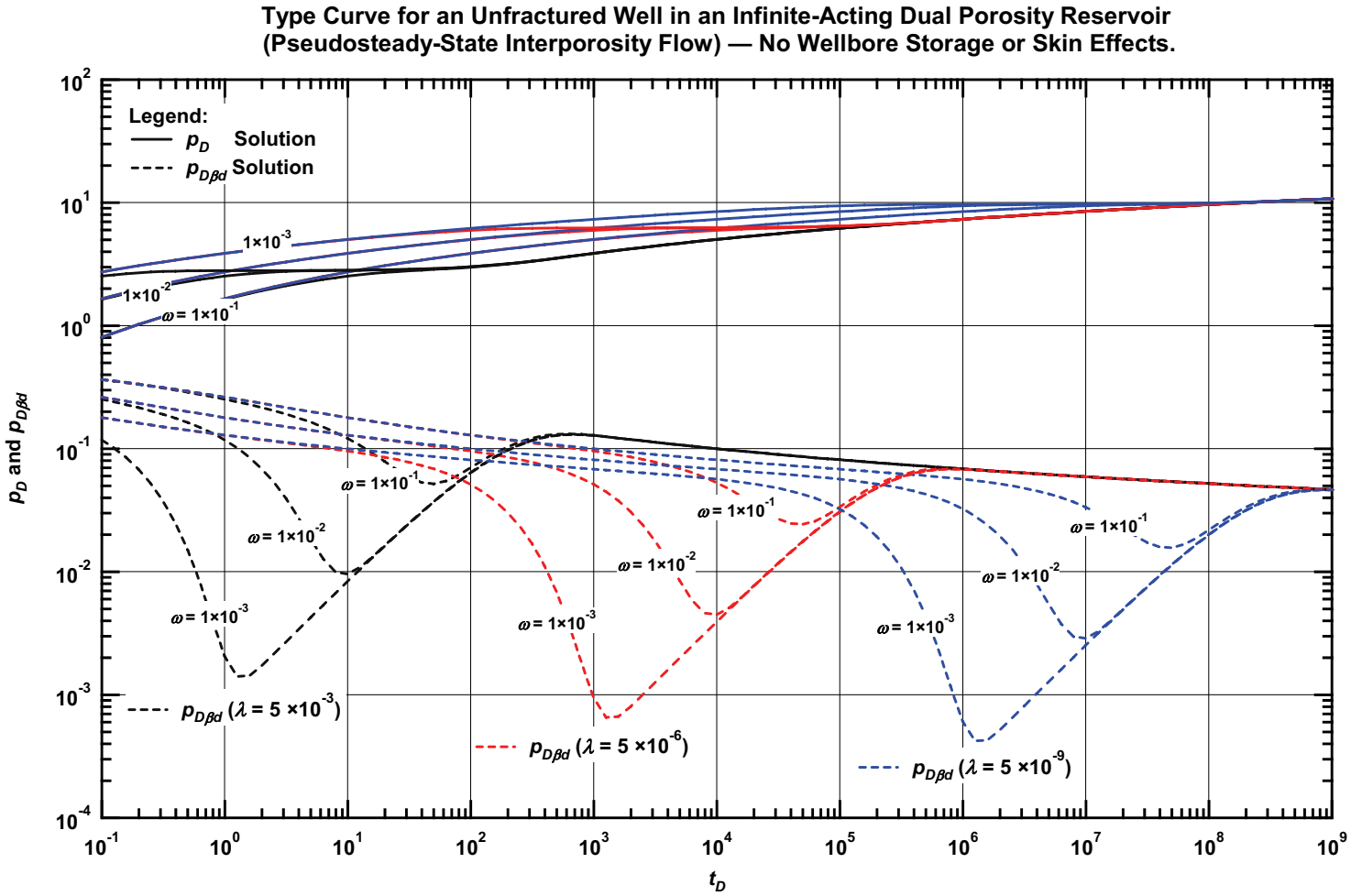

Figure 3.7 — p_D and $p_{D\beta d}$ vs. t_D — solutions for an unfractured well in an infinite-acting dual porosity system — no wellbore storage or skin effects (various λ and ω values).

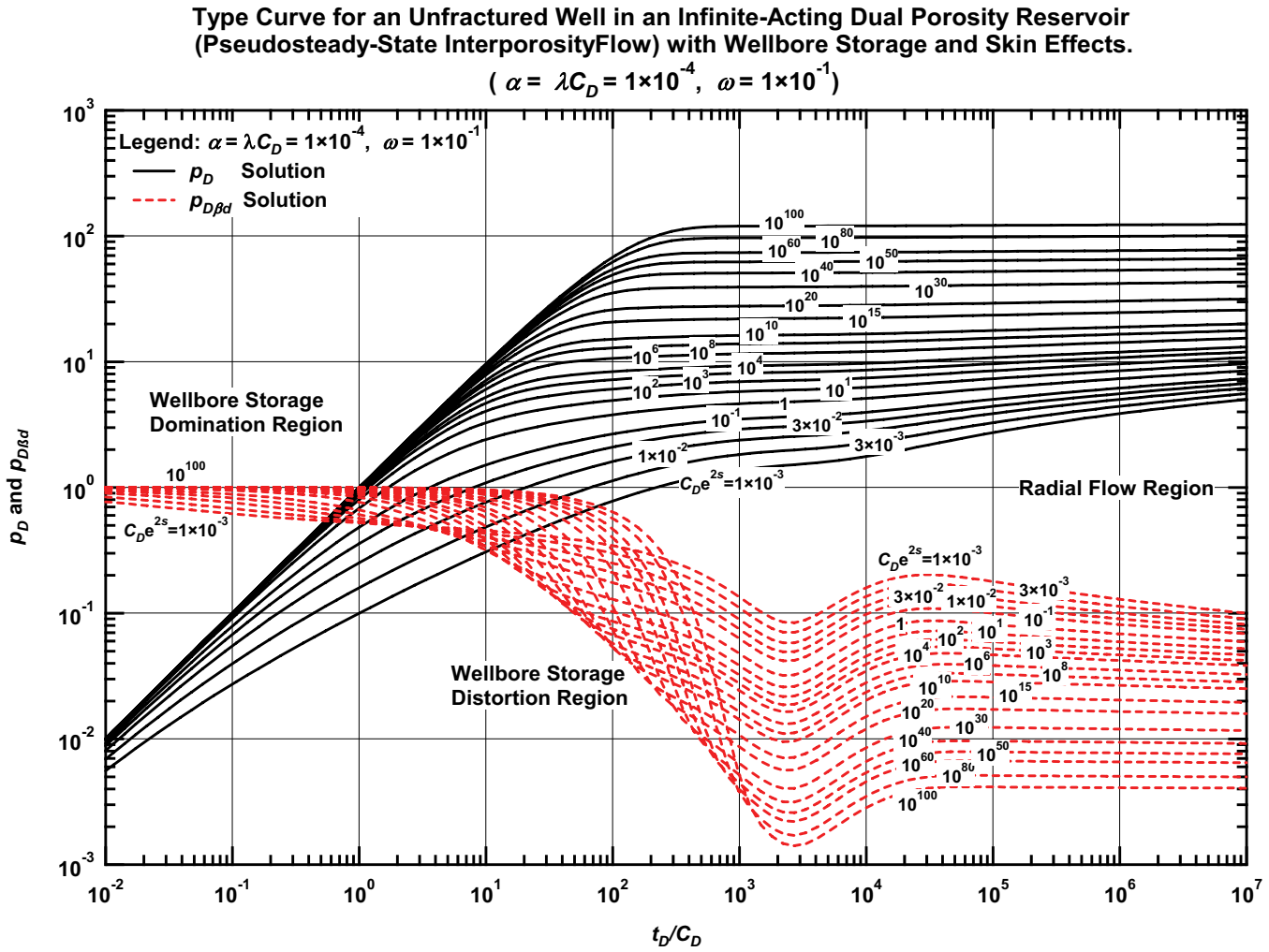

Figure 3.8 — p_D and $p_{D\beta d}$ vs. t_D/C_D — $\omega = 1\times10^{-1}$, $\alpha = \lambda C_D = 1\times10^{-4}$ (dual porosity case — includes wellbore storage and skin effects).

3.6 Fractured Wells — Dual Porosity/Naturally Fractured Reservoir System

To generate the case of a hydraulically fractured well in a naturally fractured reservoir we use the Cinco and Meng semi-analytical solution [ref. 15, Cinco and Meng] derived for a hydraulically fractured well, then adapted for a dual porosity/naturally fractured reservoir system:

$$\bar{p}_D(s)=\frac{1}{2}\int_0^1 \bar{q}_{fD}(x',s)\left[K_0(|x_D-x'|\sqrt{sf(s)})+K_0(|x_D+x'|\sqrt{sf(s)})\right]dx'-\frac{\pi}{C_{fD}}\int_0^{x_D}\int_0^{x'}\bar{q}_{fD}(x',s)dx''dx'+\frac{\pi x_D}{sC_{fD}} \qquad ...(3.16)$$

$$p_{D\beta d}(t_{Dxf})=t_{Dxf}\frac{\dfrac{dp_D(t_{Dxf})}{dt_{Dxf}}}{p_D(t_{Dxf})}=t_{Dxf}\frac{\mathcal{L}^{-1}\left\{\begin{array}{l}\dfrac{s}{2}\int_0^1\bar{q}_{fD}(x',s)\left[K_0(|x_D-x'|\sqrt{sf(s)})+K_0(|x_D+x'|\sqrt{sf(s)})\right]dx'\\ -\dfrac{s\pi}{C_{fD}}\int_0^{x_D}\int_0^{x'}\bar{q}_{fD}(x',s)\,dx''dx'+\dfrac{\pi x_D}{C_{fD}}\end{array}\right\}}{\mathcal{L}^{-1}\left\{\begin{array}{l}\dfrac{1}{2}\int_0^1\bar{q}_{fD}(x',s)\left[K_0(|x_D-x'|\sqrt{sf(s)})+K_0(|x_D+x'|\sqrt{sf(s)})\right]dx'\\ -\dfrac{\pi}{C_{fD}}\int_0^{x_D}\int_0^{x'}\bar{q}_{fD}(x',s)\,dx''dx'+\dfrac{\pi x_D}{sC_{fD}}\end{array}\right\}}$$

.....(3.17)

We have again used the pseudosteady-state interporosity flow model for dual porosity/naturally fractured reservoir flow behavior (see Eq. 3.14). **Figs. 3.9** and **3.10** are two examples of the β-derivative solution for a fractured well in a naturally fractured system with wellbore storage effects — it can easily be seen that these type curves exhibit a combination of both system characteristics. In Appendix D we present all of the type curve solutions that were generated for this case — with different fracture conductivities and a variety of dual porosity system properties (various ω and α).

3.7 Horizontal Wells — Infinite-Acting Homogeneous Reservoirs

Ozkan [ref. 16] created a line-source solution (*i.e.*, using an integration of continuous point sources) for modeling horizontal well performance. We used this solution to generate β-derivative type-curves for the case of a horizontal well of infinite conductivity, where the well is *vertically-centered* within an infinite-acting, homogeneous (and isotropic) reservoir.

$$\bar{p}_D(s)=\frac{1}{2s}\int_{-1}^{+1}K_0\left[\sqrt{s}\sqrt{(0.732-\alpha)^2}\right]d\alpha$$
$$+\frac{1}{s}\sum_{n=1}^{\infty}\cos n\pi z_D\cos n\pi z_{wD}\int_{-1}^{+1}K_0\left[\sqrt{s+n^2\pi^2L_D^2}\sqrt{(0.732-\alpha)^2}\right]d\alpha$$

.....(3.18)

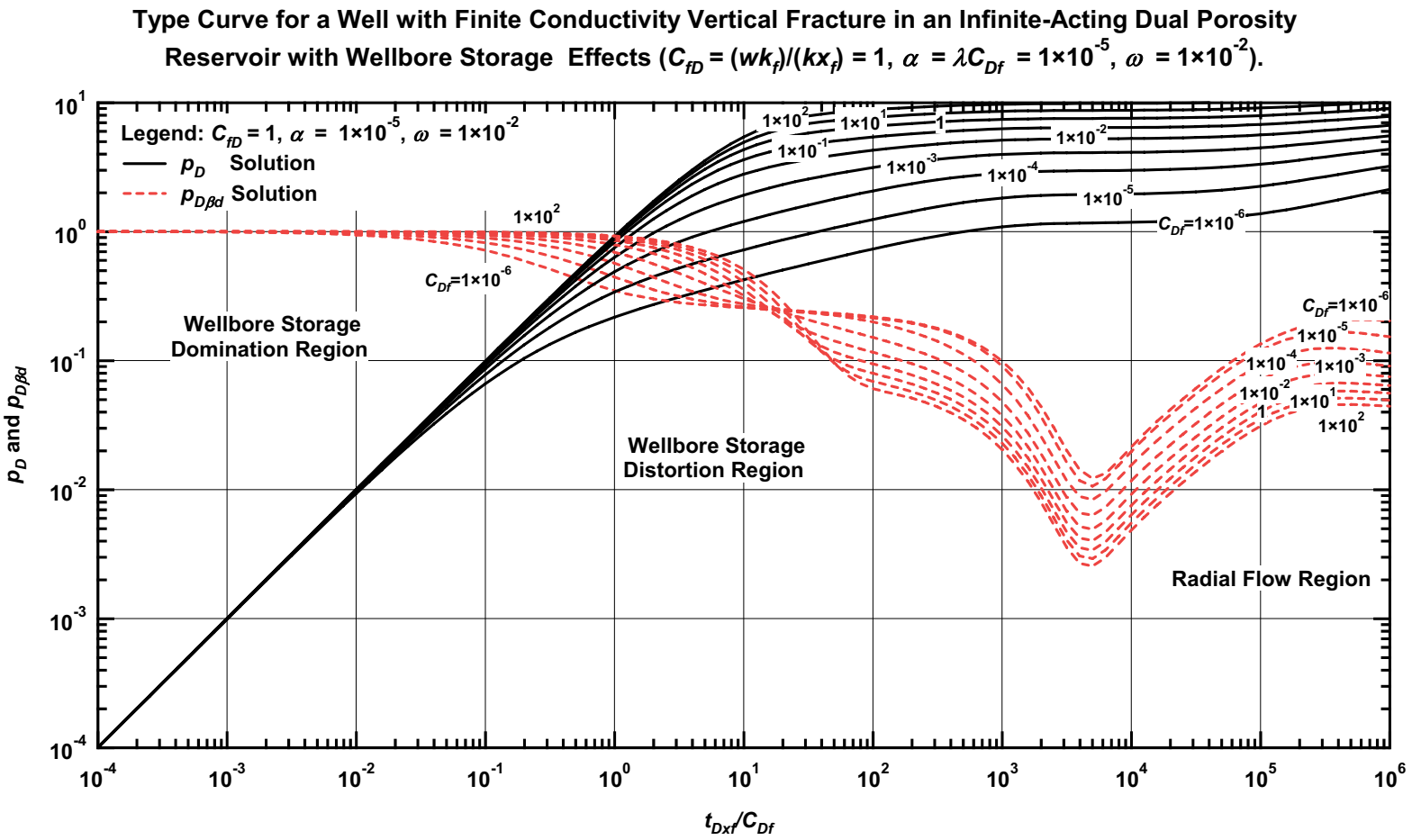

Figure 3.9 — p_D and $p_{D\beta d}$ vs. t_{Dxf}/C_{Df} — C_{fD} =1, $\omega = 1\times10^{-2}$, $\alpha = \lambda C_{Df} = 1\times10^{-5}$ (fractured well in dual porosity system case — includes wellbore storage effects).

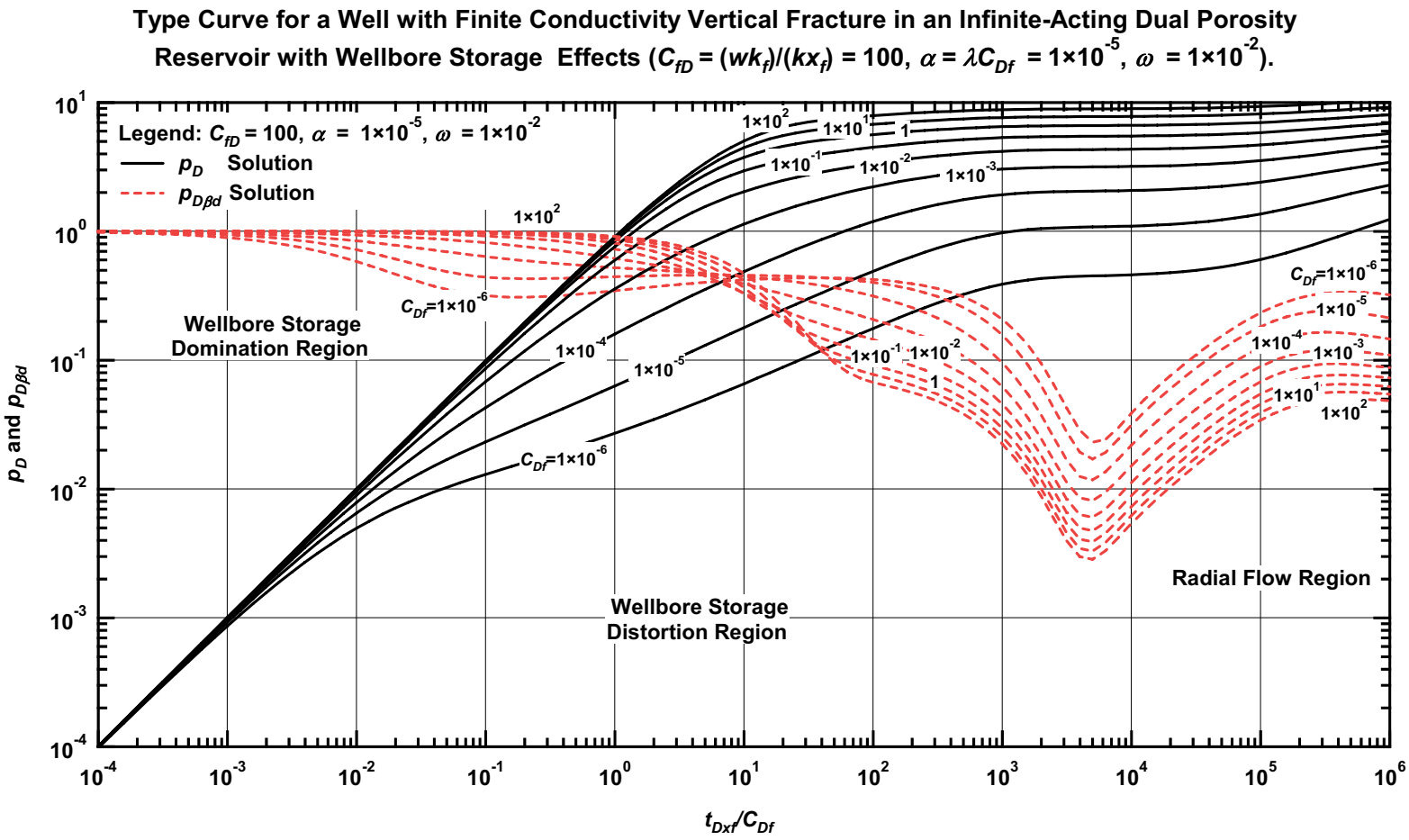

Figure 3.10 — p_D and $p_{D\beta d}$ vs. t_{Dxf}/C_{Df} — C_{fD} =100, $\omega = 1\times10^{-2}$, $\alpha = \lambda C_D = 1\times10^{-5}$ (fractured well in dual porosity system case — includes wellbore storage effects).

The real time domain formulation of Eq. 3.18 is given as:

$$p_D(t_{DL}) = \frac{\sqrt{\pi}}{4}\int_0^{t_{DL}} \left[\text{erf}\left[\frac{0.866}{\sqrt{\tau}}\right] + \text{erf}\left[\frac{0.134}{\sqrt{\tau}}\right]\right] \times \left[1 + 2\sum_{n=1}^{\infty} \exp(-n^2\pi^2 L_D^2 \tau)\cos n\pi z_D \cos n\pi z_{wD}\right] \frac{d\tau}{\sqrt{\tau}} \quad \text{.....(3.19)}$$

From which we derived the β-pressure derivative relation for this case:

$$p_{D\beta d}(t_{DL}) = t_D \frac{\frac{dp_D(t_D)}{dt_D}}{p_D(t_D)} = \frac{\left[\sqrt{t_{DL}}\left[\text{erf}\left[\frac{0.866}{\sqrt{t_{DL}}}\right] + \text{erf}\left[\frac{0.134}{\sqrt{t_{DL}}}\right]\right] \times \left[1 + 2\sum_{n=1}^{\infty} \exp(-n^2\pi^2 L_D^2 t_{DL})\cos n\pi z_D \cos n\pi z_{wD}\right]\right]}{\left[\int_0^{t_{DL}}\left[\text{erf}\left[\frac{0.866}{\sqrt{t_{DL}}}\right] + \text{erf}\left[\frac{0.134}{\sqrt{t_{DL}}}\right]\right] \times \left[1 + 2\sum_{n=1}^{\infty} \exp(-n^2\pi^2 L_D^2 \tau)\cos n\pi z_D \cos n\pi z_{wD}\right]\frac{d\tau}{\sqrt{\tau}}\right]} \quad \text{.....(3.20)}$$

In **Fig. 3.11** we present the $p_{D,}$ $p_{Dd,}$ and $p_{D\beta d}$ solutions for the case of a horizontal well with no wellbore storage or skin effects — only the influence of the L_D parameter (*i.e.*, $L_D = L/2h$) is included in order to illustrate the performance of horizontal wells with respect to reservoir thickness [thick reservoir (low L_D); thin reservoir (high L_D)].

While we do not observe any features in **Fig. 3.11** where the $p_{D\beta d}$ function is constant, we do observe unique characteristic behavior in the $p_{D\beta d}$ function, which should be of value in the diagnostic interpretation of pressure transient test data obtained from horizontal wells.

The p_{Dd} and $p_{D\beta d}$ solutions for the case of a horizontal well with wellbore storage effects are shown in **Fig. 3.12** (L_D=100, *i.e.*, a thin reservoir). As expected, we do observe the strong signature of the $p_{D\beta d}$ function for the *wellbore storage domination regime* (*i.e.*, $p_{D\beta d} = 1$). We also note an *apparent* formation linear flow regime for low values of the wellbore storage coefficient (*i.e.*, $C_{DL} < 1\text{x}10^{-2}$). We believe that this is a transition from the wellbore storage influence to linear flow (which is brief for this case), then on through the transition regime towards pseudo-radial flow. For reference, other type curve solutions which were generated using different dimensionless well lengths are presented in Appendix E.

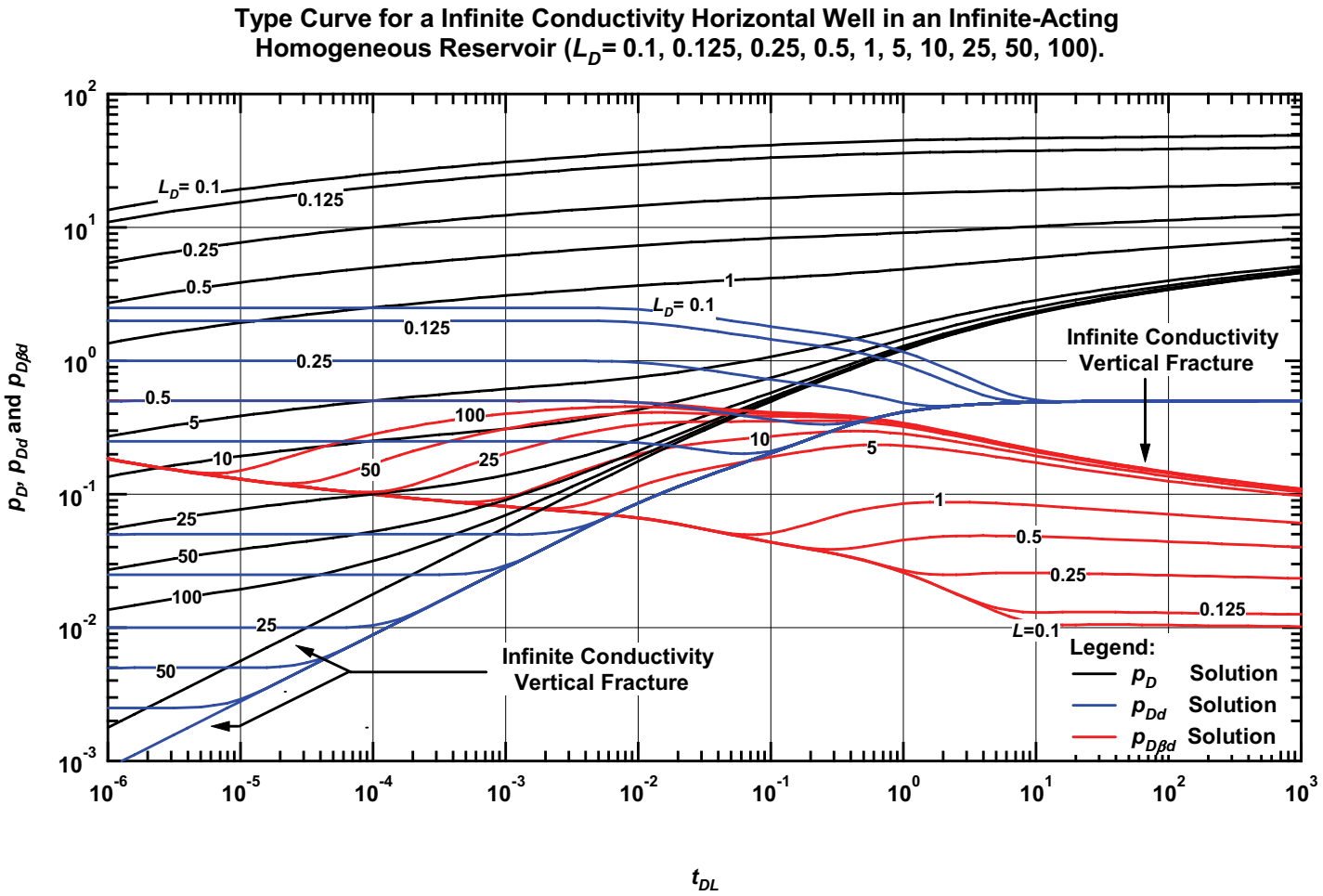

Figure 3.11 — p_D, p_{Dd}, and $p_{D\beta d}$ vs. t_{DL} — solutions for an infinite conductivity horizontal well in an infinite-acting homogeneous reservoir — no wellbore storage or skin effects (various L_D values).

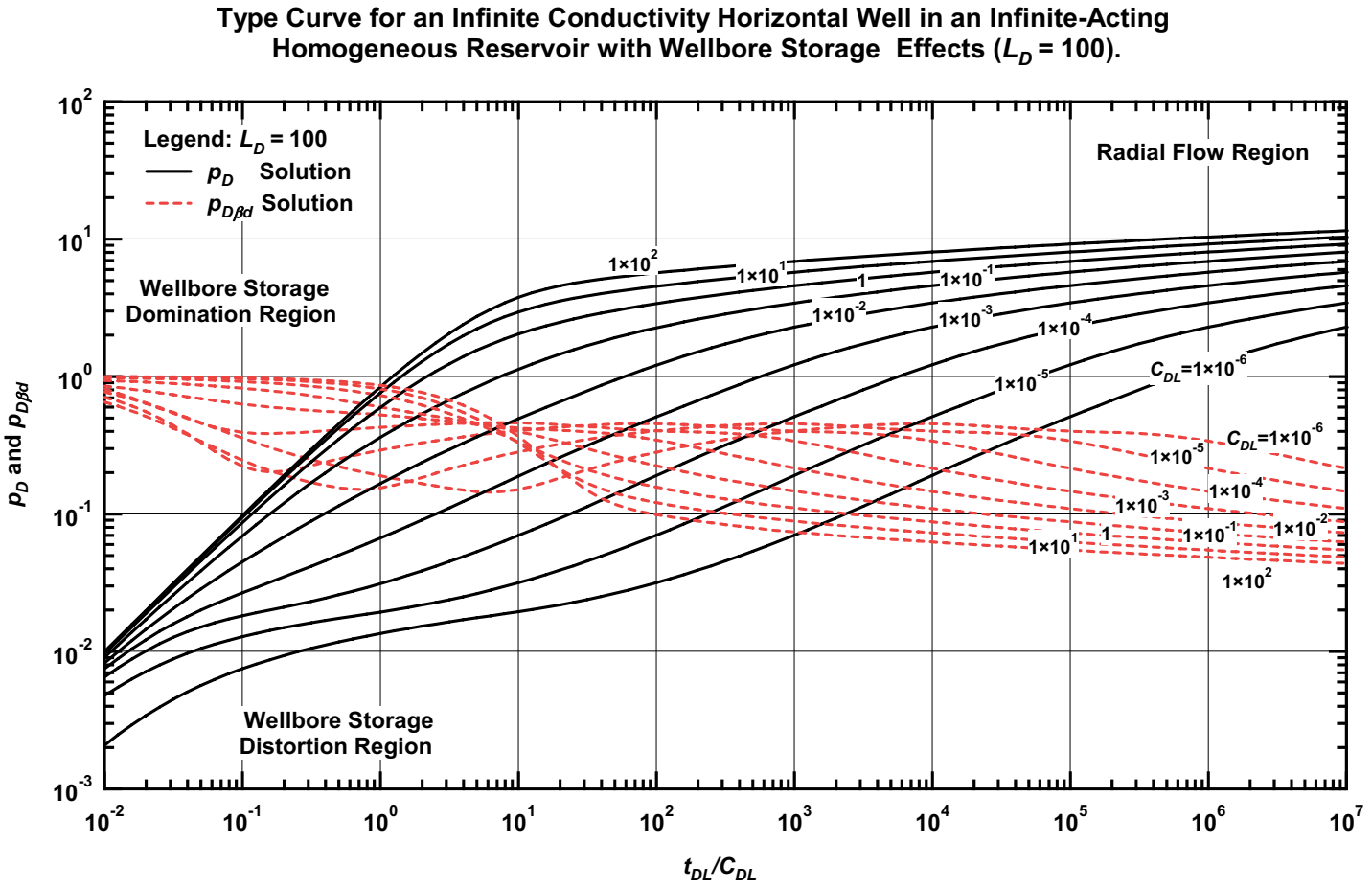

Figure 3.12 — p_D and $p_{D\beta d}$ vs. t_{DL}/C_{DL} — L_D=100 (horizontal well case — includes wellbore storage effects).

3.8 Application Procedure for the β-Derivative Type Curves

The β-derivative is a ratio function — the dimensionless formulation of the β-derivative ($p_{D\beta d}$) is exactly the same function as the "data" formulation of the β-derivative [$\Delta p_{\beta d}(t)$]. Therefore, when we plot the $\Delta p_{\beta d}(t)$ (data) function onto the grid of the $p_{D\beta d}$ function (*i.e.*, the type curve match) the y-axis functions are identical (and hence, fixed). As such, the vertical "match" is not a match at all — but rather, the model and the data functions are defined to be the same — so the vertical "match" is fixed.

At this point, the time axis match is the only remaining task, so the $\Delta p_{\beta d}(t)$ data function is shifted on top of the $p_{D\beta d}$ function — but only in the horizontal direction. The time (or horizontal) match is then used to diagnose the flow regimes and provide an auxiliary match of the time axis. When the $\Delta p_{\beta d}(t)$ function is plotted with the $\Delta p(t)$ and the $\Delta p_d(t)$ functions, we achieve a "harmony" in that the 3 functions are matched simultaneously, and one portion of the match (*i.e.*, $\Delta p_{\beta d}(t)$ — $p_{D\beta d}$) is fixed.

The procedures for type curve matching the β-derivative data and models are essentially identical the process given for the pressure derivative ratio functions [ref. 9, Onur and Reynolds; and ref. 10, Doung]. As with the "pressure derivative ratio" function, the $\Delta p_{\beta d}(t)$ — $p_{D\beta d}$ "match" is fixed, which then also fixes the $\Delta p(t)$ and the $\Delta p_d(t)$ functions on the vertical scale, and only the x-axis needs to be resolved — exactly like any other type curve for that particular case. If type curves are not used, and some sort of software-driven, model-based matching procedure is used (*i.e.*, event/history matching), then the $\Delta p_{\beta d}(t)$ and $p_{D\beta d}$ functions are matched simultaneously, in the same manner that the dimensionless pressure/derivative functions would be matched.

CHAPTER IV

APPLICATION OF THE NEW TECHNIQUE TO FIELD DATA

4.1 Introduction

To demonstrate/validate the β-derivative function, we present the results of 12 field examples obtained from the literature [refs. 1, 19-23]. **Table 4.1** below provides orientation for our examples.

Table 4.1 — List of the field examples from the literature.

Case		Field Example	**Fig.**	ref.
[oil]	Unfractured well (buildup)	1	**11**	20
[oil]	Unfractured well (buildup)	2	**12**	1
[oil]	Dual porosity (drawdown)	3	**13**	21
[oil]	Dual porosity (buildup)	4	**14**	22
[gas]	Fractured well (buildup)	5	**15**	23
[gas]	Fractured well (buildup)	6	**16**	23
[gas]	Fractured well (buildup)	7	**17**	23
[water]	Fractured well (falloff)	8	**18**	24
[water]	Fractured well (falloff)	9	**19**	24
[water]	Fractured well (falloff)	10	**20**	24
[water]	Fractured well (falloff)	11	**21**	24
[water]	Fractured well (falloff)	12	**22**	24

In all of the example cases we were able to successfully interpret and analyze the well test data objectively using the β-derivative function [$\Delta p_{\beta d}(t)$] in conjunction with the $\Delta p(t)$ and $\Delta p_d(t)$ functions. As a comment, for all of the example cases we considered, the β-derivative function [$\Delta p_{\beta d}(t)$] provided a direct analysis (*i.e.*, the "match" was obvious using the $\Delta p_{\beta d}(t)$ function — the vertical axis match was fixed, and only horizontal shifting was required). These examples and the model-based type curves validate the theory and application of the β-derivative function as a diagnostic mechanism for the analysis and interpretation of pressure transient test data.

4.2 Field Examples

In this section we present the application of the β-derivative function to well test analysis of 12 field examples as mentioned above. We note that all of the field examples are conventional well tests which were taken from literature.

4.2.1 Field Example 1

Example 1 is presented in **Fig. 4.1** [ref. 19, Meunier *et al*] and shows the field data and model matches for the $\Delta p(t)$, $\Delta p_d(t)$, and $\Delta p_{\beta d}(t)$ functions in dimensionless format (*i.e.*, the p_D, p_{Dd}, and $p_{D\beta d}$ "data" functions are given as symbols), along with the corresponding dimensionless solution functions (*i.e.*, p_D, p_{Dd}, and $p_{D\beta d}$ "model" functions given by the solid lines). This is the common format used to view the example cases in this work.

As noted in ref. 19, in this case wellbore storage effects are evident, and for the purpose of demonstrating a variable-rate procedure, downhole rates were measured. In **Fig. 4.1** we note a strong wellbore storage signature, and we find that the $p_{D\beta d}$ data function (squares) does yield the required value of unity. The $p_{D\beta d}$ data function does not yield a quantitative interpretation — other than the wellbore storage domination region ($p_{D\beta d} = 1$), but this function does provide some resolution for the data in the transition region from wellbore storage and infinite-acting radial flow.

4.2.2 Field Example 2

In **Fig. 4.2** we consider the initial literature article regarding well test analysis using the Bourdet pressure derivative function (Δp_d) [ref. 1, Bourdet *et al*]. This is a pressure buildup test where the appropriate rate history superposition is used for the time function axis. This result is an excellent match of all functions, but in particular, the β-derivative function ($p_{D\beta d}$) is an excellent diagnostic function for the wellbore storage and transition flow regimes.

Particular to this case **(Fig. 4.2)** is the fact that the duration of the pressure buildup was almost twice as long as the reported pressure drawdown. We note this issue because we believe that in order to validate the use of the β-derivative function ($p_{D\beta d}$) then we must ensure that the analyst recognizes that this function will be affected by all of the same phenomena which affect the "Bourdet" derivative function — in particular, the rate history must be accounted for, most likely using the effective time concept where a radial flow superposition function is used for the time axis.

4.2.3 Field Example 3

The next example case shown in **Fig. 4.3** is taken from a well in a known dual porosity/naturally fractured reservoir [ref. 20, DaPrat *et al*]. As we note in **Fig. 4.3**, the "late" portion of the data is not matched well with the specified reservoir model (infinite-acting radial flow with dual porosity effects). We contend that part of the less-than-perfect late time data match may be due to rate history effects (only a single production rate was reported — it is unlikely that the rate remained constant during the entire drawdown sequence).

However, we believe that this example illustrates the challenges typical of what an analyst faces in practice, and as such, we believe the β-derivative function to be of significant practical value. We note that the β-derivative provides a clear match of the wellbore storage domination/distortion period, and the function also works well in the transition to system radial flow.

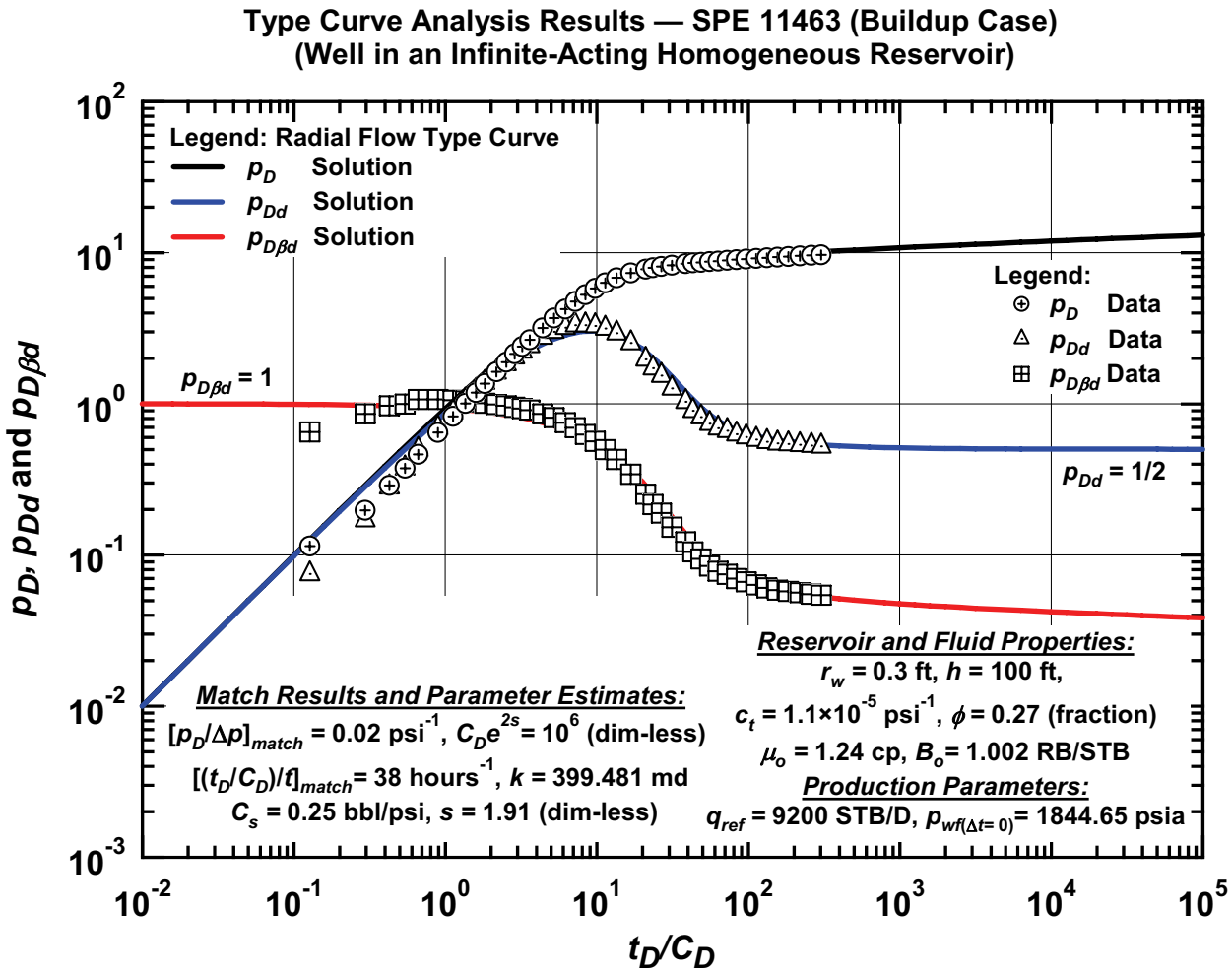

Figure 4.1 — Field example 1 type curve match — SPE 11463 [ref. 19, Meunier *et al*] (pressure build-up case).

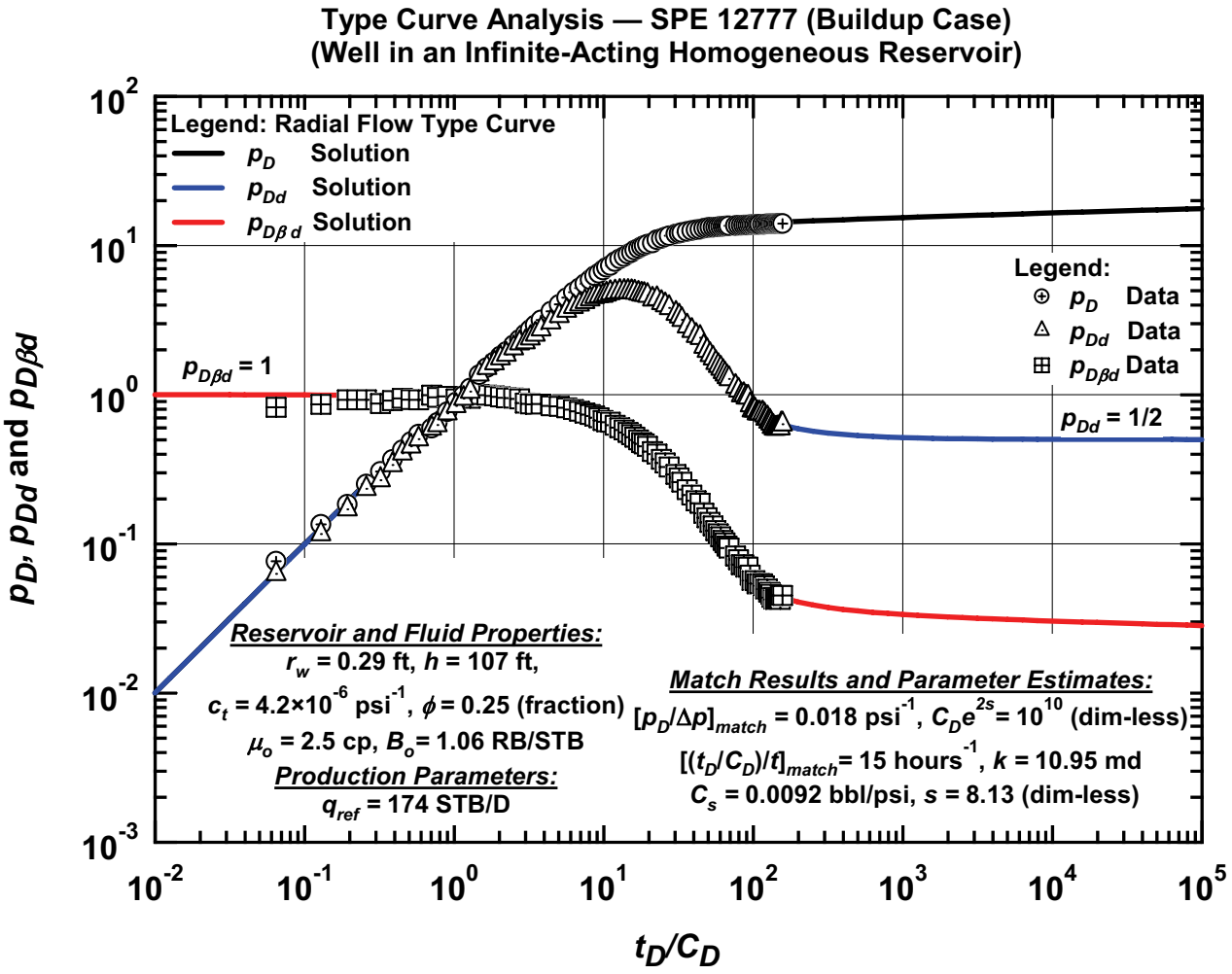

Figure 4.2 — Field example 2 type curve match — SPE 12777 [ref. 1, Bourdet *et al*] (pressure buildup case).

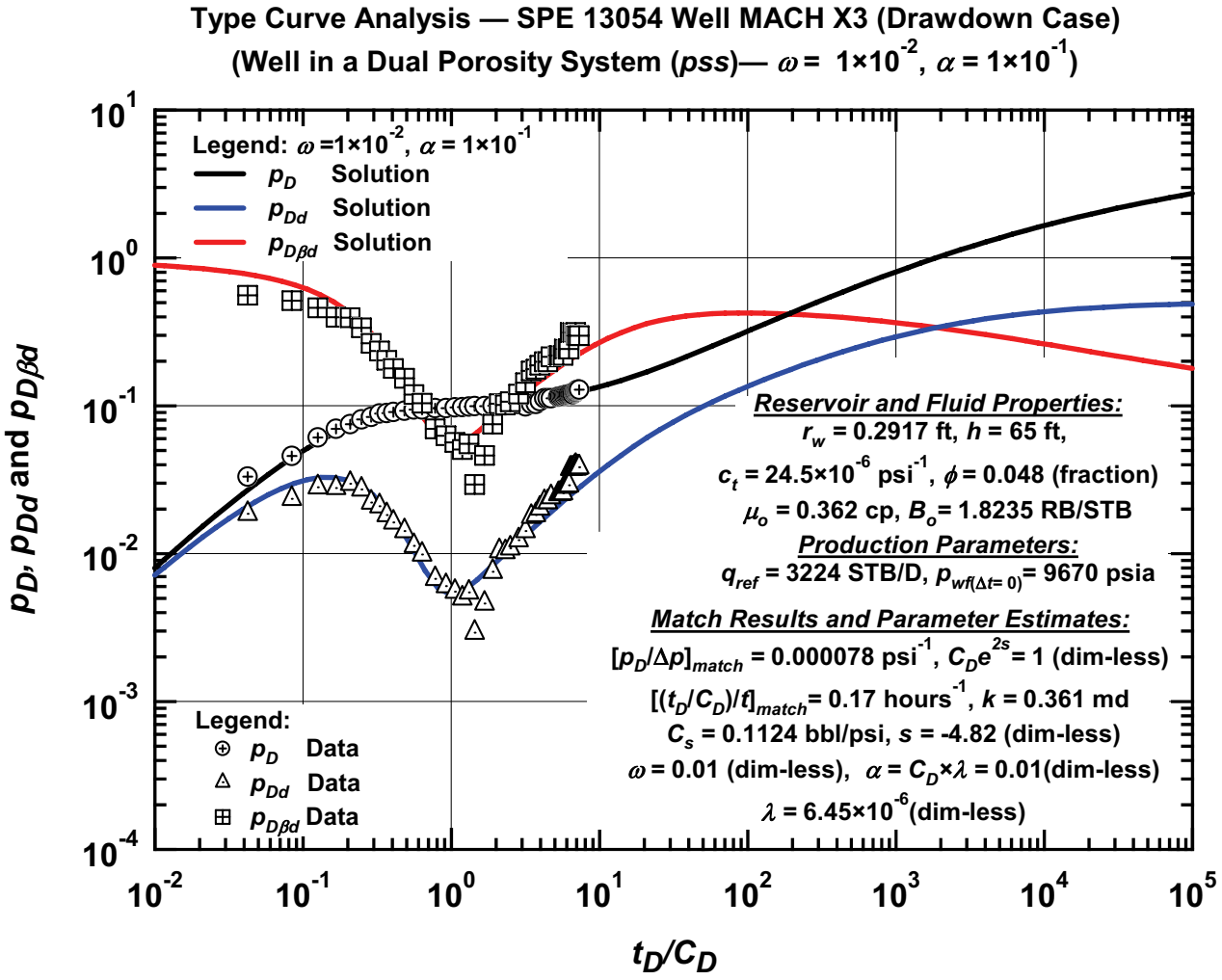

Figure 4.3 — Field example 3 type curve match — SPE 13054 [ref. 20, DaPrat *et al*] (pressure drawdown case).

4.2.4 Field Example 4

Our next case (Example 4) also considers well performance in a dual porosity/naturally fractured reservoir (see **Fig. 4.4**) [ref. 21, Allain and Horne]. From these data we again note a very strong performance of the β-derivative function — particularly in the region defined by transition from wellbore storage to transient interporosity flow. Cases such as these validate the application of the β-derivative for the interpretation of well test data obtained from dual porosity/naturally fractured reservoirs.

4.2.5 Field Example 5

In **Fig. 4.5** we investigate the use of the β-derivative function for the case of a well in a low permeability gas reservoir with an *apparent* infinite conductivity vertical fracture ["Well 5" from ref. 22, Lee and Holditch]. This is the type of case where the β-derivative function provides a unique interpretation for a difficult case. Most importantly, the β-derivative function supports the existence (and influence) of the hydraulic fracture.

4.2.6 Field Example 6

Another application of the β-derivative function is also to prove when a flow regime does not (or at least probably does not) exist — the example shown in **Fig. 4.6** is just such a case. From ref. 22 [Lee and Holditch], "Well 10" is designated as a hydraulically fractured well in a gas reservoir. In **Fig. 4.6** we observe *no evidence of a hydraulic fracture treatment* from any of the dimensionless plotting functions, in particular, the β-derivative function shows no evidence of a hydraulic fracture. The well is either poorly fracture-stimulated, or a "skin effect" has obscured any evidence of a fracture treatment — in either case, the performance of the well is significantly impaired.

4.2.7 Field Example 7

"Well 12" from ref. 22 [Lee and Holditch] is also designated as a hydraulically fractured well in a gas reservoir. In **Fig. 4.7** we note that there is no absolute signature given by the β-derivative function (*i.e.*, we do not observe $p_{D\beta d} = 1/2$ (infinite fracture conductivity) nor $p_{D\beta d} = 1/4$ (finite fracture conductivity)). We do note that $p_{D\beta d} = 1$ at early times, which confirms the wellbore storage domination regime. The p_{Dd} and $p_{D\beta d}$ signatures during mid-to-late times confirm the well is highly stimulated — and the infinite fracture conductivity vertical fracture model is used for analysis and interpretation in this case.

4.2.8 Field Example 8

In **Fig. 4.8** we present Well 207 from ref. 23 [Samad], another hydraulically fractured well case — this time the well is a water injection well in an oil field, and a "falloff test" is conducted. In this case there are no data at very early times so we cannot confirm the wellbore storage domination flow regime. However; we can use the β-derivative function to confirm the existence of an infinite conductivity vertical fracture for this case, which is an important diagnostic.

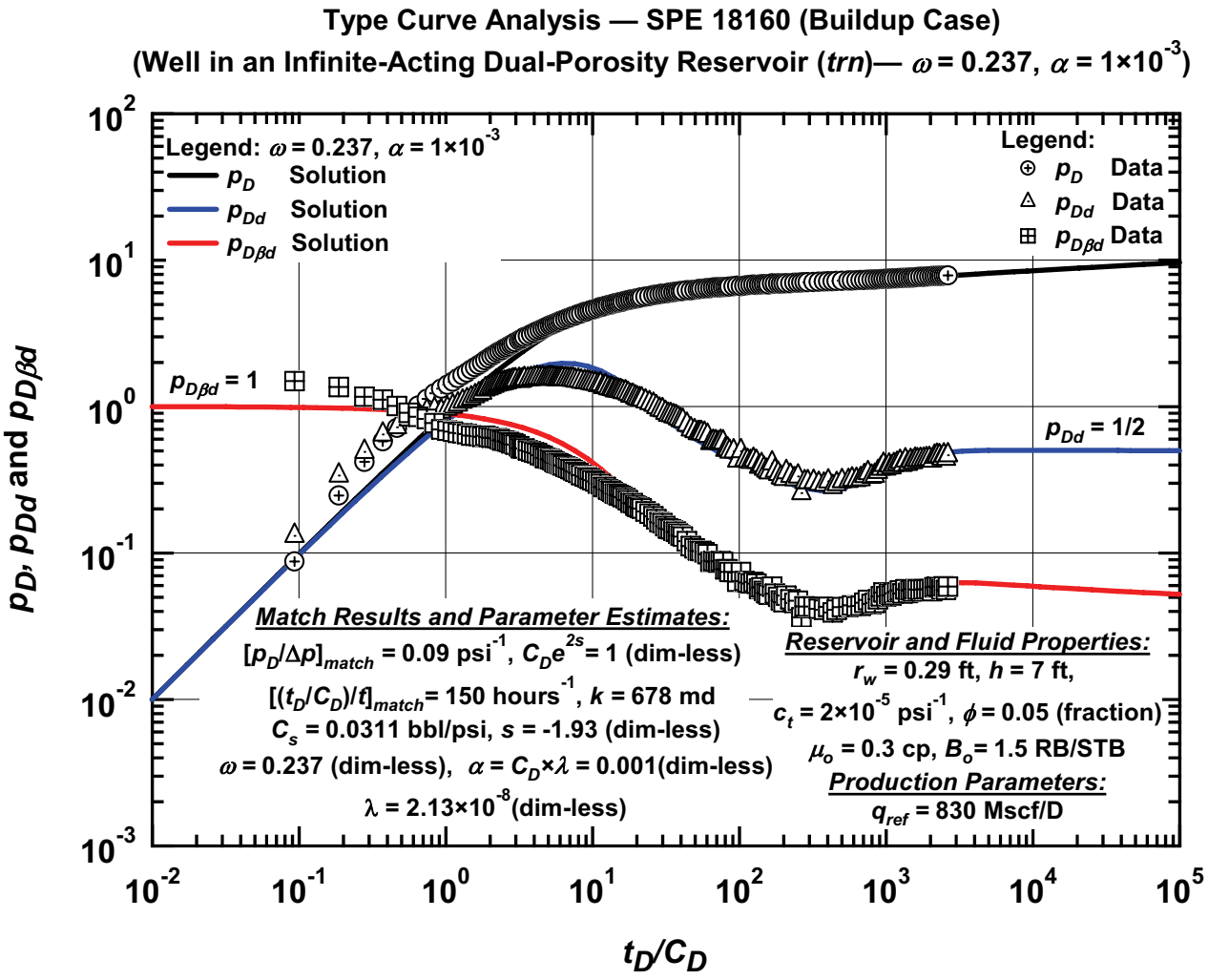

Figure 4.4 — Field example 4 type curve match — SPE 18160 [ref. 21, Allain and Horne] (pressure buildup case).

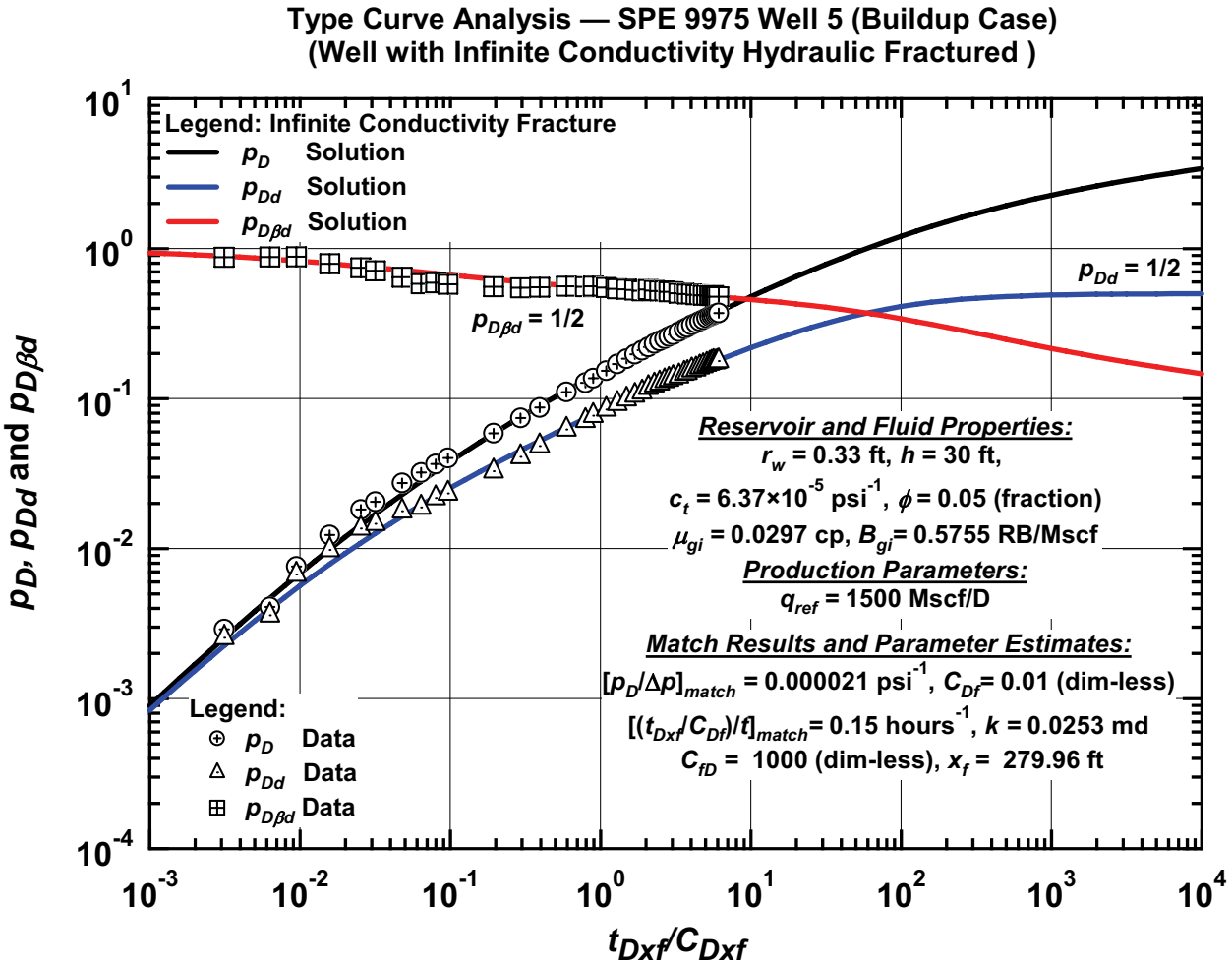

Figure 4.5 — Field example 5 type curve match — SPE 9975 Well 5 (ref. 22, Lee and Holditch) (pressure buildup case).

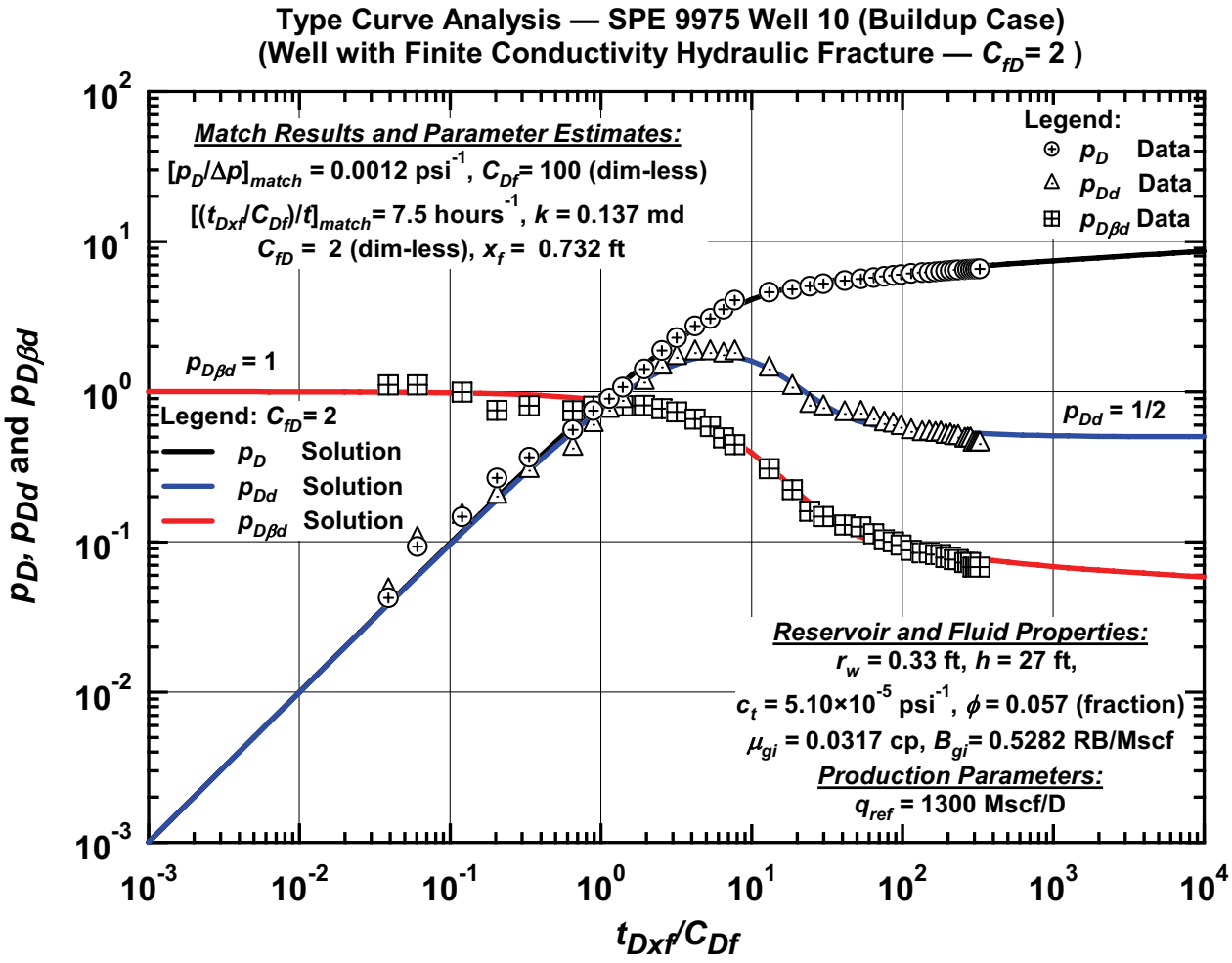

Figure 4.6 — Field example 6 type curve match — SPE 9975 Well 10 (ref. 22, Lee and Holditch) (pressure buildup case).

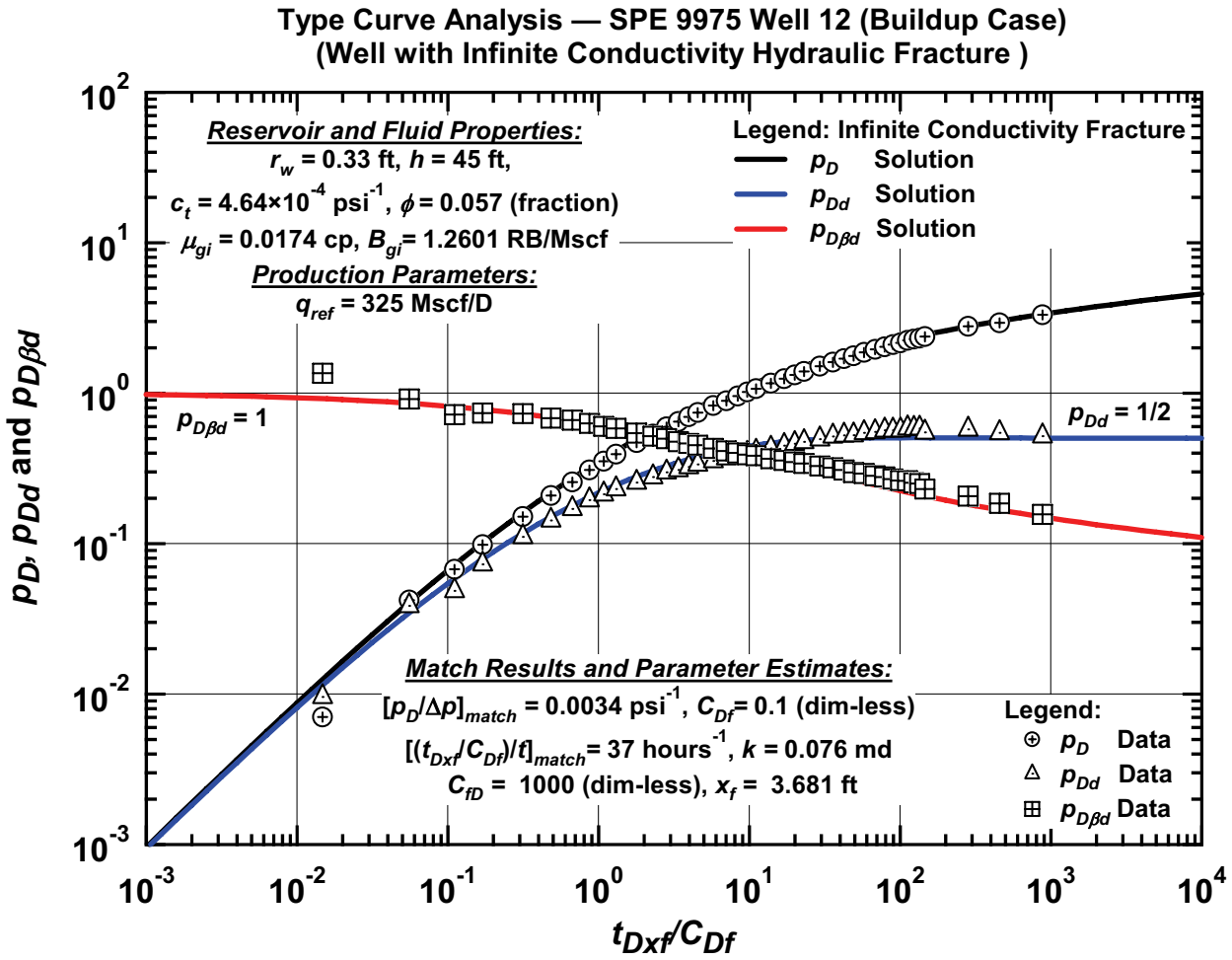

Figure 4.7 — Field example 7 type curve match — SPE 9975 Well 12 (ref. 22, Lee and Holditch) (pressure buildup case).

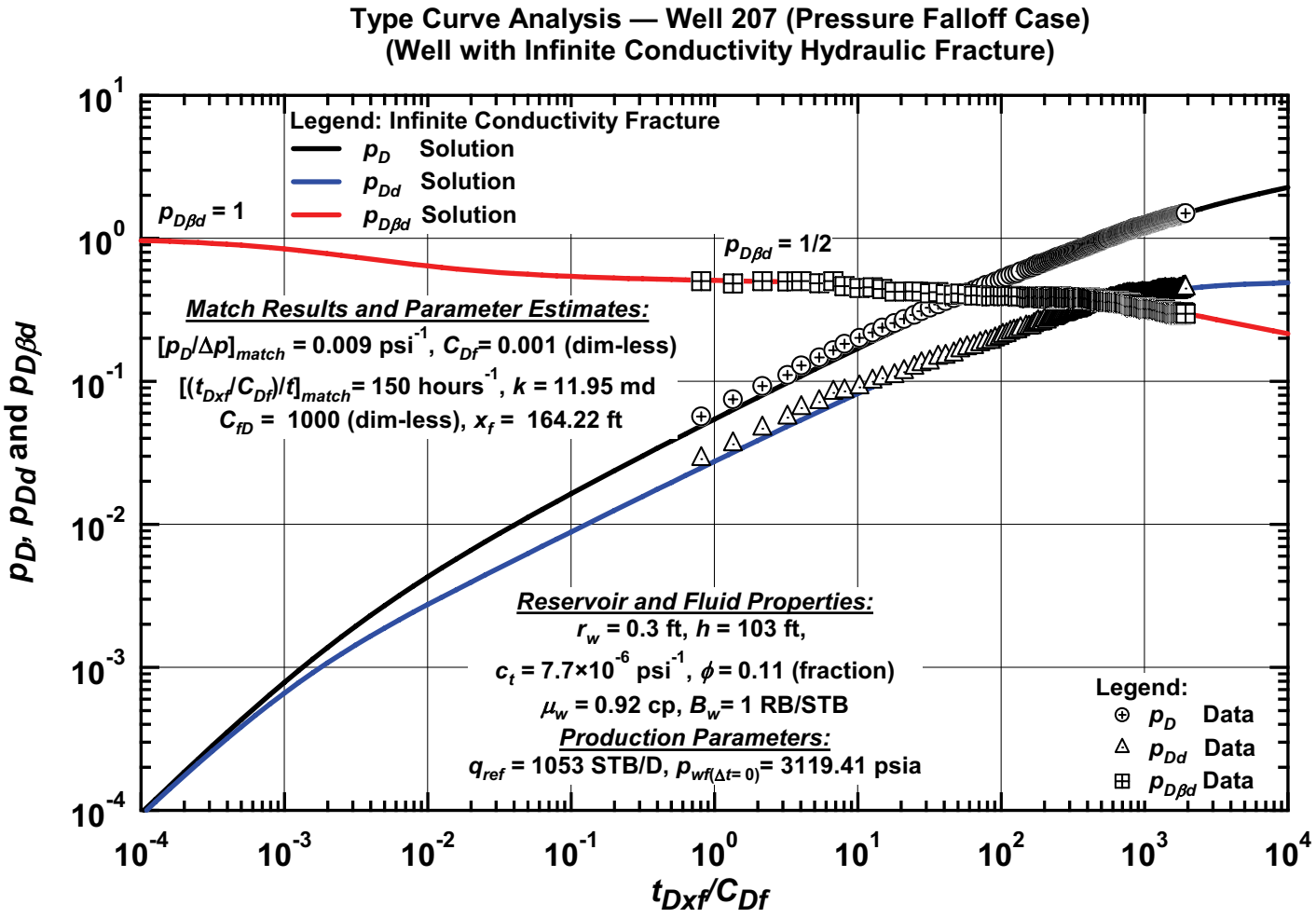

Figure 4.8 — Field example 8 type curve match — Well 207 (ref. 23, Samad) (pressure falloff case).

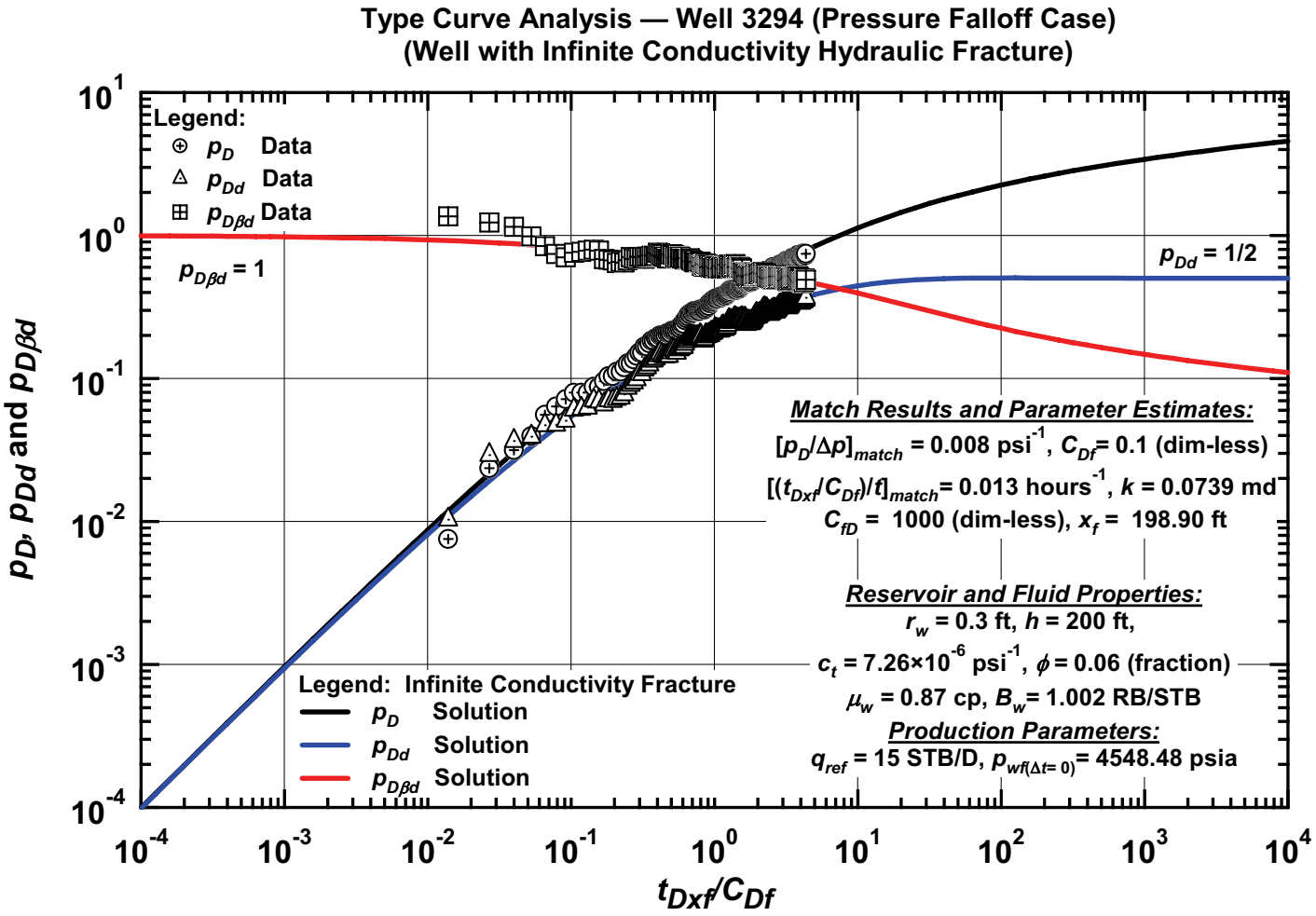

Figure 4.9 — Field example 9 type curve match — Well 3294 (ref. 23, Samad) (pressure falloff case).

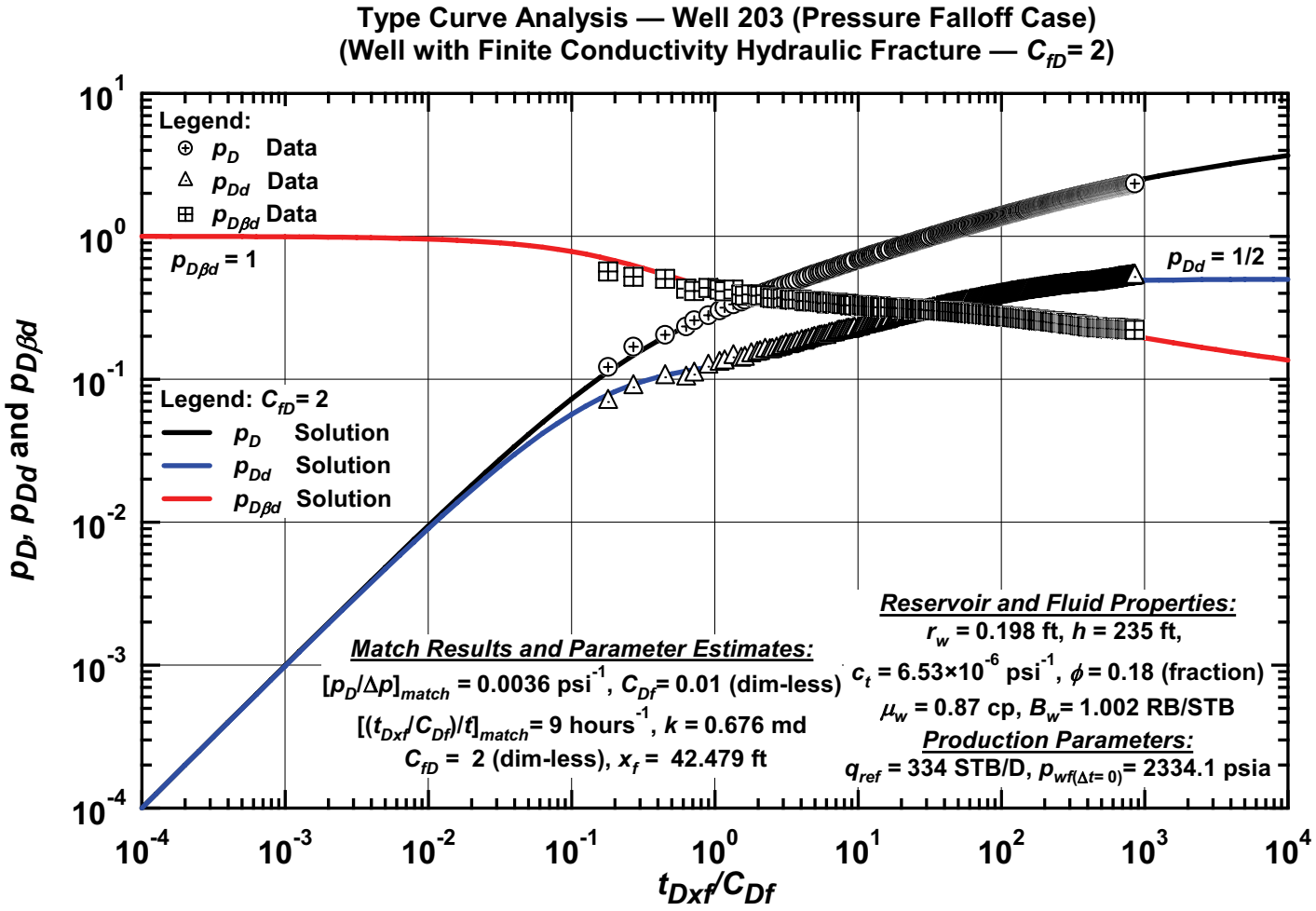

Figure 4.10 — Field example 10 type curve match — Well 203 (ref. 23, Samad) (pressure falloff case).

4.2.9 Field Example 9

In **Fig. 4.9** we present Well 3294 from ref. 23 [Samad], where the data for this case are somewhat erratic due to acquisition at the surface (*i.e.*, only surface pressures are used). Using the β-derivative function we can identify the wellbore storage domination regime (*i.e.*, $p_{D\beta d} = 1$) and we can also reasonably confirm the existence of an infinite conductivity vertical fracture ($p_{D\beta d} = 1/2$). The quality of these data impairs our ability to define the reservoir model uniquely, but we can presume that our assessment of the flow regimes is reasonable, based on the character of the β-derivative function.

4.2.10 Field Example 10

The data for Well 203, taken from ref. 23 [Samad] are presented in **Fig. 4.10.** The signature given by the p_D, p_{Dd}, and $p_{D\beta d}$ functions does not appear to be that of a high conductivity vertical fracture. In this case the p_D and p_{Dd} functions suggest a finite conductivity vertical fracture (note that these functions are less than 1/2 slope). The analysis of these data yields a fairly low estimate for the fracture conductivity (*i.e.*, $C_{fD} = 2$), where this result could suggest that the injection process is not continuing to propagate the fracture, and that the fracture is of low conductivity.

4.2.11 Field Example 11

In **Fig. 4.11** we present the data for Well 5408, a pressure falloff test obtained from ref. 23 [Samad]. This case also exhibits no unique character in the p_D, p_{Dd}, and $p_{D\beta d}$ functions, other than wellbore storage domination ($p_{D\beta d} = 1$) and infinite-acting radial flow ($p_{Dd} = 1/2$). Based on the given data, we know that this well was hydraulically fractured — and again, based on the injection history, we can conclude that the well has an infinite conductivity vertical fracture where wellbore storage domination and radial flow exists (which was the model used to provide the match in **Fig. 4.11**).

4.2.12 Field Example 12

Our last field example is a pressure falloff test performed on Well 2403, also taken from ref. 23 [Samad]. These data are presented in **Fig. 4.12** and we observe the flow regimes for wellbore storage domination ($p_{D\beta d} = 1$), and infinite-acting radial flow ($p_{Dd} = 1/2$). As for characterization of the well efficiency, we can only conclude that the signature appears to be that of a well with a high conductivity vertical fracture, hence our match using the model for a well with an infinite conductivity vertical fracture.

4.3 Summary

In closing this chapter on the example application of the β-derivative function, we conclude that the β-derivative can provide unique insight, particularly for pressure transient data from fractured wells, pressure transient data which are influenced by wellbore storage, and pressure transient data (and likely production data) which are influenced by closed boundary effects. In addition, the β-derivative function exhibits some diagnostic character for the pressure transient behavior of dual porosity/naturally fractured reservoir systems, although these diagnostics are less quantitative in such cases [*i.e.*, the $\Delta p_{\beta d}(t)$ and $p_{D\beta d}$ functions do not exhibit "constant" behavior as with other cases (*e.g.*, wellbore storage, fracture flow regimes, and boundary-dominated flow)].

We believe that these examples confirm the utility and relevance of the β-derivative function — and we expect the β-derivative to find considerable practical application in the analysis/interpretation of pressure transient test data and (eventually) production data.

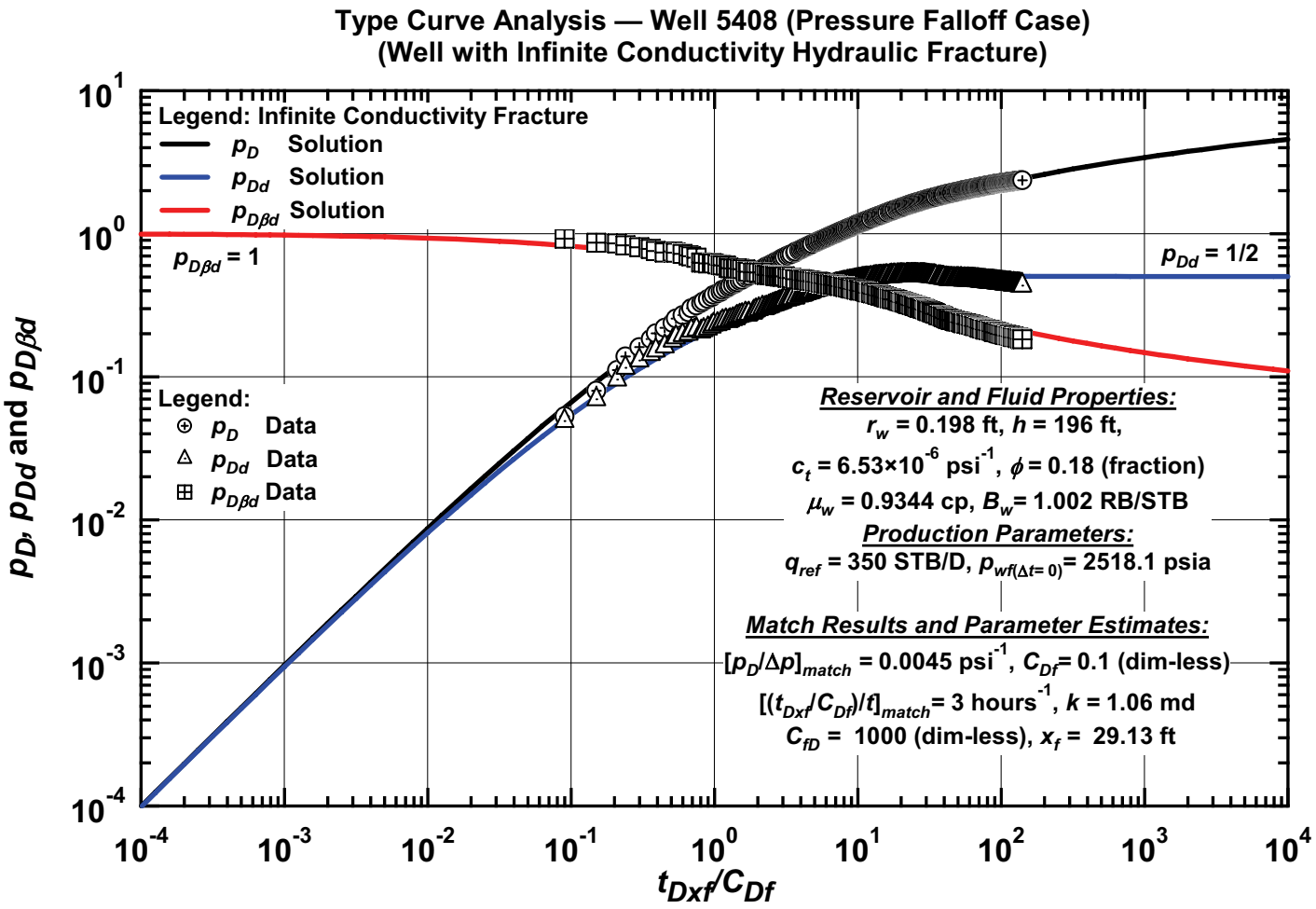

Figure 4.11 — Field example 11 type curve match — Well 5408 (ref. 23, Samad) (pressure falloff case).

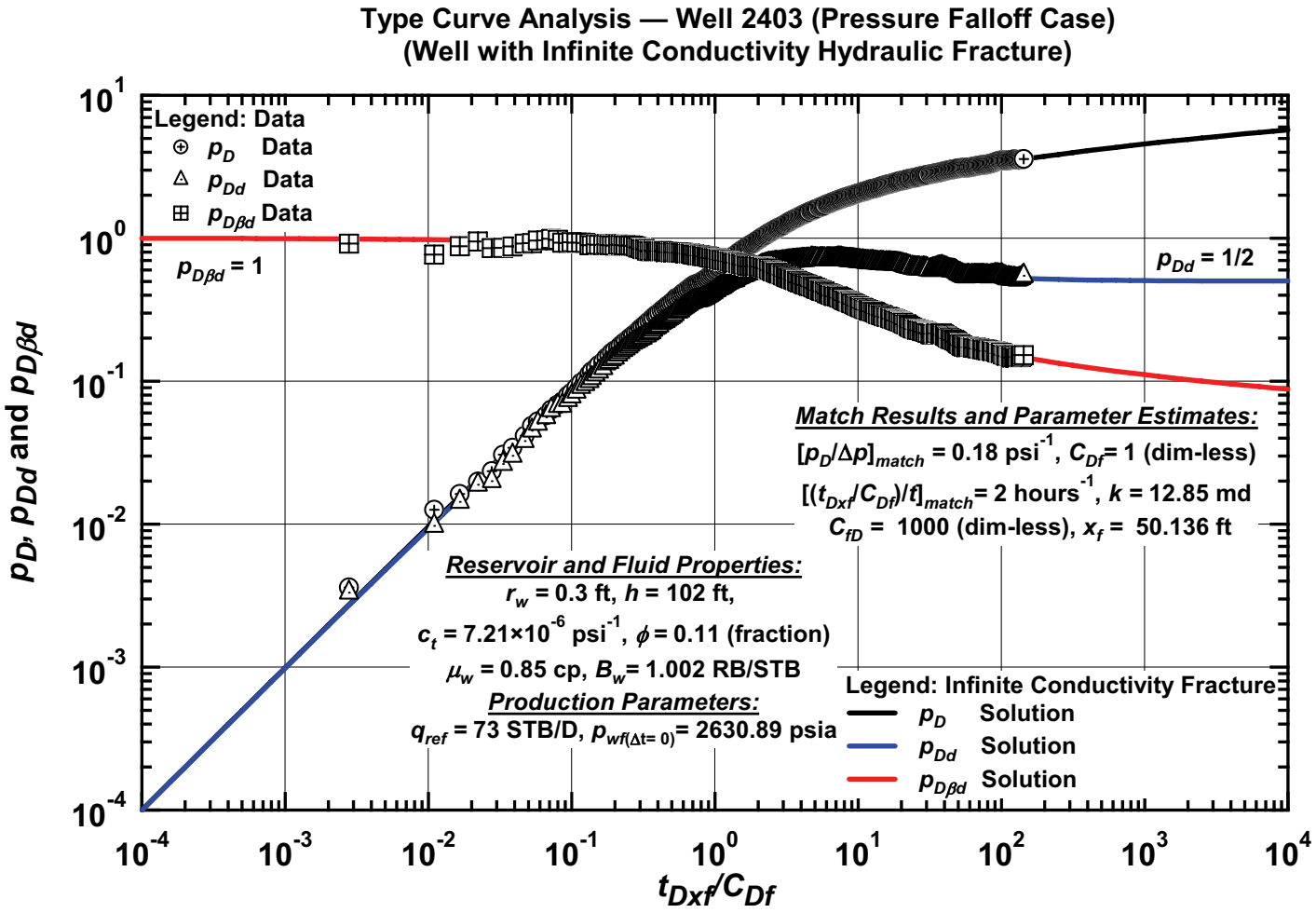

Figure 4.12 — Field example 12 type curve match — Well 2403 (ref. 23, Samad) (pressure falloff case).

CHAPTER V

SUMMARY, CONCLUSIONS, AND RECOMMENDATIONS FOR FUTURE WORK

5.1 Summary

The primary purpose of this work is the presentation of the new power-law or β-derivative formulation — which is given by:

$$\Delta p_{\beta d}(t) = \frac{d\ln(\Delta p)}{d\ln(t)} = \frac{1}{\Delta p} t \frac{d\Delta p}{dt} = \frac{\Delta p_d(t)}{\Delta p} \quad \text{.....(1.1)}$$

The work of Sowers [ref. 2] confirms that using the β-derivative definition (Eq. 1.1) *does provide a slightly more accurate derivative function than extracting the $\Delta p_{\beta d}(t)$ function from the $\Delta p_d(t)$ function* as defined in Eq. 1.1. However, the benefit derived from using Eq. 1.1 is likely to be outweighed by the popularity (and availability) of the Bourdet (or semilog) pressure derivative function [$\Delta p_d(t)$]. In short, if a derivative computation module is being developed from nothing, Eq. 1.1 should be used. Otherwise, the "Bourdet" derivative function [$\Delta p_d(t)$] should be adequate to "extract" the β-derivative function [$\Delta p_{\beta d}(t)$] via Eq. 2.2.

Our goal is the presentation/demonstration of the β-derivative formulation. We have presented the β-derivative solutions (graphical representations) for some of the most popular well test analysis cases in the form of "type curves." The β-derivative has been shown to provide much improved resolution for certain well test analysis cases — in particular, the β-derivative yields a constant value (*i.e.*, $\Delta p_{\beta d}(t)$ = *constant*) for the following cases:

Case	$\Delta p_{\beta d}(t)$
● Wellbore storage domination:	1
● Reservoir boundaries:	
— Closed reservoir (circle, rectangle, etc.).	1
— 2-Parallel faults (large time).	1/2
— 3-Perpendicular faults (large time).	1/2
● Fractured wells:	
— Infinite conductivity vertical fracture.	1/2
— Finite conductivity vertical fracture.	1/4
● Horizontal wells:	
— Formation linear flow.	1/2

In addition, the β-derivative also provides a unique characterization of well test behavior in dual porosity/naturally fractured reservoirs (although the β-derivative is never constant for these cases — except for the possibility of a rare fractured or horizontal well case).

Finally, we also provide a *schematic* "diagnosis worksheet" for the interpretation of the β-derivative function (see **Fig 5.1**).

5.2 Conclusions

The following conclusions are derived from this work:

- We have successfully developed and verified a new form of derivative function type curves for the following cases: (*i.e.*, the β-derivative function [$\Delta p_{\beta d}(t)$])
  - — Unfractured well in an infinite-acting homogenous reservoir (including wellbore storage and skin effects).
  - — Fractured well with a finite or infinite conductivity vertical fracture in an infinite-acting homogenous reservoir (with/without wellbore storage effects).
  - — Unfractured well in a homogenous reservoir with single or multiple sealing boundaries — including closed boundary cases:
    - ■ Circular boundary (without wellbore storage and skin effects).
    - ■ Single sealing fault (without wellbore storage and skin effects).
    - ■ 2-parallel sealing faults (without wellbore storage and skin effects).
    - ■ 2-perpendicular sealing faults (without wellbore storage and skin effects).
    - ■ 3-perpendicular sealing faults (without wellbore storage and skin effects).
  - — Unfractured well in an infinite-acting dual porosity/naturally fractured reservoir (with/without wellbore storage and skin effects).
  - — Fractured well with a finite or infinite conductivity vertical fracture in an infinite-acting dual porosity/naturally fractured reservoir (with/without wellbore storage effects).
  - — Unfractured horizontal well (infinite conductivity well condition) in an infinite-acting homogeneous and isotropic reservoir (with/without wellbore storage effects).
- We have shown the diagnostic value of the β-derivative function via type curves for different flow regimes. Specifically, we have illustrated regimes where the β-derivative is constant, as well as regimes where the β-derivative can be used to identify the transition between regimes.
- We have successfully demonstrated the application of the new β-derivative type curves for field data taken from literature.

5.3 Recommendations for Future Work

The future work on this topic should focus on the application of the β-derivative concept for production data analysis. Auxiliary functions (pressure integral, pressure integral-derivative) will be required in order to create similar diagnostic tools for production data as those which exist for pressure transient data.

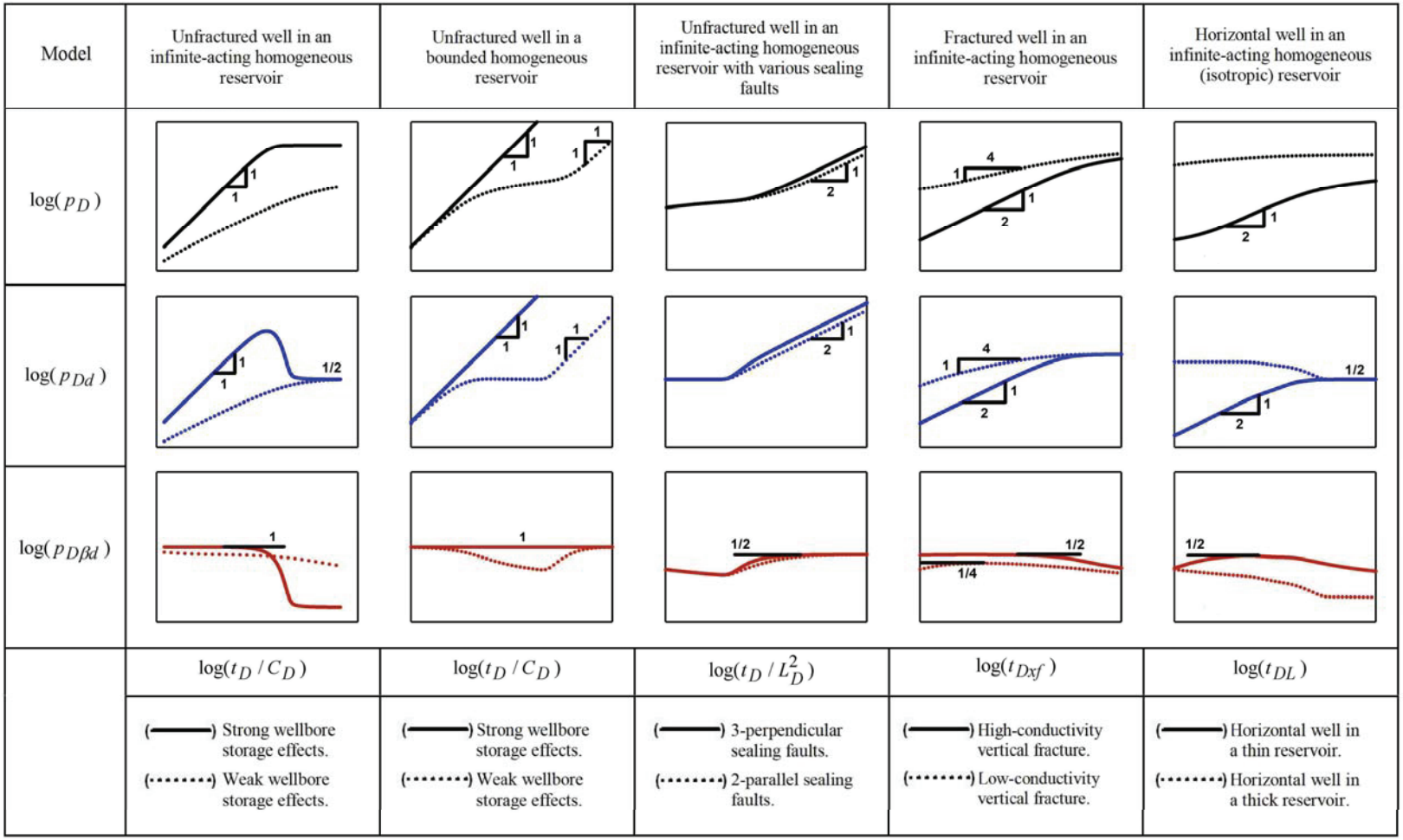

Figure 5.1 — Summary of schematic well test responses for the β-derivative formulation.

NOMENCLATURE

Variables

b_{pss} = Pseudosteady-state constant, dimensionless

B = Formation volume factor, RB/STB

c_t = total system compressibility, psi^{-1}

C_A = shape factor, dimensionless

C_s = wellbore storage coefficient, bbl/psi

C_D = dimensionless wellbore storage coefficient — unfractured well

C_{Df} = dimensionless wellbore storage coefficient — horizontal well

C_{DL} = dimensionless wellbore storage coefficient — fractured well

C_{fD} = fracture conductivity, dimensionless

f = Interporosity flow function

h = pay thickness, ft

h_{ma} = matrix height, ft

$I_0(x)$ = modified Bessel function of the first kind, zero order

$I_1(x)$ = modified Bessel function of the first kind, first order

$K_0(x)$ = modified Bessel function of the second kind, zero order

$K_1(x)$ = modified Bessel function of the second kind, first order

k = permeability, md

k_f = fracture permeability, md

k_{fb} = dual porosity fracture permeability, md

k_{ma} = matrix permeability, md

L = horizontal well length, ft

L_D = dimensionless horizontal well length

L_{Df} = dimensionless distance from fault

n = positive integer

p = pressure, psi

p_D = dimensionless pressure

$\overline{p_D}$ = dimensionless pressure in Laplace domain

p_{Dd} = dimensionless pressure derivative

$p_{D\beta d}$ = dimensionless β-pressure derivative

p_i = initial reservoir pressure, psi

p_{wf} = well flowing pressure, psi

p_{wfd} = well flowing pressure derivative, psi

$p_{wf\beta d}$ = well flowing β–pressure derivative, dimensionless

p_{ws} = well shut-in pressure, psi

p_{wsd} = well shut-in pressure derivative, psi

$p_{ws\beta d}$ = well shut-in β–pressure derivative, dimensionless

q = flow rate, STB/Day

$\overline{q_{fD}}$ = fracture flow rate in Laplace domain , dimensionless

r_e = reservoir outer boundary radius, ft

r_{eD} = outer reservoir boundary radius, dimensionless

r_w = wellbore radius, ft

r_{wD} = dimensionless wellbore radius

r_{wzD} = dimensionless wellbore radius

s = Laplace domain variable, dimensionless

t = time, hr

t_D = dimensionless time

t_{DA} = dimensionless time with respect to drainage area

t_{DL} = dimensionless time in horizontal well case

t_{Dxf} = dimensionless time in fractured well case

x = distance from wellbore along fracture, ft

x_D = dimensionless distance along fracture, ft

x_f = fracture length, ft

z = distance in z direction, ft

z_D = dimensionless distance in z direction

z_w = well location, ft

z_{wD} = dimensionless well location

Greek Symbols

ϕ = porosity, fraction

ϕ_f = fracture porosity, fraction

ϕ_{ma} = matrix porosity, fraction

γ = Euler's constant, 0.577216…

η_{fD} = hydraulic diffusivity, dimensionless

μ = viscosity, cp

λ = interporosity flow parameter

ω	=	storativity parameter

Subscript

g	=	gas
o	=	oil
w		water
wbs	=	wellbore storage
pss	=	pseudosteady-state

REFERENCES

1. Bourdet, D., Ayoub, J.A., and Pirad, Y.M.: "Use of Pressure Derivative in Well-Test Interpretation," *SPEFE* (June 1989) 293.
2. Sowers, S.: *The Bourdet Derivative Algorithm Revisited — Introduction and Validation of the Power-Law Derivative Algorithm for Applications in Well-Test Analysis*, (internal) B.S. Report, Texas A&M U., College Station, Texas (2005).
3. Mattar, L. and Zaoral, K.: "The Primary Pressure Derivative (*PPD*) A New Diagnostic Tool in Well Test Interpretation," *JCPT*, (April 1992) 63.
4. Clark, D.G and van Golf-Racht, T.D.: "Pressure-Derivative Approach to Transient Test Analysis: A High-Permeability North Sea Reservoir Example," *JPT* (Nov. 1985), 2023.
5. Lane, H.S., Lee, J.W., and Watson, A.T.: "An Algorithm for Determining Smooth, Continuous Pressure Derivatives from Well Test Data," *SPEFE* (December 1991) 493.
6. Escobar, F.H., Navarrete, J.M., and Losada, H.D.: "Evaluation of Pressure Derivative Algorithms for Well-Test Analysis," paper SPE 86936 presented at the 2004 SPE International Thermal Operations and Heavy Oil Symposium and Western Regional Meeting, Bakersfield, California, 16-18 March.
7. Gonzales-Tamez, F., Camacho-Velazquez, R., and Escalante-Ramirez, B.: "Truncation Denoising in Transient Pressure Tests," SPE 56422 presented at the 1999 SPE Annual Technical Conference and Exhibition, Houston, Texas, 3-6 October.
8. Cheng, Y., Lee, J.W., and McVay, D.A.: "Determination of Optimal Window Size in Pressure-Derivative Computation Using Frequency-Domain Constraints," SPE 96026 presented at the 2005 SPE Annual Technical Conference and Exhibition, Dallas, Texas, 9-12 October.
9. Onur, M. and Reynolds, A.C.: "A New Approach for Constructing Derivative Type Curves for Well Test Analysis," *SPEFE* (March 1988) 197.
10. Doung, A.N.: "A New Set of Type Curves for Well Test Interpretation with the Pressure/Pressure-Derivative Ratio," *SPEFE* (June 1989) 264.
11. van Everdingen, A.F. and Hurst, W.: "The Application of the Laplace Transformation to Flow Problems in Reservoirs," *Trans*., AIME (1949) 186.
12. Stehfest, H.: "Numerical Inversion of Laplace Transforms," *Communication of the ACM* (Jan. 1970) **13**, No. 1, 47. (Algorithm 368 with correction (October 1970), **13**, No.10).

13. Valko, P.P. and Abate, J.: "Comparison of Sequence Accelerators for the Gaver Method of Numerical Laplace Transform Inversion," *Computers and Mathematics with Application,* Vol. 48 (Iss.3-40) 2004 pp. 629-636

14. Stewart, G., Gupta, A., and Westaway, P.: "The Interpretation of Interference Tests in a Reservoir with Sealing and Partially Communicating Faults," paper SPE 12967 presented at the 1984 European Petroleum Conf. held in London, England, 25-28 October.

15. Cinco-Ley, H. and Meng, H.-Z.: "Pressure Transient Analysis of Wells with Finite Conductivity Vertical Fractures in Dual Porosity Reservoirs," SPE 18172 presented at the 1989 SPE Annual Technical Conference and Exhibition, Houston, Texas, 2-5 October.

16. Ozkan, E.: *Performance of Horizontal Wells*, Ph.D. Dissertation, U. of Tulsa, Tulsa, Oklahoma (1988).

17. Warren, J.E. and Root, P.J.: "The Behavior of Naturally Fractures reservoirs," *SPEJ* (September 1963) 228.

18. Angel, J.A.: *Type Curve Analysis for Naturally Fractures Reservoir* (*Infinite-Acting Reservoir Case*) ─ *A New Approach*, MS. thesis, Texas A&M U., College Station, Texas (2000).

19. Meunier, D., Wittmann, M.J., and Stewart, G.: "Interpretation of Pressure Buildup Test Using In-Situ Measurement of Afterflow," *JPT* (January 1985) 143.

20. DaPrat, G.D. *et al*: "Use of Pressure Transient Testing to Evaluate Fractured Reservoirs in Western Venezuela," SPE 13054 presented at the 1984 SPE Annual Technical Conference and Exhibition, Houston, Texas, 16-19 September.

21. Allain, O.F. and Horne R.N.: "Use of Artificial Intelligence in Well-Test Interpretation," *JPT* (March 1990) 342.

22. Lee, W.J. and Holditch, S.A.: "Fracture Evaluation with Pressure Transient Testing in Low-Permeability Gas Reservoirs," *JPT* (September 1981) 1776.

23. Samad, Z.: *Application of Pressure and Pressure Integral Functions for the Analysis of Well Test Data*, MS. thesis, Texas A&M U., College Station, Texas (1994).

APPENDIX A

CASES OF RADIAL FLOW WITH INFINITE AND FINITE-ACTING BOUNDARIES IN HOMOGENEOUS RESERVOIRS

In this Appendix we provide pressure, pressure derivative, and pressure β-derivative solutions (in dimensionless format) for the cases of wellbore storage, unfractured well in infinite-acting reservoir, unfractured well in bounded reservoir, and different fault configurations both in equation and graphical format (type curves).

Table A-1 — Solutions for the wellbore storage domination flow regime.

Variable	Solution Relation
Δp_{wbs}	$\Delta p_{wbs} = m_{wbs} t$ ..... (A.1.1)
$\Delta p_{d,wbs}$	$\Delta p_{d,wbs} = m_{wbs} t$ ..... (A.1.2)
$\Delta p_{\beta d,wbs}$	$\Delta p_{\beta d,wbs} = 1$ ..... (A.1.3)

Definitions: (field units)

$$m_{wbs} = \frac{1}{24}\frac{qB}{C_s} \quad \text{.....(A.1.4)}$$

Table A-2 — Solutions for a well in a finite-acting, homogeneous reservoir (closed system, any well/reservoir configuration).

Description	Relation
p_D	$p_D(t_{DA}) = 2\pi t_{DA} + \frac{1}{2}\ln\left[\frac{4}{e^{\gamma}}\frac{A}{r_w^2}\frac{1}{C_A}\right] + s = 2\pi t_{DA} + b_{pss}$ ..... (A.2.1)
p_{Dd}	$p_{Dd}(t_{DA}) = 2\pi t_{DA}$ ..... (A.2.2)
$p_{D\beta d}$ $(= p_{Dd}/p_D)$	$p_{D\beta d}(t_{DA}) = \frac{1}{1+(b_{pss}/2\pi t_{DA})} \approx 1$ (large-time) ..... (A.2.3)

Definitions: (field units)

$$t_{DA} = 2.637\times10^{-4}\frac{k}{\phi\mu c_t A}t \quad \text{.....(A.2.4)}$$

$$p_D = \frac{1}{141.2}\frac{kh}{qB\mu}(p_i - p_{wf}) \quad \text{.....(A.2.5)}$$

$$b_{pss} = \frac{1}{2}\ln\left[\frac{4}{e^{\gamma}}\frac{A}{r_w^2}\frac{1}{C_A}\right] + s \quad \text{.....(A.2.6)}$$

Table A-3 — Solutions for an unfractured well in an infinite-acting, homogeneous reservoir (radial flow).

Description	Relation
p_D	$p_D(t_D) = \frac{1}{2}\mathrm{E}_1\left[\frac{1}{4t_D}\right]$ $\left(t_D > 10\right)$ ..... (A.3.1)
p_{Dd}	$p_{Dd}(t_D) = \frac{1}{2}\exp\left[\frac{-1}{4t_D}\right]$ $\left(t_D > 10\right)$ ..... (A.3.2)
$p_{D\beta d}$ $(= p_{Dd}/p_D)$	$p_{D\beta d}(t_D) = \exp\left[\frac{1}{4t_D}\right] \Big/ \mathrm{E}_1\left[\frac{1}{4t_D}\right]$ $\left(t_D > 10\right)$ ..... (A.3.3)

Definitions: (field units)

$$t_D = 2.637\times10^{-4}\frac{kt}{\phi c_t \mu r_w^2} \quad \text{..... (A.3.4)}$$

$$p_D = \frac{1}{141.2}\frac{kh}{qB\mu}(p_i - p_{wf}) \quad \text{..... (A.3.5)}$$

$$C_D = \frac{0.8936 C_s}{\phi h c_t r_w^2} \quad \text{..... (A.3.6)}$$

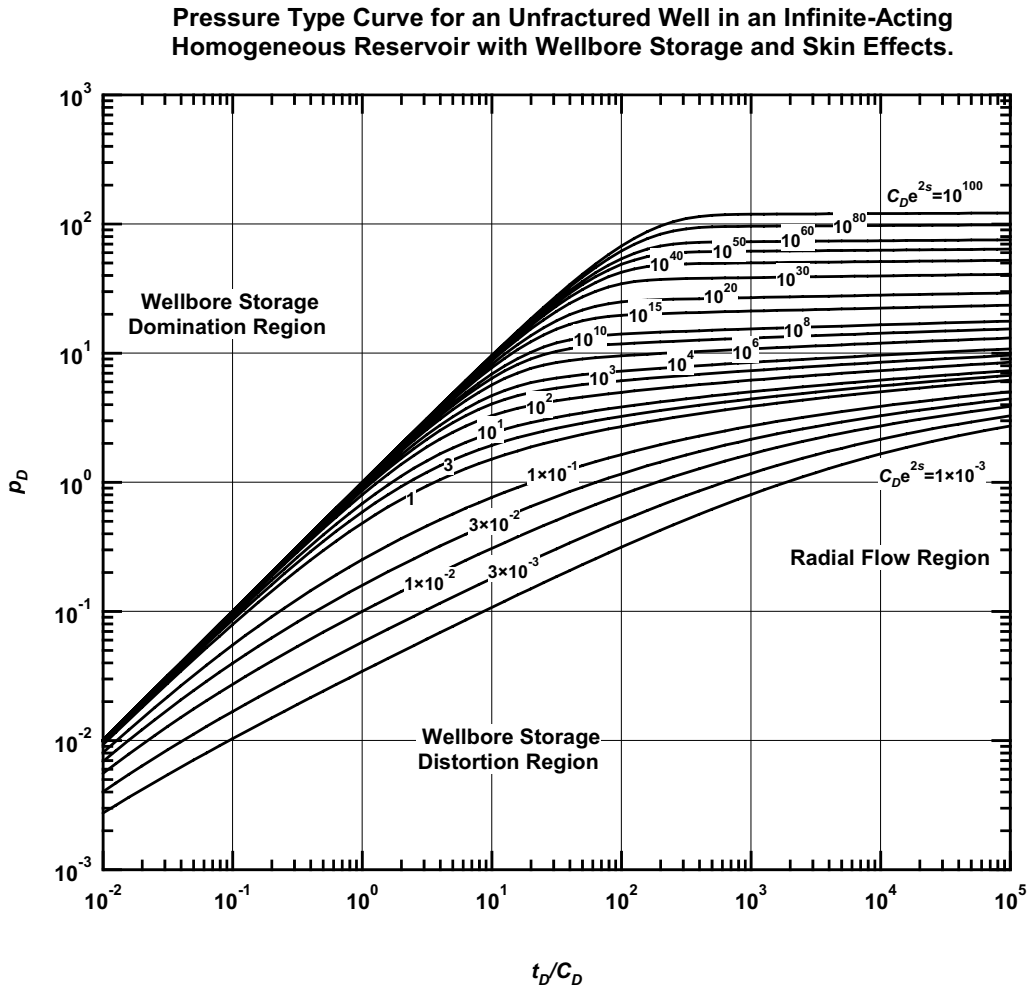

Figure A.1 — p_D vs. t_D/C_D — solutions for an unfractured well in an infinite-acting homogeneous reservoir— wellbore storage and skin effects included (various C_D values).

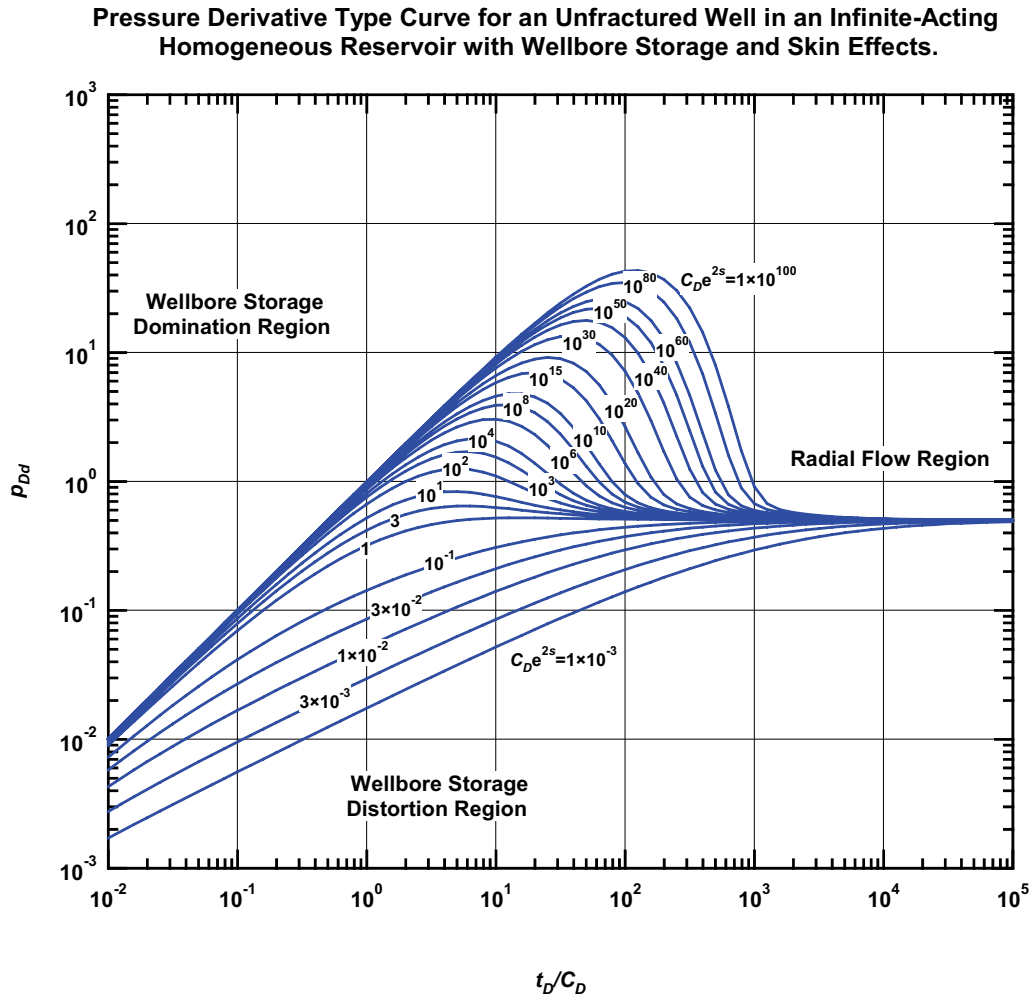

Figure A.2— p_{Dd} vs. t_D/C_D — solutions for an unfractured well in an infinite-acting homogeneous reservoir— wellbore storage and skin effects included (various C_D values).

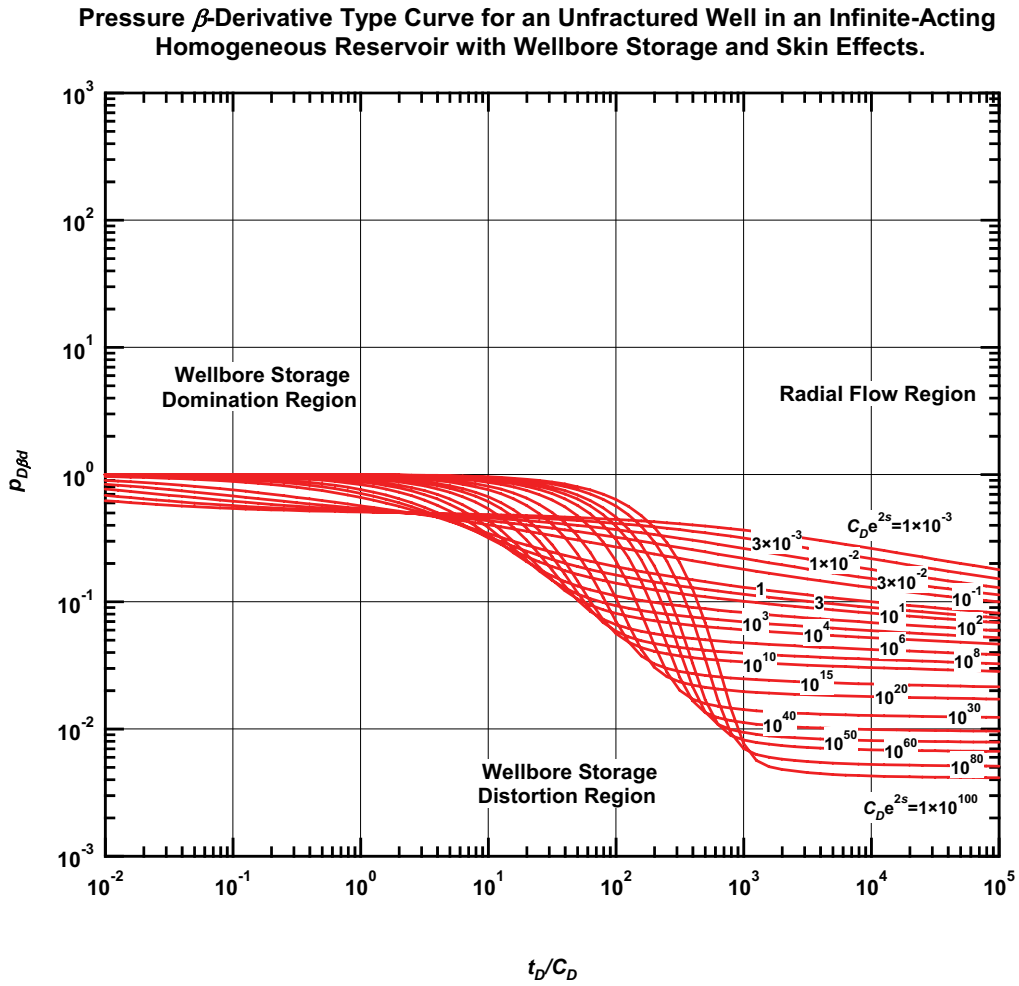

Figure A.3— $p_{D\beta d}$ vs. t_D/C_D — solutions for an unfractured well in an infinite-acting homogeneous reservoir— wellbore storage and skin effects included (various C_D values).

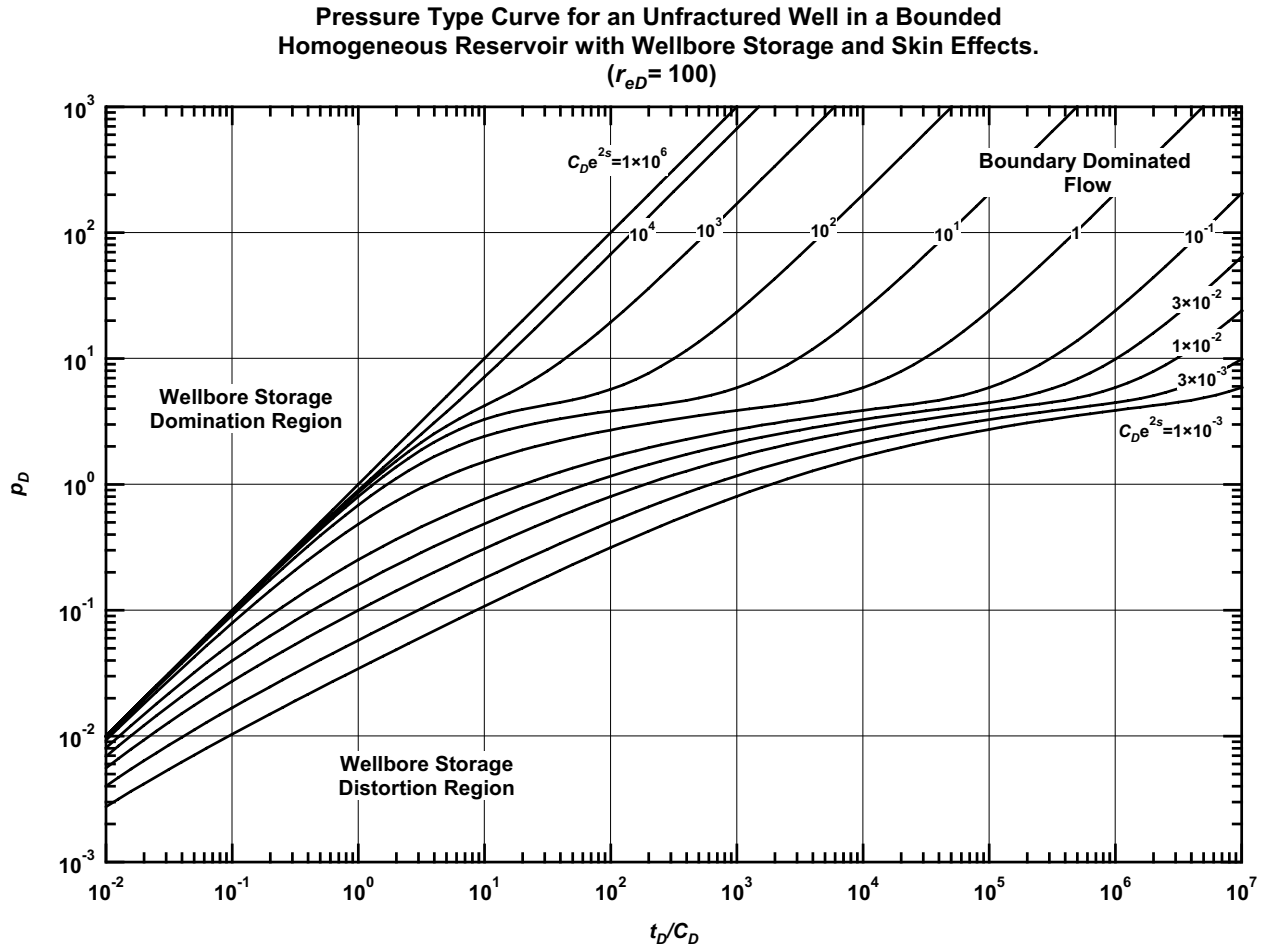

Figure A.4— p_D vs. t_D/C_D — r_{eD} =100, bounded circular reservoir case — includes wellbore storage and skin effects.

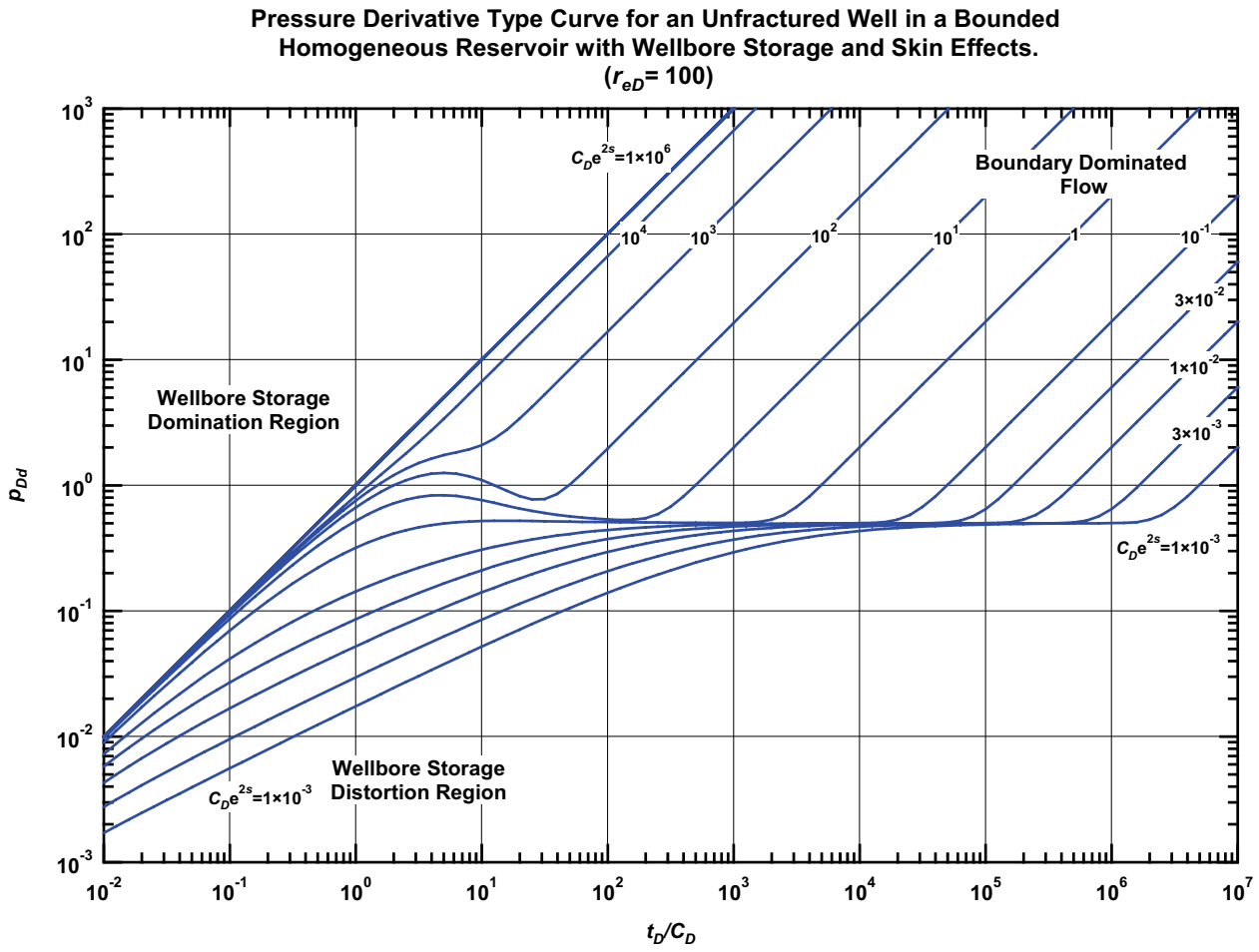

Figure A.5— p_{Dd} vs. t_D/C_D — r_{eD} =100, bounded circular reservoir case — includes wellbore storage and skin effects.

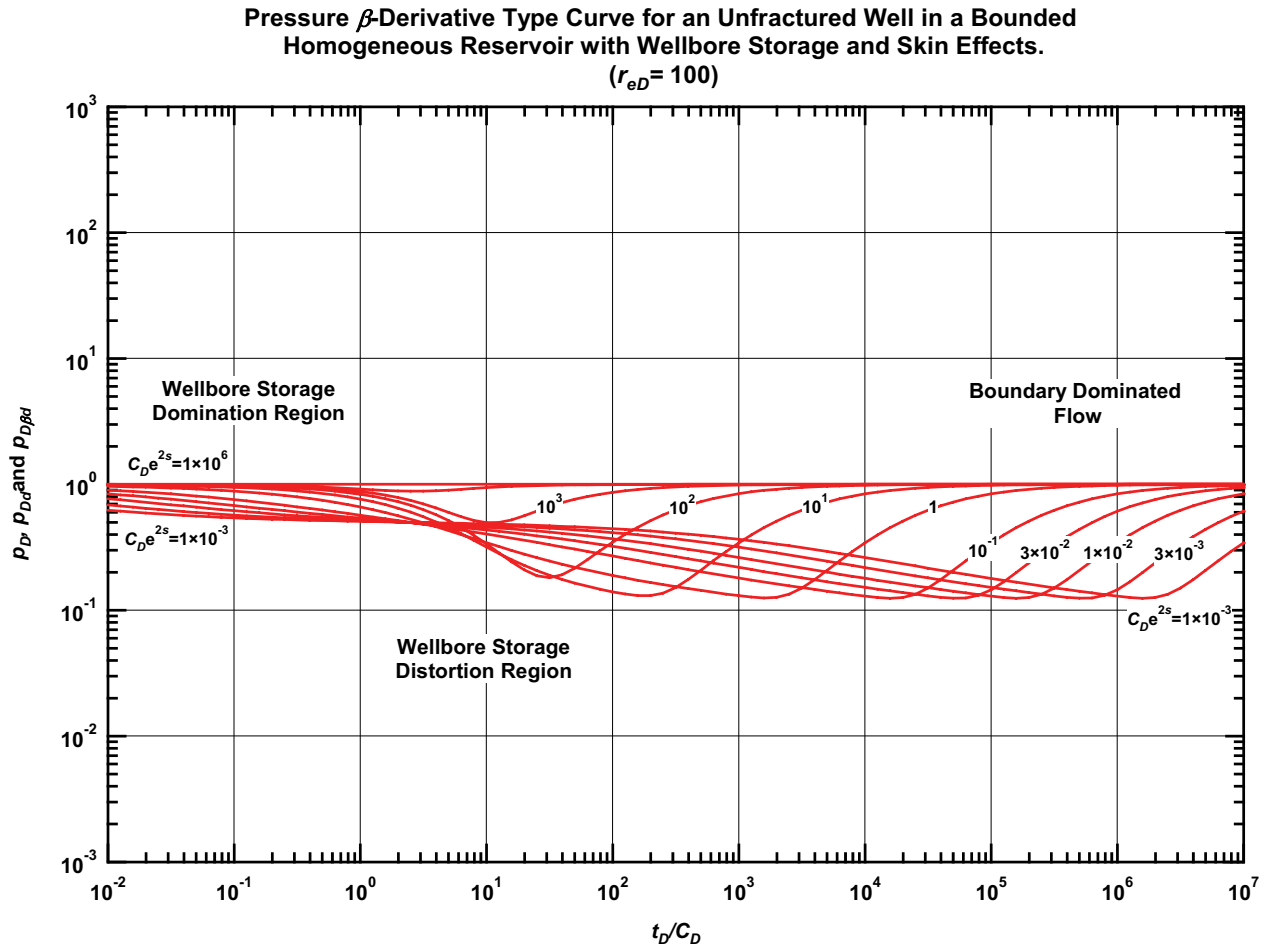

Figure A.6— $p_{D\beta d}$ vs. t_D/C_D — r_{eD} =100, bounded circular reservoir case — includes wellbore storage and skin effects.

Table A-4 — Solutions for a single well in an infinite-acting homogeneous reservoir system with a single or multiple sealing faults.

Description	Relation
p_D	$p_D(t_D) = \frac{1}{2}\left[\mathrm{E}_1\left[\frac{1}{4t_D}\right] + \mathrm{E}_1\left[\frac{L_{Df}^2}{t_D}\right]\right]$ (single fault) ..... (A.4.1)
	$p_D(t_D) = \frac{1}{2}\left[\mathrm{E}_1\left[\frac{1}{4t_D}\right] + 2\mathrm{E}_1\left[\frac{L_{Df}^2}{t_D}\right] + \mathrm{E}_1\left[\frac{2L_{Df}^2}{t_D}\right]\right]$ (two perpendicular faults)..... (A.4.2)
	$p_D(t_D) = \frac{1}{2}\left[\mathrm{E}_1\left[\frac{1}{4t_D}\right] + 2\sum_{i=1}^{\infty}\mathrm{E}_1\left[\frac{iL_{Df}^2}{t_D}\right]\right]$ (two parallel faults) ..... (A.4.3)
	$p_D(t_D) = \frac{1}{2}\left[\mathrm{E}_1\left[\frac{1}{4t_D}\right] + 2\sum_{i=1}^{\infty}\mathrm{E}_1\left[\frac{(i^2+1)L_{Df}^2}{t_D}\right] + 2\sum_{i=1}^{\infty}\mathrm{E}_1\left[\frac{iL_{Df}^2}{t_D}\right] + \mathrm{E}_1\left[\frac{L_{Df}^2}{t_D}\right]\right]$ (three perpendicular faults) ..... (A.4.4)
p_{Dd}	$p_{Dd}(t_D) = \frac{1}{2}e^{-1/4t_D} + \frac{1}{2}e^{-L_{Df}^2/t_D} \approx 1$ (single fault, complete solution and large-time approximation) ..... (A.4.5)
	$p_{Dd}(t_D) = \frac{1}{2}e^{-1/4t_D} + e^{-L_{Df}^2/t_D} + \frac{1}{2}e^{-2L_{Df}^2/t_D} \approx 2$ (two perpendicular faults, complete solution and large-time approximation) ..... (A.4.6)
	$p_{Dd}(t_D) = \frac{1}{2}e^{-1/4t_D} + \sum_{i=1}^{\infty}e^{-iL_{Df}^2/t_D}$ (two parallel faults, complete solution and large-time approximation) ..... (A.4.7)
	$p_{Dd}(t_D) = \frac{1}{2}e^{-1/4t_D} + \sum_{i=1}^{\infty}e^{-(i^2+1)L_{Df}^2/t_D} + \sum_{i=1}^{\infty}e^{-iL_{Df}^2/t_D} + \frac{1}{2}e^{-L_{Df}^2/t_D}$ (three perpendicular faults) ..... (A.4.8)

Table A-4 — Continued

Description	Relation
$p_{D\beta d}$ $(= p_{Dd}/p_D)$	$p_{D\beta d}(t_D) = \dfrac{e^{-1/4t_D} + e^{-L_{Df}^2/t_D}}{\mathrm{E}_1\left[\dfrac{1}{4t_D}\right] + \mathrm{E}_1\left[\dfrac{L_{Df}^2}{t_D}\right]} \approx \dfrac{2}{\mathrm{E}_1\left[\dfrac{1}{4t_D}\right] + \mathrm{E}_1\left[\dfrac{L_{Df}^2}{t_D}\right]}$ (single fault, complete solution and large-time approximation) ..... (A.4.9)
	$p_{D\beta d}(t_D) = \dfrac{e^{-1/4t_D} + 2e^{-L_{Df}^2/t_D} + e^{-2L_{Df}^2/t_D}}{\mathrm{E}_1\left[\dfrac{1}{4t_D}\right] + 2\mathrm{E}_1\left[\dfrac{L_{Df}^2}{t_D}\right] + \mathrm{E}_1\left[\dfrac{2L_{Df}^2}{t_D}\right]}$ $\approx \dfrac{4}{\mathrm{E}_1\left[\dfrac{1}{4t_D}\right] + 2\mathrm{E}_1\left[\dfrac{L_{Df}^2}{t_D}\right] + \mathrm{E}_1\left[\dfrac{2L_{Df}^2}{t_D}\right]}$ (two perpendicular faults, complete solution and large-time approximation) ..... (A.4.10)
	$p_{D\beta d}(t_D) = \dfrac{e^{-1/4t_D} + 2\sum_{i=1}^{\infty} e^{-iL_{Df}^2/t_D}}{\mathrm{E}_1\left[\dfrac{1}{4t_D}\right] + 2\sum_{i=1}^{\infty} \mathrm{E}_1\left[\dfrac{iL_{Df}^2}{t_D}\right]} \approx 1/2$ (two parallel faults, complete solution and large-time approximation) .. (A.4.11)
	$p_{D\beta d}(t_D) = \dfrac{e^{-1/4t_D} + 2\sum_{i=1}^{\infty}\left[e^{-(i^2+1)L_{Df}^2/t_D} + e^{-iL_{Df}^2/t_D}\right] + e^{-L_{Df}^2/t_D}}{\mathrm{E}_1\left[\dfrac{1}{4t_D}\right] + 2\sum_{i=1}^{\infty}\left[\mathrm{E}_1\left[\dfrac{(i^2+1)L_{Df}^2}{t_D}\right] + \mathrm{E}_1\left[\dfrac{iL_{Df}^2}{t_D}\right]\right] + \mathrm{E}_1\left[\dfrac{L_{Df}^2}{t_D}\right]}$ $\approx 1/2$ (three perpendicular faults, complete solution and large-time approximation) ..... (A.4.12)

Definitions: (field units)

$$t_D = 2.637\times10^{-4}\frac{kt}{\phi c_t \mu r_w^2} \quad \text{(A.4.13)}$$

$$p_D = \frac{1}{141.2}\frac{kh}{qB\mu}(p_i - p_{wf}) \quad \text{(A.4.14)}$$

$$L_{Df} = L_{fault} / r_w \quad \text{(A.4.15)}$$

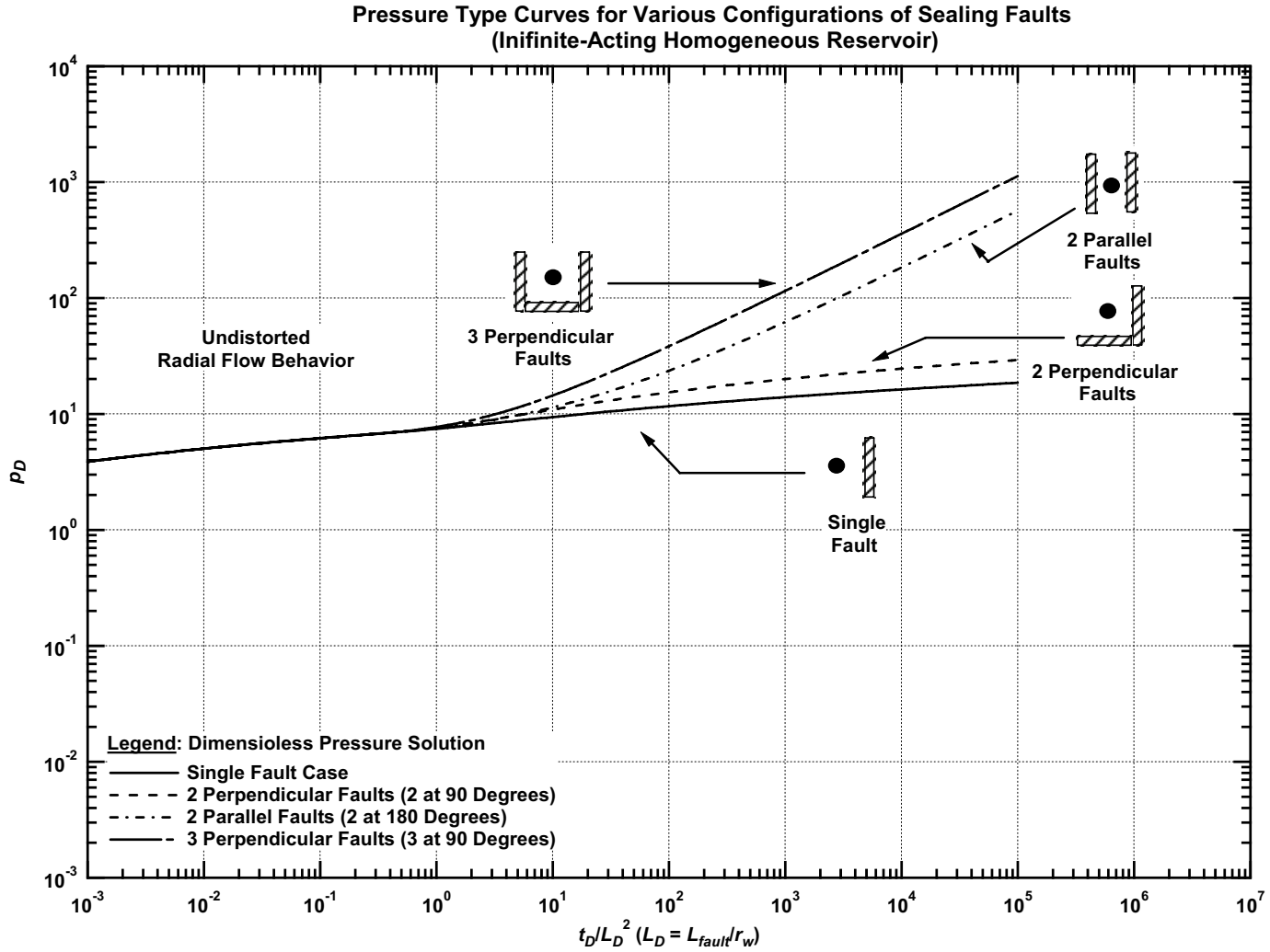

Figure A.7 — p_D vs. t_D/L_D^2 — various sealing faults configurations (wellbore storage and skin effects are NOT included).

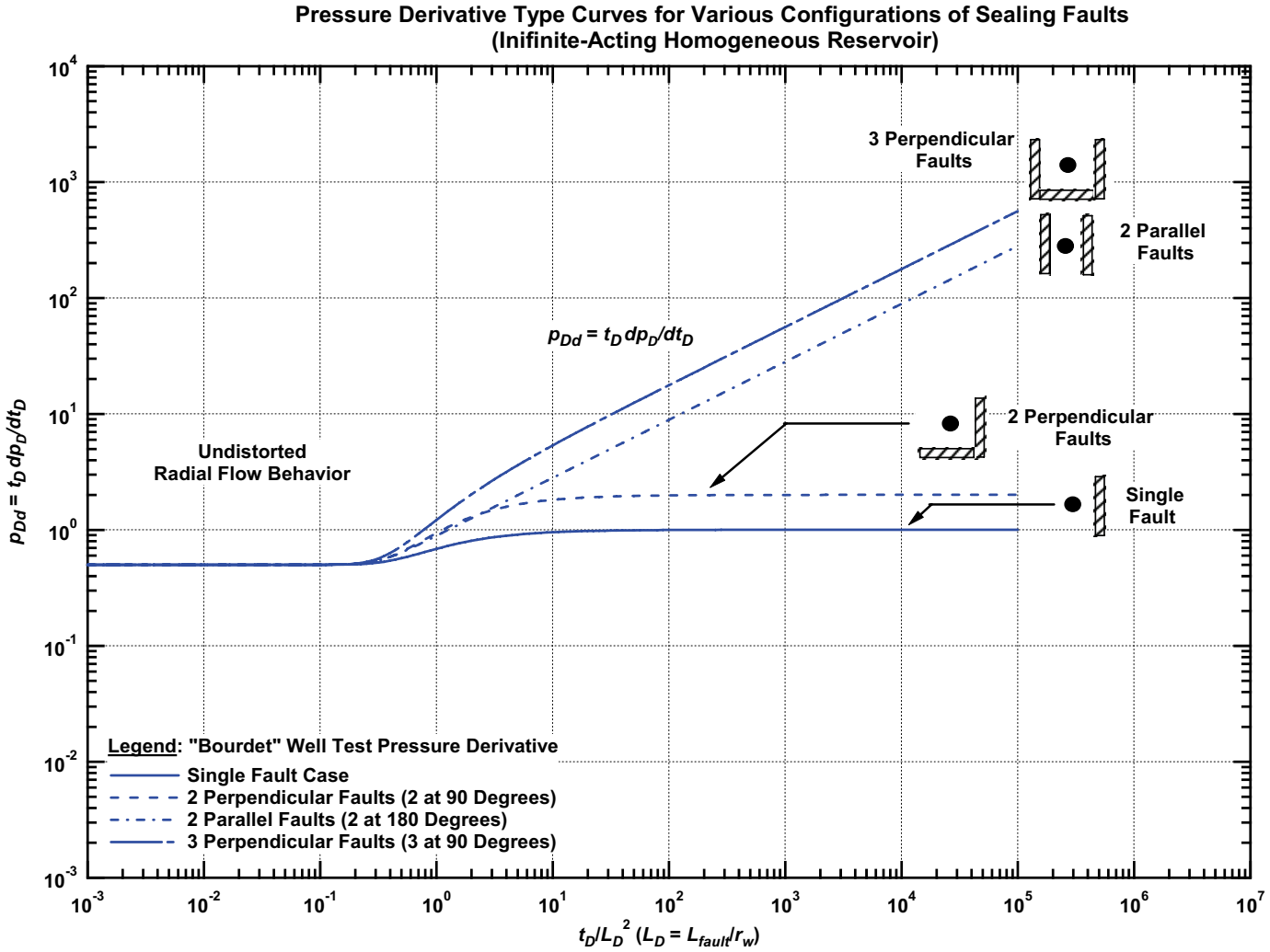

Figure A.8 — p_{Dd} vs. t_D/L_D^2 — various sealing faults configurations (wellbore storage and skin effects are NOT included).

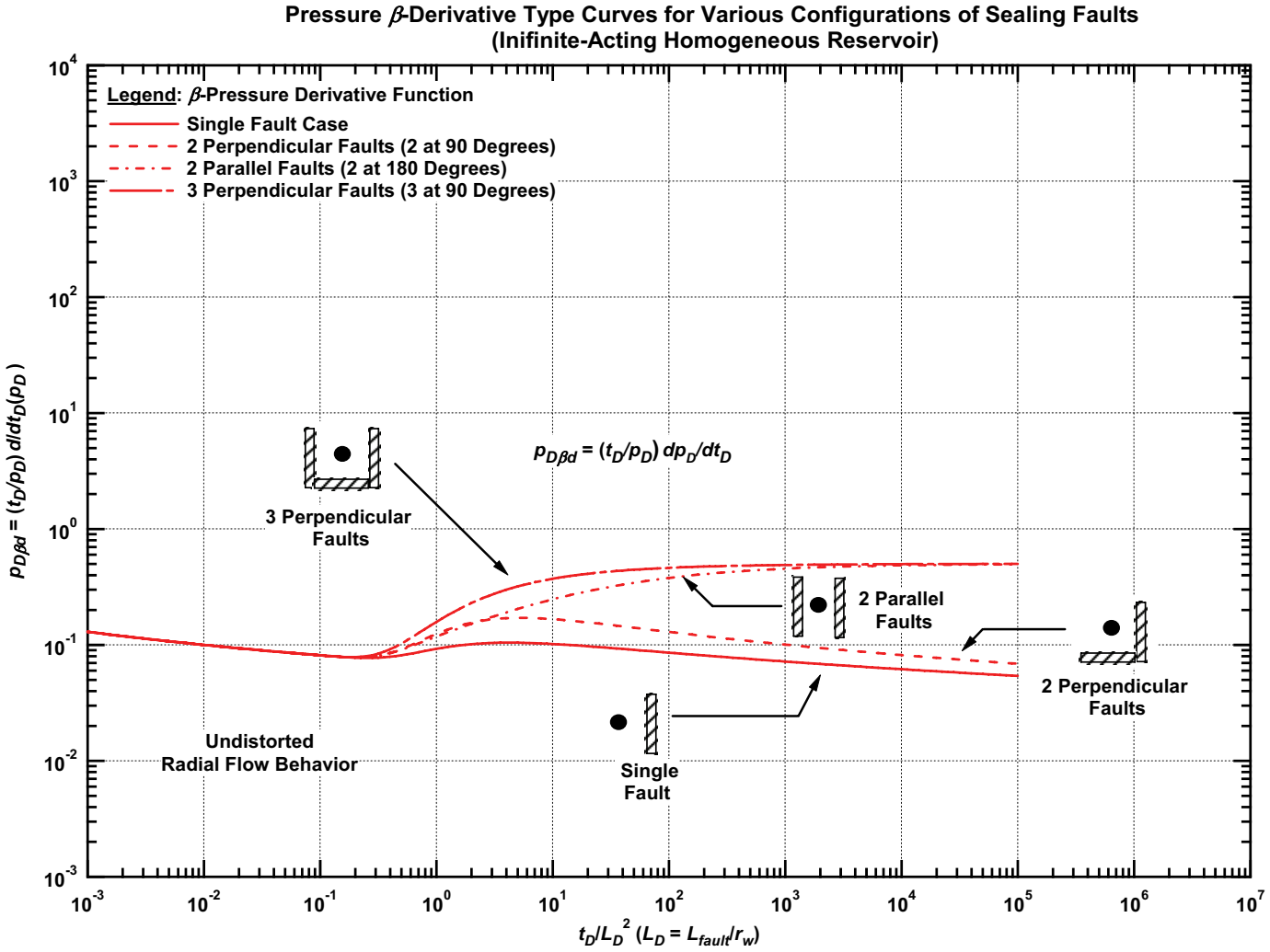

Figure A.9 — $p_{D\beta d}$ vs. t_D/L_D^2 — various sealing faults configurations (wellbore storage and skin effects are NOT included).

APPENDIX B

CASES OF HYDRAULICALLY FRACTURED WELLS WITH INFINITE OR FINITE CONDUCTIVITY IN AN INFINITE-ACTING HOMOGENEOUS RESERVOIR

In this appendix we provide pressure, pressure derivative, and β-derivative solutions (in dimensionless format) for the cases of hydraulically fractured well with infinite and finite conductivity in an infinite-acting homogeneous reservoir both in the form of equations and graphical type curve solutions. For graphical presentation of the solution, we generated type curves using dimensionless fracture conductivity (C_{fD}) values range from 1 to 1000, with and without wellbore storage effects.

Table B-1 — Solutions for a hydraulically fractured well with an infinite conductivity fracture in an infinite-acting reservoir.

Description	Relation
p_D	$p_D(t_{Dxf}) = \frac{\sqrt{\pi t_{Dxf}}}{2}\left[\mathrm{erf}\left[\frac{1-x_D}{2\sqrt{t_{Dxf}}}\right]+\mathrm{erf}\left[\frac{1+x_D}{2\sqrt{t_{Dxf}}}\right]\right]$ $+\frac{(1-x_D)}{4}\mathrm{E}_1\left[\frac{(1-x_D)^2}{4t_{Dxf}}\right]+\frac{(1+x_D)}{4}\mathrm{E}_1\left[\frac{(1+x_D)^2}{4t_{Dxf}}\right]$ (Uniform-flux (x_D=0) or infinite conductivity(x_D=0.732)) ..... (B.1.1)
	$p_D(t_{Dxf}) = \sqrt{\pi t_{Dxf}}$ (early time, linear flow)..... (B.1.2)
	$p_D(t_{Dxf}) = \frac{1}{2}[\ln(t_{Dxf}) + 2.80907]$ (late time, uniform flux fracture)..... (B.1.3)
	$p_D(t_{Dxf}) = \frac{1}{2}[\ln(t_{Dxf}) + 2.20000]$ (late time, infinite conductivity fracture)..... (B.1.4)
p_{Dd}	$p_{Dd}(t_{Dxf}) = \frac{\sqrt{\pi t_{Dxf}}}{4}\left[\mathrm{erf}\left[\frac{1-x_D}{2\sqrt{t_{Dxf}}}\right]+\mathrm{erf}\left[\frac{1+x_D}{2\sqrt{t_{Dxf}}}\right]\right]$ (Uniform-flux (x_D=0) or infinite conductivity(x_D=0.732)) ..... (B.1.5)
	$p_{Dd}(t_{Dxf}) = \frac{\sqrt{\pi t_{Dxf}}}{4}$ (early time, linear flow)..... (B.1.6)
	$p_{Dd}(t_{Dxf}) = 0.5$ (late time)..... (B.1.7)

Table B-1 — Continued

$$p_{D\beta d}\ (t_{Dxf}) = \left[\frac{\sqrt{\pi t_{Dxf}}}{4}\left[\operatorname{erf}\left[\frac{1-x_D}{2\sqrt{t_{Dxf}}}\right]+\operatorname{erf}\left[\frac{1+x_D}{2\sqrt{t_{Dxf}}}\right]\right]\right] \Bigg/ \left[\begin{array}{l}\dfrac{\sqrt{\pi t_{Dxf}}}{2}\left[\operatorname{erf}\left[\dfrac{1-x_D}{2\sqrt{t_{Dxf}}}\right]+\operatorname{erf}\left[\dfrac{1+x_D}{2\sqrt{t_{Dxf}}}\right]\right] \\ +\dfrac{(1-x_D)}{4}\mathrm{E}_1\left[\dfrac{(1-x_D)^2}{4t_{Dxf}}\right]+\dfrac{(1+x_D)}{4}\mathrm{E}_1\left[\dfrac{(1+x_D)^2}{4t_{Dxf}}\right]\end{array}\right]$$

$p_{D\beta d}\ (= p_{Dd}/p_D)$

(Uniform-flux (x_D=0) or infinite conductivity(x_D=0.732)) ..... (B.1.8)

$$p_{D\beta d}\ (t_{Dxf}) = 0.5$$

(early time, linear flow)..... (B.1.9)

$$p_{D\beta d}\ (t_{Dxf}) = \frac{1}{\ln(t_{Dxf}) + 2.80907}$$

(late time, uniform flux fracture)..... (B.1.10)

$$p_{D\beta d}\ (t_{Dxf}) = \frac{1}{\ln(t_{Dxf}) + 2.20000}$$

(late time, infinite conductivity fracture)..... (B.1.11)

Definitions: (field units)

$$t_{Dxf} = 2.637\times10^{-4}\frac{kt}{\phi c_t \mu x_f^2} \quad \text{..... (B.1.12)}$$

$$p_D = \frac{1}{141.2}\frac{kh}{qB\mu}(p_i - p_{wf}) \quad \text{..... (B.1.13)}$$

$$x_D = x/x_f \quad \text{..... (B.1.14)}$$

$$C_{Df} = \frac{0.8936 C_s}{\phi h c_t x_f^2} \quad \text{..... (B.1.15)}$$

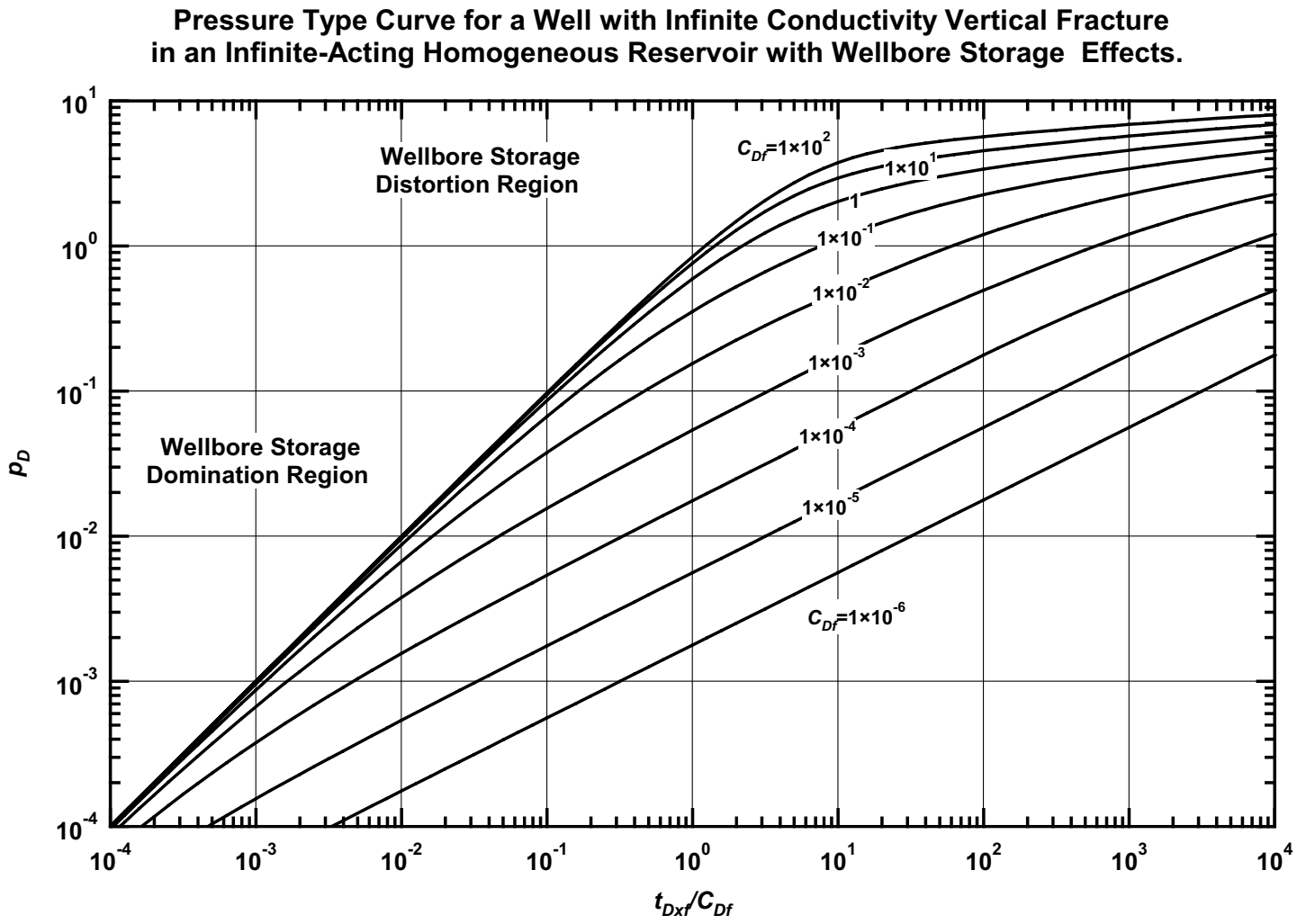

Figure B.1— p_D vs. t_{Dxf}/C_{Df} — C_{fD} = ∞ (fractured well case — includes wellbore storage effects).

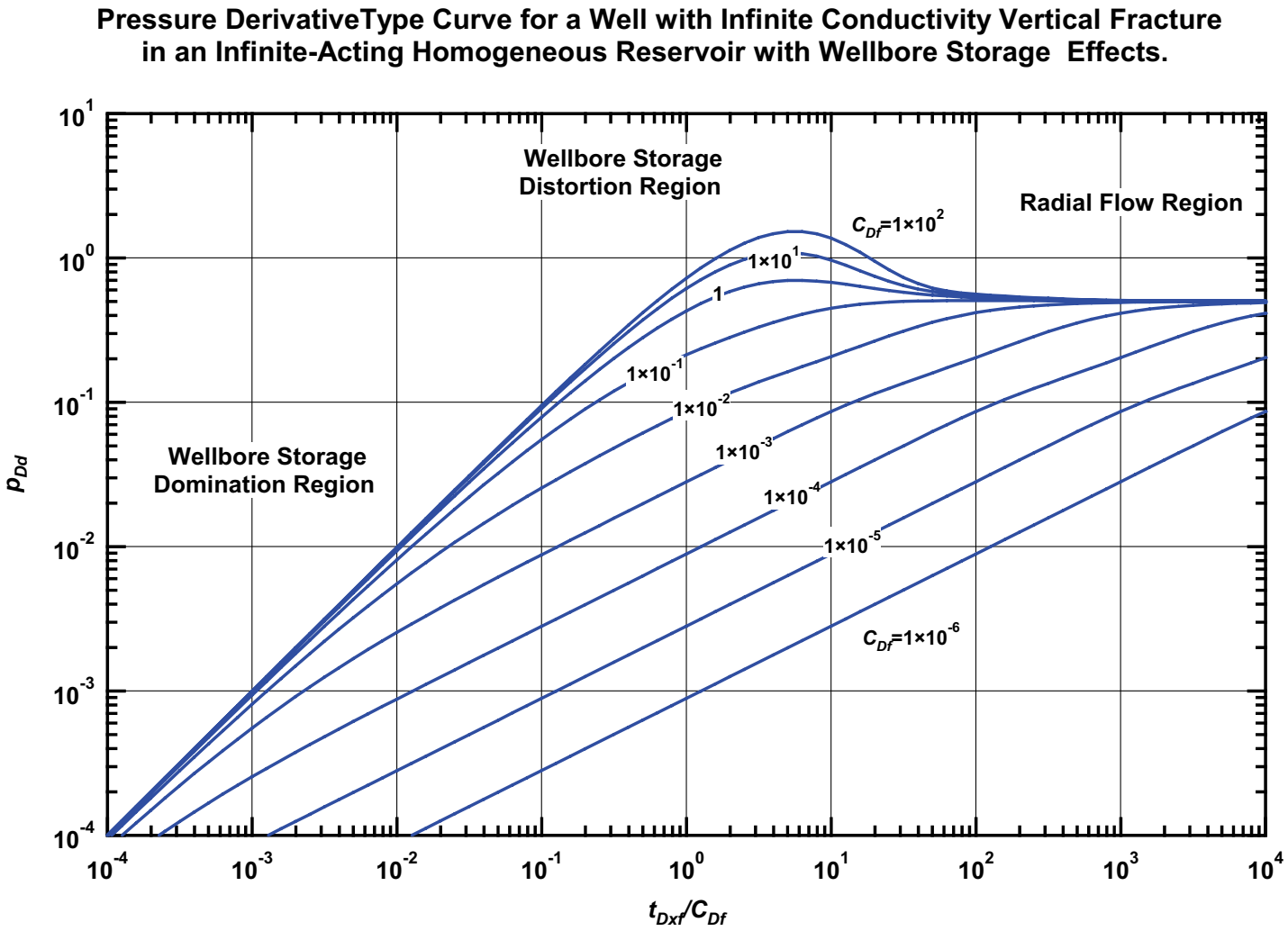

Figure B.2— p_{Dd} vs. t_{Dxf}/C_{Df} — C_{fD} = ∞ (fractured well case — includes wellbore storage effects).

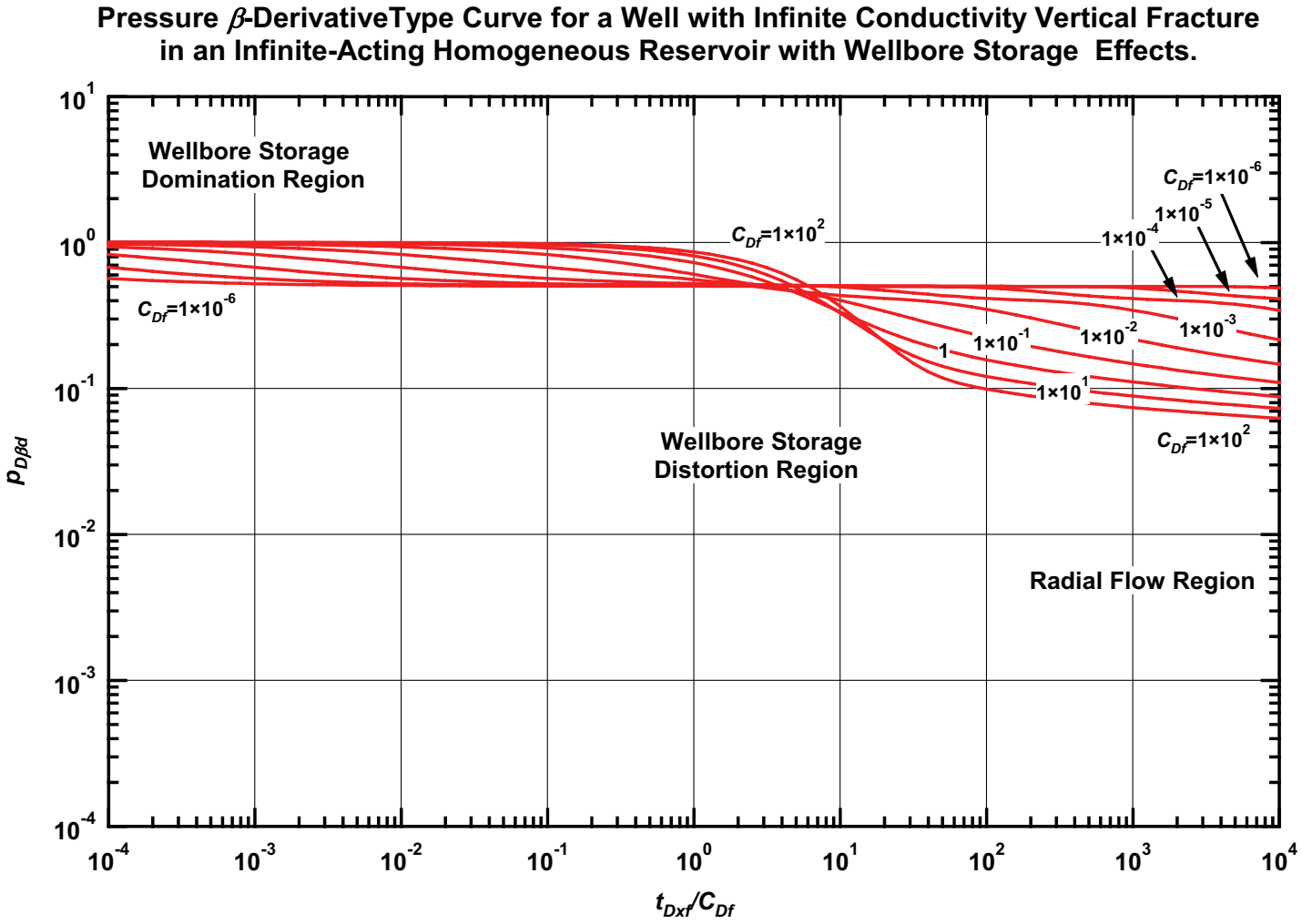

Figure B.3— $p_{D\beta d}$ vs. t_{Dxf}/C_{Df} — C_{fD} = ∞ (fractured well case — includes wellbore storage effects).

Table B-2 — Early time solutions for a hydraulically fractured well with a finite conductivity fracture — infinite-acting homogeneous reservoir (includes wellbore storage effects).

Description	Relation
p_D	$p_D(t_{Dxf}) = \frac{\sqrt{\pi\eta_{fD}}}{C_{fD}} \int_0^{t_{Dxf}} \frac{\operatorname{erfc}\left[\frac{\eta_{fD} z}{C_{fD}(t_{Dfx} - z)^{0.5}}\right]}{\sqrt{z}} dz$ (General solution) ..... (B.2.1)
	$p_D(t_{Dxf}) = \frac{2}{C_{fD}}\sqrt{\pi\eta_{fD} t_{Dxf}}$ (Short-time approximation), $t_{Dxf} \le \frac{0.01 C_{fD}^2}{\eta_{fD}^2}$ ..... (B.2.2)
	$p_D(t_{Dxf}) = \frac{\pi}{\Gamma(1.25)\sqrt{2C_{fD}}} t_{Dxf}^{\frac{1}{4}}$ (Large-time approximation), $\begin{cases} t_{Dxf} \le \frac{0.1}{C_{fD}^2} & C_{fD} \ge 3 \\ t_{Dxf} \le 0.0205(C_{fD} - 1.5)^{-1.53} & 1.6 \le C_{fD} \le 3 \\ t_{Dxf} \le \left[\frac{4.55}{\sqrt{C_{fD}}} - 2.5\right]^4 & C_{fD} \le 1.6 \end{cases}$ ..... (B.2.3)
p_{Dd}	$p_{Dd}(t_{Dxf}) = \frac{\sqrt{\pi\eta_{fD} t_{Dxf}}}{C_{fD}}$ (Short-time approximation) ..... (B.2.4)
	$p_{Dd}(t_{Dxf}) = \frac{0.612708}{\sqrt{C_{fD}}} t_{Dxf}^{\frac{1}{4}}$ (Large-time approximation) ..... (B.2.5)
$p_{D\beta d}$ $(= p_{Dd}/p_D)$	$p_{D\beta d}(t_{Dxf}) = \frac{1}{2}$ (Short-time approximation) ..... (B.2.6)
	$p_{D\beta d}(t_{Dxf}) = \frac{1}{4}$ (Large-time approximation) ..... (B.2.7)

Table B-2 — Continued

Definitions: (field units)

$$t_{Dxf} = 2.637\times10^{-4}\frac{kt}{\phi c_t \mu x_f^2} \quad \text{(B.2.8)}$$

$$p_D = \frac{1}{141.2}\frac{kh}{qB\mu}(p_i - p_{wf}) \quad \text{(B.2.9)}$$

$$\eta_{fD} = \frac{k_f \phi c_t}{k\phi_f c_{ft}} \quad \text{(B.2.10)}$$

$$C_{fD} = \frac{k_f w}{k x_f} \quad \text{(B.2.11)}$$

$$C_{Df} = \frac{0.8936 C_s}{\phi h c_t x_f^2} \quad \text{(B.2.12)}$$

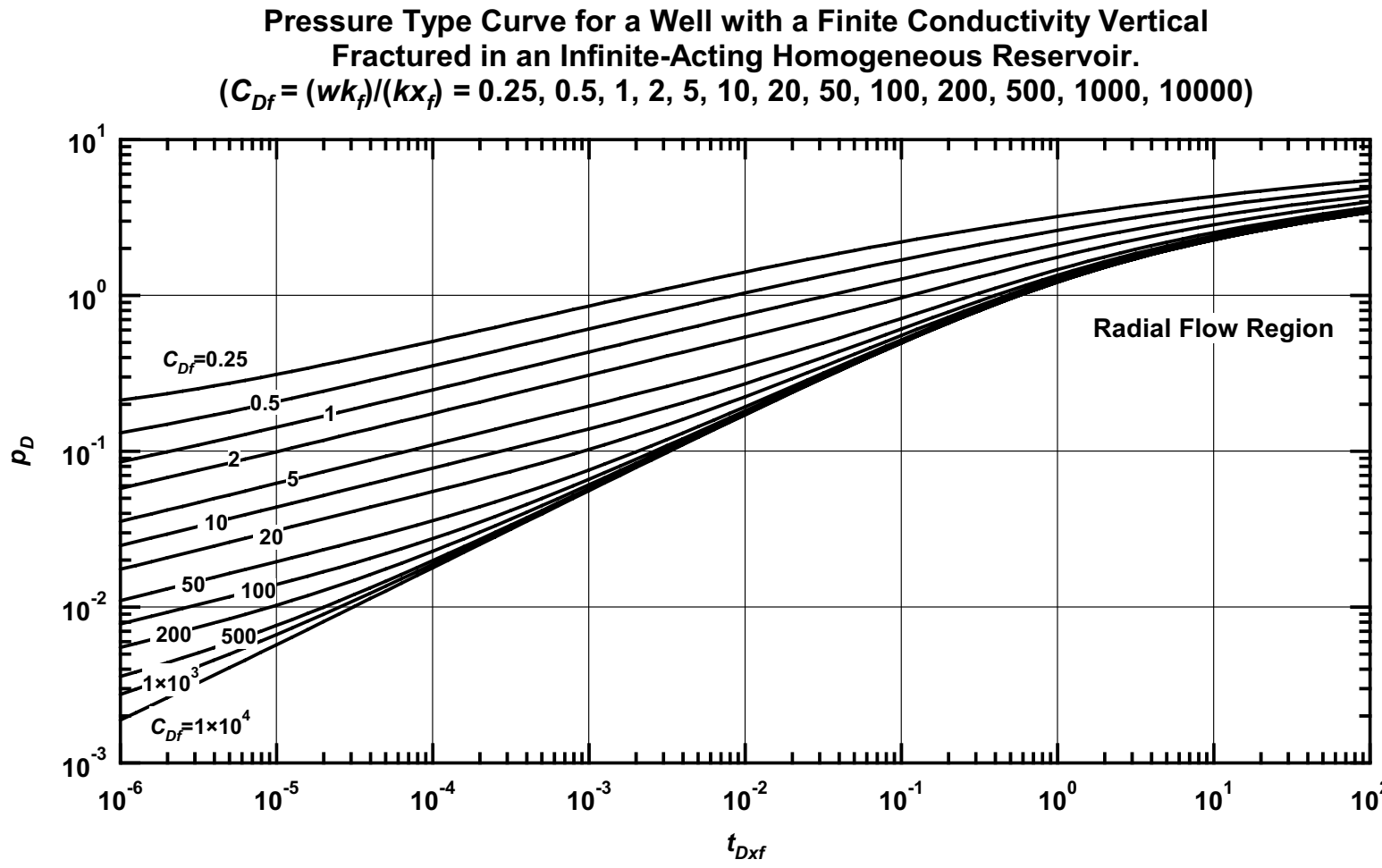

Figure B.4— p_D vs. t_{Dxf} — solutions for a fractured well in an infinite-acting homogeneous reservoir— no wellbore storage or skin effects (various C_{fD} values).

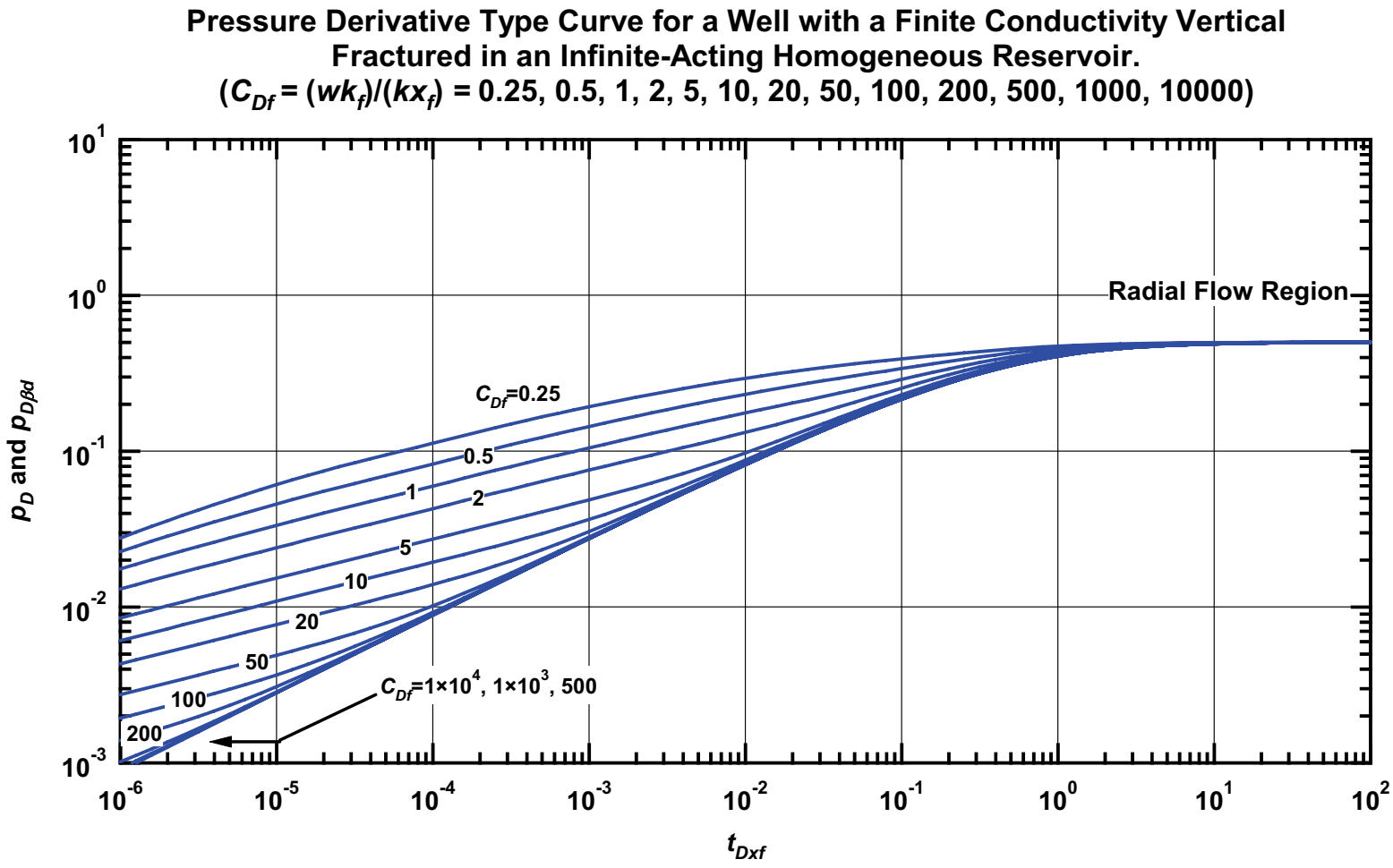

Figure B.5— p_{Dd} vs. t_{Dxf} — solutions for a fractured well in an infinite-acting homogeneous reservoir— no wellbore storage or skin effects (various C_{fD} values).

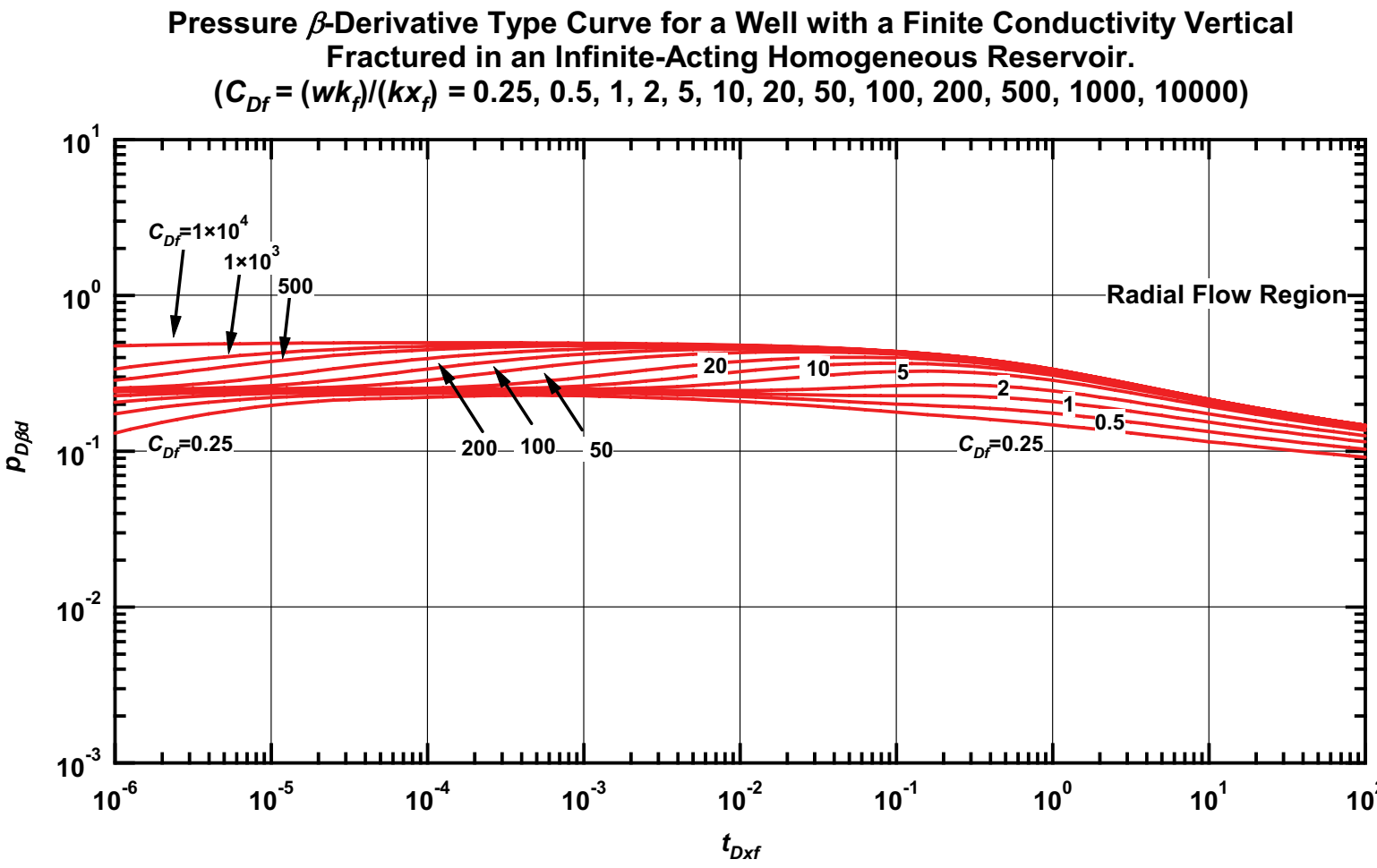

Figure B.6— $p_{D\beta d}$ vs. t_{Dxf} — solutions for a fractured well in an infinite-acting homogeneous reservoir— no wellbore storage or skin effects (various C_{fD} values).

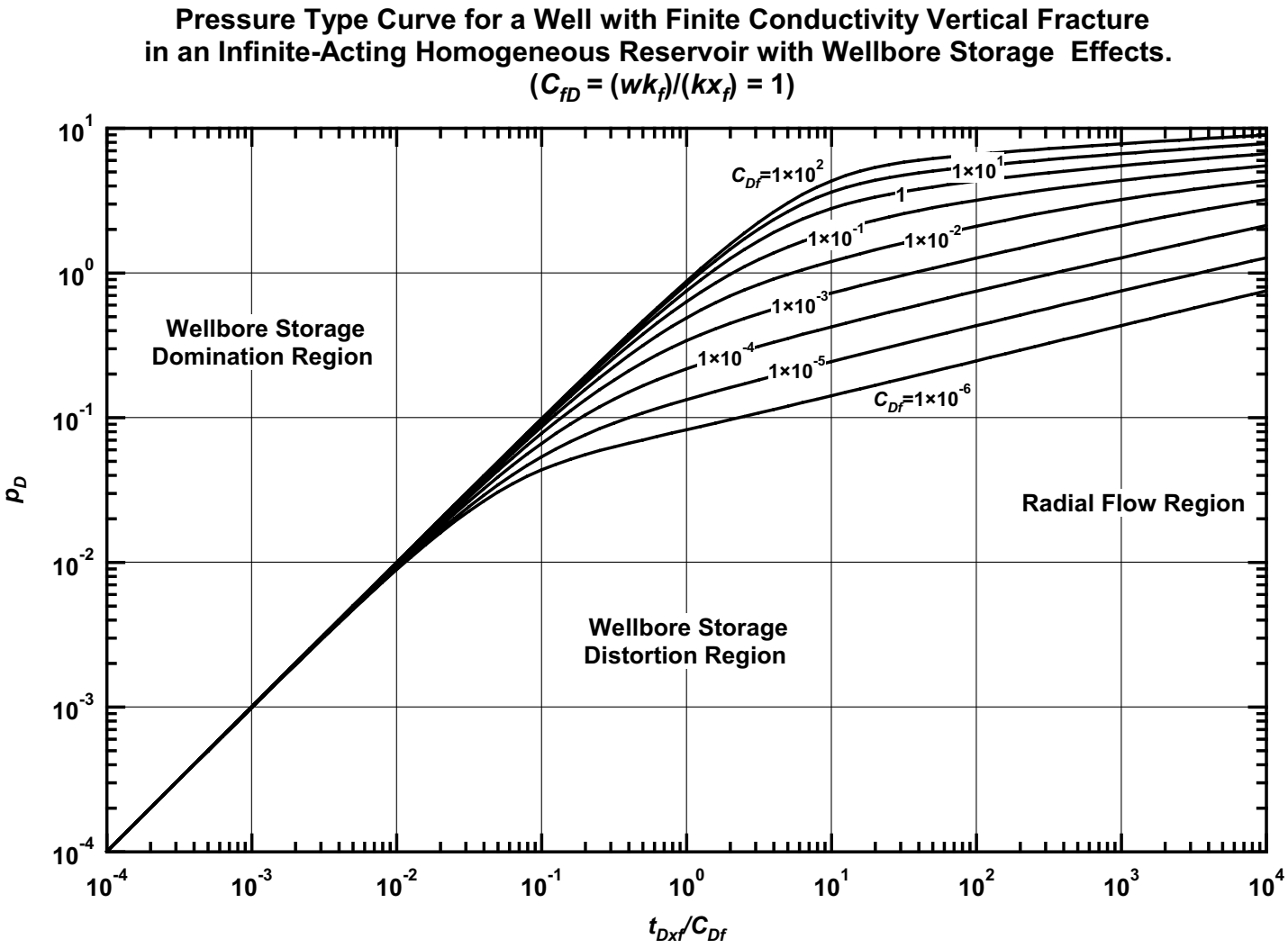

Figure B.7 — p_D vs. t_{Dxf}/C_{Df} — C_{fD} = 1 (fractured well case — includes wellbore storage effects).

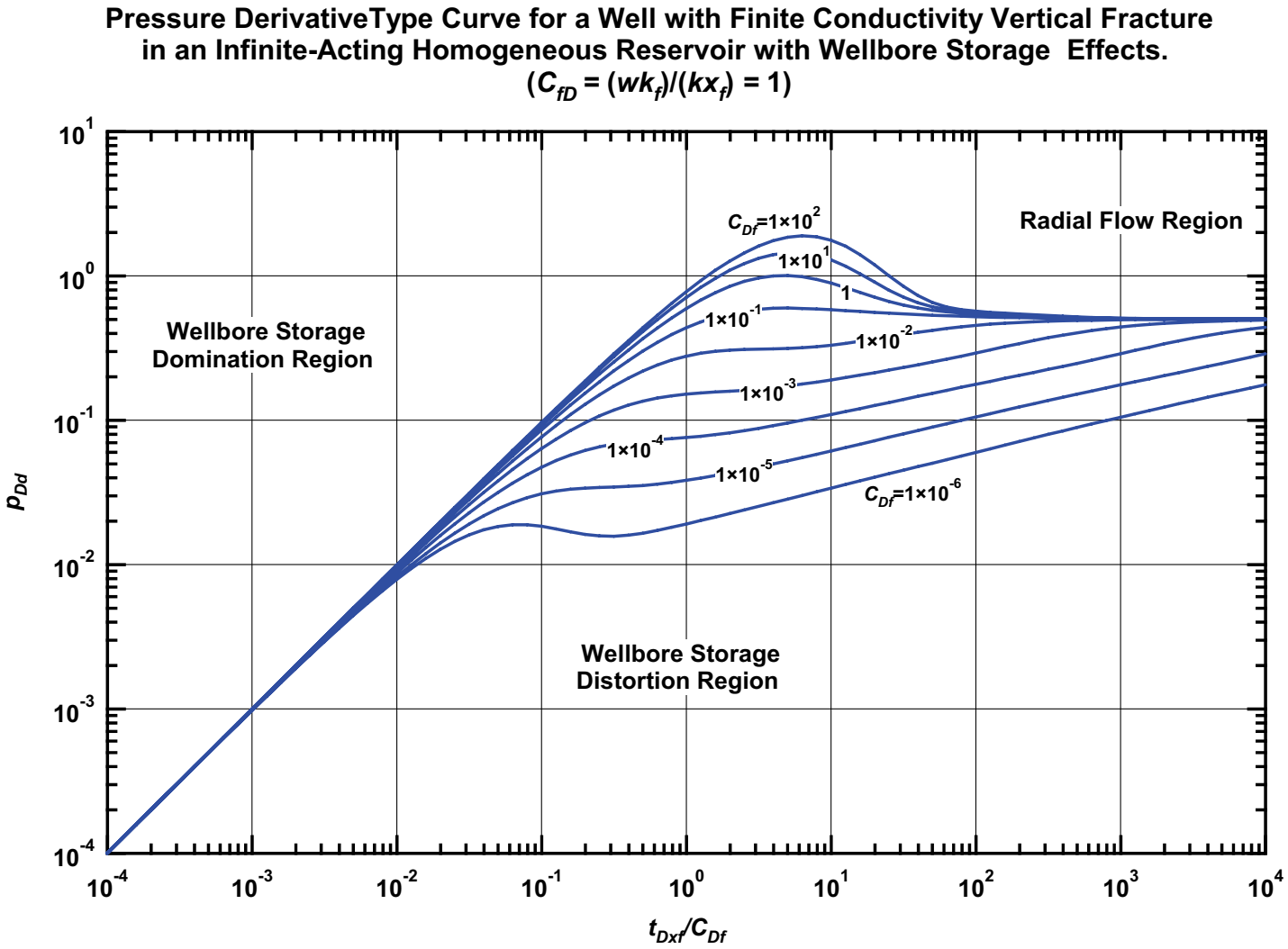

Figure B.8— p_{Dd} vs. t_{Dxf}/C_{Df} — C_{fD} = 1 (fractured well case — includes wellbore storage effects).

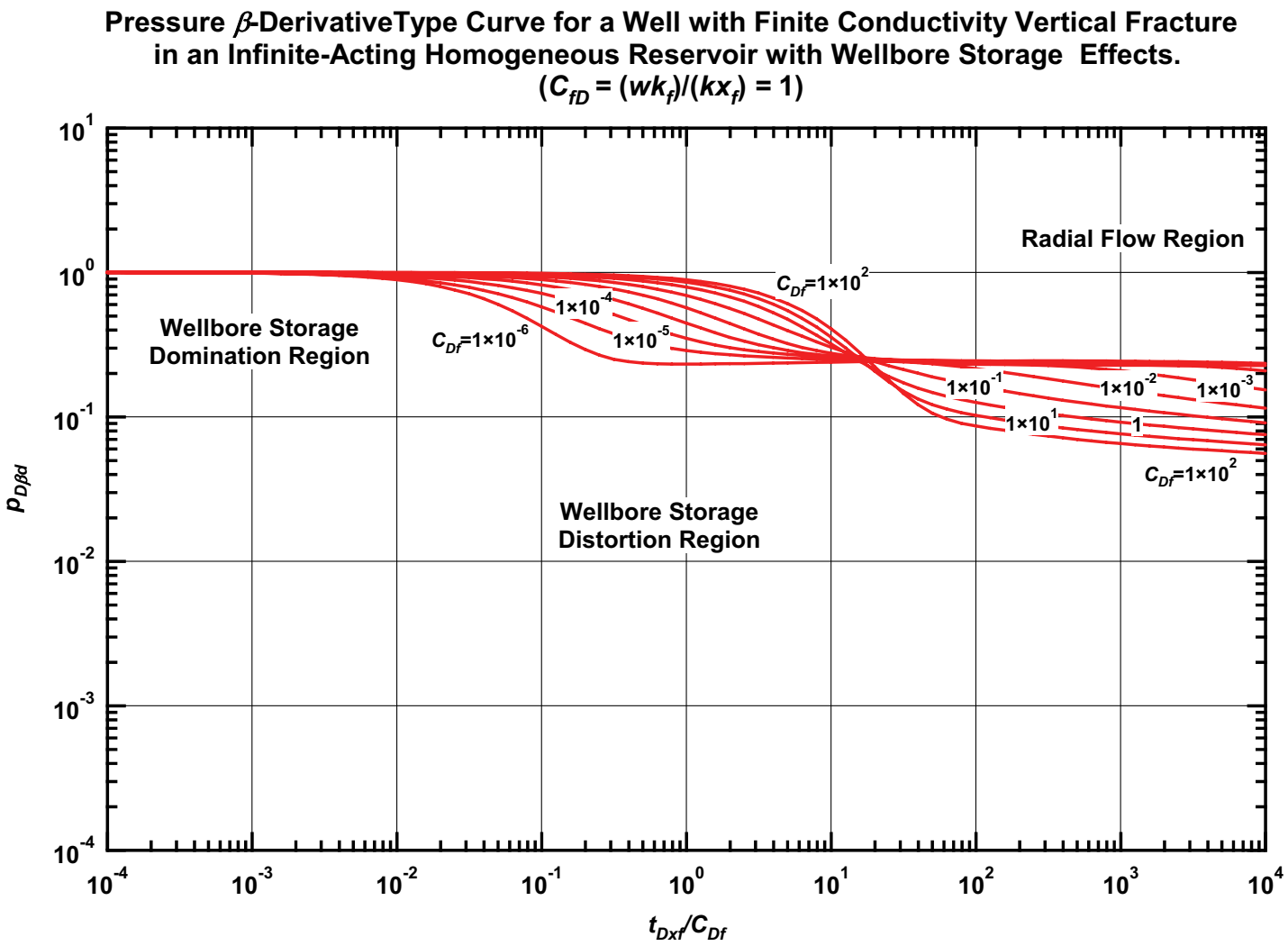

Figure B.9 — $p_{D\beta d}$ vs. t_{Dxf}/C_{Df} — C_{fD} = 1 (fractured well case — includes wellbore storage effects).

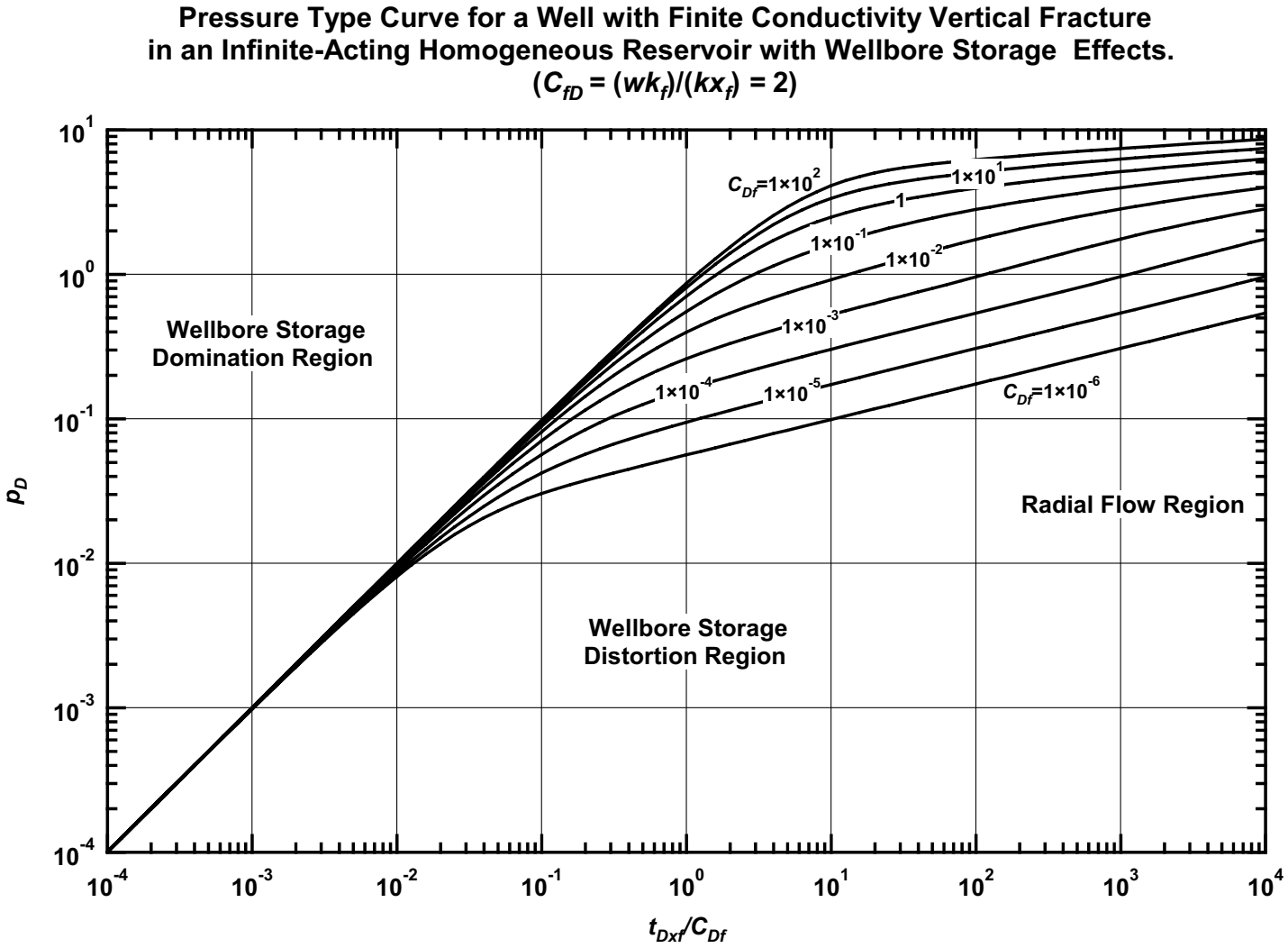

Figure B.10 — p_D vs. t_{Dxf}/C_{Df} — C_{fD} = 2 (fractured well case — includes wellbore storage effects).

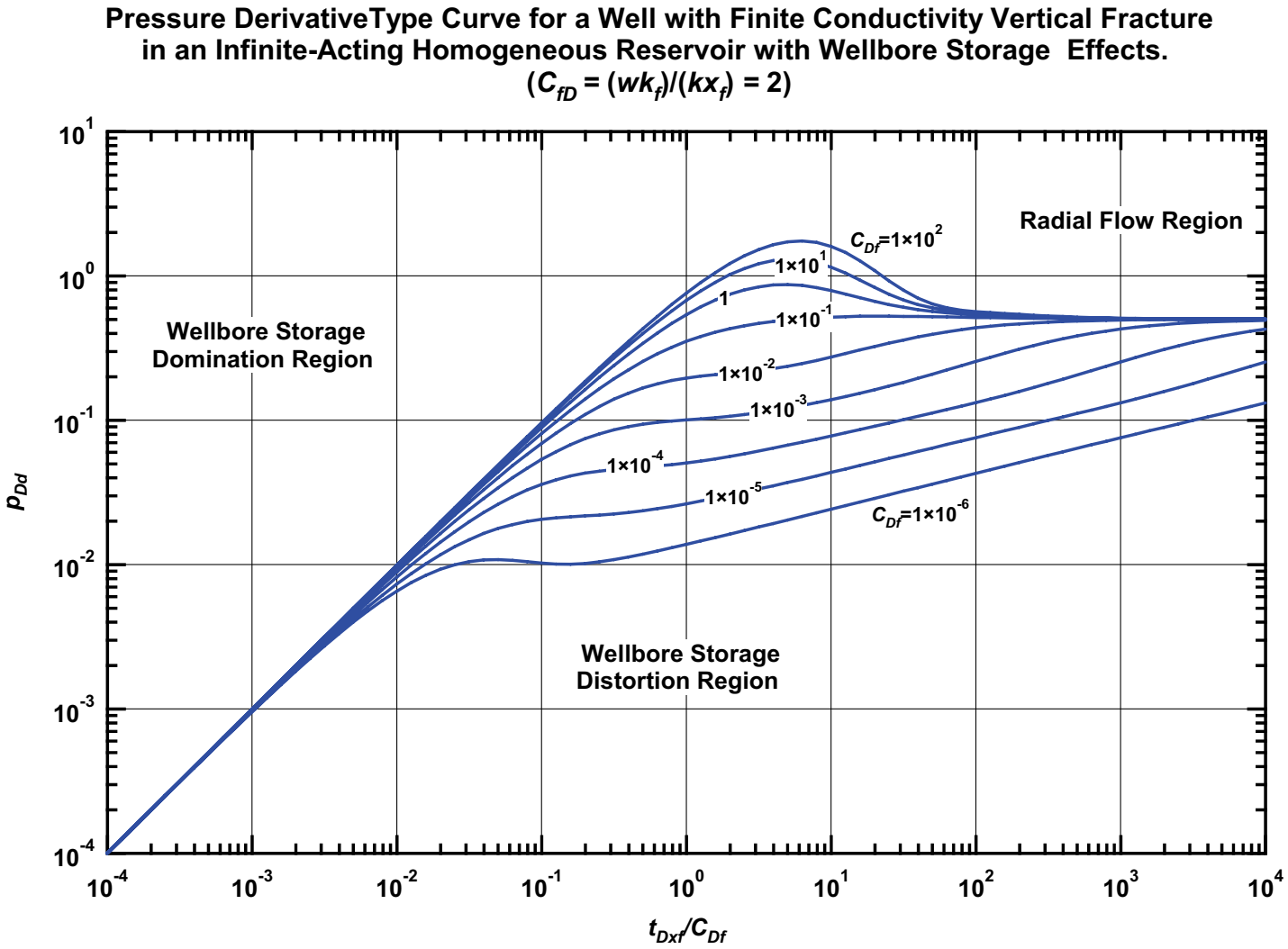

Figure B.11 — p_{Dd} vs. t_{Dxf}/C_{Df} — C_{fD} = 2 (fractured well case — includes wellbore storage effects).

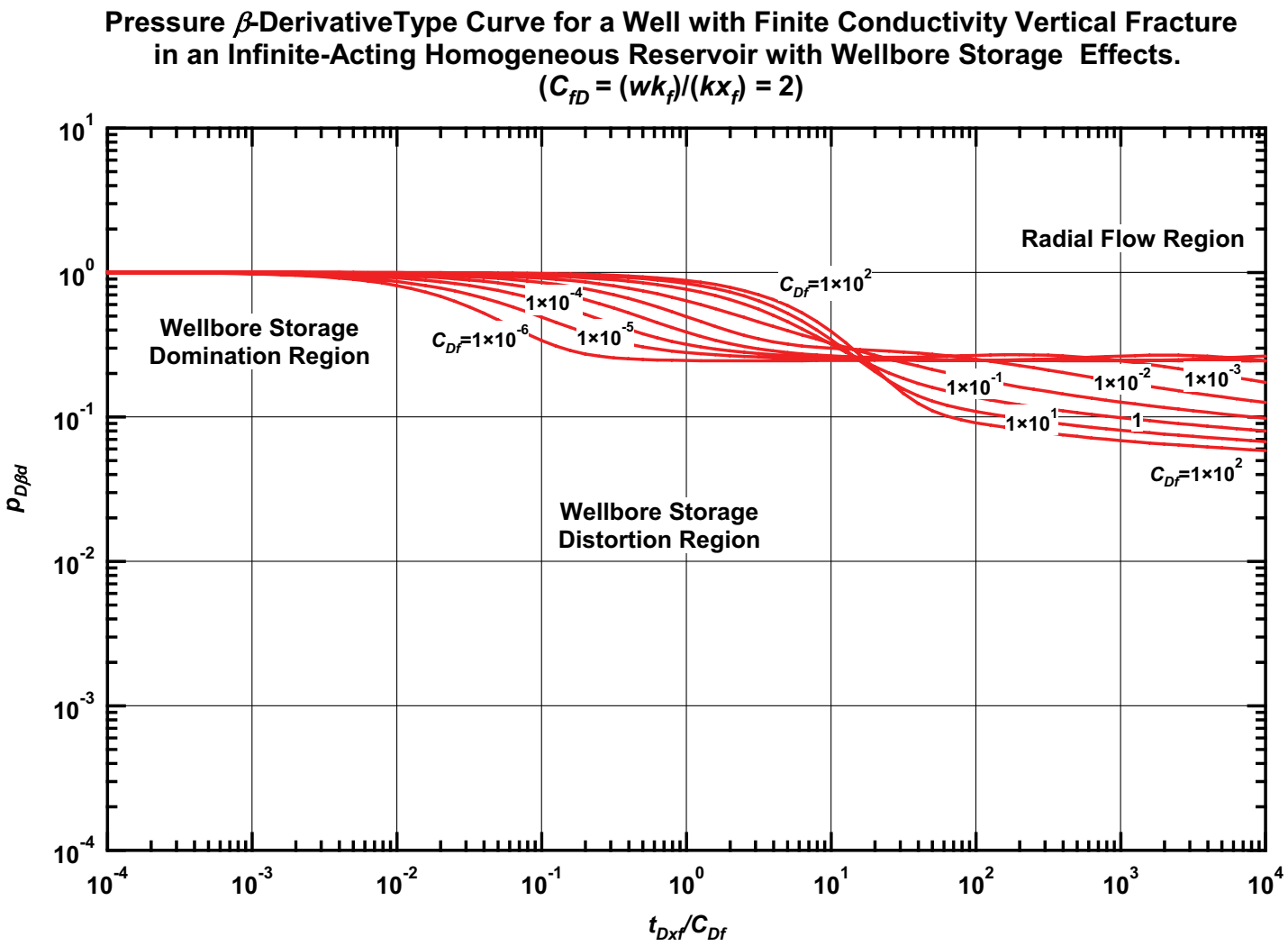

Figure B.12 — $p_{D\beta d}$ vs. t_{Dxf}/C_{Df} — C_{fD} = 2 (fractured well case — includes wellbore storage effects).

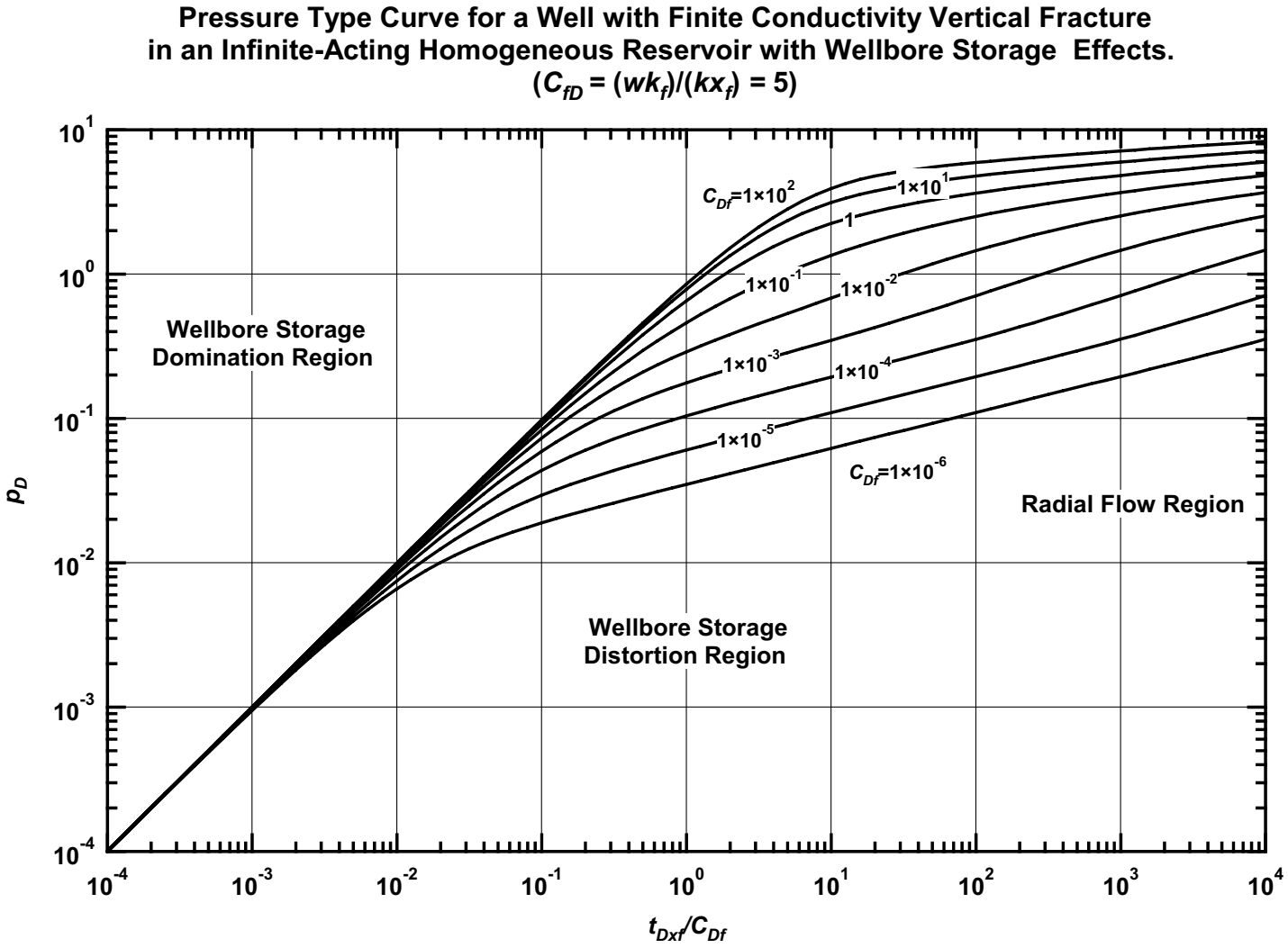

Figure B.13 — p_D vs. t_{Dxf}/C_{Df} — C_{fD} = 5 (fractured well case — includes wellbore storage effects).

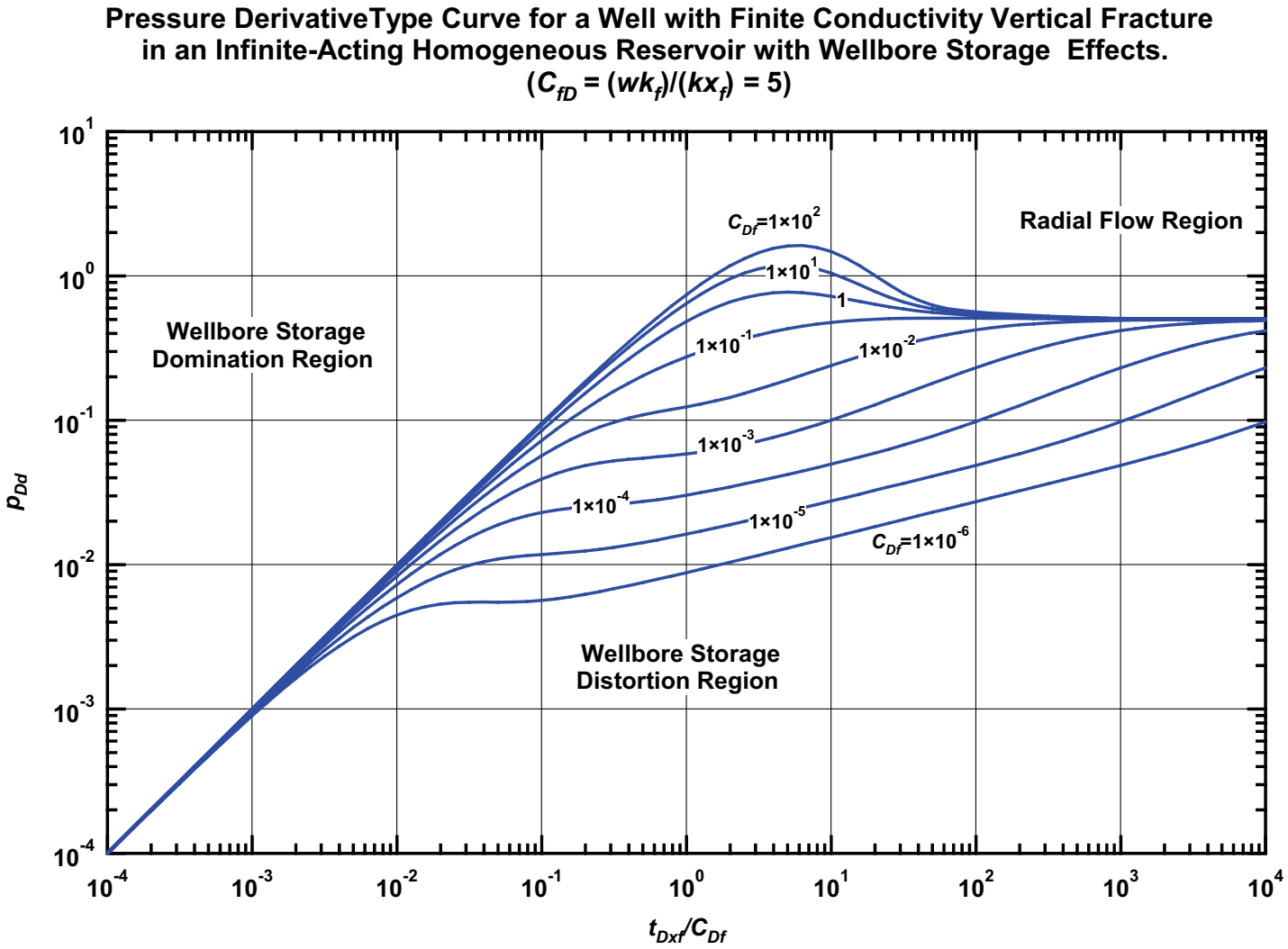

Figure B.14 — p_{Dd} vs. t_{Dxf}/C_{Df} — C_{fD} = 5 (fractured well case — includes wellbore storage effects).

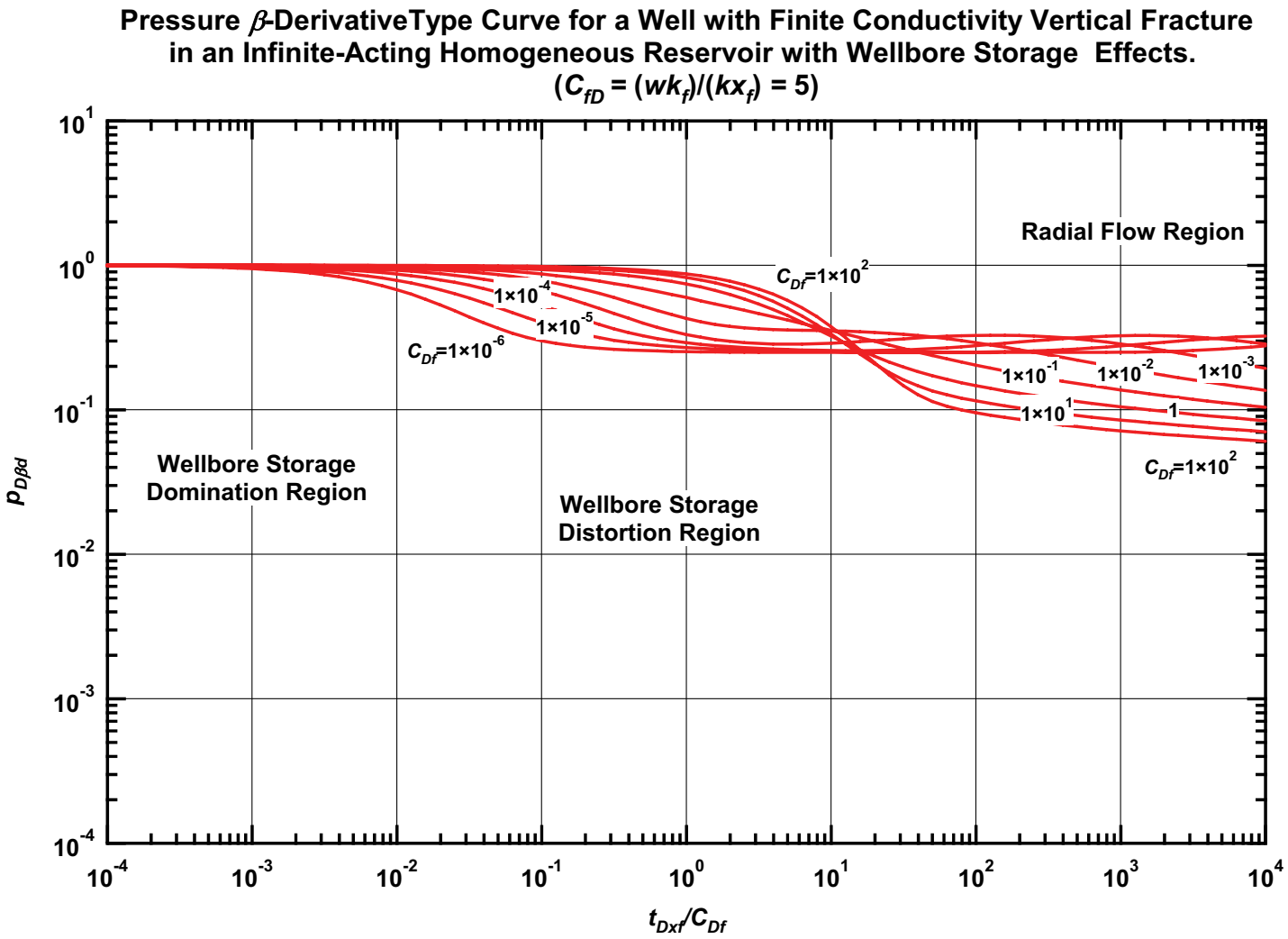

Figure B.15 — $p_{D\beta d}$ vs. t_{Dxf}/C_{Df} — C_{fD} = 5 (fractured well case — includes wellbore storage effects).

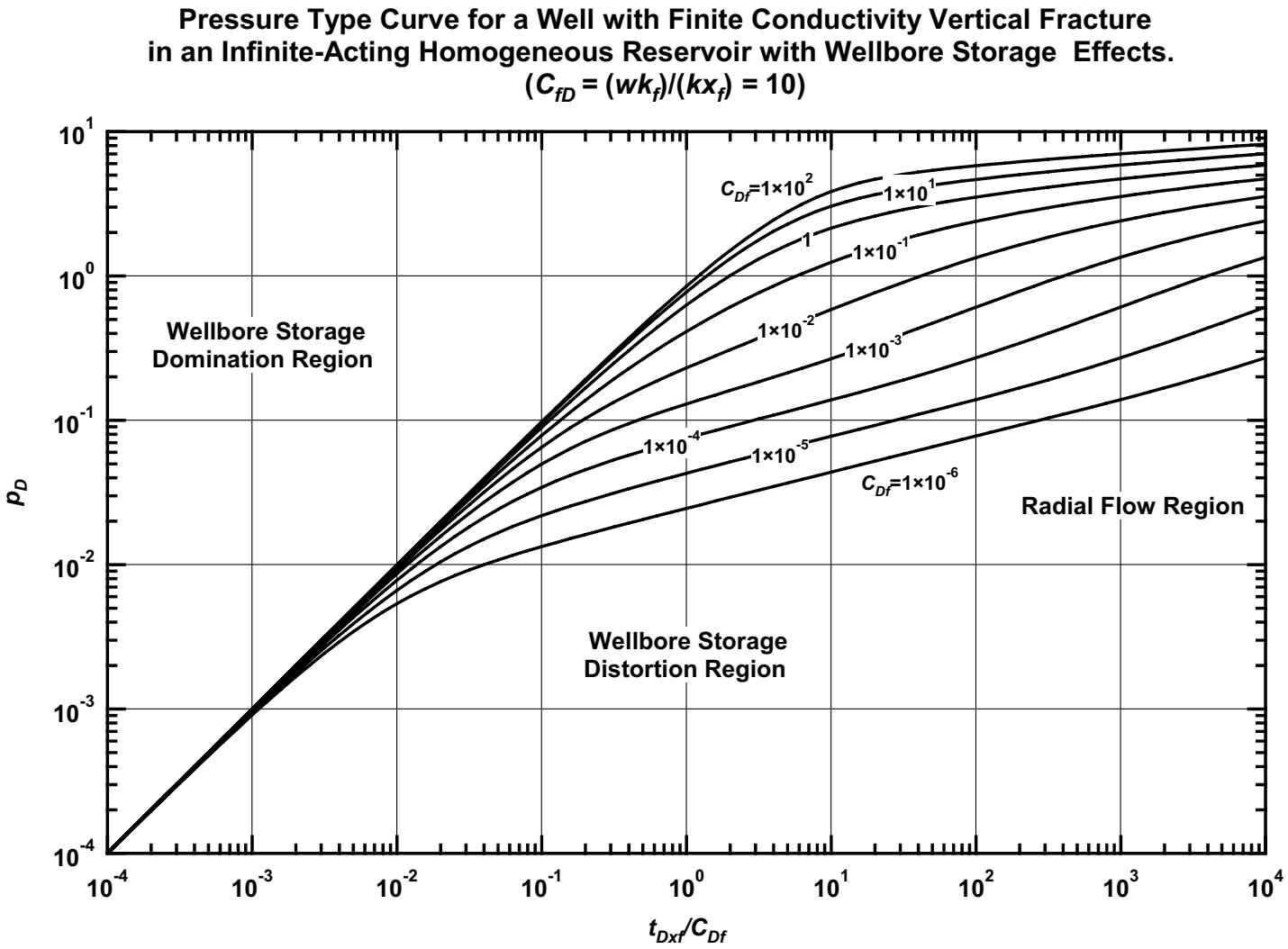

Figure B.16 — p_D vs. t_{Dxf}/C_{Df} — C_{fD} = 10 (fractured well case — includes wellbore storage effects).

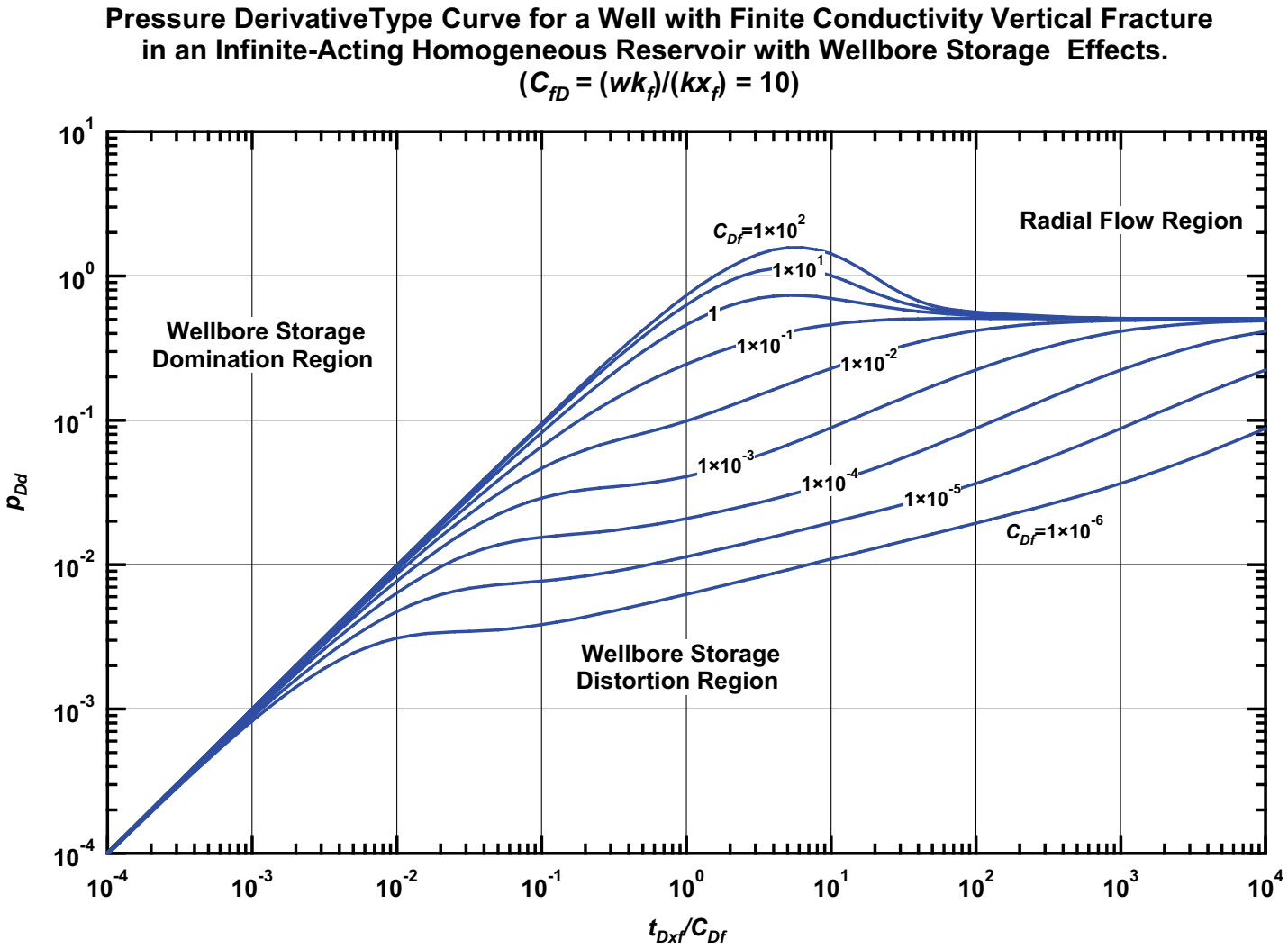

Figure B.17 — p_{Dd} vs. t_{Dxf}/C_{Df} — C_{fD} = 10 (fractured well case — includes wellbore storage effects).

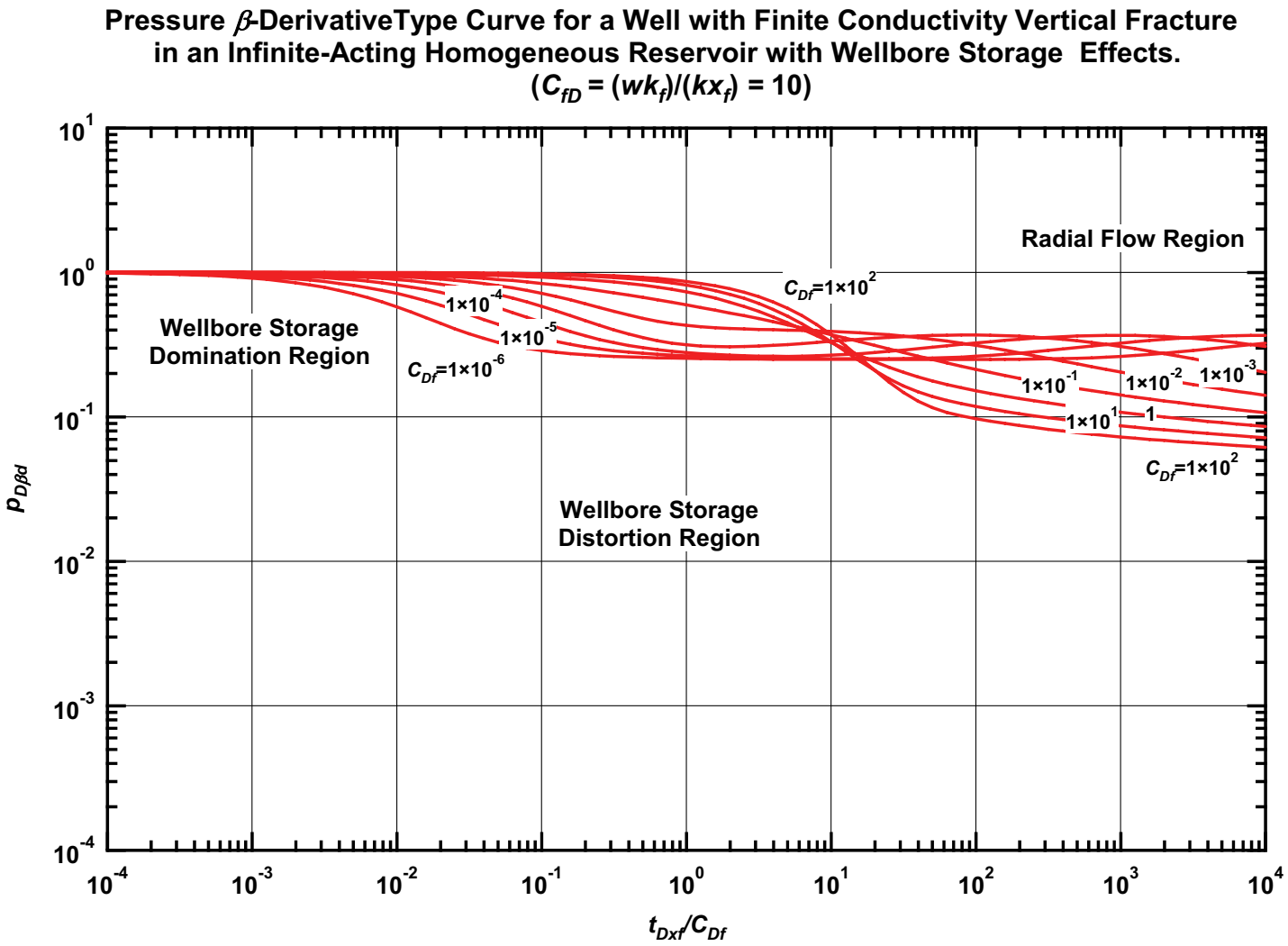

Figure B.18 — $p_{D\beta d}$ vs. t_{Dxf}/C_{Df} — C_{fD} = 10 (fractured well case — includes wellbore storage effects).

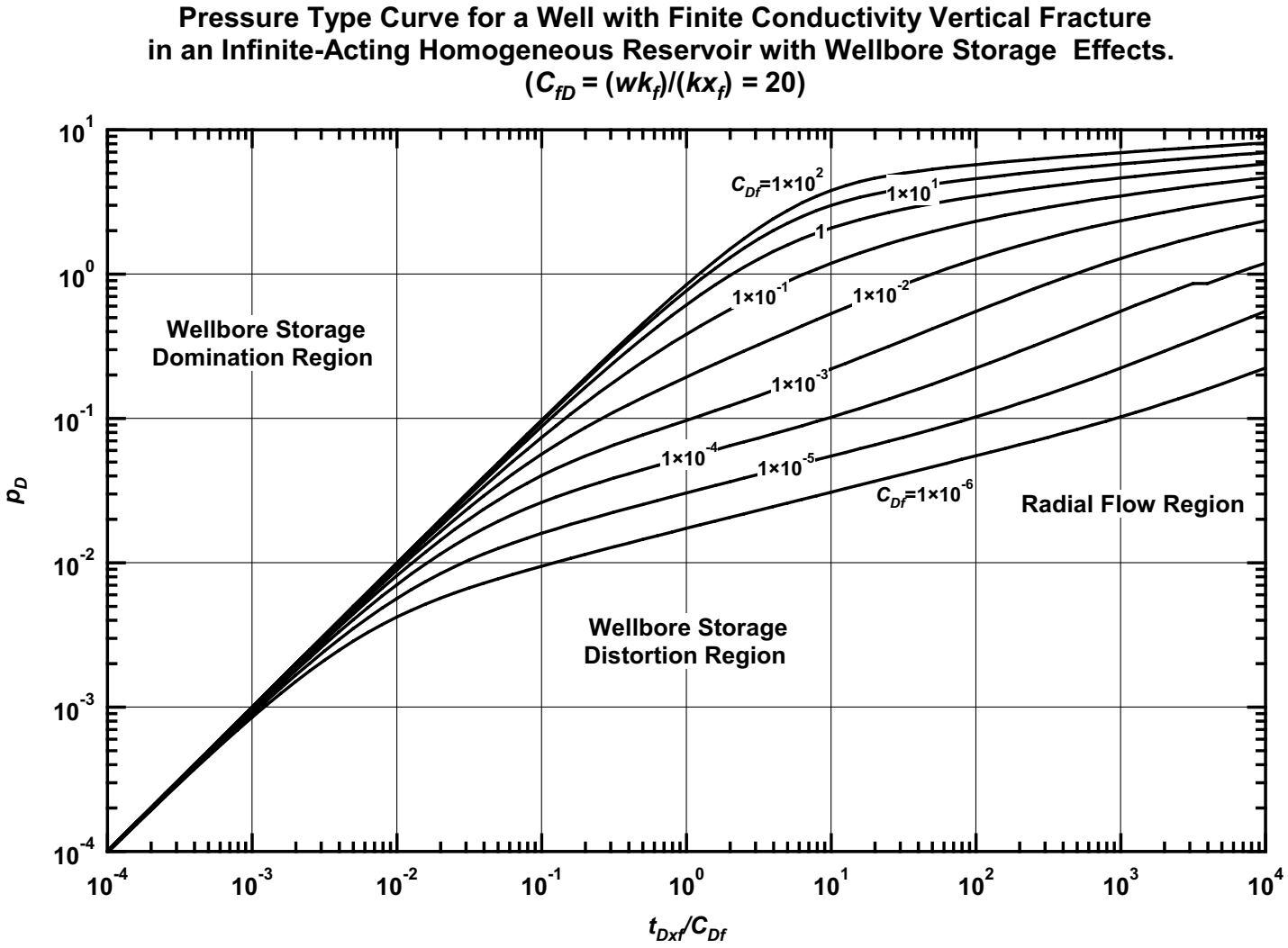

Figure B.19 — p_D vs. t_{Dxf}/C_{Df} — C_{fD} = 20 (fractured well case — includes wellbore storage effects).

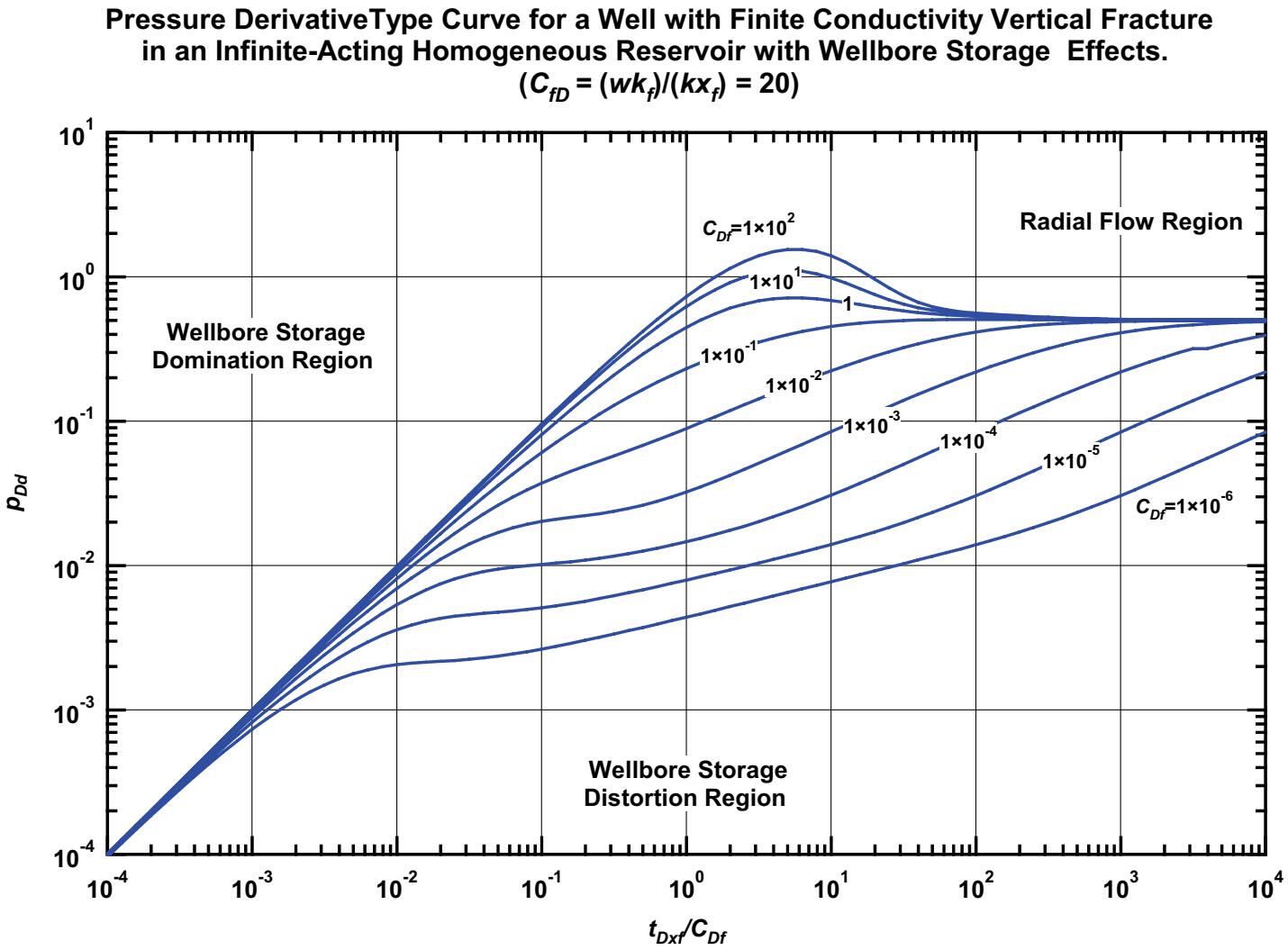

Figure B.20 — p_{Dd} vs. t_{Dxf}/C_{Df} — C_{fD} = 20 (fractured well case — includes wellbore storage effects).

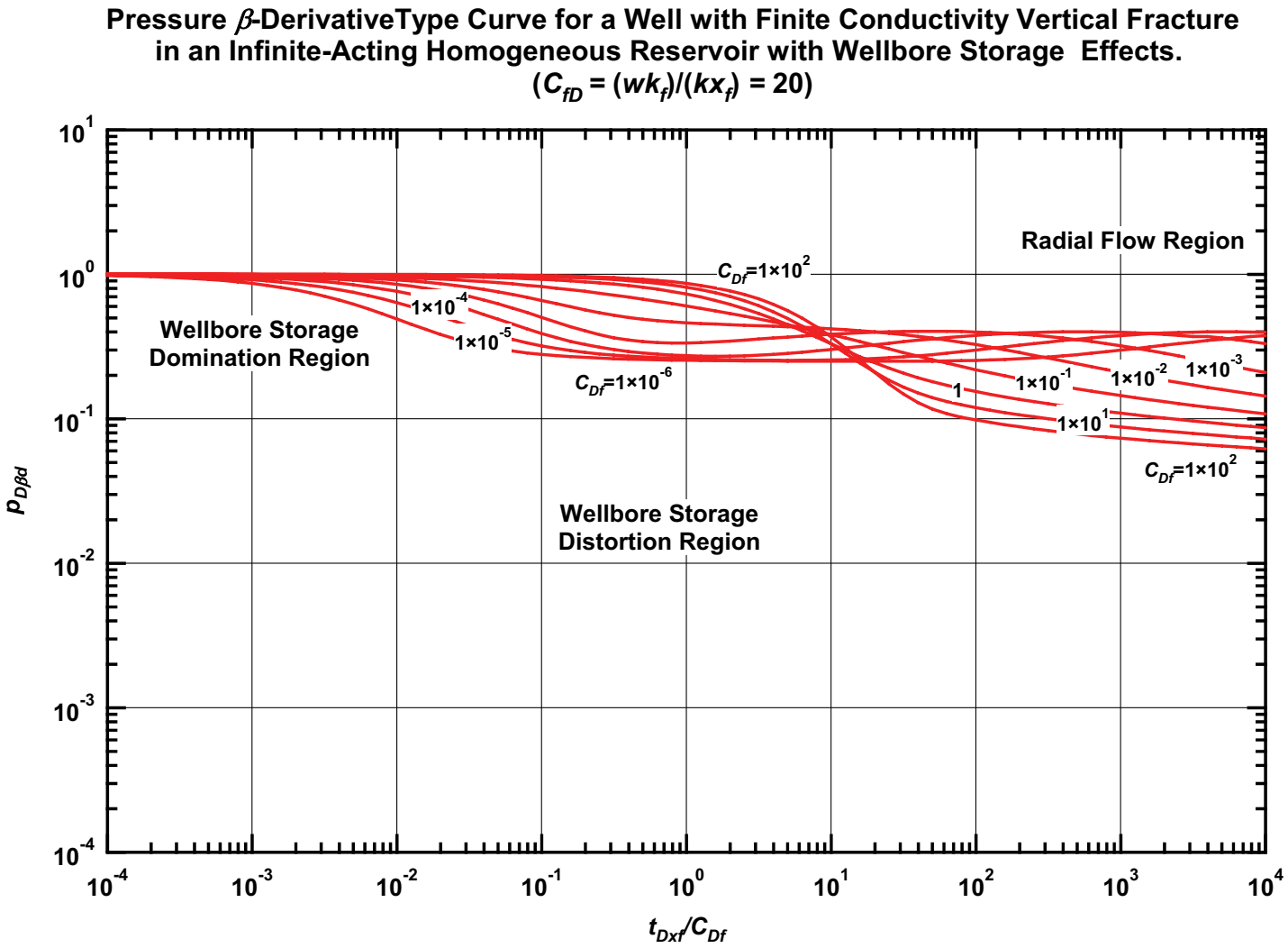

Figure B.21 — $p_{D\beta d}$ vs. t_{Dxf}/C_{Df} — C_{fD} = 20 (fractured well case — includes wellbore storage effects).

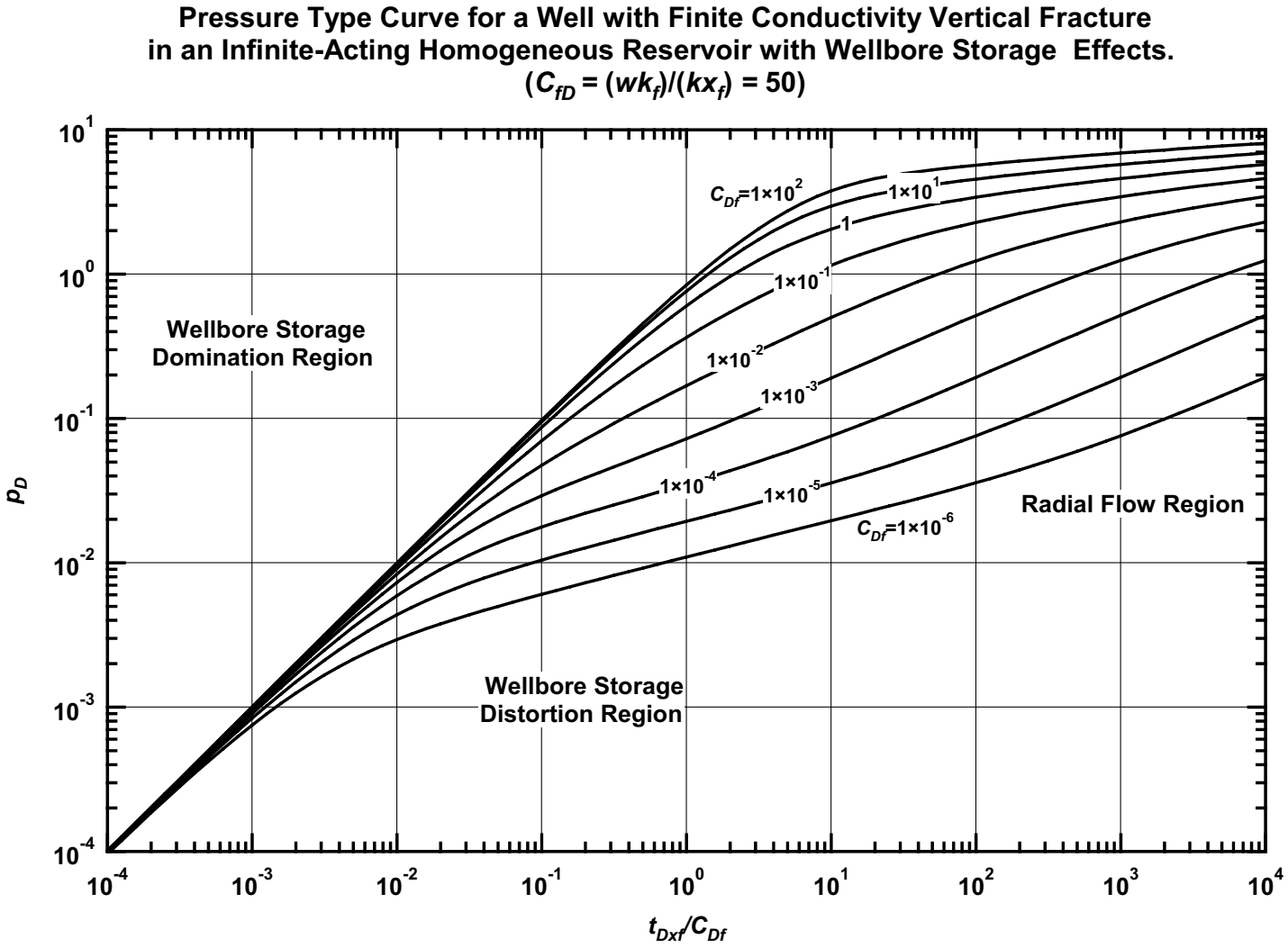

Figure B.22 — p_D vs. t_{Dxf}/C_{Df} — C_{fD} = 50 (fractured well case — includes wellbore storage effects).

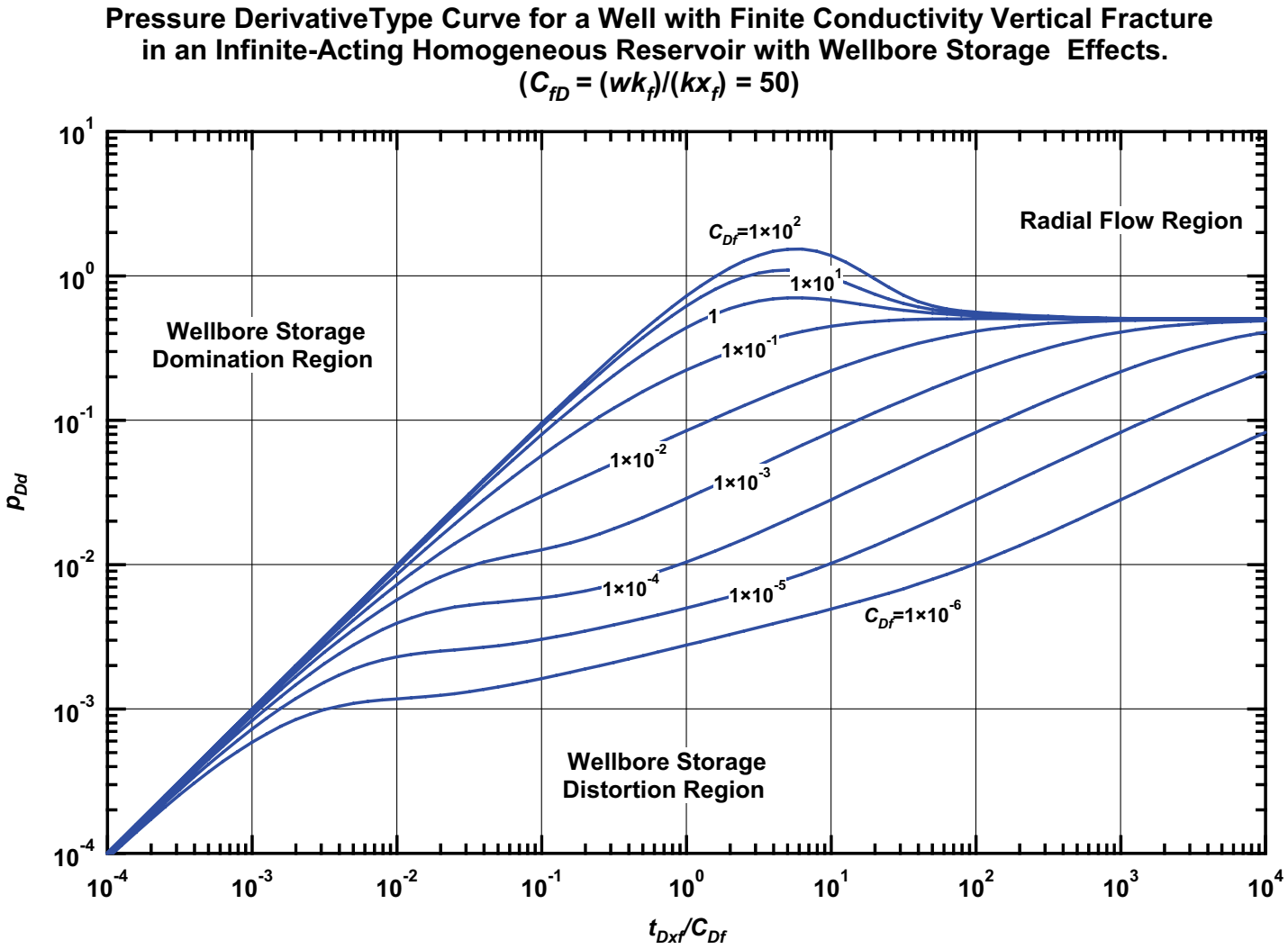

Figure B.23 — p_{Dd} vs. t_{Dxf}/C_{Df} — C_{fD} = 50 (fractured well case — includes wellbore storage effects).

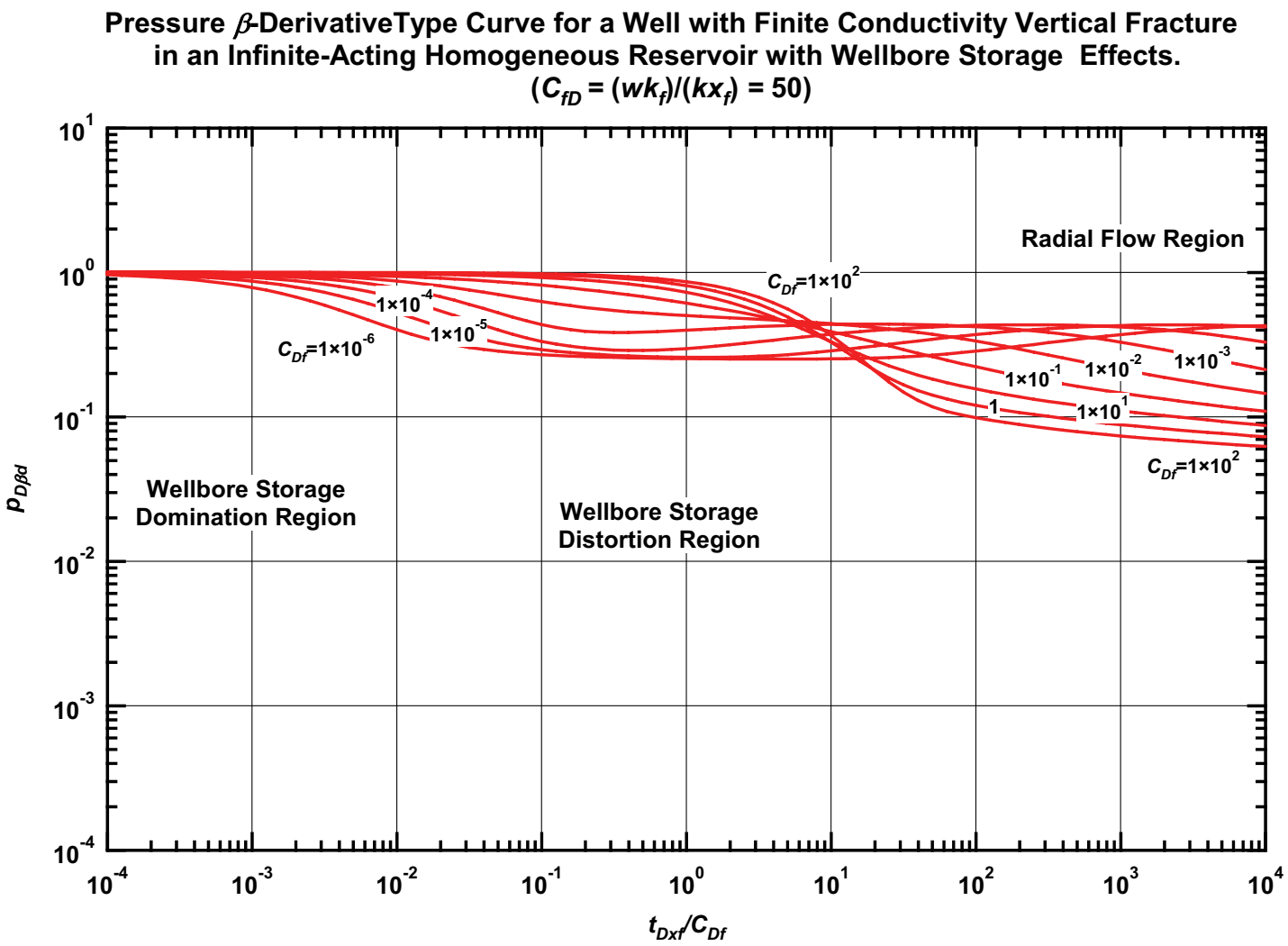

Figure B.24 — $p_{D\beta d}$ **vs.** t_{Dxf}/C_{Df} **—** C_{fD} **= 50 (fractured well case — includes wellbore storage effects).**

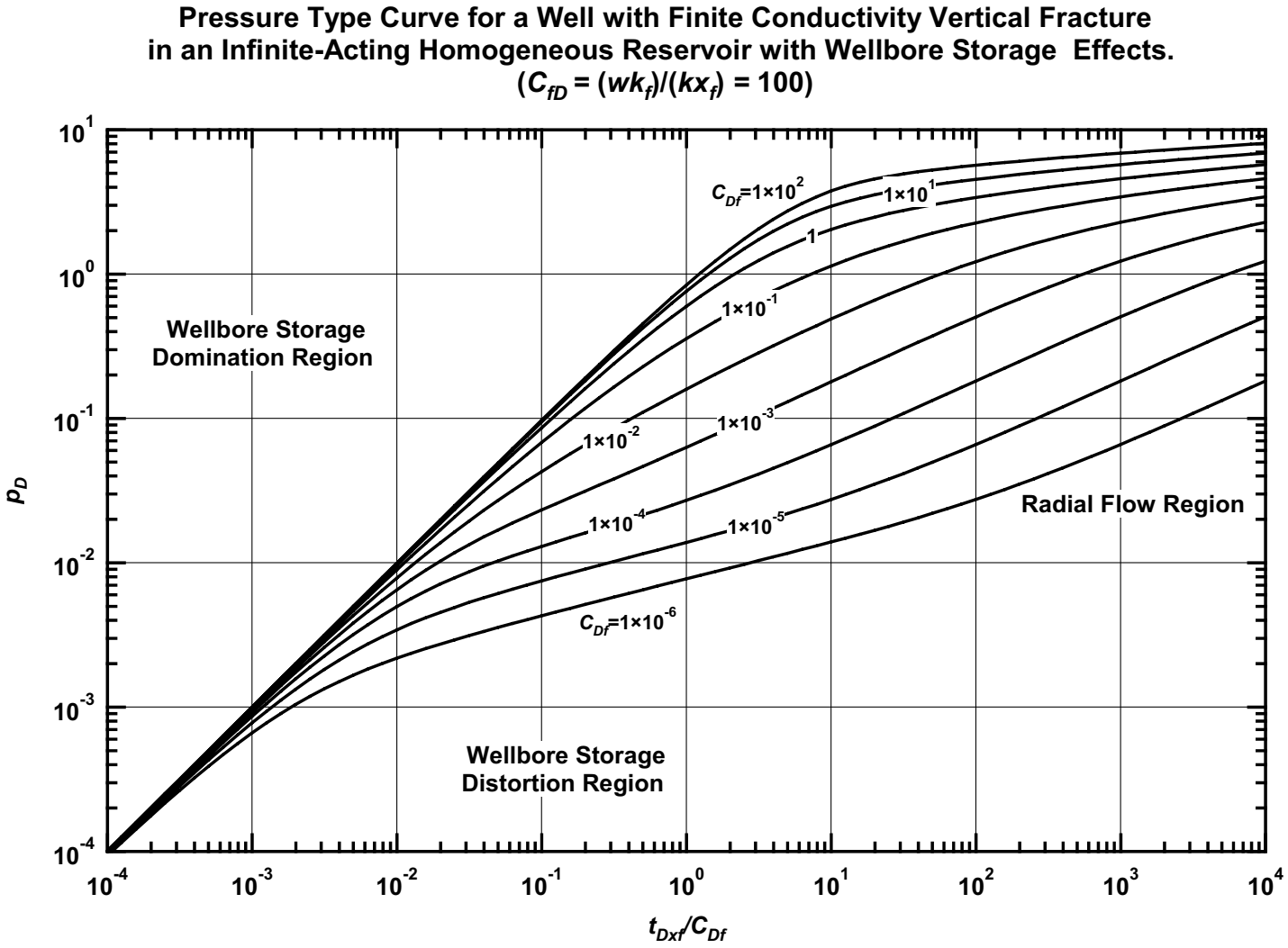

Figure B.25 — p_D vs. t_{Dxf}/C_{Df} — C_{fD} = 100 (fractured well case — includes wellbore storage effects).

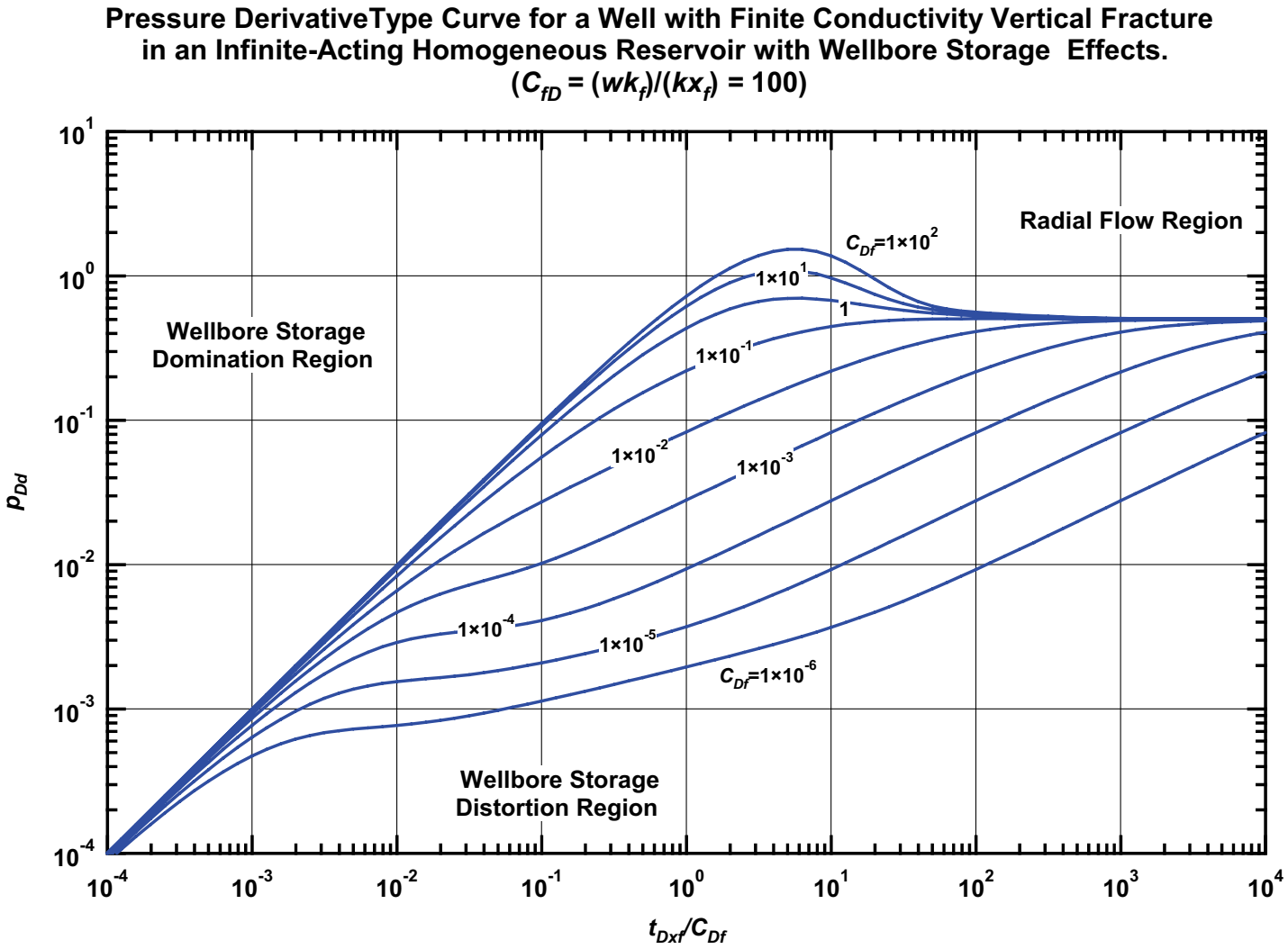

Figure B.26 — p_{Dd} vs. t_{Dxf}/C_{Df} — C_{fD} = 100 (fractured well case — includes wellbore storage effects).

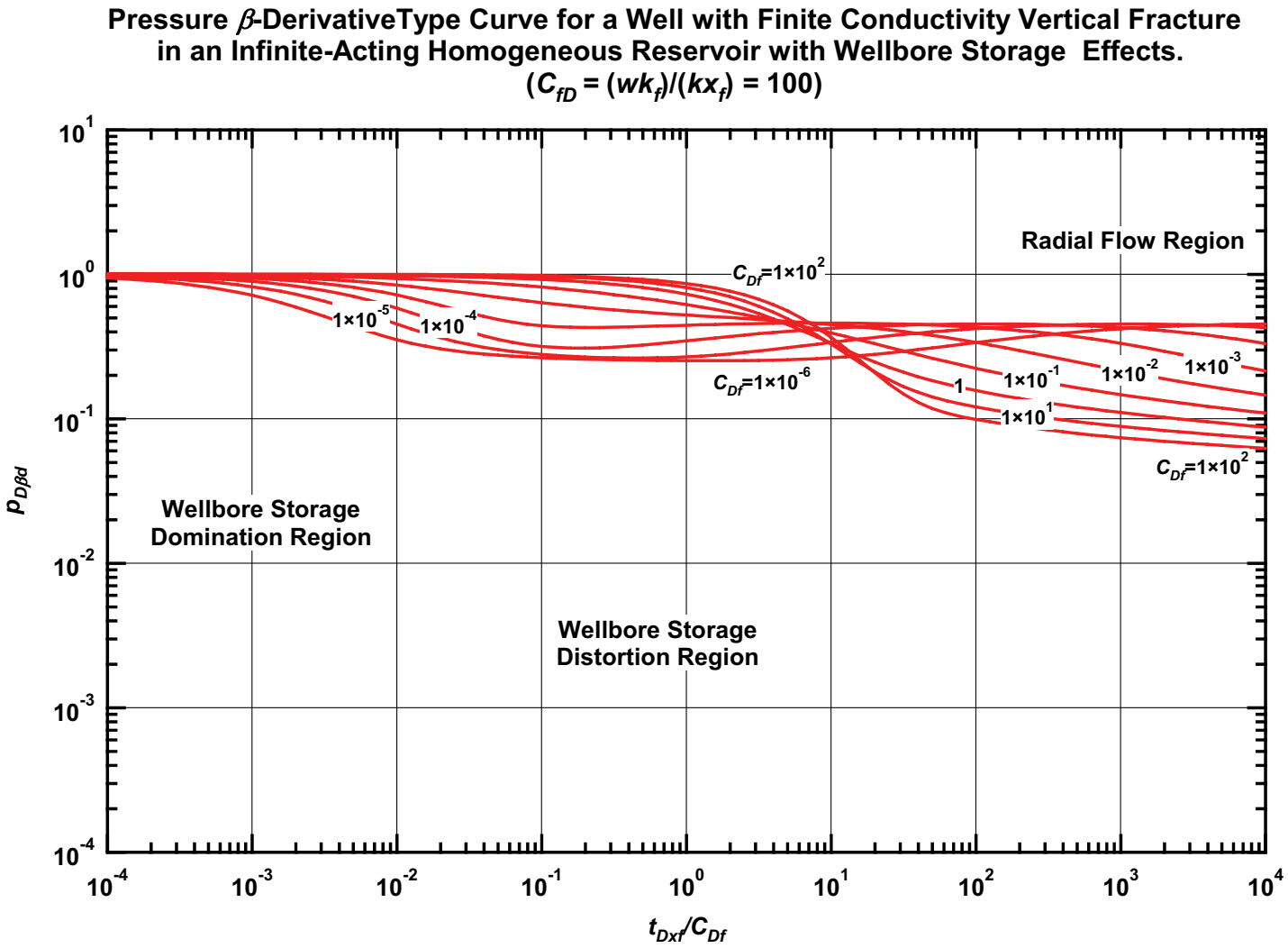

Figure B.27 — $p_{D\beta d}$ vs. t_{Dxf}/C_{Df} — C_{fD} = 100 (fractured well case — includes wellbore storage effects).

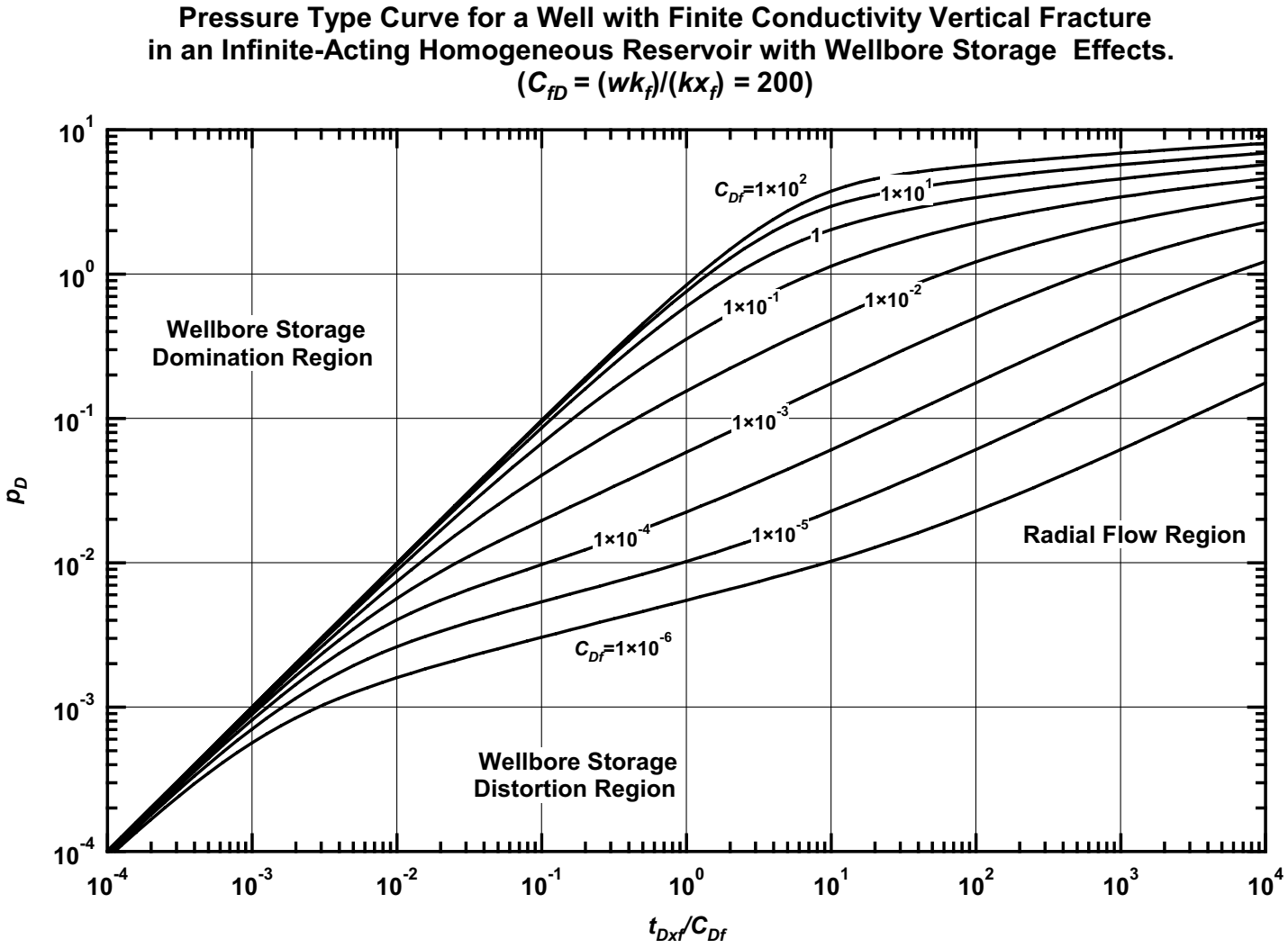

Figure B.28 — p_D vs. t_{Dxf}/C_{Df} — C_{fD} = 200 (fractured well case — includes wellbore storage effects).

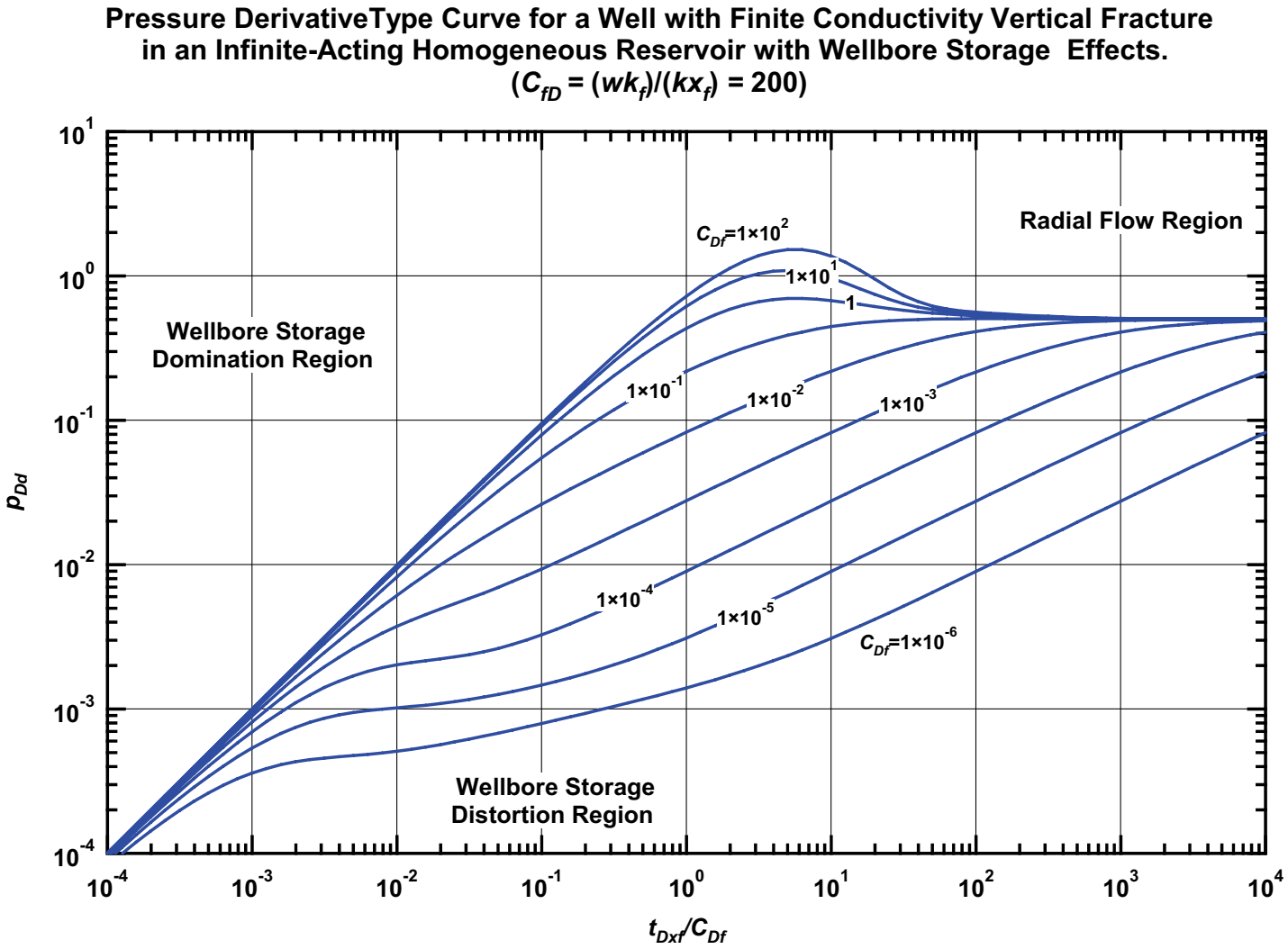

Figure B.29 — p_{Dd} vs. t_{Dxf}/C_{Df} — C_{fD} = 200 (fractured well case — includes wellbore storage effects).

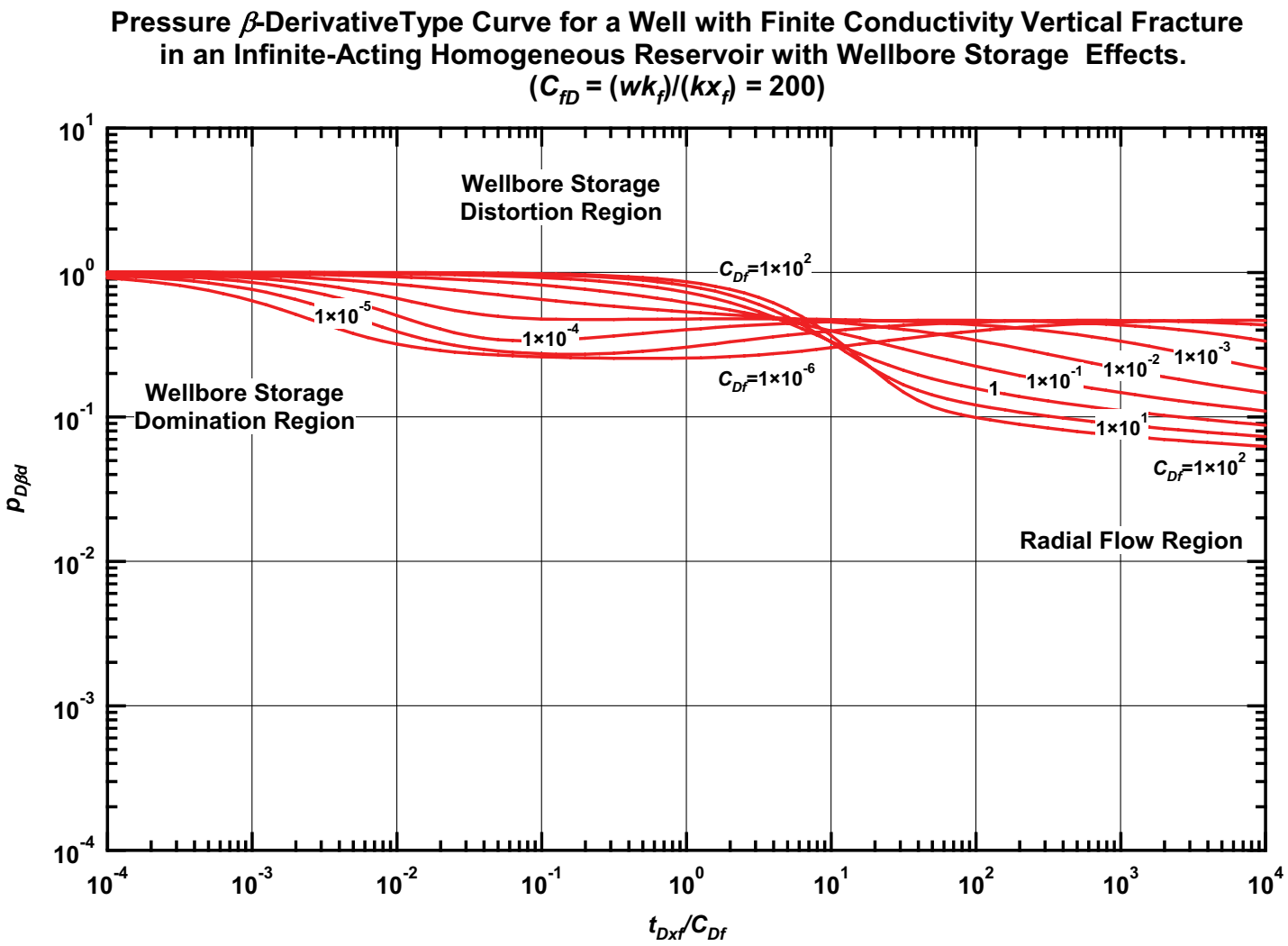

Figure B.30 — $p_{D\beta d}$ vs. t_{Dxf}/C_{Df} — C_{fD} = 200 (fractured well case — includes wellbore storage effects).

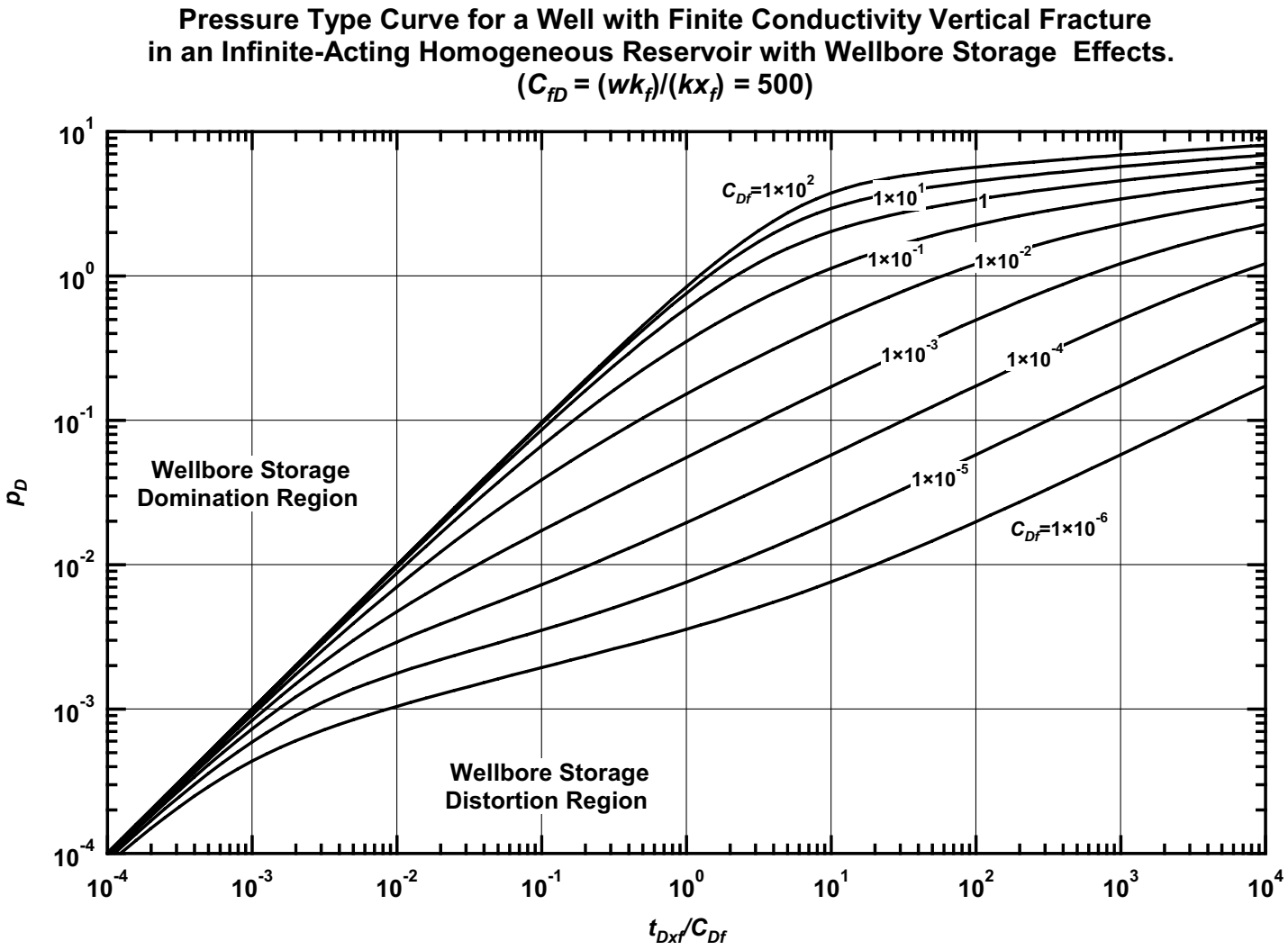

Figure B.31 — p_D vs. t_{Dxf}/C_{Df} — C_{fD} = 500 (fractured well case — includes wellbore storage effects).

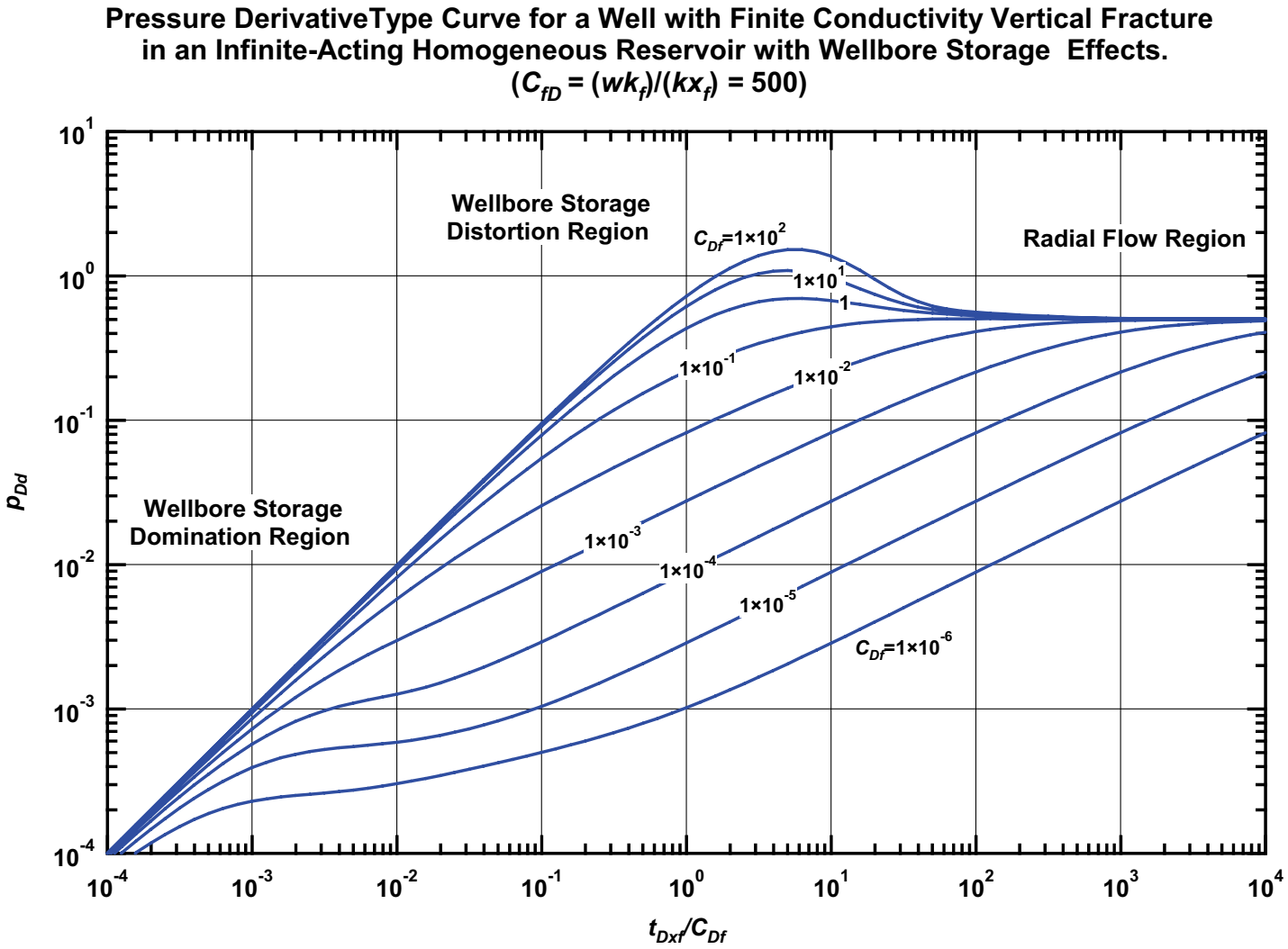

Figure B.32 — p_{Dd} vs. t_{Dxf}/C_{Df} — C_{fD} = 500 (fractured well case — includes wellbore storage effects).

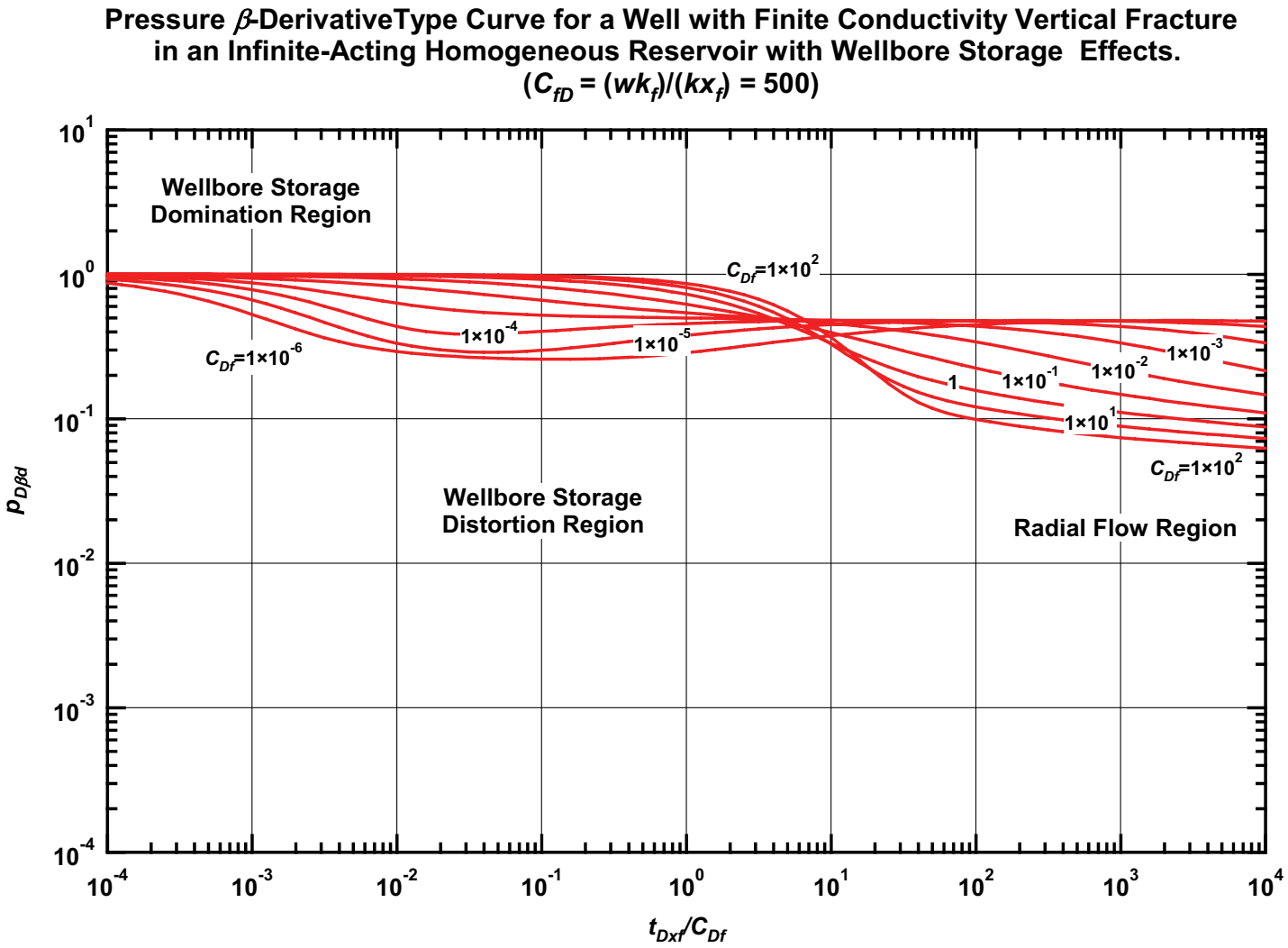

Figure B.33 — $p_{D\beta d}$ vs. t_{Dxf}/C_{Df} — C_{fD} = 500 (fractured well case — includes wellbore storage effects).

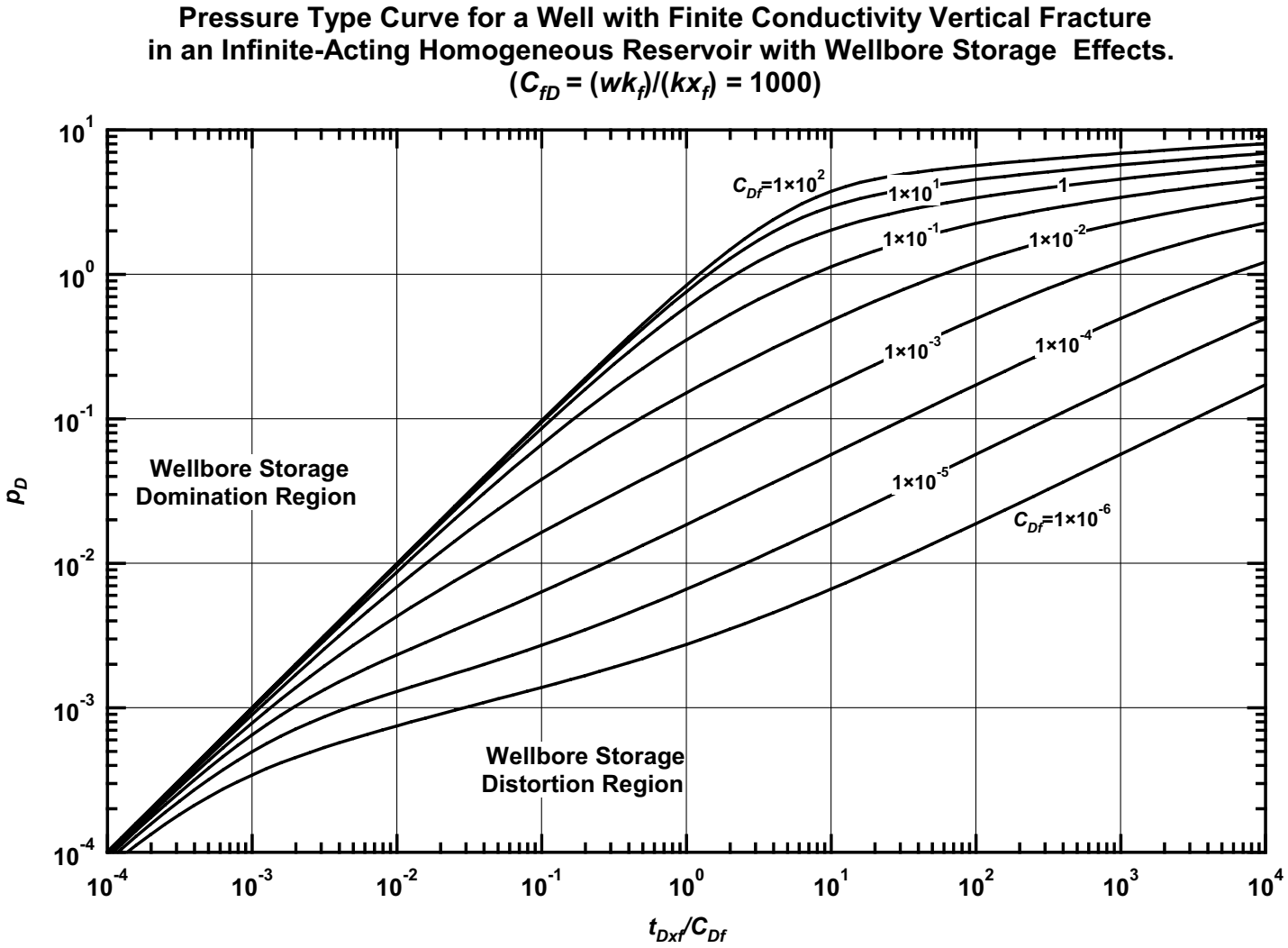

Figure B.34 — p_D vs. t_{Dxf}/C_{Df} — C_{fD} = 1000 (fractured well case — includes wellbore storage effects).

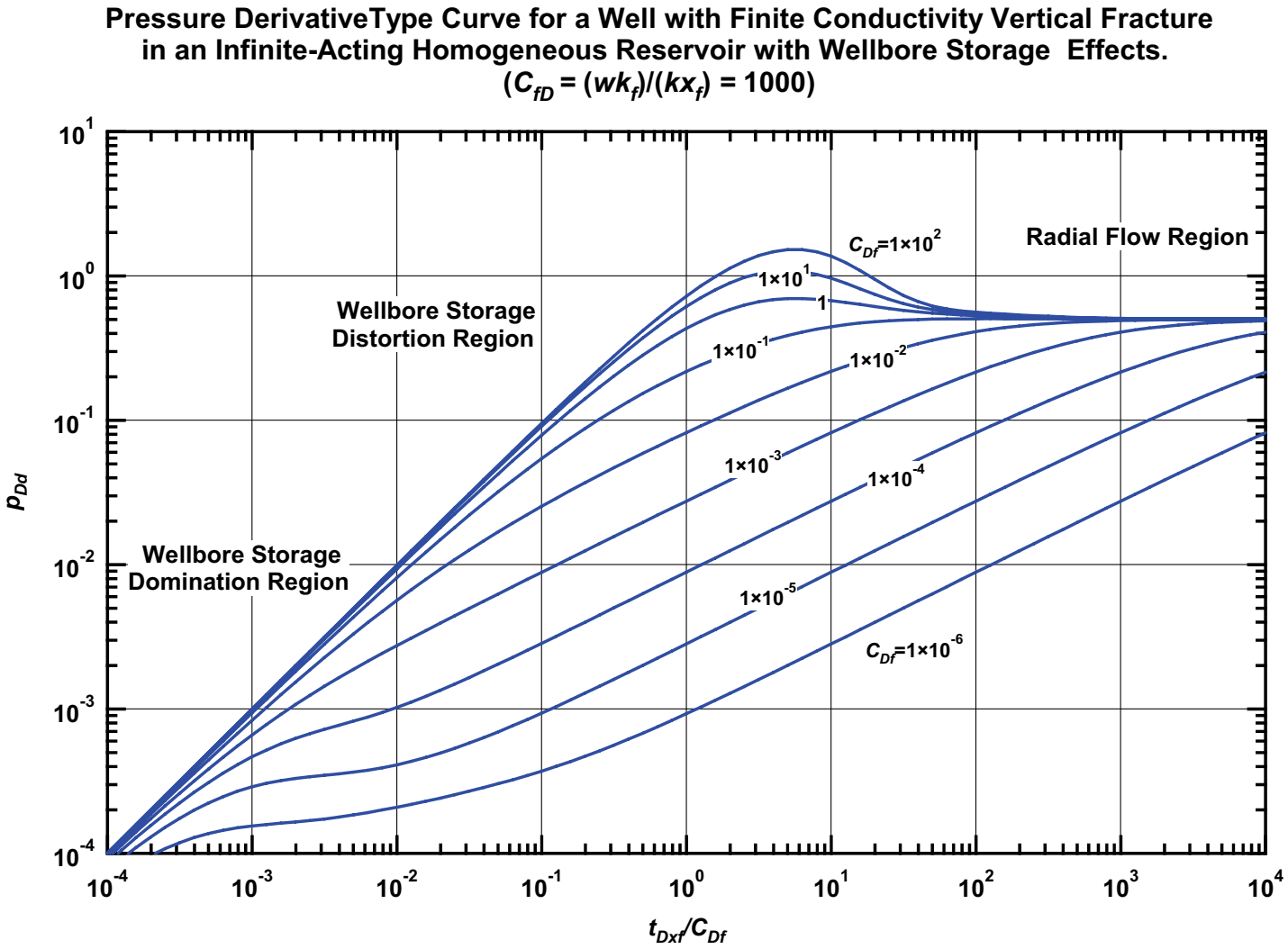

Figure B.35 — p_{Dd} vs. t_{Dxf}/C_{Df} — C_{fD} = 1000 (fractured well case — includes wellbore storage effects).

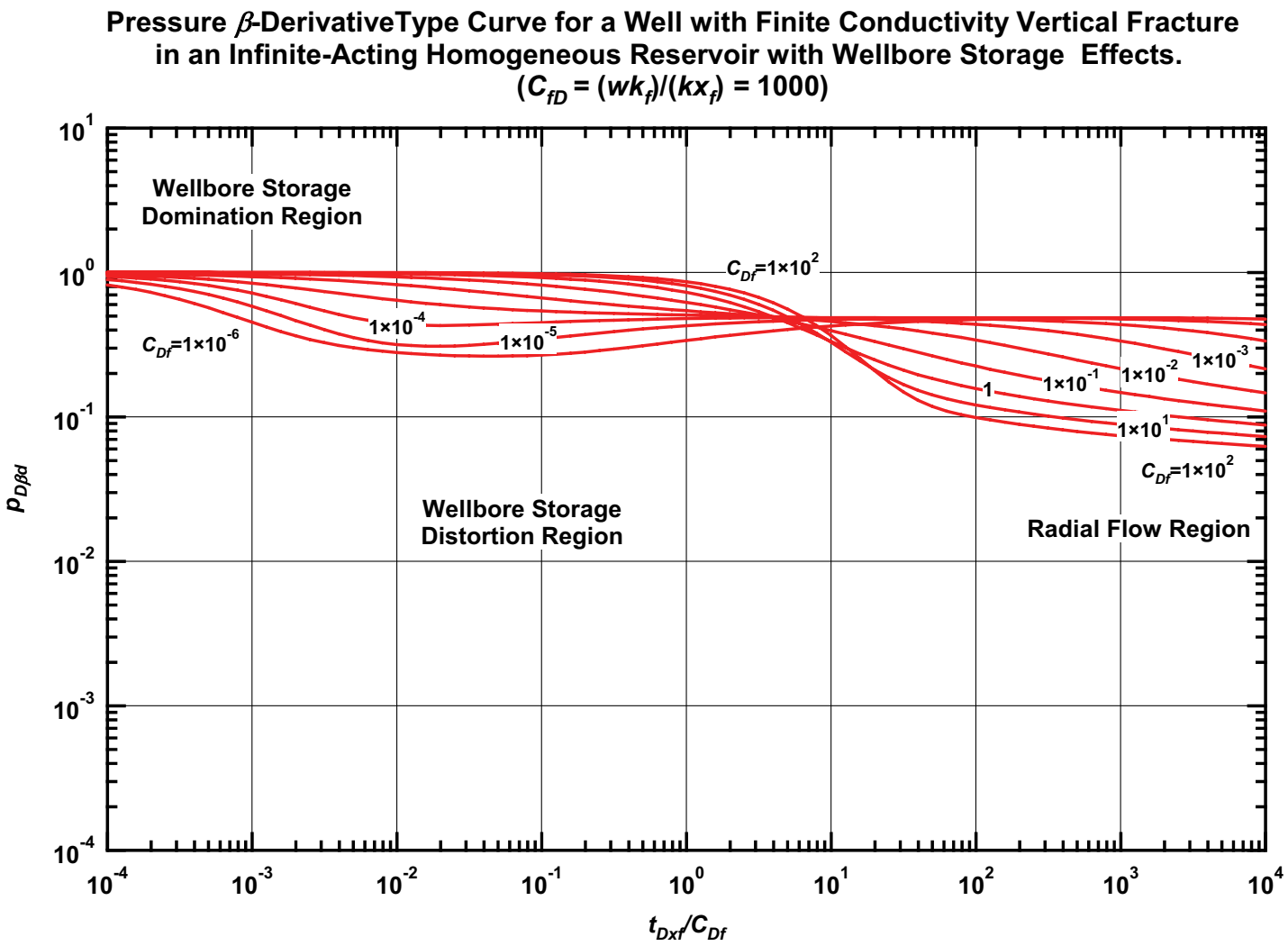

Figure B.36 — $p_{D\beta d}$ vs. t_{Dxf}/C_{Df} — C_{fD} = 1000 (fractured well case — includes wellbore storage effects).

APPENDIX C

CASE OF AN UNFRACTURED WELL IN AN INFINITE-ACTING DUAL POROSITY (NATURALLY FRACTURED) RESERVOIR

In this appendix we provide pressure, pressure derivative, and β-derivative solutions (in dimensionless format) for the case of a well in a naturally fractured reservoir in the form of equations and type curve plots (graphical solutions). To describe the dual porosity reservoir system, we used the pseudosteady-state interporosity flow model, and for graphical presentation of the solutions we generated type curves for ω varying from 10^{-1} to 10^{-4} and λ varying from 10^{-1} to 10^{-8}.

Table C-1 — Solutions for an unfractured well in an infinite-acting, dual porosity (naturally fractured) reservoir system (pseudosteady-state interporosity flow model).

Description	Relation
p_D	$p_D(t_D) = \frac{1}{2}\ln\left[\frac{4}{e^{\gamma}}t_D\right] - \frac{1}{2}\mathrm{E}_1\left[\frac{\lambda}{\omega(1-\omega)}t_D\right] + \frac{1}{2}\mathrm{E}_1\left[\frac{\lambda}{(1-\omega)}t_D\right]$ (logarithmic approximation) (C.1.1)
p_{Dd}	$p_{Dd}(t_D) = \frac{1}{2} + \frac{1}{2}\exp\left[\frac{-\lambda}{\omega(1-\omega)}t_D\right] - \frac{1}{2}\exp\left[\frac{-\lambda}{(1-\omega)}t_D\right]$ (C.1.2) $p_{Dd}(t_D) \approx \frac{1}{2}$ (large-time) (C.1.3)
$p_{D\beta d}$ $(= p_{Dd}/p_D)$	$p_{D\beta d}(t_D) = \left[1 + \exp\left[\frac{-\lambda}{\omega(1-\omega)}t_D\right] - \exp\left[\frac{-\lambda}{(1-\omega)}t_D\right]\right] \Big/ \left[\ln\left[\frac{4}{e^{\gamma}}t_D\right] - \mathrm{E}_1\left[\frac{\lambda}{\omega(1-\omega)}t_D\right] + \mathrm{E}_1\left[\frac{\lambda}{(1-\omega)}t_D\right]\right]$ (C.1.4) $p_{D\beta d}(t_D) \approx \frac{1}{\left[\ln\left[\frac{4}{e^{\gamma}}t_D\right] - \mathrm{E}_1\left[\frac{\lambda}{\omega(1-\omega)}t_D\right] + \mathrm{E}_1\left[\frac{\lambda}{(1-\omega)}t_D\right]\right]}$ (large-time) (C.1.5)

Definitions: (field units)

$$t_D = 2.637\times10^{-4}\frac{kt}{(\phi_{fb}c_{tfb} + \phi_{ma}c_{tma})\mu r_w^2} \quad \text{(C.1.6)}$$

$$p_D = \frac{1}{141.2}\frac{kh}{qB\mu}(p_i - p_{wf}) \quad \text{(C.1.7)}$$

$$\omega = \frac{\phi_{fb}c_{tfb}}{\phi_{fb}c_{tfb} + \phi_{ma}c_{tma}} \quad \text{(C.1.8)}$$

$$\lambda = 12\frac{r_w^2}{h_{ma}^2}\frac{k_{ma}}{k_{fb}} \quad \text{(C.1.9)}$$

$$C_D = \frac{0.8936C_s}{\phi h c_t r_w^2} \quad \text{(C.1.10)}$$

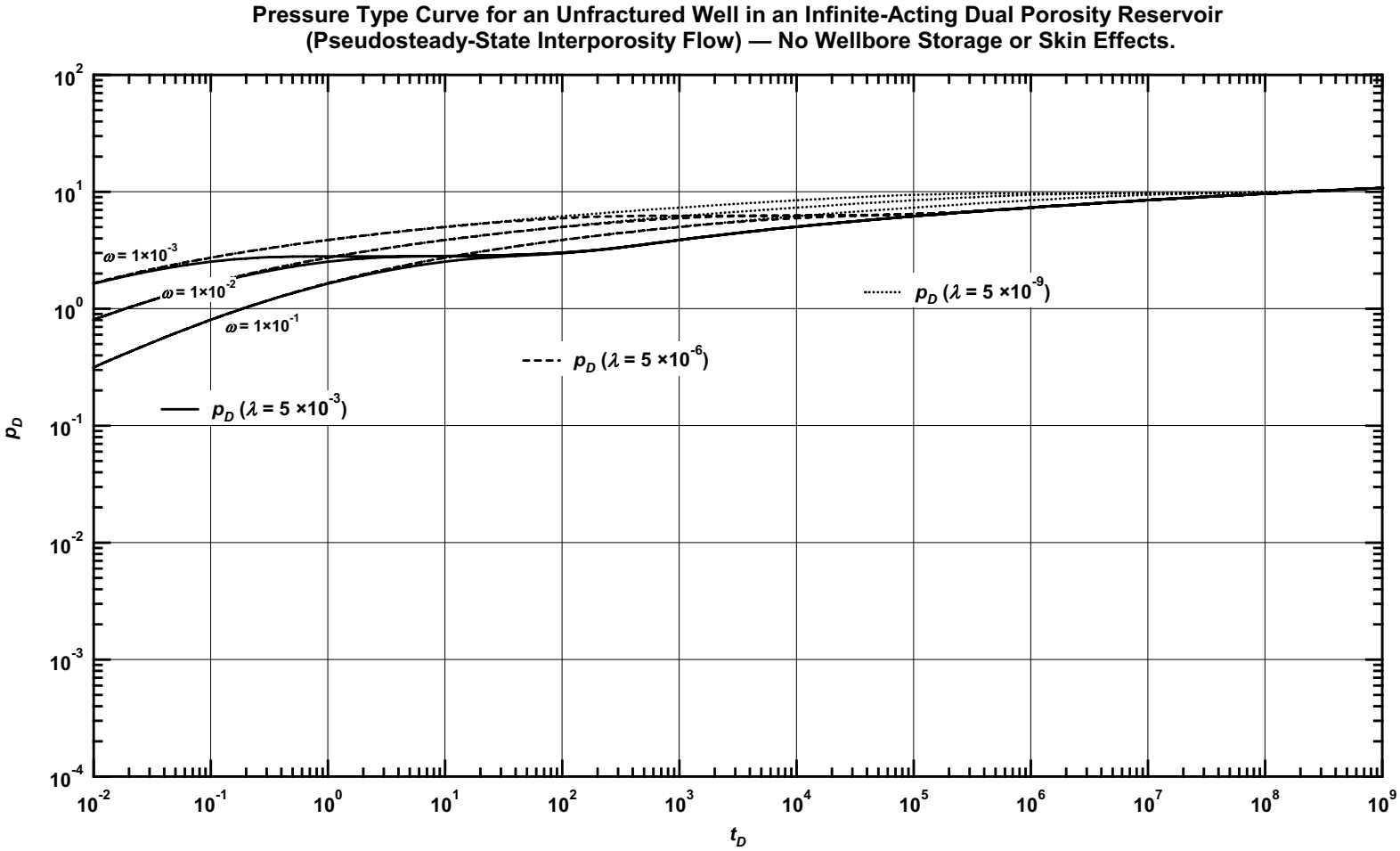

Figure C.1— p_D vs. t_D — solutions for an unfractured well in an infinite-acting dual porosity system — no wellbore storage or skin effects (various λ and ω values).

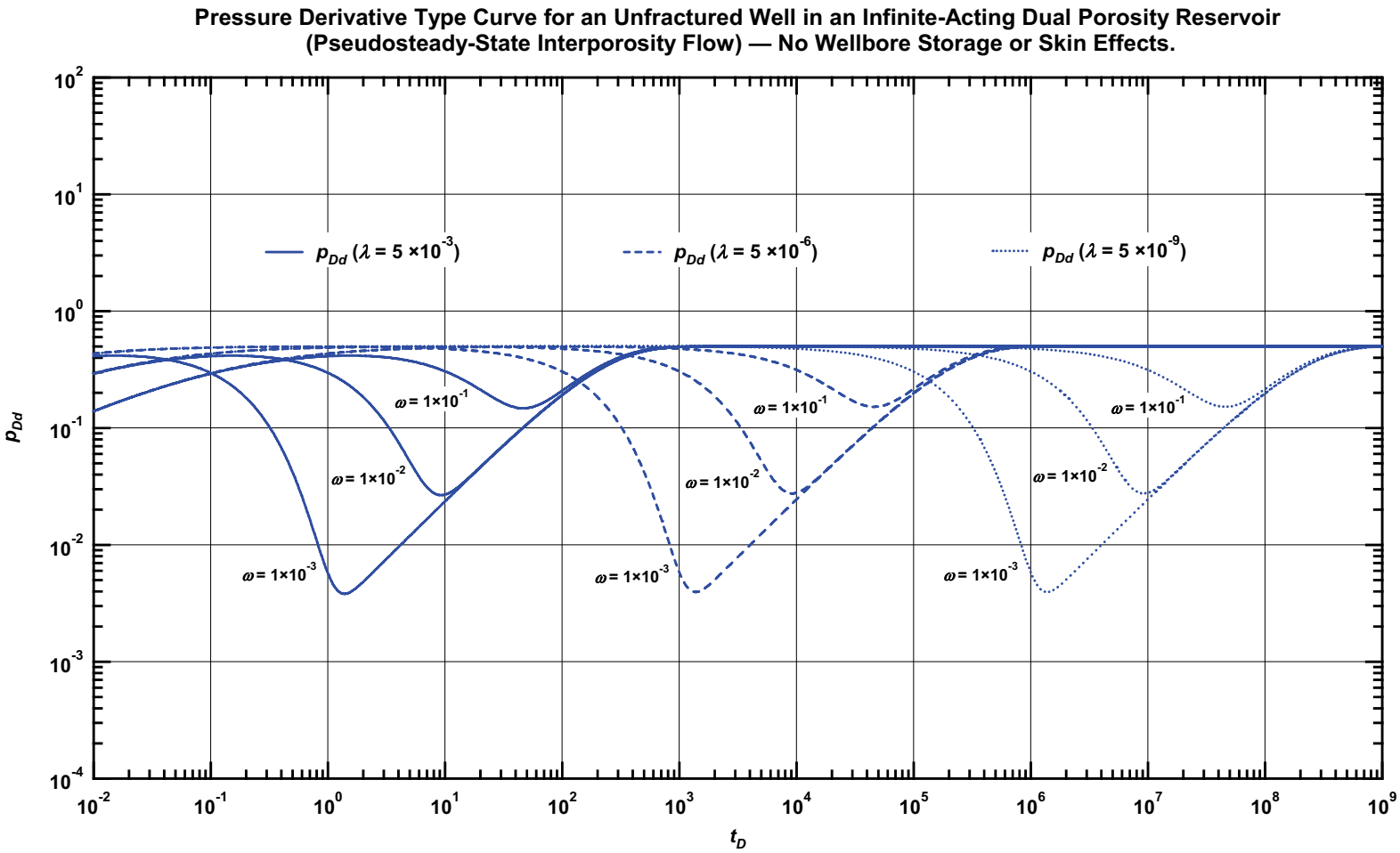

Figure C.2— p_{Dd} vs. t_D — solutions for an unfractured well in an infinite-acting dual porosity system — no wellbore storage or skin effects (various λ and ω values).

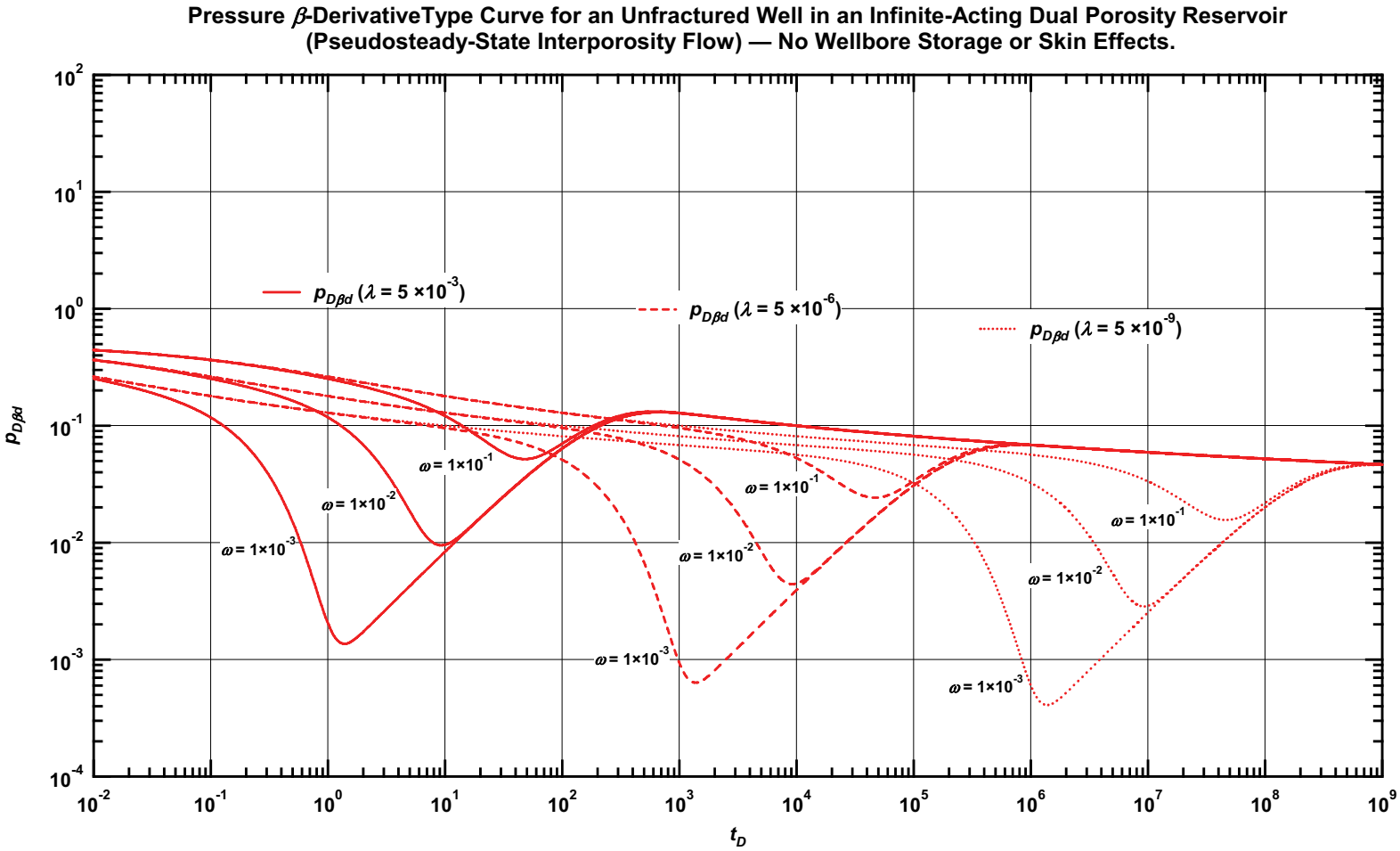

Figure C.3— $p_{D\beta d}$ vs. t_D — solutions for an unfractured well in an infinite-acting dual porosity system — no wellbore storage or skin effects (various λ and ω values).

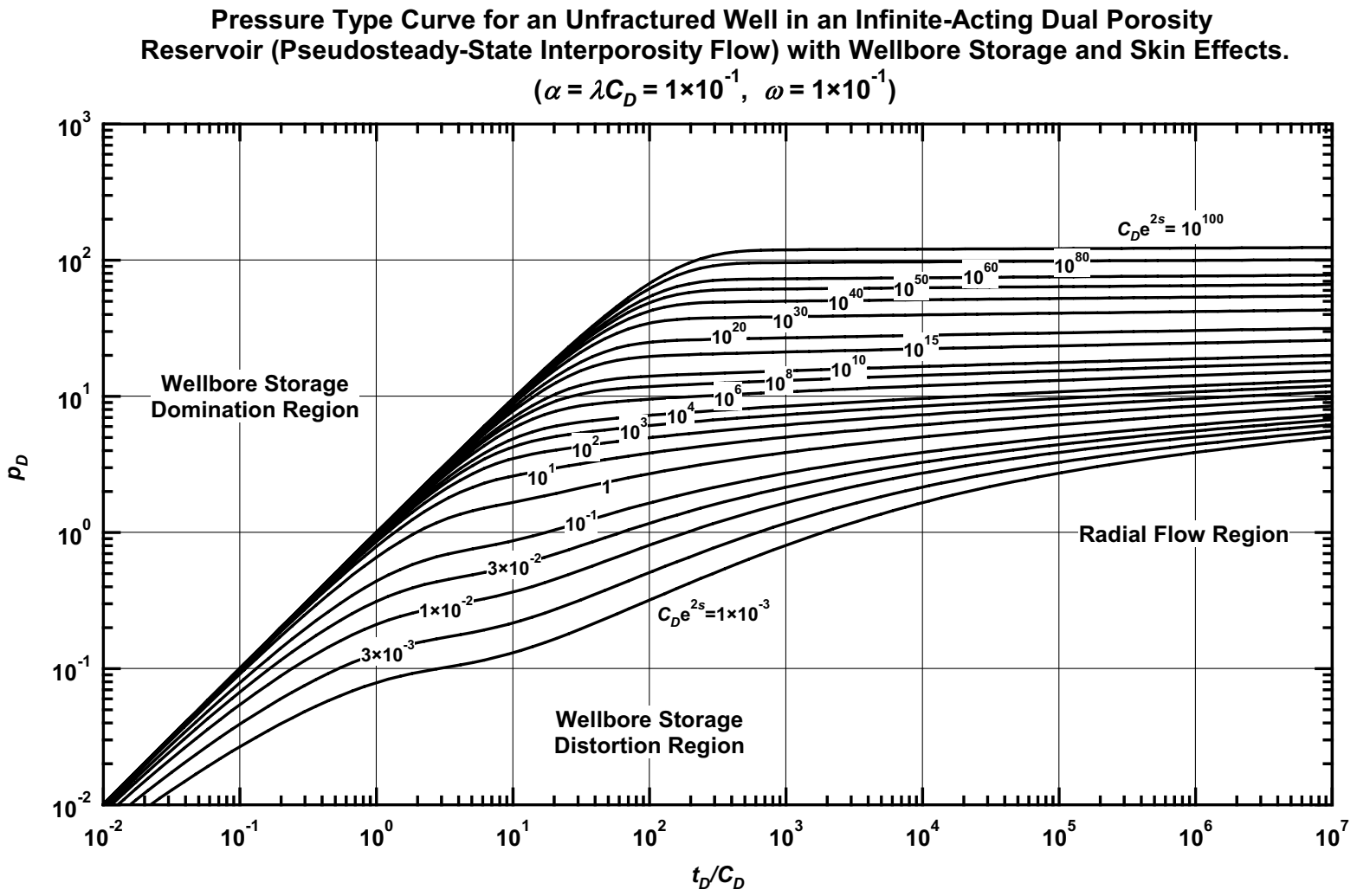

Figure C.4— p_D vs. t_D/C_D — $\omega = 1\times10^{-1}$, $\alpha = \lambda C_D = 1\times10^{-1}$ (dual porosity case — includes wellbore storage and skin effects).

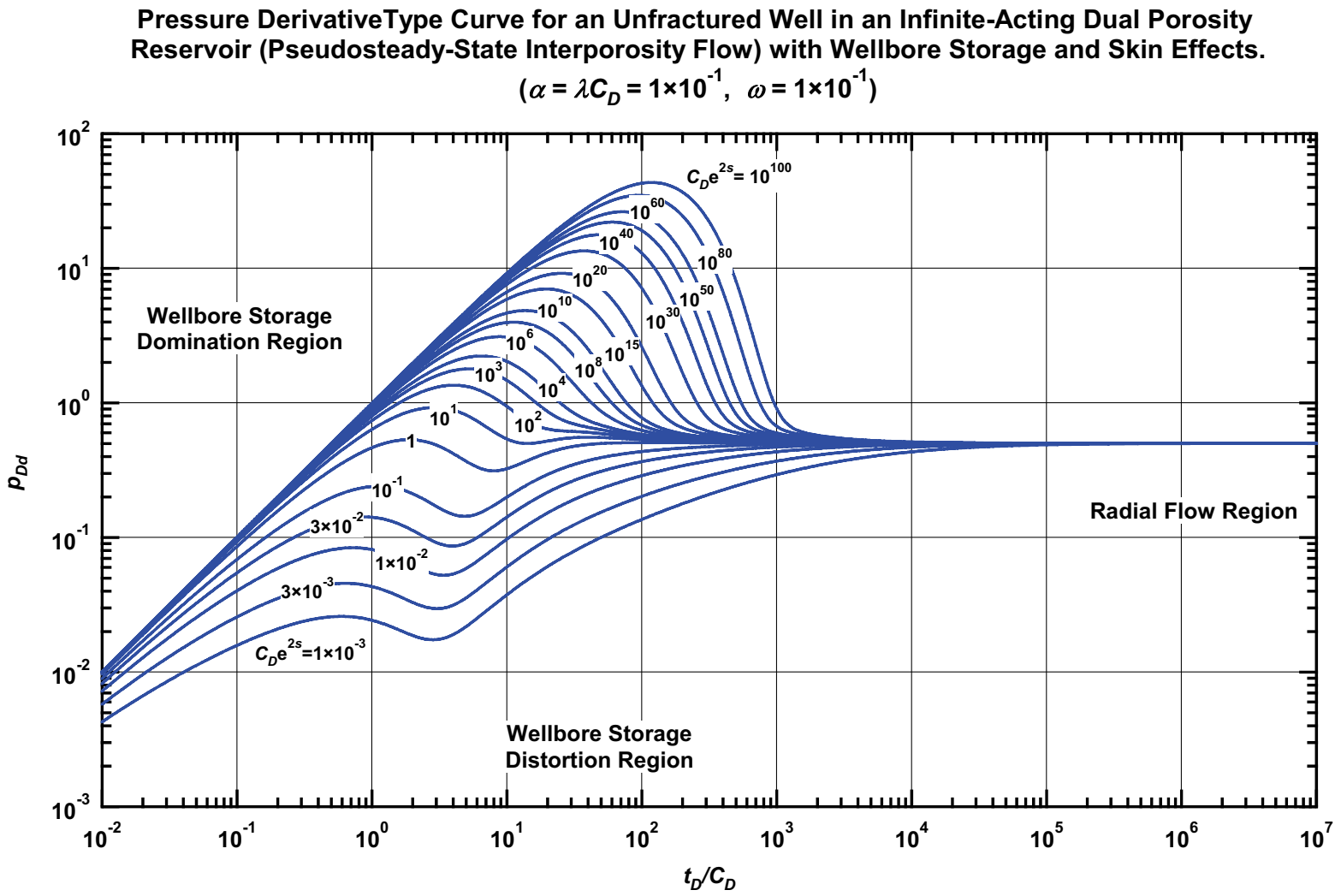

Figure C.5— p_{Dd} vs. t_D/C_D — $\omega = 1\times10^{-1}$, $\alpha = \lambda C_D = 1\times10^{-1}$ (dual porosity case — includes wellbore storage and skin effects).

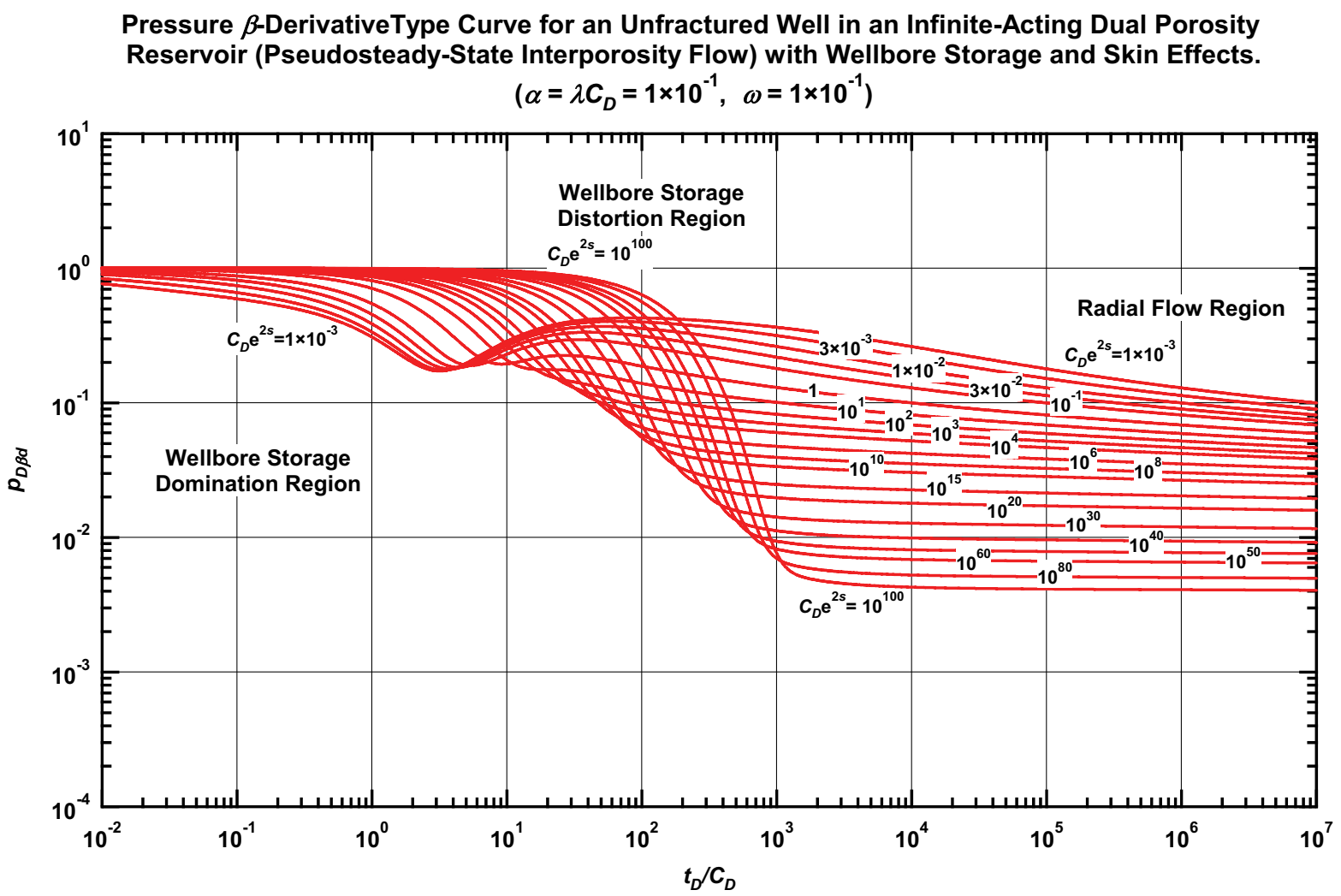

Figure C.6— $p_{D\beta d}$ vs. t_D/C_D — $\omega = 1\times10^{-1}$, $\alpha = \lambda C_D = 1\times10^{-1}$ (dual porosity case — includes wellbore storage and skin effects).

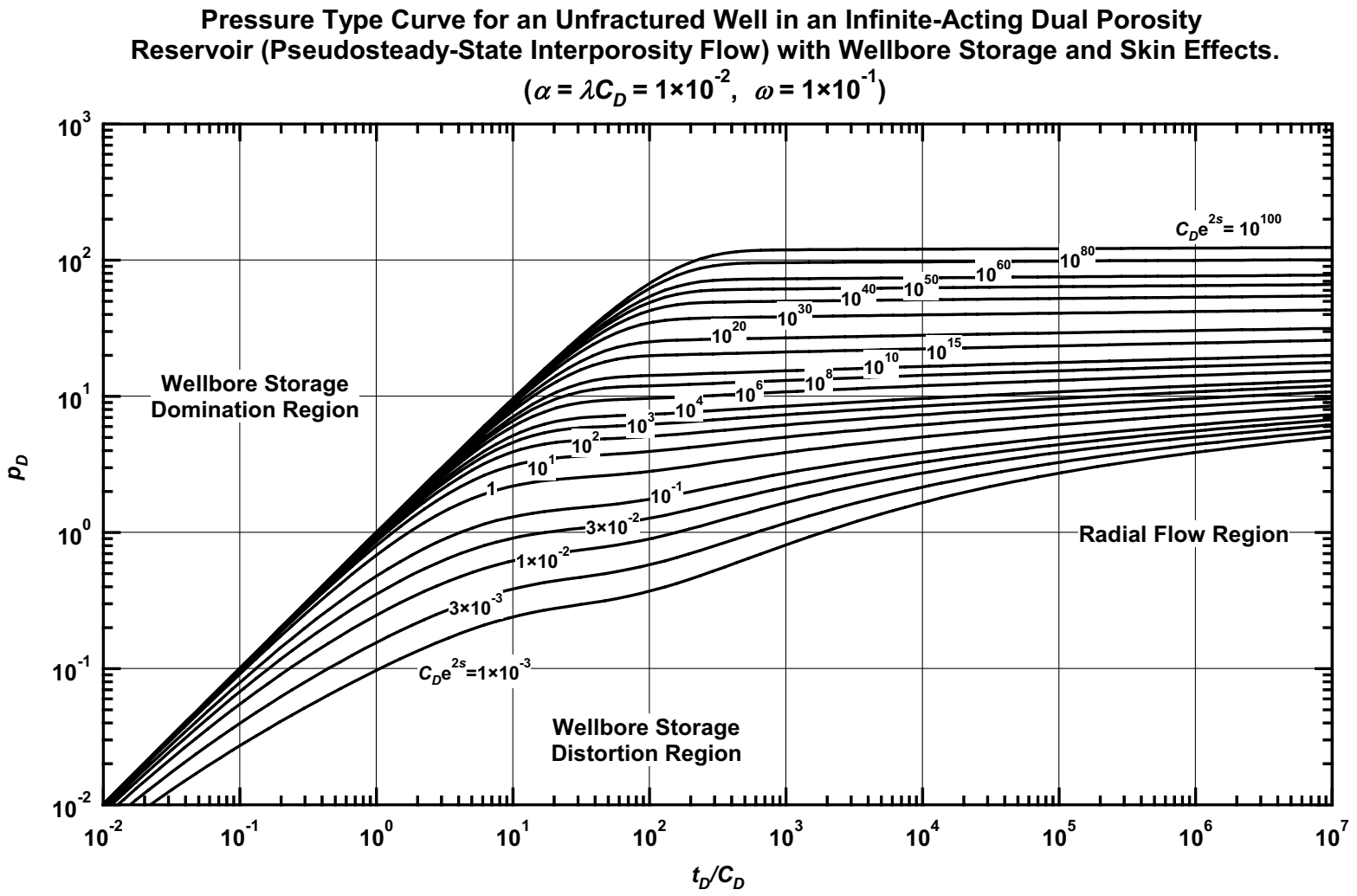

Figure C.7 — p_D vs. t_D/C_D — $\omega = 1\times10^{-1}$, $\alpha = \lambda C_D = 1\times10^{-2}$ (dual porosity case — includes wellbore storage and skin effects).

Pressure DerivativeType Curve for an Unfractured Well in an Infinite-Acting Dual Porosity Reservoir (Pseudosteady-State Interporosity Flow) with Wellbore Storage and Skin Effects.

($\alpha = \lambda C_D = 1\times10^{-2}$, $\omega = 1\times10^{-1}$)

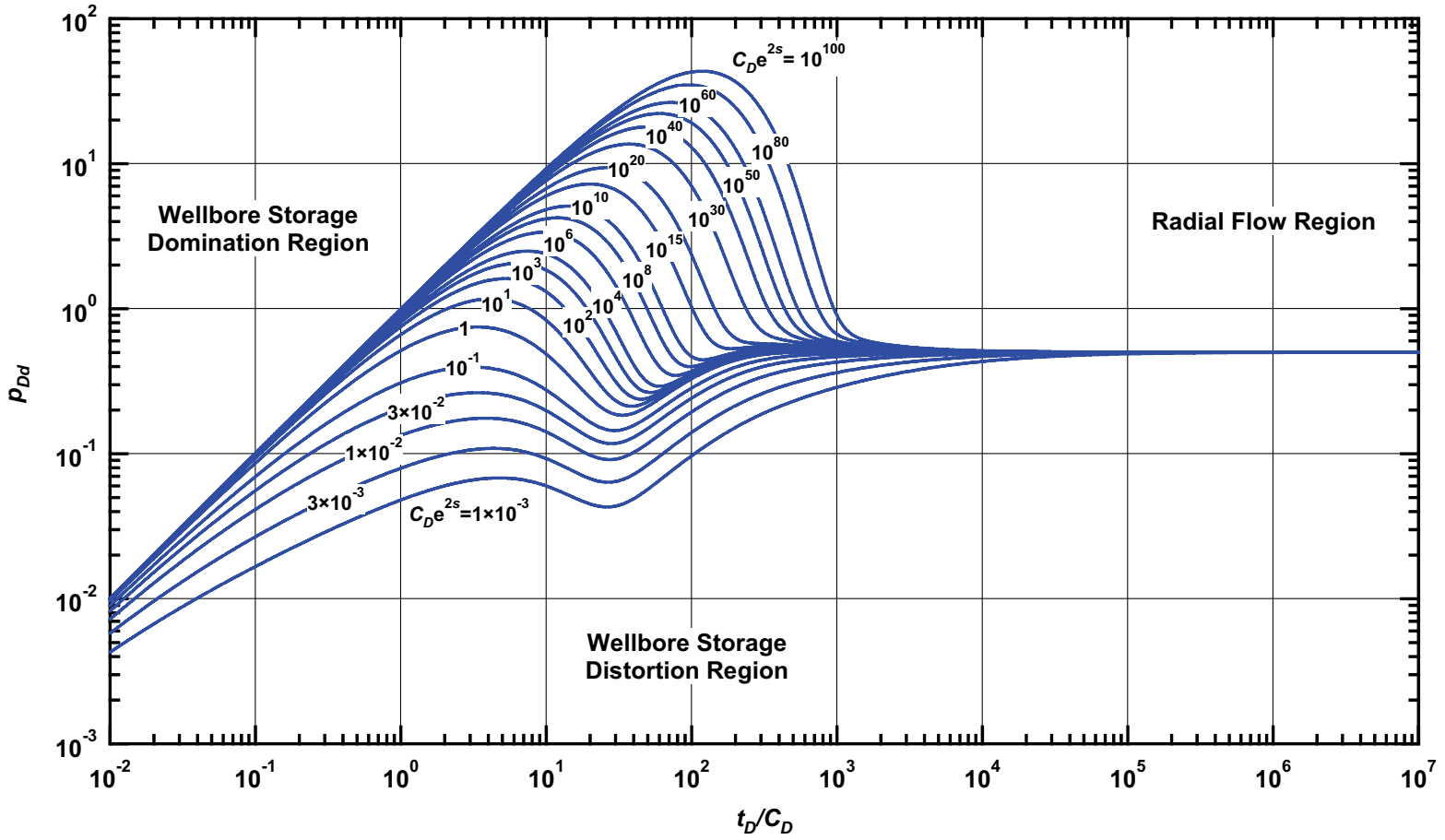

Figure C.8 — p_{Dd} vs. t_D/C_D — $\omega = 1\times10^{-1}$, $\alpha = \lambda C_D = 1\times10^{-2}$ (dual porosity case — includes wellbore storage and skin effects).

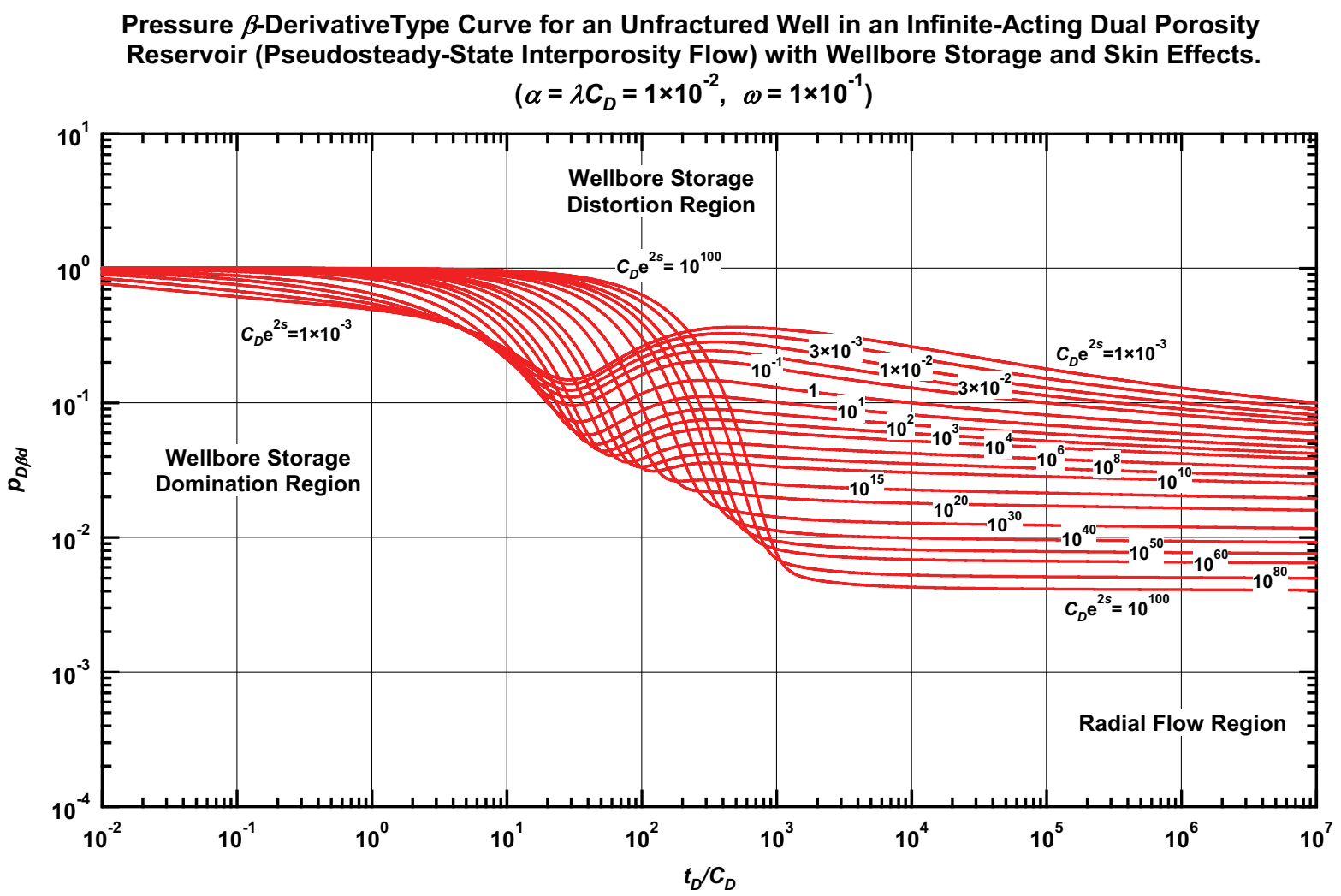

Figure C.9— $p_{D\beta d}$ vs. t_D/C_D — $\omega = 1\times10^{-1}$, $\alpha = \lambda C_D = 1\times10^{-2}$ (dual porosity case — includes wellbore storage and skin effects).

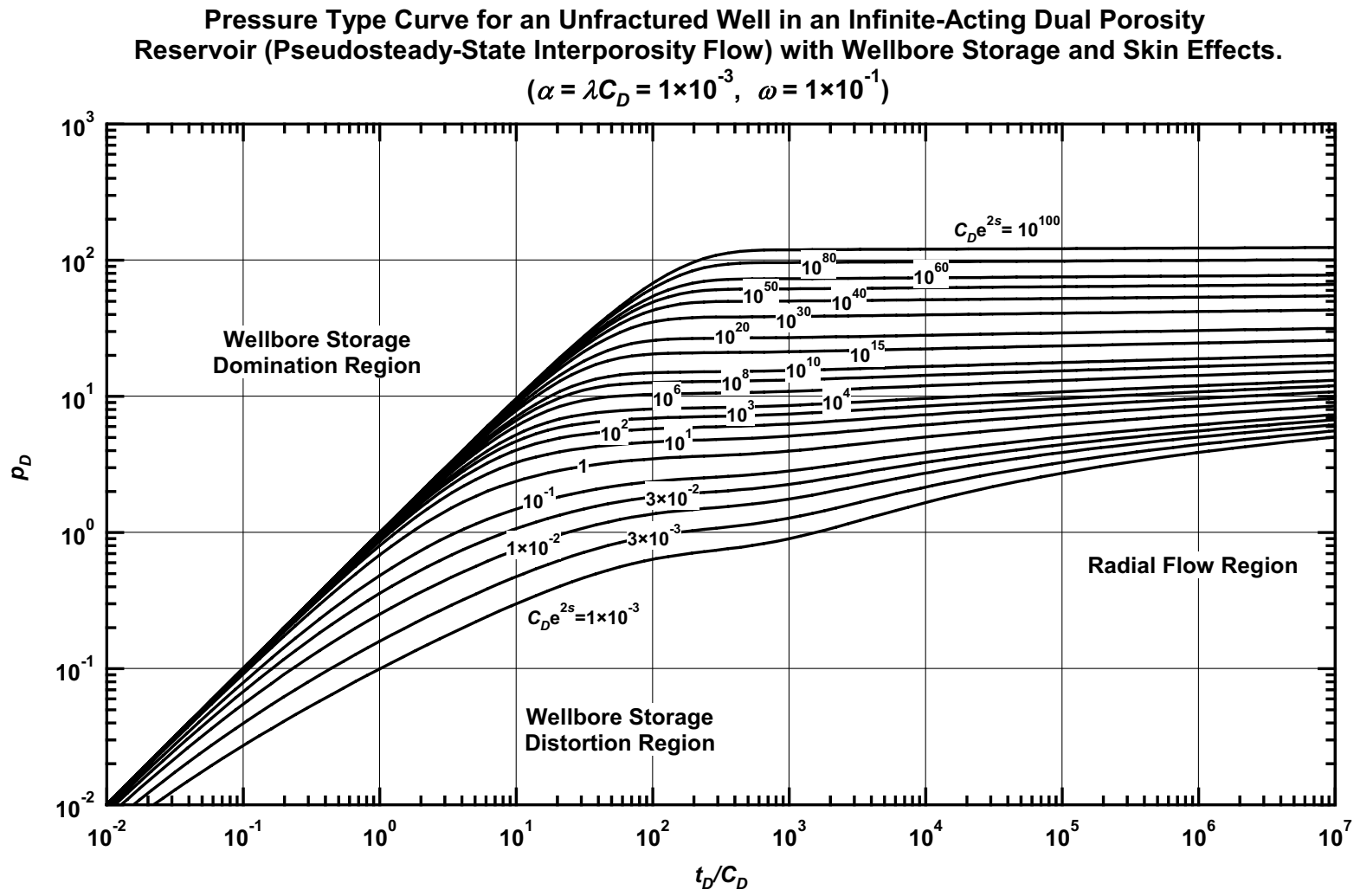

Figure C.10 — p_D vs. t_D/C_D — $\omega = 1\times10^{-1}$, $\alpha = \lambda C_D = 1\times10^{-3}$ (dual porosity case — includes wellbore storage and skin effects).

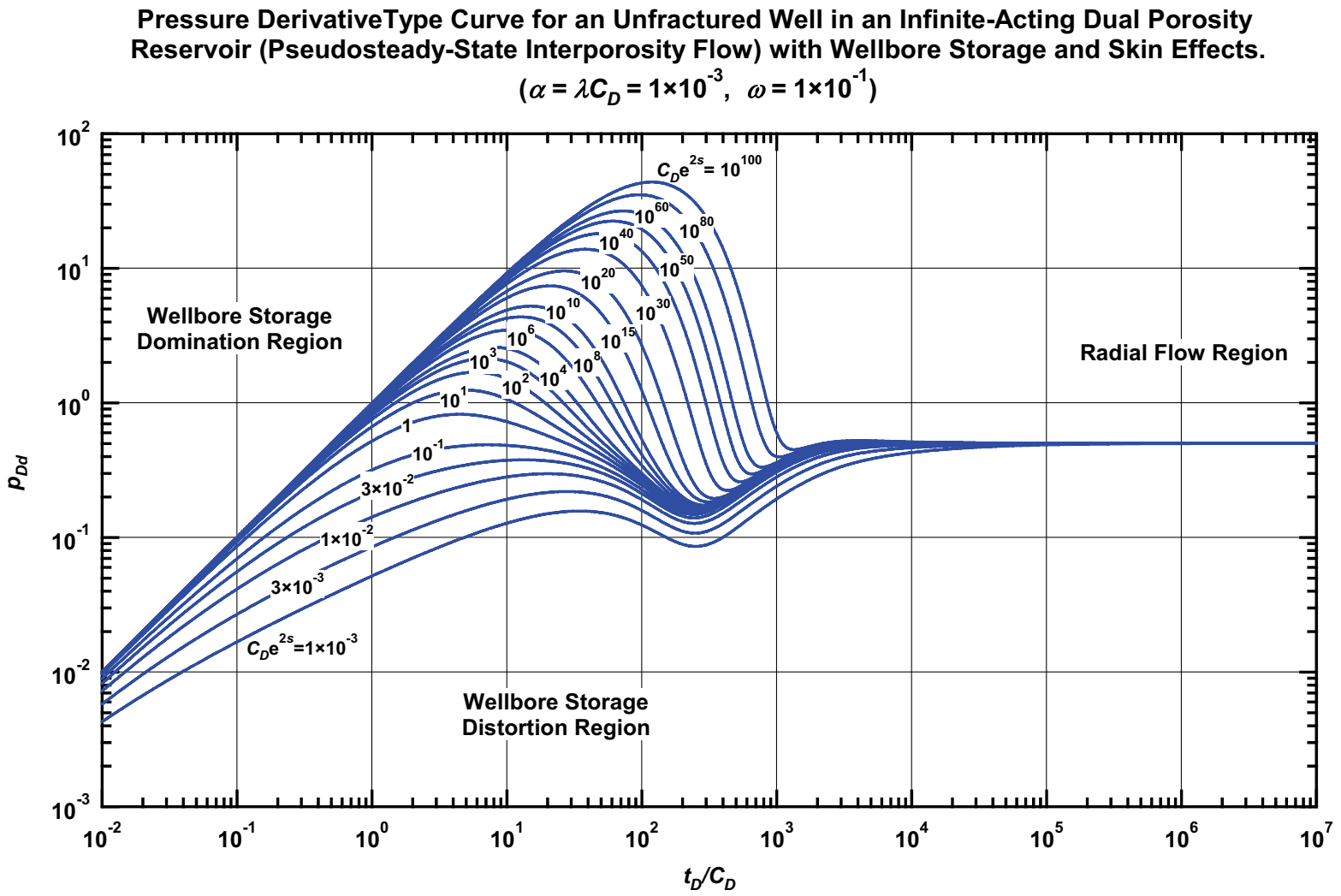

Figure C.11 — p_{Dd} vs. t_D/C_D — $\omega = 1\times10^{-1}$, $\alpha = \lambda C_D = 1\times10^{-3}$ (dual porosity case — includes wellbore storage and skin effects).

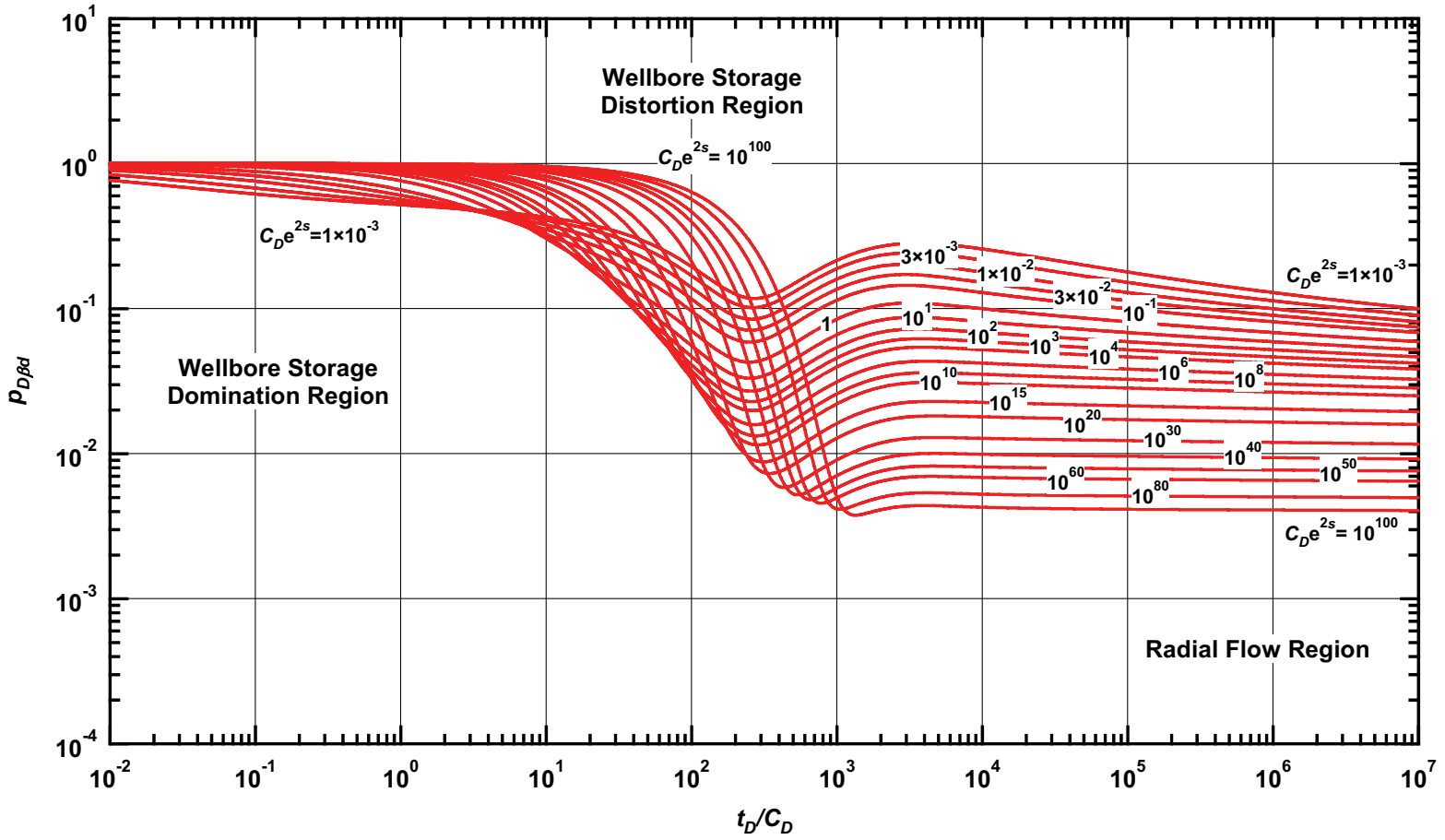

Figure C.12 — $p_{D\beta d}$ vs. t_D/C_D — $\omega = 1\times10^{-1}$, $\alpha = \lambda C_D = 1\times10^{-3}$ (dual porosity case — includes wellbore storage and skin effects).

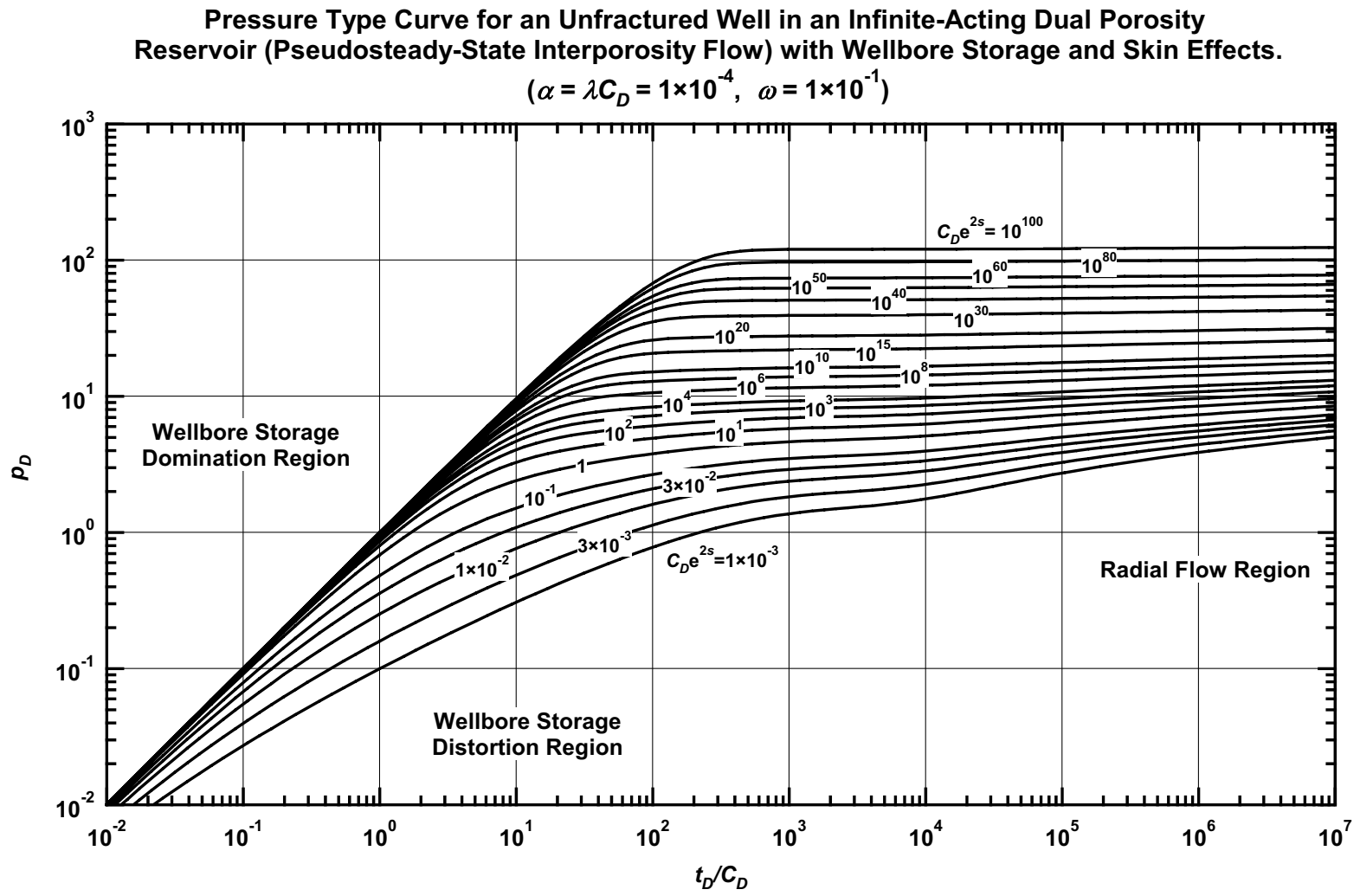

Figure C.13 — p_D vs. t_D/C_D — $\omega = 1\times10^{-1}$, $\alpha = \lambda C_D = 1\times10^{-4}$ (dual porosity case — includes wellbore storage and skin effects).

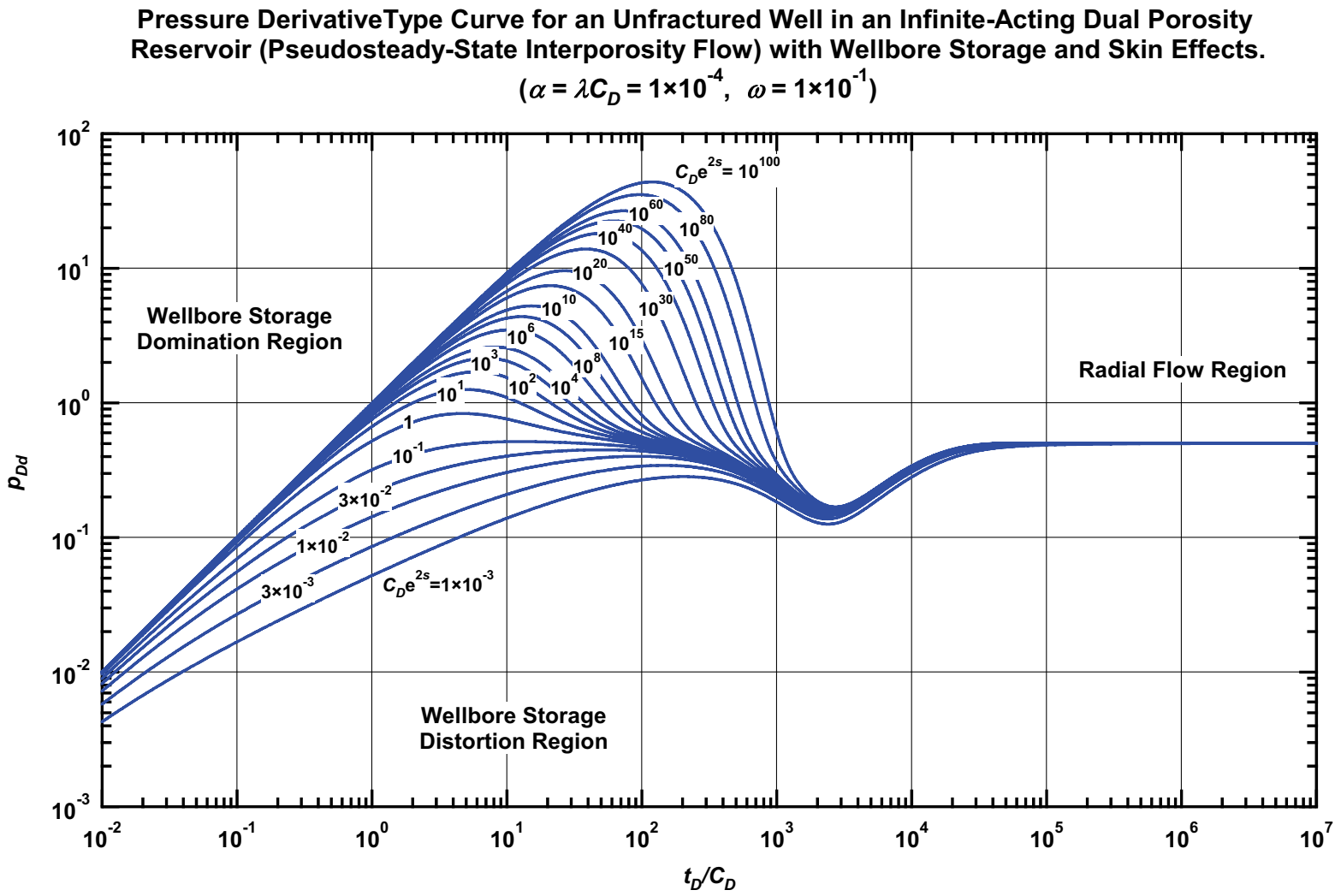

Figure C.14 — p_{Dd} **vs.** t_D/C_D **—** $\omega = 1\times10^{-1}$, $\alpha = \lambda C_D = 1\times10^{-4}$ **(dual porosity case — includes wellbore storage and skin effects).**

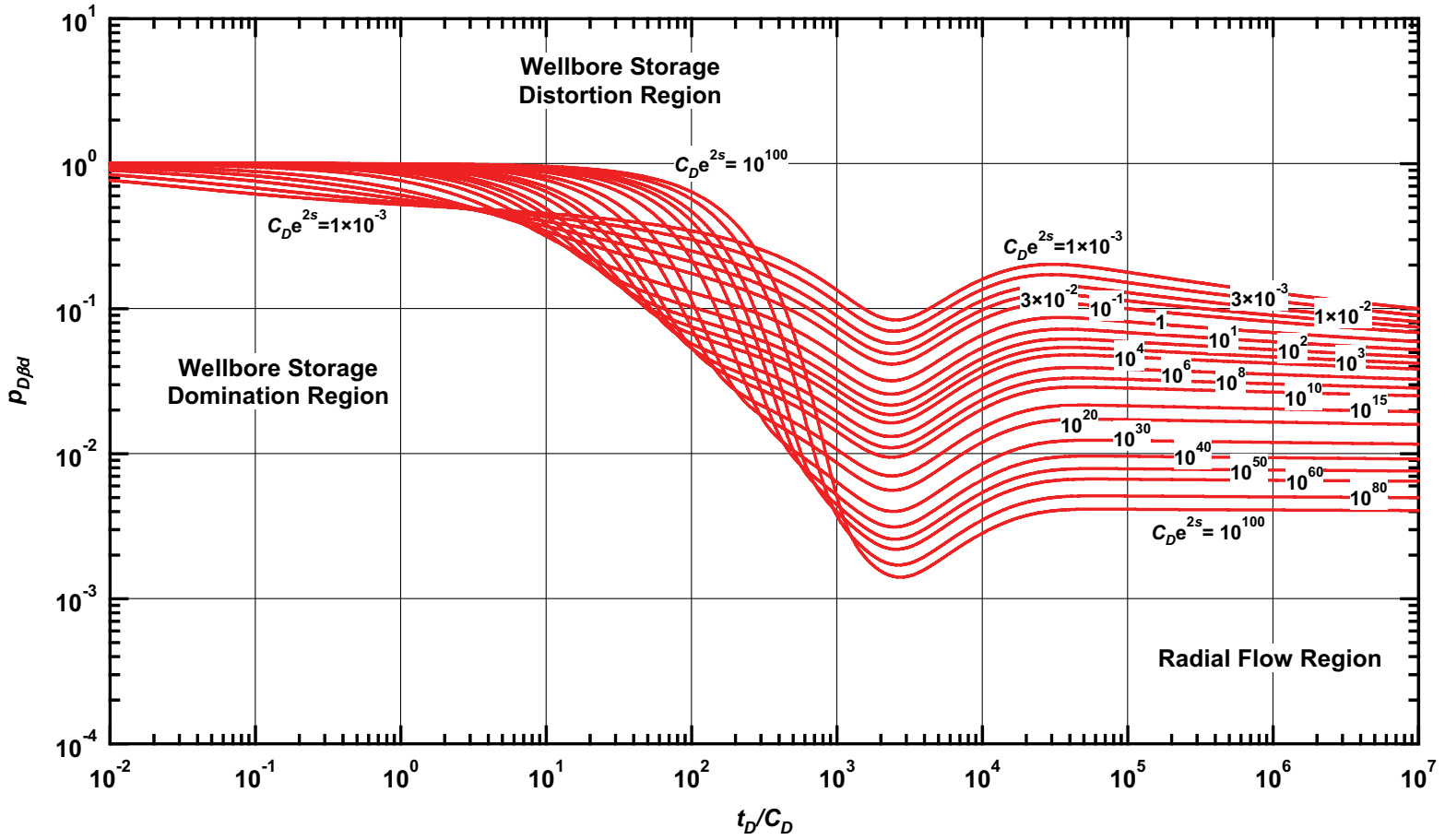

Figure C.15 — $p_{D\beta d}$ vs. t_D/C_D — $\omega = 1\times10^{-1}$, $\alpha = \lambda C_D = 1\times10^{-4}$ (dual porosity case — includes wellbore storage and skin effects).

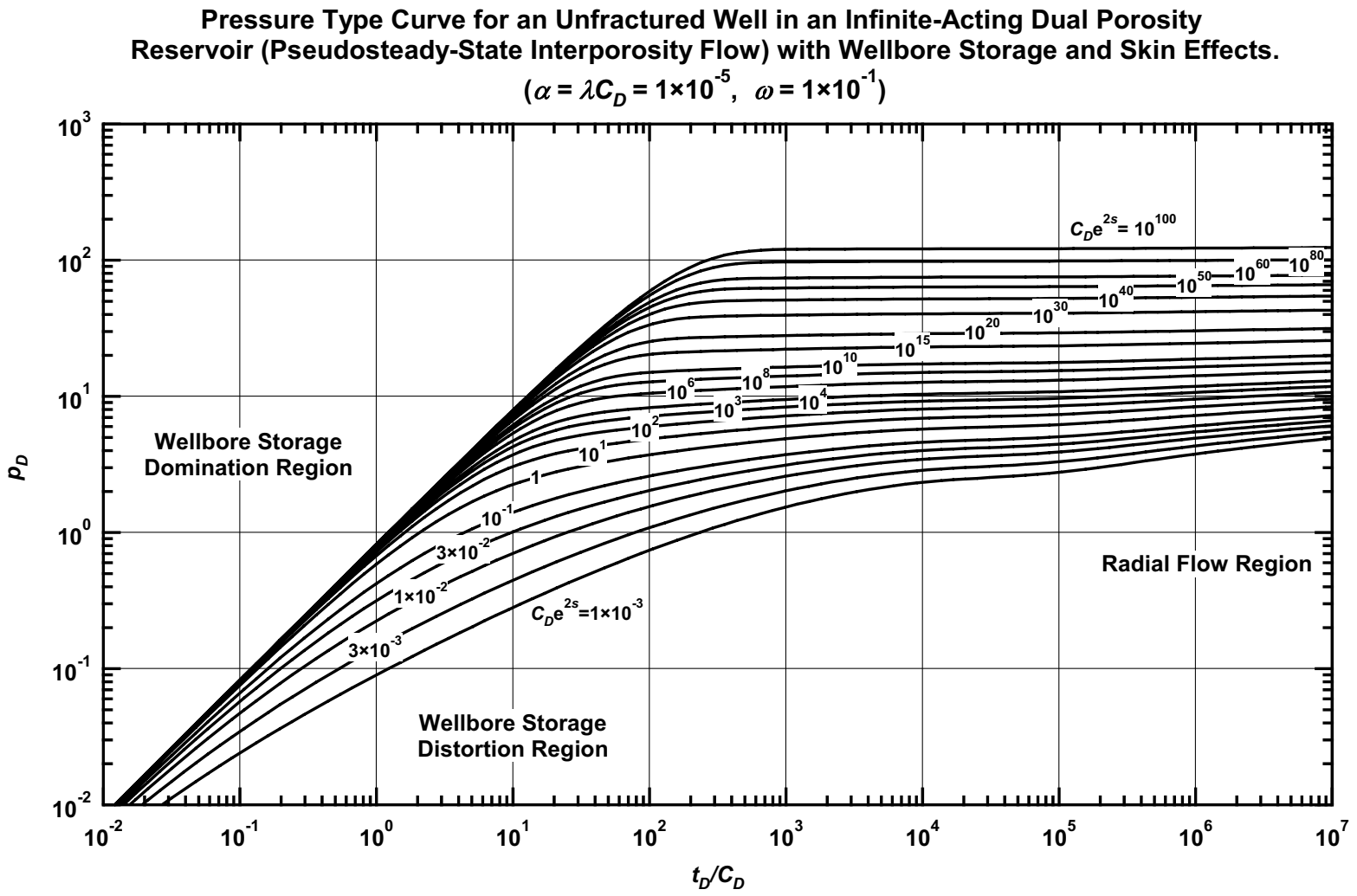

Figure C.16 — p_D vs. t_D/C_D — $\omega = 1\times10^{-1}$, $\alpha = \lambda C_D = 1\times10^{-5}$ (dual porosity case — includes wellbore storage and skin effects).

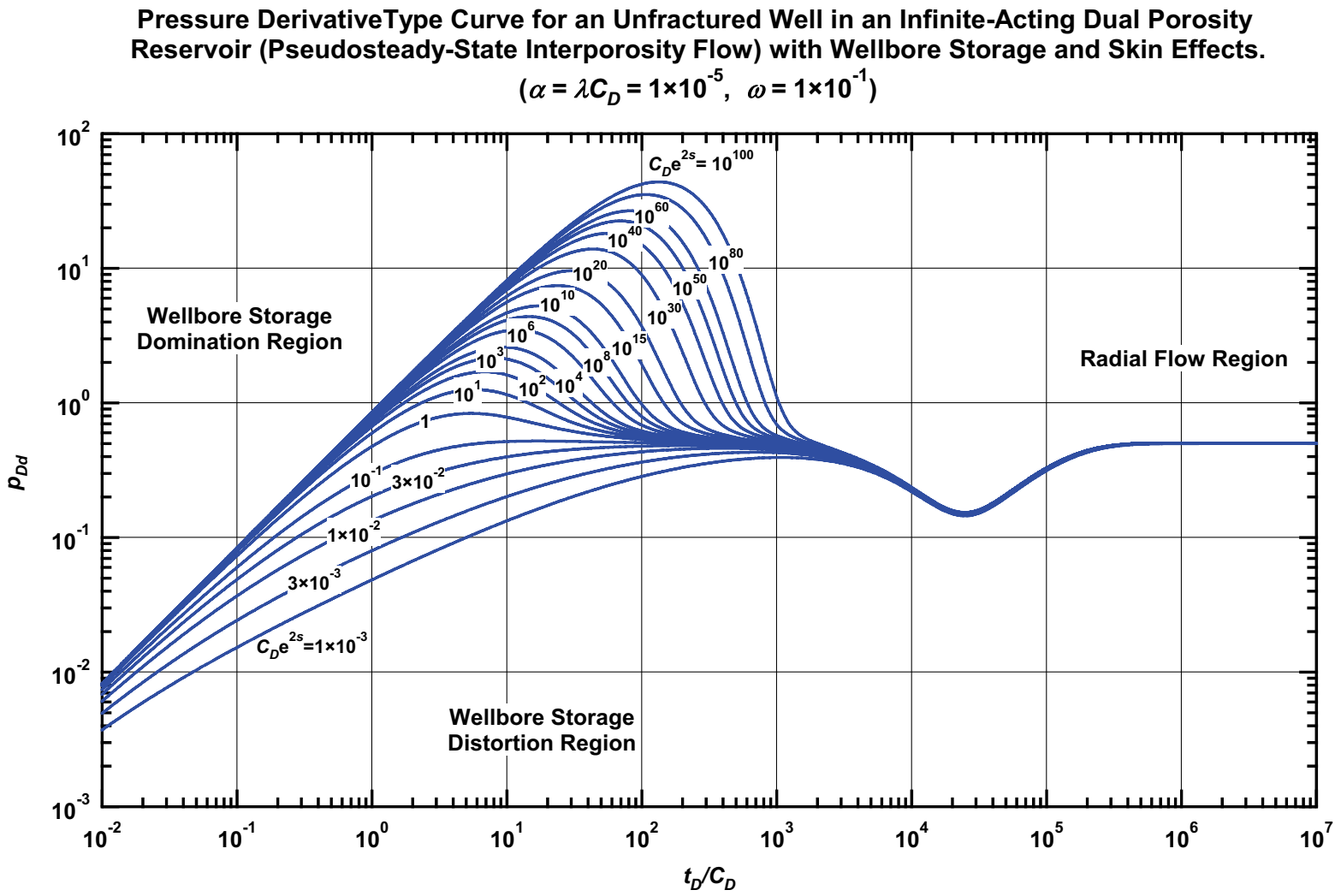

Figure C.17 — p_{Dd} vs. t_D/C_D — $\omega = 1\times10^{-1}$, $\alpha = \lambda C_D = 1\times10^{-5}$ (dual porosity case — includes wellbore storage and skin effects).

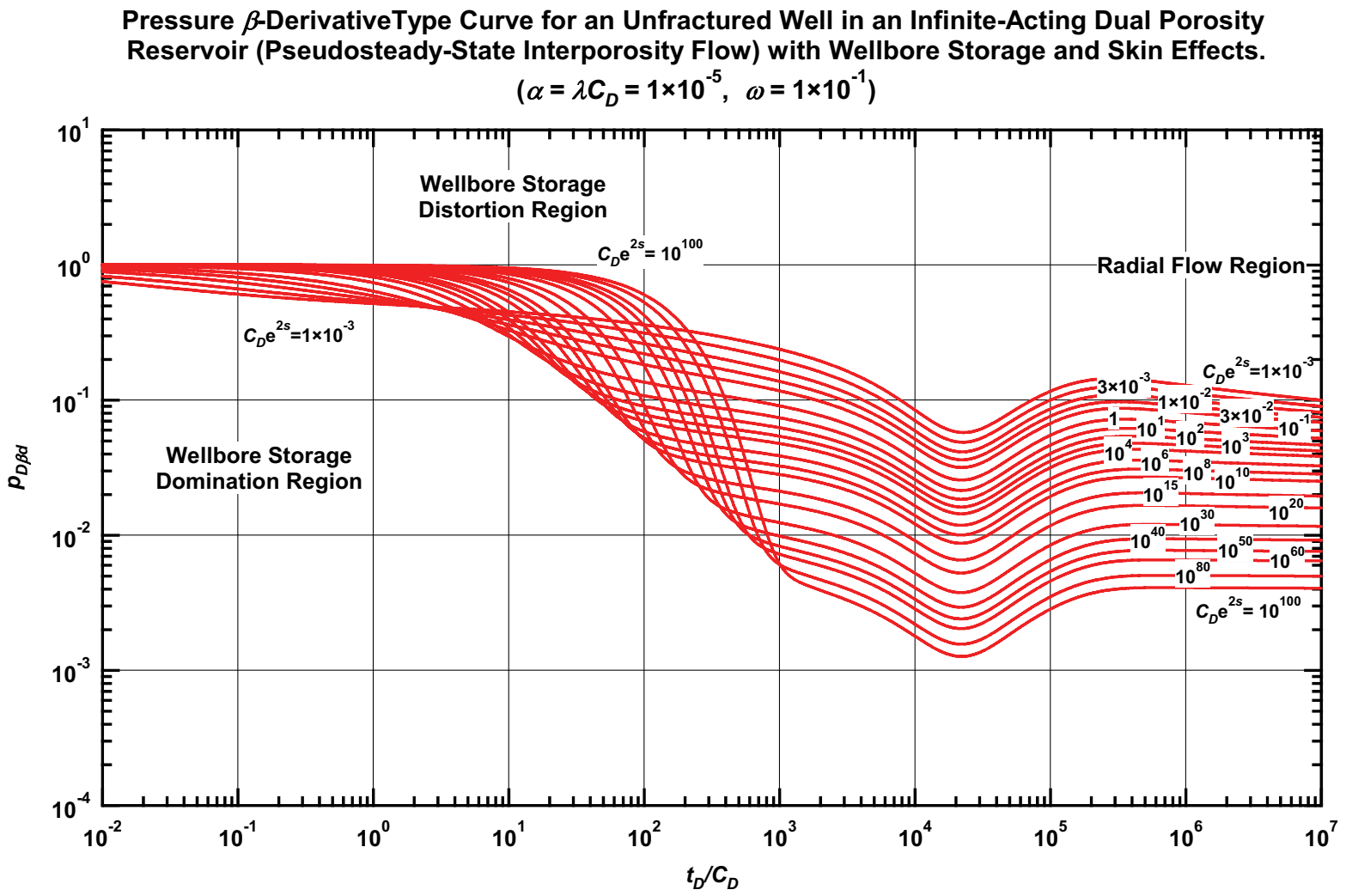

Figure C.18 — $p_{D\beta d}$ vs. t_D/C_D — $\omega = 1\times10^{-1}$, $\alpha = \lambda C_D = 1\times10^{-5}$ (dual porosity case — includes wellbore storage and skin effects).

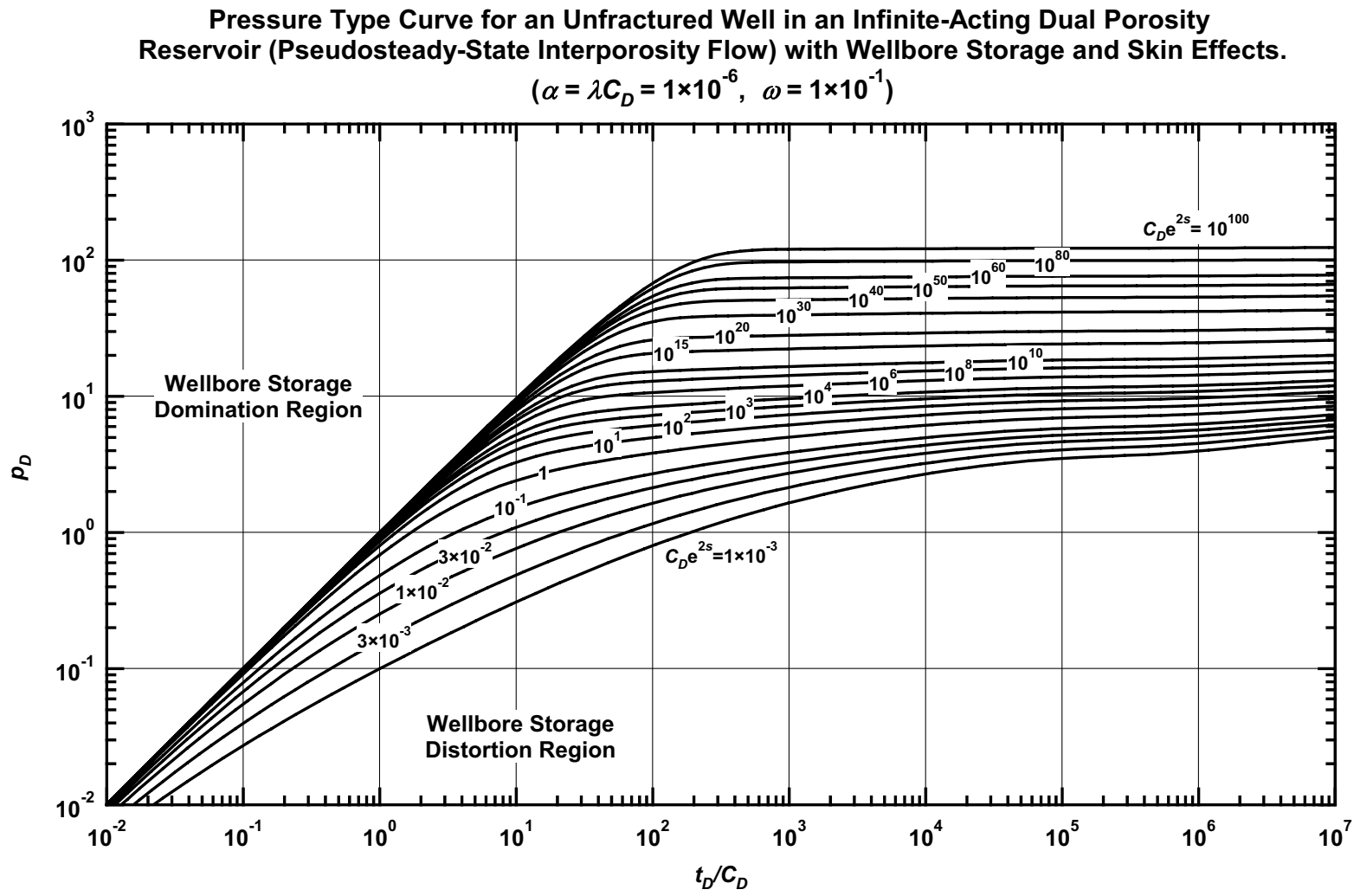

Figure C.19 — p_D vs. t_D/C_D — $\omega = 1\times10^{-1}$, $\alpha = \lambda C_D = 1\times10^{-6}$ (dual porosity case — includes wellbore storage and skin effects).

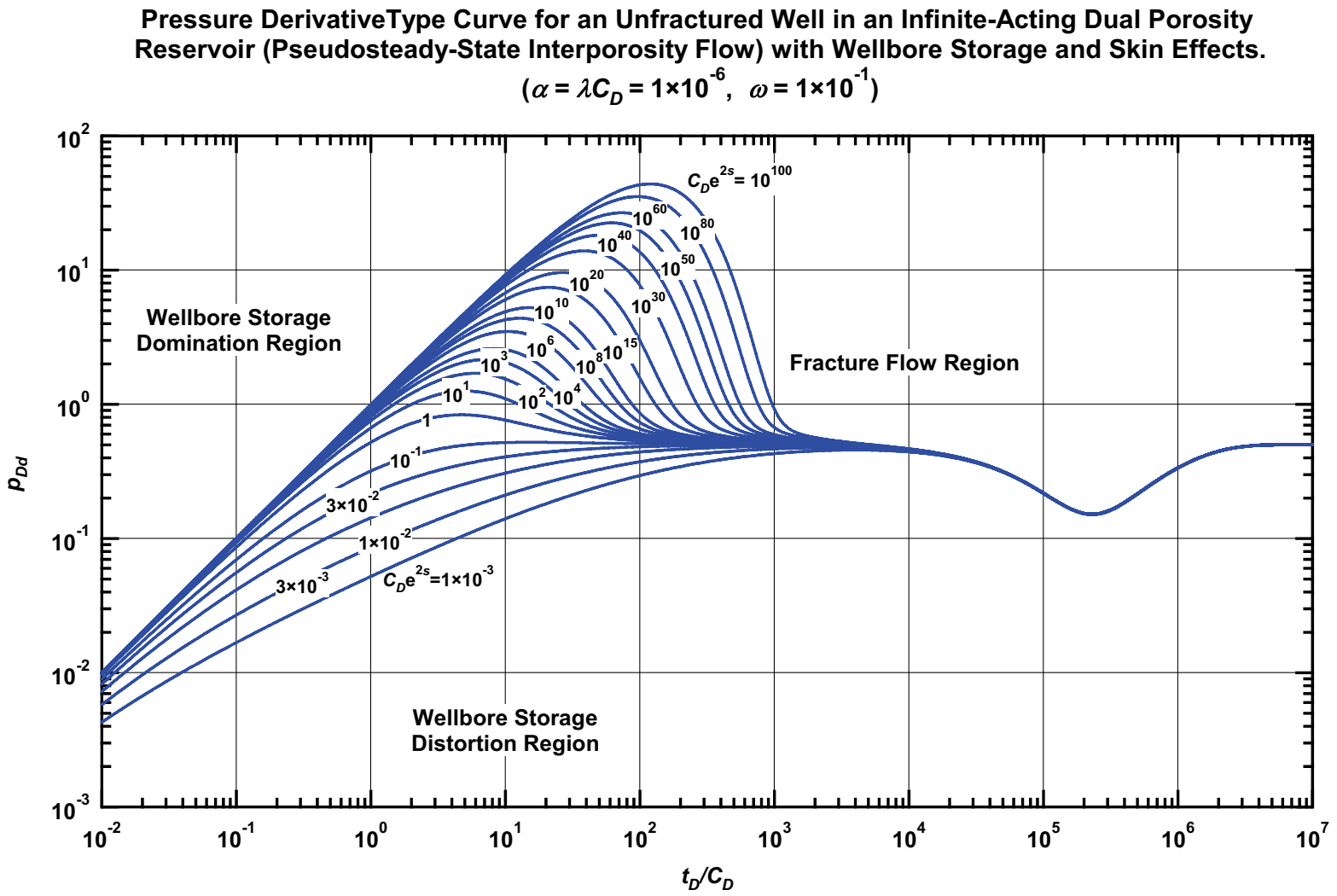

Figure C.20 — p_{Dd} vs. t_D/C_D — $\omega = 1\times10^{-1}$, $\alpha = \lambda C_D = 1\times10^{-6}$ (dual porosity case — includes wellbore storage and skin effects).

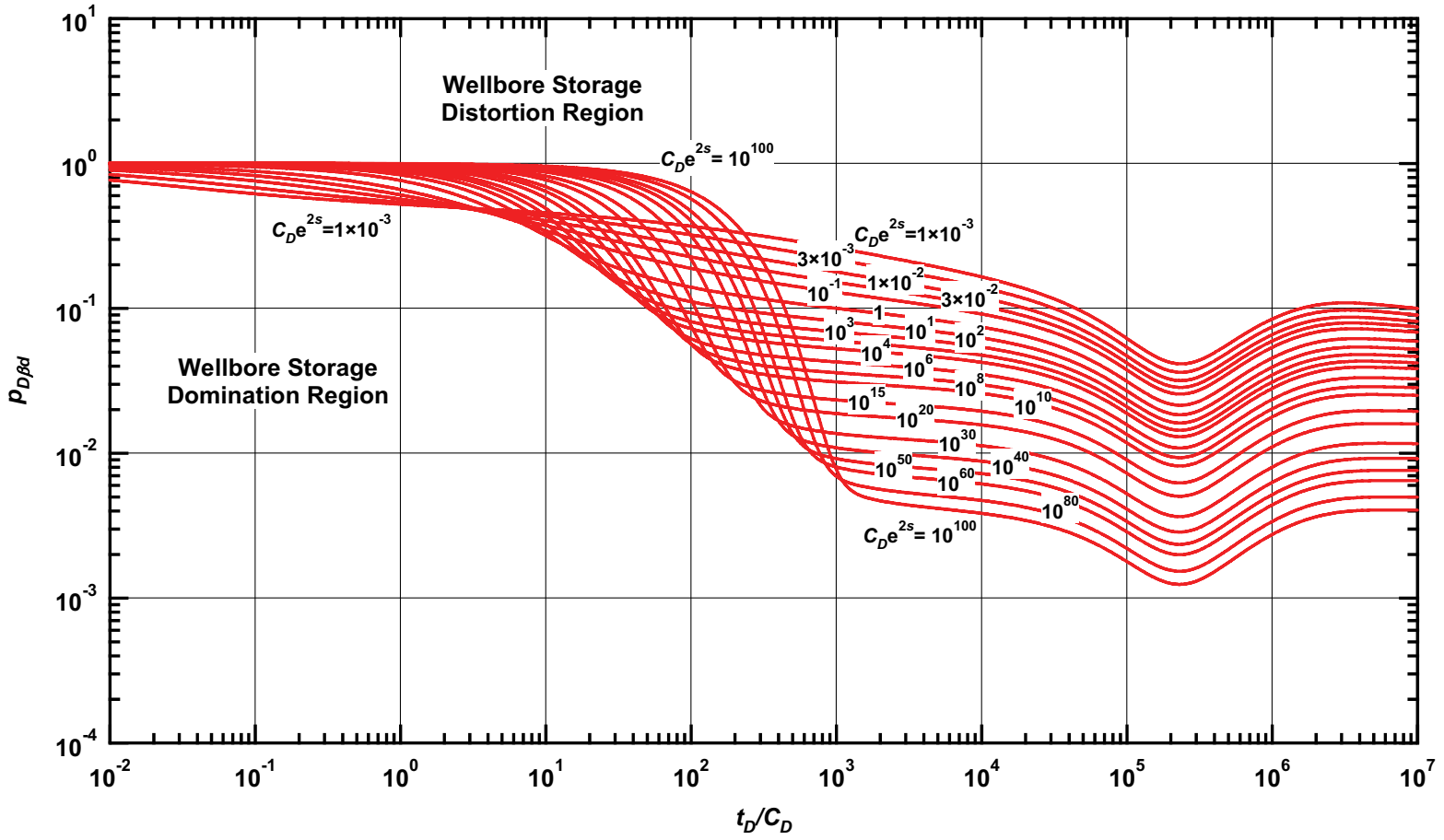

Figure C.21 — $p_{D\beta d}$ vs. t_D/C_D — $\omega = 1\times10^{-1}$, $\alpha = \lambda C_D = 1\times10^{-6}$ (dual porosity case — includes wellbore storage and skin effects).

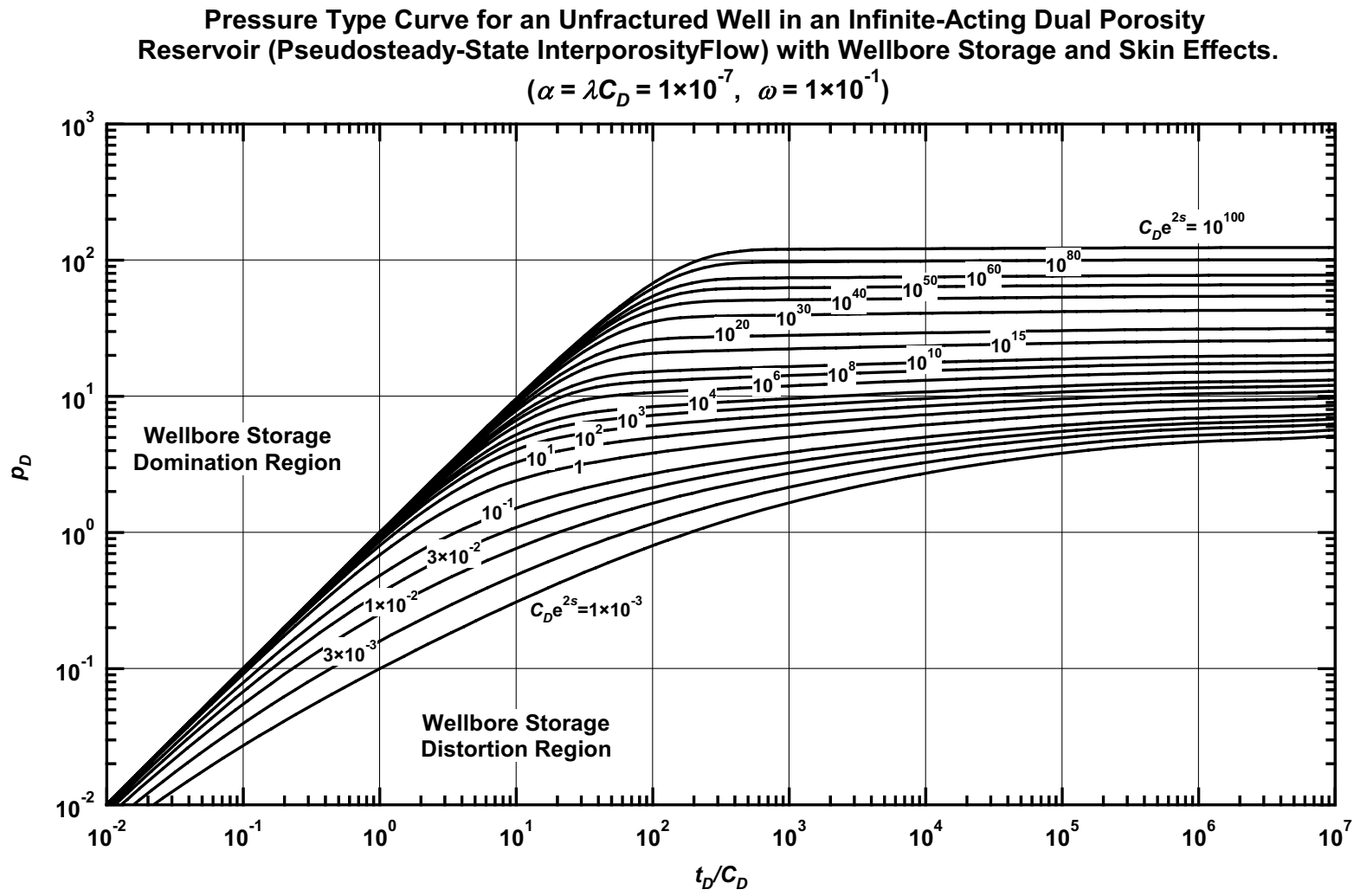

Figure C.22 — p_D vs. t_D/C_D — $\omega = 1\times10^{-1}$, $\alpha = \lambda C_D = 1\times10^{-7}$ (dual porosity case — includes wellbore storage and skin effects).

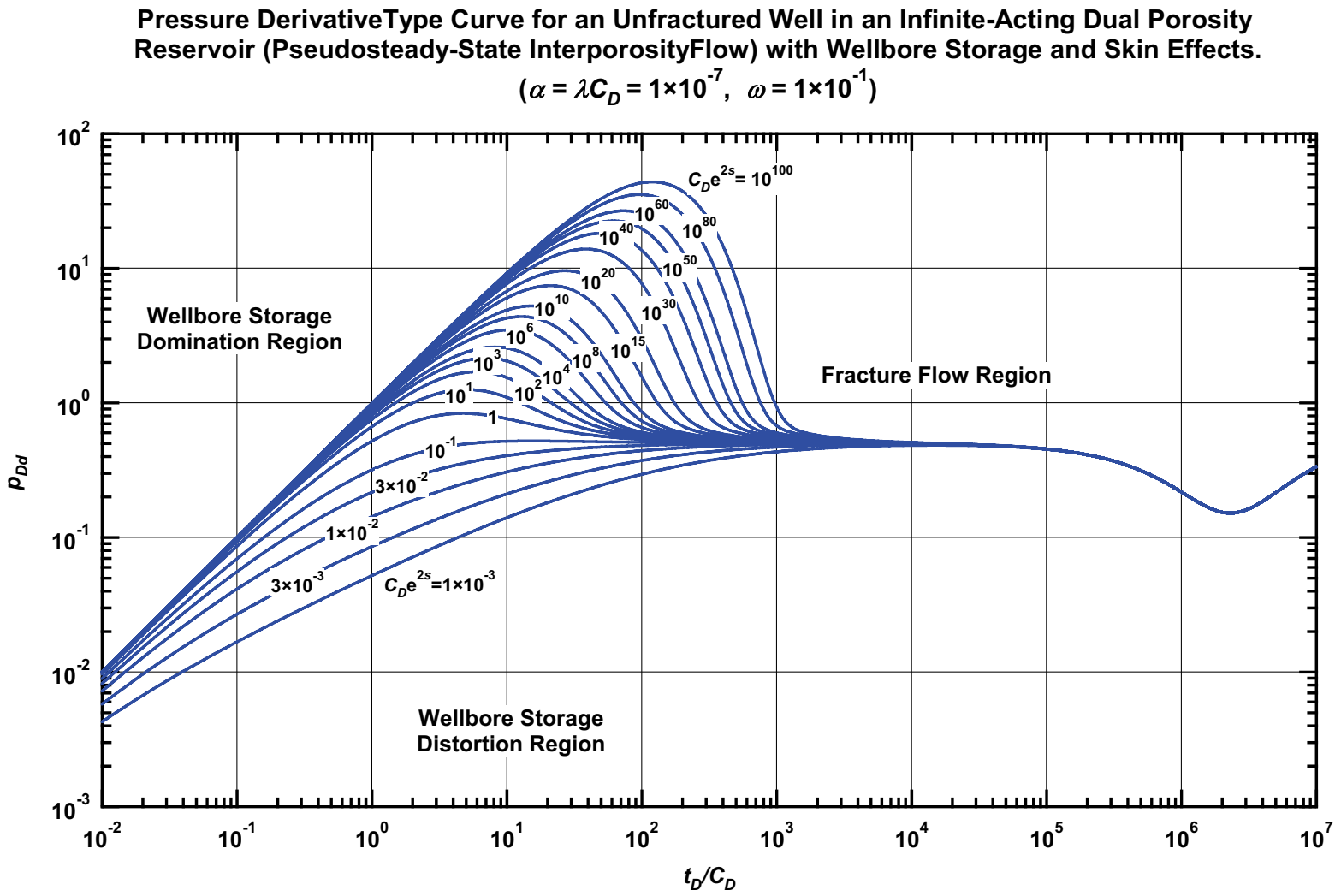

Figure C.23 — p_{Dd} vs. t_D/C_D — $\omega = 1\times10^{-1}$, $\alpha = \lambda C_D = 1\times10^{-7}$ (dual porosity case — includes wellbore storage and skin effects).

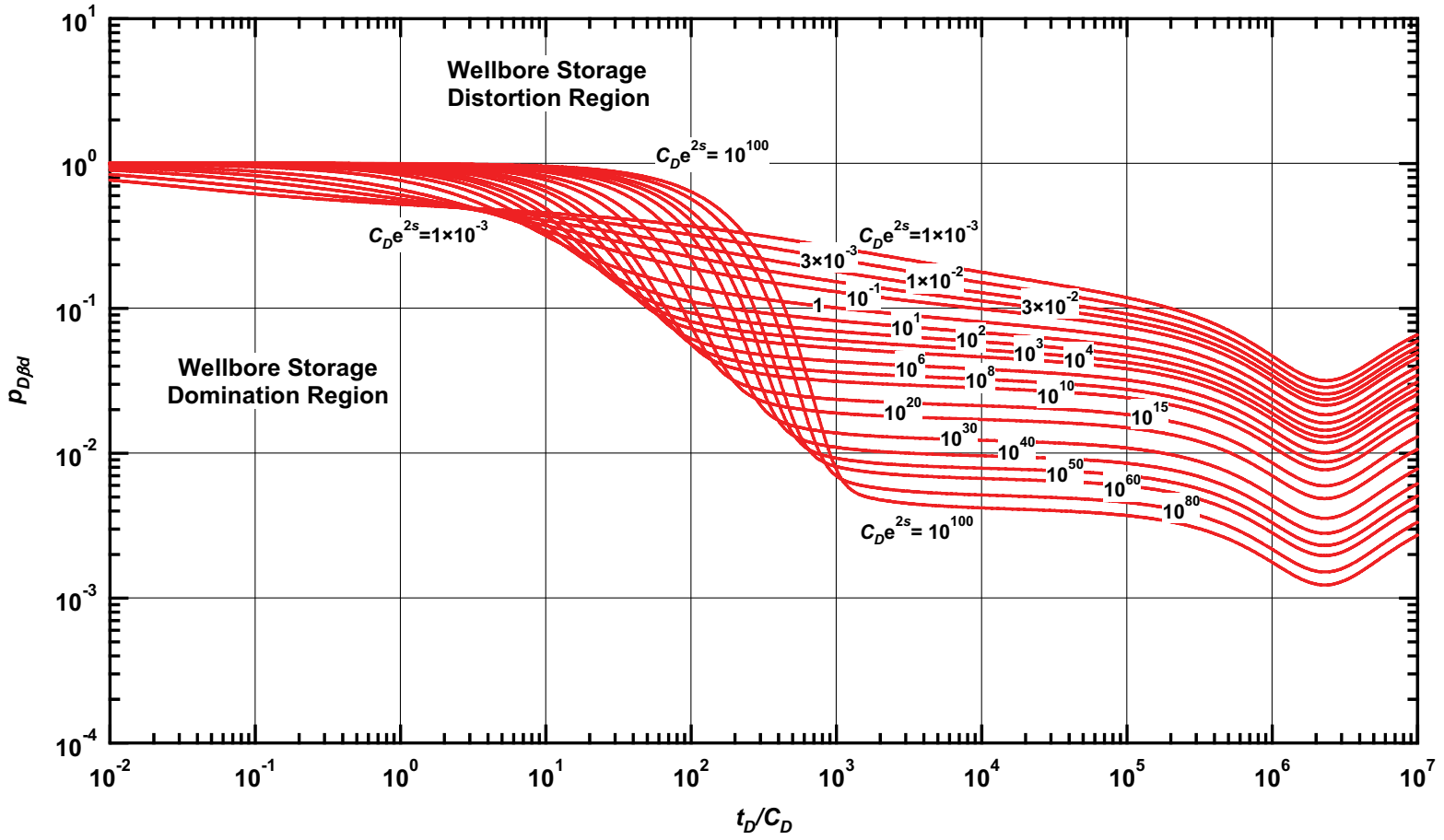

Figure C.24 — $p_{D\beta d}$ vs. t_D/C_D — $\omega = 1\times10^{-1}$, $\alpha = \lambda C_D = 1\times10^{-7}$ (dual porosity case — includes wellbore storage and skin effects).

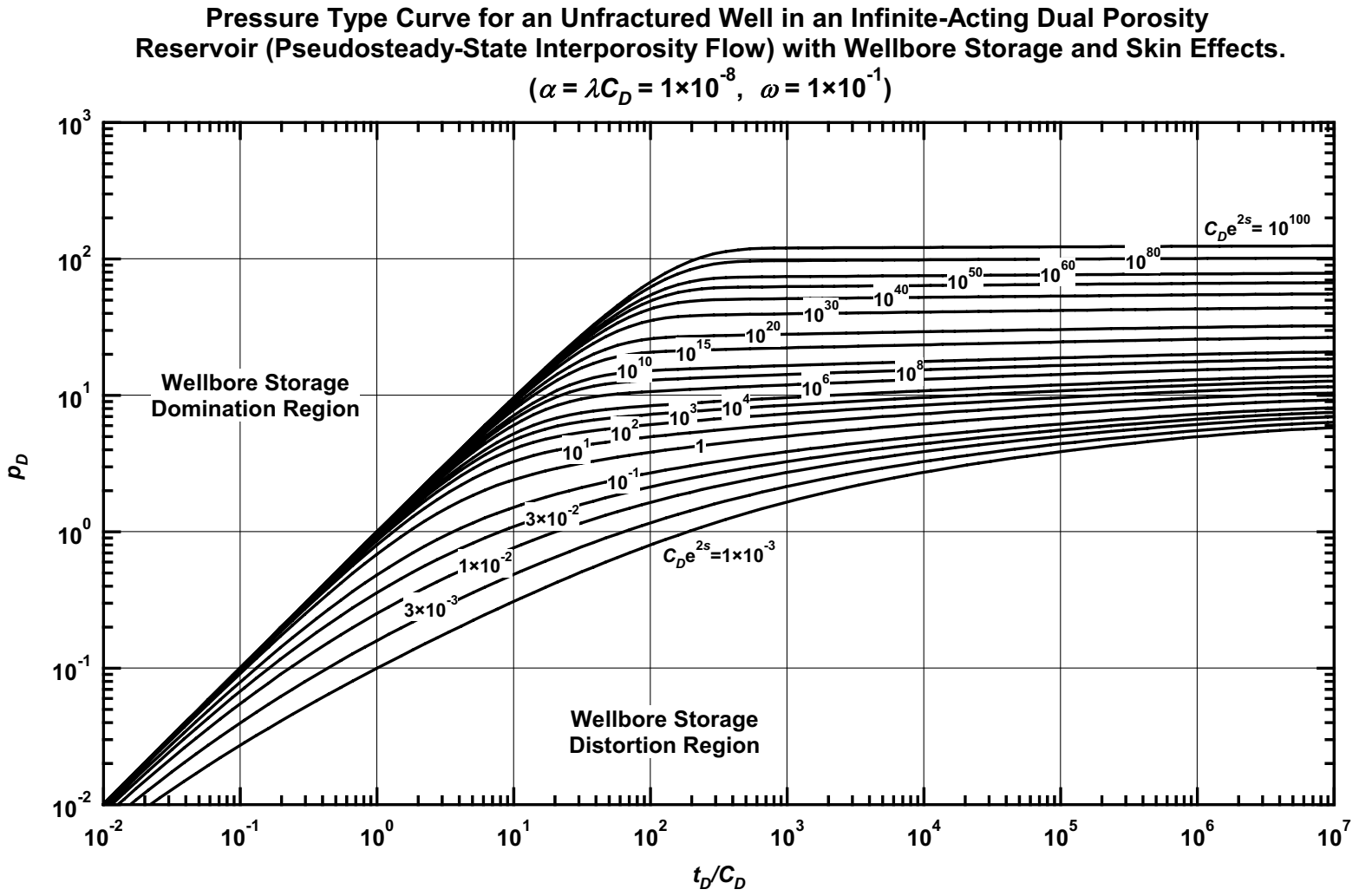

Figure C.25 — p_D vs. t_D/C_D — $\omega = 1\times10^{-1}$, $\alpha = \lambda C_D = 1\times10^{-8}$ (dual porosity case — includes wellbore storage and skin effects).

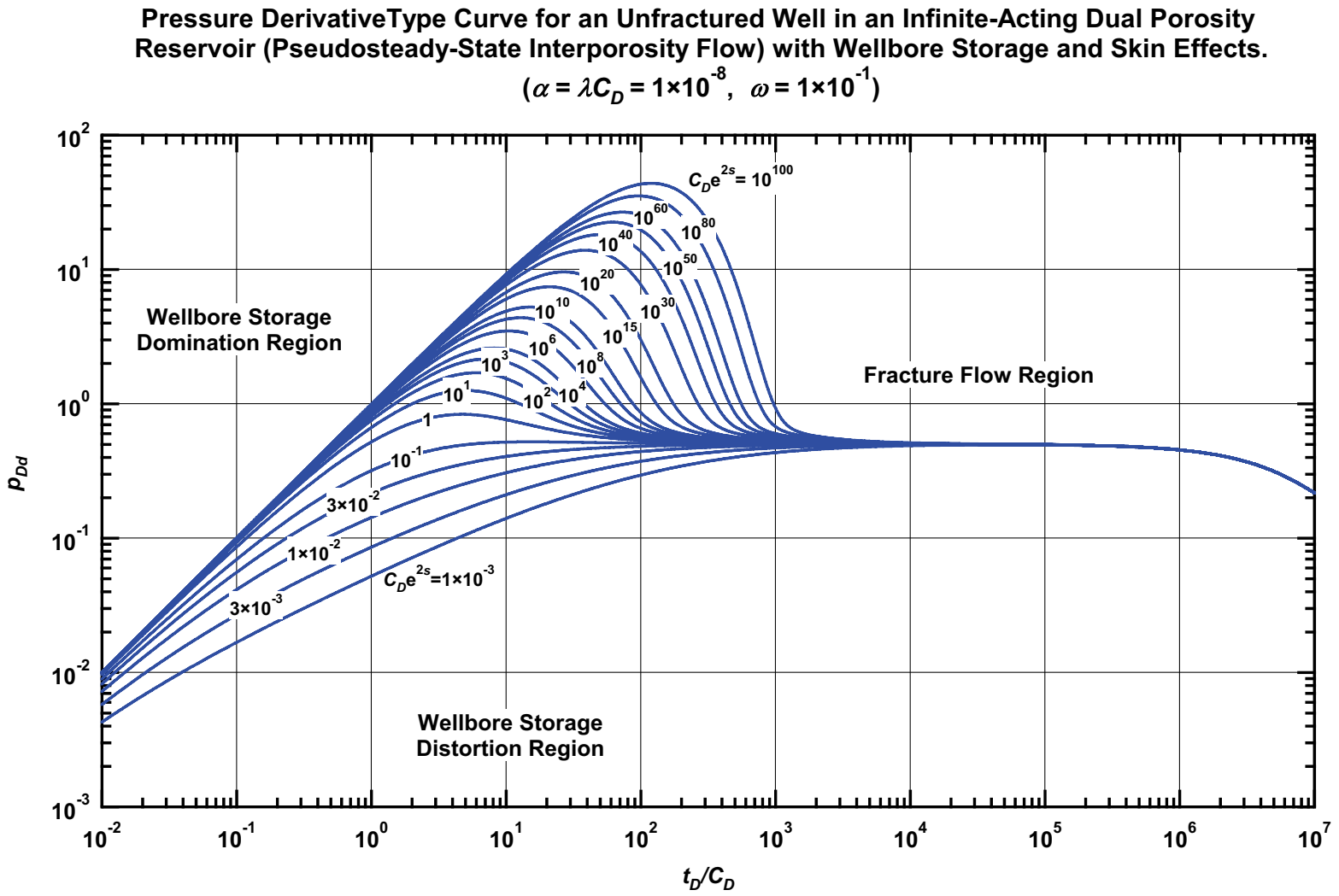

Figure C.26 — p_{Dd} vs. t_D/C_D — $\omega = 1\times10^{-1}$, $\alpha = \lambda C_D = 1\times10^{-8}$ (dual porosity case — includes wellbore storage and skin effects).

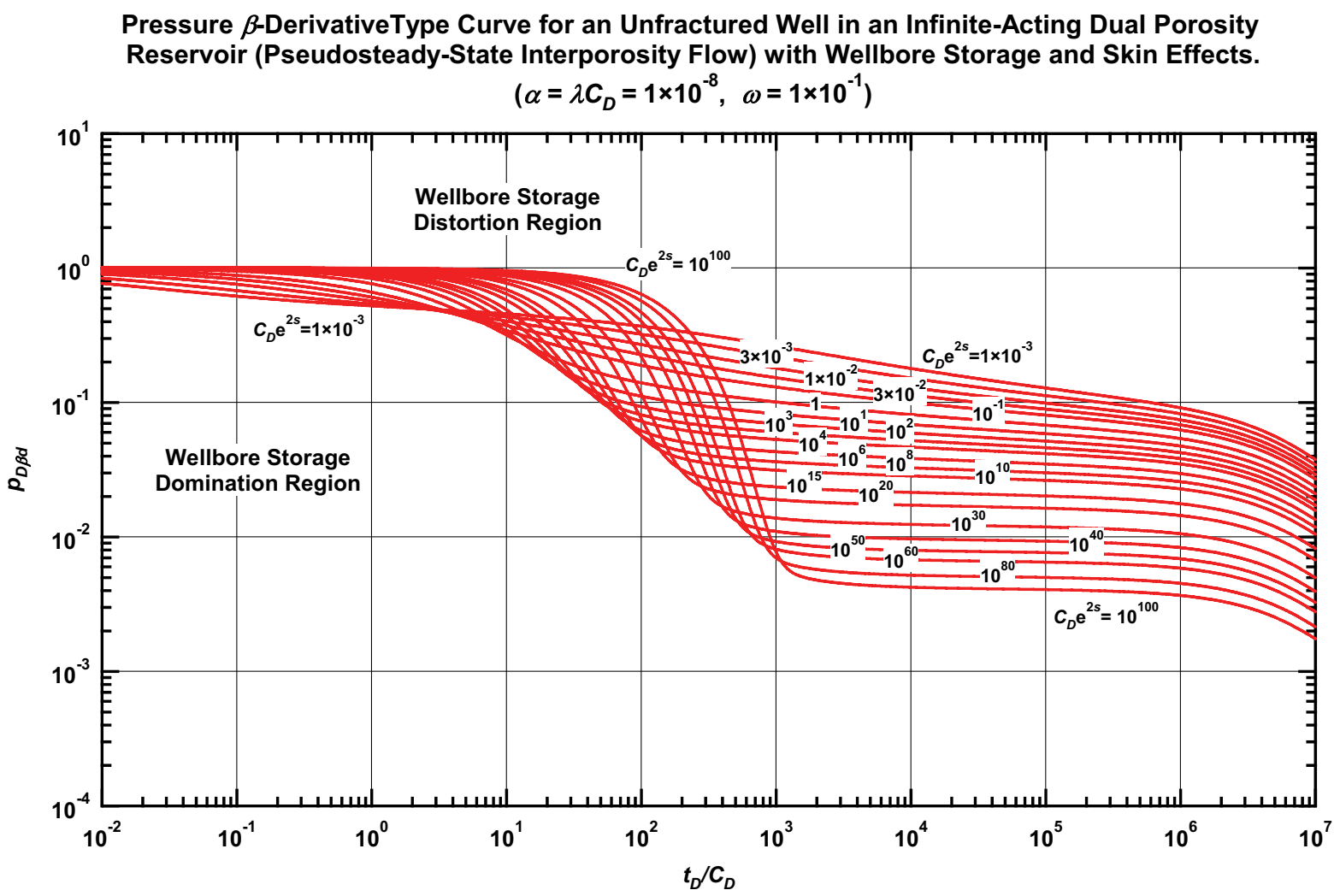

Figure C.27 — $p_{D\beta d}$ vs. t_D/C_D — $\omega = 1\times10^{-1}$, $\alpha = \lambda C_D = 1\times10^{-8}$ (dual porosity case — includes wellbore storage and skin effects).

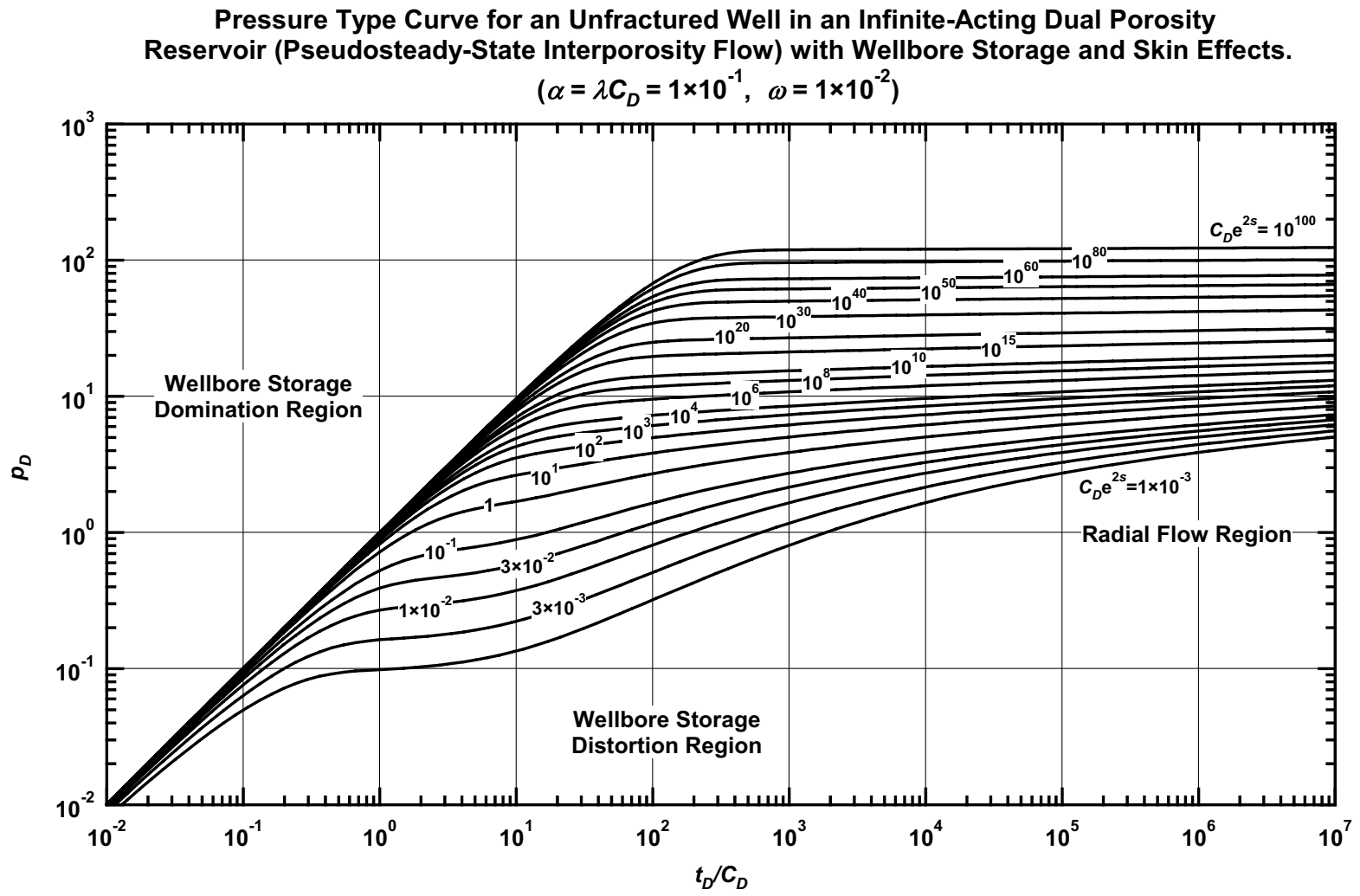

Figure C.28 — p_D vs. t_D/C_D — $\omega = 1\times10^{-2}$, $\alpha = \lambda C_D = 1\times10^{-1}$ (dual porosity case — includes wellbore storage and skin effects).

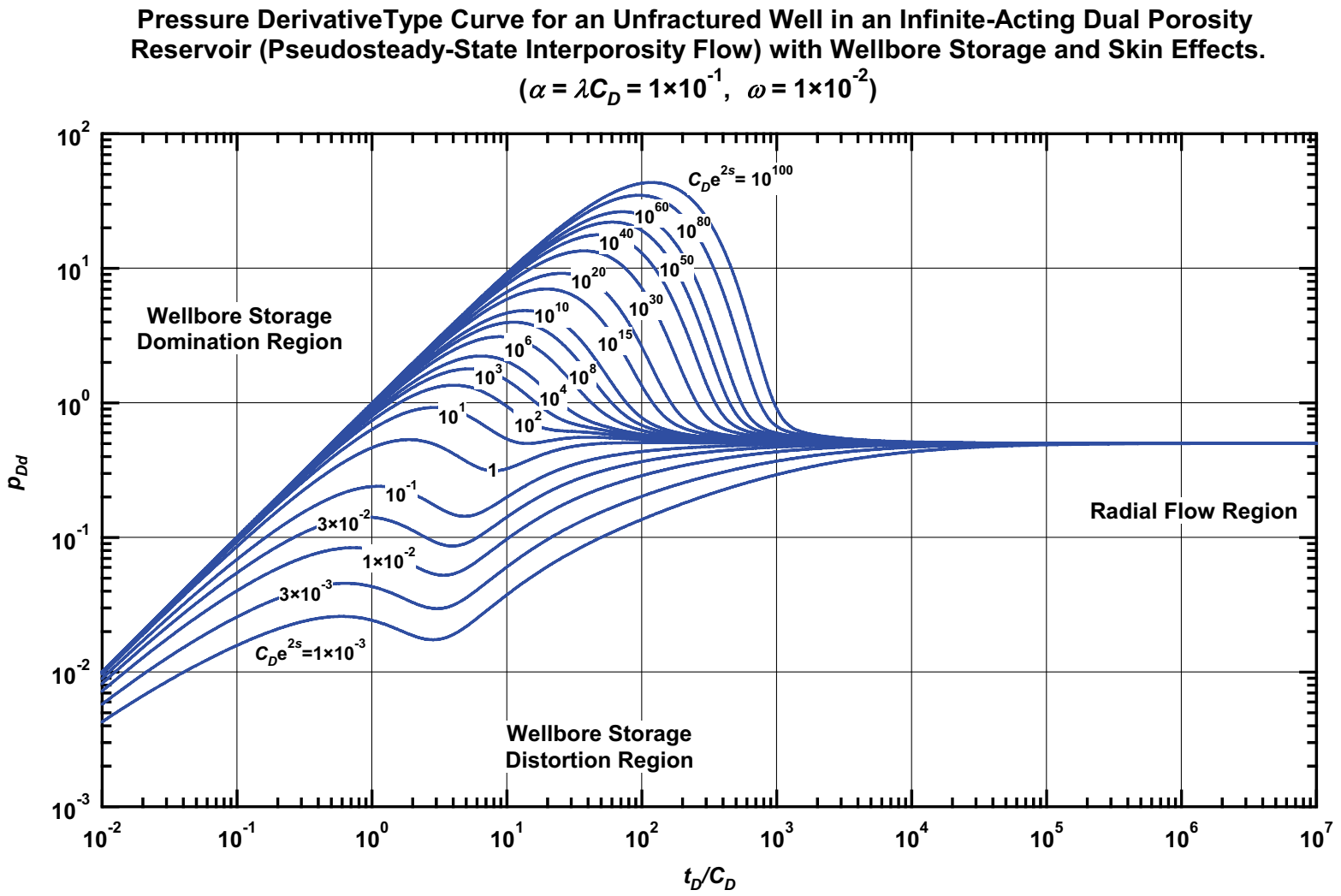

Figure C.29 — p_{Dd} vs. t_D/C_D — $\omega = 1\times10^{-2}$, $\alpha = \lambda C_D = 1\times10^{-1}$ (dual porosity case — includes wellbore storage and skin effects).

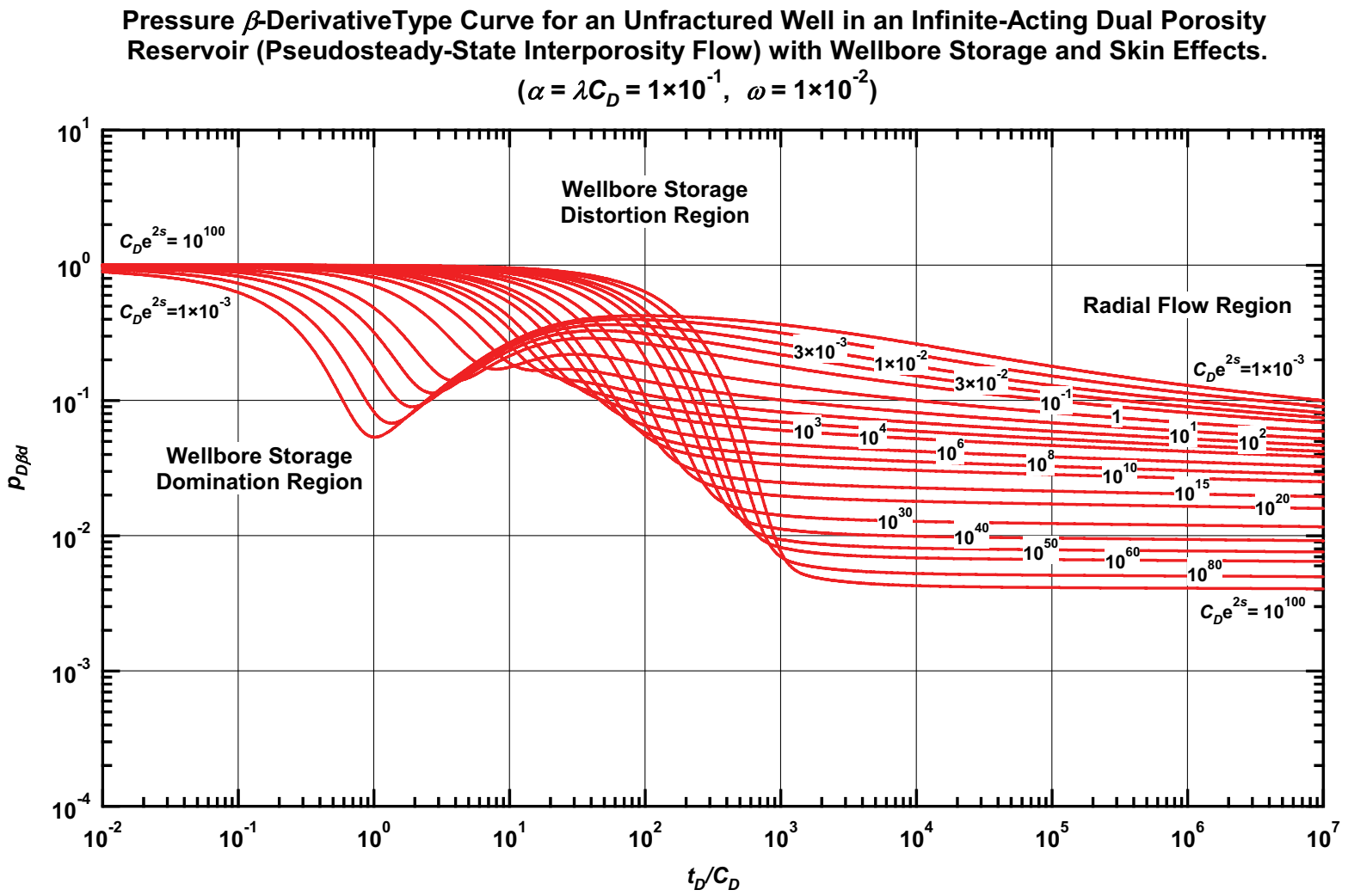

Figure C.30 — $p_{D\beta d}$ vs. t_D/C_D — $\omega = 1\times10^{-2}$, $\alpha = \lambda C_D = 1\times10^{-1}$ (dual porosity case — includes wellbore storage and skin effects).

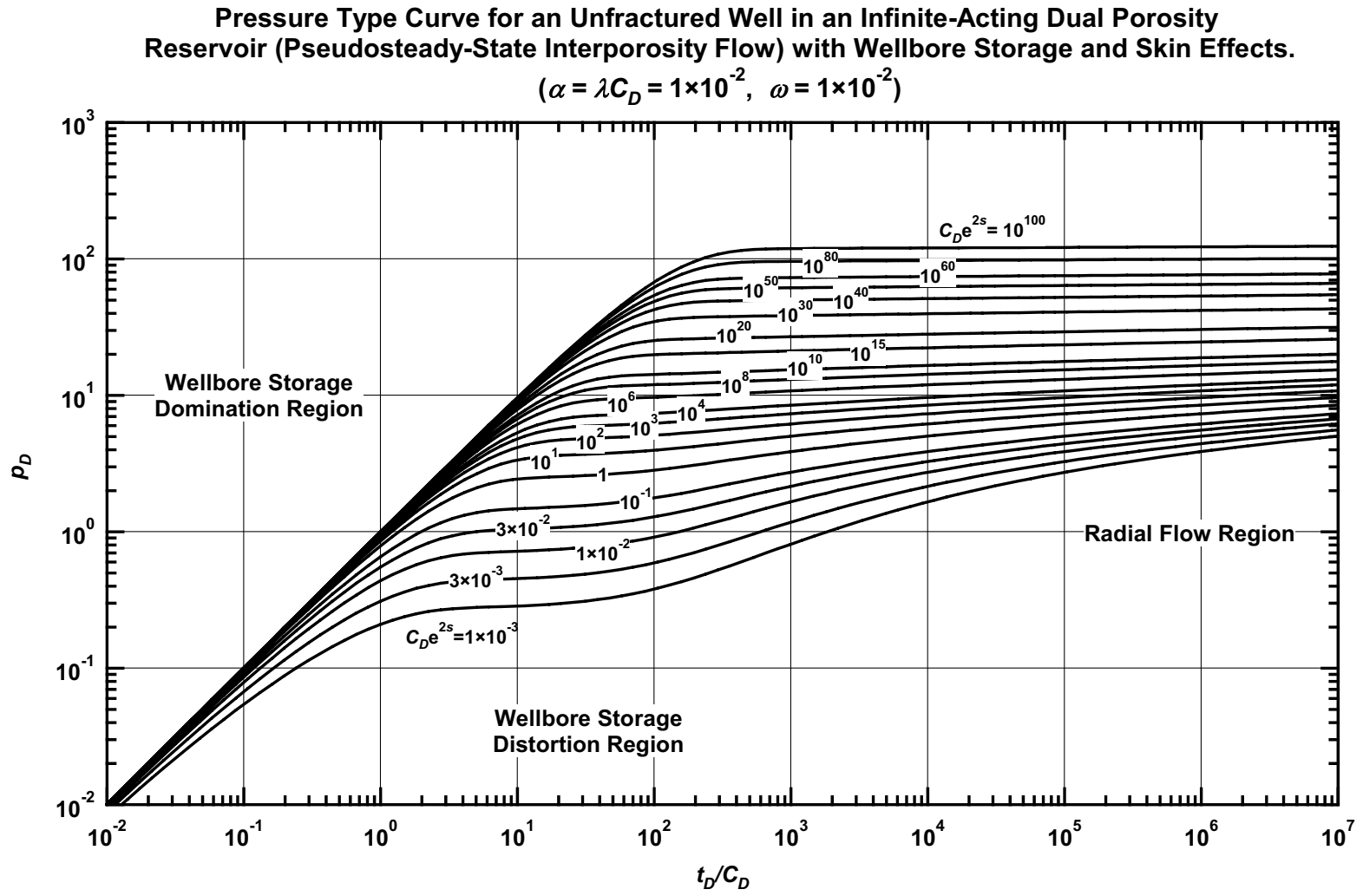

Figure C.31 — p_D vs. t_D/C_D — $\omega = 1\times10^{-2}$, $\alpha = \lambda C_D = 1\times10^{-2}$ (dual porosity case — includes wellbore storage and skin effects).

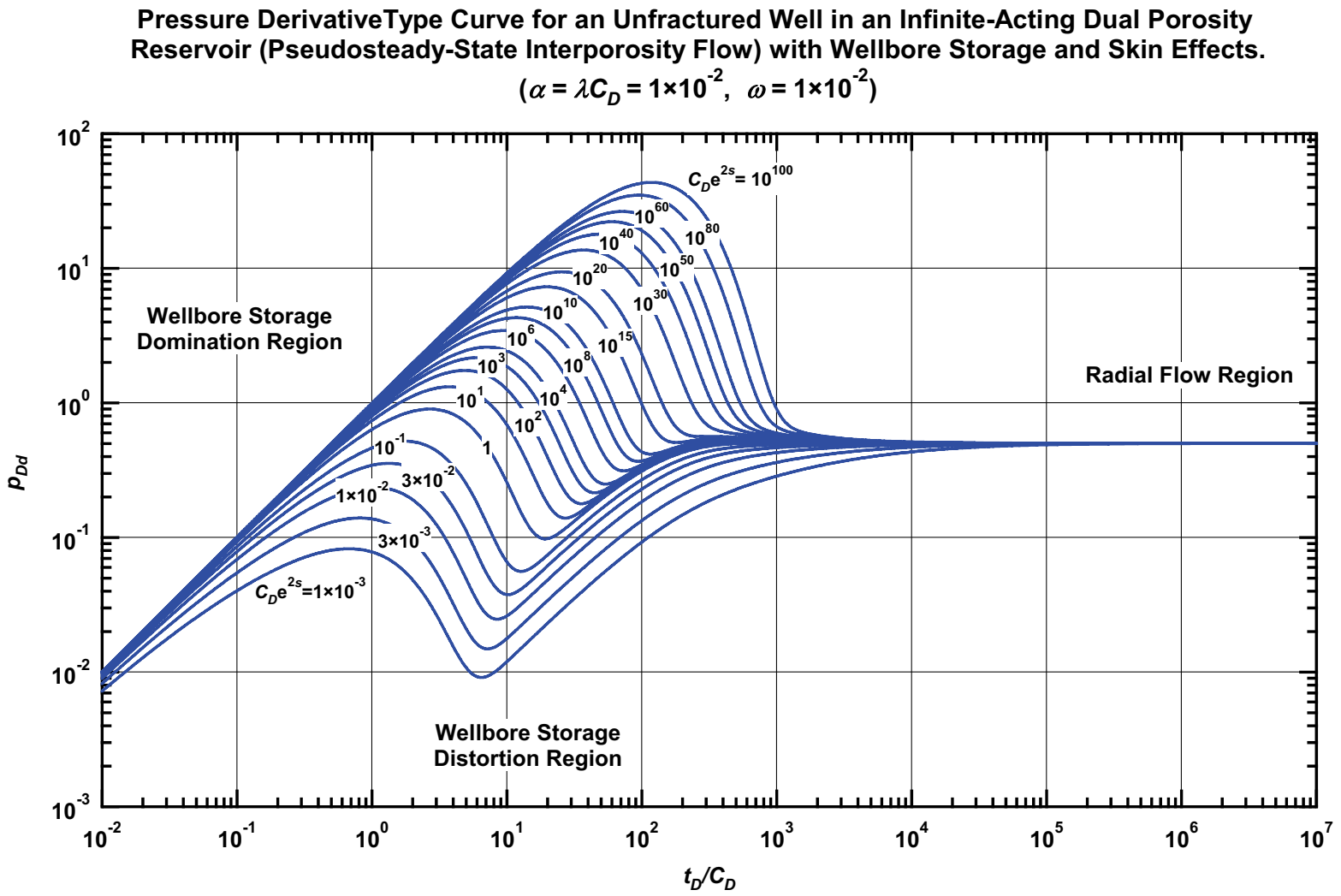

Figure C.32 — p_{Dd} vs. t_D/C_D — $\omega = 1\times10^{-2}$, $\alpha = \lambda C_D = 1\times10^{-2}$ (dual porosity case — includes wellbore storage and skin effects).

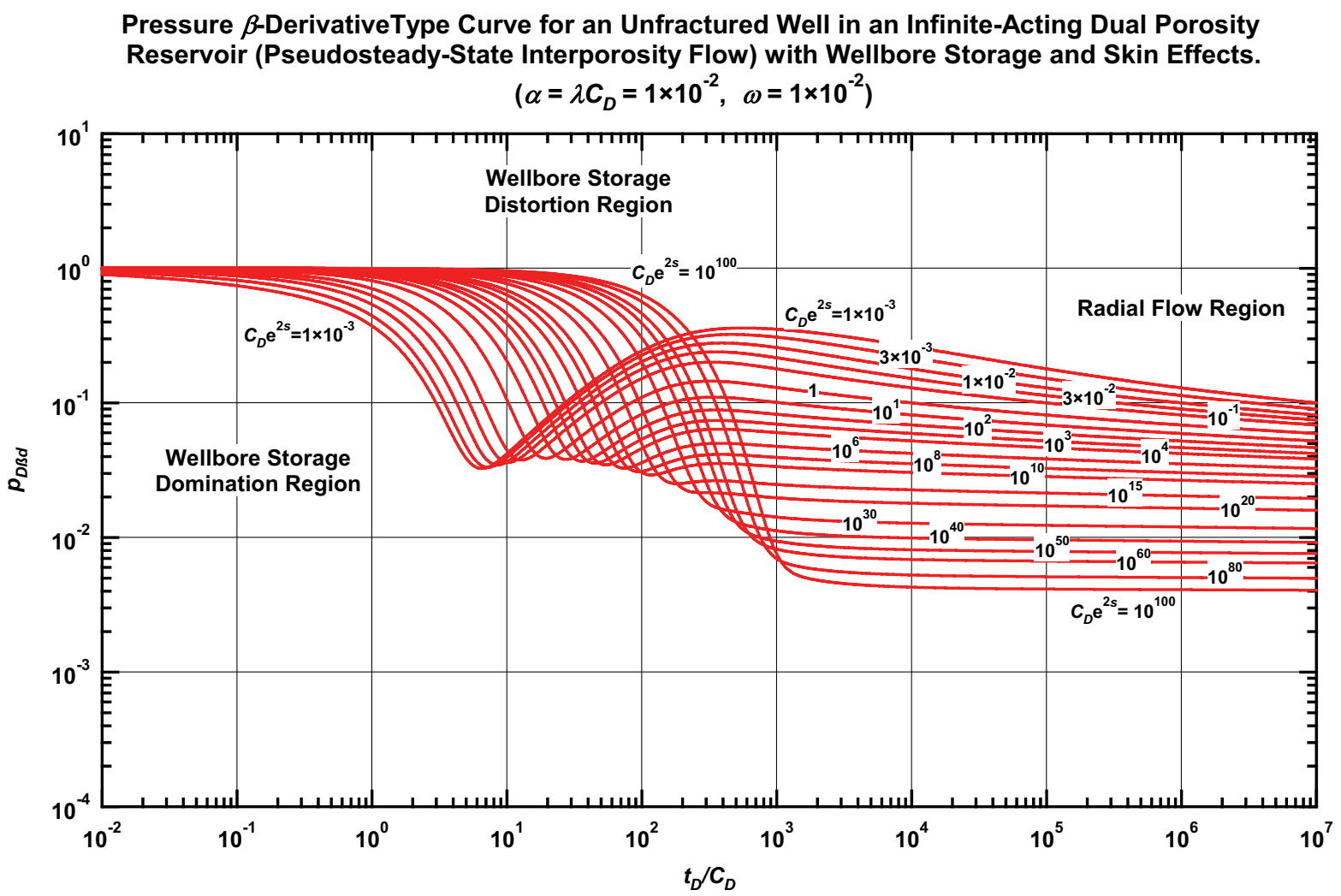

Figure C.33 — $p_{D\beta d}$ vs. t_D/C_D — $\omega = 1\times10^{-2}$, $\alpha = \lambda C_D = 1\times10^{-2}$ (dual porosity case — includes wellbore storage and skin effects).

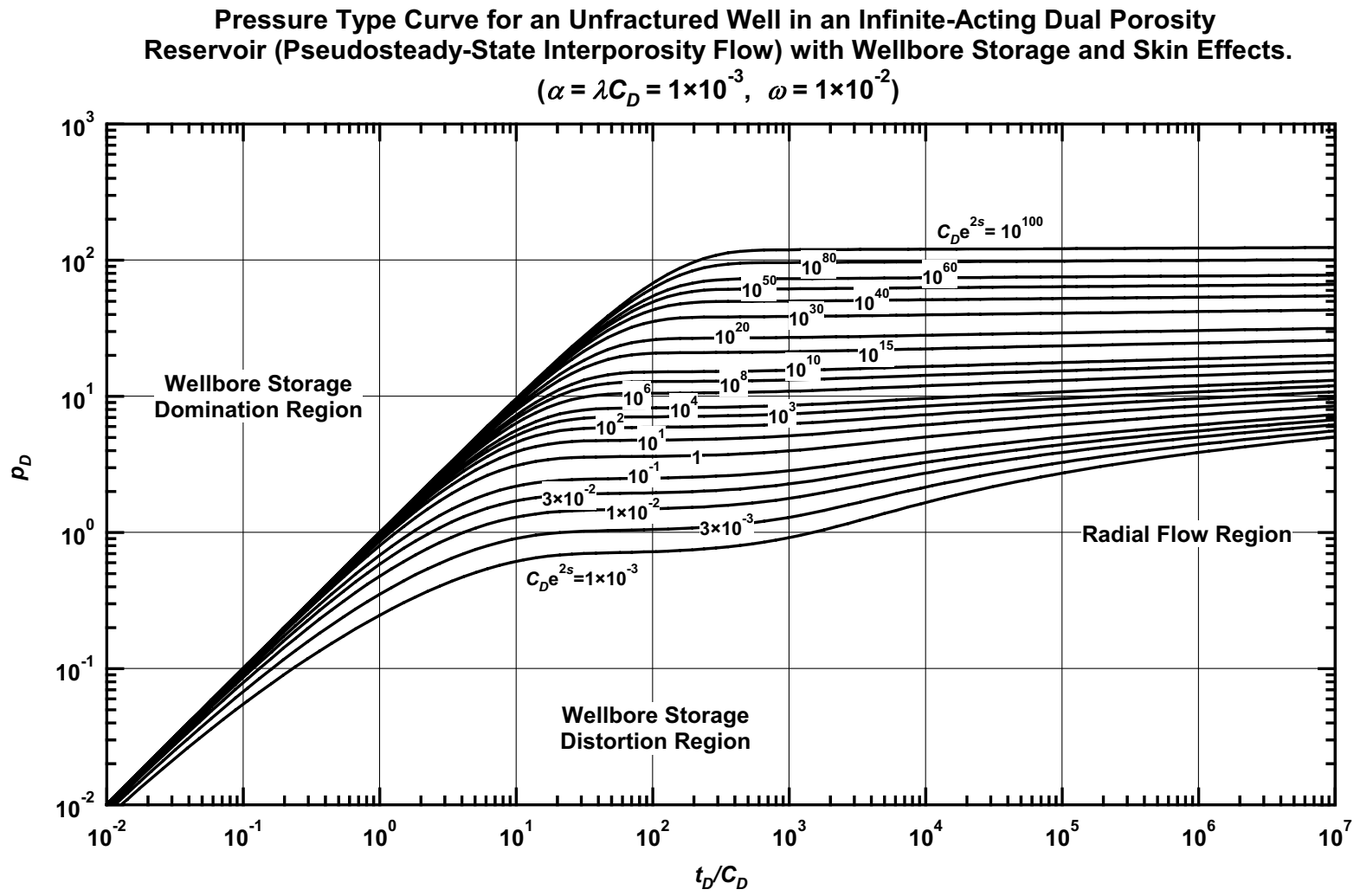

Figure C.34 — p_D vs. t_D/C_D — $\omega = 1\times10^{-2}$, $\alpha = \lambda C_D = 1\times10^{-3}$ (dual porosity case — includes wellbore storage and skin effects).

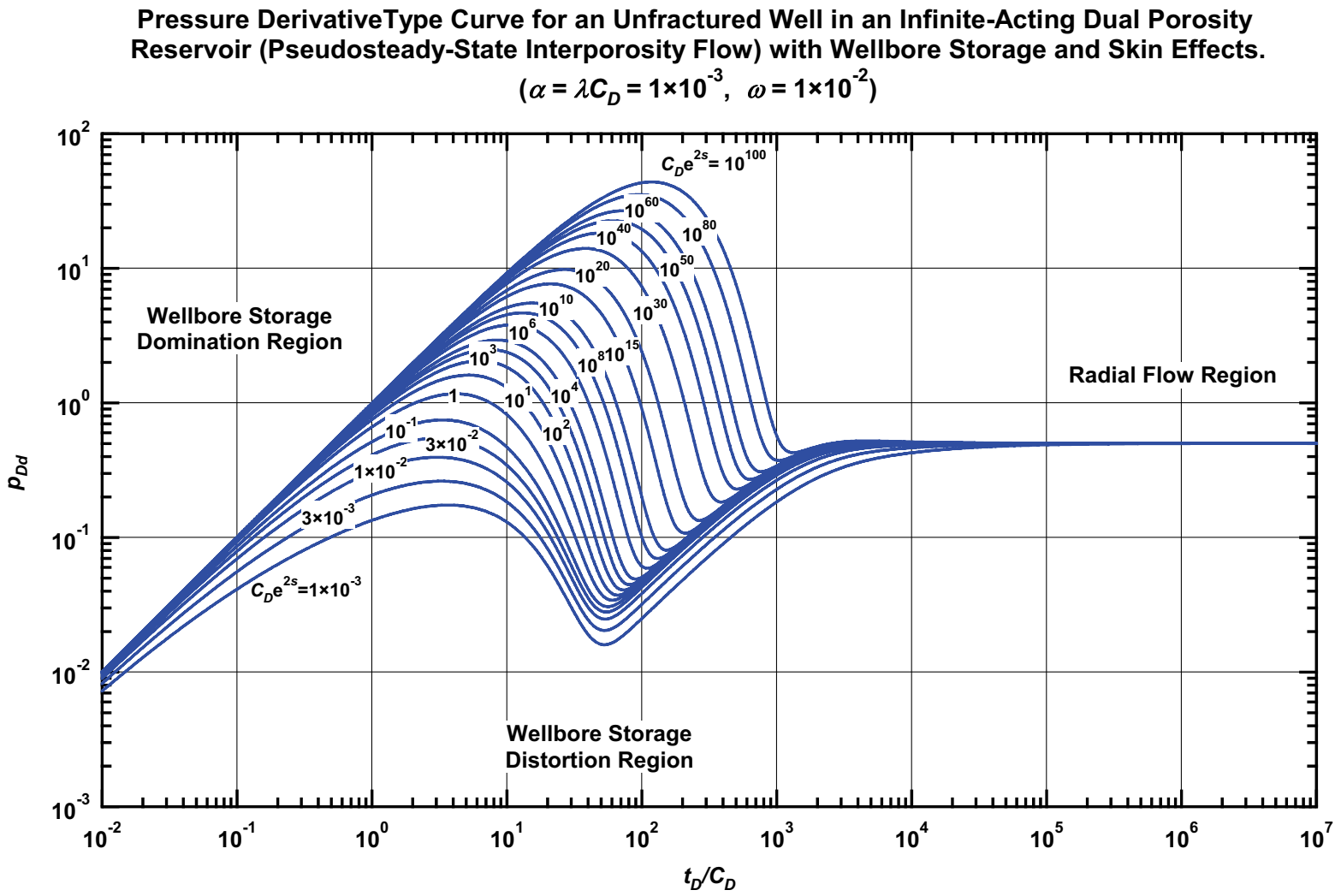

Figure C.35 — p_{Dd} vs. t_D/C_D — $\omega = 1\times10^{-2}$, $\alpha = \lambda C_D = 1\times10^{-3}$ (dual porosity case — includes wellbore storage and skin effects).

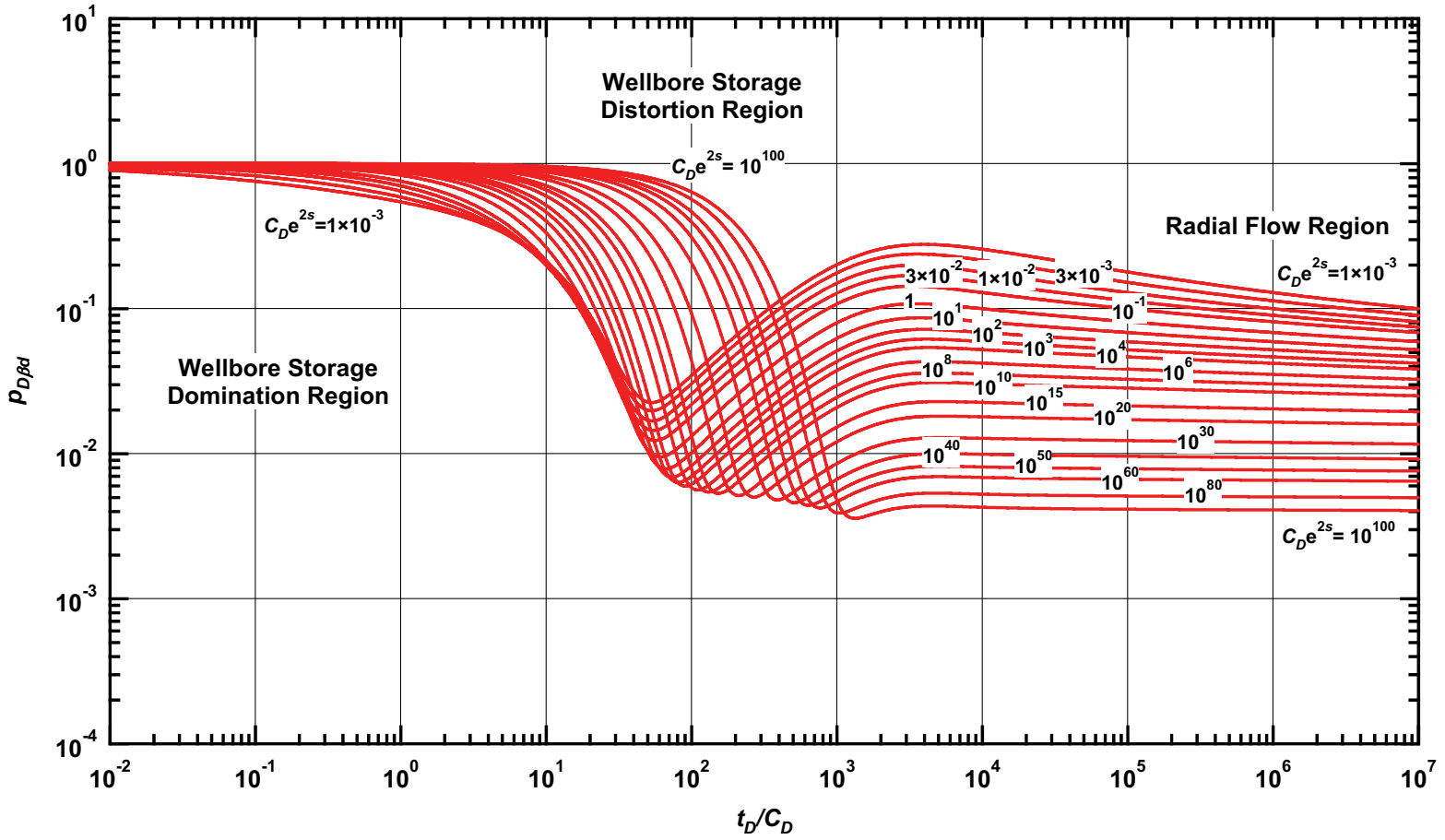

Figure C.36 — $p_{D\beta d}$ vs. t_D/C_D — $\omega = 1\times10^{-2}$, $\alpha = \lambda C_D = 1\times10^{-3}$ (dual porosity case — includes wellbore storage and skin effects).

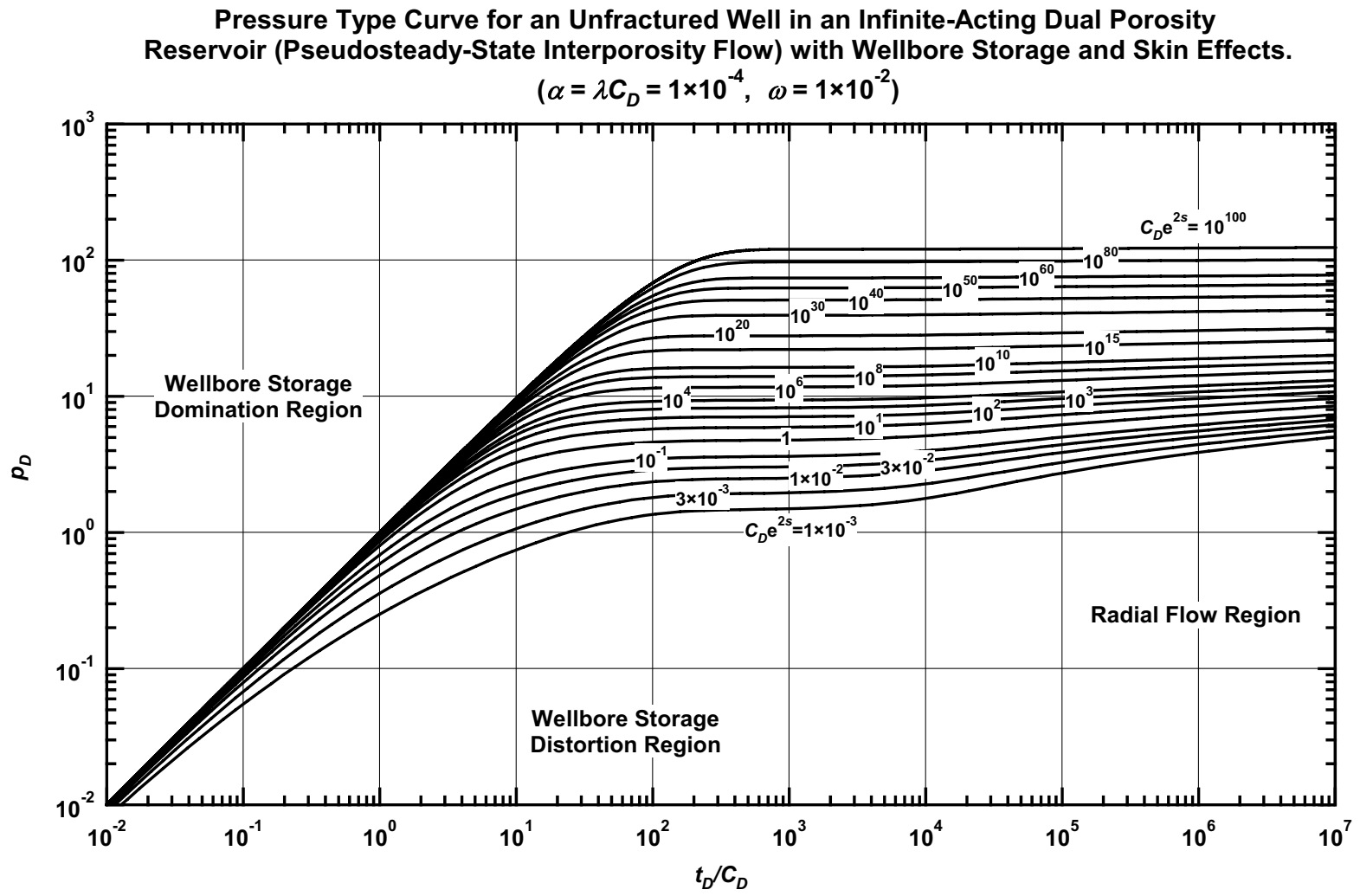

Figure C.37 — p_D vs. t_D/C_D — $\omega = 1\times10^{-2}$, $\alpha = \lambda C_D = 1\times10^{-4}$ (dual porosity case — includes wellbore storage and skin effects).

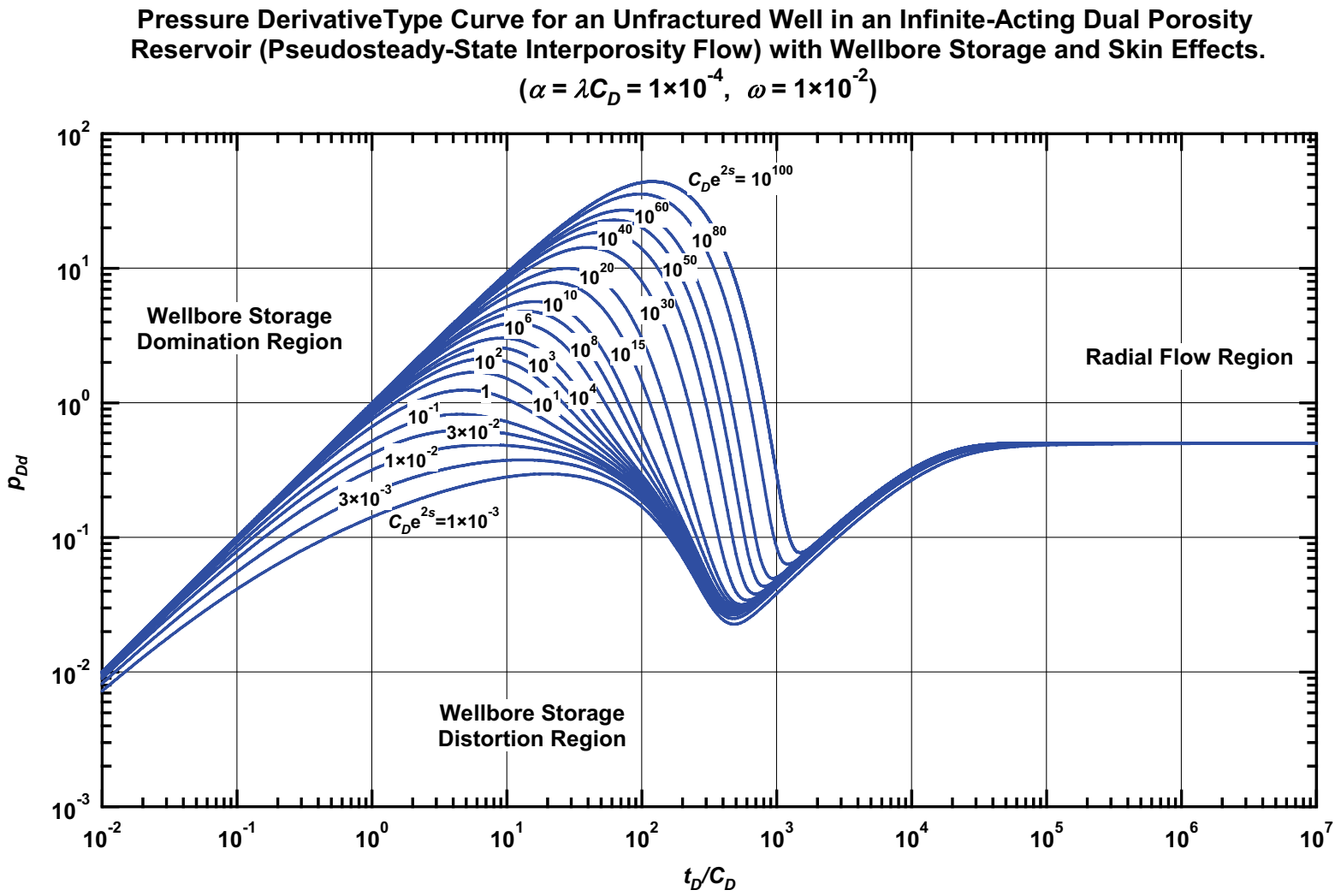

Figure C.38 — p_{Dd} vs. t_D/C_D — $\omega = 1\times10^{-2}$, $\alpha = \lambda C_D = 1\times10^{-4}$ (dual porosity case — includes wellbore storage and skin effects).

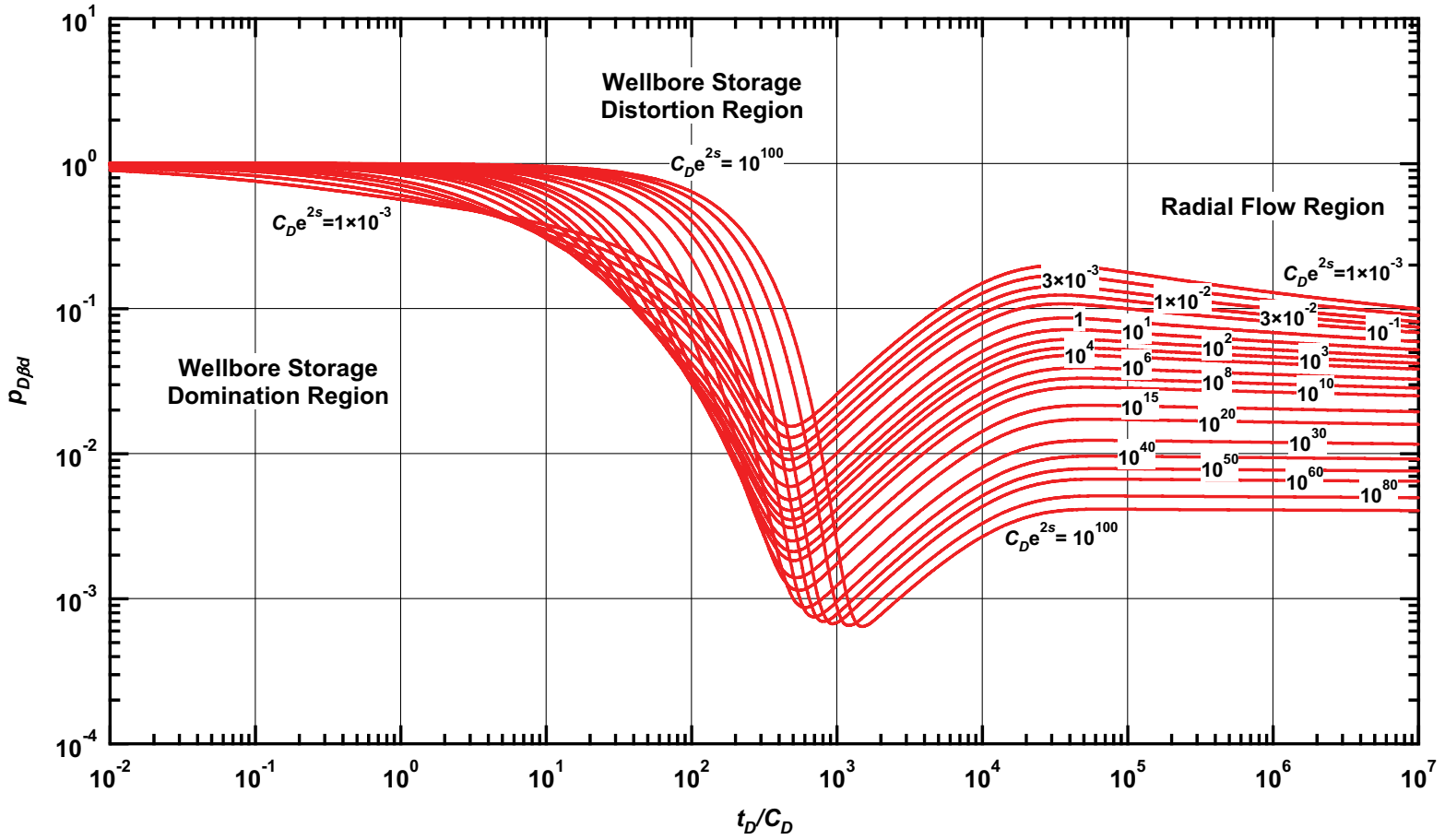

Figure C.39 — $p_{D\beta d}$ vs. t_D/C_D — $\omega = 1\times10^{-2}$, $\alpha = \lambda C_D = 1\times10^{-4}$ (dual porosity case — includes wellbore storage and skin effects).

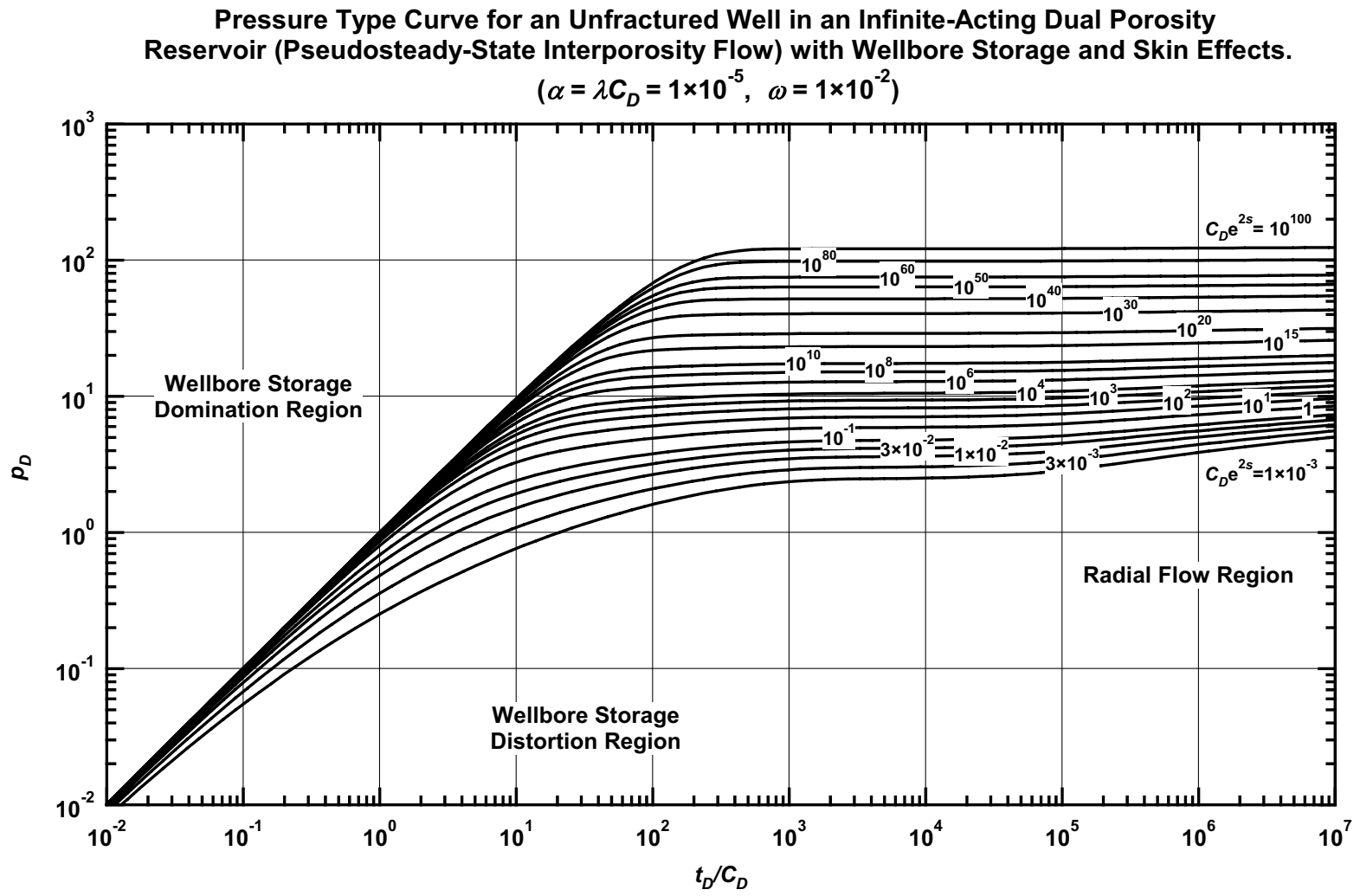

Figure C.40 — p_D vs. t_D/C_D — $\omega = 1\times10^{-2}$, $\alpha = \lambda C_D = 1\times10^{-5}$ (dual porosity case — includes wellbore storage and skin effects).

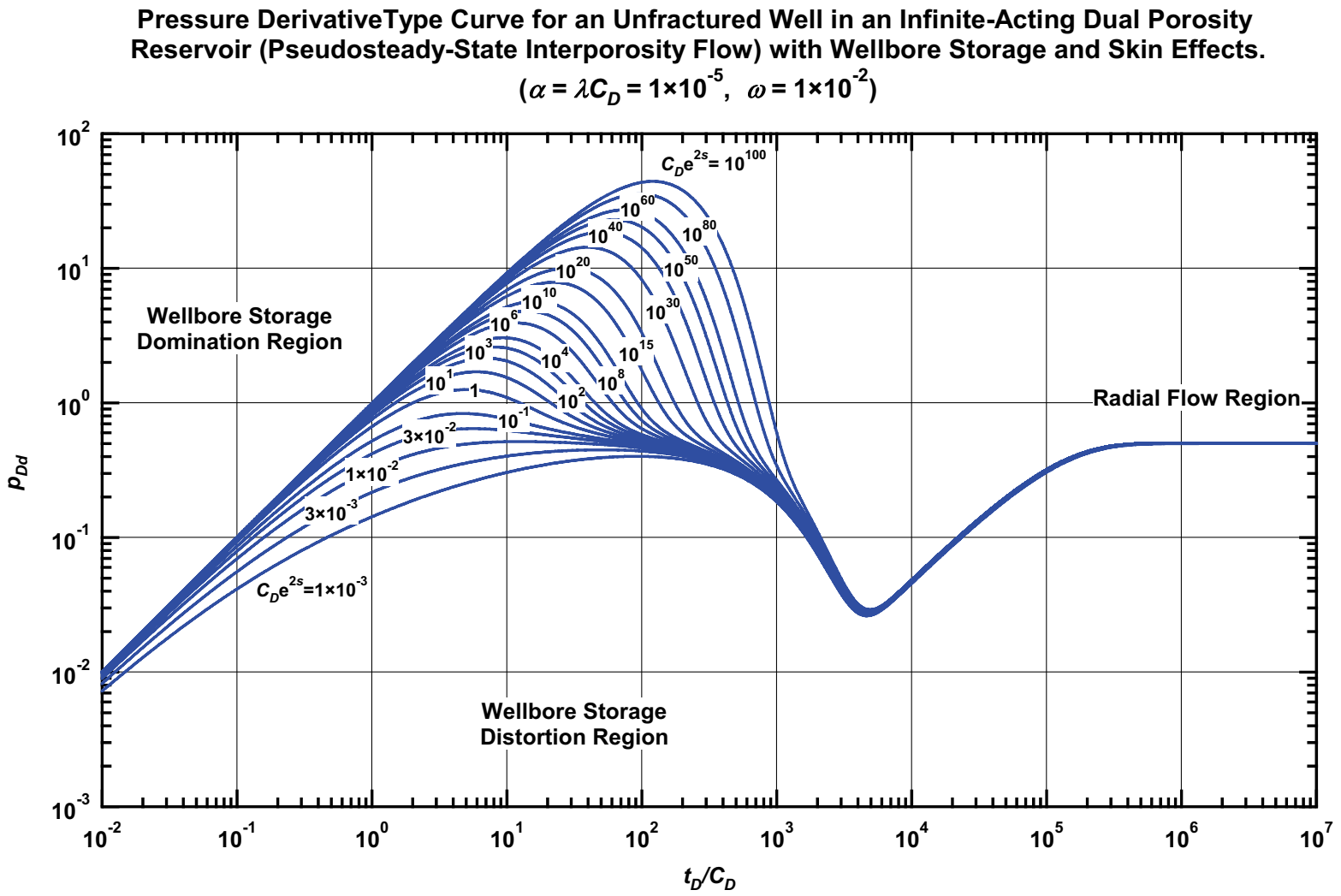

Figure C.41 — p_{Dd} vs. t_D/C_D — $\omega = 1\times10^{-2}$, $\alpha = \lambda C_D = 1\times10^{-5}$ (dual porosity case — includes wellbore storage and skin effects).

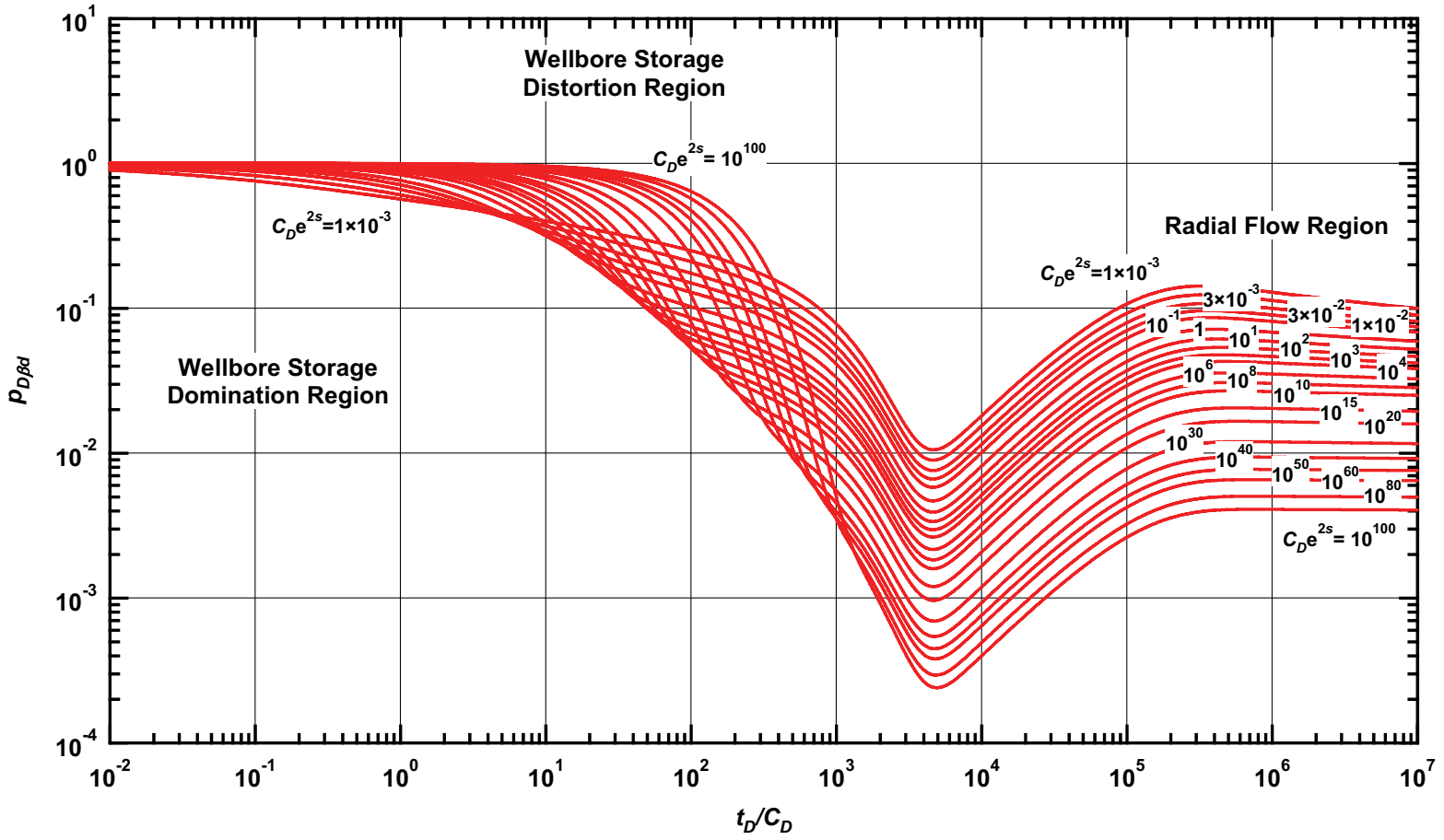

Figure C.42 — $p_{D\beta d}$ vs. t_D/C_D — $\omega = 1\times10^{-2}$, $\alpha = \lambda C_D = 1\times10^{-5}$ (dual porosity case — includes wellbore storage and skin effects).

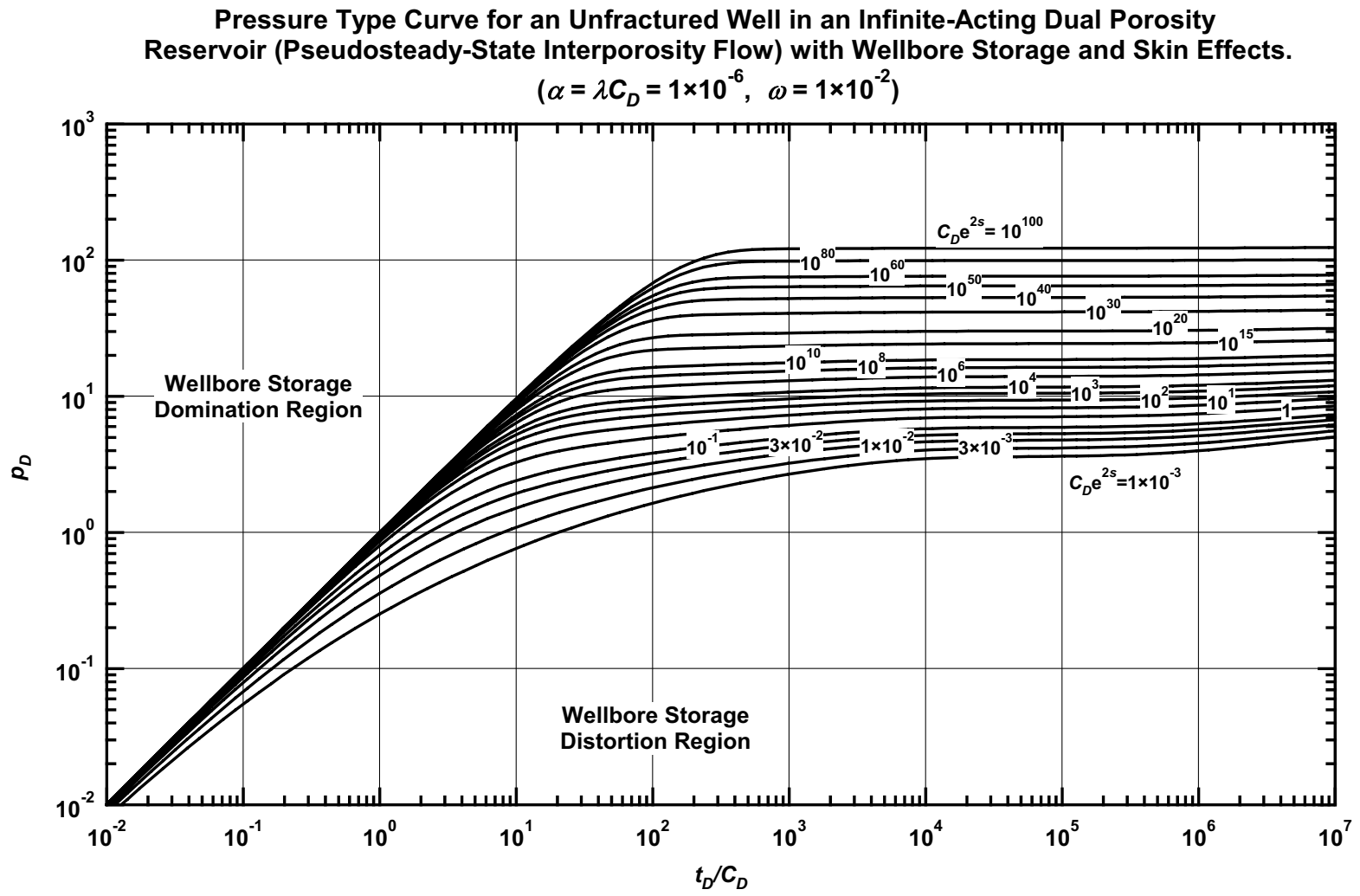

Figure C.43 — p_D vs. t_D/C_D — $\omega = 1\times10^{-2}$, $\alpha = \lambda C_D = 1\times10^{-6}$ (dual porosity case — includes wellbore storage and skin effects).

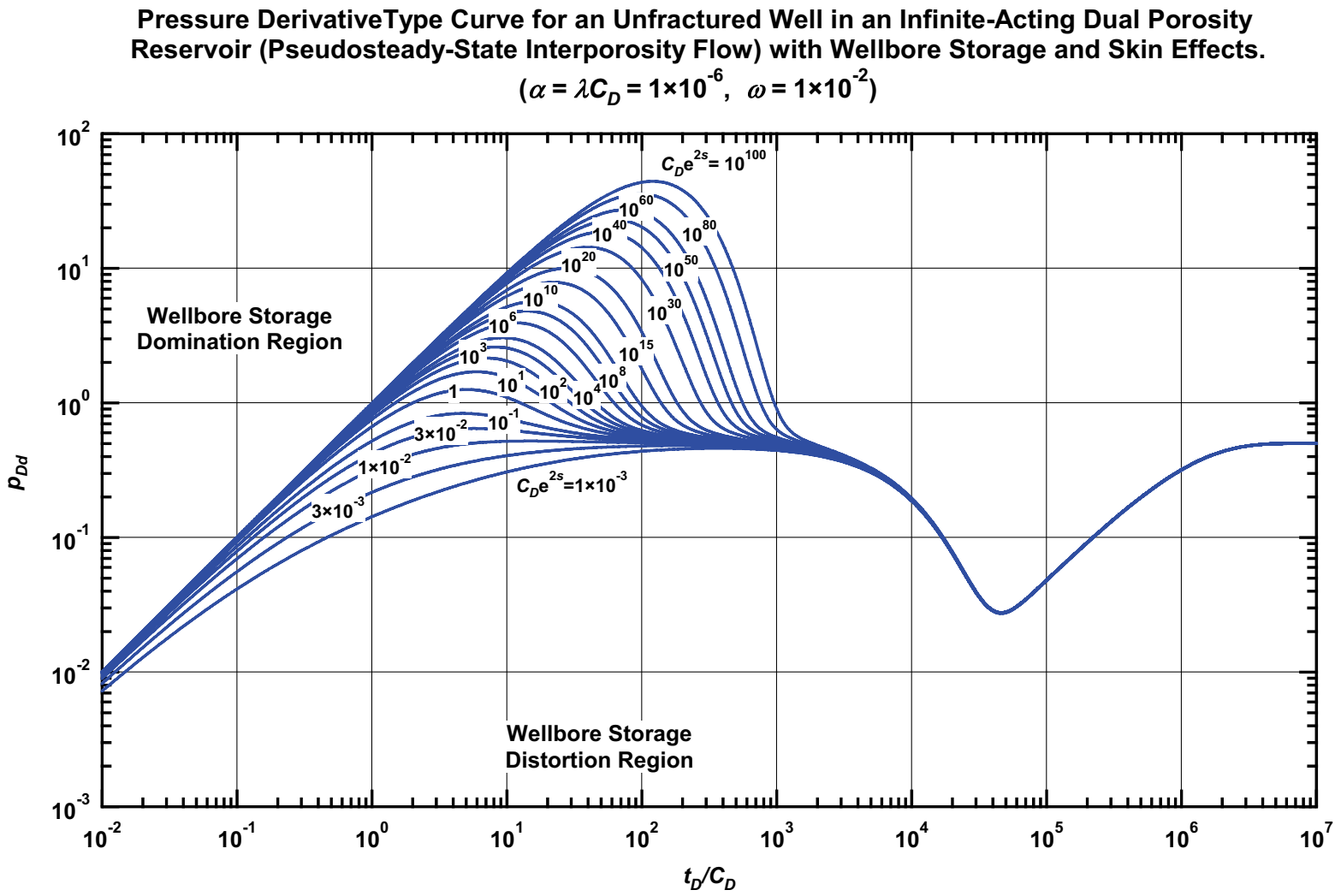

Figure C.44 — p_{Dd} vs. t_D/C_D — $\omega = 1\times10^{-2}$, $\alpha = \lambda C_D = 1\times10^{-6}$ (dual porosity case — includes wellbore storage and skin effects).

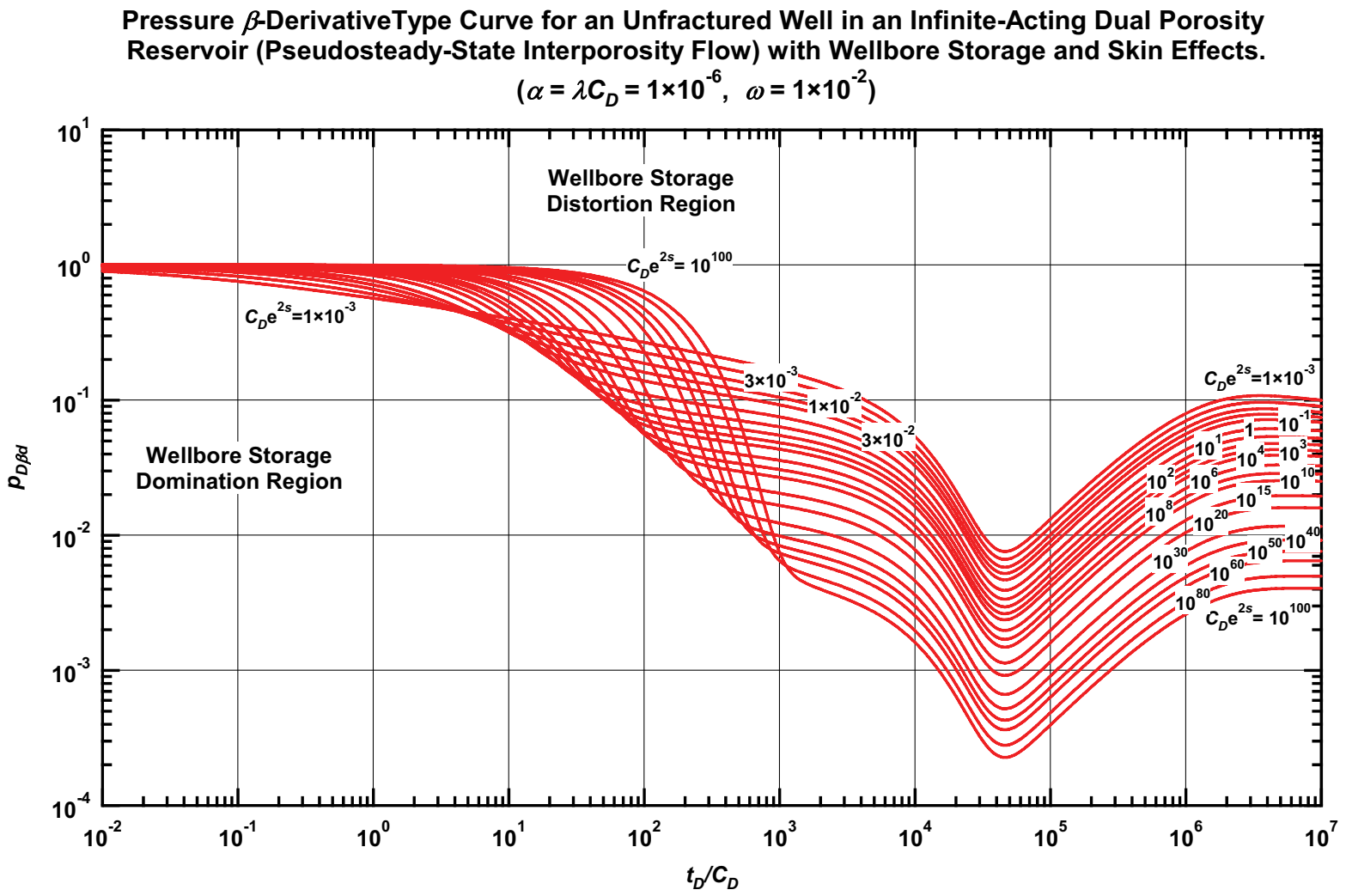

Figure C.45 — $p_{D\beta d}$ vs. t_D/C_D — $\omega = 1\times10^{-2}$, $\alpha = \lambda C_D = 1\times10^{-6}$ (dual porosity case — includes wellbore storage and skin effects).

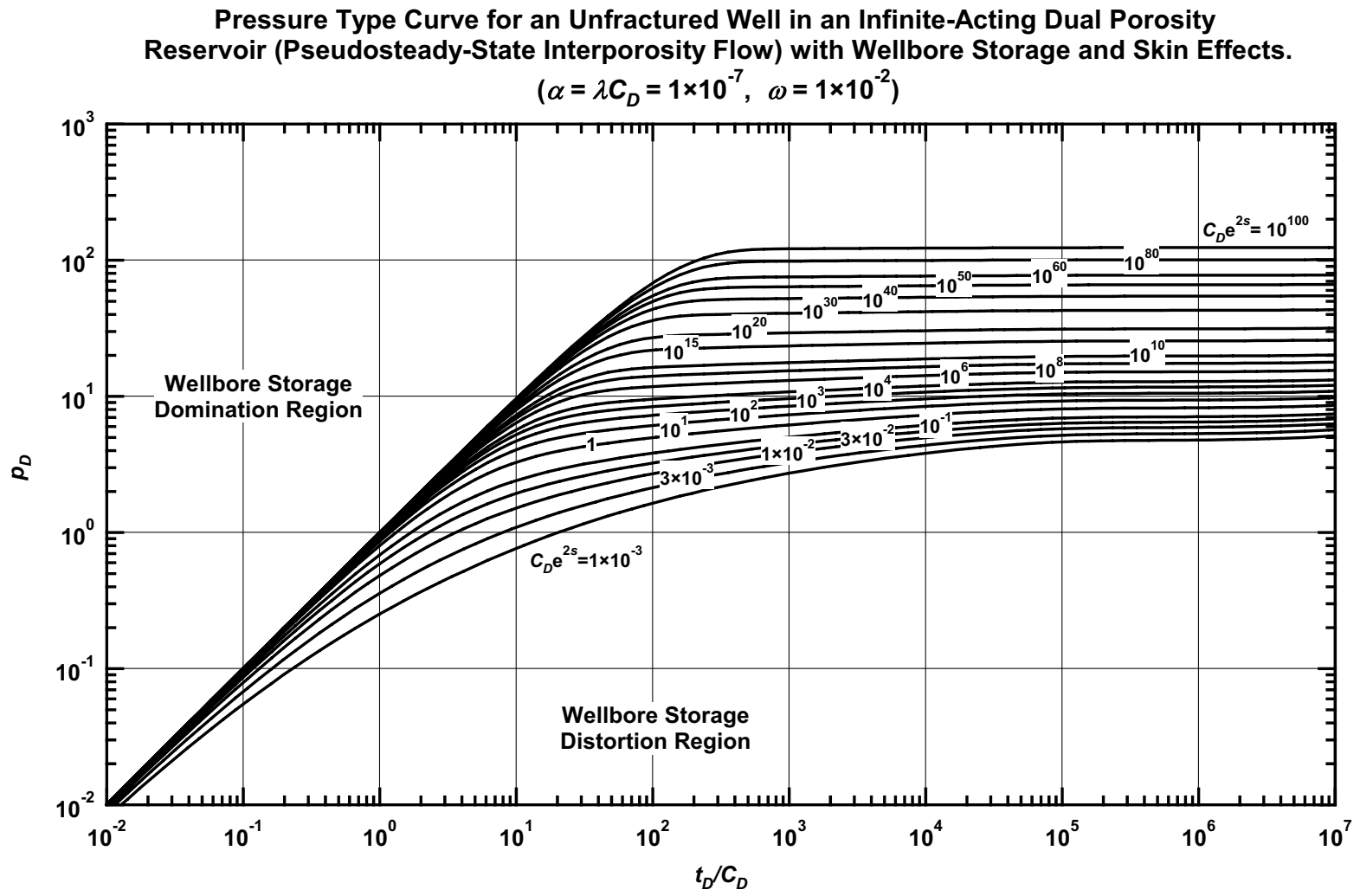

Figure C.46 — p_D vs. t_D/C_D — $\omega = 1\times10^{-2}$, $\alpha = \lambda C_D = 1\times10^{-7}$ (dual porosity case — includes wellbore storage and skin effects).

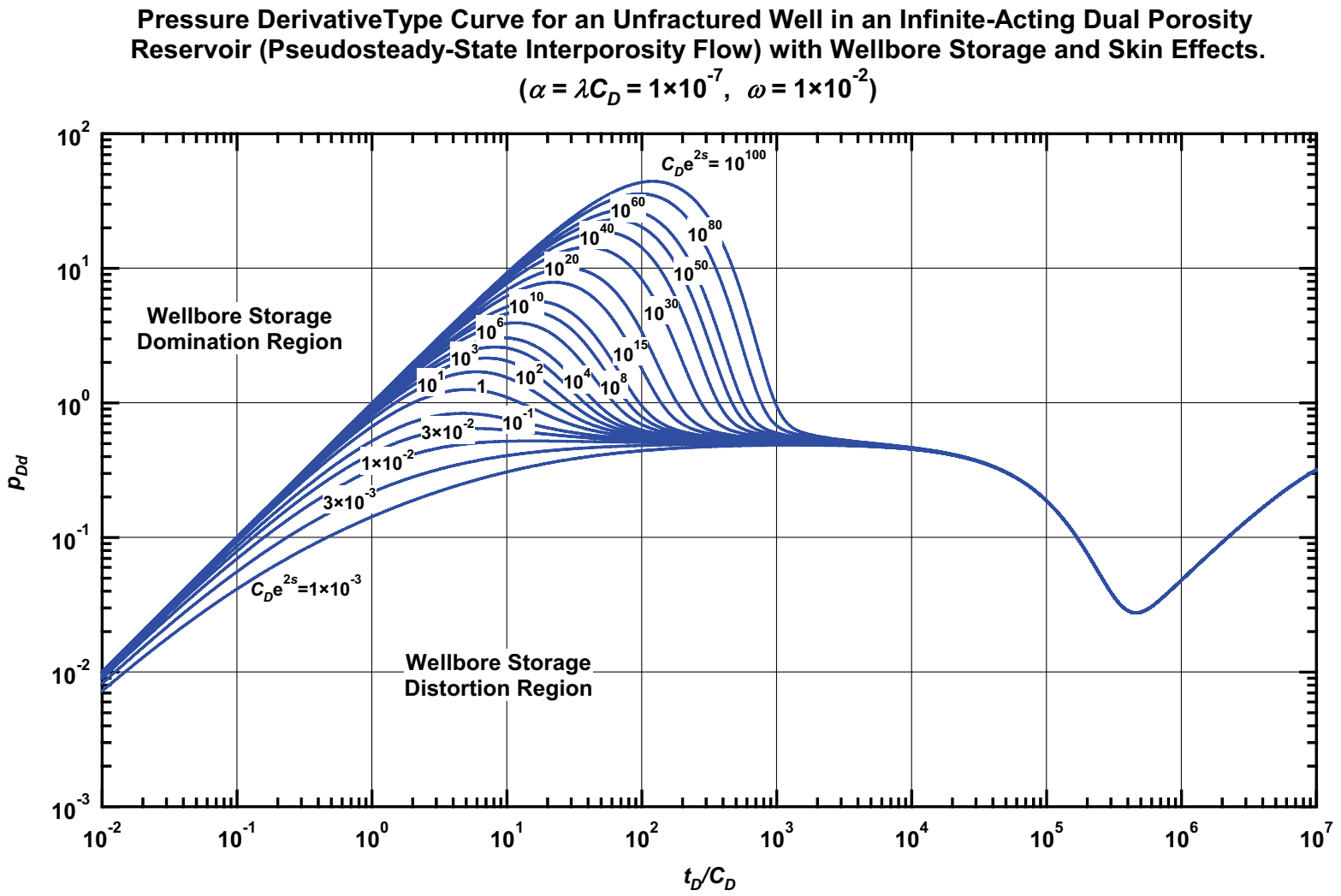

Figure C.47 — p_{Dd} vs. t_D/C_D — $\omega = 1\times10^{-2}$, $\alpha = \lambda C_D = 1\times10^{-7}$ (dual porosity case — includes wellbore storage and skin effects).

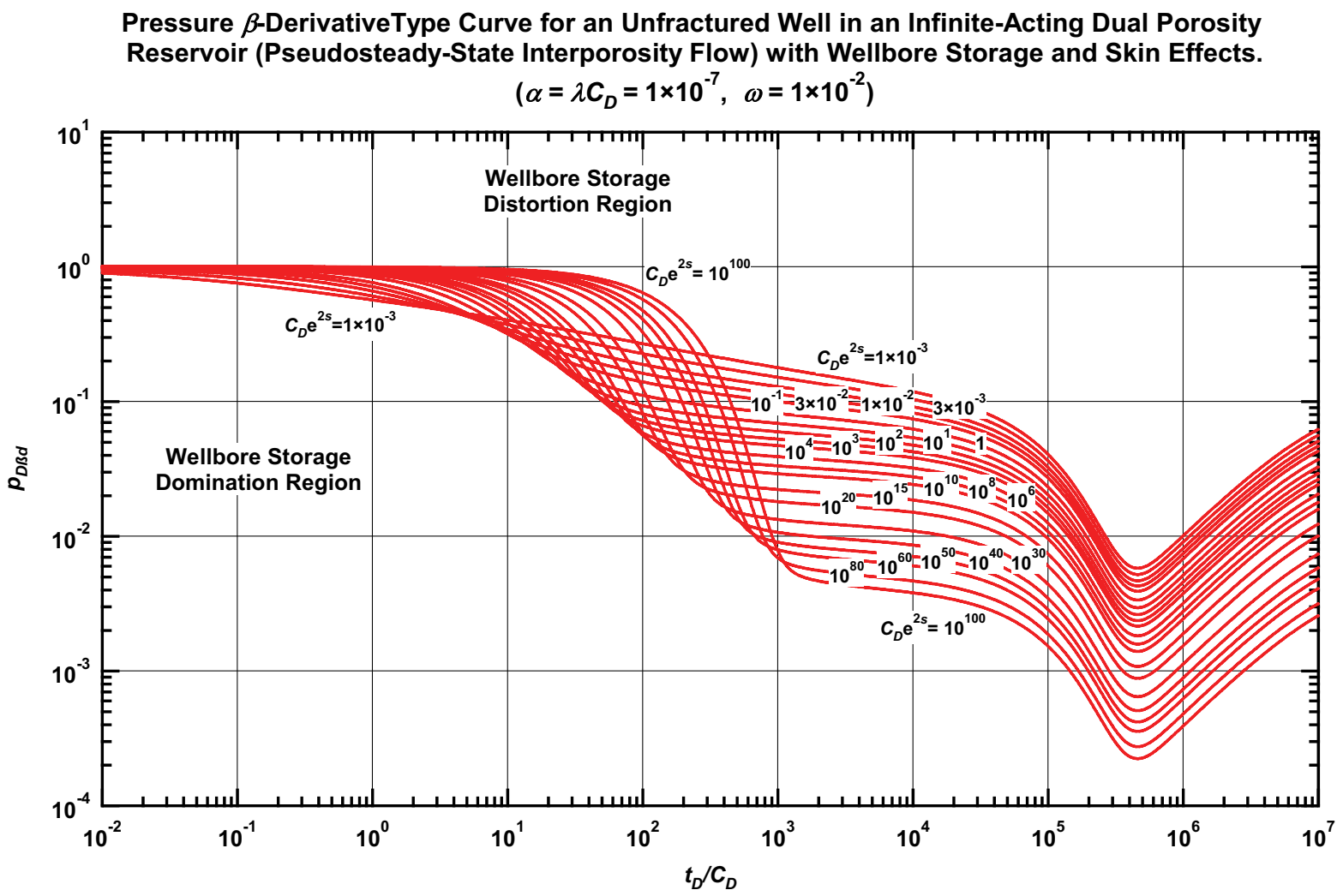

Figure C.48 — $p_{D\beta d}$ vs. t_D/C_D — $\omega = 1\times10^{-2}$, $\alpha = \lambda C_D = 1\times10^{-7}$ (dual porosity case — includes wellbore storage and skin effects).

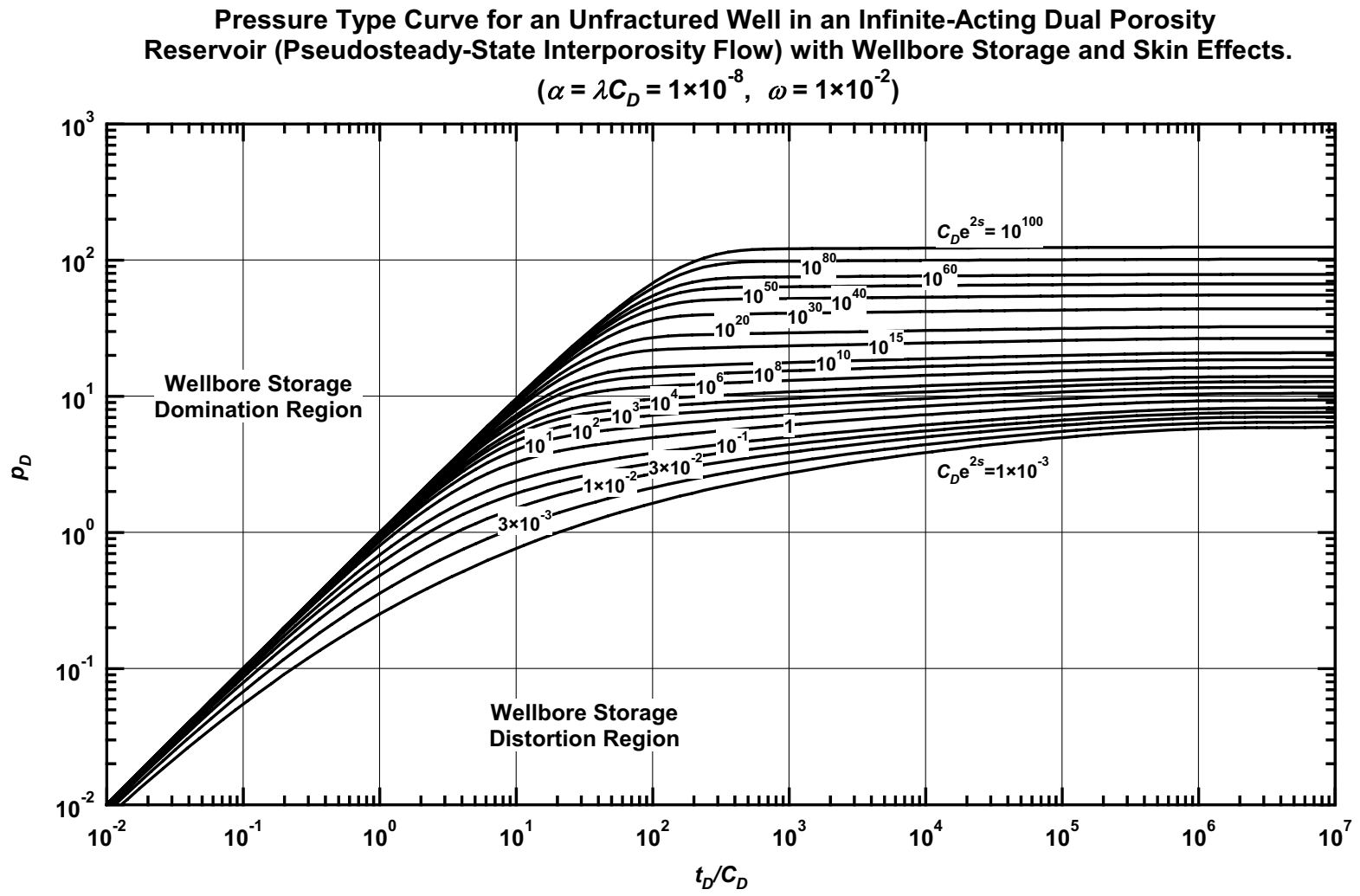

Figure C.49 — p_D vs. t_D/C_D — $\omega = 1\times10^{-2}$, $\alpha = \lambda C_D = 1\times10^{-8}$ (dual porosity case — includes wellbore storage and skin effects).

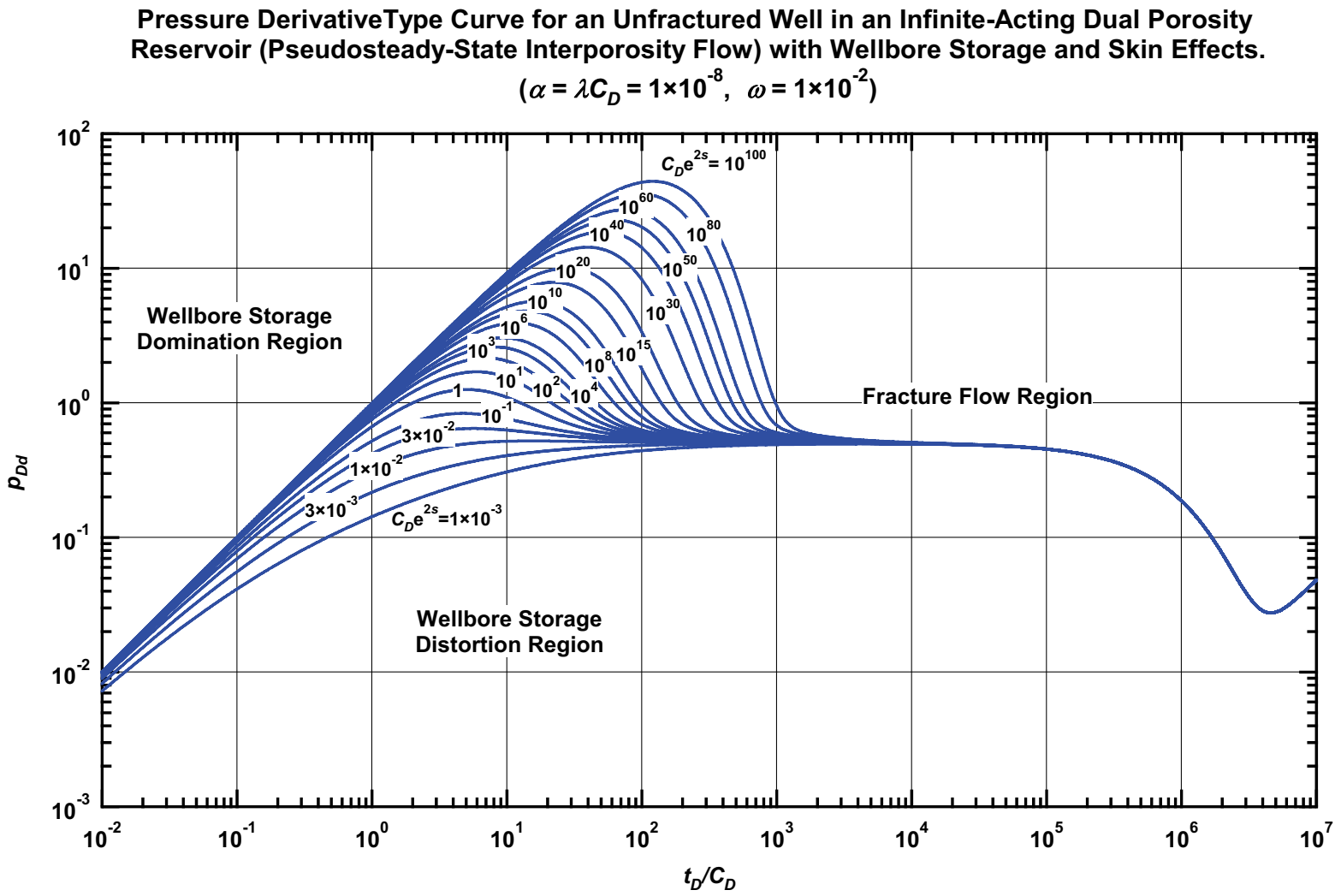

Figure C.50 — p_{Dd} vs. t_D/C_D — $\omega = 1\times10^{-2}$, $\alpha = \lambda C_D = 1\times10^{-8}$ (dual porosity case — includes wellbore storage and skin effects).

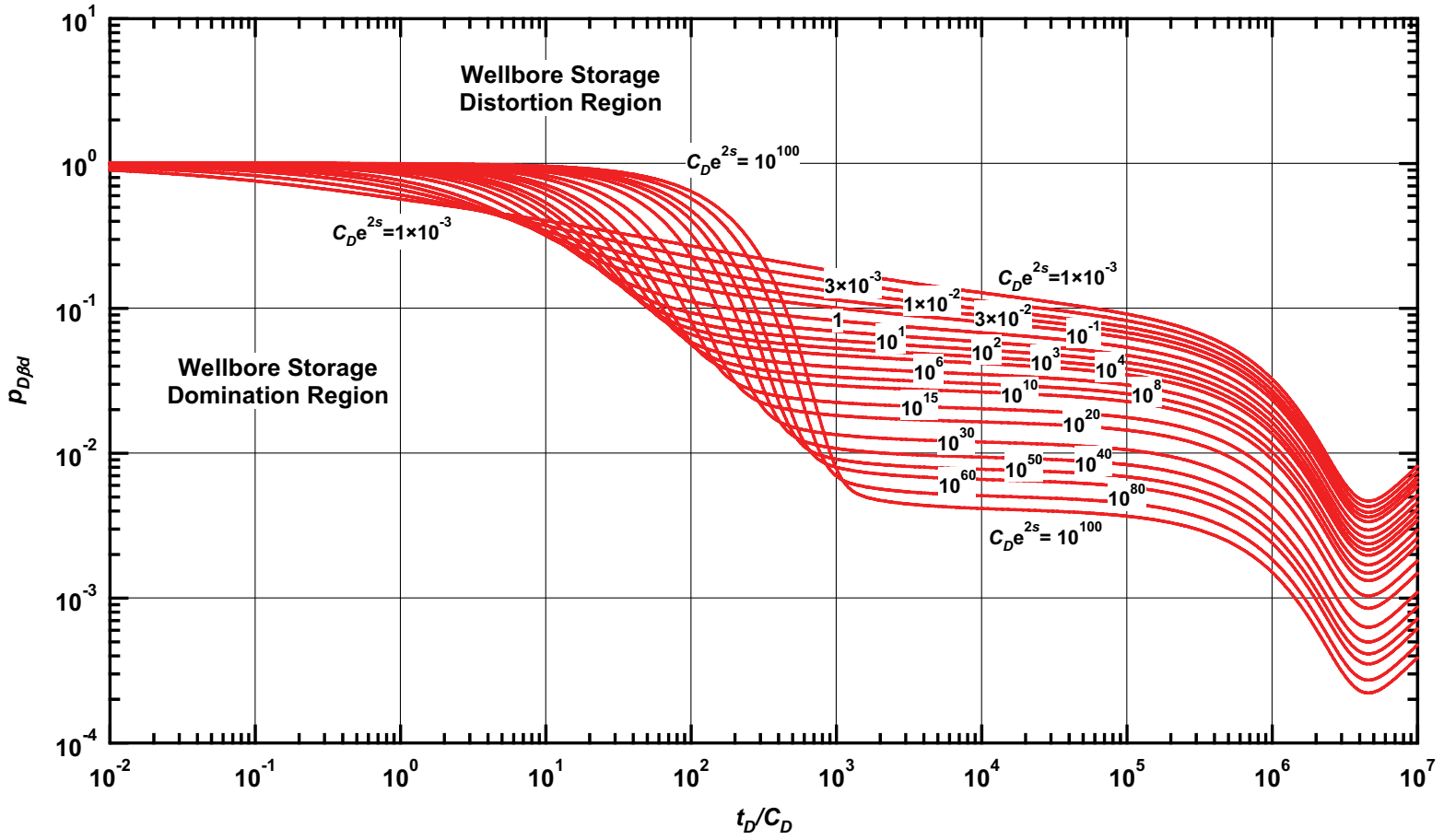

Figure C.51 — $p_{D\beta d}$ vs. t_D/C_D — $\omega = 1\times10^{-2}$, $\alpha = \lambda C_D = 1\times10^{-8}$ (dual porosity case — includes wellbore storage and skin effects).

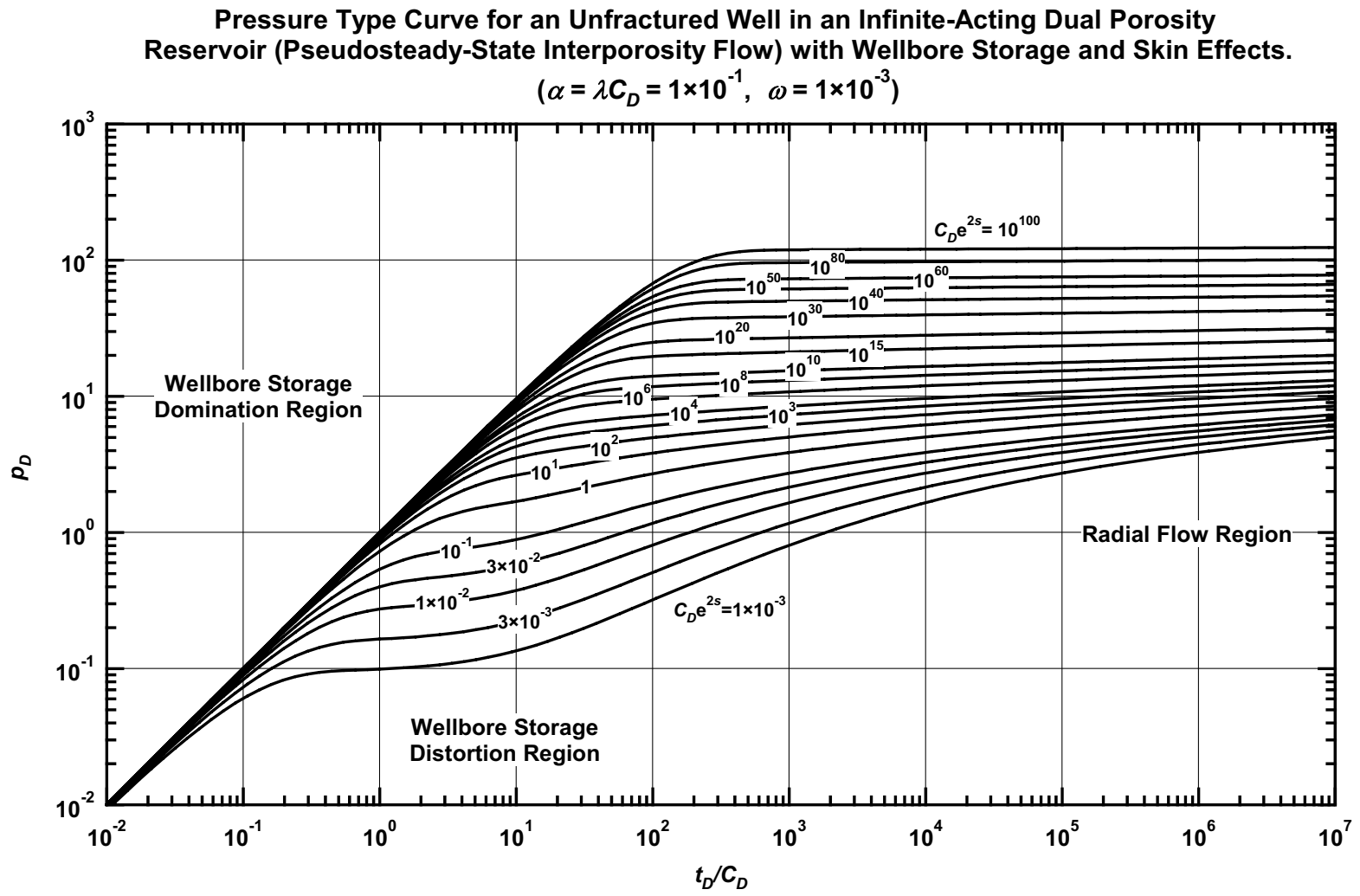

Figure C.52 — p_D vs. t_D/C_D — $\omega = 1\times10^{-3}$, $\alpha = \lambda C_D = 1\times10^{-1}$ (dual porosity case — includes wellbore storage and skin effects).

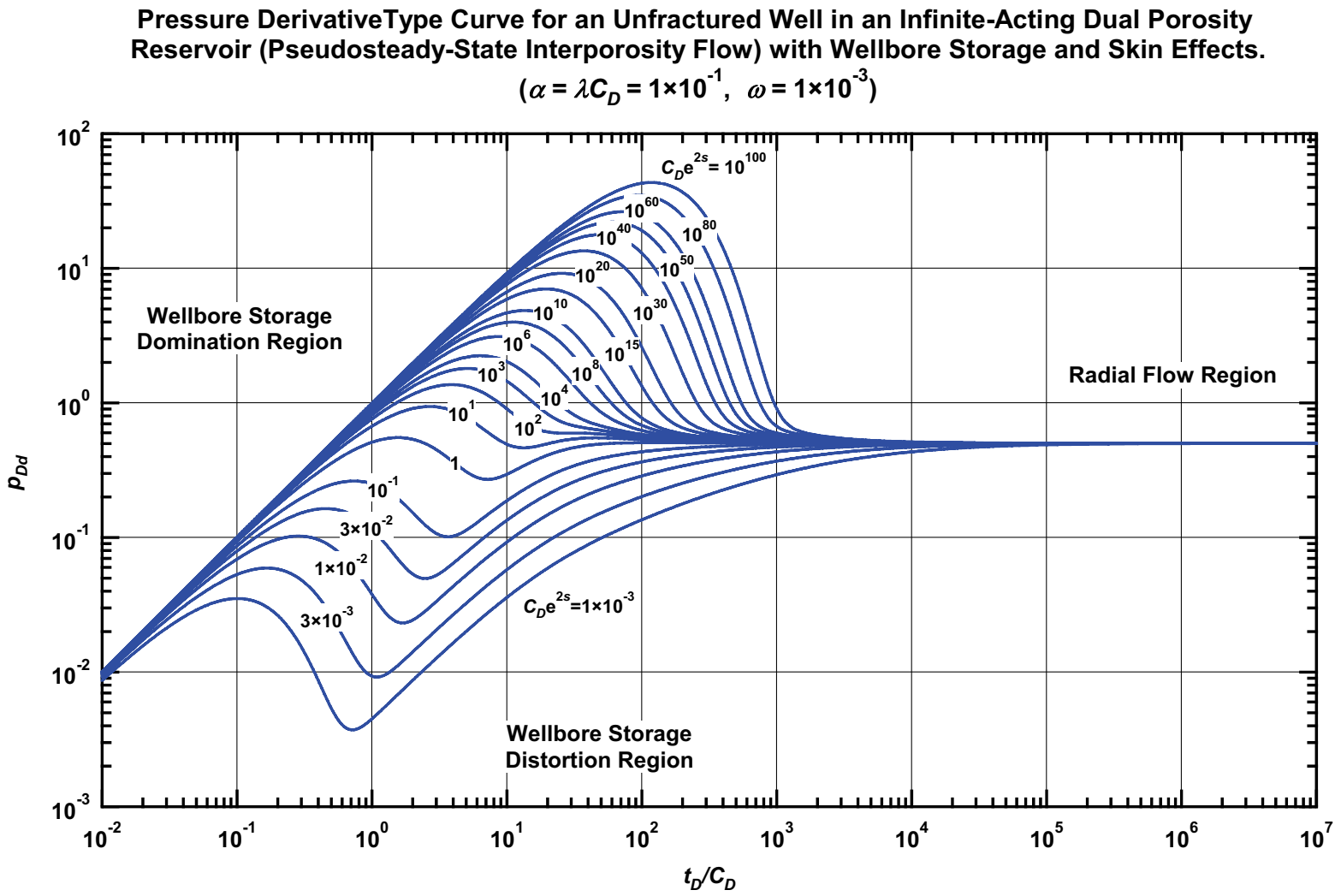

Figure C.53 — p_{Dd} vs. t_D/C_D — $\omega = 1\times10^{-3}$, $\alpha = \lambda C_D = 1\times10^{-1}$ (dual porosity case — includes wellbore storage and skin effects).

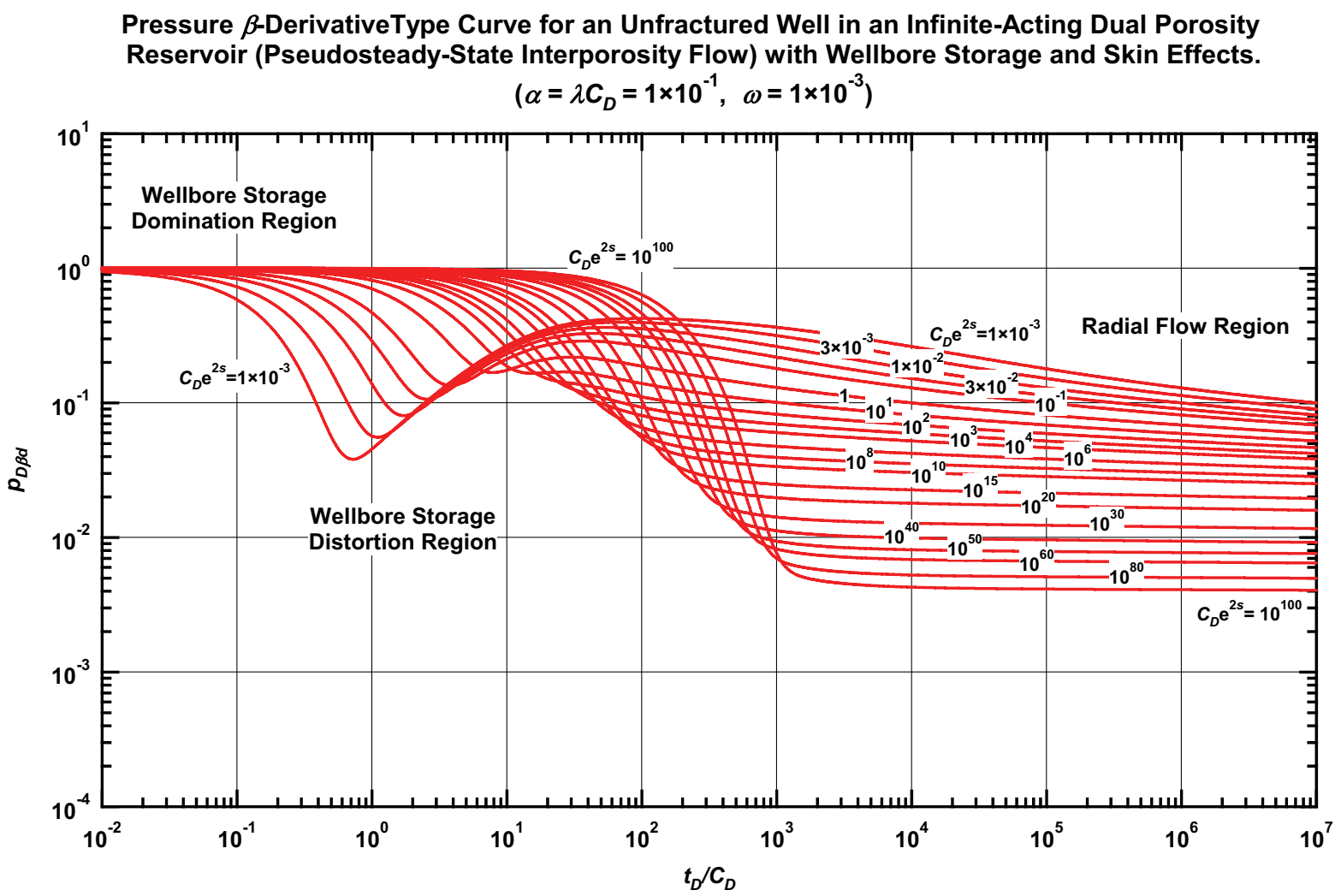

Figure C.54 — $p_{D\beta d}$ vs. t_D/C_D — $\omega = 1\times10^{-3}$, $\alpha = \lambda C_D = 1\times10^{-1}$ (dual porosity case — includes wellbore storage and skin effects).

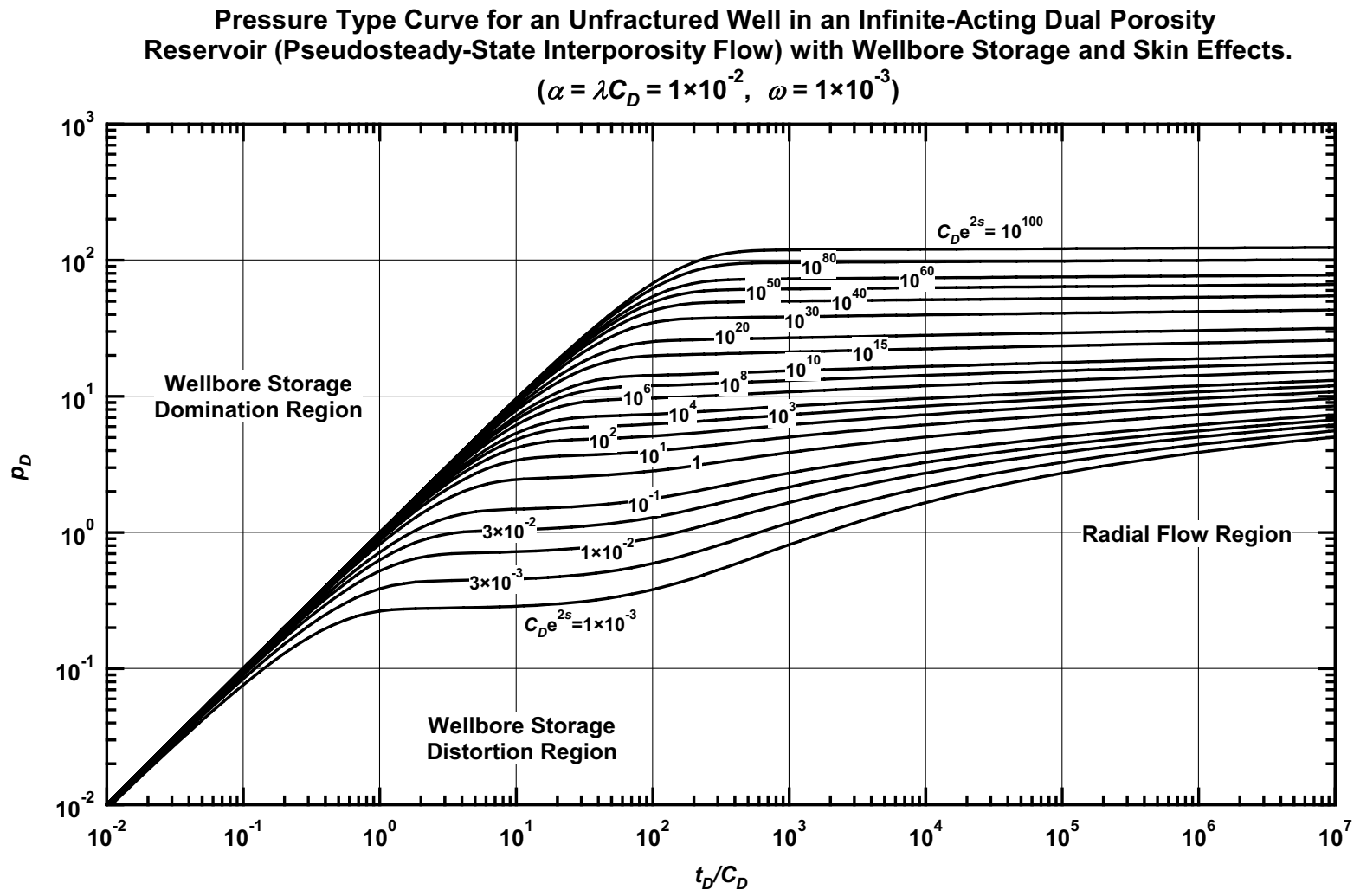

Figure C.55 — p_D vs. t_D/C_D — $\omega = 1\times10^{-3}$, $\alpha = \lambda C_D = 1\times10^{-2}$ (dual porosity case — includes wellbore storage and skin effects).

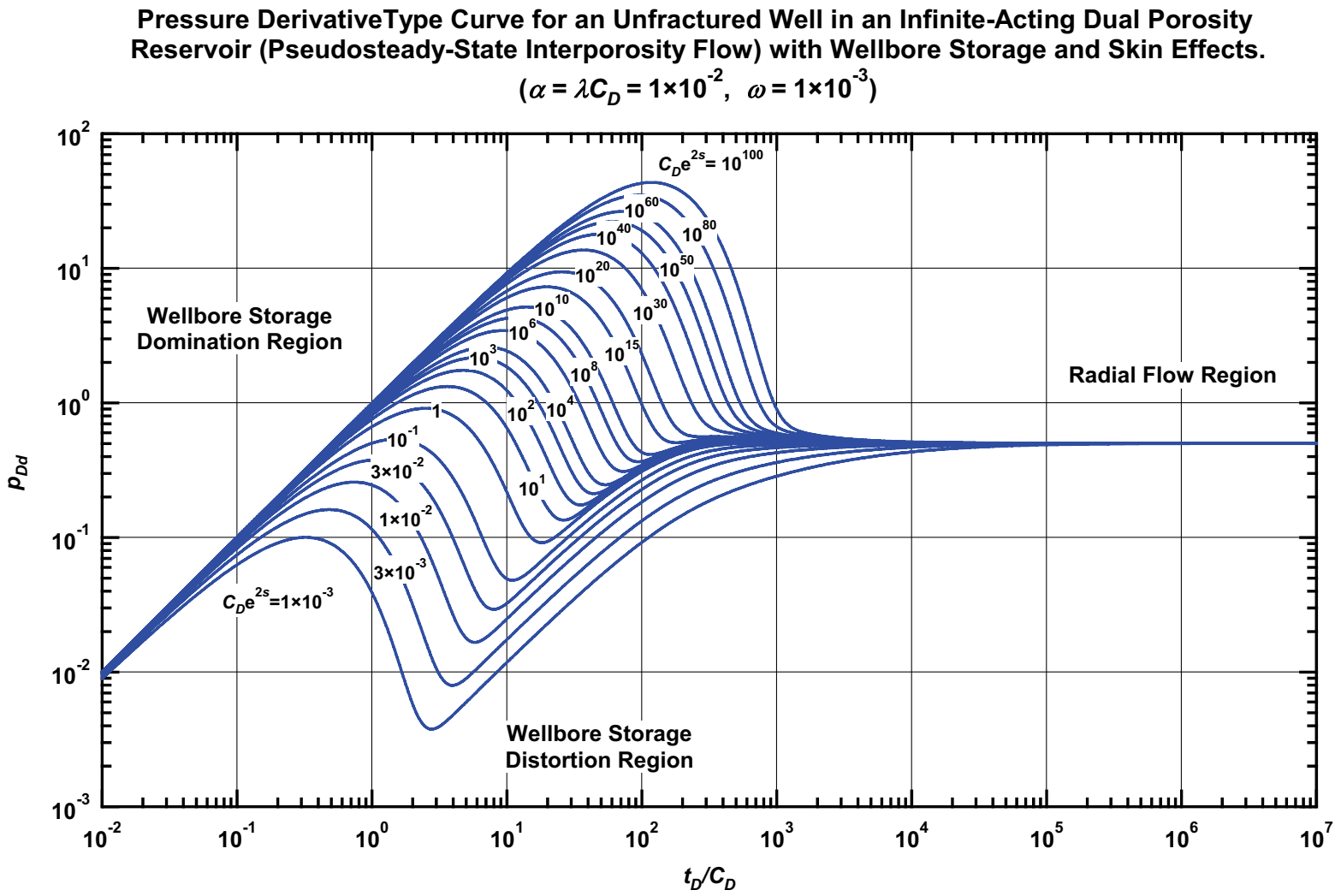

Figure C.56 — p_{Dd} vs. t_D/C_D — $\omega = 1\times10^{-3}$, $\alpha = \lambda C_D = 1\times10^{-2}$ (dual porosity case — includes wellbore storage and skin effects).

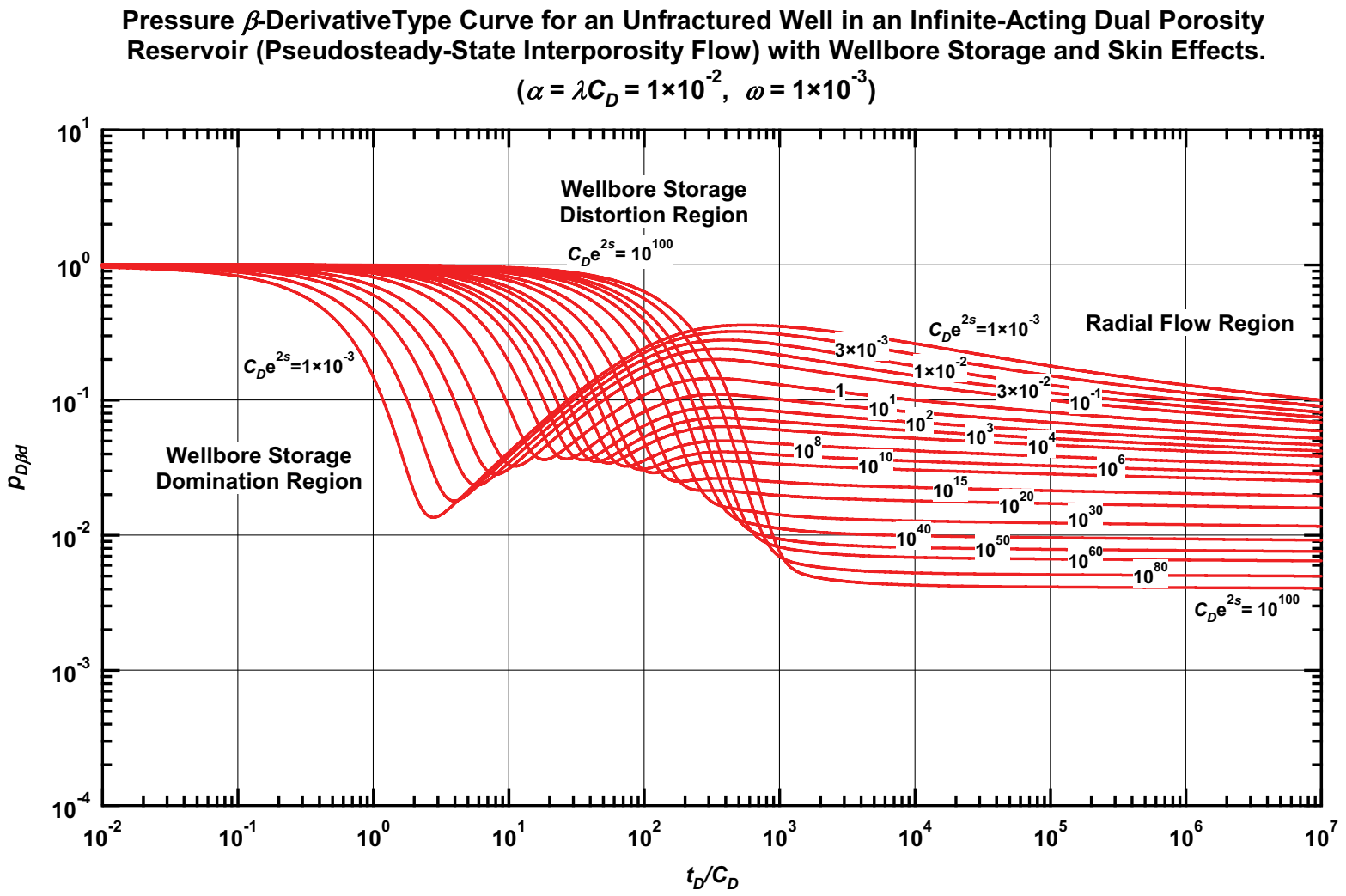

Figure C.57 — $p_{D\beta d}$ vs. t_D/C_D — $\omega = 1\times10^{-3}$, $\alpha = \lambda C_D = 1\times10^{-2}$ (dual porosity case — includes wellbore storage and skin effects).

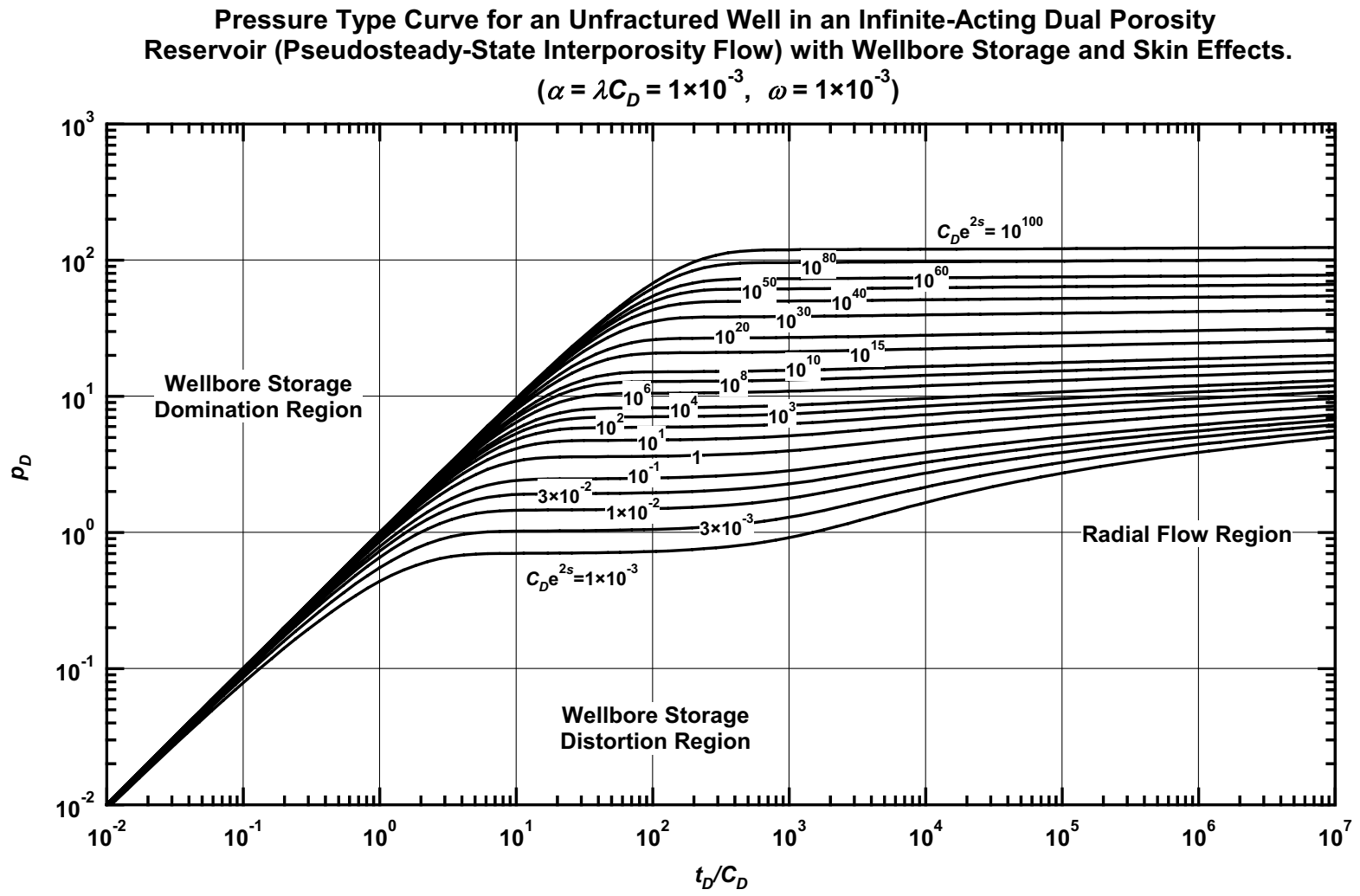

Figure C.58 — p_D vs. t_D/C_D — $\omega = 1\times10^{-3}$, $\alpha = \lambda C_D = 1\times10^{-3}$ (dual porosity case — includes wellbore storage and skin effects).

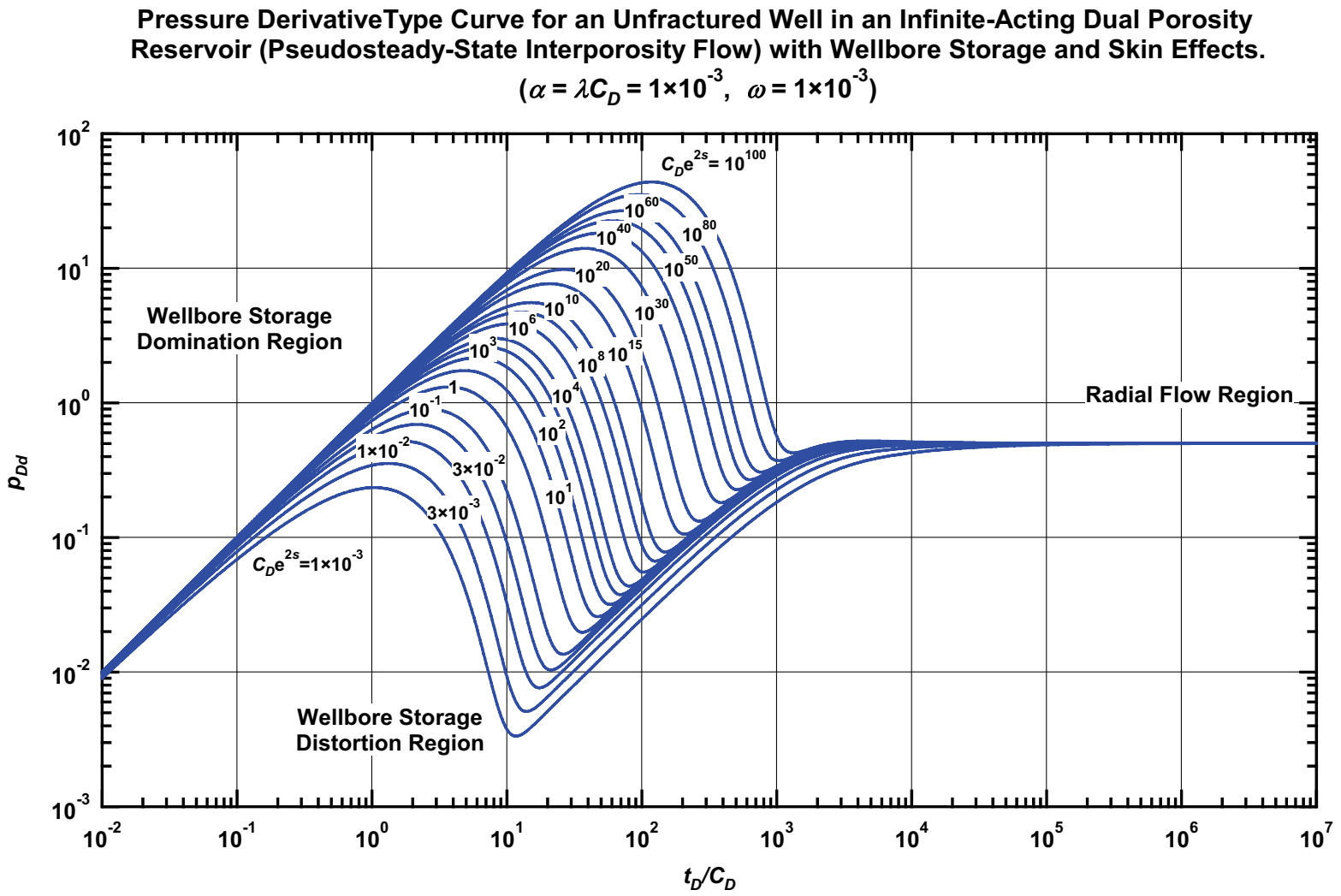

Figure C.59 — p_{Dd} vs. t_D/C_D — $\omega = 1\times10^{-3}$, $\alpha = \lambda C_D = 1\times10^{-3}$ (dual porosity case — includes wellbore storage and skin effects).

Pressure β-DerivativeType Curve for an Unfractured Well in an Infinite-Acting Dual Porosity Reservoir (Pseudosteady-State Interporosity Flow) with Wellbore Storage and Skin Effects.
($\alpha = \lambda C_D = 1\times10^{-3}$, $\omega = 1\times10^{-3}$)

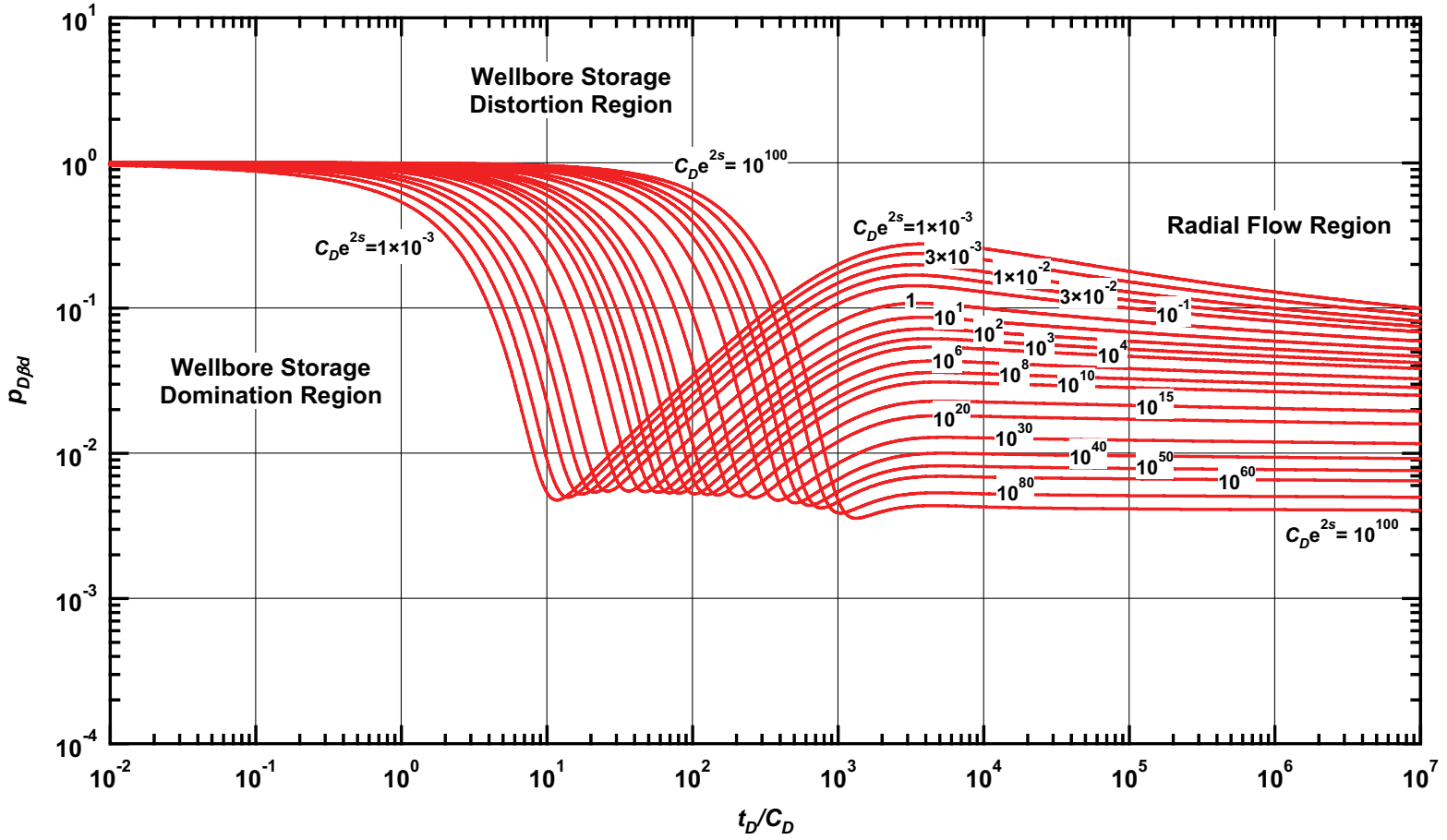

Figure C.60 — $p_{D\beta d}$ vs. t_D/C_D — $\omega = 1\times10^{-3}$, $\alpha = \lambda C_D = 1\times10^{-3}$ (dual porosity case — includes wellbore storage and skin effects).

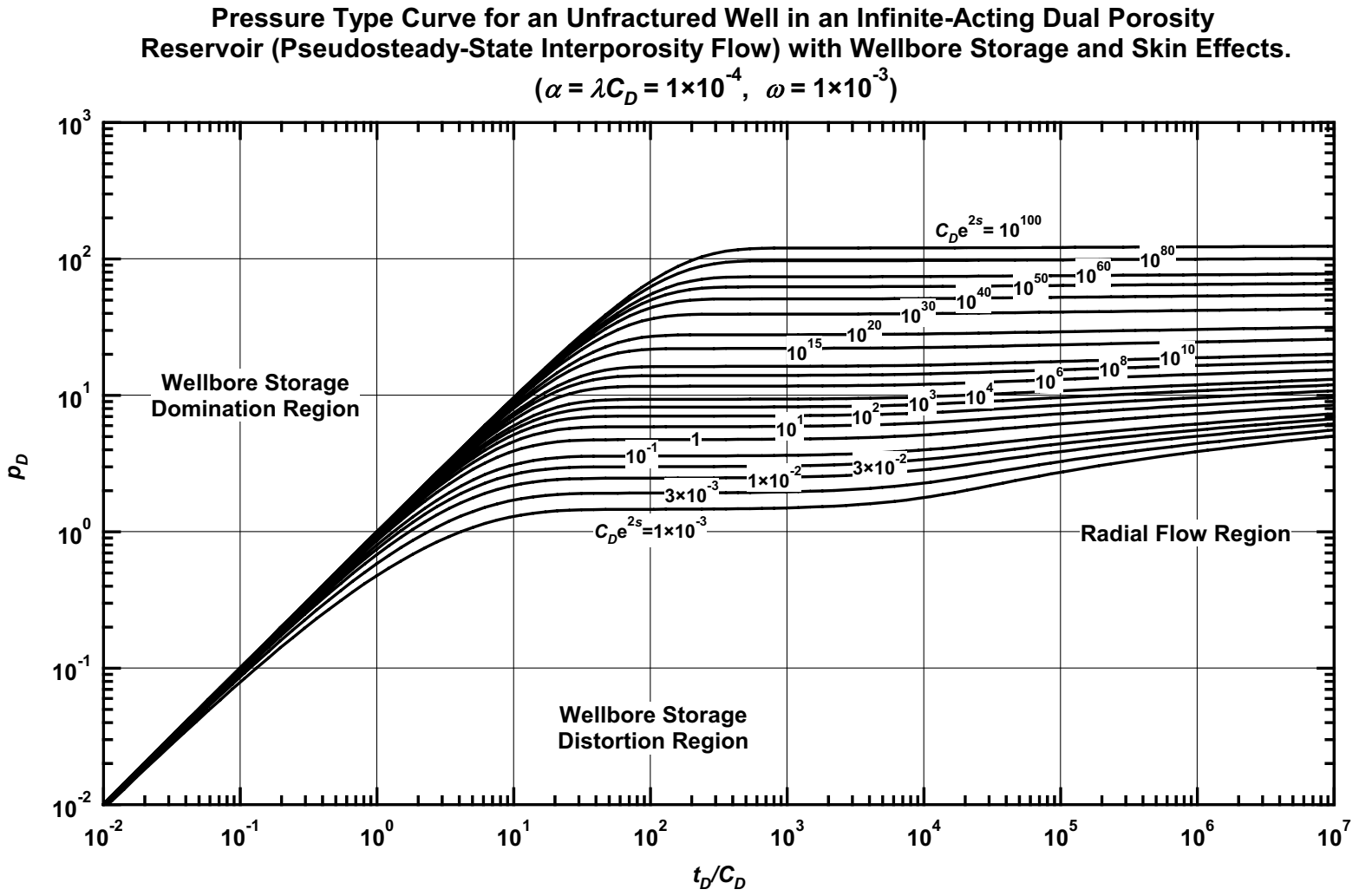

Figure C.61 — p_D vs. t_D/C_D — $\omega = 1\times10^{-3}$, $\alpha = \lambda C_D = 1\times10^{-4}$ (dual porosity case — includes wellbore storage and skin effects).

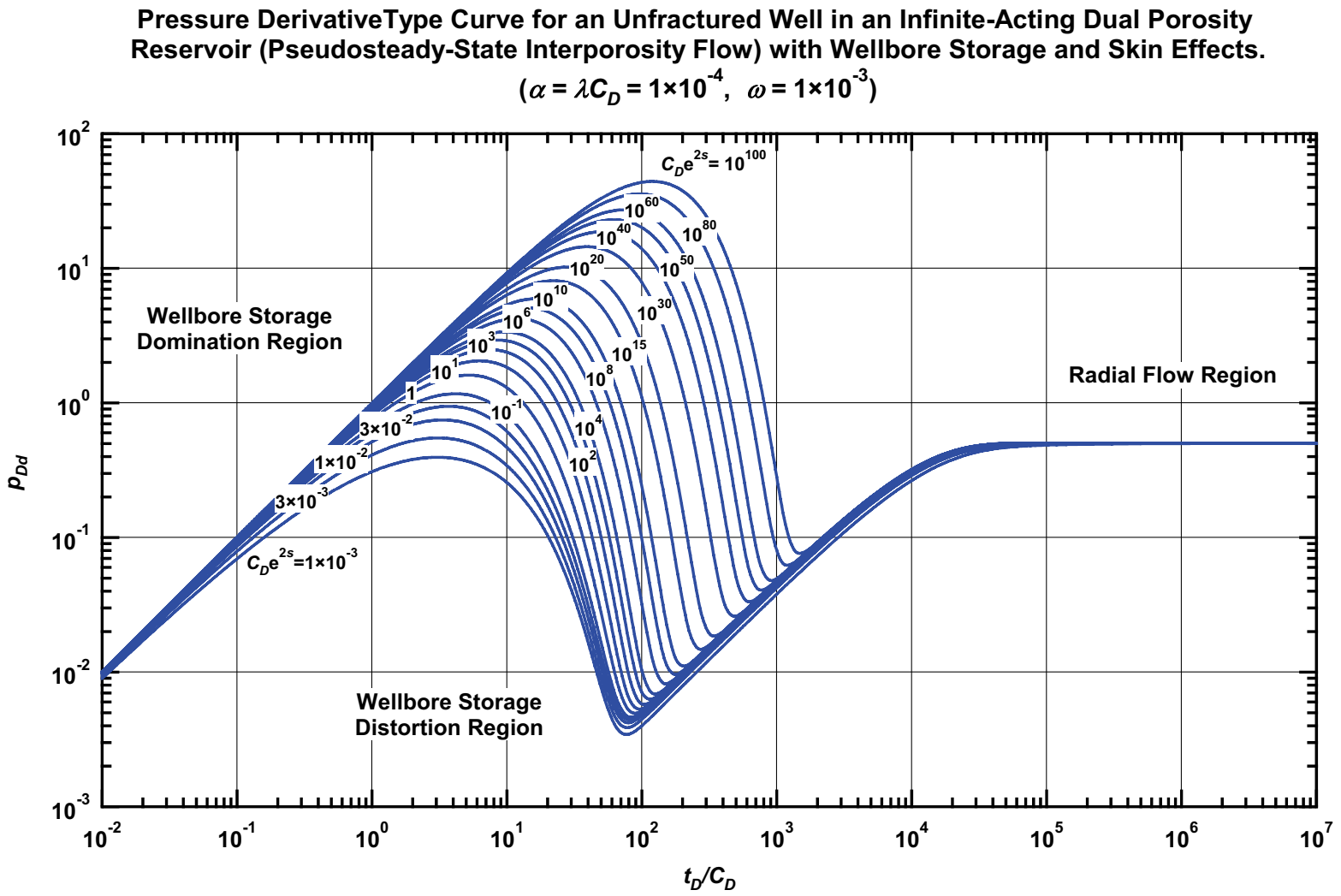

Figure C.62 — p_{Dd} vs. t_D/C_D — $\omega = 1\times10^{-3}$, $\alpha = \lambda C_D = 1\times10^{-4}$ (dual porosity case — includes wellbore storage and skin effects).

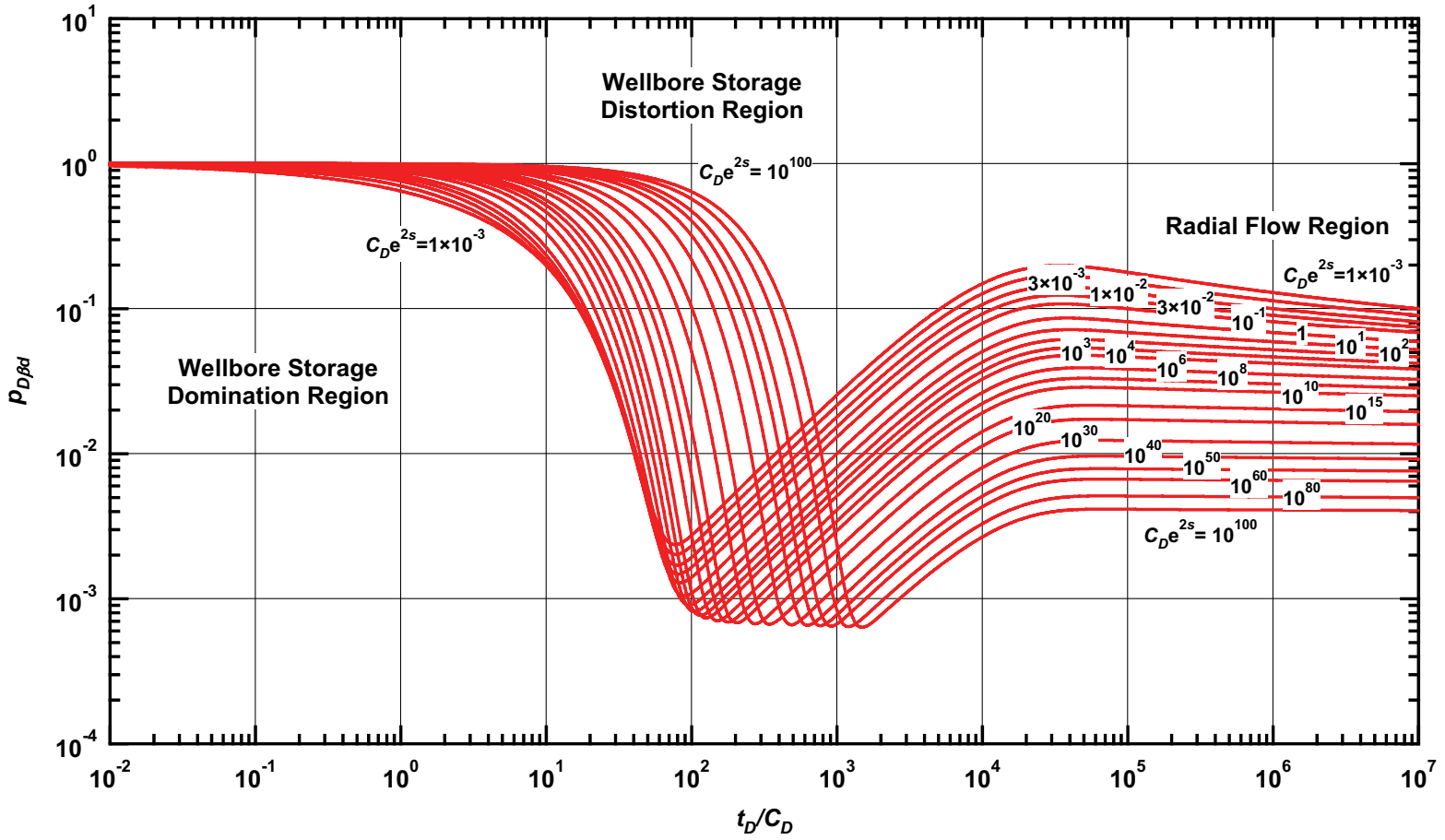

Figure C.63 — $p_{D\beta d}$ vs. t_D/C_D — $\omega = 1\times10^{-3}$, $\alpha = \lambda C_D = 1\times10^{-4}$ (dual porosity case — includes wellbore storage and skin effects).

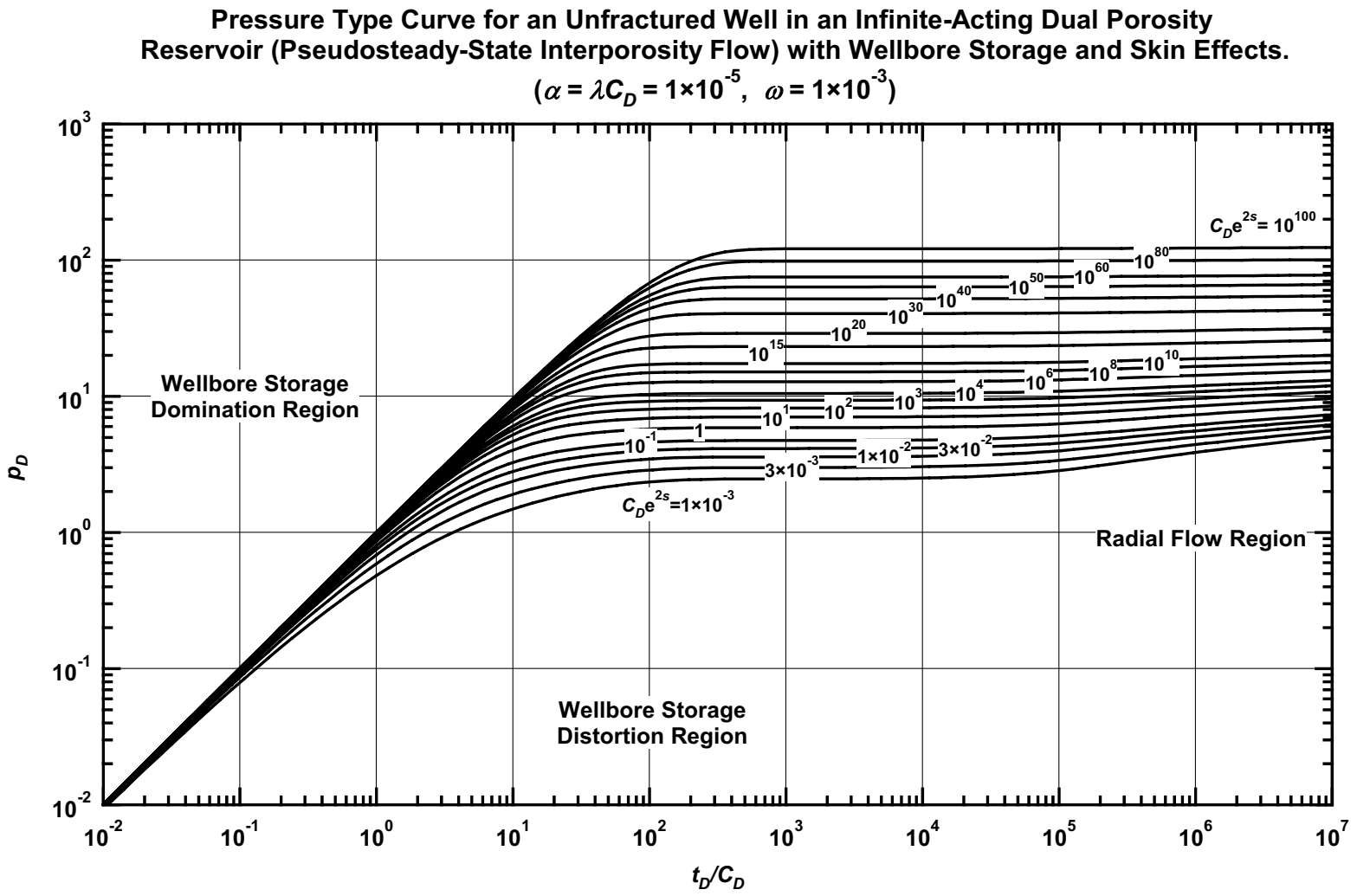

Figure C.64 — p_D vs. t_D/C_D — $\omega = 1\times10^{-3}$, $\alpha = \lambda C_D = 1\times10^{-5}$ (dual porosity case — includes wellbore storage and skin effects).

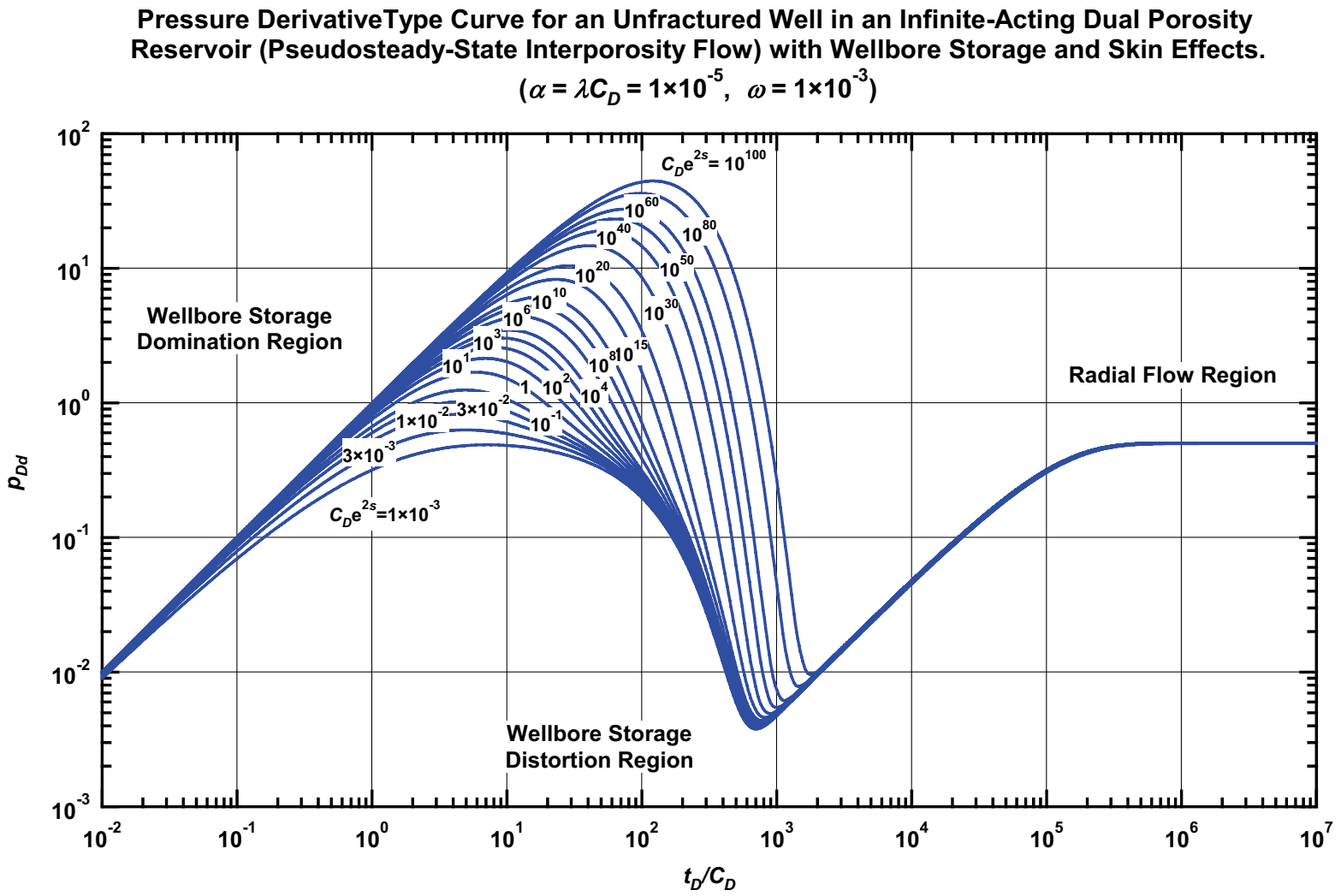

Figure C.65 — p_{Dd} vs. t_D/C_D — $\omega = 1\times10^{-3}$, $\alpha = \lambda C_D = 1\times10^{-5}$ (dual porosity case — includes wellbore storage and skin effects).

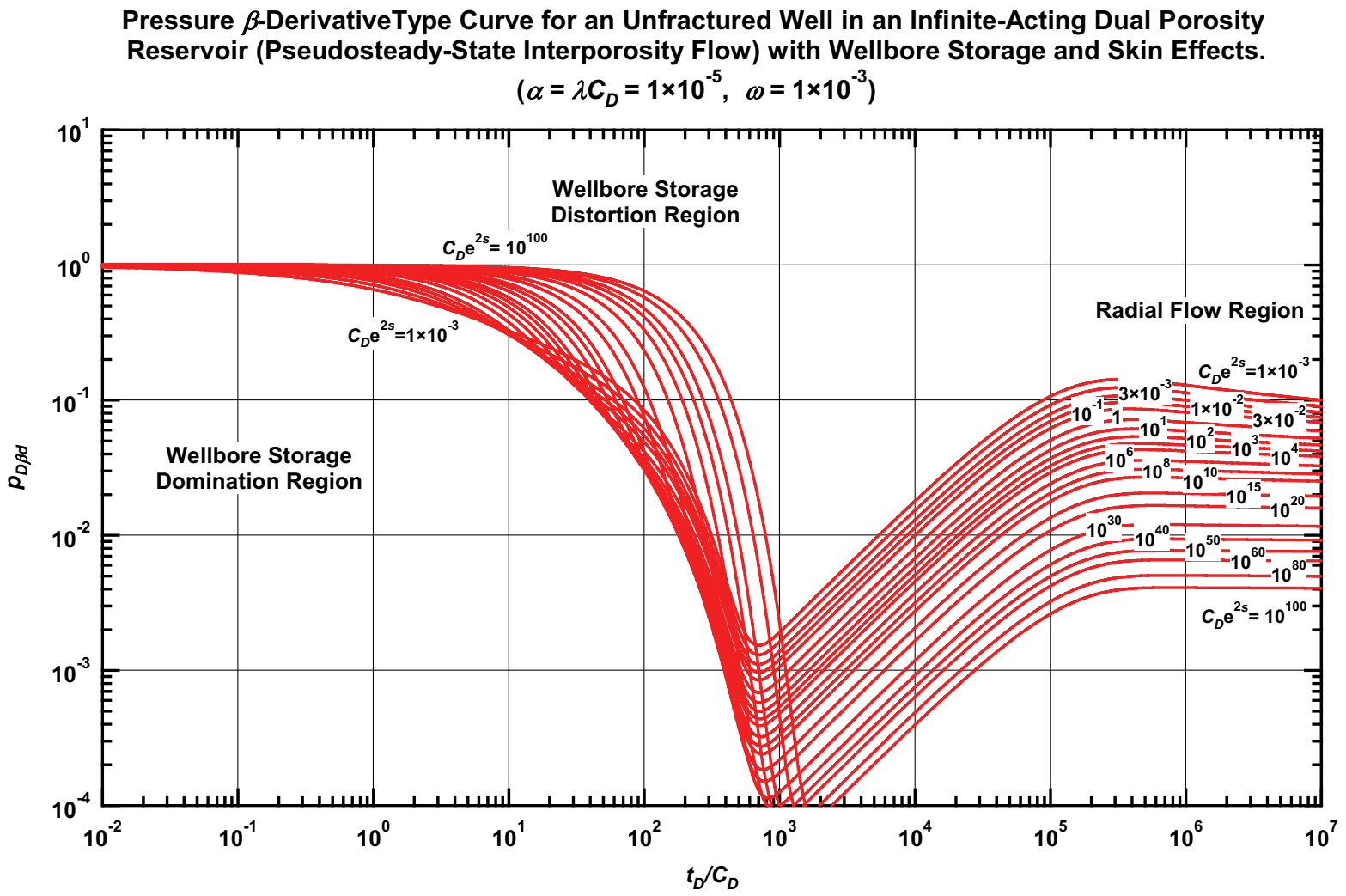

Figure C.66 — $p_{D\beta d}$ vs. t_D/C_D — $\omega = 1\times10^{-3}$, $\alpha = \lambda C_D = 1\times10^{-5}$ (dual porosity case — includes wellbore storage and skin effects).

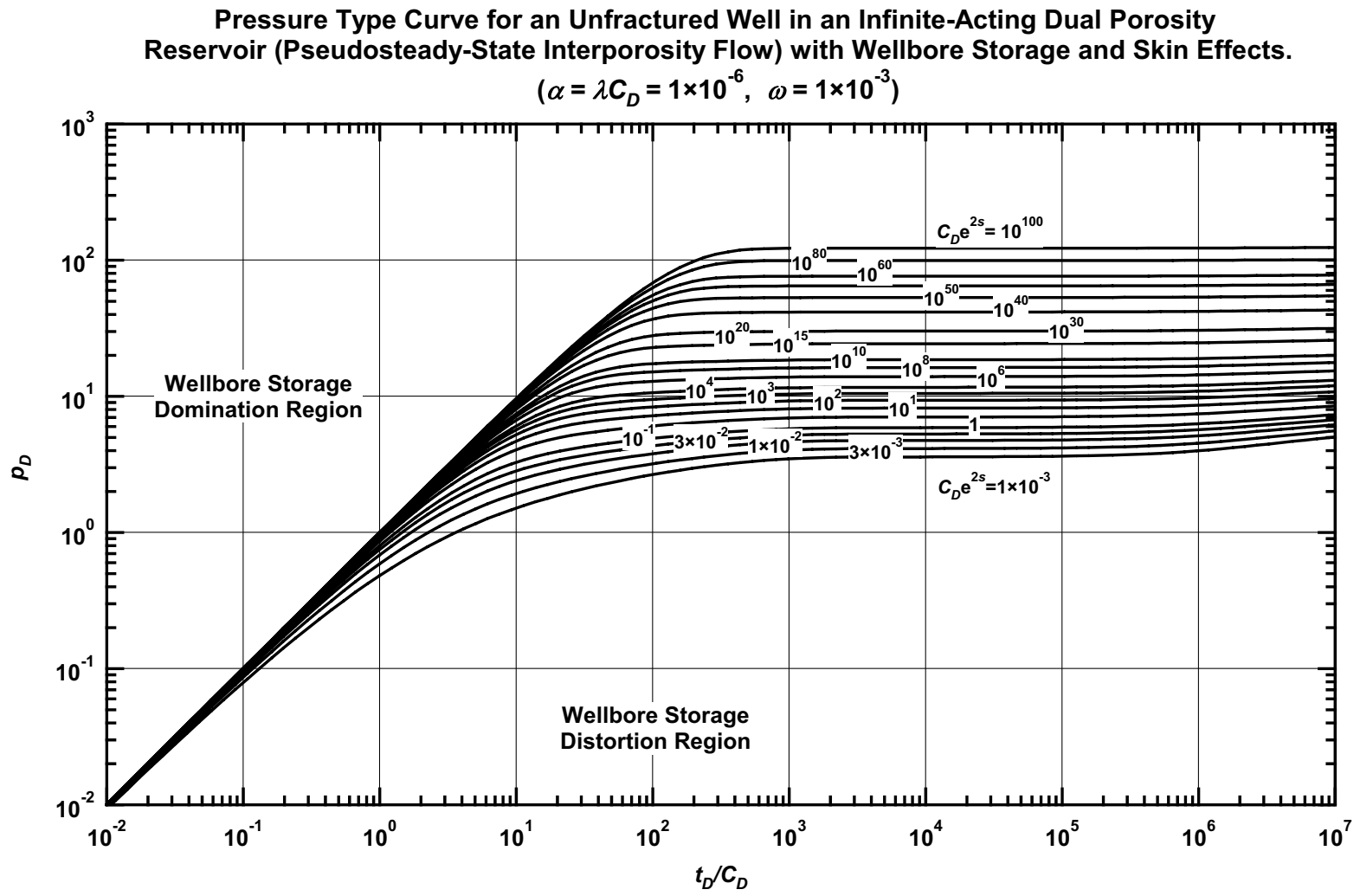

Figure C.67 — p_D vs. t_D/C_D — $\omega = 1\times10^{-3}$, $\alpha = \lambda C_D = 1\times10^{-6}$ (dual porosity case — includes wellbore storage and skin effects).

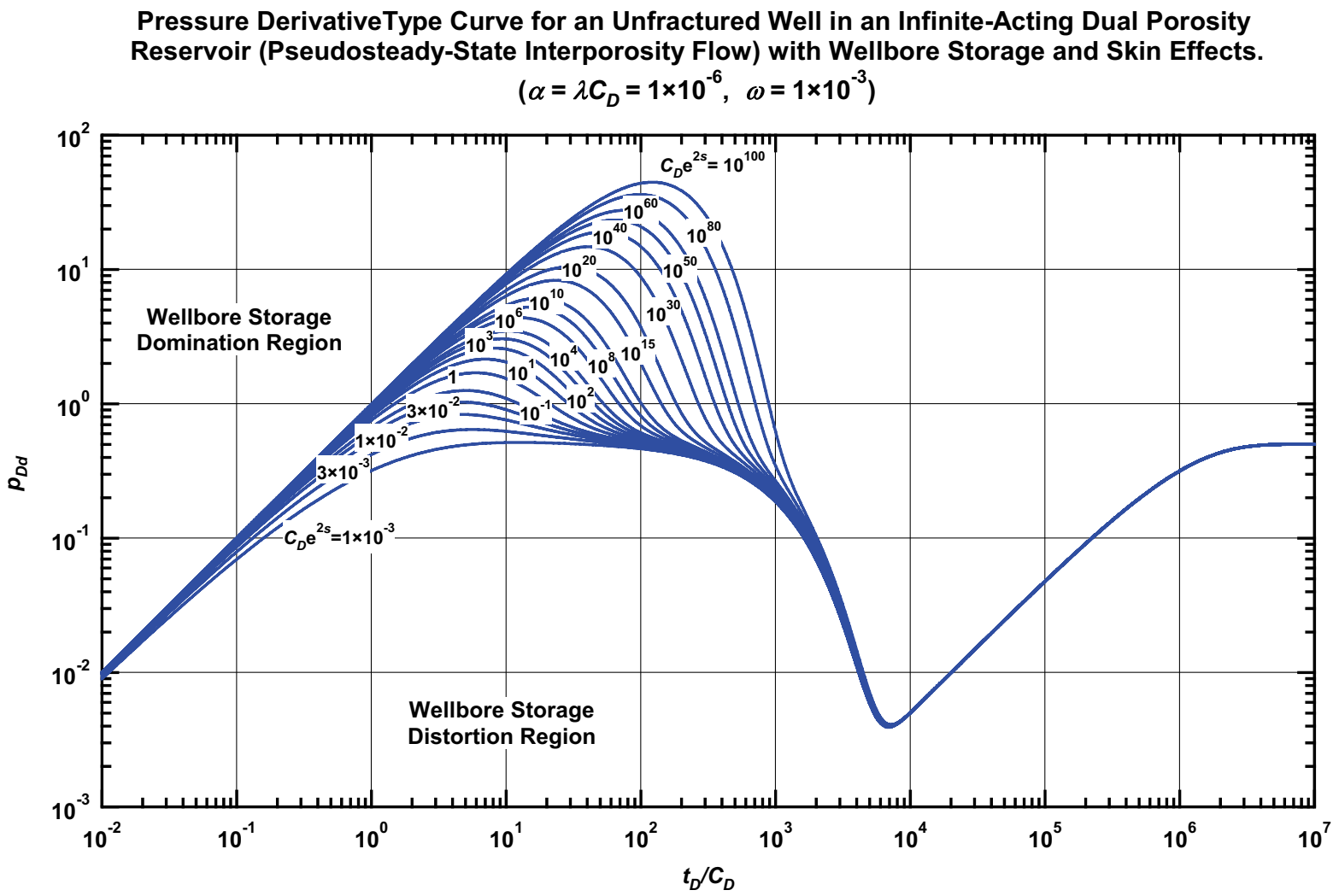

Figure C.68 — p_{Dd} vs. t_D/C_D — $\omega = 1\times10^{-3}$, $\alpha = \lambda C_D = 1\times10^{-6}$ (dual porosity case — includes wellbore storage and skin effects).

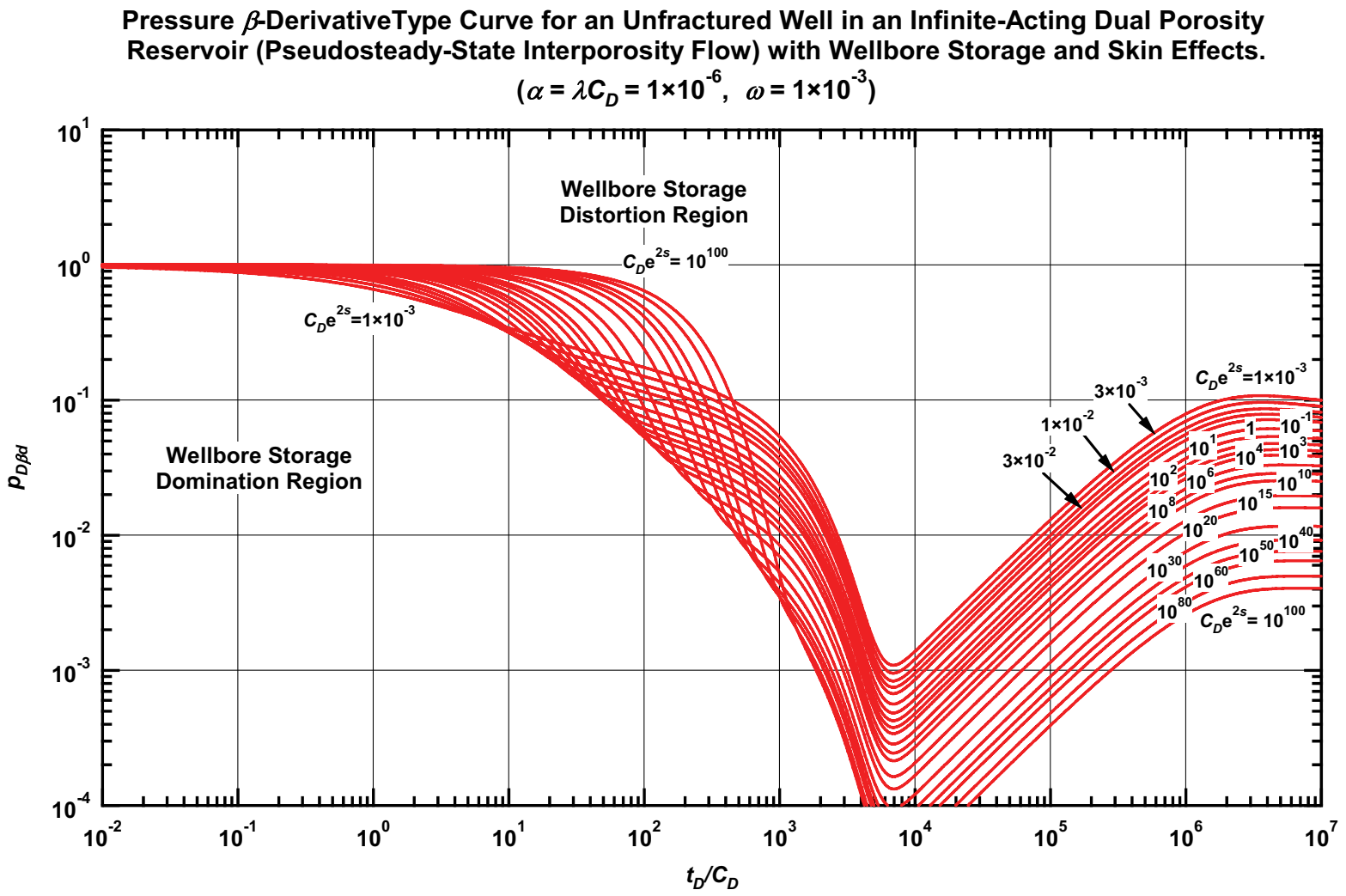

Figure C.69 — $p_{D\beta d}$ vs. t_D/C_D — $\omega = 1\times10^{-3}$, $\alpha = \lambda C_D = 1\times10^{-6}$ (dual porosity case — includes wellbore storage and skin effects).

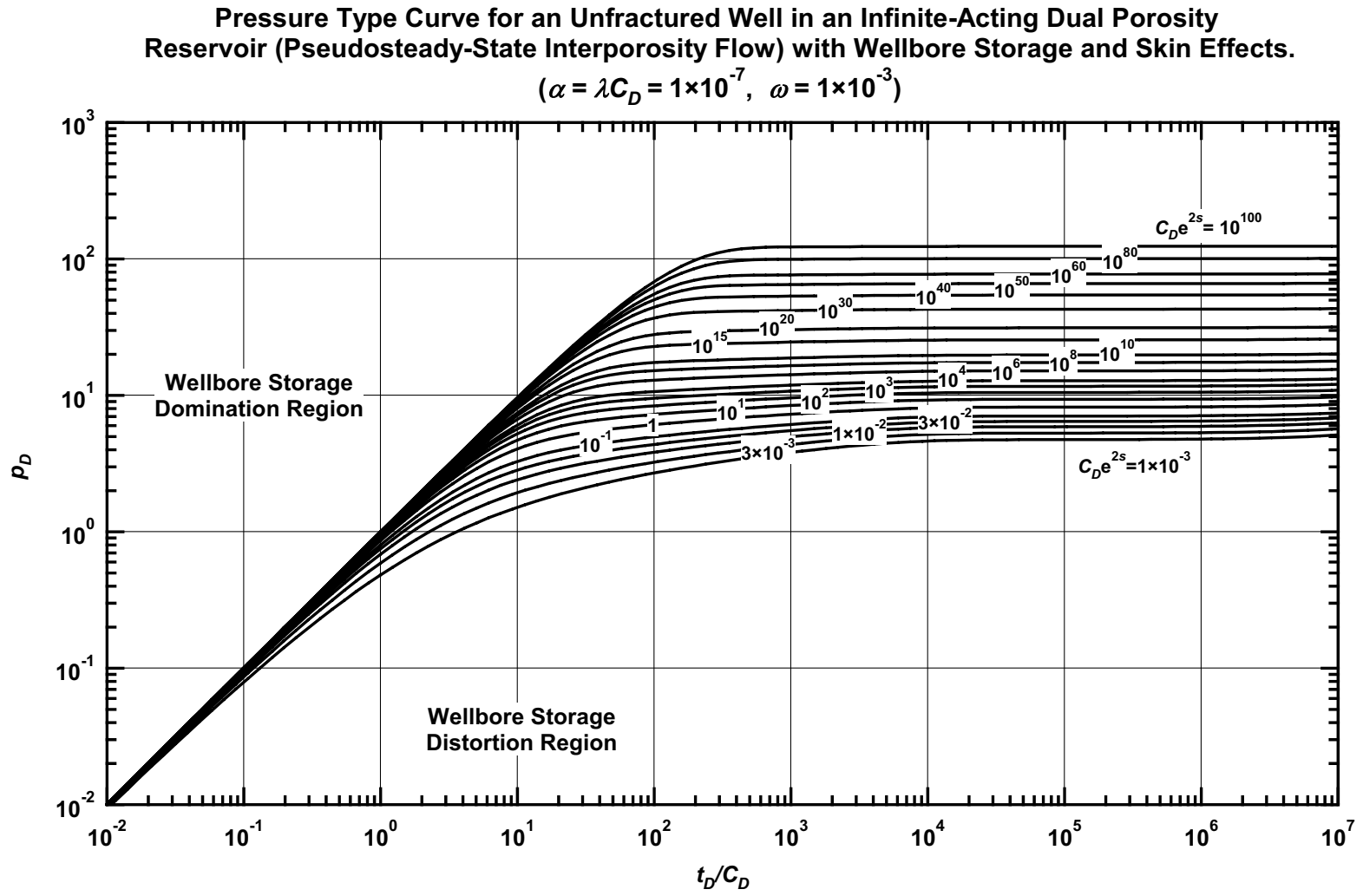

Figure C.70 — p_D vs. t_D/C_D — $\omega = 1\times10^{-3}$, $\alpha = \lambda C_D = 1\times10^{-7}$ (dual porosity case — includes wellbore storage and skin effects).

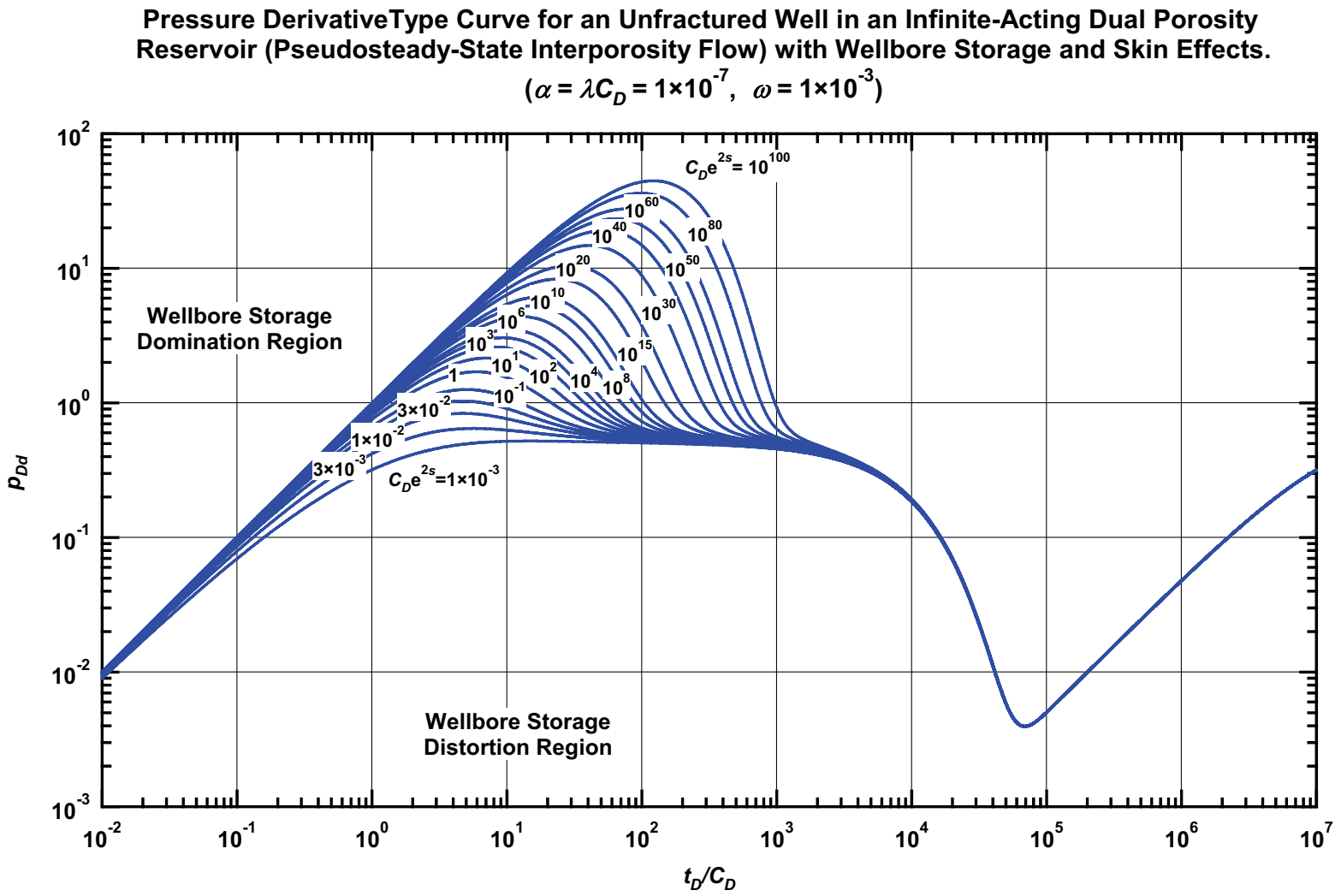

Figure C.71 — p_{Dd} vs. t_D/C_D — $\omega = 1\times10^{-3}$, $\alpha = \lambda C_D = 1\times10^{-7}$ (dual porosity case — includes wellbore storage and skin effects).

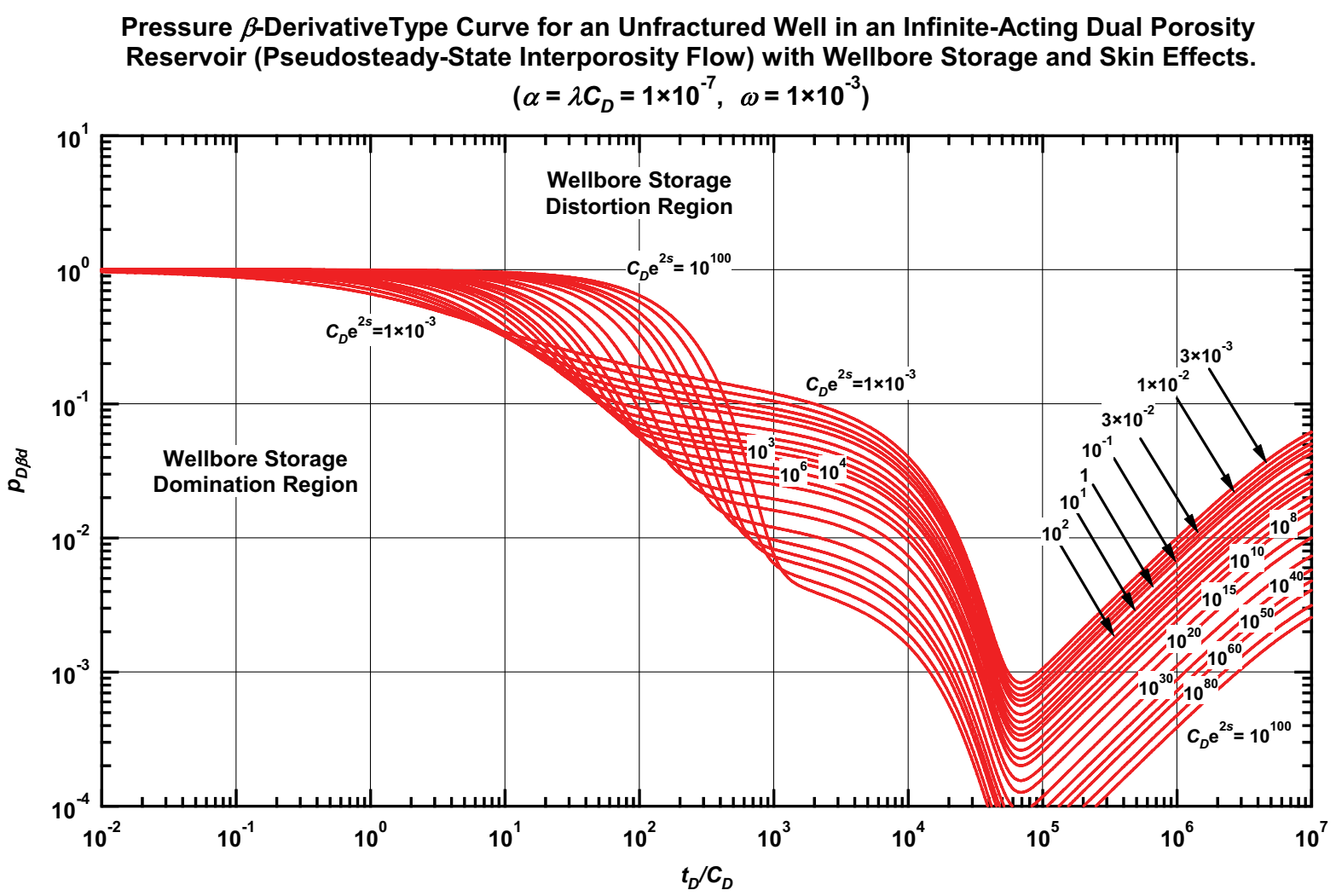

Figure C.72 — $p_{D\beta d}$ vs. t_D/C_D — $\omega = 1\times10^{-3}$, $\alpha = \lambda C_D = 1\times10^{-7}$ (dual porosity case — includes wellbore storage and skin effects).

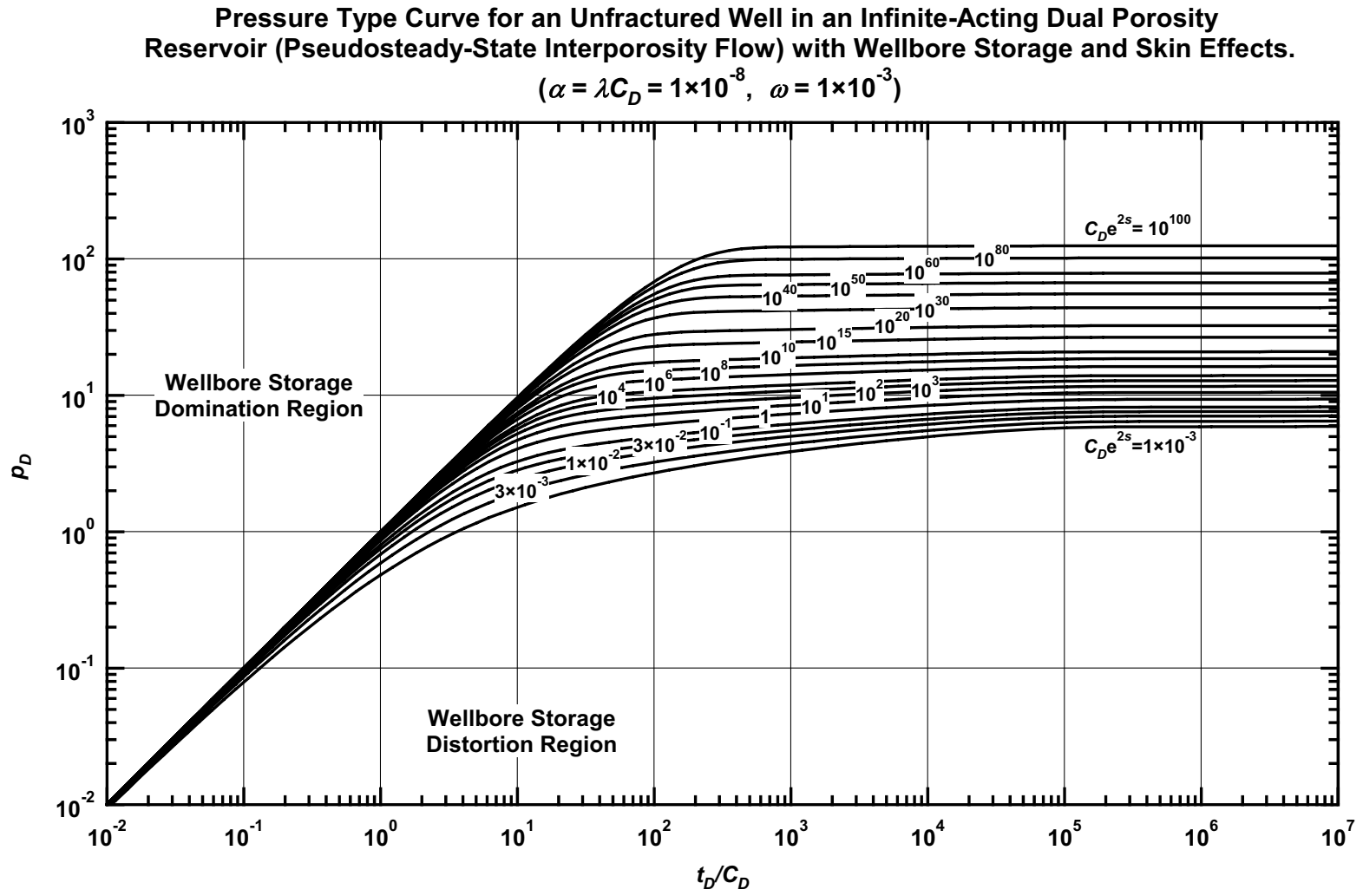

Figure C.73 — p_D vs. t_D/C_D — $\omega = 1\times10^{-3}$, $\alpha = \lambda C_D = 1\times10^{-8}$ (dual porosity case — includes wellbore storage and skin effects).

Pressure DerivativeType Curve for an Unfractured Well in an Infinite-Acting Dual Porosity Reservoir (Pseudosteady-State Interporosity Flow) with Wellbore Storage and Skin Effects.

($\alpha = \lambda C_D = 1\times10^{-8}$, $\omega = 1\times10^{-3}$)

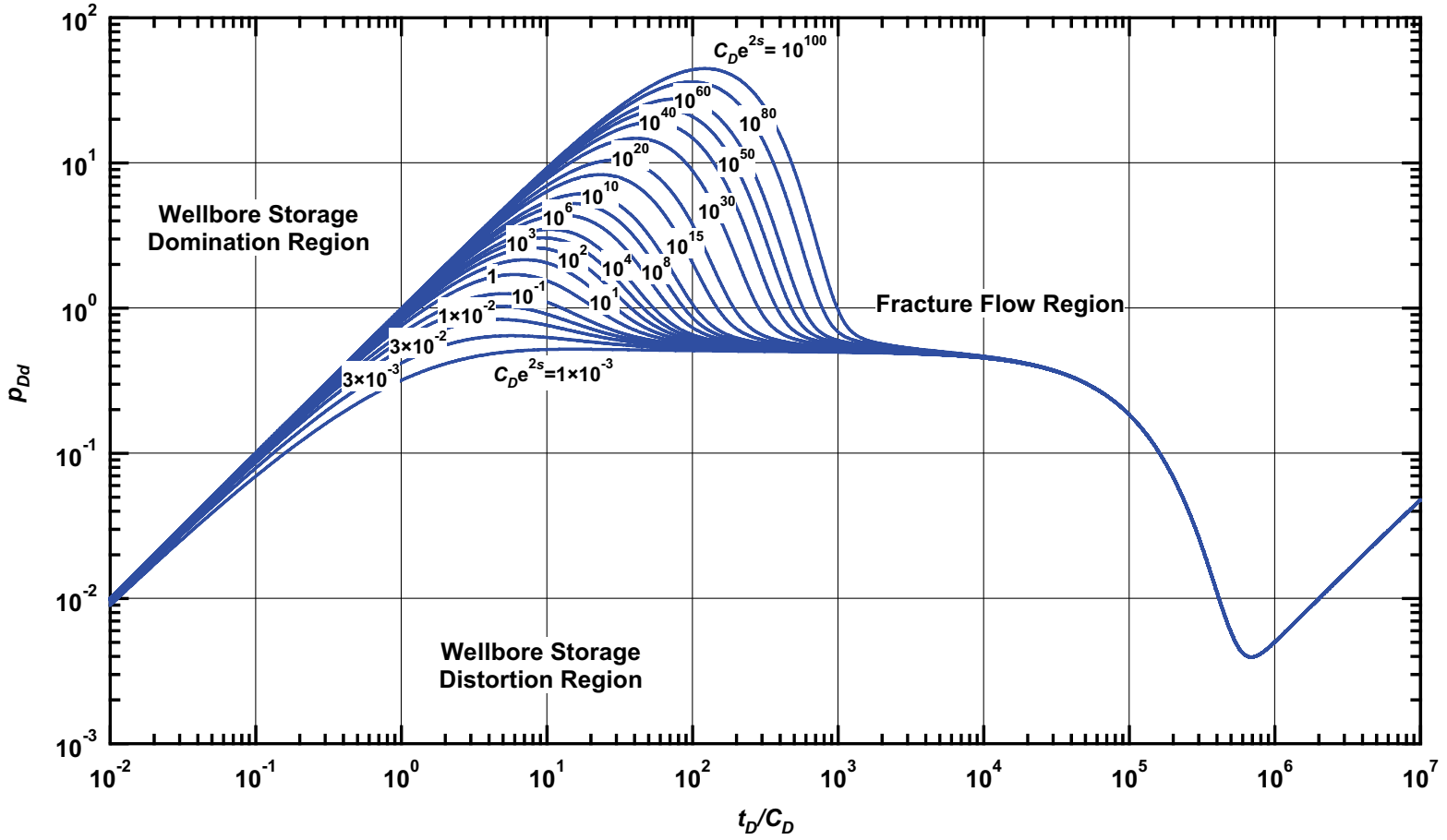

Figure C.74 — p_{Dd} vs. t_D/C_D — $\omega = 1\times10^{-3}$, $\alpha = \lambda C_D = 1\times10^{-8}$ (dual porosity case — includes wellbore storage and skin effects).

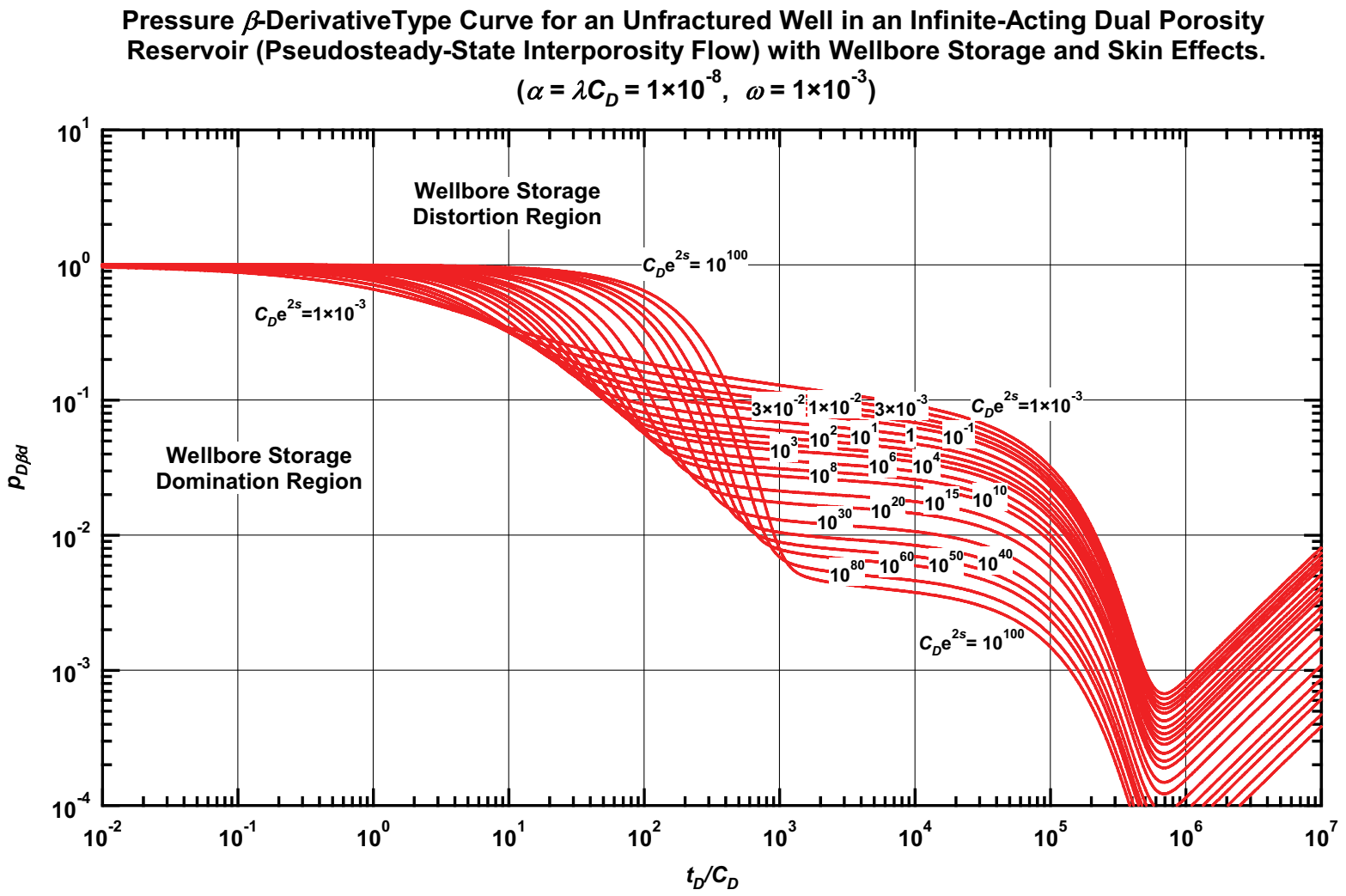

Figure C.75 — $p_{D\beta d}$ **vs.** t_D/C_D **—** $\omega = 1\times10^{-3}$, $\alpha = \lambda C_D = 1\times10^{-8}$ **(dual porosity case — includes wellbore storage and skin effects).**

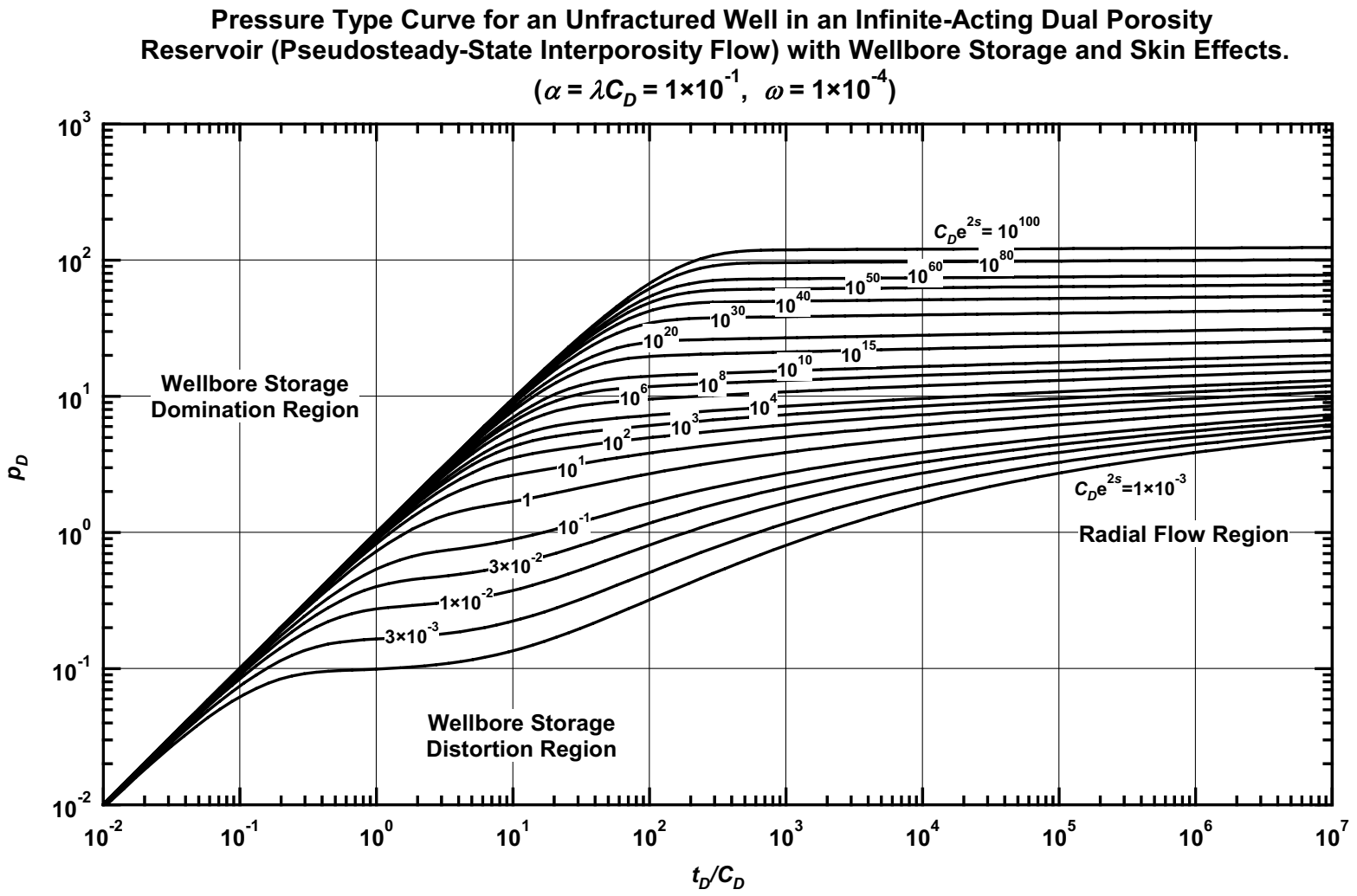

Figure C.76 — p_D vs. t_D/C_D — $\omega = 1\times10^{-4}$, $\alpha = \lambda C_D = 1\times10^{-1}$ (dual porosity case — includes wellbore storage and skin effects).

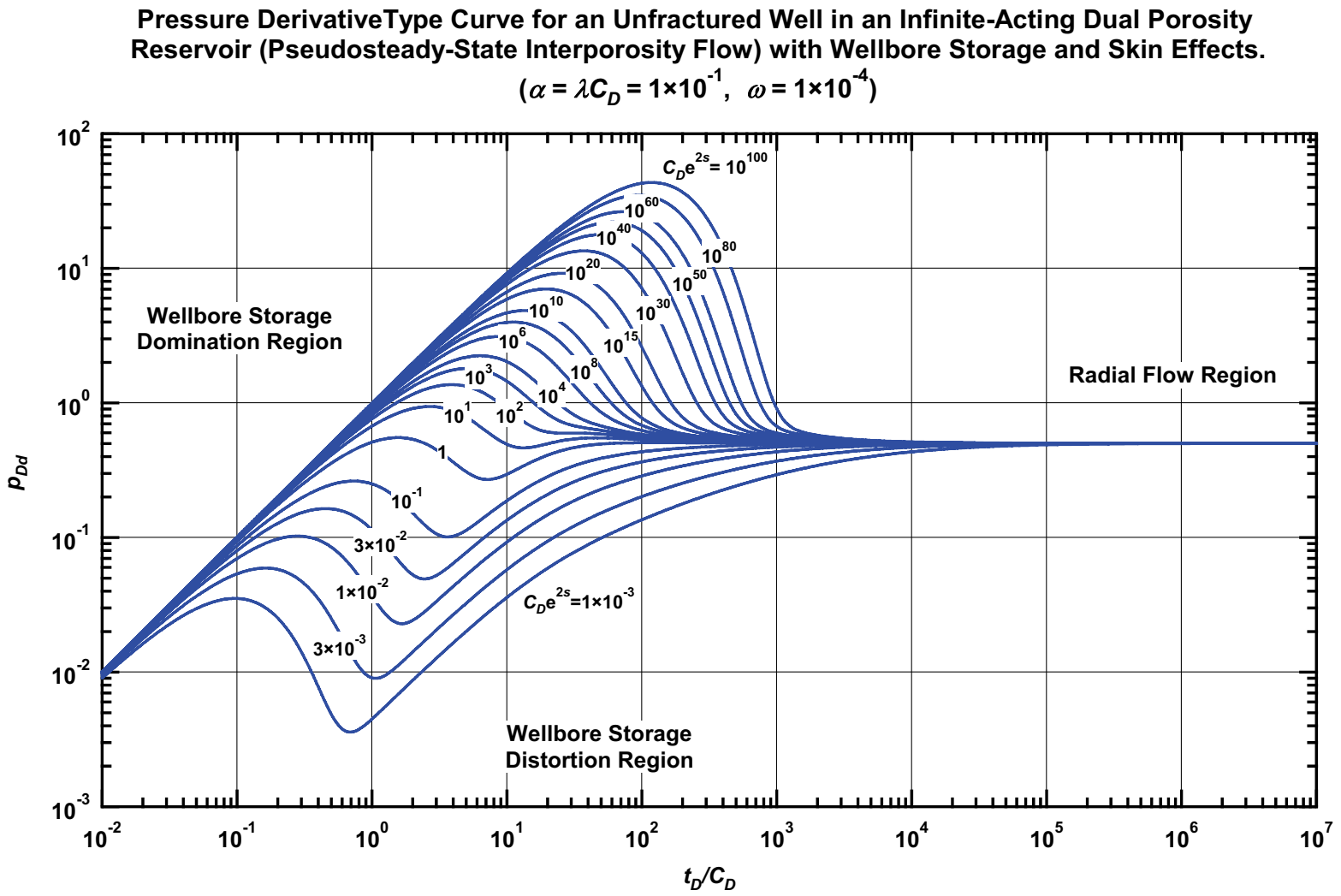

Figure C.77 — p_{Dd} vs. t_D/C_D — $\omega = 1\times10^{-4}$, $\alpha = \lambda C_D = 1\times10^{-1}$ (dual porosity case — includes wellbore storage and skin effects).

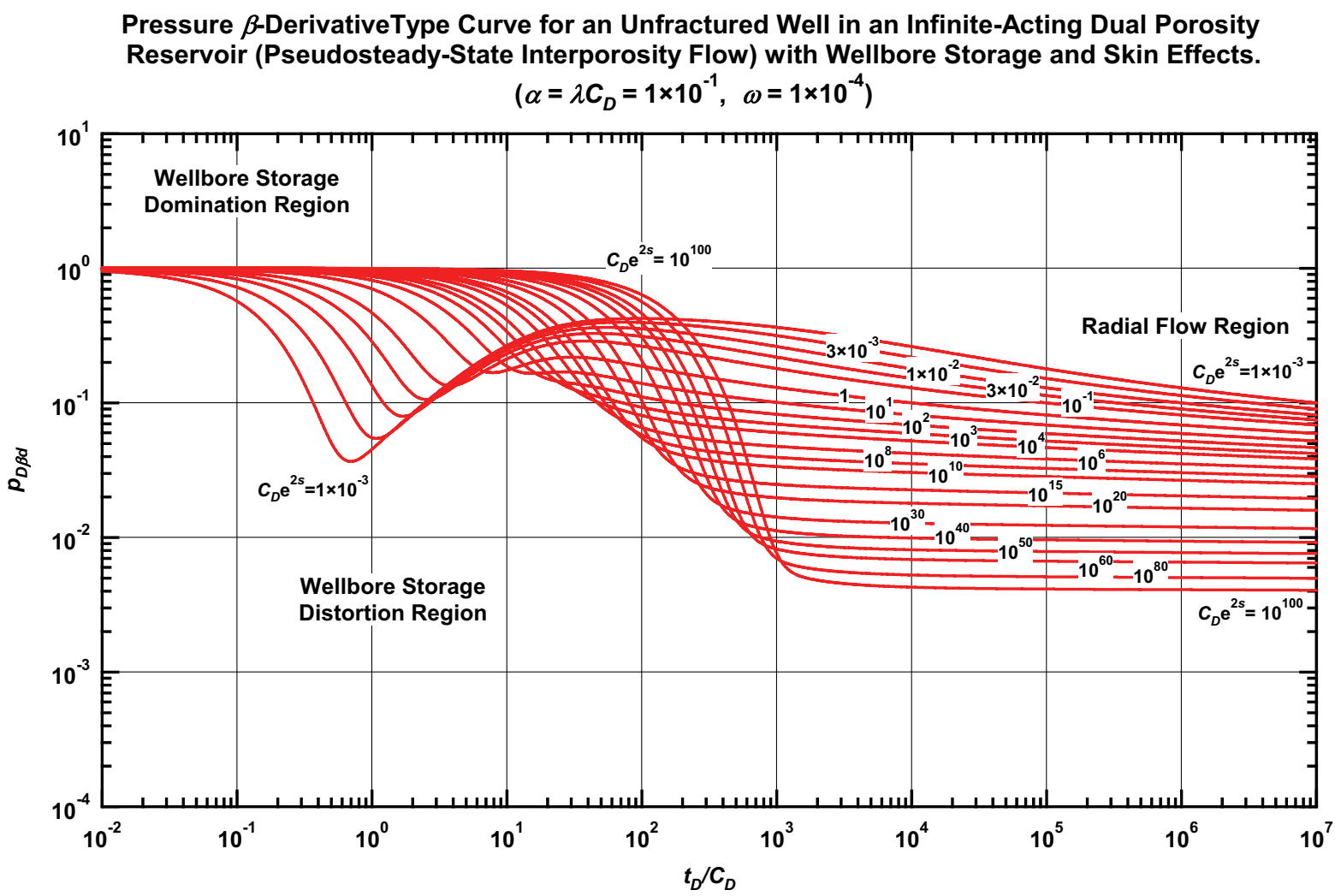

Figure C.78 — $p_{D\beta d}$ vs. t_D/C_D — $\omega = 1\times10^{-4}$, $\alpha = \lambda C_D = 1\times10^{-1}$ (dual porosity case — includes wellbore storage and skin effects).

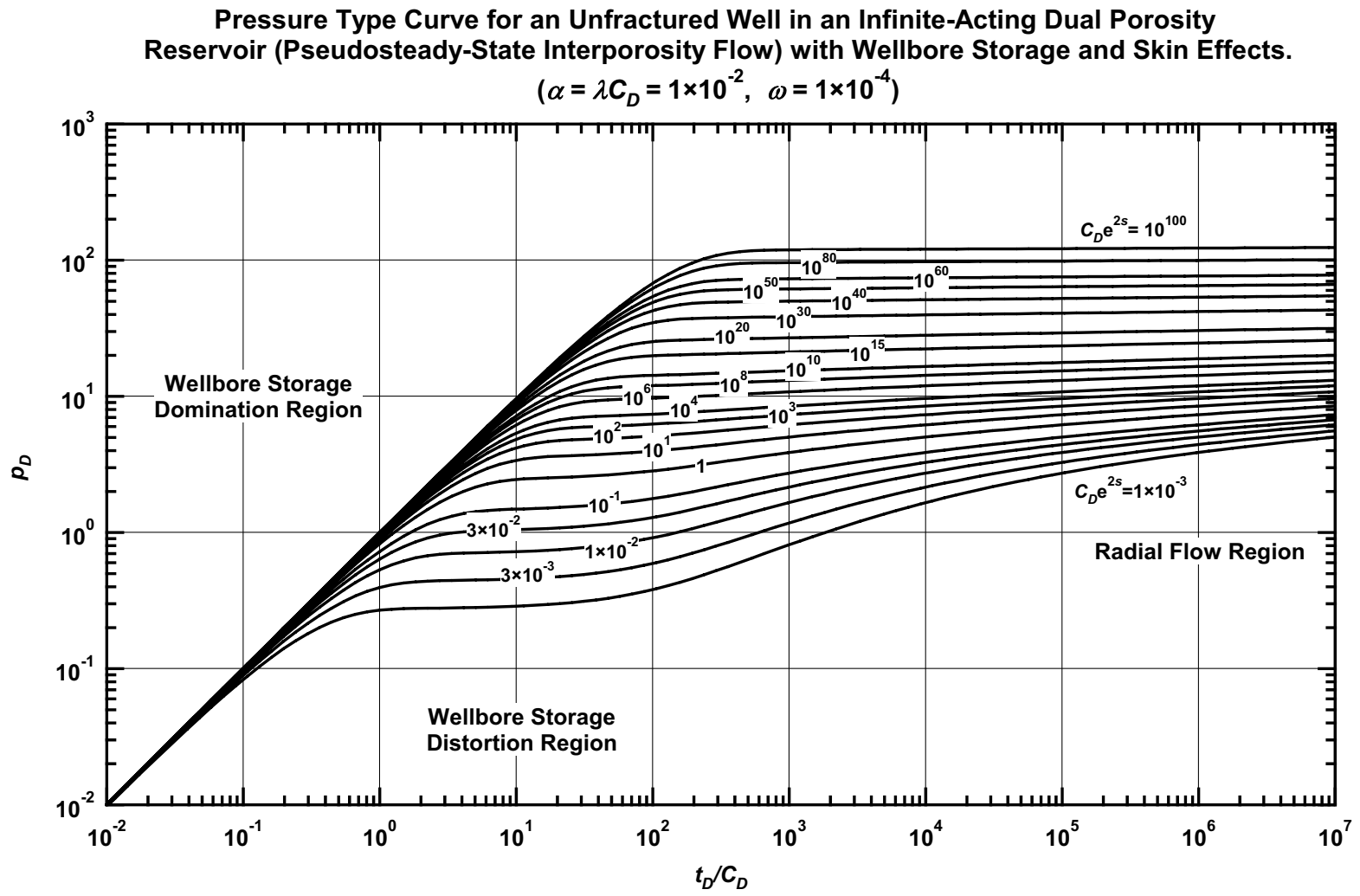

Figure C.79 — p_D vs. t_D/C_D — $\omega = 1\times10^{-4}$, $\alpha = \lambda C_D = 1\times10^{-2}$ (dual porosity case — includes wellbore storage and skin effects).

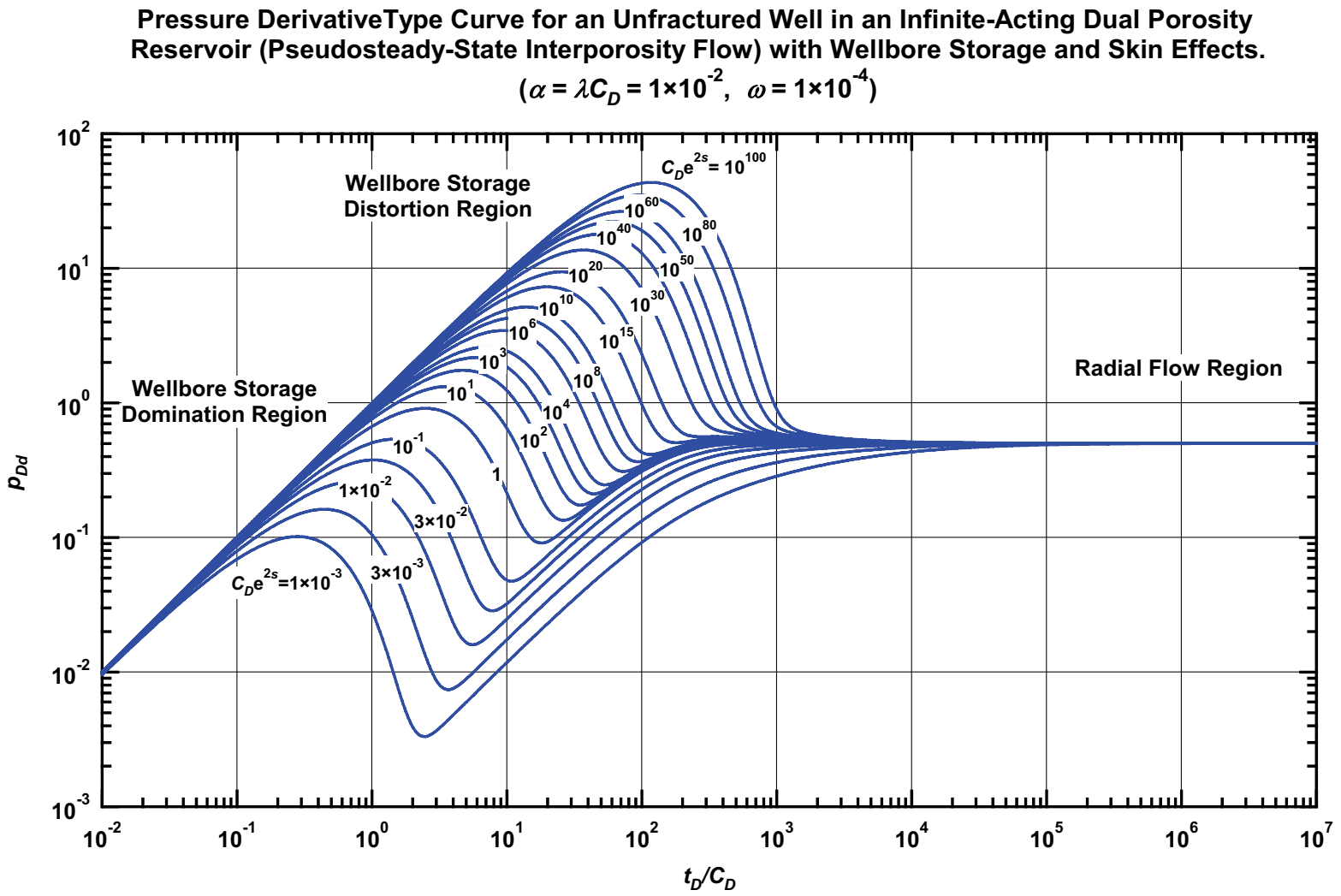

Figure C.80 — p_{Dd} vs. t_D/C_D — $\omega = 1\times10^{-4}$, $\alpha = \lambda C_D = 1\times10^{-2}$ (dual porosity case — includes wellbore storage and skin effects).

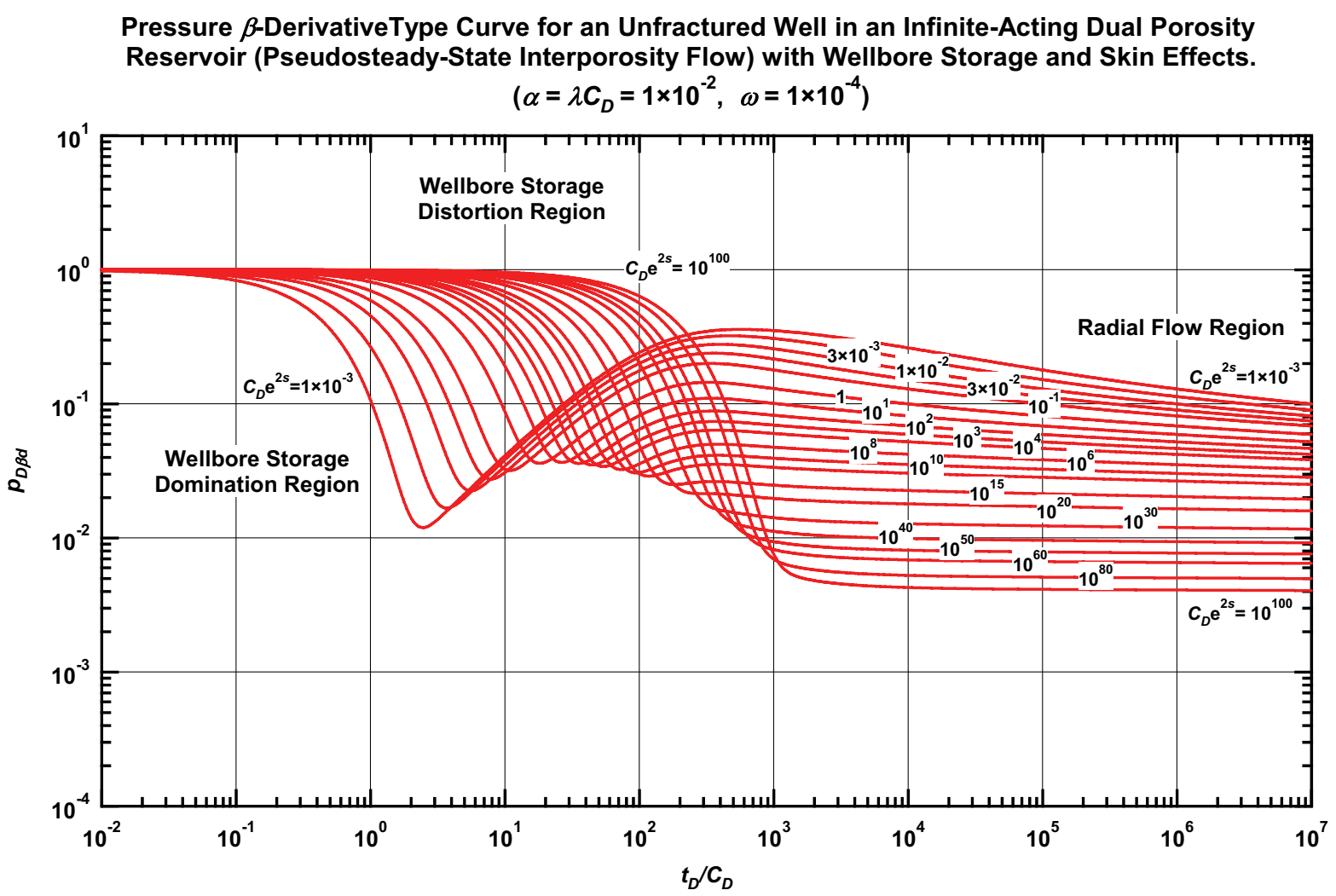

Figure C.81 — $p_{D\beta d}$ vs. t_D/C_D — $\omega = 1\times10^{-4}$, $\alpha = \lambda C_D = 1\times10^{-2}$ (dual porosity case — includes wellbore storage and skin effects).

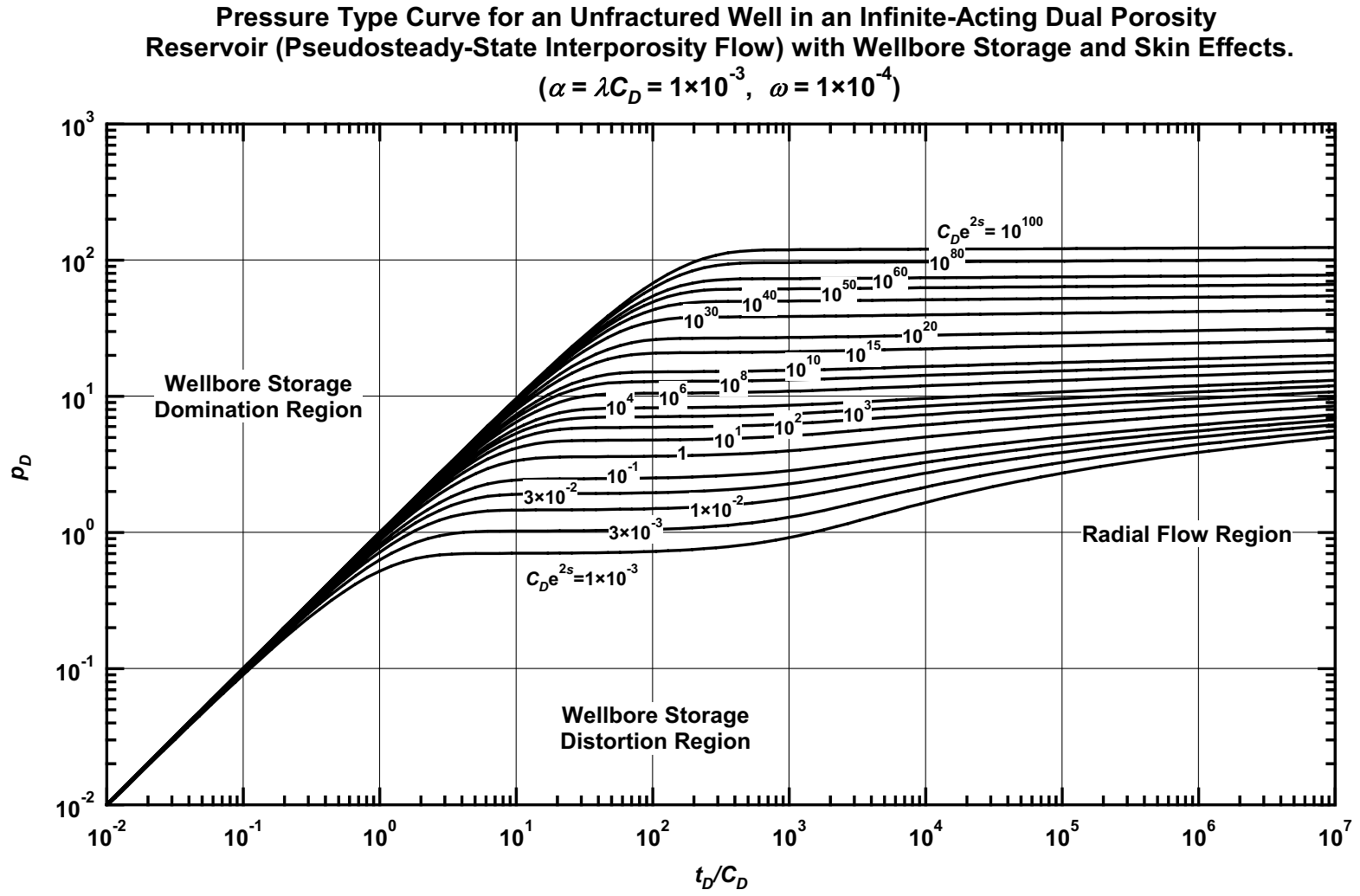

Figure C.82 — p_D vs. t_D/C_D — $\omega = 1\times10^{-4}$, $\alpha = \lambda C_D = 1\times10^{-3}$ (dual porosity case — includes wellbore storage and skin effects).

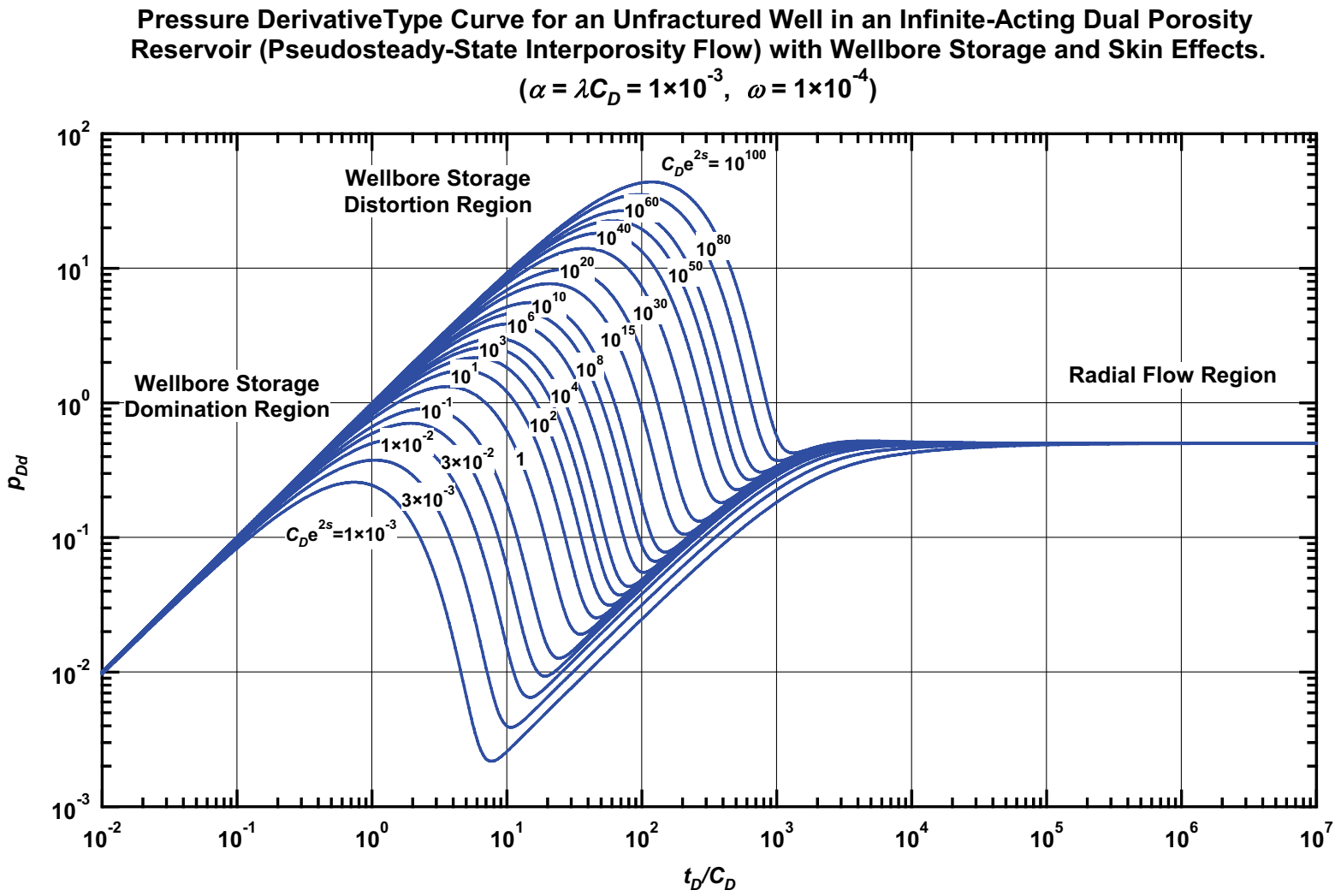

Figure C.83 — p_{Dd} vs. t_D/C_D — $\omega = 1\times10^{-4}$, $\alpha = \lambda C_D = 1\times10^{-3}$ (dual porosity case — includes wellbore storage and skin effects).

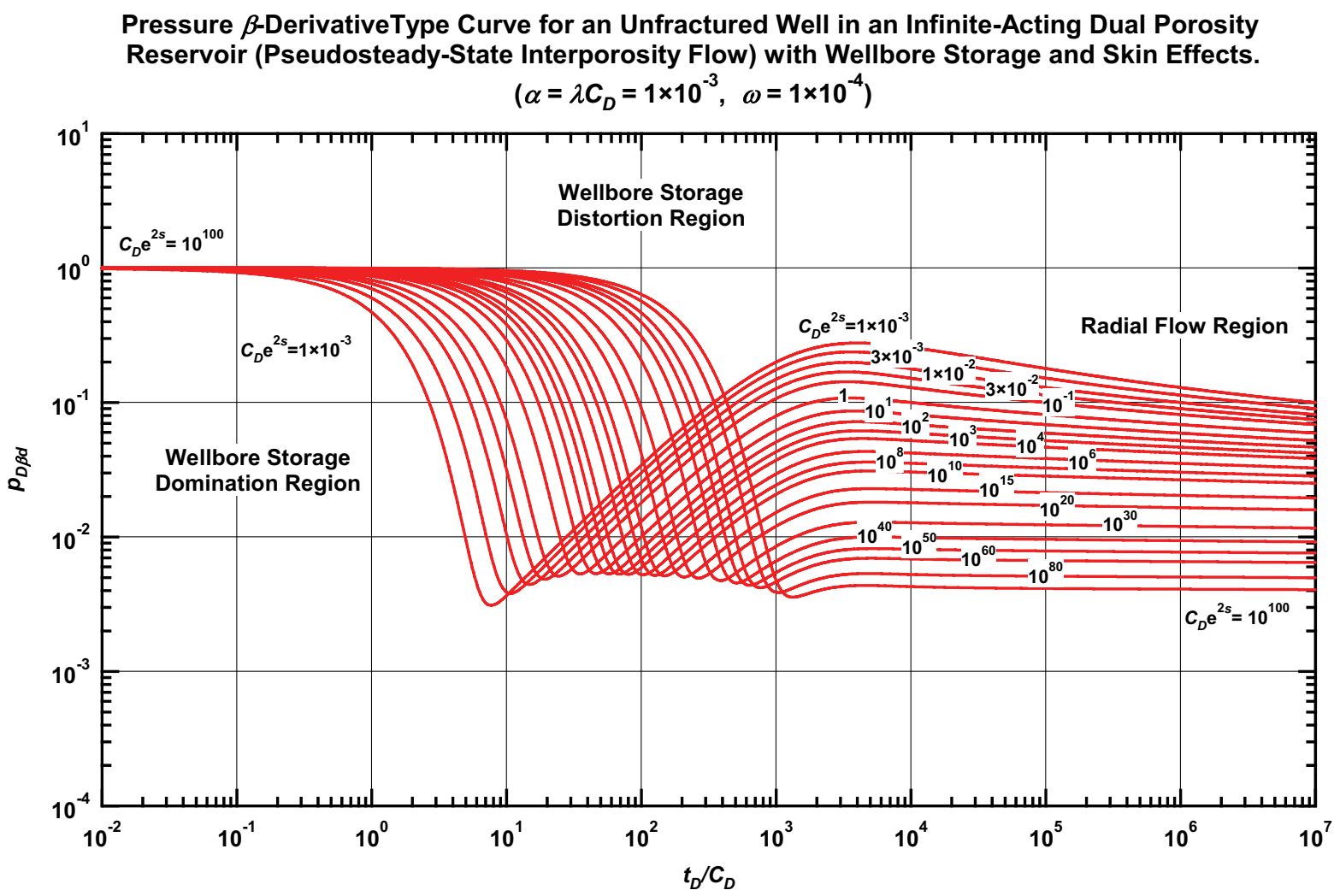

Figure C.84 — $p_{D\beta d}$ vs. t_D/C_D — $\omega = 1\times10^{-4}$, $\alpha = \lambda C_D = 1\times10^{-3}$ (dual porosity case — includes wellbore storage and skin effects).

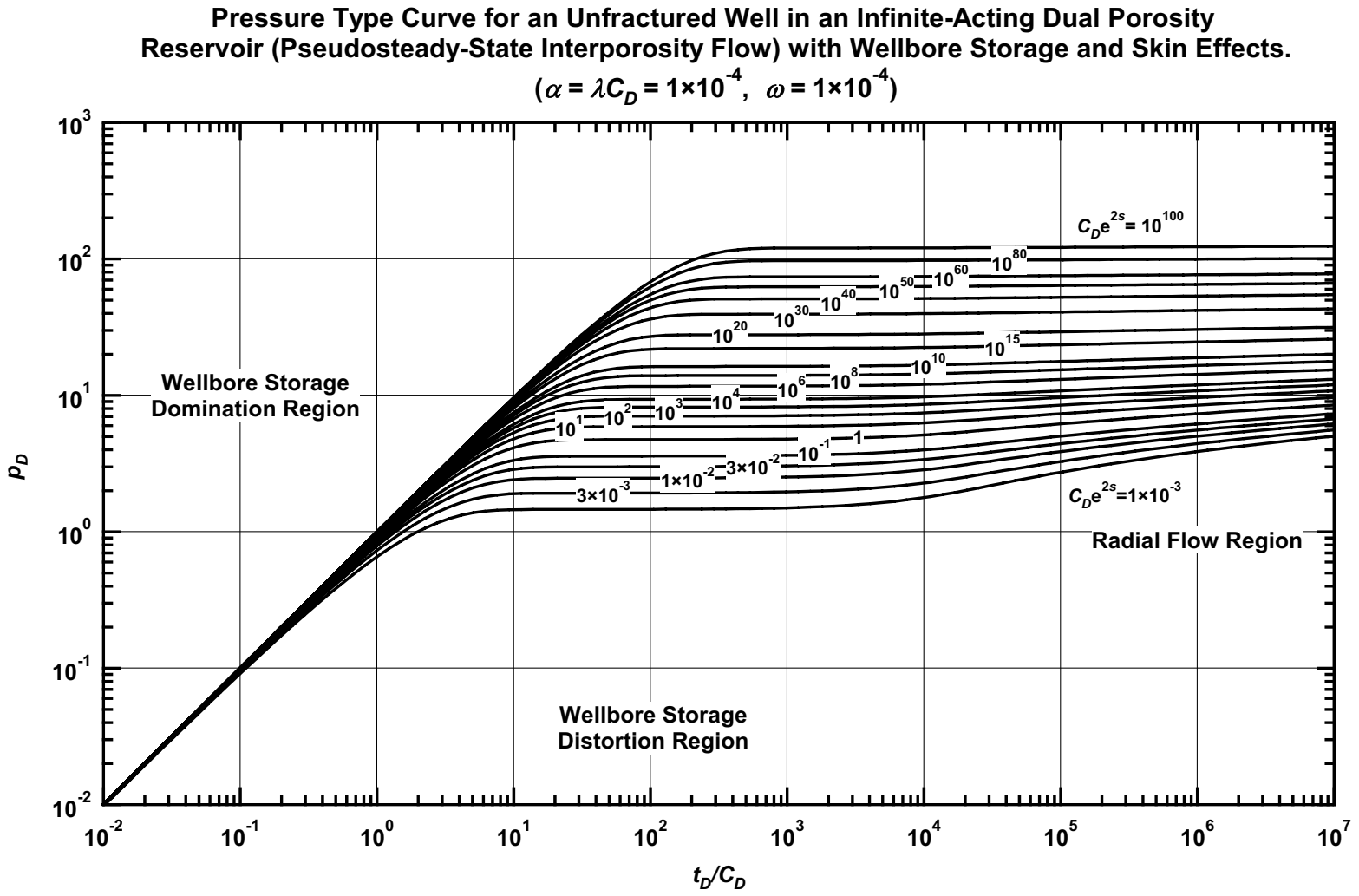

Figure C.85 — p_D vs. t_D/C_D — $\omega = 1\times10^{-4}$, $\alpha = \lambda C_D = 1\times10^{-4}$ (dual porosity case — includes wellbore storage and skin effects).

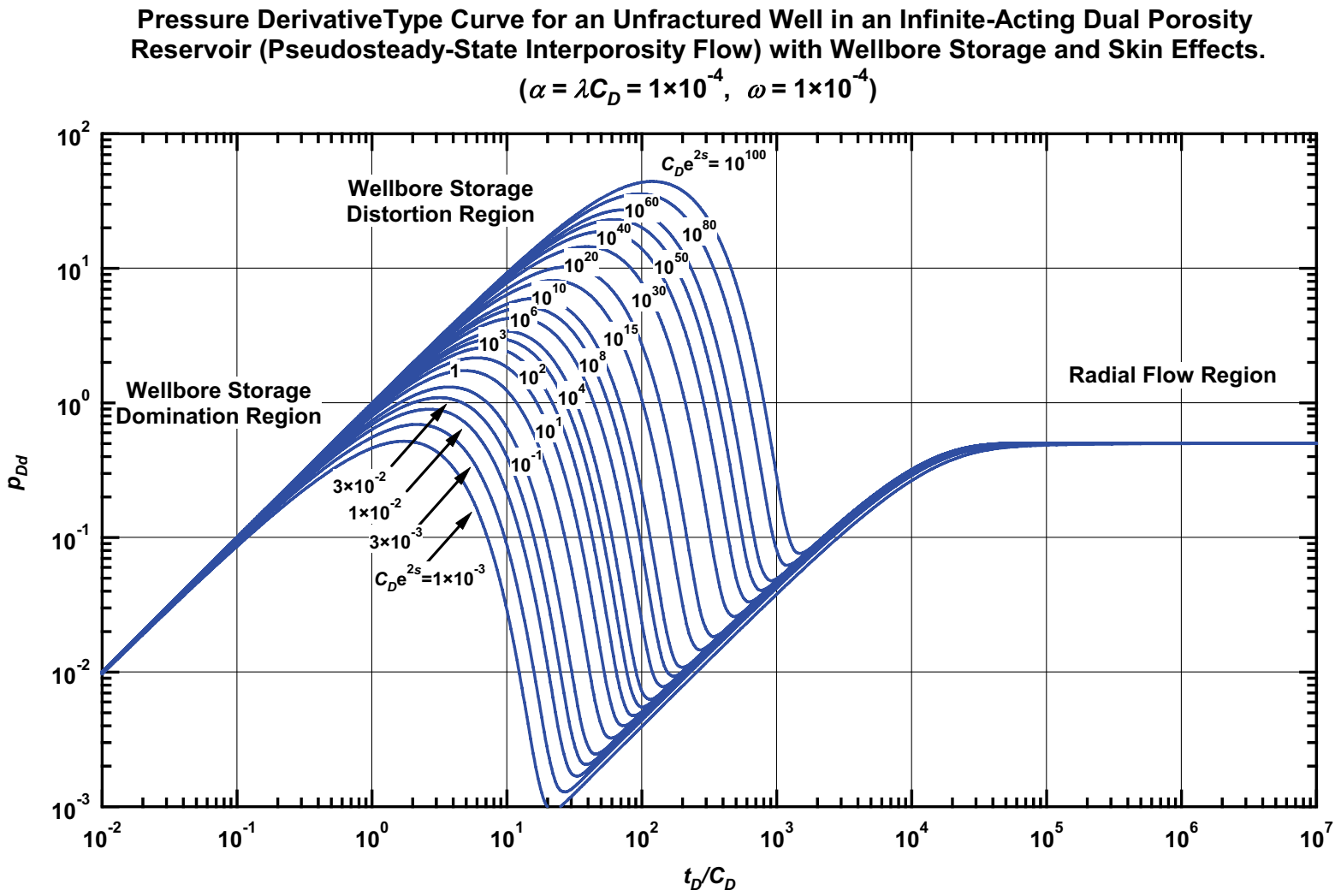

Figure C.86 — p_{Dd} vs. t_D/C_D — $\omega = 1\times10^{-4}$, $\alpha = \lambda C_D = 1\times10^{-4}$ (dual porosity case — includes wellbore storage and skin effects).

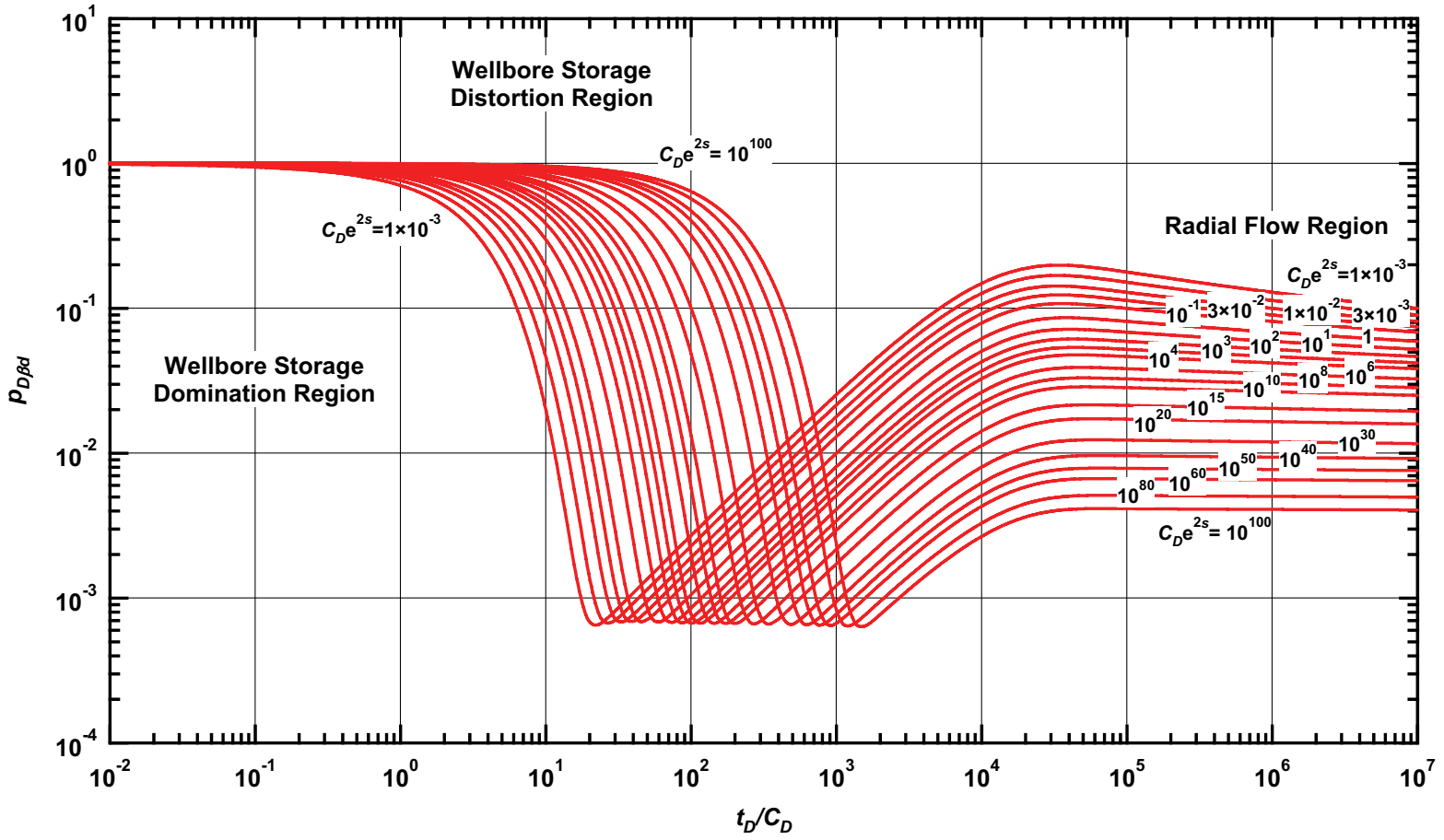

Figure C.87 — $p_{D\beta d}$ vs. t_D/C_D — $\omega = 1\times10^{-4}$, $\alpha = \lambda C_D = 1\times10^{-4}$ (dual porosity case — includes wellbore storage and skin effects).

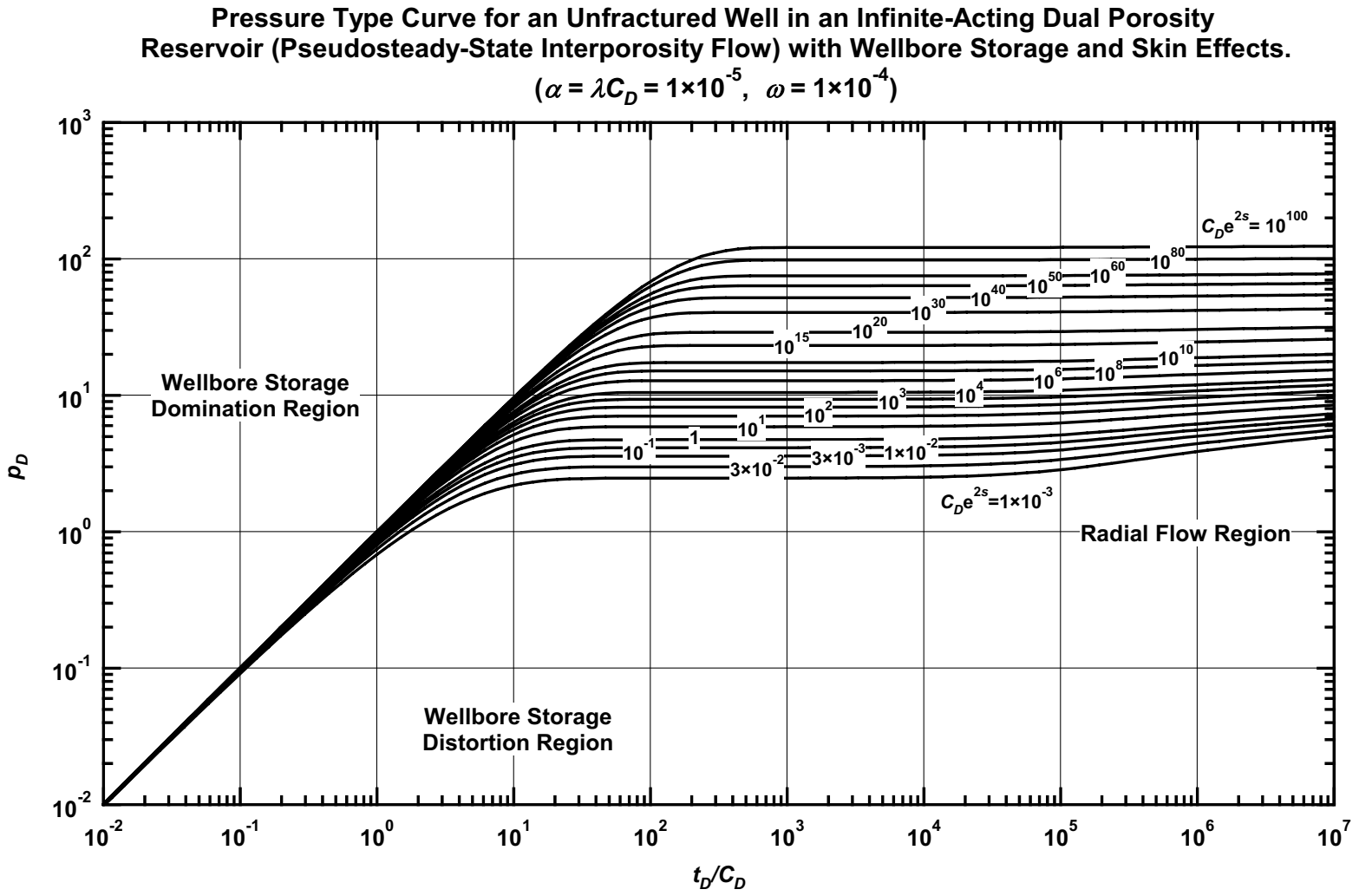

Figure C.88 — p_D vs. t_D/C_D — $\omega = 1\times10^{-4}$, $\alpha = \lambda C_D = 1\times10^{-5}$ (dual porosity case — includes wellbore storage and skin effects).

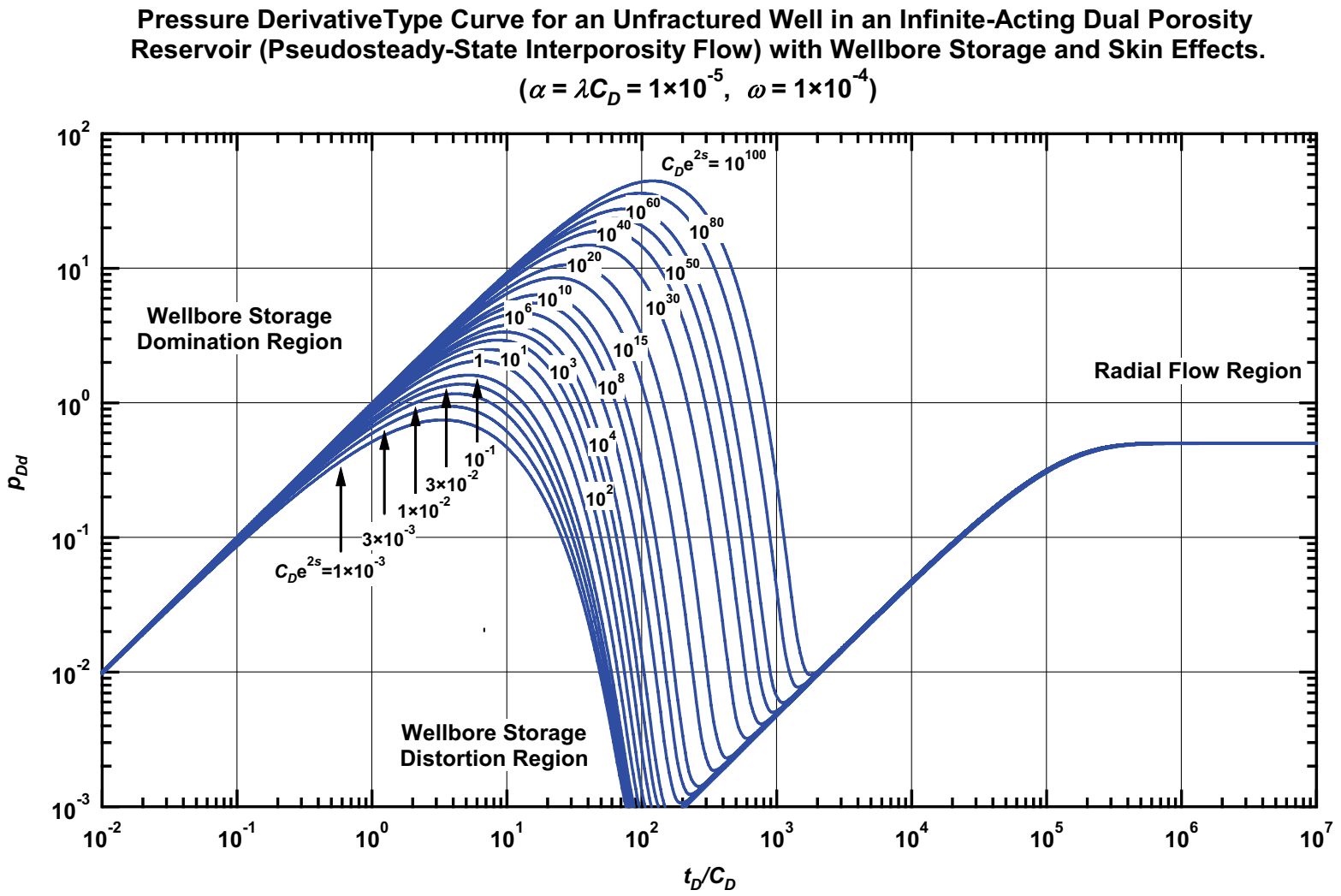

Figure C.89 — p_{Dd} vs. t_D/C_D — $\omega = 1\times10^{-4}$, $\alpha = \lambda C_D = 1\times10^{-5}$ (dual porosity case — includes wellbore storage and skin effects).

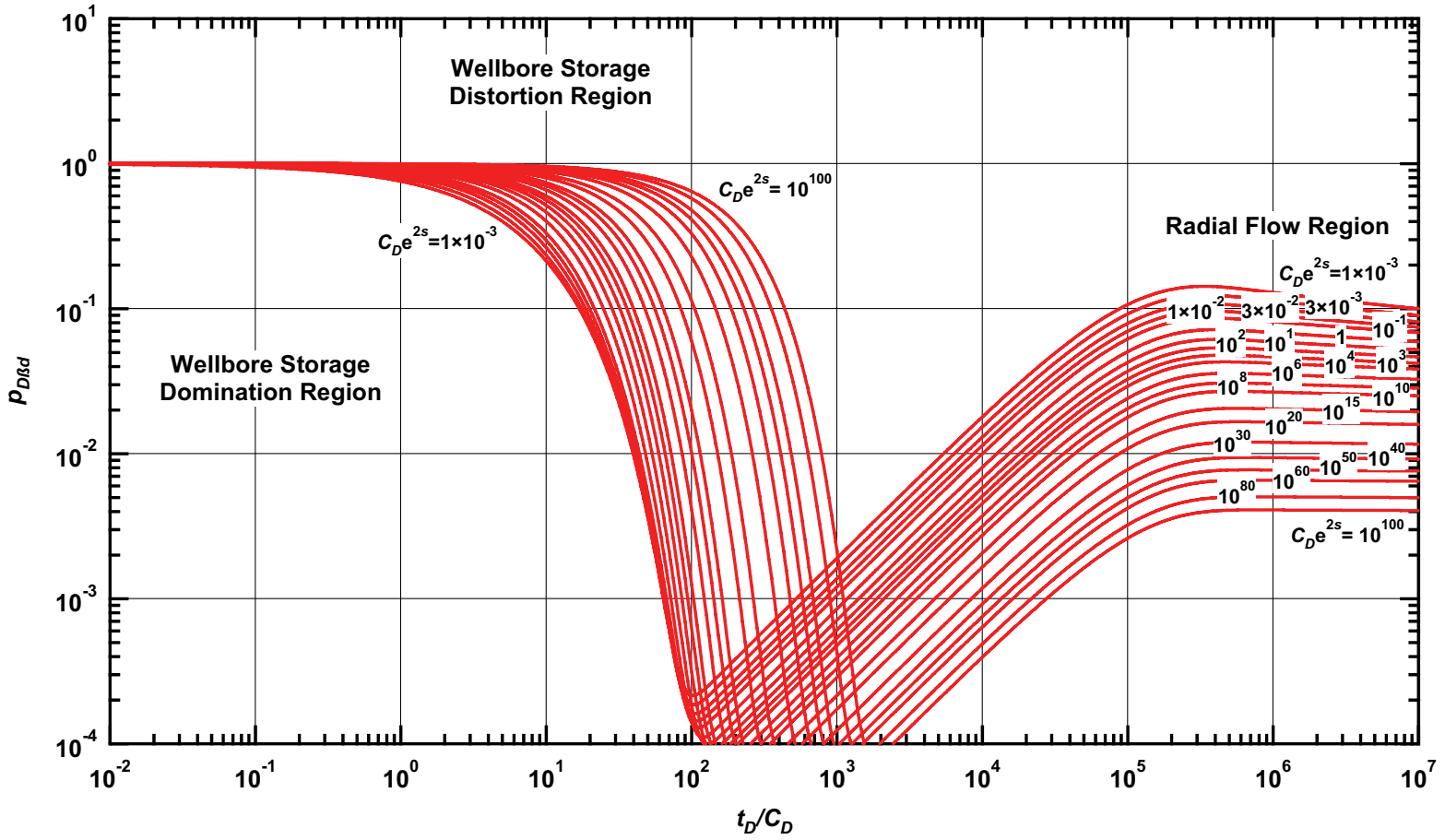

Figure C.90 — $p_{D\beta d}$ vs. t_D/C_D — $\omega = 1\times10^{-4}$, $\alpha = \lambda C_D = 1\times10^{-5}$ (dual porosity case — includes wellbore storage and skin effects).

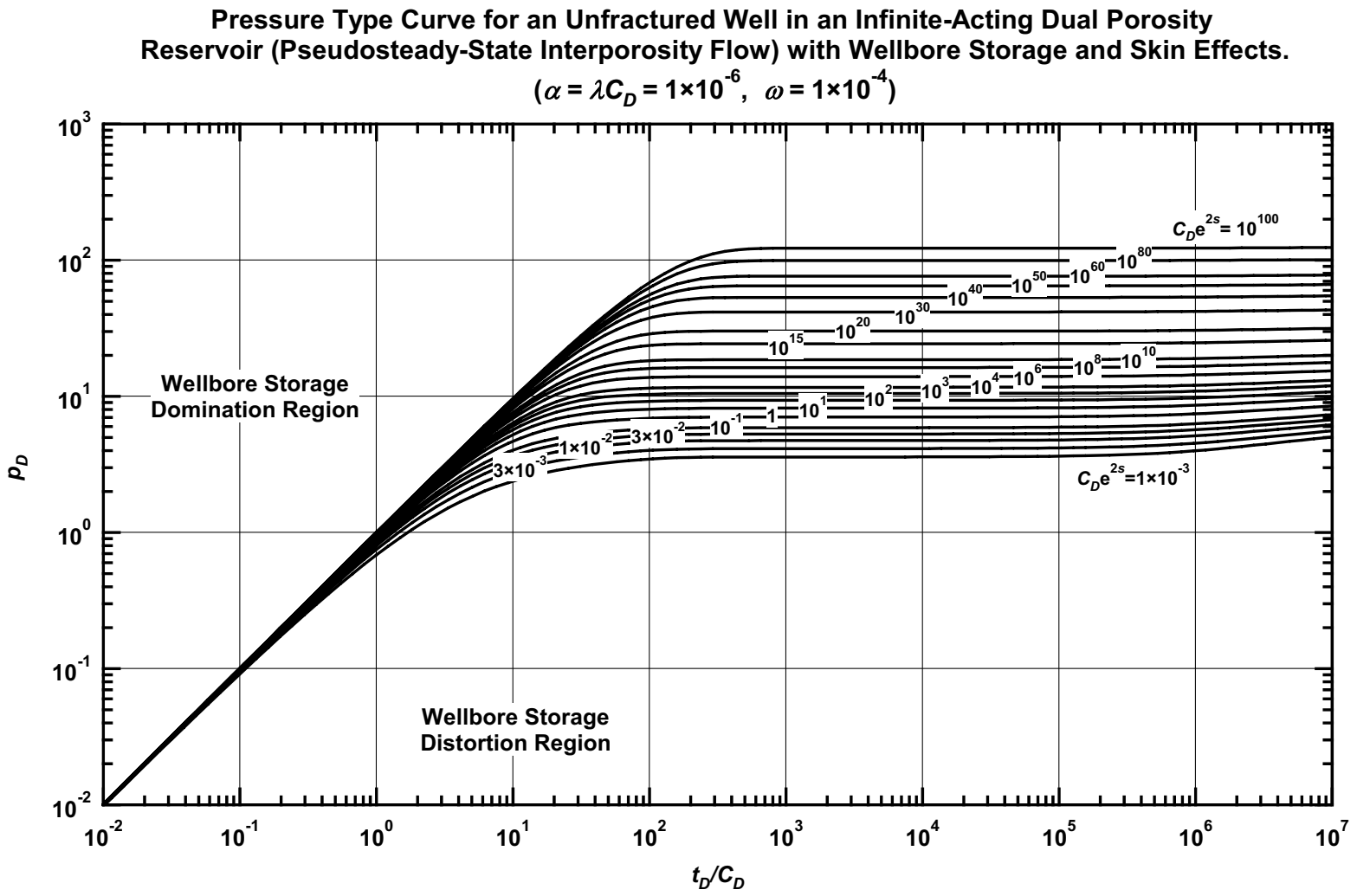

Figure C.91 — p_D vs. t_D/C_D — $\omega = 1\times10^{-4}$, $\alpha = \lambda C_D = 1\times10^{-6}$ (dual porosity case — includes wellbore storage and skin effects).

Pressure DerivativeType Curve for an Unfractured Well in an Infinite-Acting Dual Porosity Reservoir (Pseudosteady-State Interporosity Flow) with Wellbore Storage and Skin Effects.

($\alpha = \lambda C_D = 1\times10^{-6}$, $\omega = 1\times10^{-4}$)

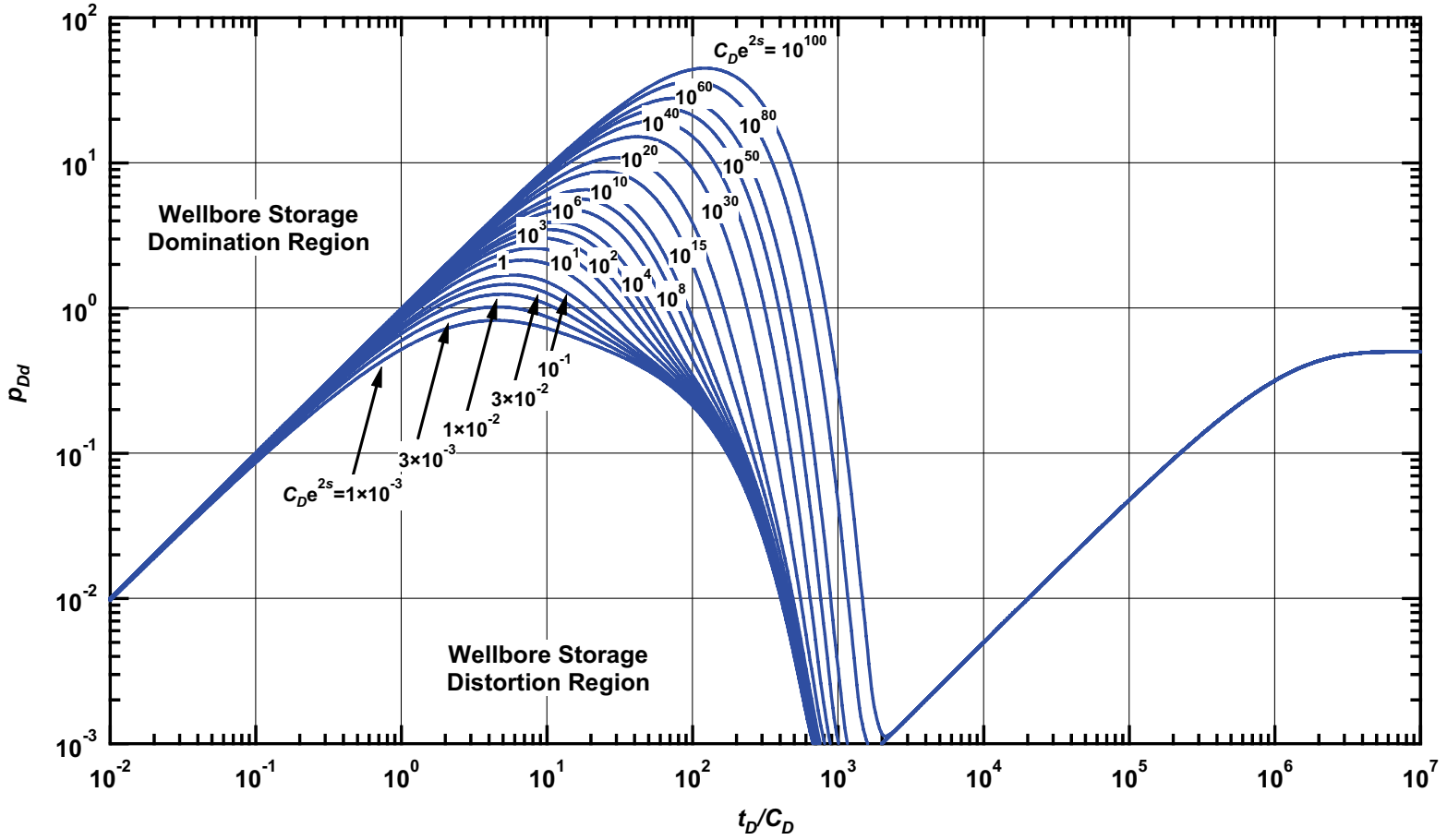

Figure C.92 — p_{Dd} vs. t_D/C_D — $\omega = 1\times10^{-4}$, $\alpha = \lambda C_D = 1\times10^{-6}$ (dual porosity case — includes wellbore storage and skin effects).

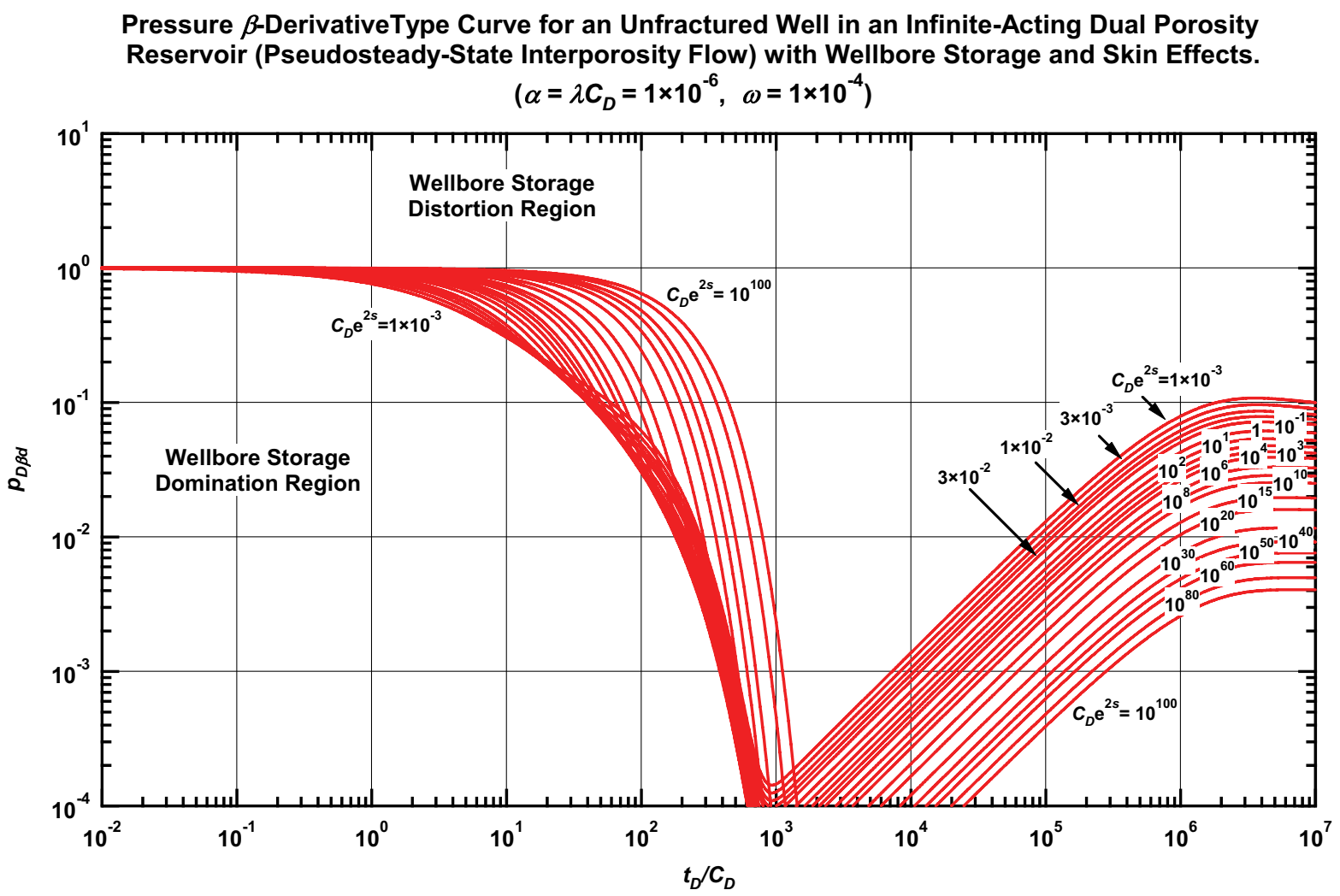

Figure C.93 — $p_{D\beta d}$ vs. t_D/C_D — $\omega = 1\times10^{-4}$, $\alpha = \lambda C_D = 1\times10^{-6}$ (dual porosity case — includes wellbore storage and skin effects).

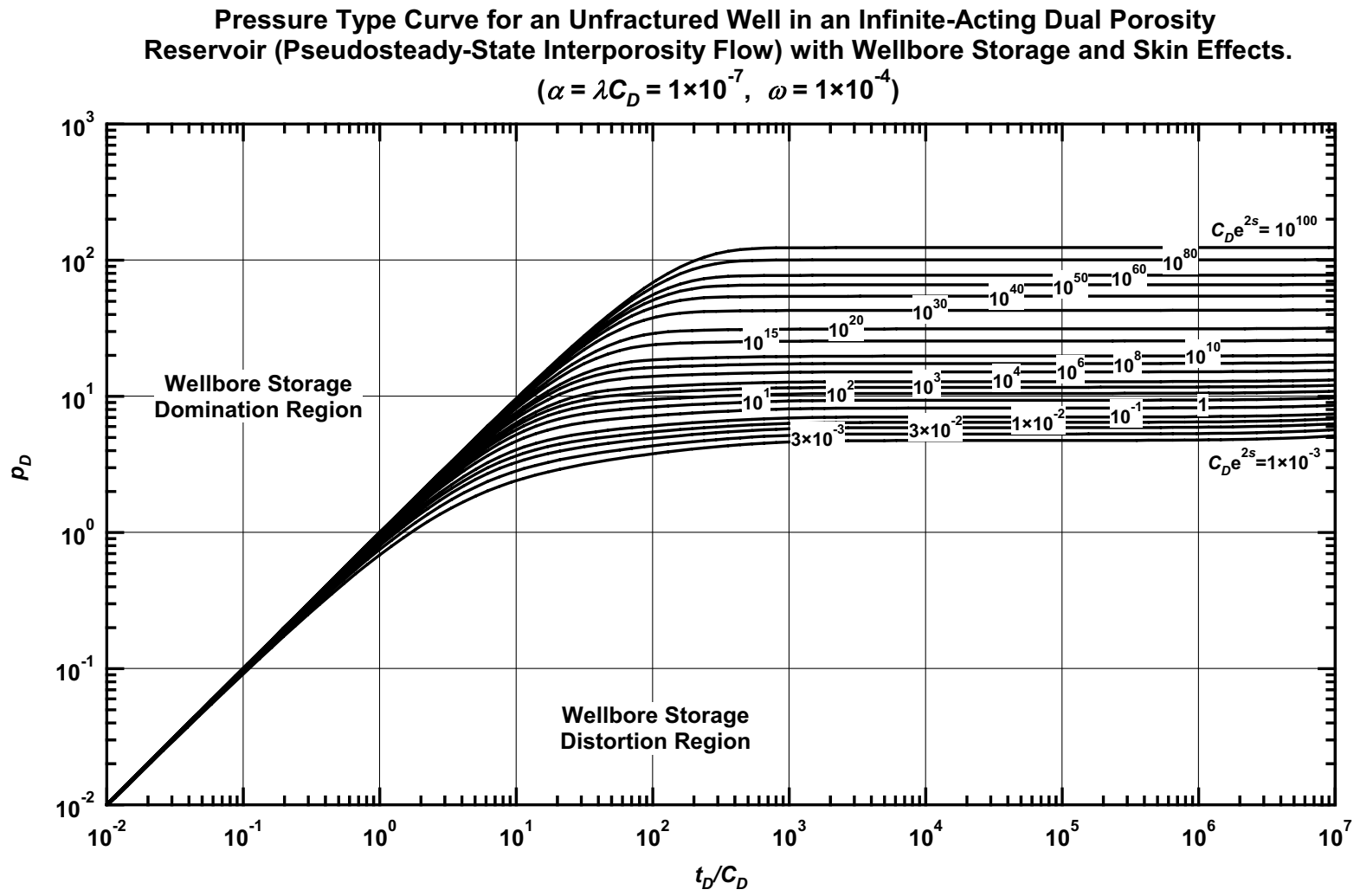

Figure C.94 — p_D vs. t_D/C_D — $\omega = 1\times10^{-4}$, $\alpha = \lambda C_D = 1\times10^{-7}$ (dual porosity case — includes wellbore storage and skin effects).

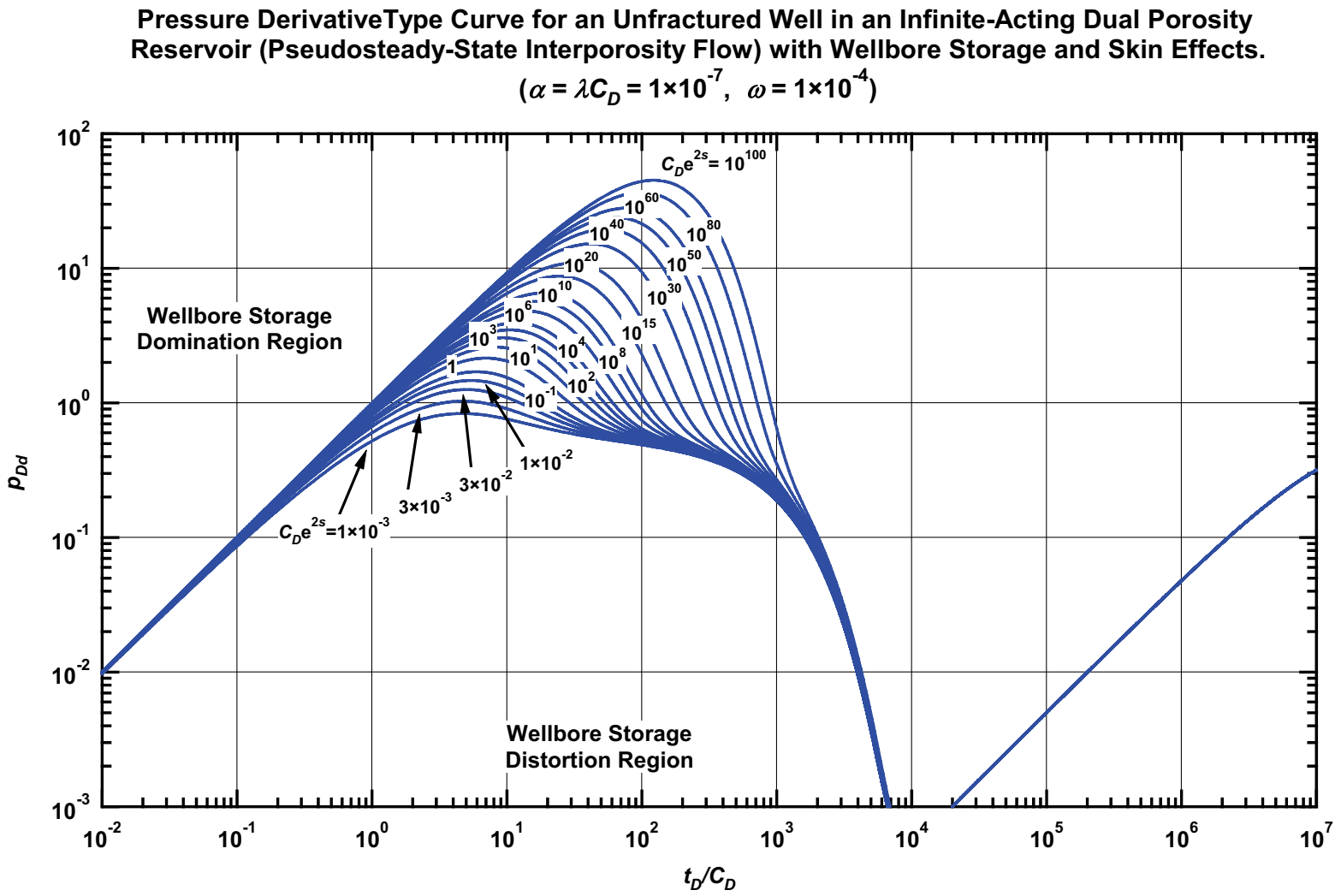

Figure C.95 — p_{Dd} vs. t_D/C_D — $\omega = 1\times10^{-4}$, $\alpha = \lambda C_D = 1\times10^{-7}$ (dual porosity case — includes wellbore storage and skin effects).

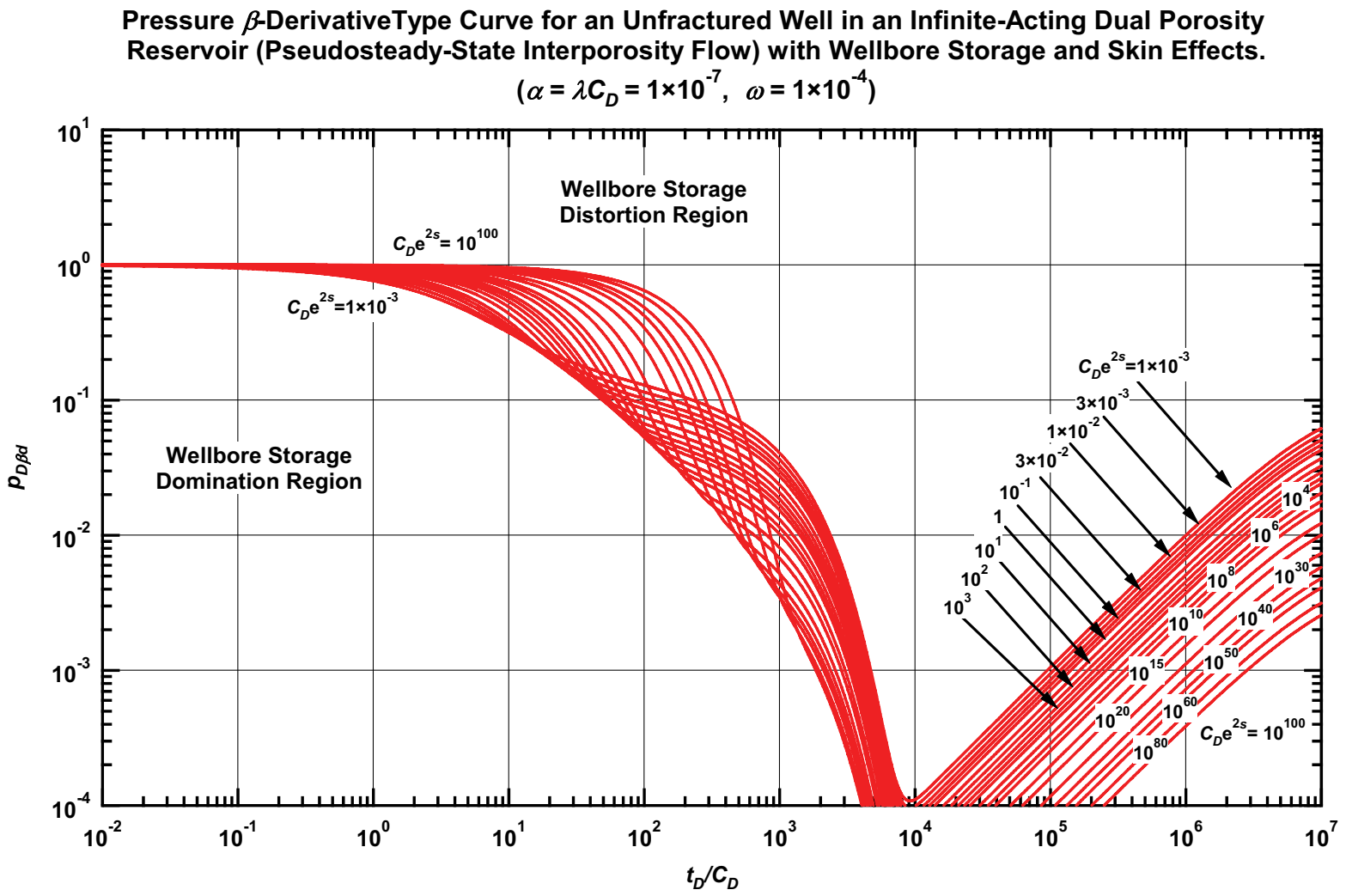

Figure C.96 — $p_{D\beta d}$ vs. t_D/C_D — $\omega = 1\times10^{-4}$, $\alpha = \lambda C_D = 1\times10^{-7}$ (dual porosity case — includes wellbore storage and skin effects).

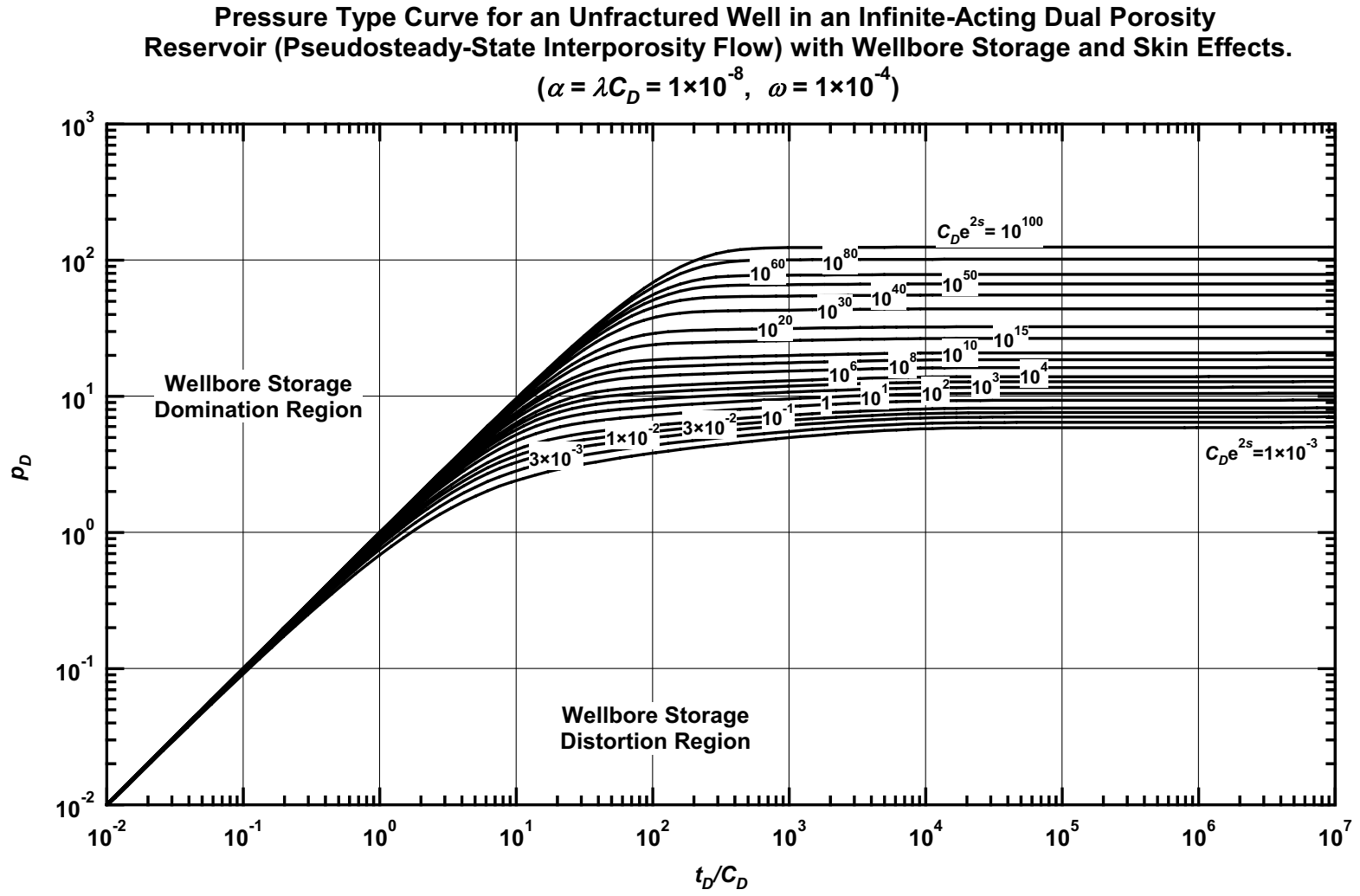

Figure C.97 — p_D vs. t_D/C_D — $\omega = 1\times10^{-4}$, $\alpha = \lambda C_D = 1\times10^{-8}$ (dual porosity case — includes wellbore storage and skin effects).

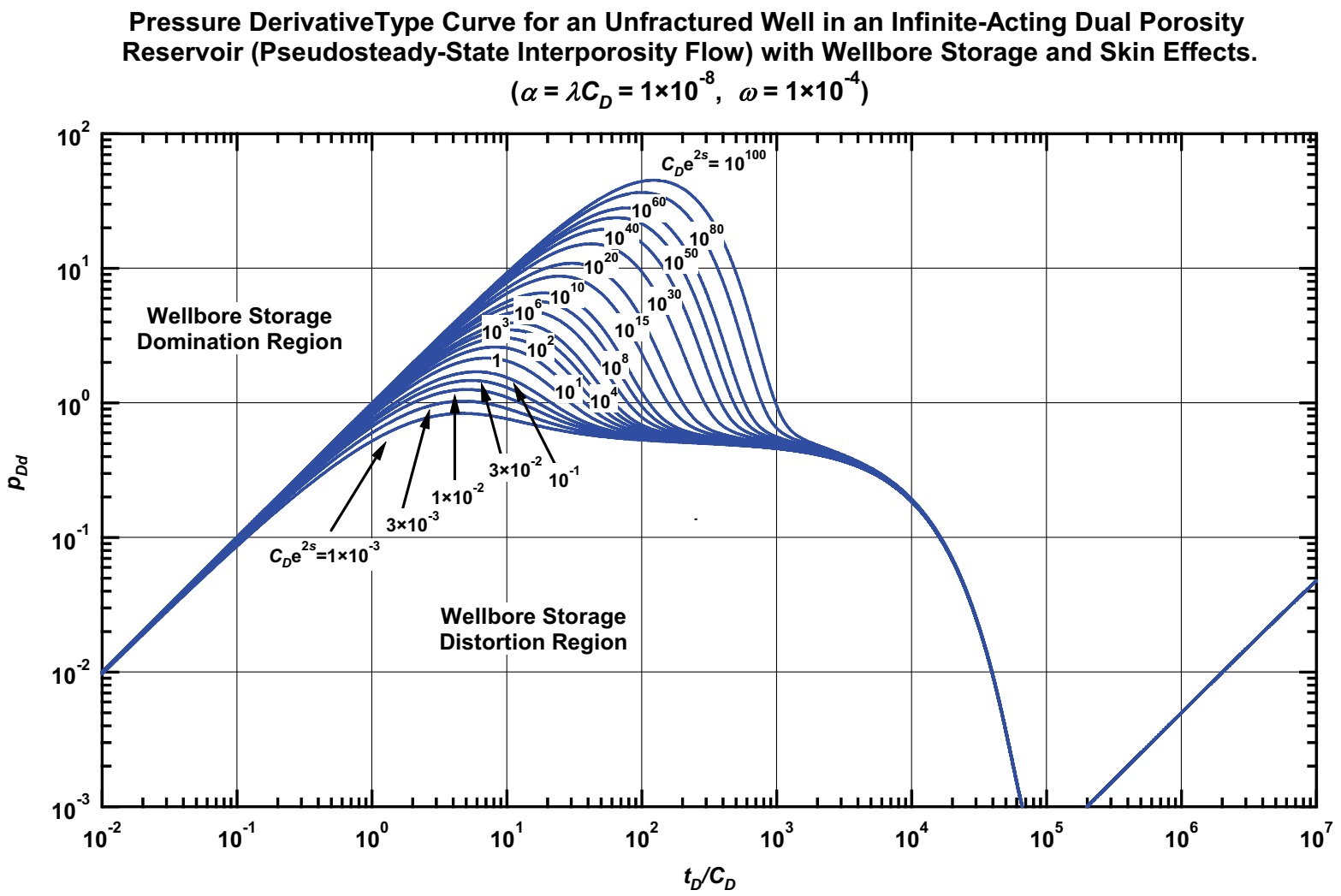

Figure C.98 — p_{Dd} vs. t_D/C_D — $\omega = 1\times10^{-4}$, $\alpha = \lambda C_D = 1\times10^{-8}$ (dual porosity case — includes wellbore storage and skin effects).

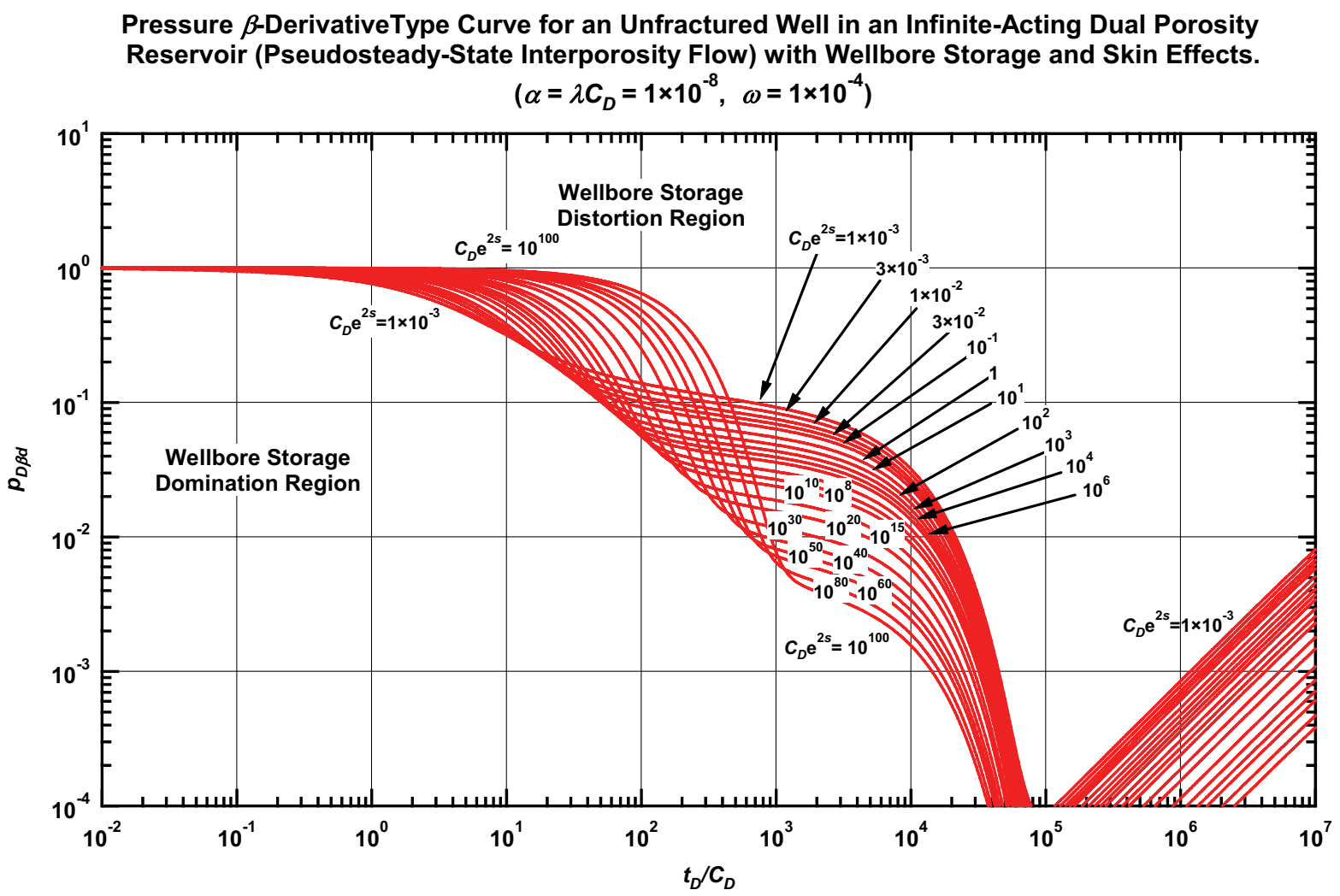

Figure C.99 —$p_{D\beta d}$ vs. t_D/C_D — $\omega = 1\times10^{-4}$, $\alpha = \lambda C_D = 1\times10^{-8}$ (dual porosity case — includes wellbore storage and skin effects).

APPENDIX D

CASE OF A FRACTURED WELL IN AN INFINITE-ACTING DUAL POROSITY (NATURALLY FRACTURED) RESERVOIR

In this appendix we provide the pressure, pressure derivative, and β-derivative solutions (in dimensionless format) for the case of a hydraulically fractured well in a naturally fractured reservoir, in the forms of equations and graphical type curve solutions. To describe the dual porosity reservoir system, we used the pseudosteady-state interporosity flow model, and for graphical presentation of the solutions we generated type curves for ω varying from 10^{-1} to 10^{-4} and λ varying from 10^{-1} to 10^{-8}, for fracture conductivity (C_{fD}) values of 1, 10, 100 and 1000.

Table D-1 — Solutions for a hydraulically fractured well in an infinite-acting, dual porosity (naturally fractured) reservoir system (pseudosteady-state interporosity flow model).

Description	Relation
p_D	$p_D(t_{Dxf}) = \frac{\pi}{\Gamma(1.25)\sqrt{2C_{fD}}}\left[\frac{t_{Dxf}}{\omega}\right]^{1/4}$ (fracture storage dominated flow period, early time) .....(D.1.1) $p_D(t_{Dxf}) = \sqrt{\frac{\pi t_{Dxf}}{\omega}} + \frac{\pi}{3C_{fD}}$ (fracture storage dominated flow period, intermediate time) .....(D.1.2) $p_D(t_{Dxf}) = \frac{\pi}{\Gamma(5/4)\sqrt{2C_{fD}}} t_{Dxf}^{1/4}$ (total system compressibility dominated flow period, early time).....(D.1.3) $p_D(t_{Dxf}) = \sqrt{\pi t_{Dxf}} + \frac{\pi}{3C_{fD}}$ (total system compressibility dominated flow period, intermediate time) ....(D.1.4)
p_{Dd}	$p_{Dd}(t_{Dxf}) = \frac{0.612708}{\sqrt{C_{fD}}}\left[\frac{t_{Dxf}}{\omega}\right]^{1/4}$ (fracture storage dominated flow period, early time) .....(D.1.5) $p_{Dd}(t_{Dxf}) = \sqrt{\frac{\pi t_{Dxf}}{\omega}} + \frac{\pi}{3C_{fD}}$ (fracture storage dominated flow period, intermediate time) .....(D.1.6) $p_{Dd}(t_{Dxf}) = \frac{\pi}{\Gamma(5/4)\sqrt{2C_{fD}}} t_{Dxf}^{1/4}$ (total system compressibility dominated flow period, early time).....(D.1.7) $p_{Dd}(t_{Dxf}) = \sqrt{\pi t_{Dxf}} + \frac{\pi}{3C_{fD}}$ (total system compressibility dominated flow period, intermediate time)..... ..... (D.1.8)

Table D-1 — Continued

	$p_{D\beta d}(t_{Dxf}) = \frac{1}{4}$ (fracture storage dominated flow period, early time) .....(D.1.9)
	$p_{D\beta d}(t_{Dxf}) = \frac{3C_{fD}t_{Dxf}}{6C_{fD}t_{Dxf} + 2\sqrt{\pi t_{Dxf}\omega}}$ (fracture storage dominated flow period, intermediate time) .....(D.1.10)
$p_{D\beta d}\ (= p_{Dd}/p_D)$	$p_{D\beta d}(t_{Dxf}) = \frac{1}{4}$ (total system compressibility dominated flow period, early time).....(D.1.11)
	$p_{D\beta d}(t_{Dxf}) = \frac{\sqrt{\pi t_{Dxf}}}{2\left[\sqrt{\pi t_{Dxf}} + \frac{\pi}{3C_{fD}}\right]}$ (total system compressibility dominated flow period, intermediate time)..... ..... (D.1.12)

Definitions: (field units)

$$t_{Dxf} = 2.637\times10^{-4}\frac{kt}{\phi c_t \mu x_f^2} \quad \text{.....(D.1.13)}$$

$$p_D = \frac{1}{141.2}\frac{kh}{qB\mu}(p_i - p_{wf}) \quad \text{.....(D.1.14)}$$

$$\omega = \frac{\phi_{fb}c_{tfb}}{\phi_{fb}c_{tfb} + \phi_{ma}c_{tma}} \quad \text{.....(D.1.15)}$$

$$\lambda = 12\frac{r_w^2}{h_{ma}^2}\frac{k_{ma}}{k_{fb}} \quad \text{.....(D.1.16)}$$

$$C_{fD} = \frac{k_f w}{kx_f} \quad \text{.....(D.1.17)}$$

$$C_{Df} = \frac{0.8936C_s}{\phi h c_t x_f^2} \quad \text{.....(D.1.18)}$$

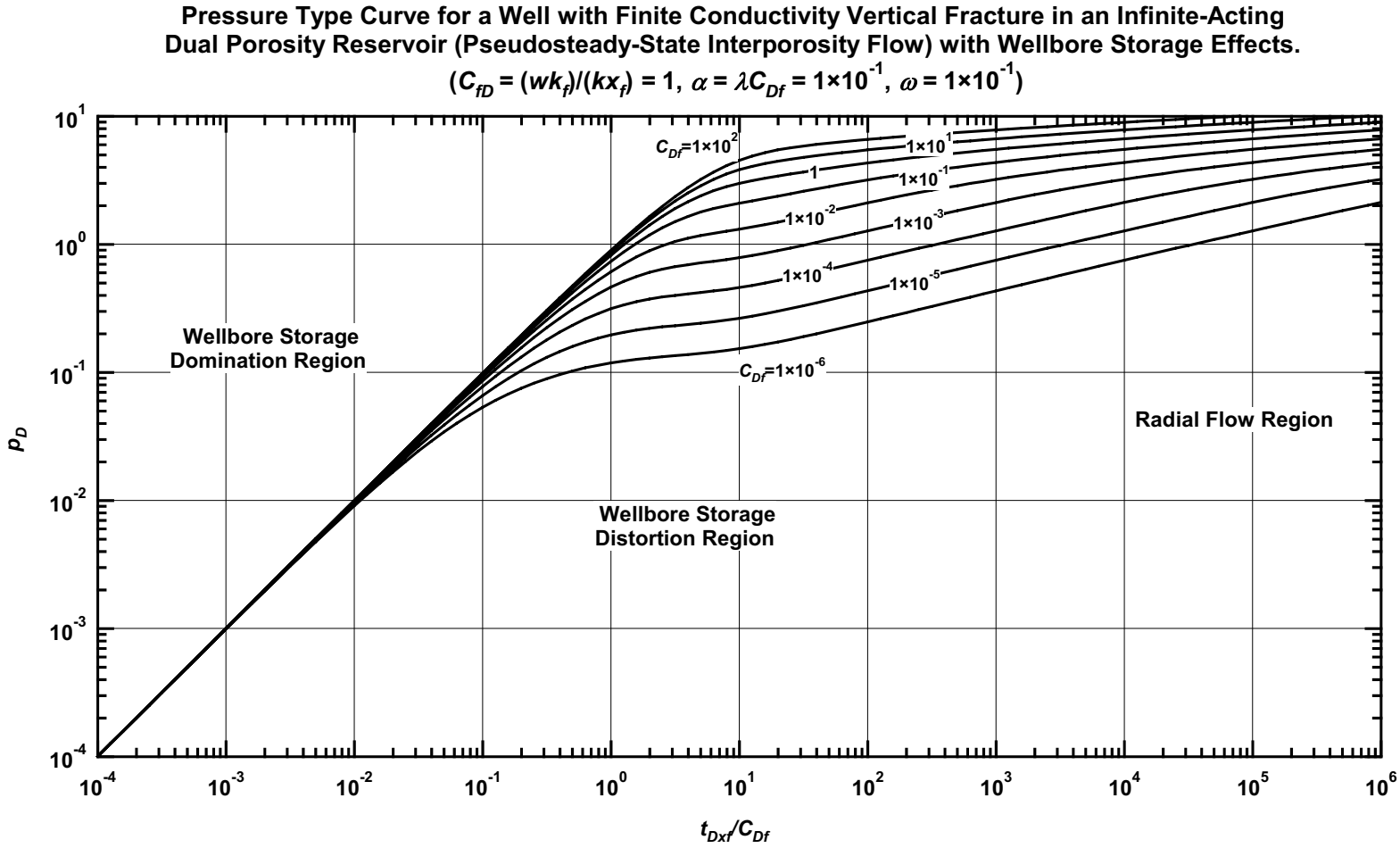

Figure D.1 — p_D vs. t_{Dxf}/C_{Df} — C_{fD} =1, $\omega = 1\times10^{-1}$, $\alpha = \lambda C_{Df} = 1\times10^{-1}$ (fractured well in dual porosity system case — includes wellbore storage effects).

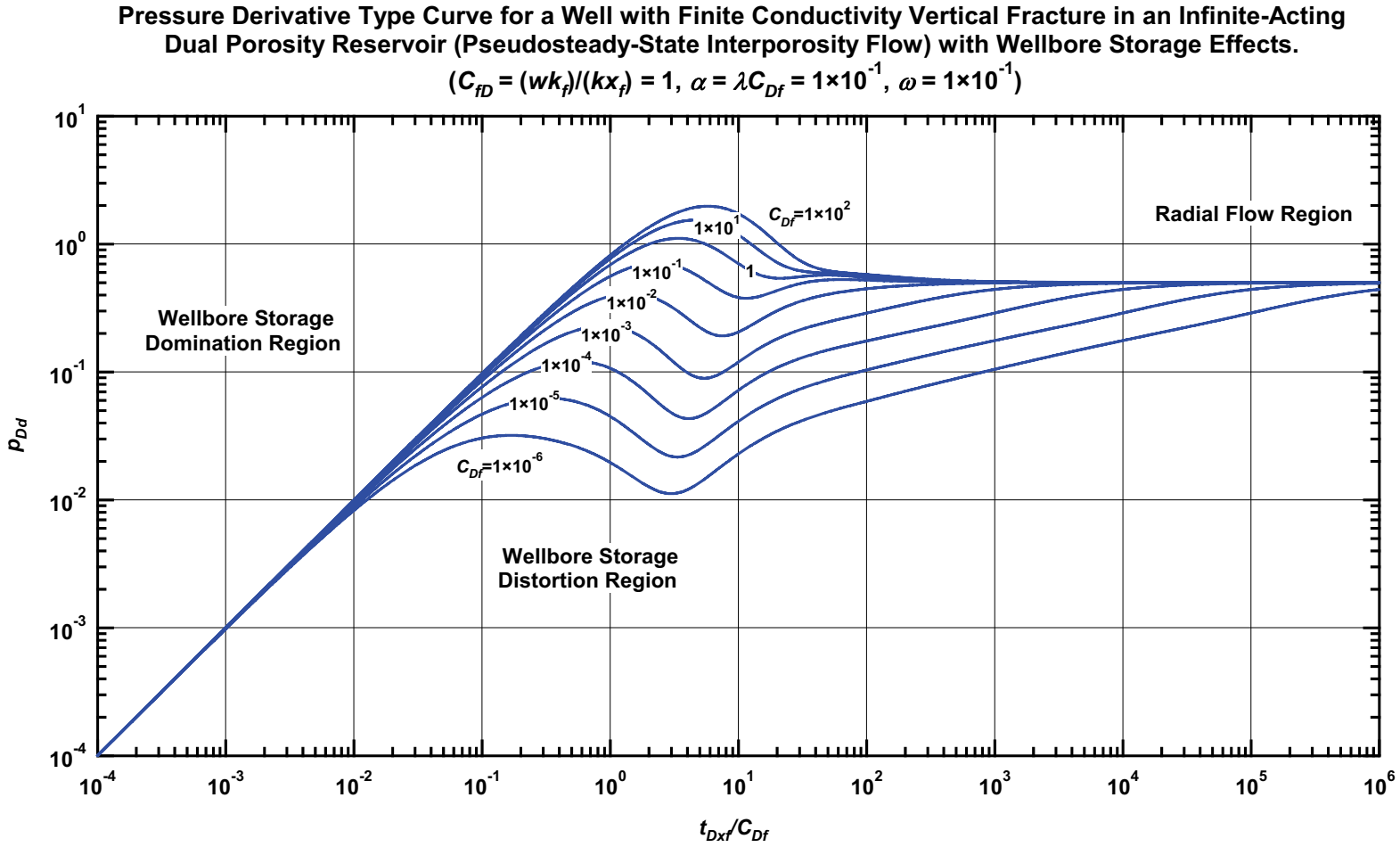

Figure D.2— p_{Dd} vs. t_{Dxf}/C_{Df} — C_{fD} =1, $\omega = 1\times10^{-1}$, $\alpha = \lambda C_{Df} = 1\times10^{-1}$ (fractured well in dual porosity system case — includes wellbore storage effects).

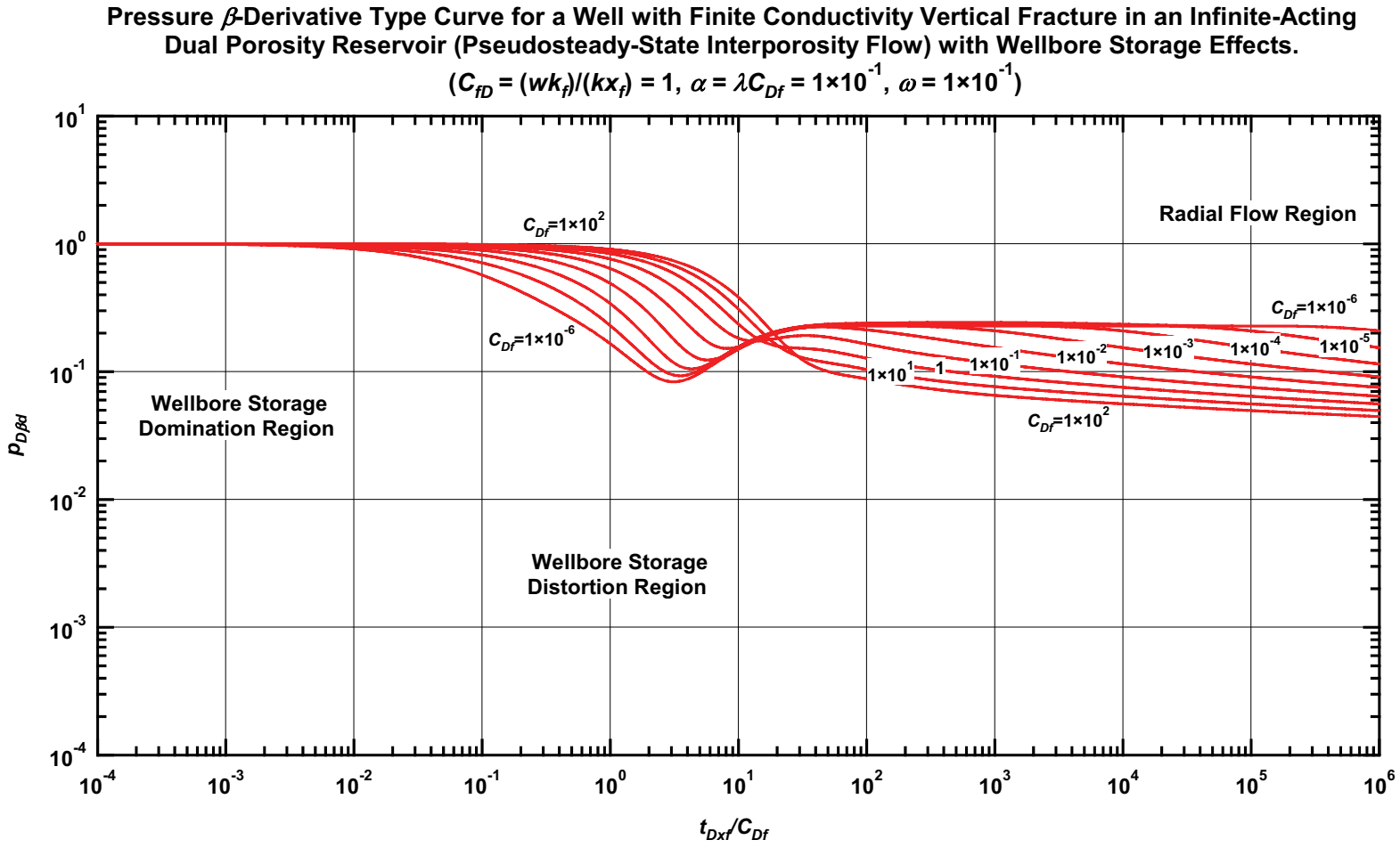

Figure D.3 — $p_{D\beta d}$ vs. t_{Dxf}/C_{Df} — C_{fD} =1, $\omega = 1\times10^{-1}$, $\alpha = \lambda C_{Df} = 1\times10^{-1}$ (fractured well in dual porosity system case — includes wellbore storage effects).

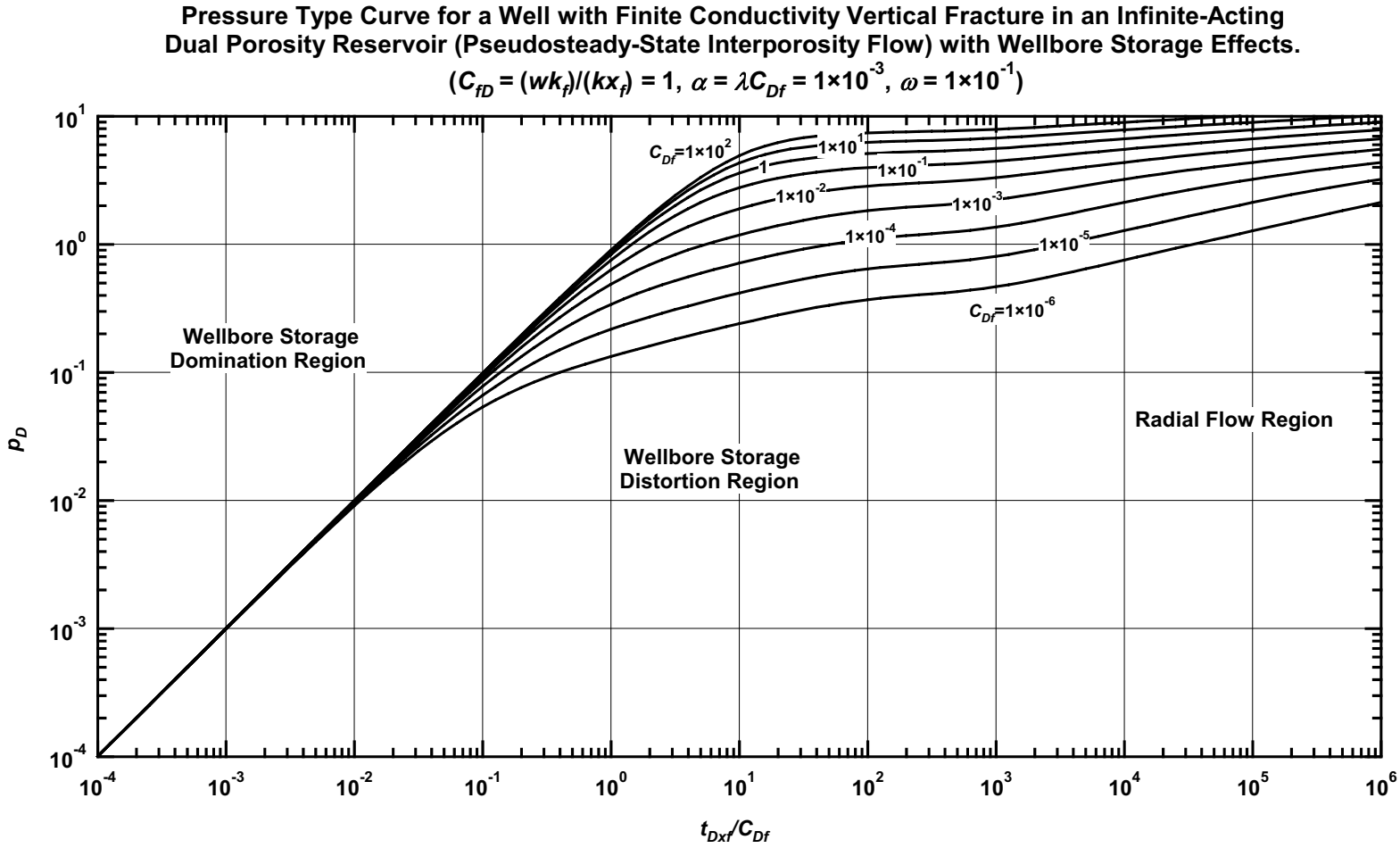

Figure D.4— p_D vs. t_{Dxf}/C_{Df} — C_{fD} =1, $\omega = 1\times10^{-1}$, $\alpha = \lambda C_{Df} = 1\times10^{-3}$ (fractured well in dual porosity system case — includes wellbore storage effects).

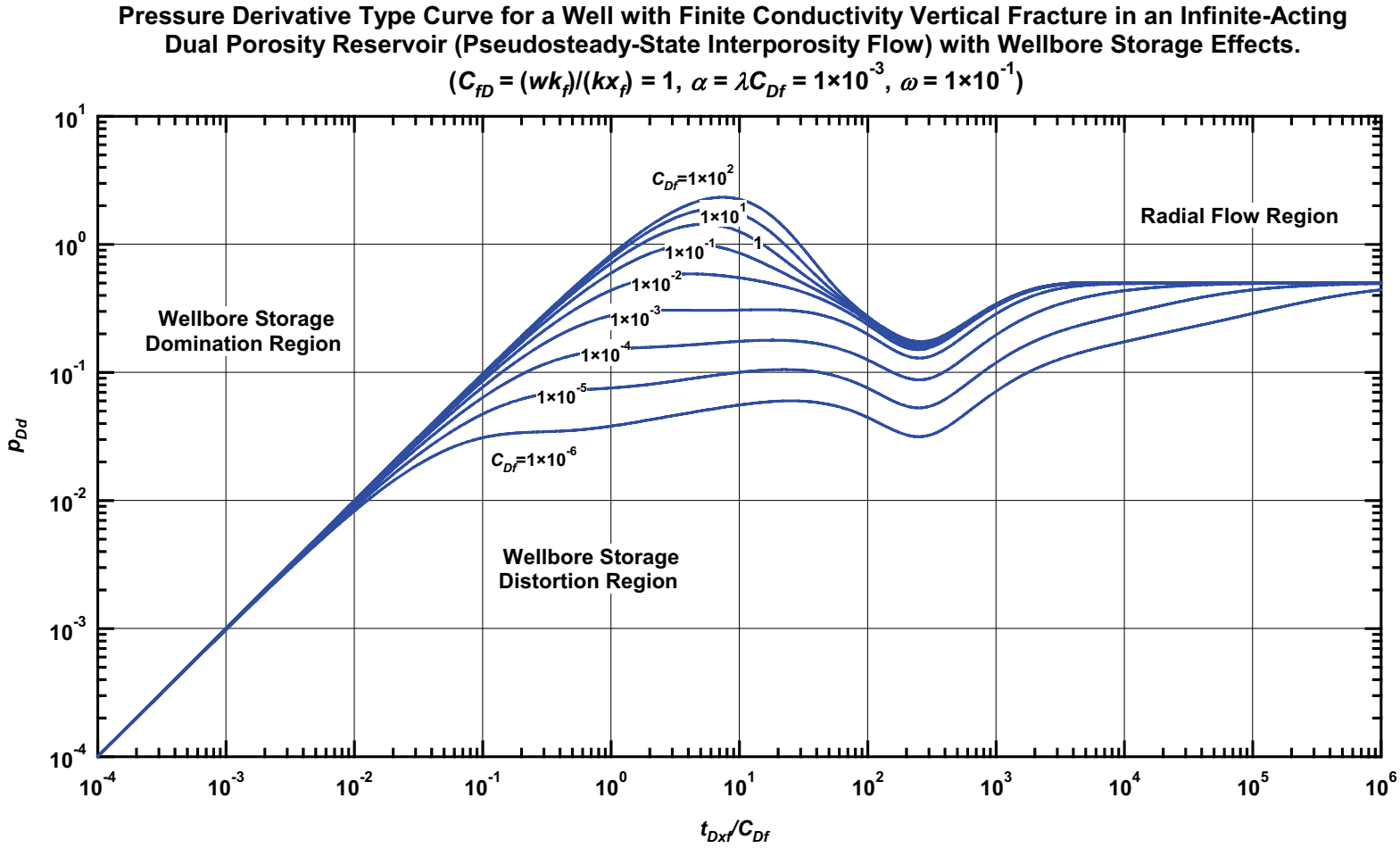

Figure D.5— p_{Dd} vs. t_{Dxf}/C_{Df} — C_{fD} =1, ω = 1×10^{-1}, $\alpha = \lambda C_{Df}$ = 1×10^{-3} (fractured well in dual porosity system case — includes wellbore storage effects).

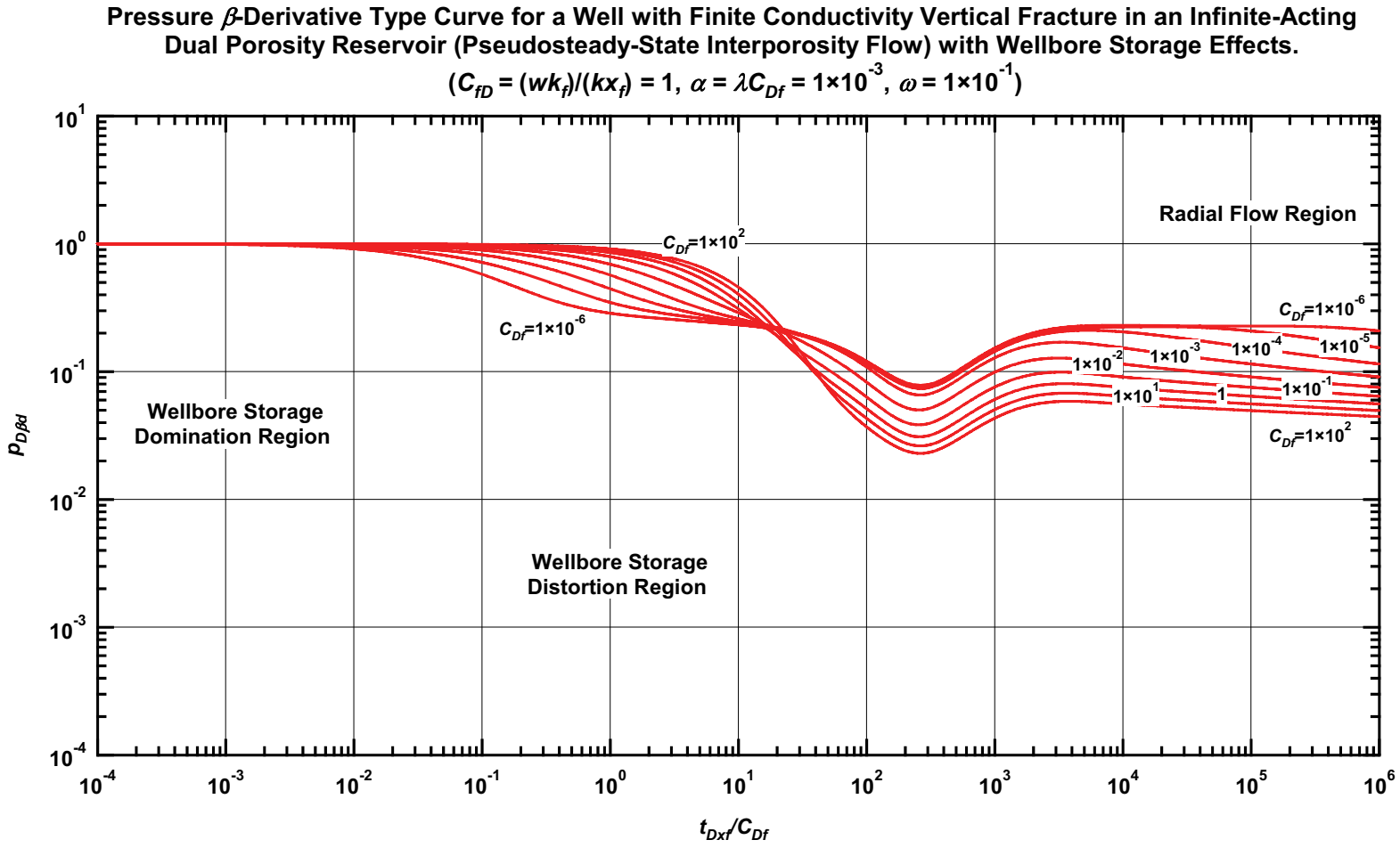

Figure D.6— $p_{D\beta d}$ vs. t_{Dxf}/C_{Df} — C_{fD} =1, $\omega = 1\times10^{-1}$, $\alpha = \lambda C_{Df} = 1\times10^{-3}$ (fractured well in dual porosity system case — includes wellbore storage effects).

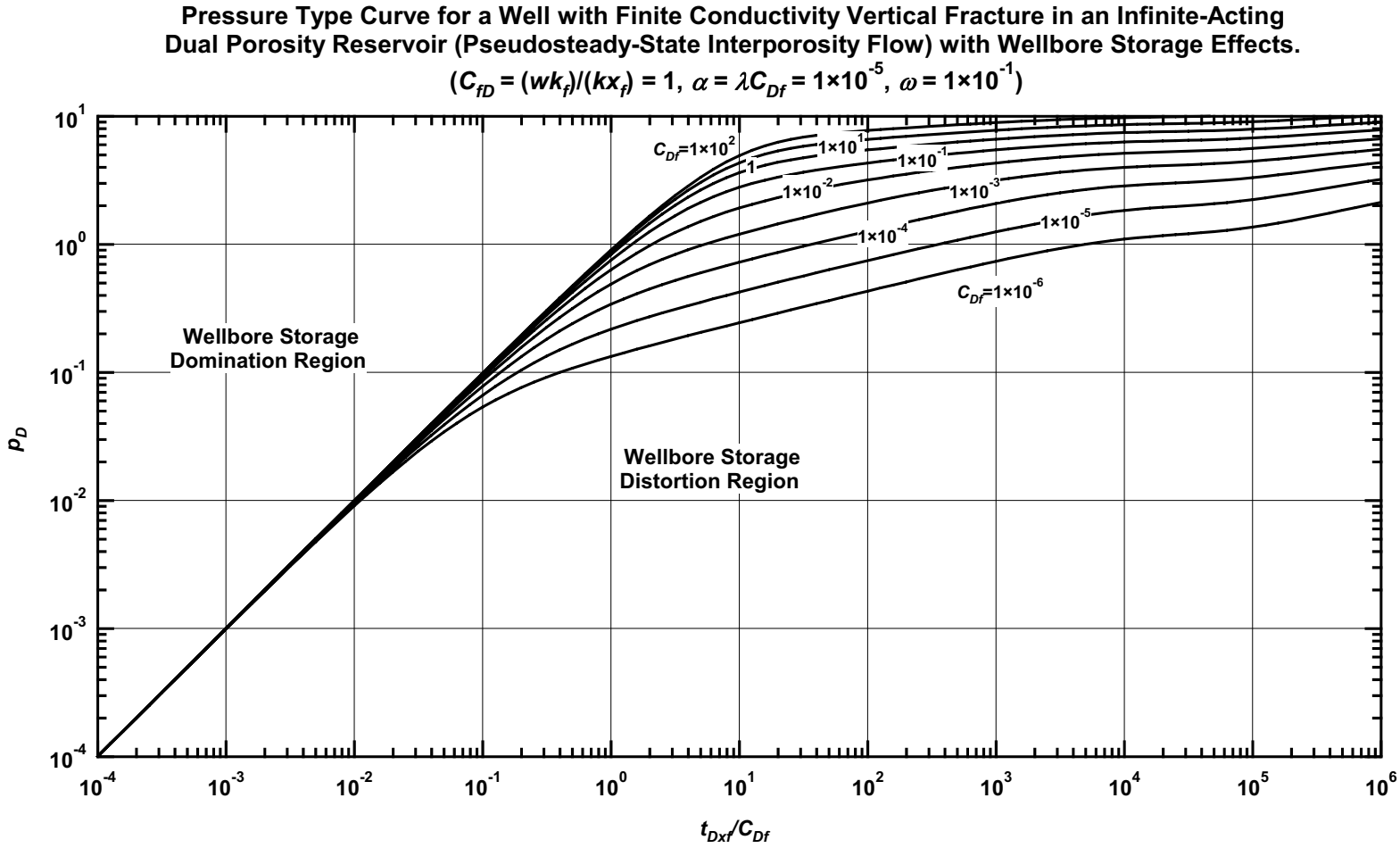

Figure D.7 — p_D vs. t_{Dxf}/C_{Df} — C_{fD} =1, $\omega = 1\times10^{-1}$, $\alpha = \lambda C_{Df} = 1\times10^{-5}$ (fractured well in dual porosity system case — includes wellbore storage effects).

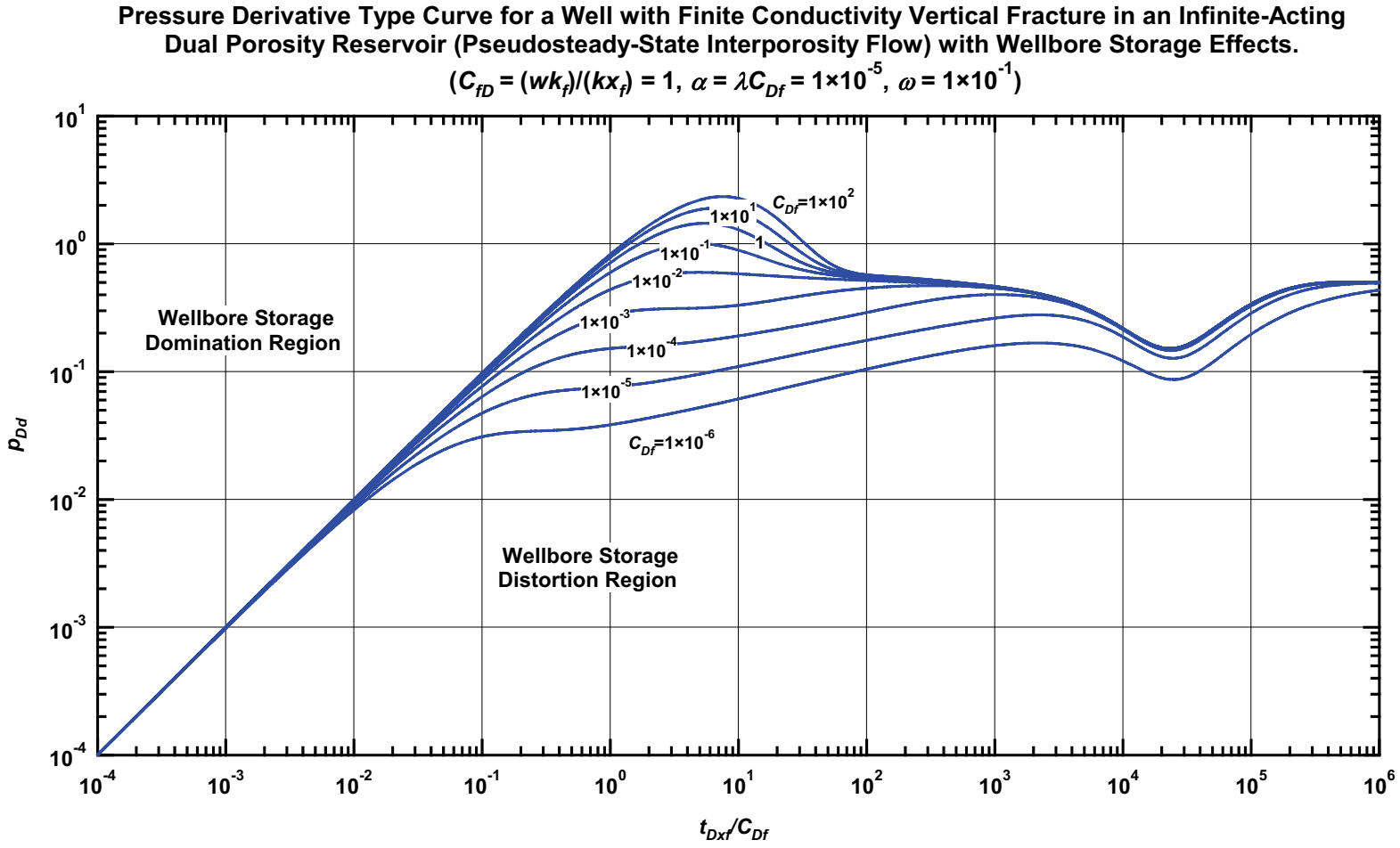

Figure D.8 — p_{Dd} vs. t_{Dxf}/C_{Df} — C_{fD} =1, $\omega = 1\times10^{-1}$, $\alpha = \lambda C_{Df} = 1\times10^{-5}$ (fractured well in dual porosity system case — includes wellbore storage effects).

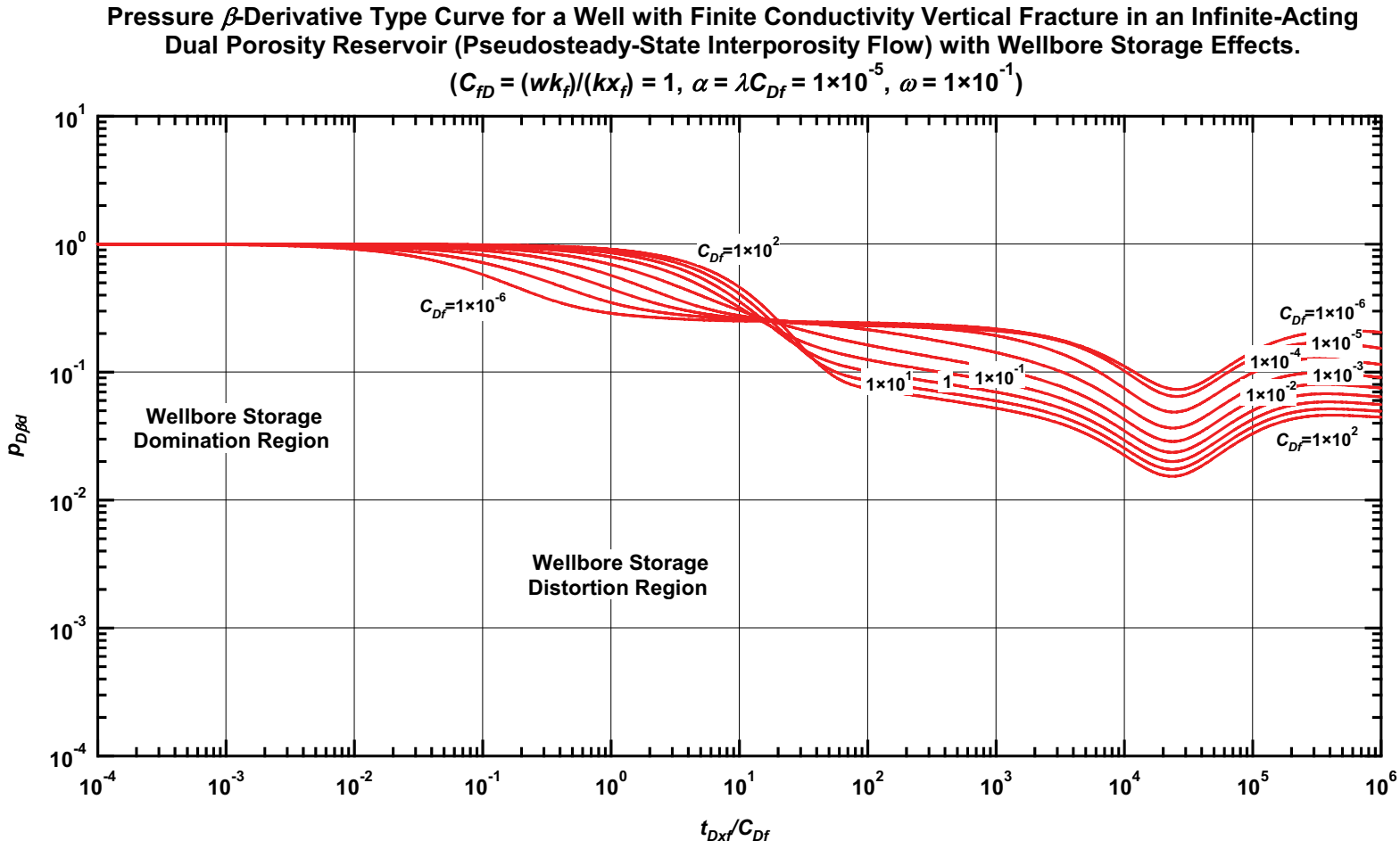

Figure D.9— $p_{D\beta d}$ vs. t_{Dxf}/C_{Df} — C_{fD} =1, $\omega = 1\times10^{-1}$, $\alpha = \lambda C_{Df} = 1\times10^{-5}$ (fractured well in dual porosity system case — includes wellbore storage effects).

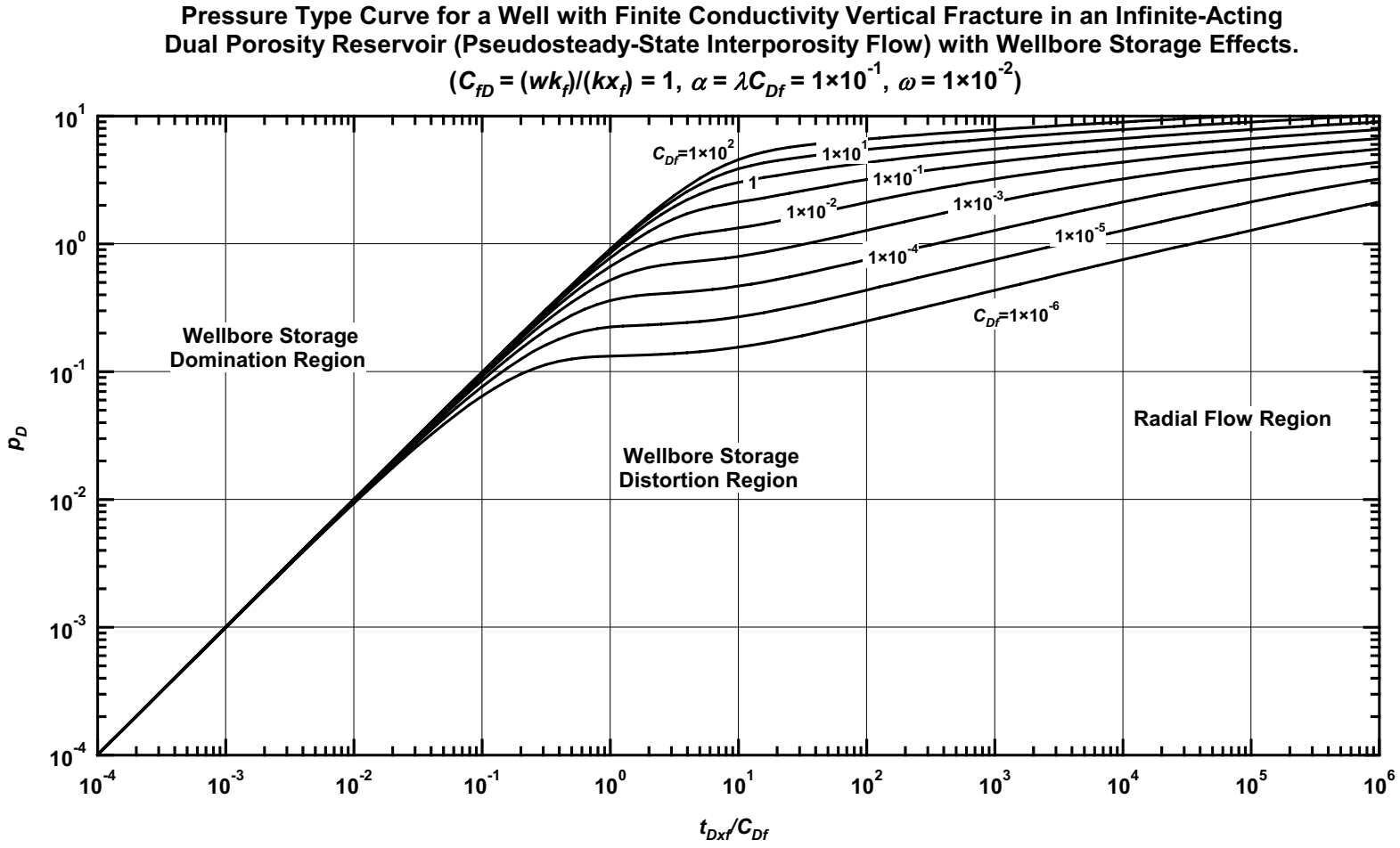

Figure D.10 — p_D **vs.** t_{Dxf}/C_{Df} **—** C_{fD} **=1,** $\omega = 1\times10^{-2}$, $\alpha = \lambda C_{Df} = 1\times10^{-1}$ **(fractured well in dual porosity system case — includes wellbore storage effects).**

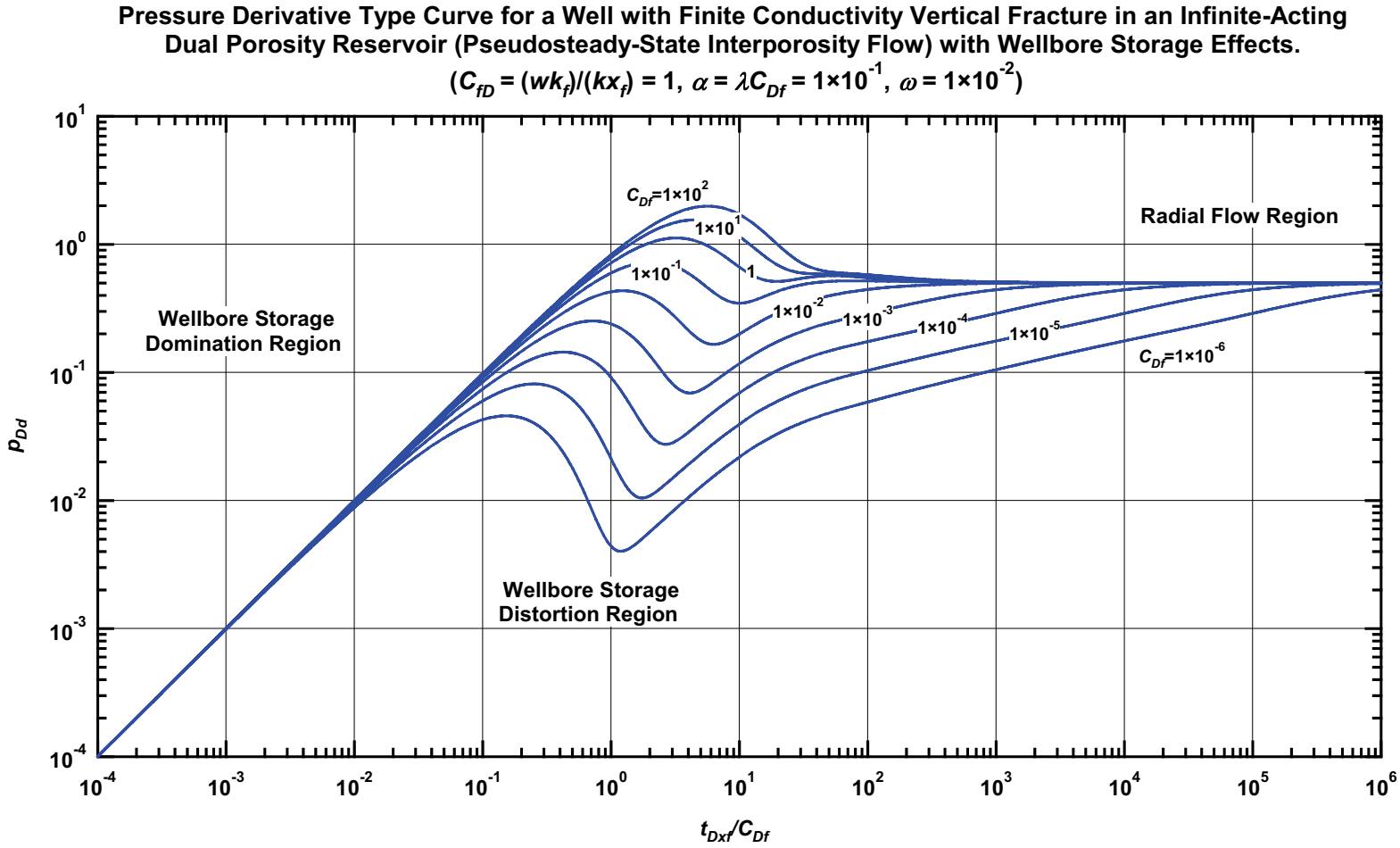

Figure D.11 — p_{Dd} vs. t_{Dxf}/C_{Df} — C_{fD} =1, $\omega = 1\times10^{-2}$, $\alpha = \lambda C_{Df} = 1\times10^{-1}$ (fractured well in dual porosity system case — includes wellbore storage effects).

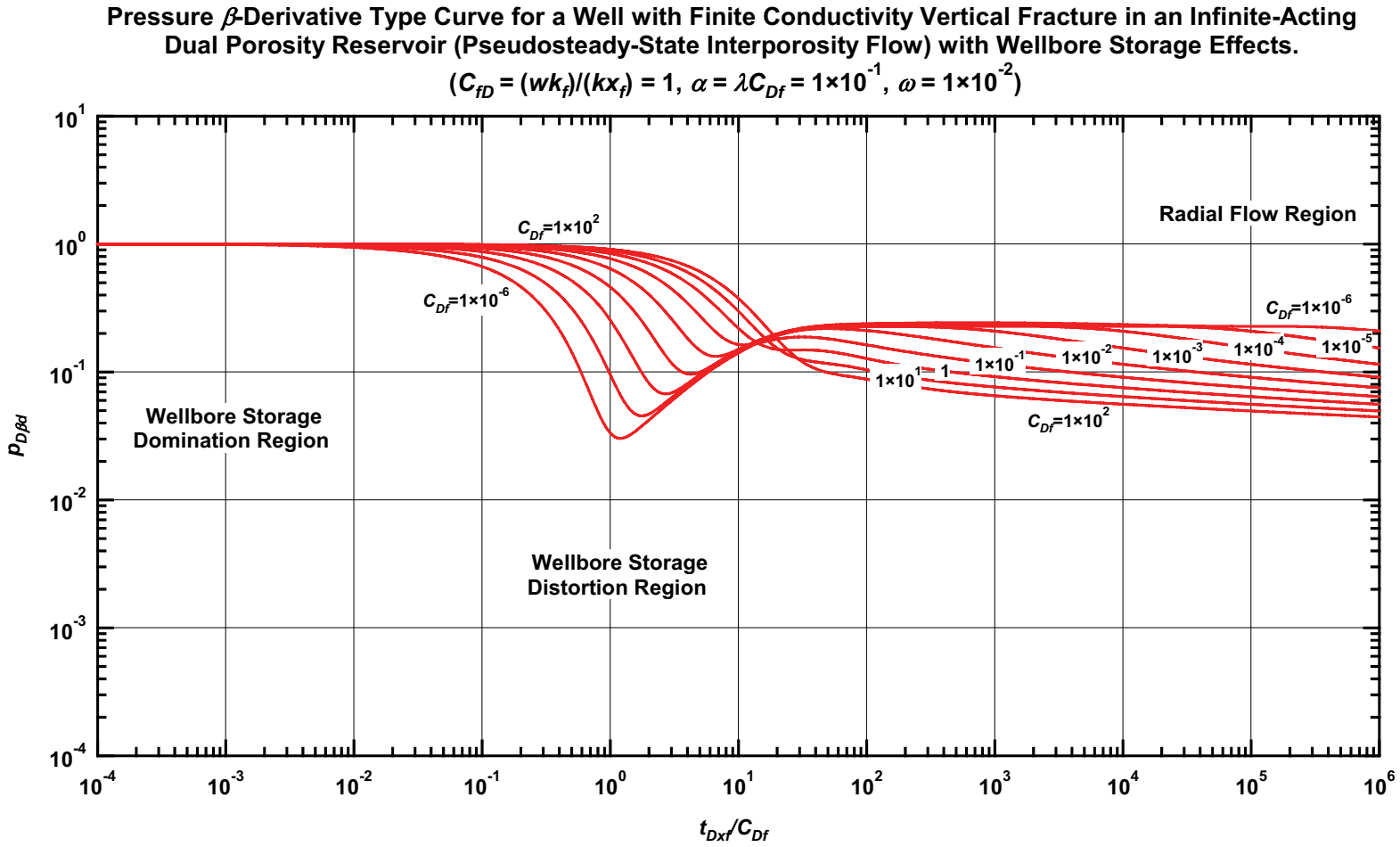

Figure D.12 — $p_{D\beta d}$ vs. t_{Dxf}/C_{Df} — C_{fD} =1, $\omega = 1\times10^{-2}$, $\alpha = \lambda C_{Df} = 1\times10^{-1}$ (fractured well in dual porosity system case — includes wellbore storage effects).

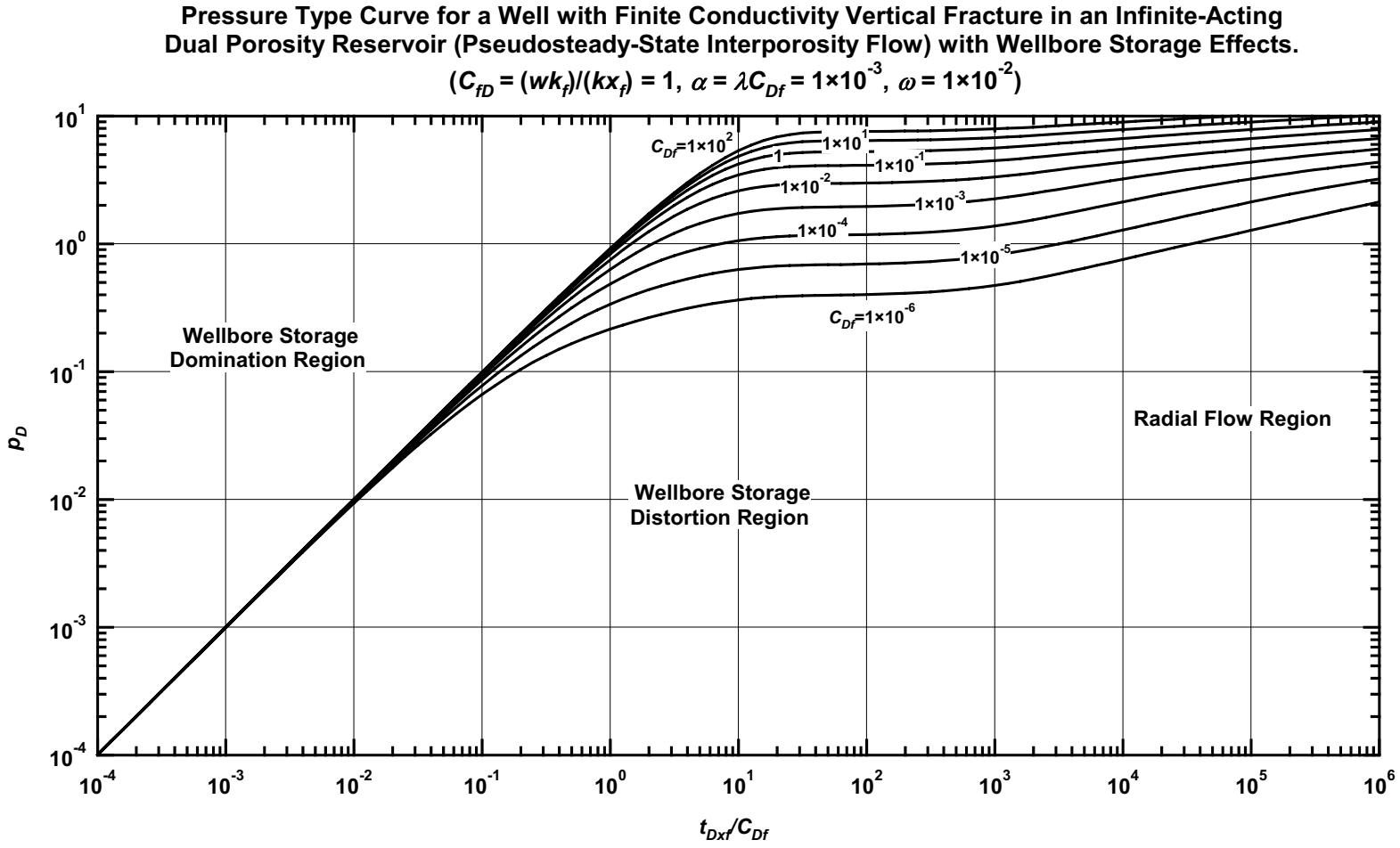

Figure D.13 — p_D vs. t_{Dxf}/C_{Df} — C_{fD} =1, $\omega = 1\times10^{-2}$, $\alpha = \lambda C_{Df} = 1\times10^{-3}$ (fractured well in dual porosity system case — includes wellbore storage effects).

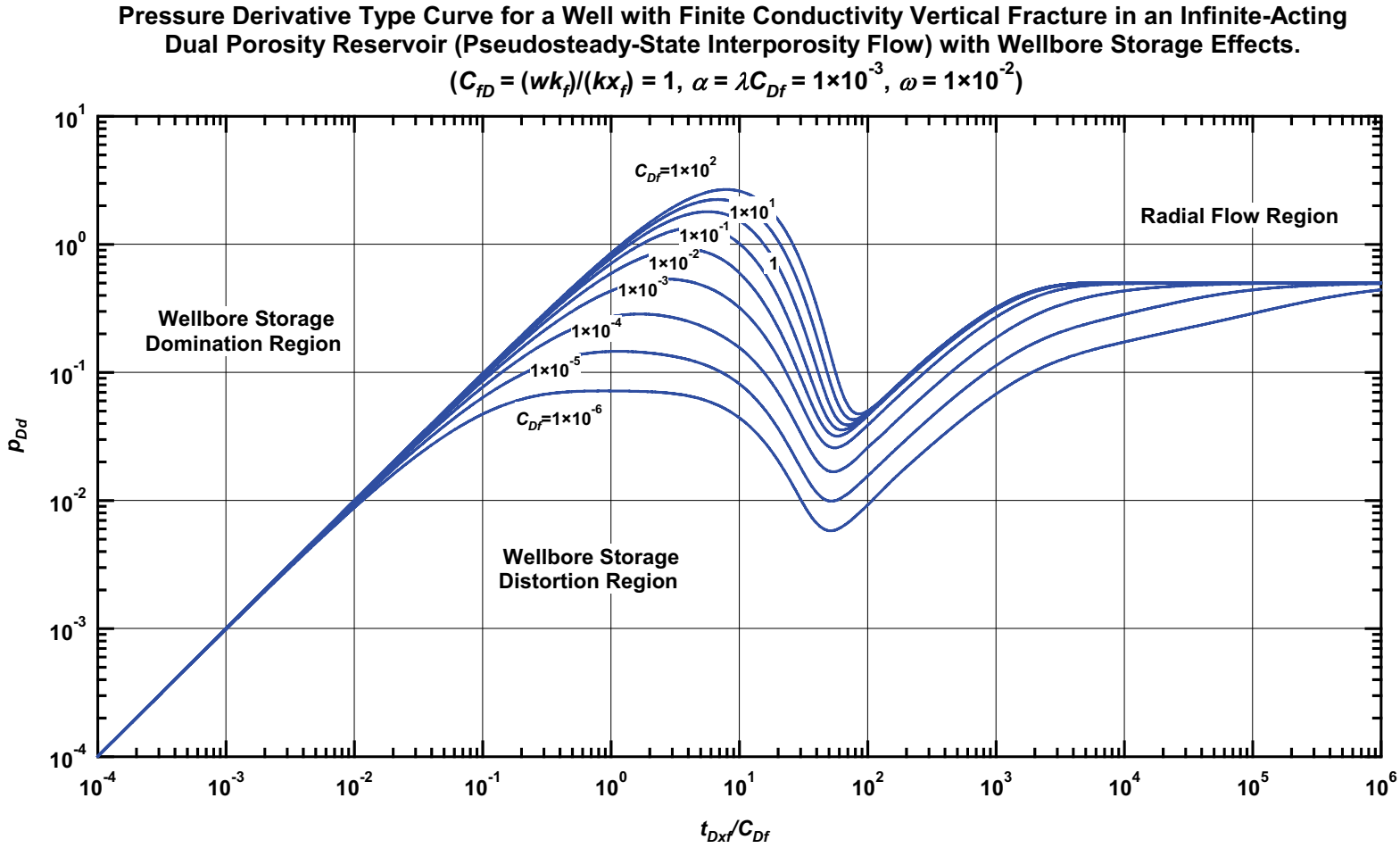

Figure D.14— p_{Dd} vs. t_{Dxf}/C_{Df} — C_{fD} =1, $\omega = 1\times10^{-2}$, $\alpha = \lambda C_{Df} = 1\times10^{-3}$ (fractured well in dual porosity system case — includes wellbore storage effects).

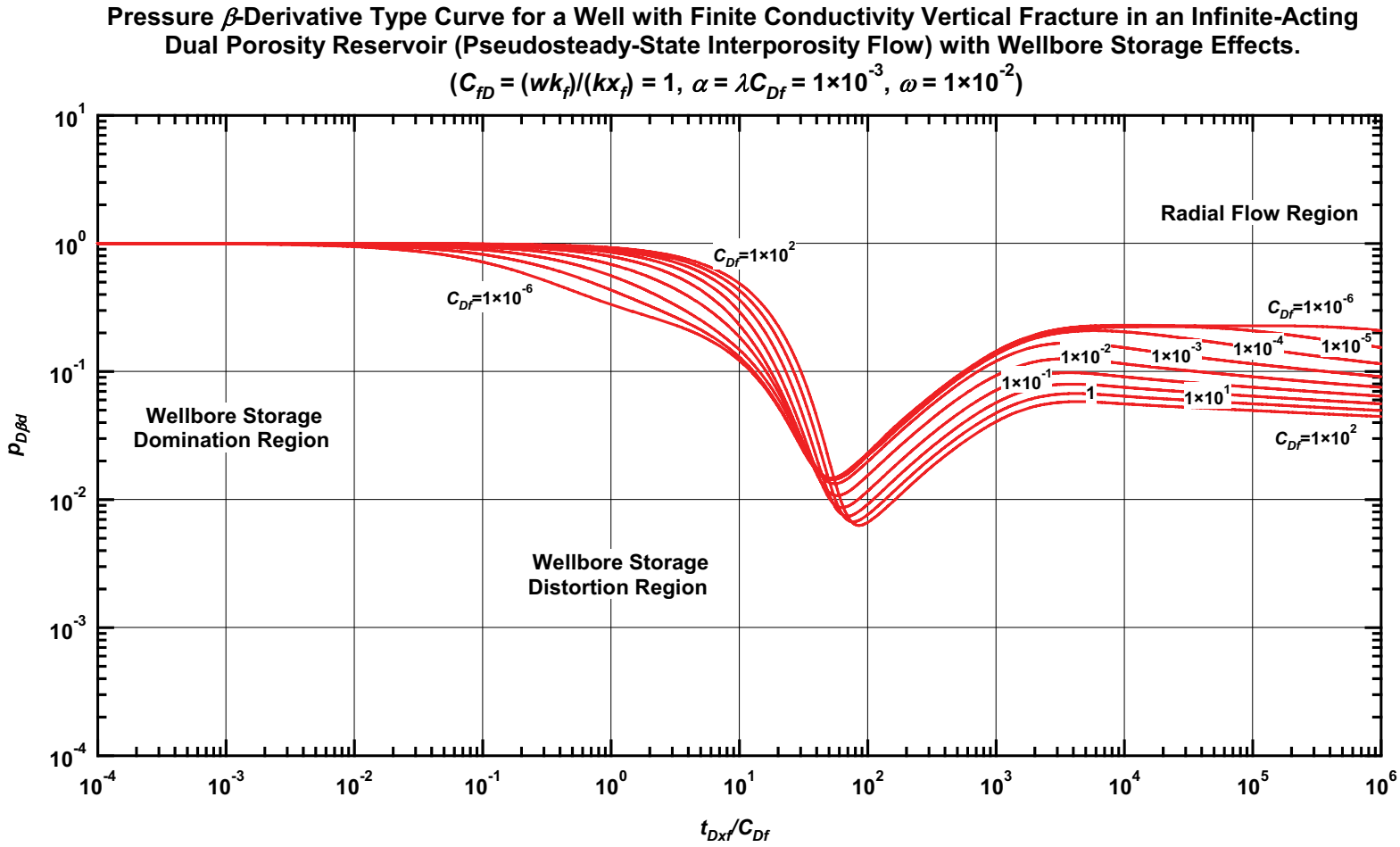

Figure D.15 — $p_{D\beta d}$ vs. t_{Dxf}/C_{Df} — C_{fD} =1, $\omega = 1\times10^{-2}$, $\alpha = \lambda C_{Df} = 1\times10^{-3}$ (fractured well in dual porosity system case — includes wellbore storage effects).

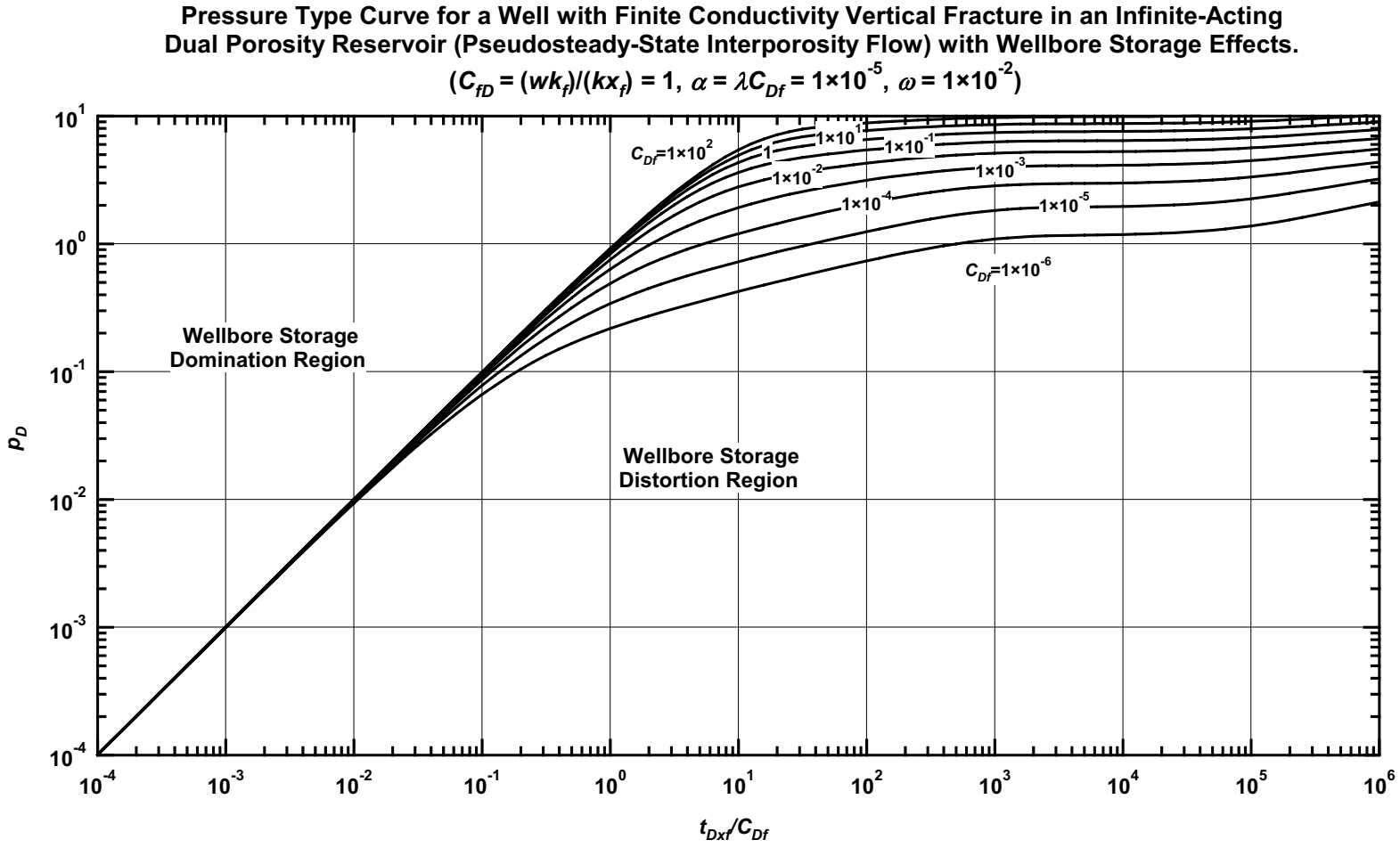

Figure D.16 — p_D vs. t_{Dxf}/C_{Df} — C_{fD} =1, $\omega = 1\times10^{-2}$, $\alpha = \lambda C_{Df} = 1\times10^{-5}$ (fractured well in dual porosity system case — includes wellbore storage effects).

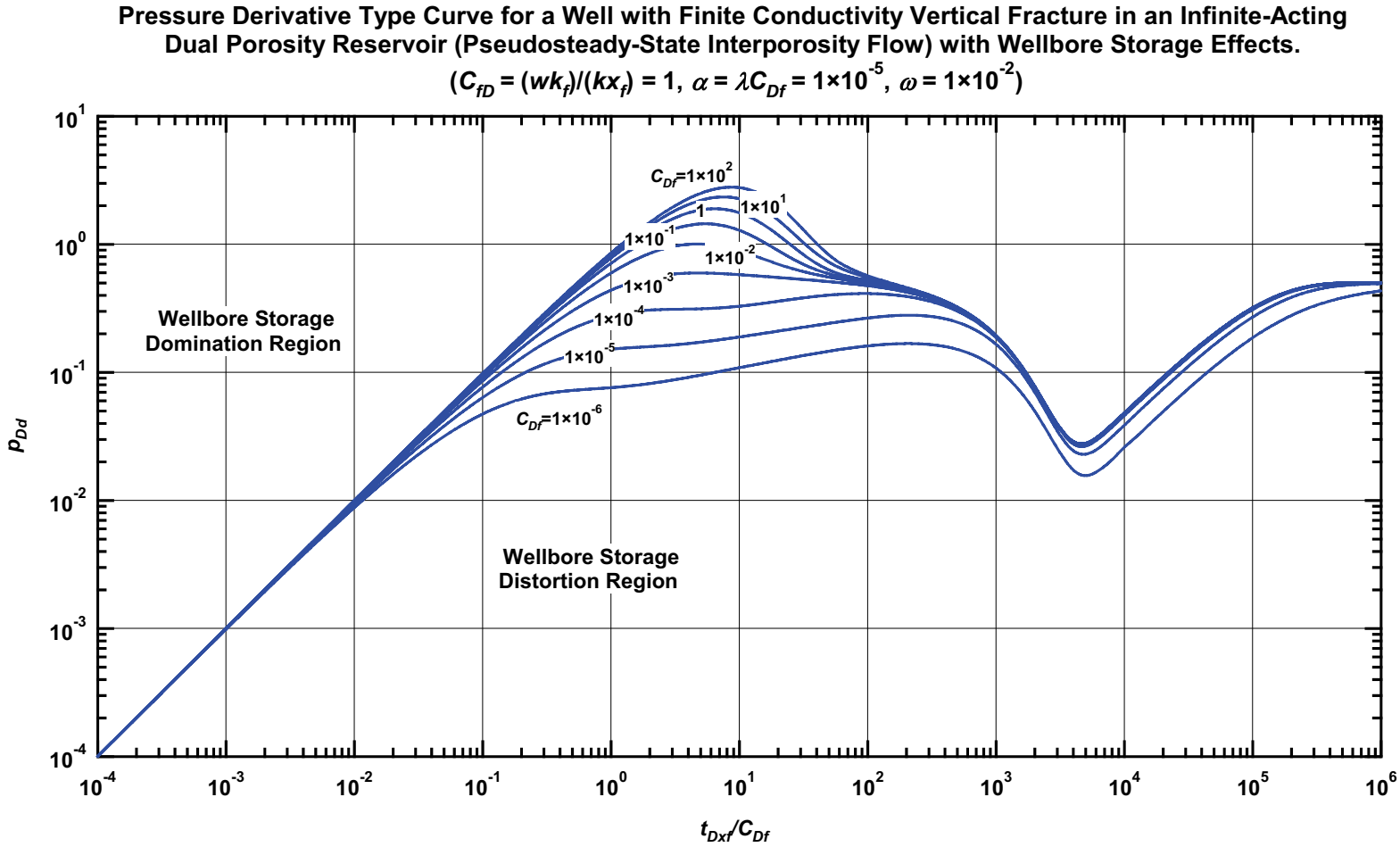

Figure D.17 — p_{Dd} vs. t_{Dxf}/C_{Df} — C_{fD} =1, $\omega = 1\times10^{-2}$, $\alpha = \lambda C_{Df} = 1\times10^{-5}$ (fractured well in dual porosity system case — includes wellbore storage effects).

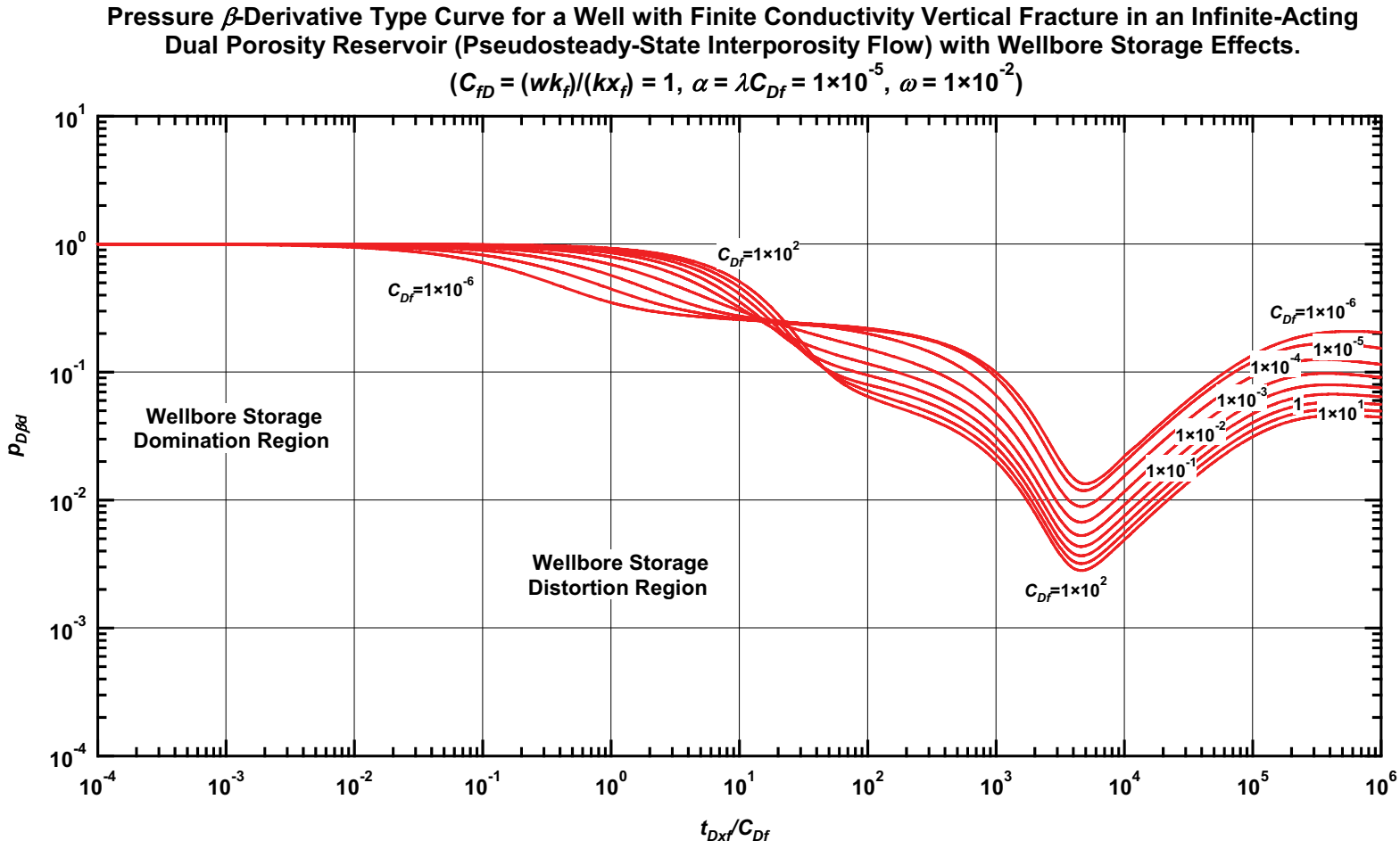

Figure D.18 — $p_{D\beta d}$ vs. t_{Dxf}/C_{Df} — C_{fD} =1, $\omega = 1\times10^{-2}$, $\alpha = \lambda C_{Df} = 1\times10^{-5}$ (fractured well in dual porosity system case — includes wellbore storage effects).

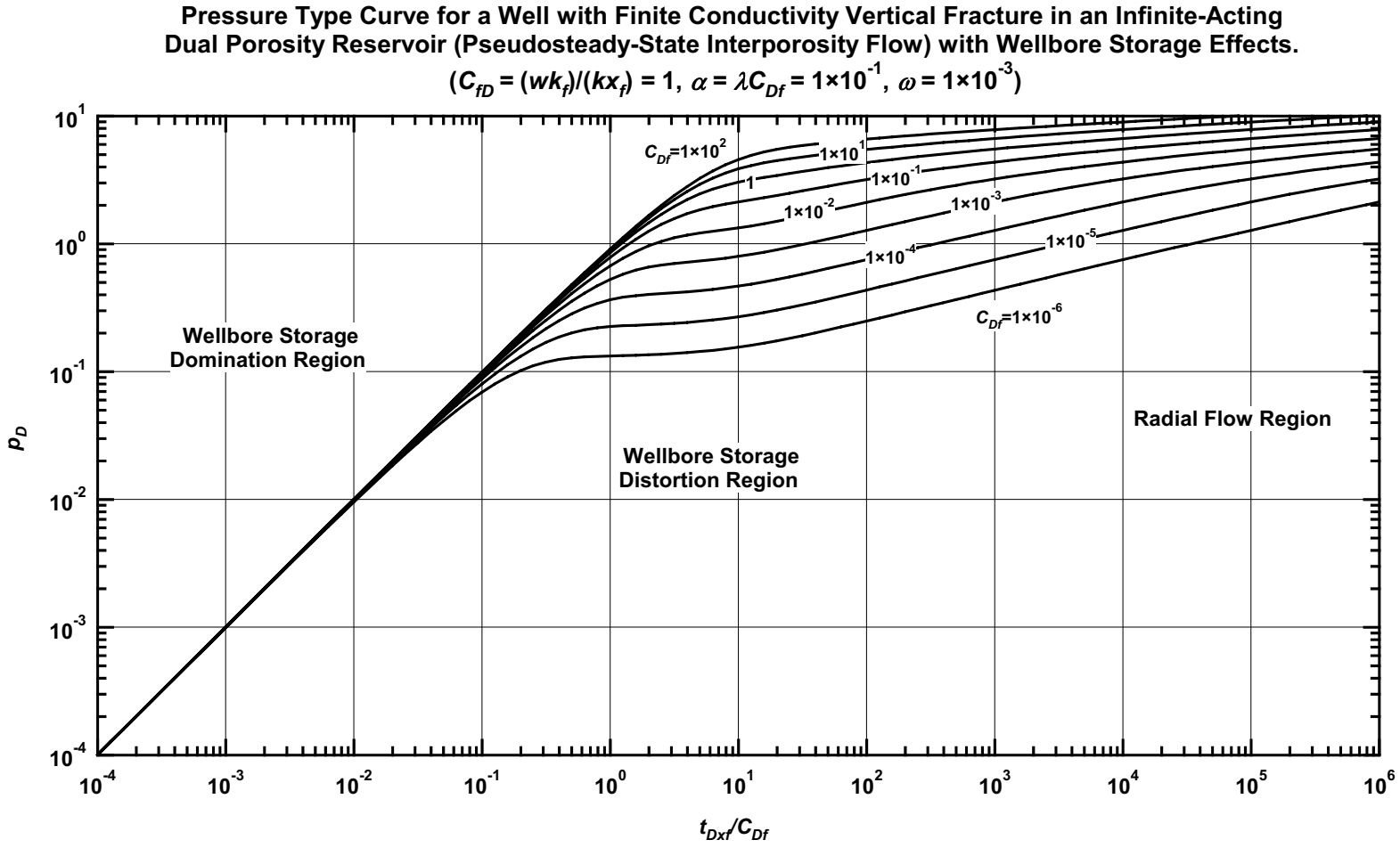

Figure D.19 — p_D **vs.** t_{Dxf}/C_{Df} **—** C_{fD} **=1,** $\omega = 1\times10^{-3}$, $\alpha = \lambda C_{Df} = 1\times10^{-1}$ **(fractured well in dual porosity system case — includes wellbore storage effects).**

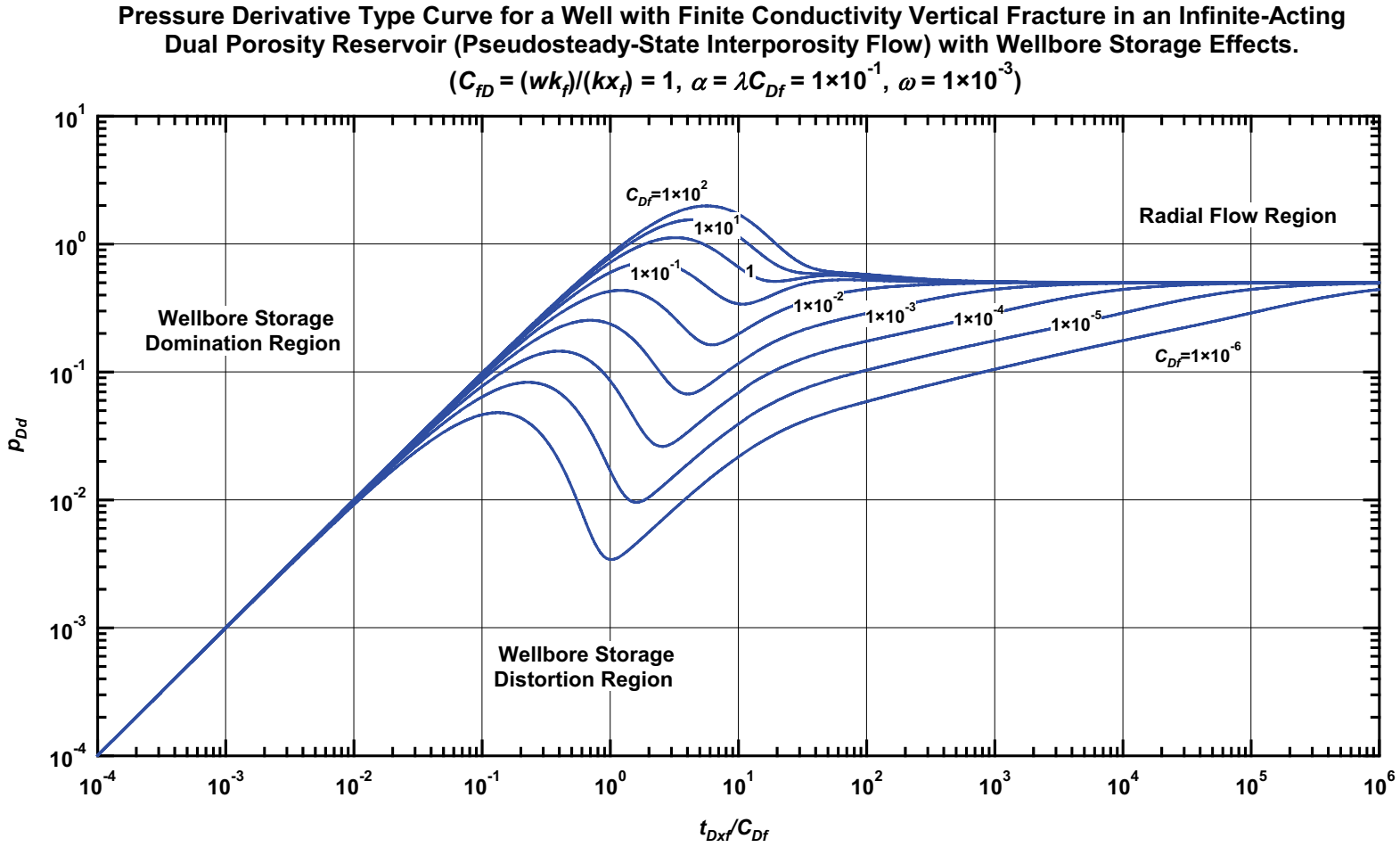

Figure D.20 — p_{Dd} vs. t_{Dxf}/C_{Df} — C_{fD} =1, $\omega = 1\times10^{-3}$, $\alpha = \lambda C_{Df} = 1\times10^{-1}$ (fractured well in dual porosity system case — includes wellbore storage effects).

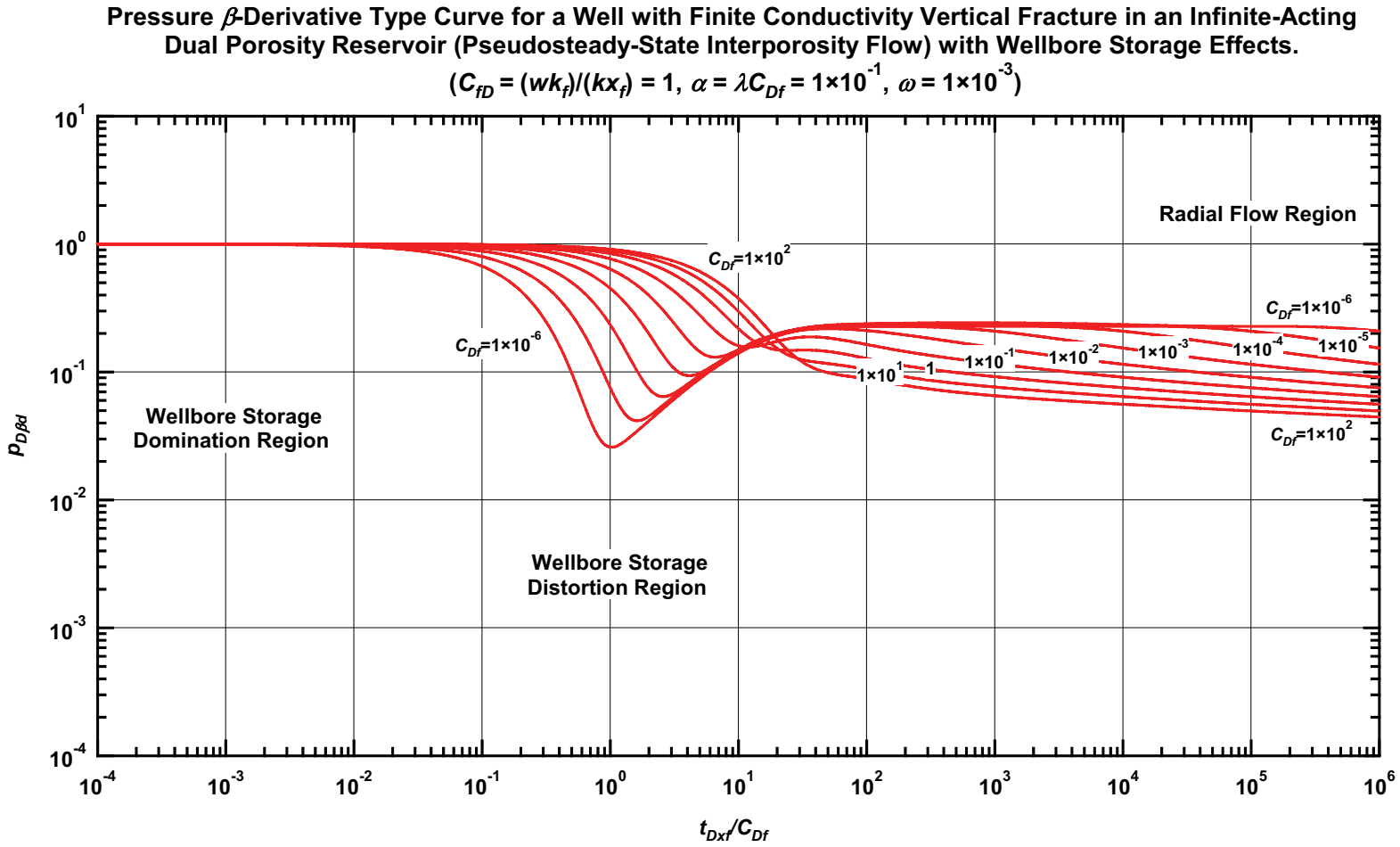

Figure D.21 — $p_{D\beta d}$ vs. t_{Dxf}/C_{Df} — C_{fD} =1, $\omega = 1\times10^{-3}$, $\alpha = \lambda C_{Df} = 1\times10^{-1}$ (fractured well in dual porosity system case — includes wellbore storage effects).

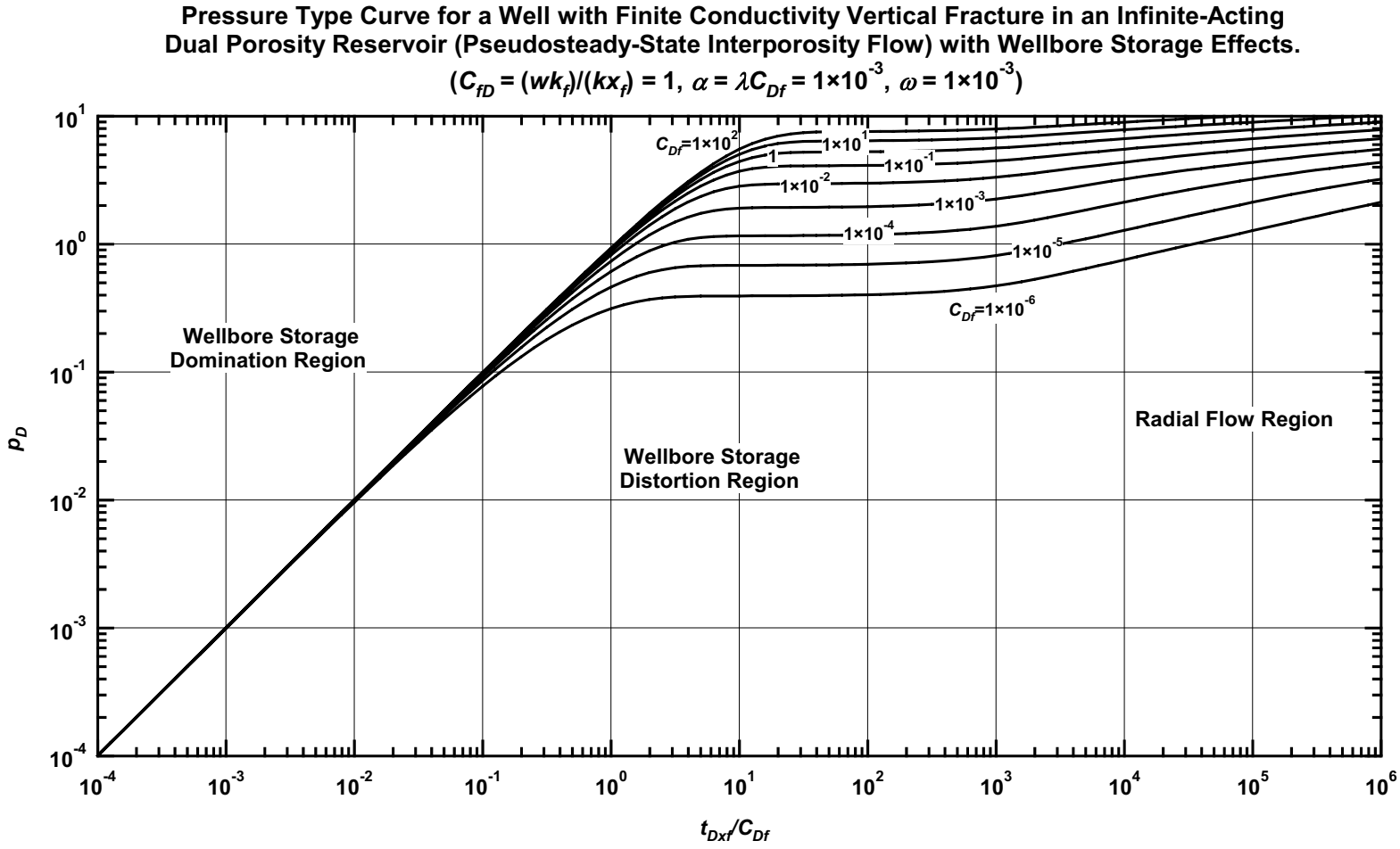

Figure D.22 — p_D **vs.** t_{Dxf}/C_{Df} **—** C_{fD} **=1,** $\omega = 1\times10^{-3}$, $\alpha = \lambda C_{Df} = 1\times10^{-3}$ **(fractured well in dual porosity system case — includes wellbore storage effects).**

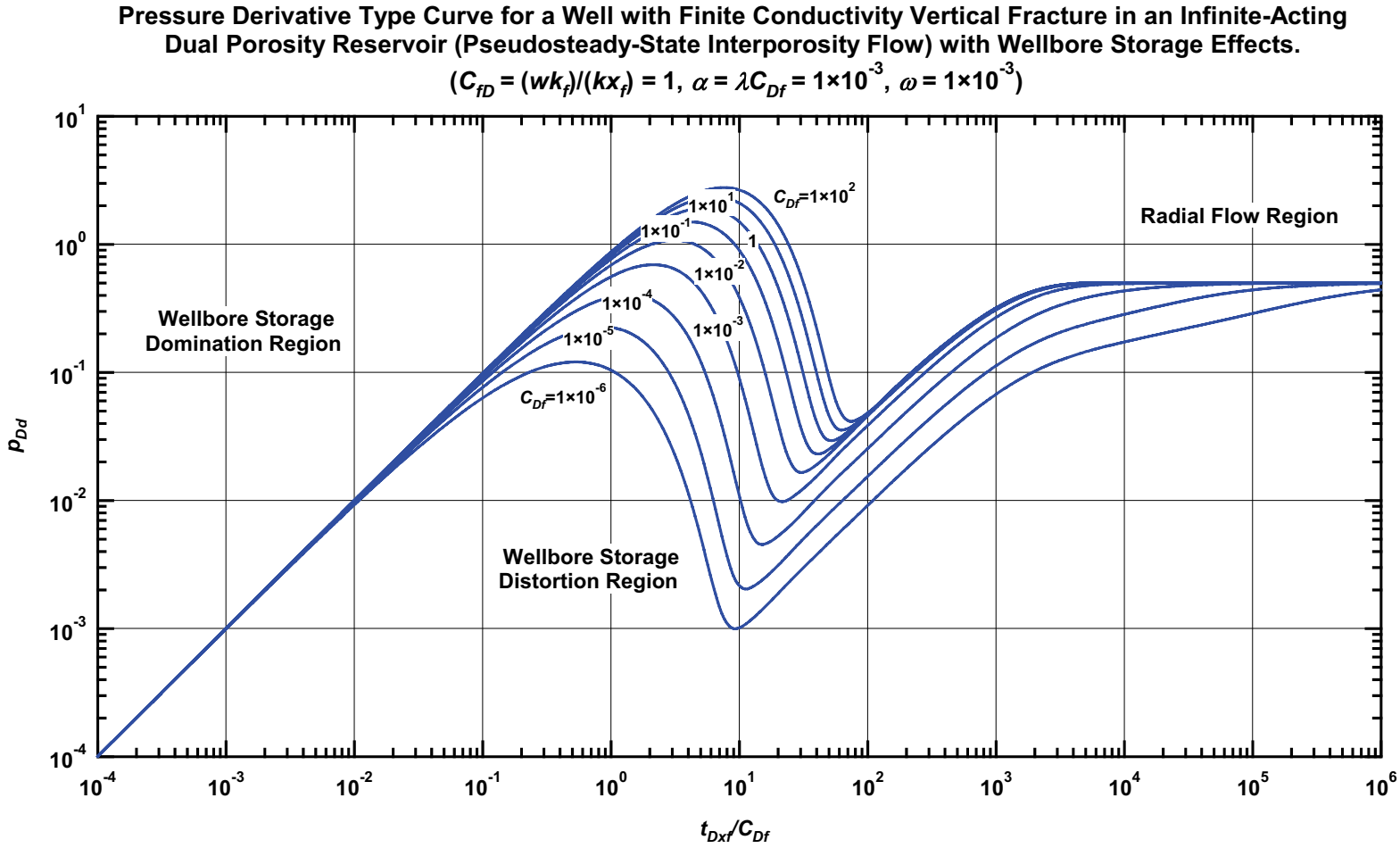

Figure D.23 — p_{Dd} **vs.** t_{Dxf}/C_{Df} **—** C_{fD} **=1,** $\omega = 1\times10^{-3}$, $\alpha = \lambda C_{Df} = 1\times10^{-3}$ **(fractured well in dual porosity system case — includes wellbore storage effects).**

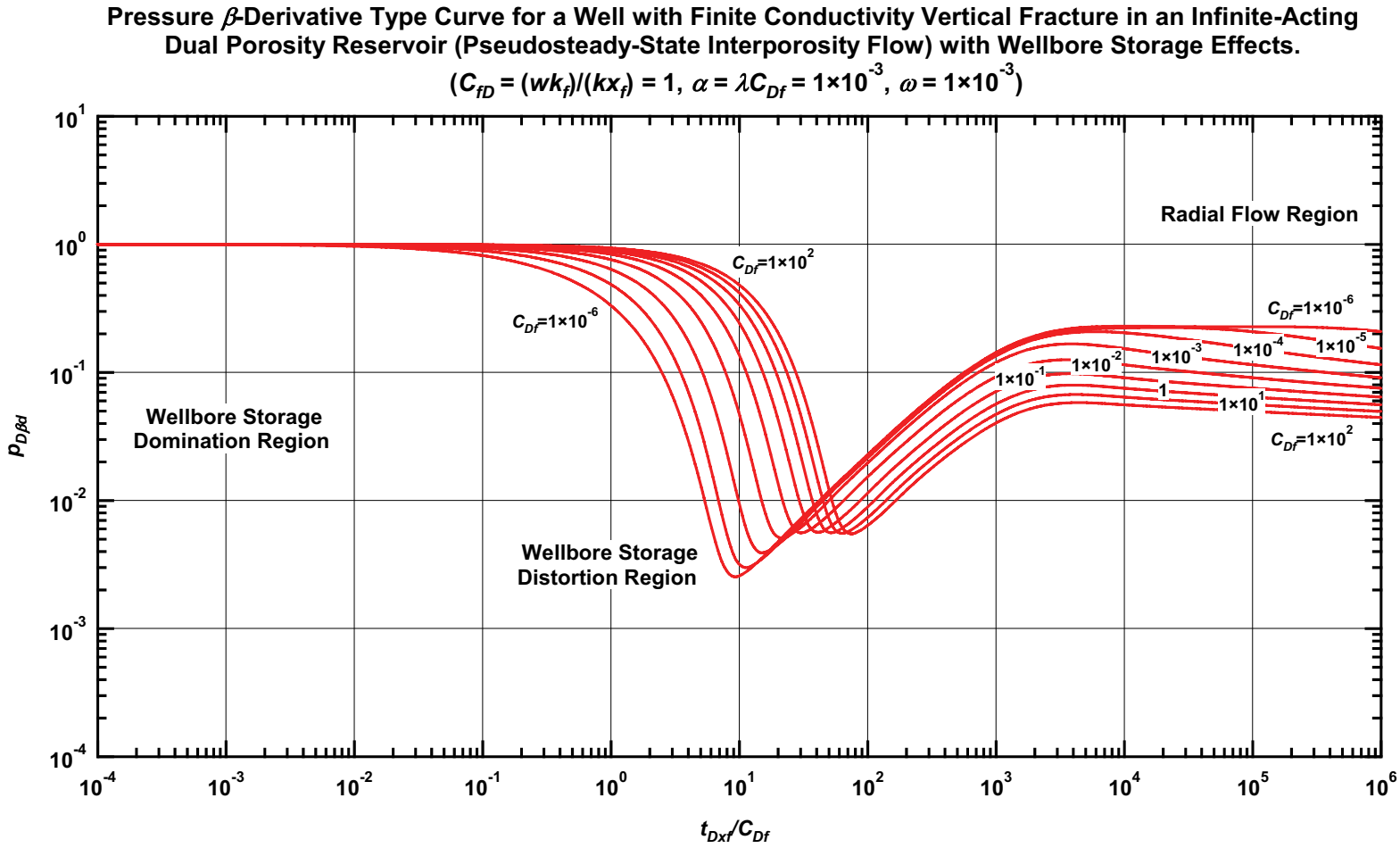

Figure D.24— $p_{D\beta d}$ vs. t_{Dxf}/C_{Df} — C_{fD} =1, $\omega = 1\times10^{-3}$, $\alpha = \lambda C_{Df} = 1\times10^{-3}$ (fractured well in dual porosity system case — includes wellbore storage effects).

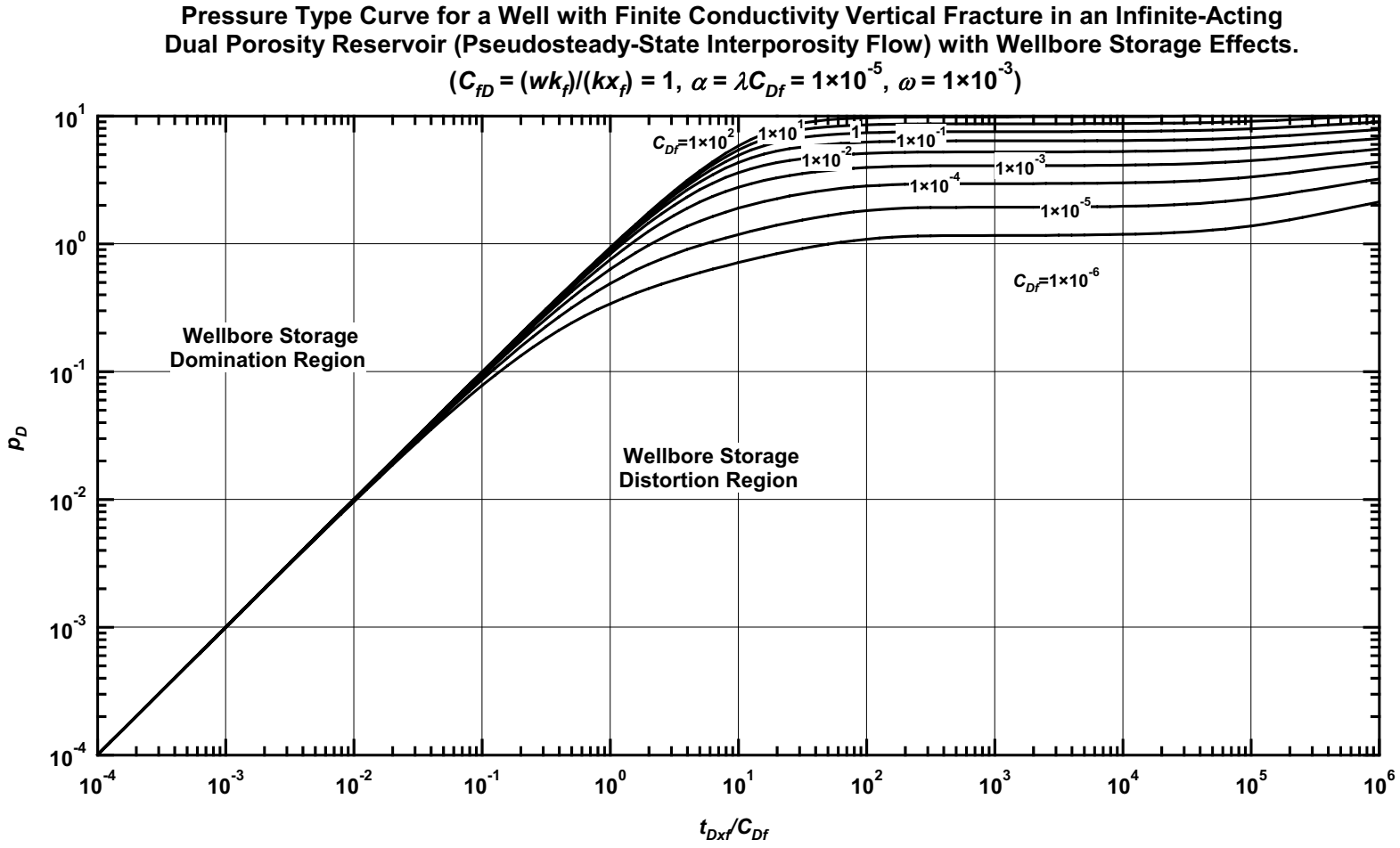

Figure D.25 — p_D vs. t_{Dxf}/C_{Df} — C_{fD} =1, $\omega = 1\times10^{-3}$, $\alpha = \lambda C_{Df} = 1\times10^{-5}$ (fractured well in dual porosity system case — includes wellbore storage effects).

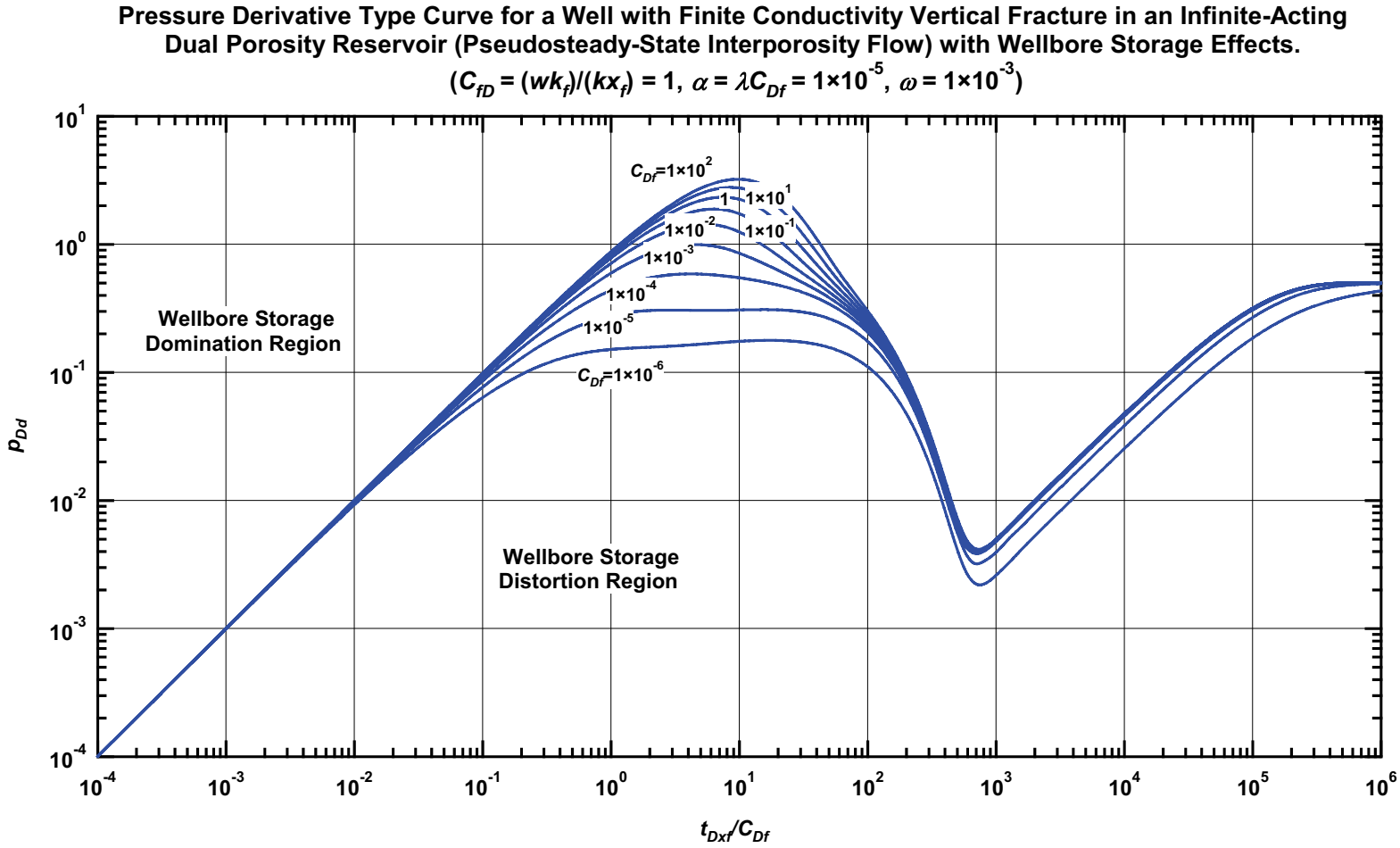

Figure D.26 — p_{Dd} **vs.** t_{Dxf}/C_{Df} **—** C_{fD} **=1,** $\omega = 1\times10^{-3}$, $\alpha = \lambda C_{Df} = 1\times10^{-5}$ **(fractured well in dual porosity system case — includes wellbore storage effects).**

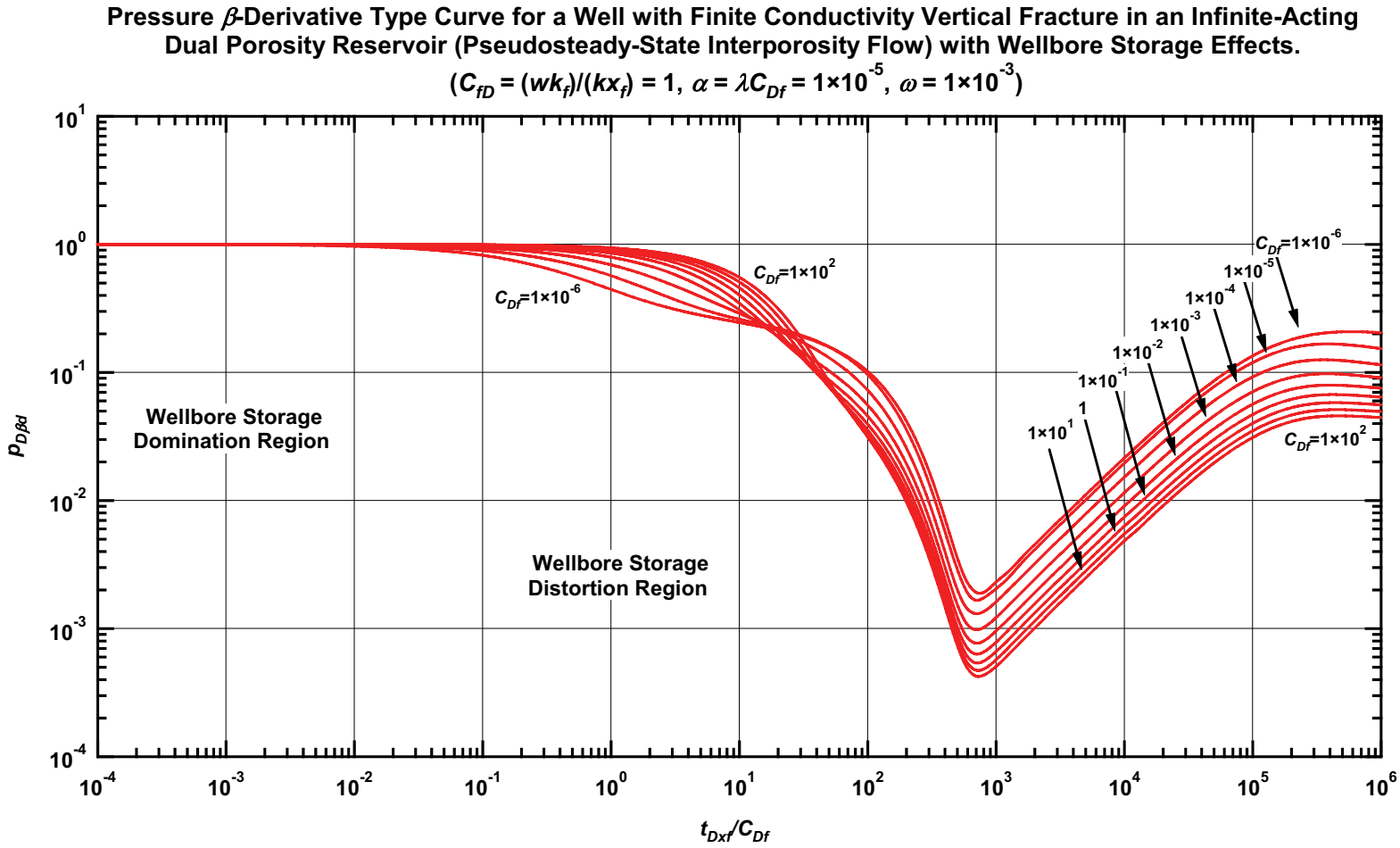

Figure D.27 — $p_{D\beta d}$ vs. t_{Dxf}/C_{Df} — C_{fD} =1, $\omega = 1\times10^{-3}$, $\alpha = \lambda C_{Df} = 1\times10^{-5}$ (fractured well in dual porosity system case — includes wellbore storage effects).

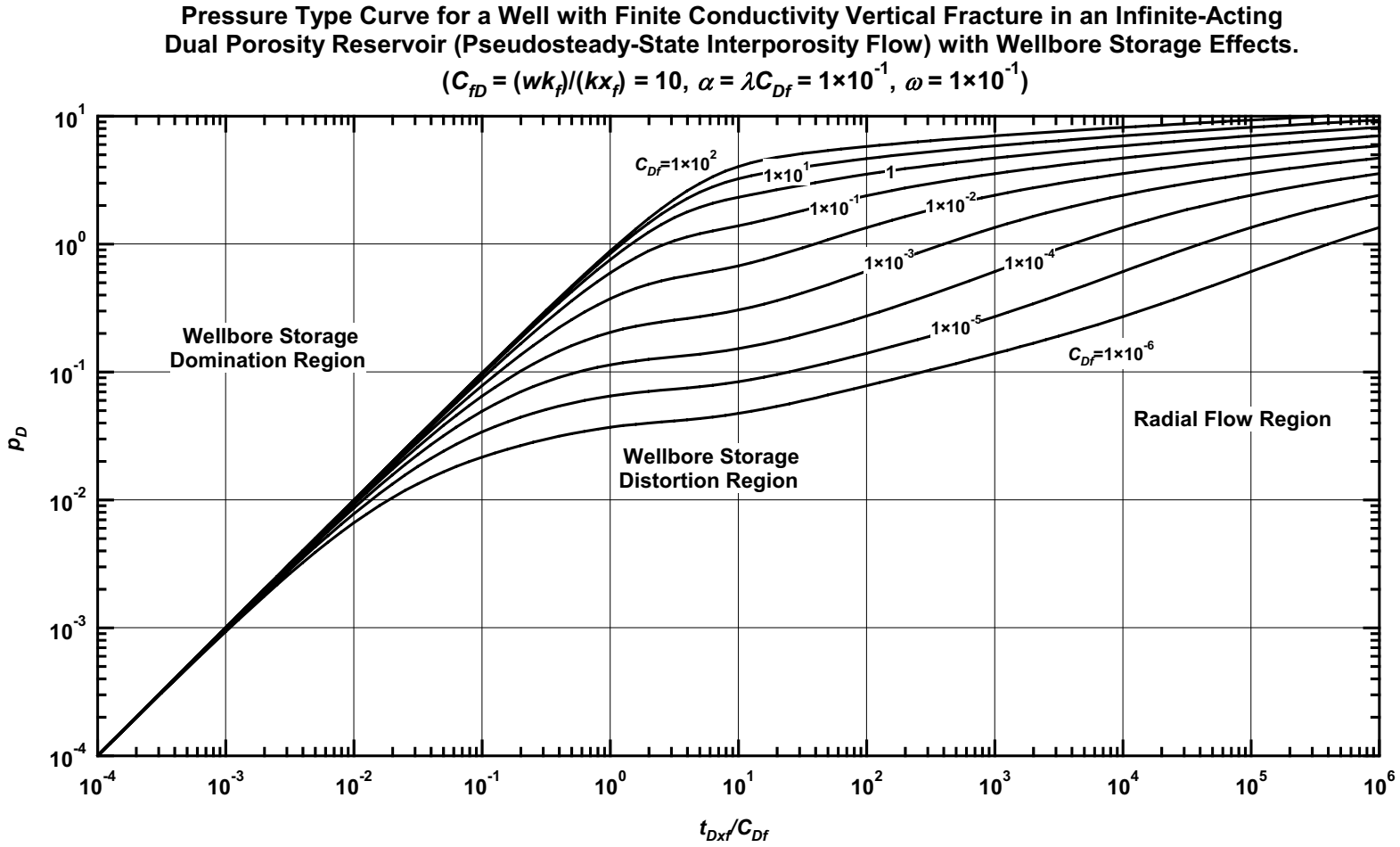

Figure D.28 — p_D vs. t_{Dxf}/C_{Df} — C_{fD} =10, $\omega = 1\times10^{-1}$, $\alpha = \lambda C_{Df} = 1\times10^{-1}$ (fractured well in dual porosity system case — includes wellbore storage effects).

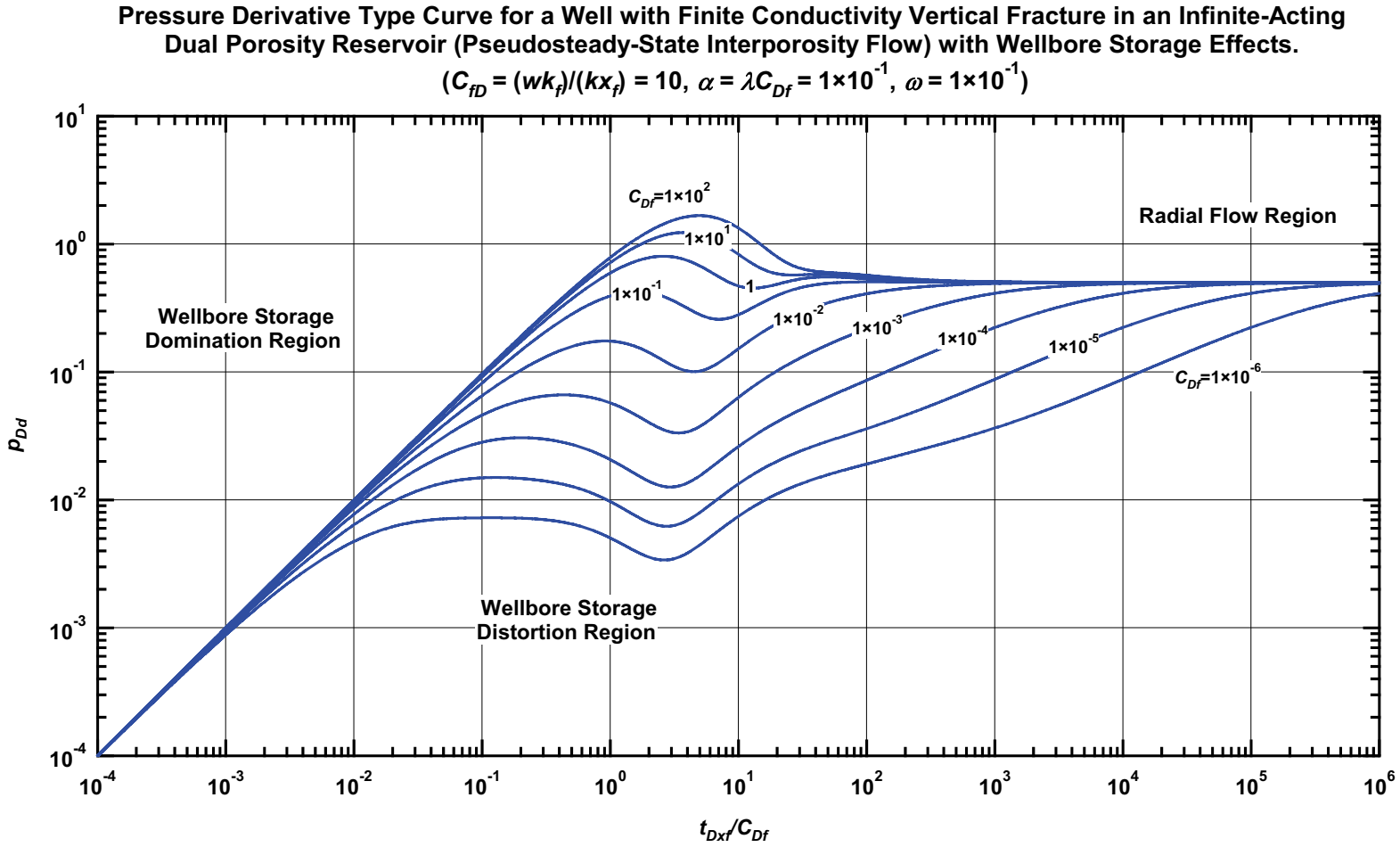

Figure D.29 — p_{Dd} vs. t_{Dxf}/C_{Df} — C_{fD} =10, $\omega = 1\times10^{-1}$, $\alpha = \lambda C_{Df} = 1\times10^{-1}$ (fractured well in dual porosity system case — includes wellbore storage effects).

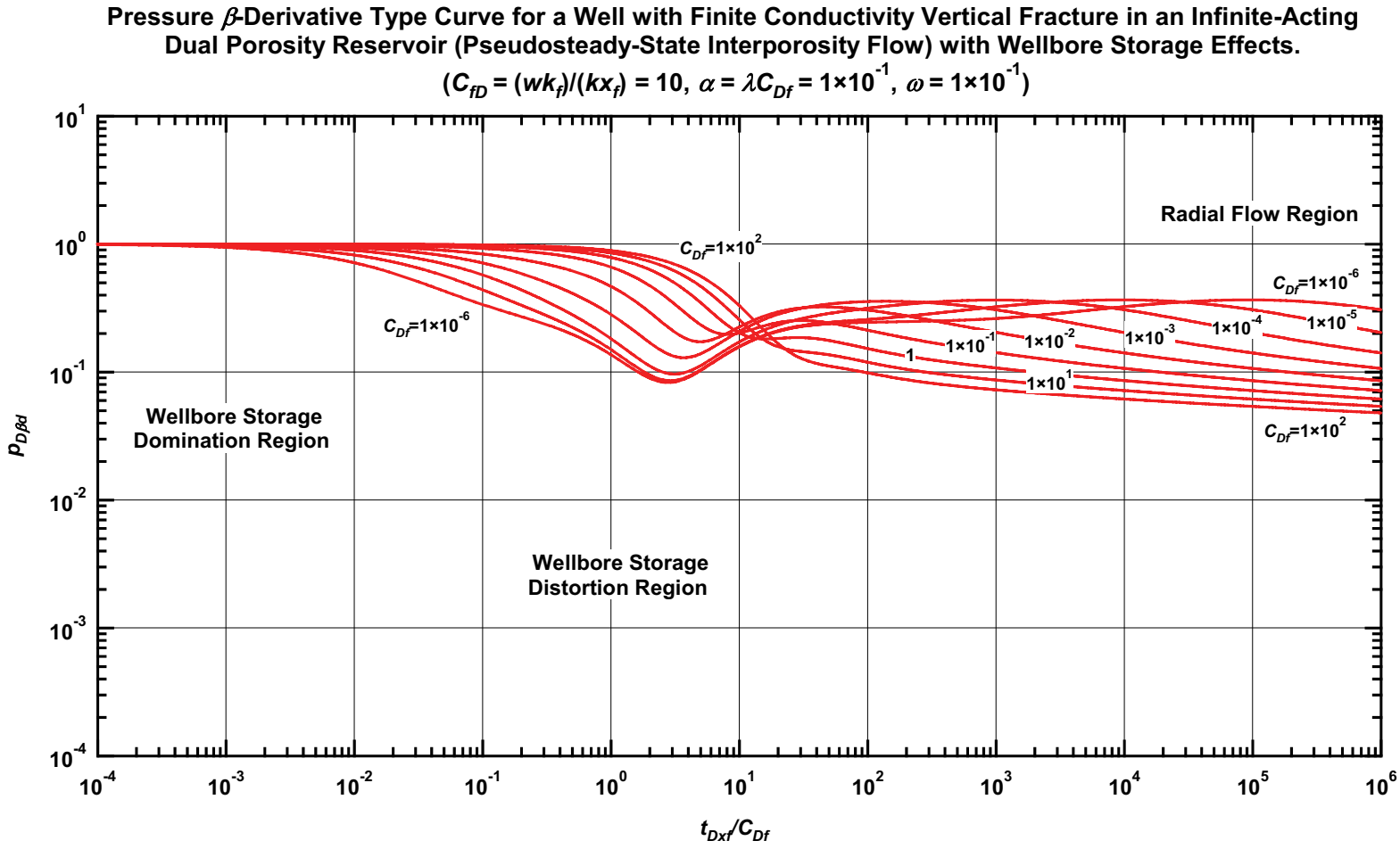

Figure D.30 — $p_{D\beta d}$ vs. t_{Dxf}/C_{Df} — C_{fD} =10, $\omega = 1\times10^{-1}$, $\alpha = \lambda C_{Df} = 1\times10^{-1}$ (fractured well in dual porosity system case — includes wellbore storage effects).

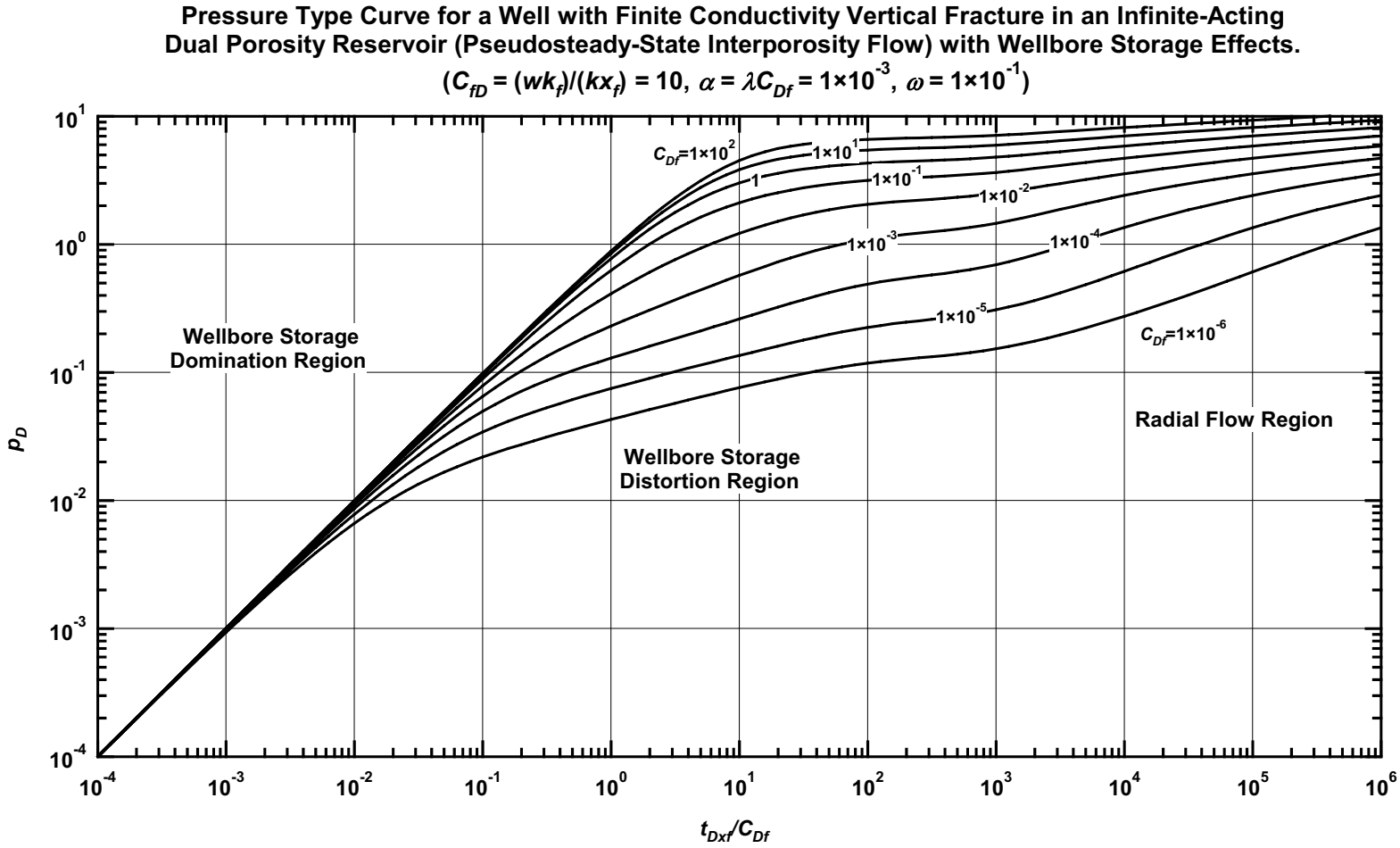

Figure D.31 — p_D **vs.** t_{Dxf}/C_{Df} **—** C_{fD} **=10,** $\omega = 1\times10^{-1}$, $\alpha = \lambda C_{Df} = 1\times10^{-3}$ **(fractured well in dual porosity system case — includes wellbore storage effects).**

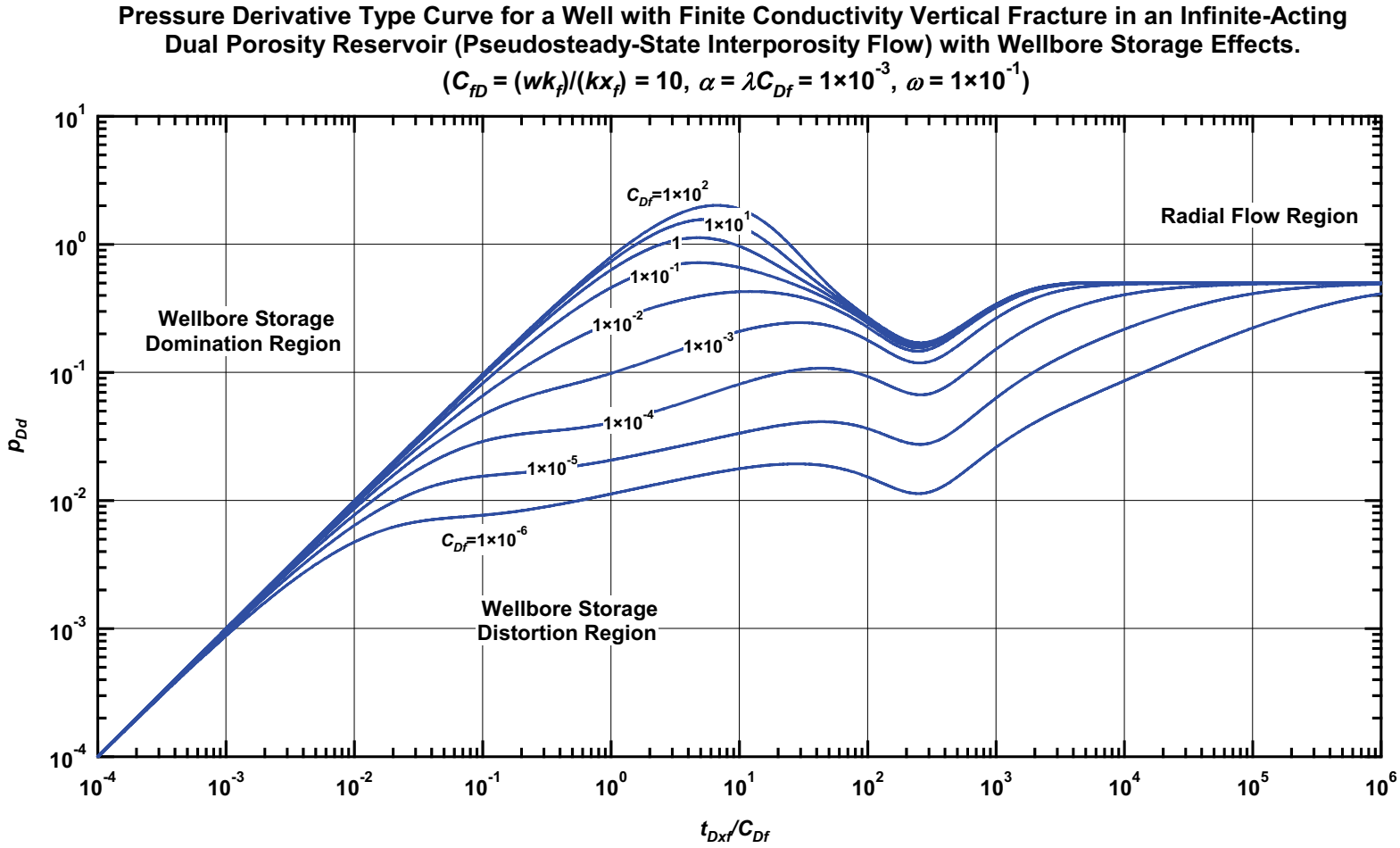

Figure D.32 — p_{Dd} **vs.** t_{Dxf}/C_{Df} **—** C_{fD} **=10,** $\omega = 1\times10^{-1}$, $\alpha = \lambda C_{Df} = 1\times10^{-3}$ **(fractured well in dual porosity system case — includes wellbore storage effects).**

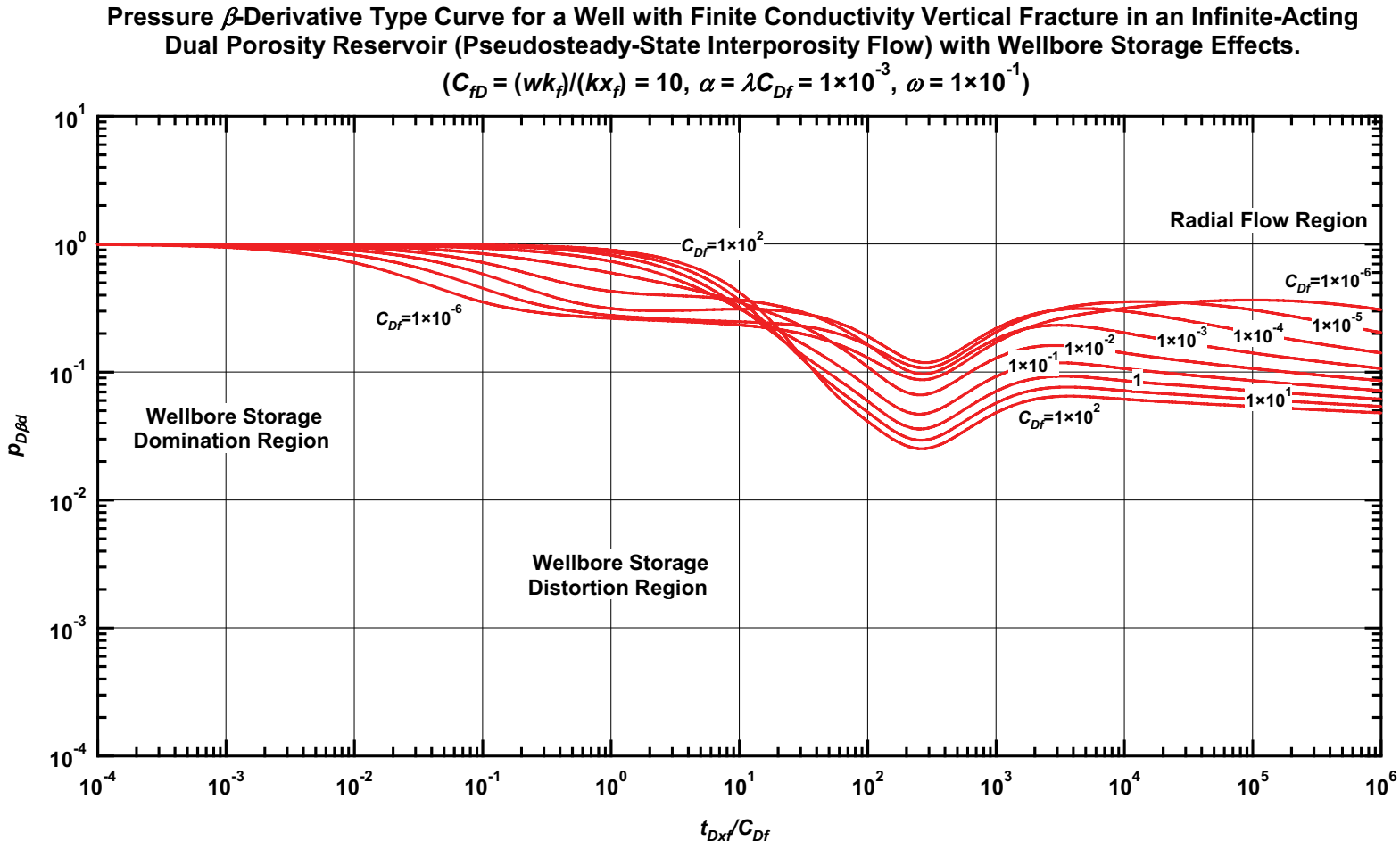

Figure D.33 — $p_{D\beta d}$ vs. t_{Dxf}/C_{Df} — C_{fD} =10, $\omega = 1\times10^{-1}$, $\alpha = \lambda C_{Df} = 1\times10^{-3}$ (fractured well in dual porosity system case — includes wellbore storage effects).

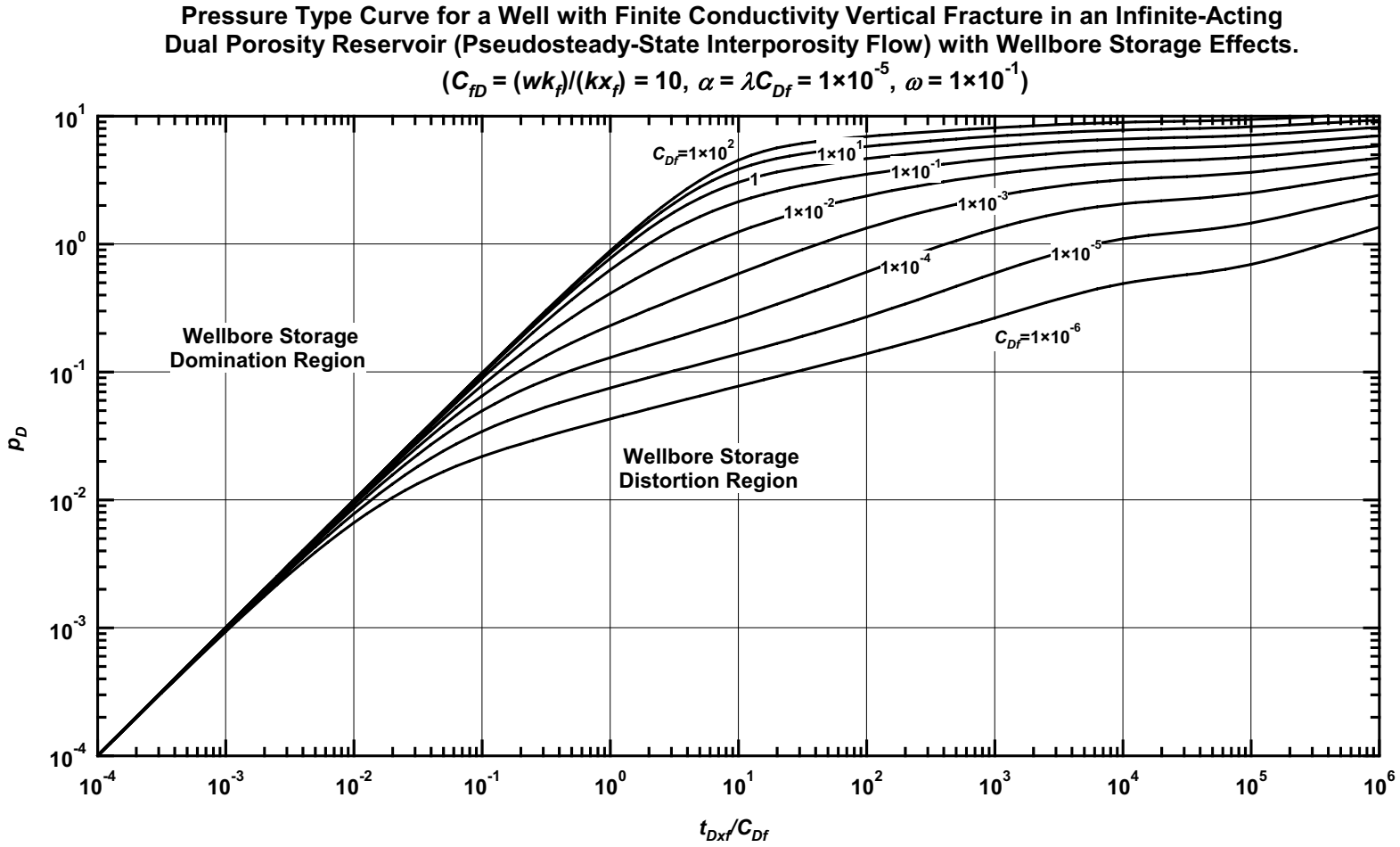

Figure D.34 — p_D vs. t_{Dxf}/C_{Df} — C_{fD} =10, $\omega = 1\times10^{-1}$, $\alpha = \lambda C_{Df} = 1\times10^{-5}$ (fractured well in dual porosity system case — includes wellbore storage effects).

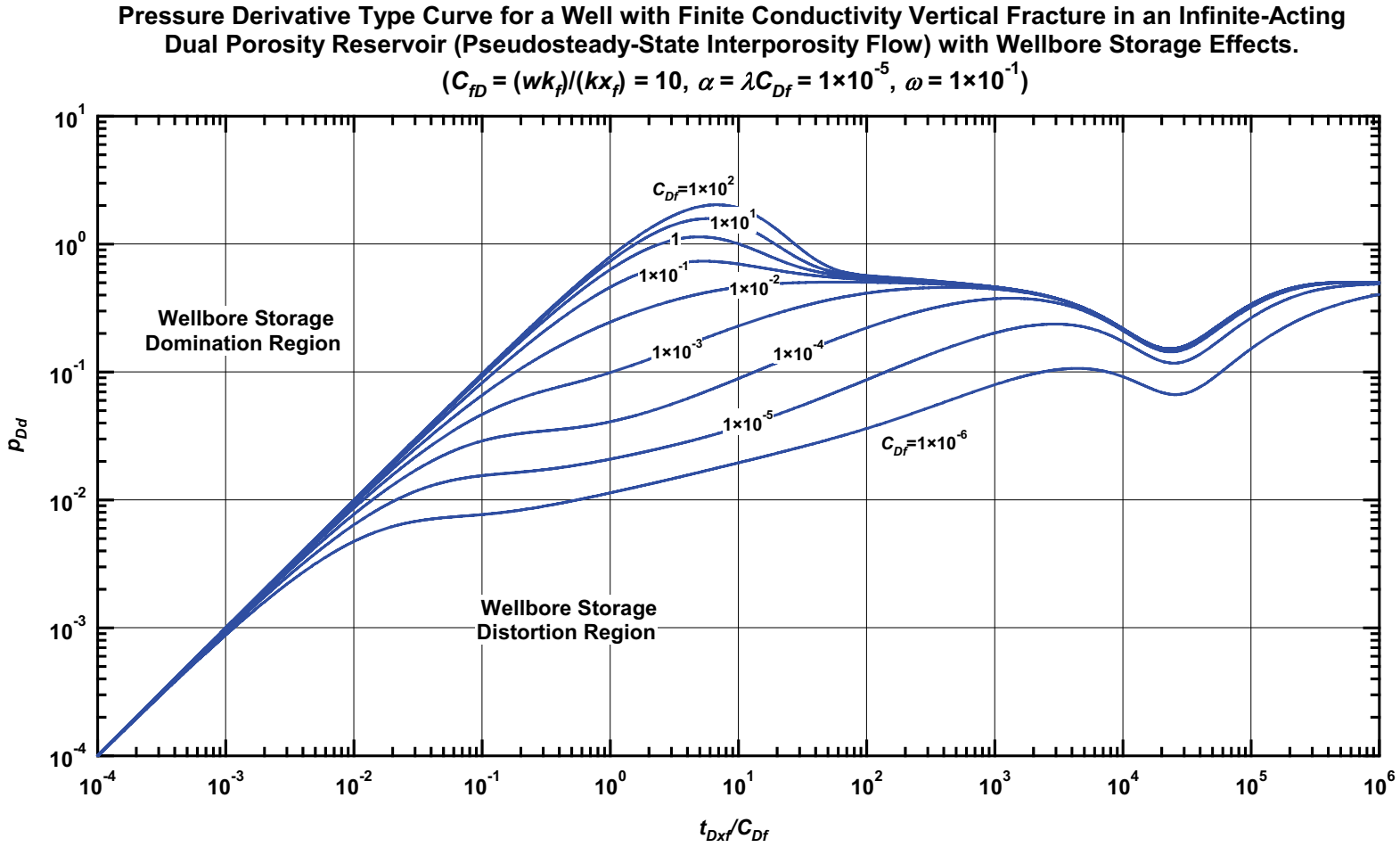

Figure D.35 — p_{Dd} **vs.** t_{Dxf}/C_{Df} **—** C_{fD} **=10,** $\omega = 1\times10^{-1}$, $\alpha = \lambda C_{Df} = 1\times10^{-5}$ **(fractured well in dual porosity system case — includes wellbore storage effects).**

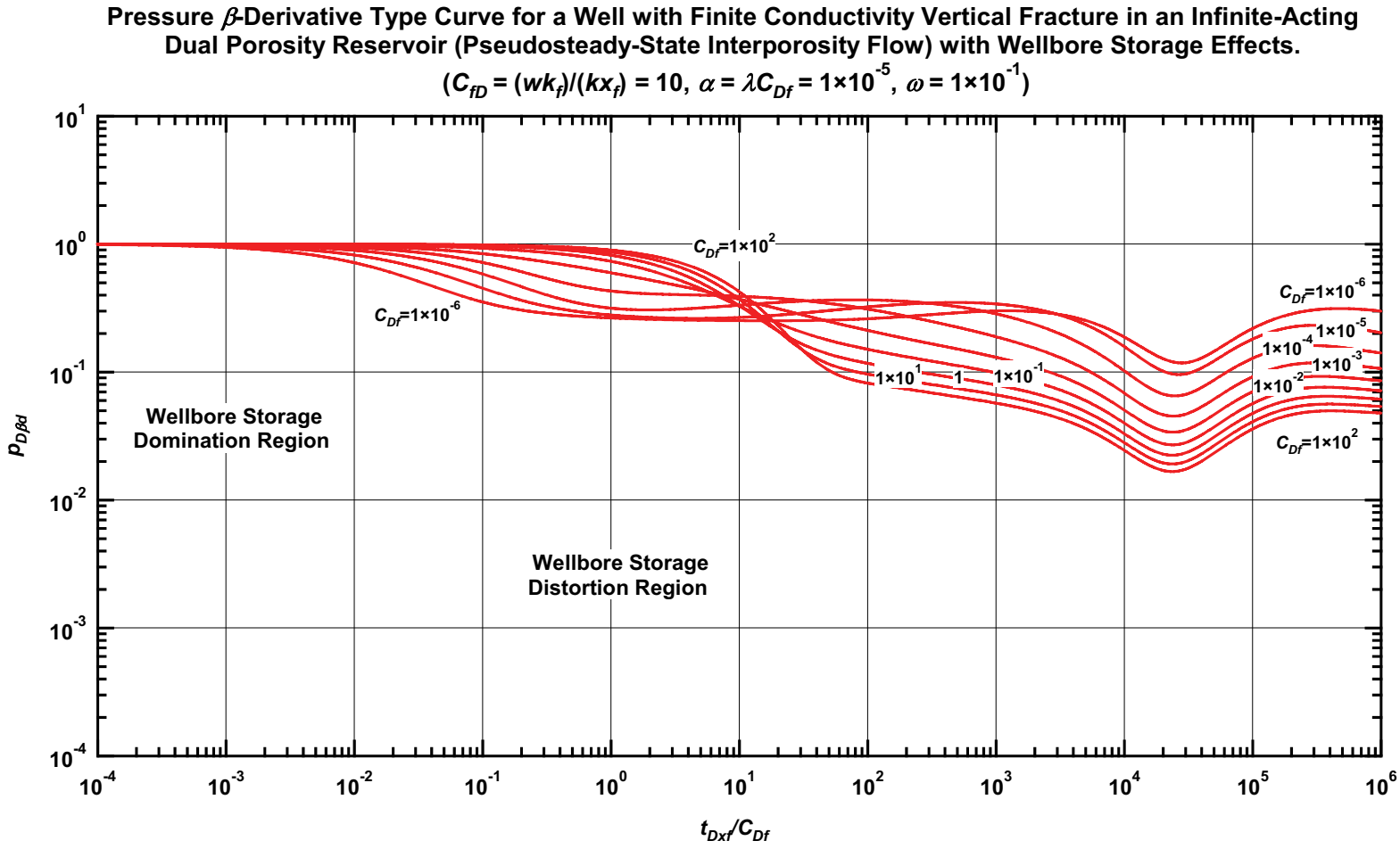

Figure D.36— $p_{D\beta d}$ vs. t_{Dxf}/C_{Df} — C_{fD} =10, $\omega = 1\times10^{-1}$, $\alpha = \lambda C_{Df} = 1\times10^{-5}$ (fractured well in dual porosity system case — includes wellbore storage effects).

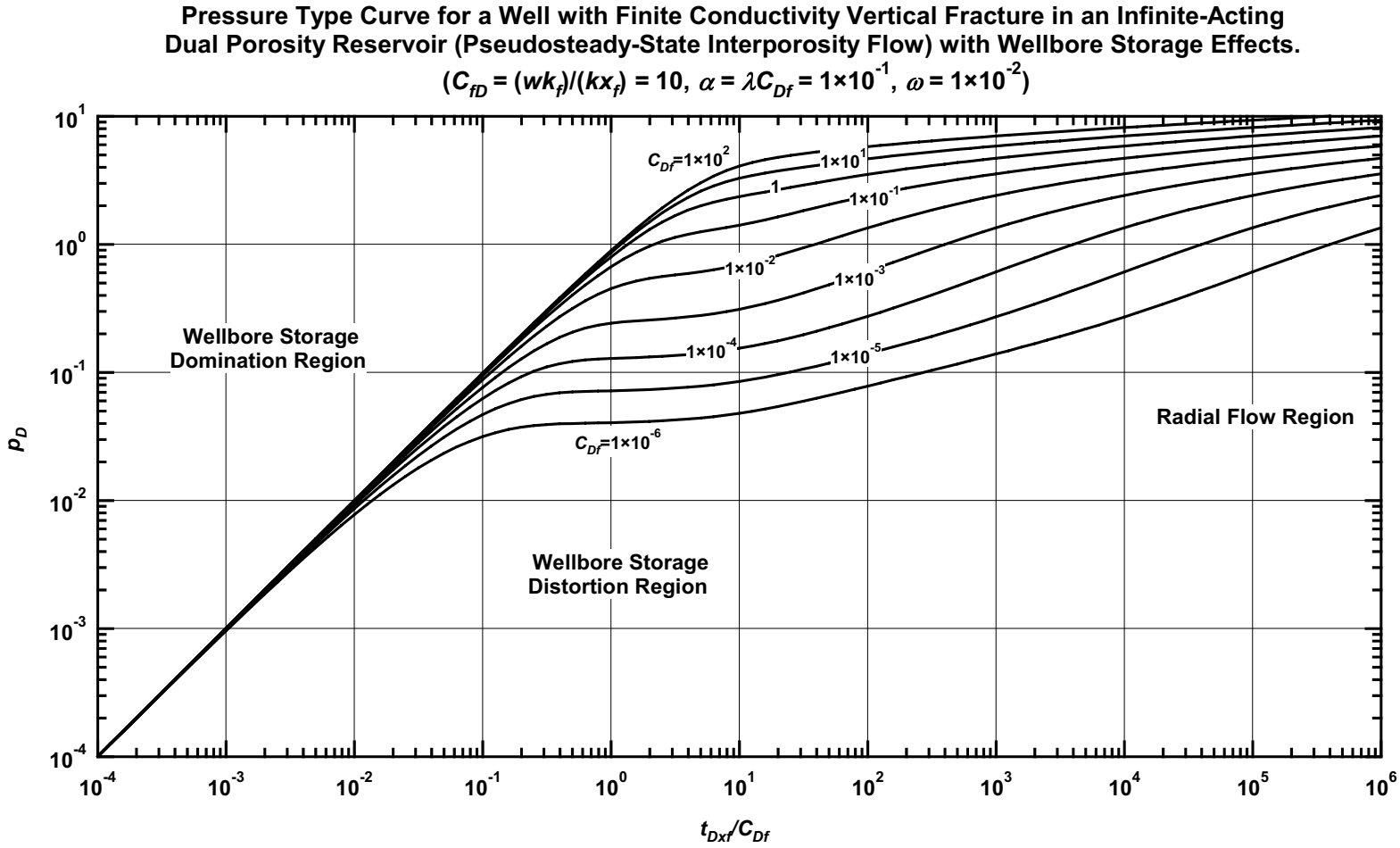

Figure D.37 — p_D vs. t_{Dxf}/C_{Df} — C_{fD} =10, $\omega = 1\times10^{-2}$, $\alpha = \lambda C_{Df} = 1\times10^{-1}$ (fractured well in dual porosity system case — includes wellbore storage effects).

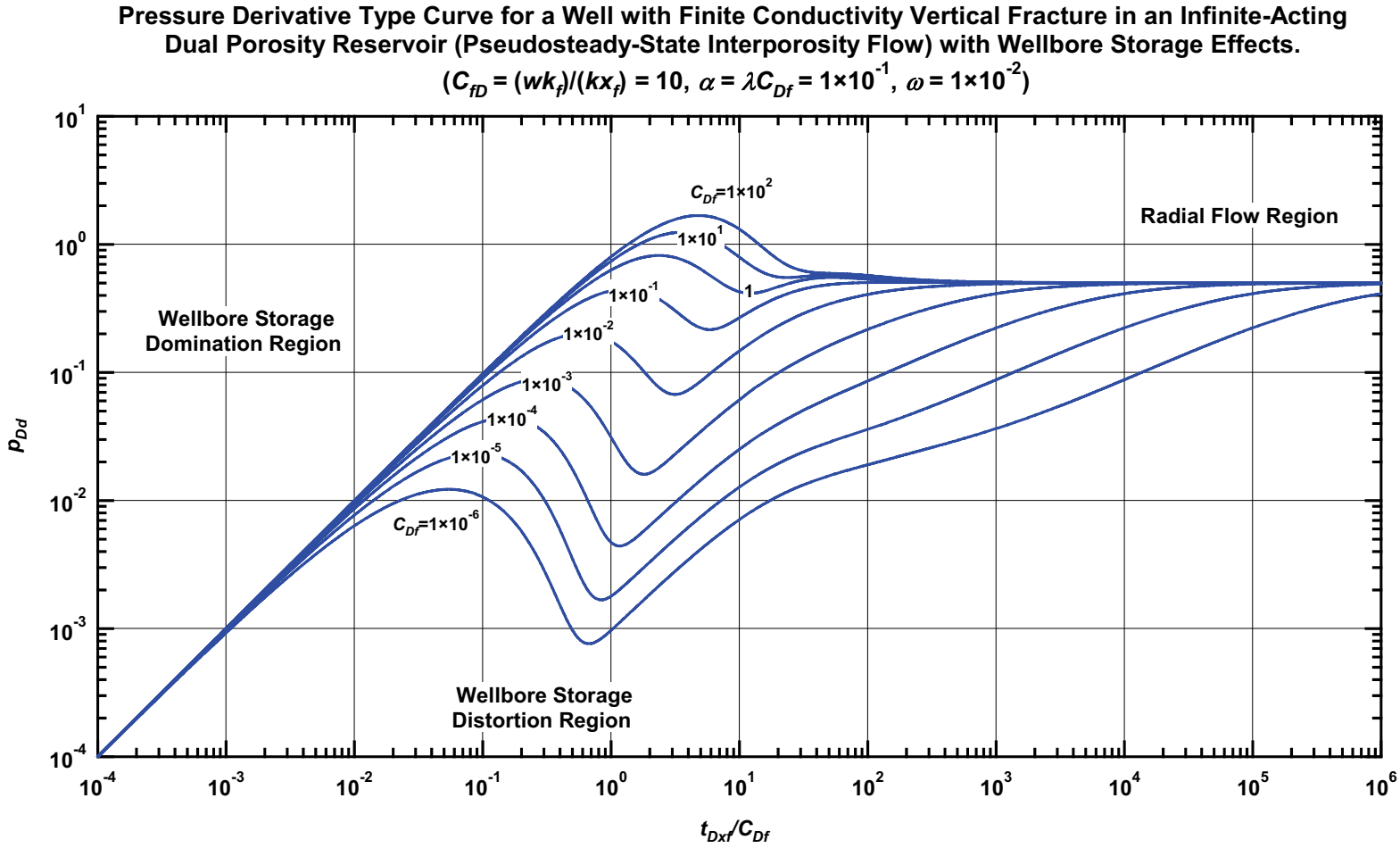

Figure D.38 — p_{Dd} vs. t_{Dxf}/C_{Df} — C_{fD} =10, $\omega = 1\times10^{-2}$, $\alpha = \lambda C_{Df} = 1\times10^{-1}$ (fractured well in dual porosity system case — includes wellbore storage effects).

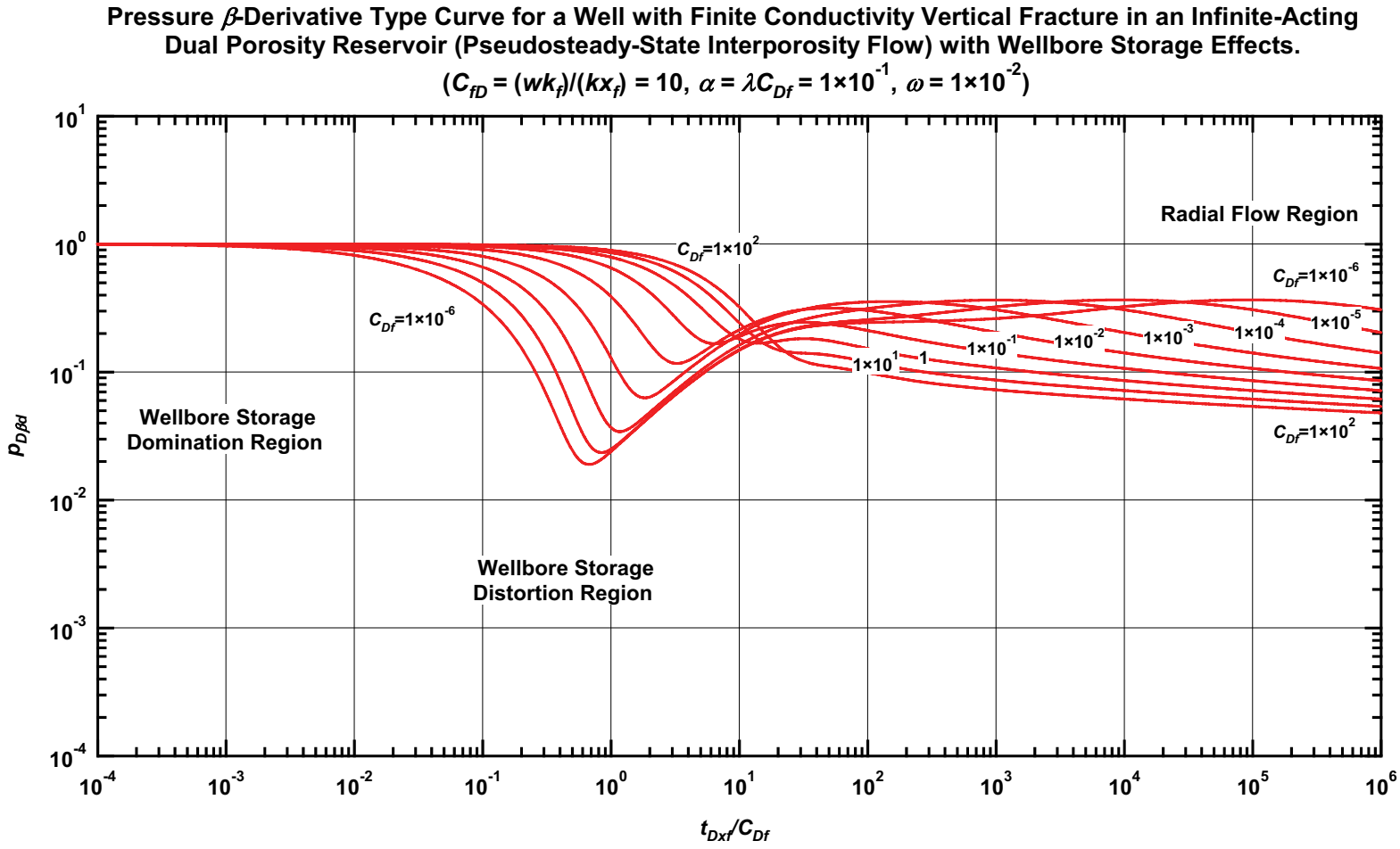

Figure D.39 — $p_{D\beta d}$ vs. t_{Dxf}/C_{Df} — C_{fD} =10, $\omega = 1\times10^{-2}$, $\alpha = \lambda C_{Df} = 1\times10^{-1}$ (fractured well in dual porosity system case — includes wellbore storage effects).

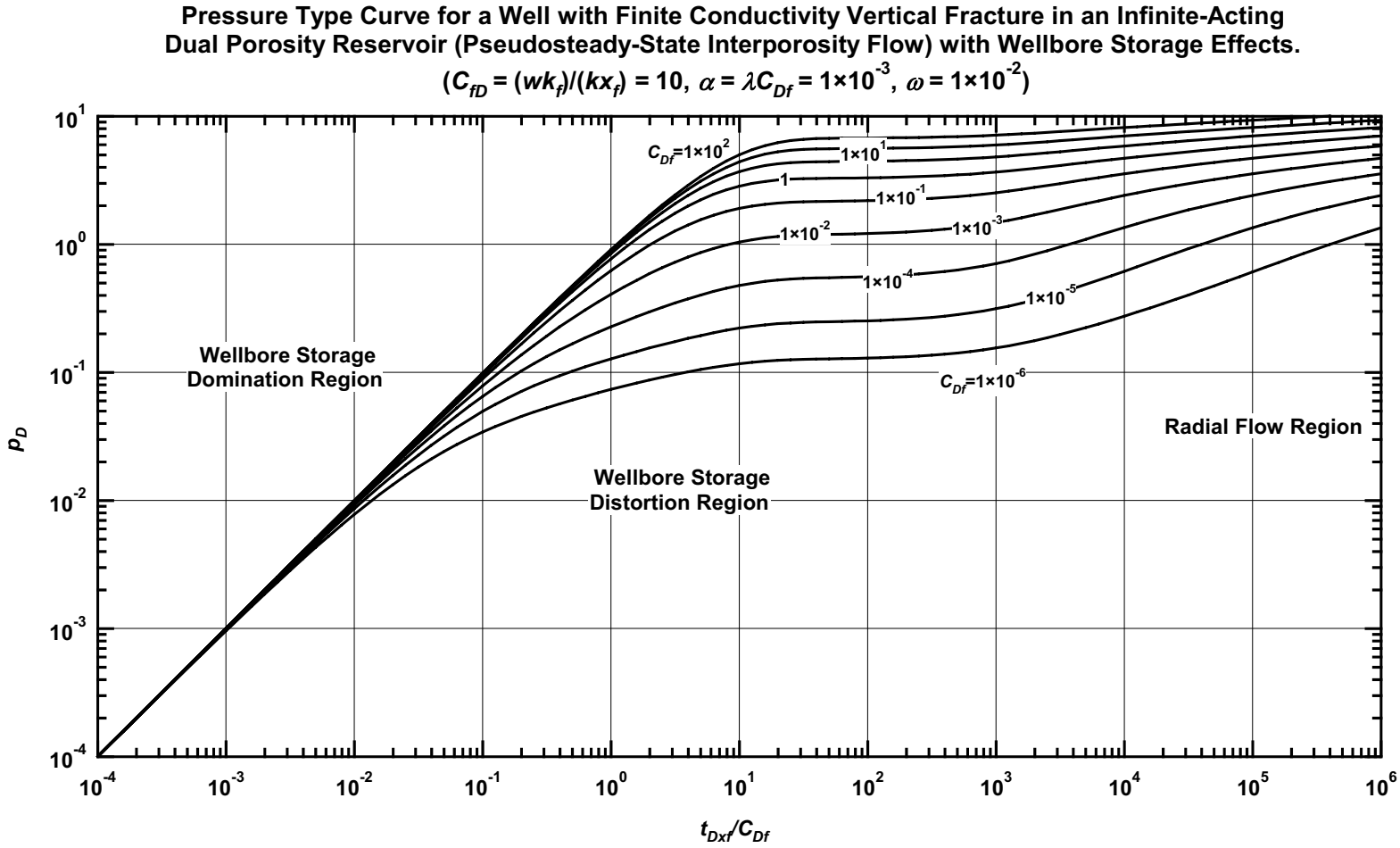

Figure D.40 — p_D vs. t_{Dxf}/C_{Df} — C_{fD} =10, $\omega = 1\times10^{-2}$, $\alpha = \lambda C_{Df} = 1\times10^{-3}$ (fractured well in dual porosity system case — includes wellbore storage effects).

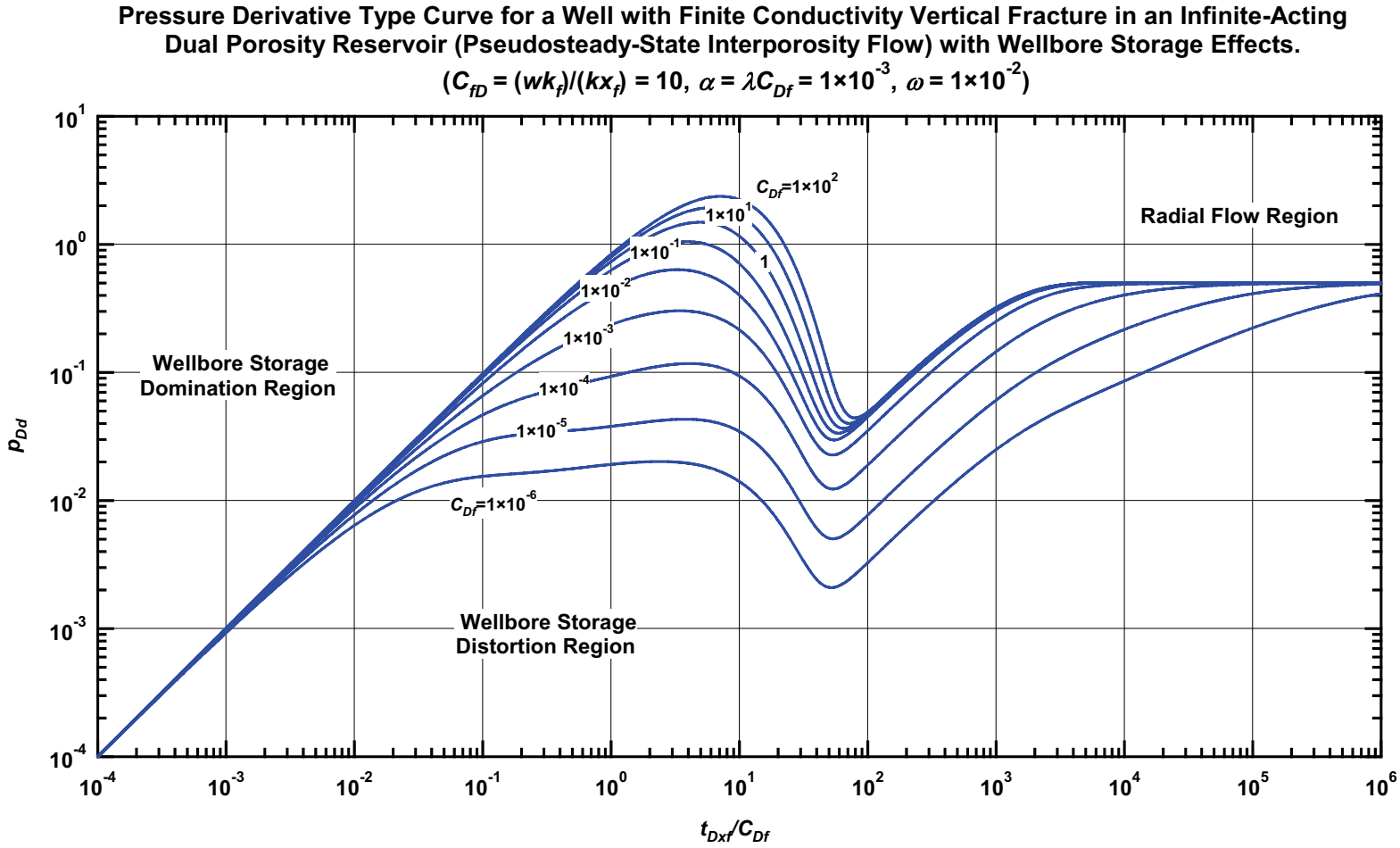

Figure D.41 — p_{Dd} vs. t_{Dxf}/C_{Df} — C_{fD} =10, $\omega = 1\times10^{-2}$, $\alpha = \lambda C_{Df} = 1\times10^{-3}$ (fractured well in dual porosity system case — includes wellbore storage effects).

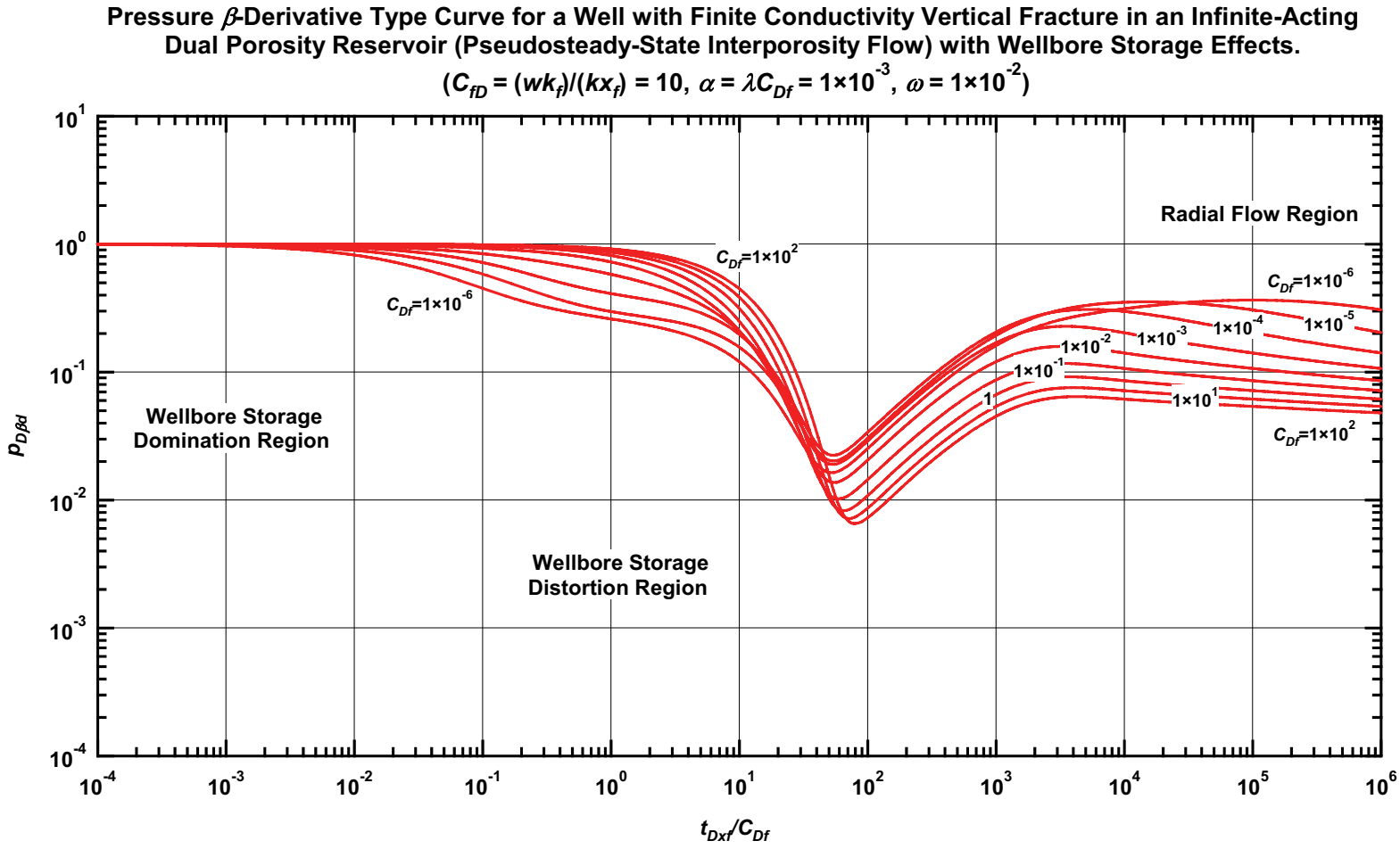

Figure D.42 — $p_{D\beta d}$ **vs.** t_{Dxf}/C_{Df} **—** C_{fD} **=10,** $\omega = 1\times10^{-2}$, $\alpha = \lambda C_{Df} = 1\times10^{-3}$ **(fractured well in dual porosity system case — includes wellbore storage effects).**

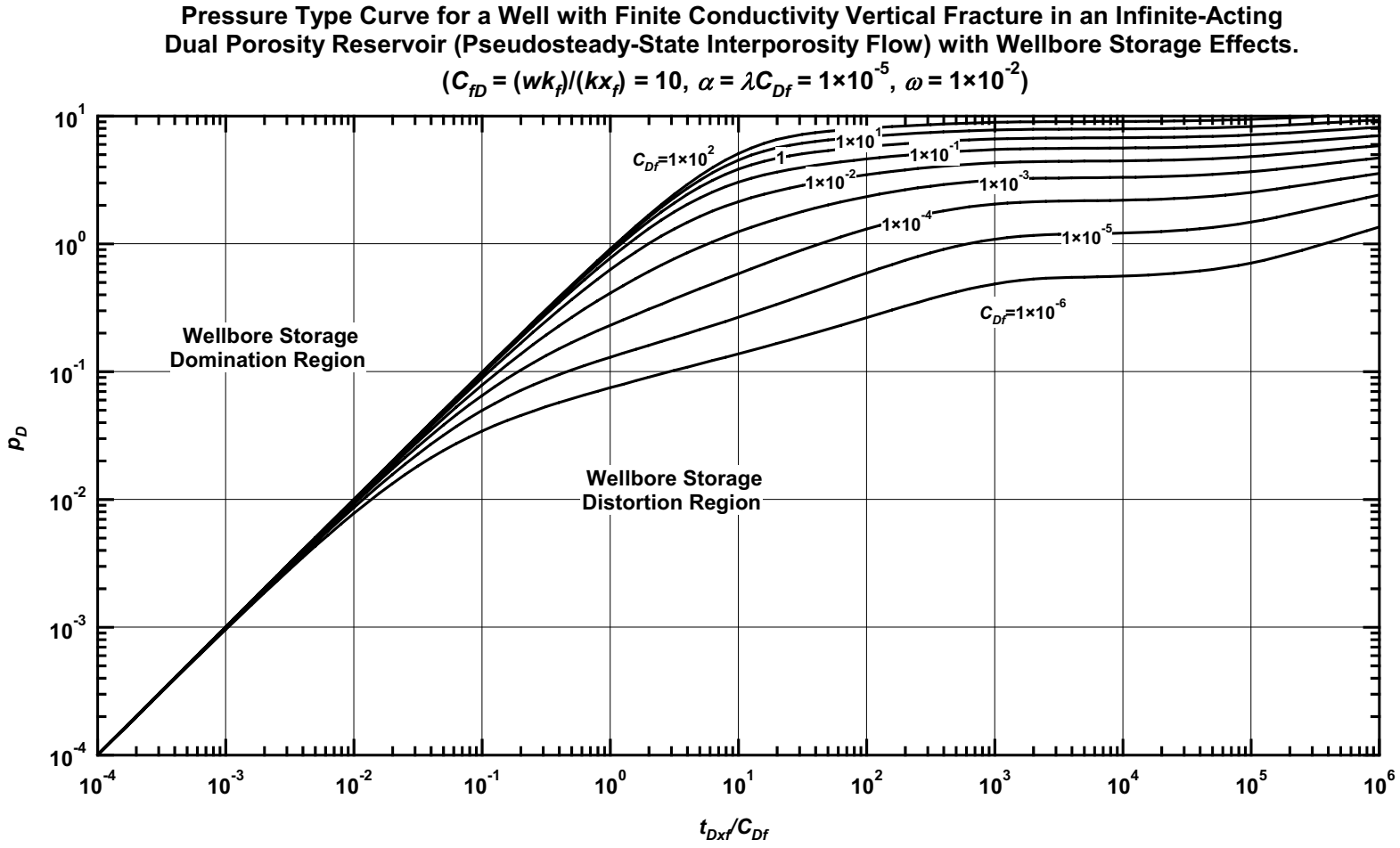

Figure D.43 — p_D vs. t_{Dxf}/C_{Df} — C_{fD} =10, $\omega = 1\times10^{-2}$, $\alpha = \lambda C_{Df} = 1\times10^{-5}$ (fractured well in dual porosity system case — includes wellbore storage effects).

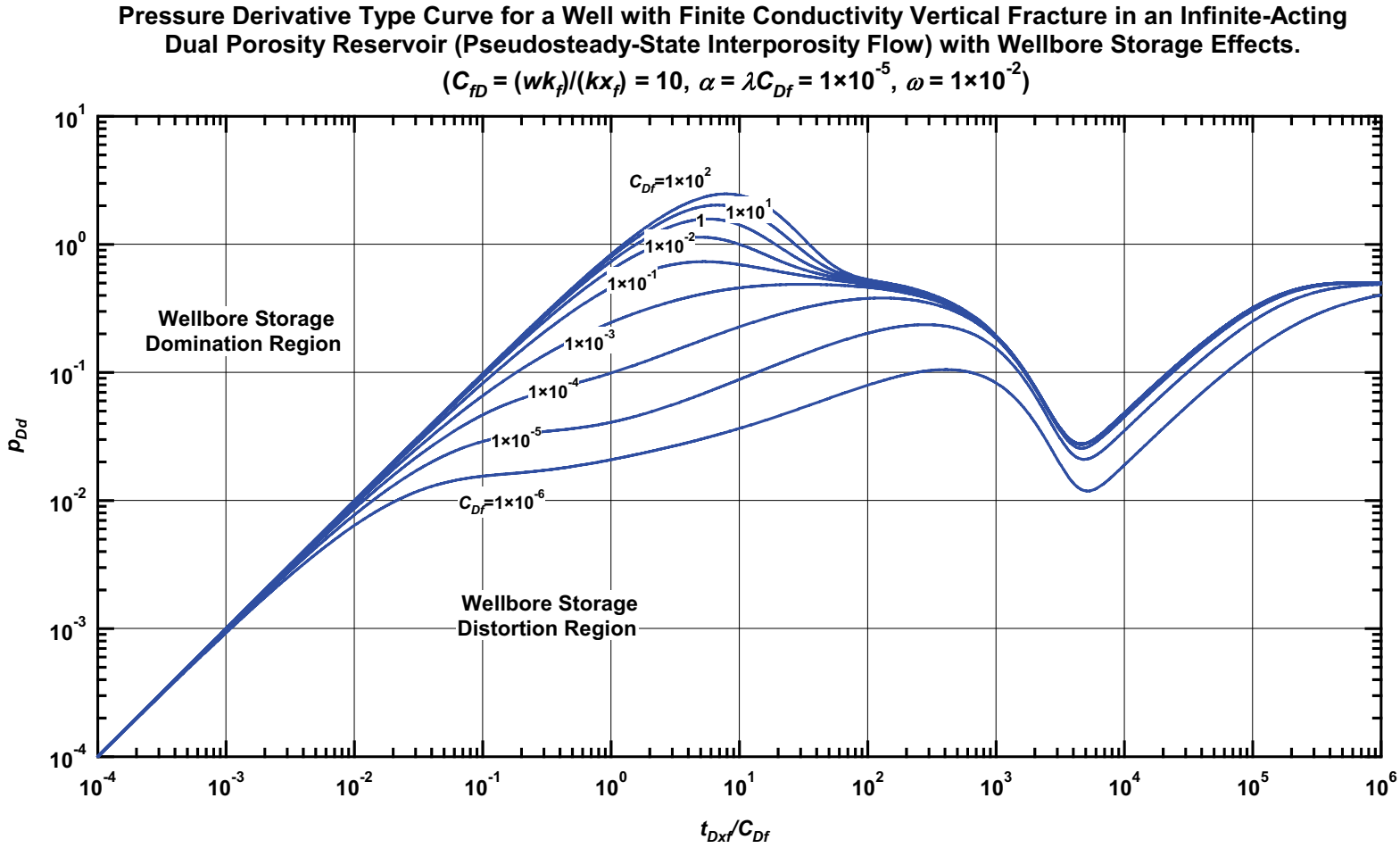

Figure D.44 — p_{Dd} **vs.** t_{Dxf}/C_{Df} **—** C_{fD} **=10,** $\omega = 1\times10^{-2}$, $\alpha = \lambda C_{Df} = 1\times10^{-5}$ **(fractured well in dual porosity system case — includes wellbore storage effects).**

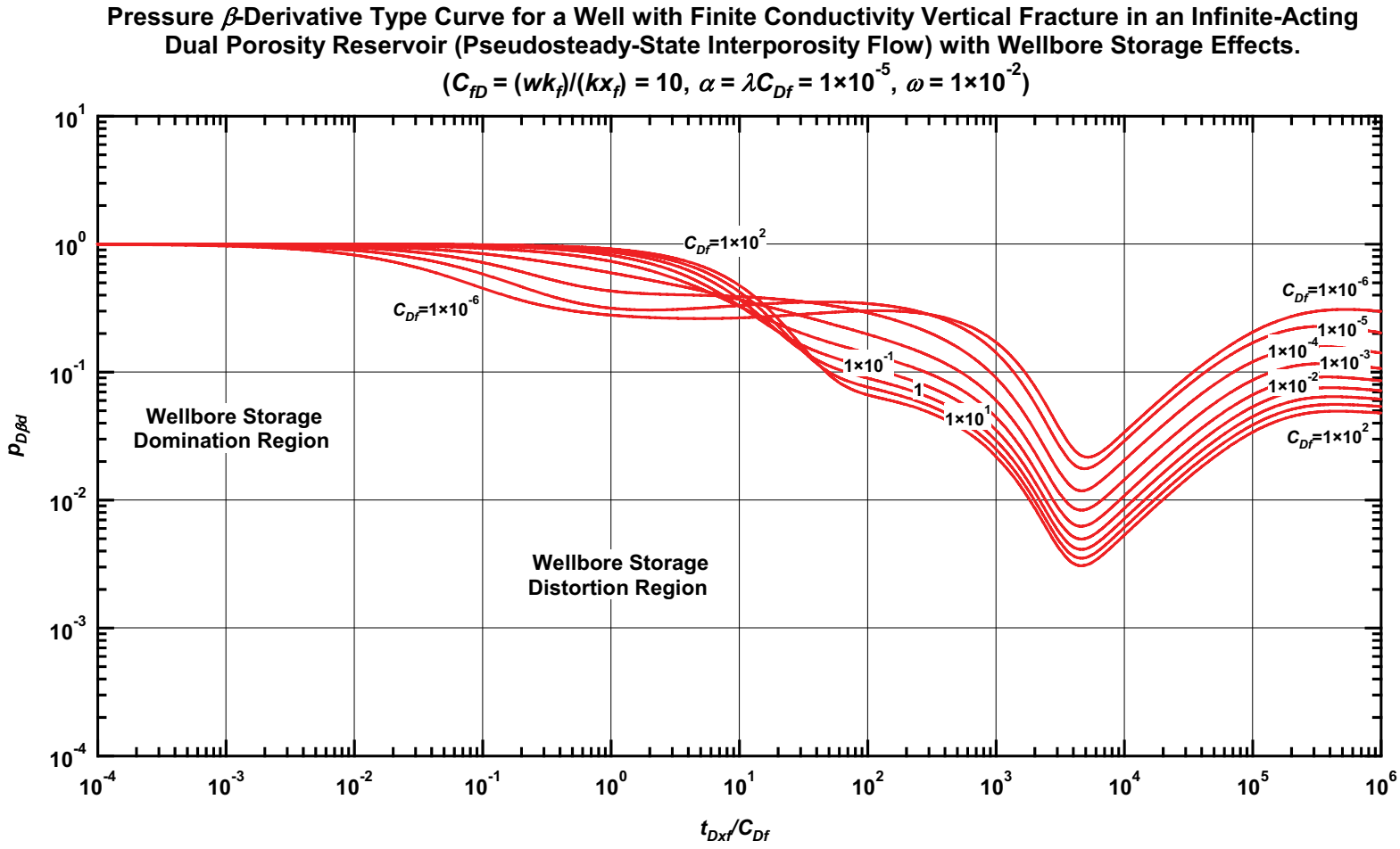

Figure D.45— $p_{D\beta d}$ vs. t_{Dxf}/C_{Df} — C_{fD} =10, $\omega = 1\times10^{-2}$, $\alpha = \lambda C_{Df} = 1\times10^{-5}$ (fractured well in dual porosity system case — includes wellbore storage effects).

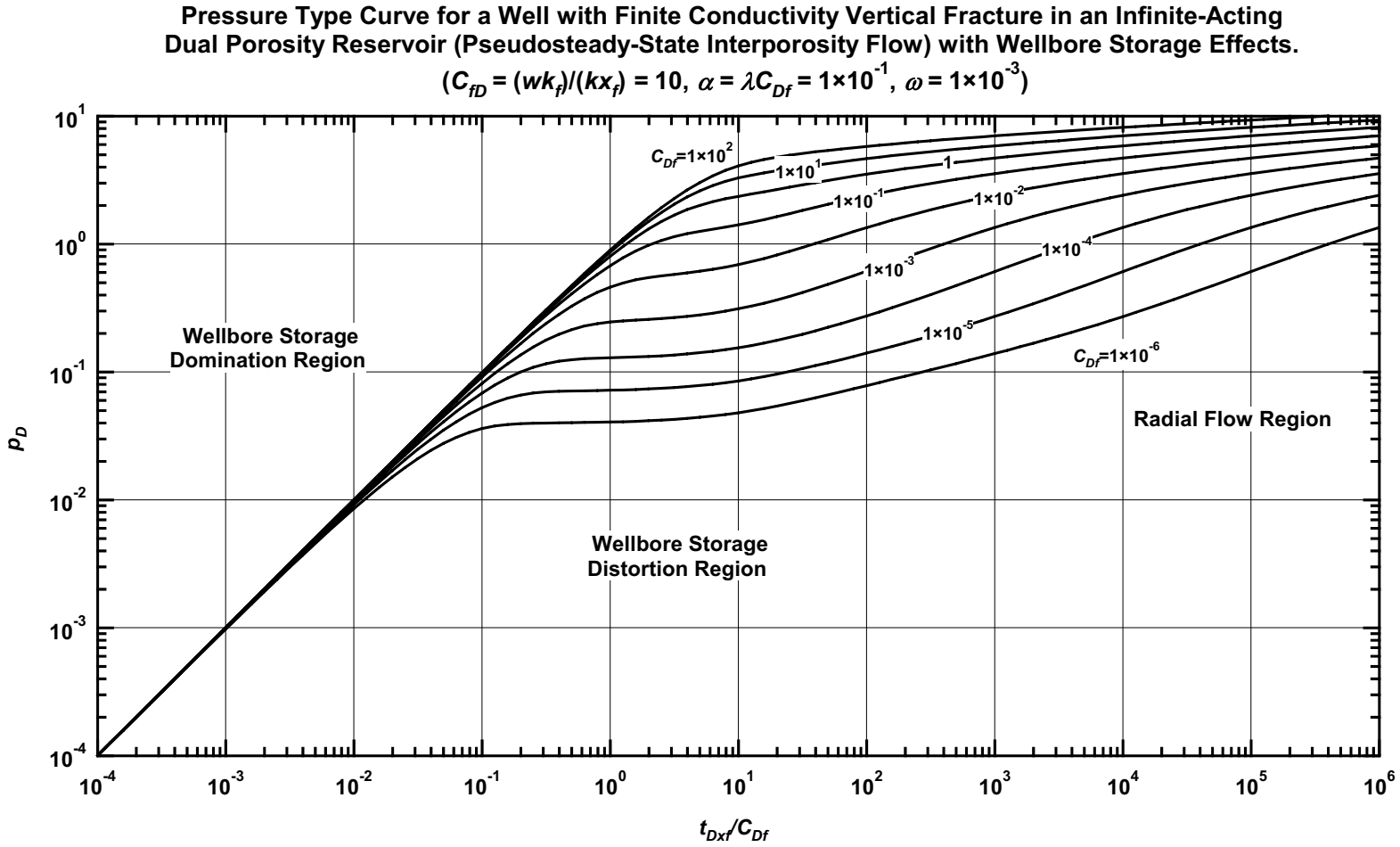

Figure D.46 — p_D **vs.** t_{Dxf}/C_{Df} **—** C_{fD} **=10,** $\omega = 1\times10^{-3}$, $\alpha = \lambda C_{Df} = 1\times10^{-1}$ **(fractured well in dual porosity system case — includes wellbore storage effects).**

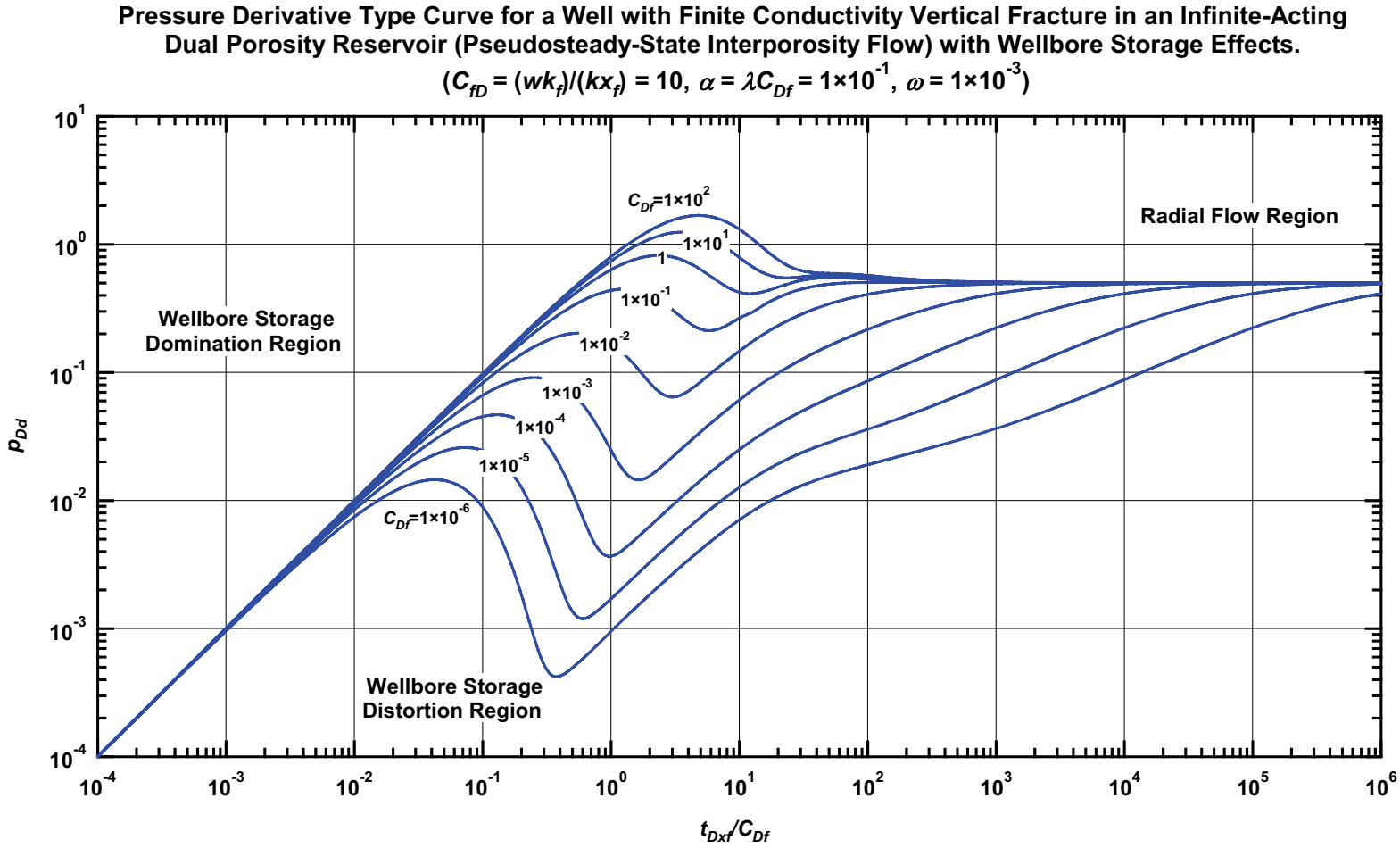

Figure D.47 — p_{Dd} vs. t_{Dxf}/C_{Df} — C_{fD} =10, $\omega = 1\times10^{-3}$, $\alpha = \lambda C_{Df} = 1\times10^{-1}$ (fractured well in dual porosity system case — includes wellbore storage effects).

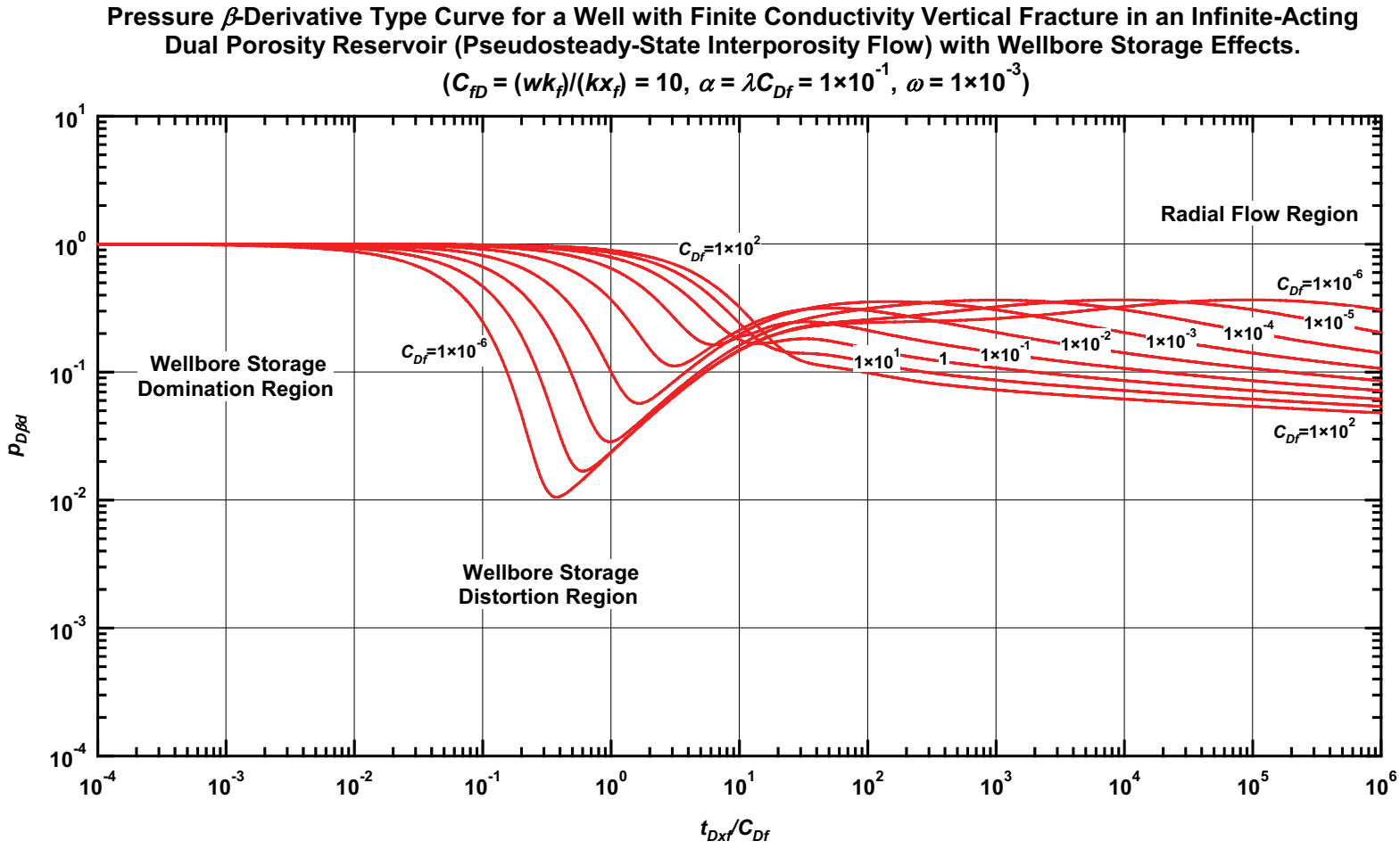

Figure D.48 — $p_{D\beta d}$ vs. t_{Dxf}/C_{Df} — C_{fD} =10, $\omega = 1\times10^{-3}$, $\alpha = \lambda C_{Df} = 1\times10^{-1}$ (fractured well in dual porosity system case — includes wellbore storage effects).

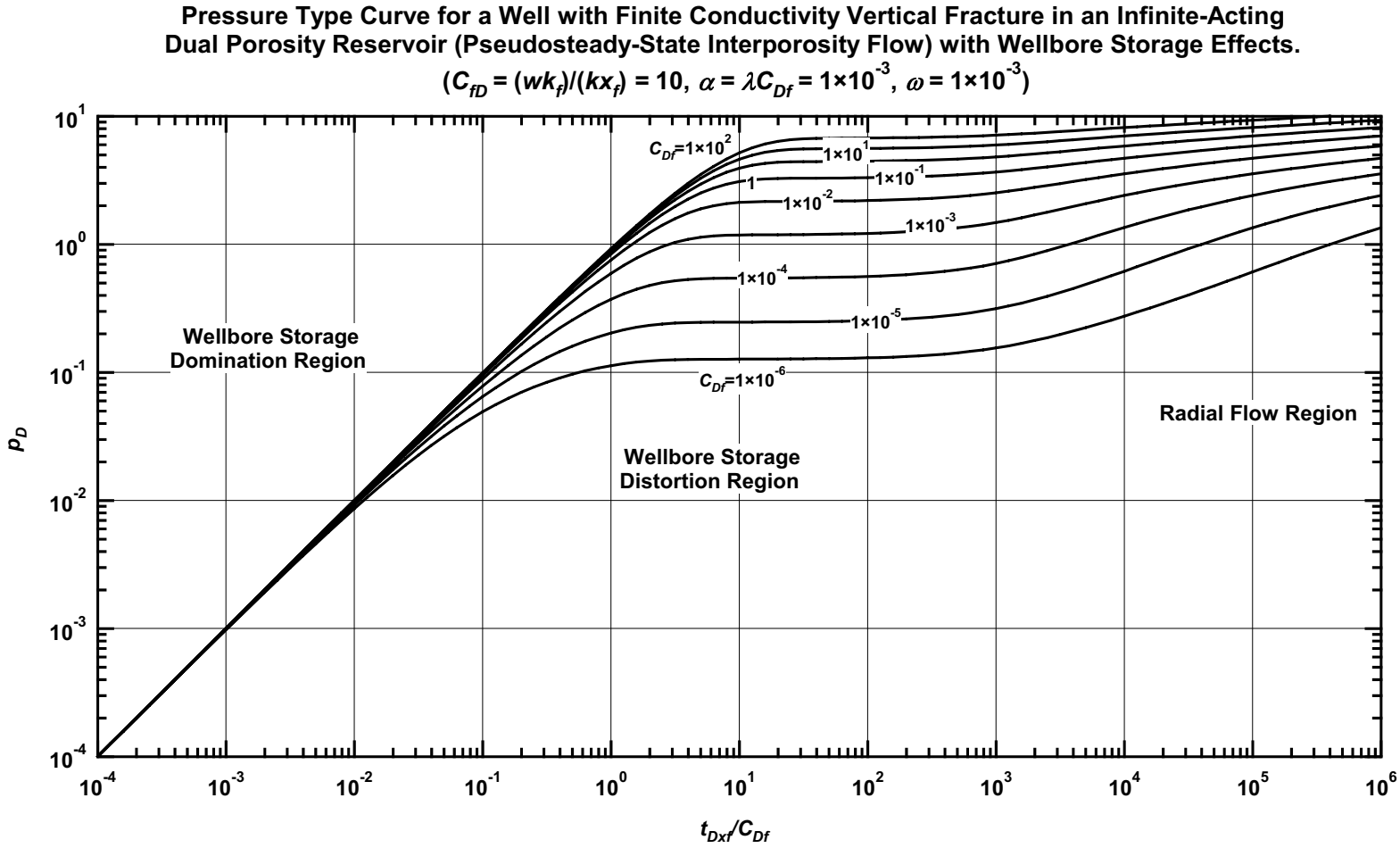

Figure D.49 — p_D vs. t_{Dxf}/C_{Df} — C_{fD} =10, $\omega = 1\times10^{-3}$, $\alpha = \lambda C_{Df} = 1\times10^{-3}$ (fractured well in dual porosity system case — includes wellbore storage effects).

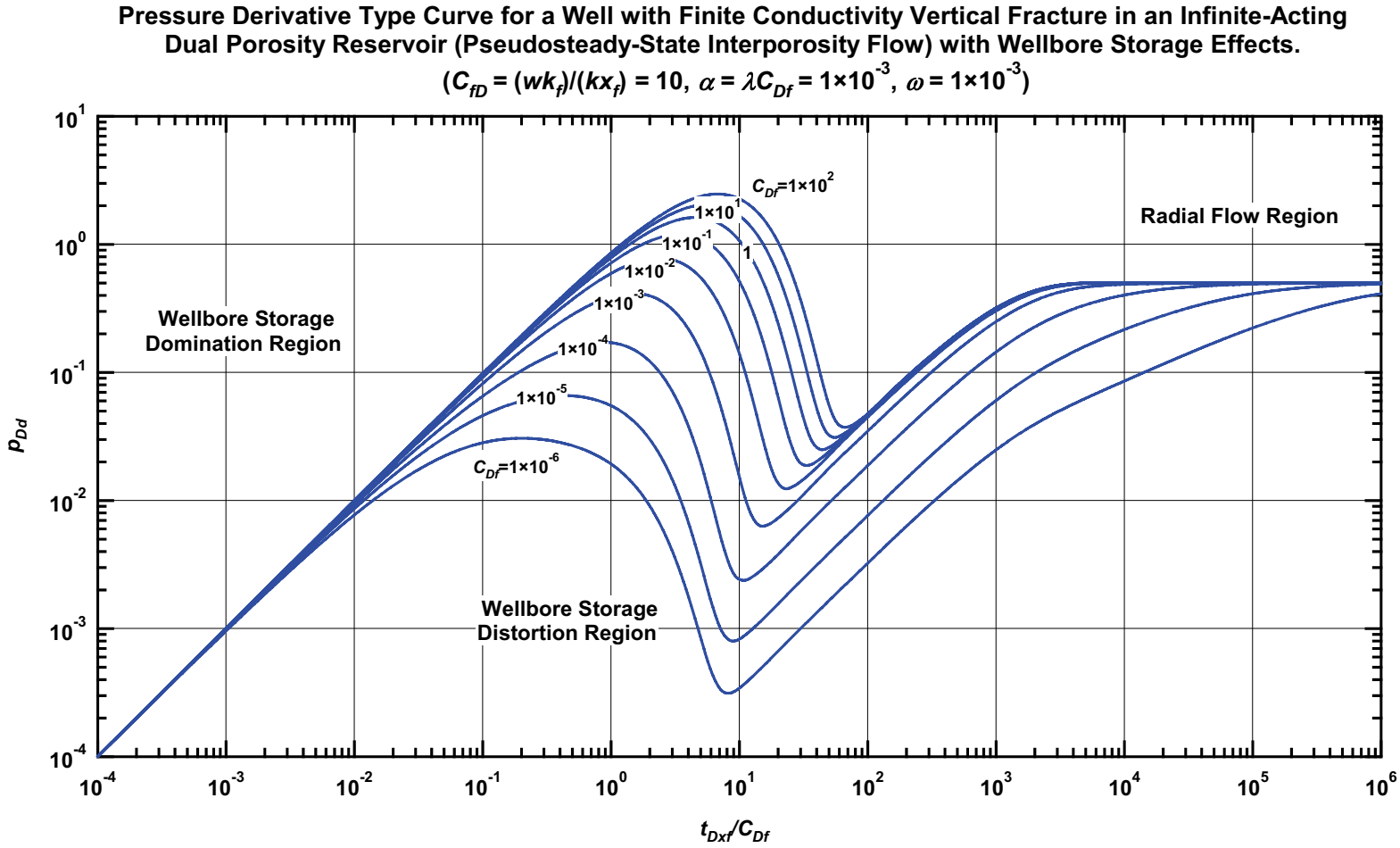

Figure D.50 — p_{Dd} **vs.** t_{Dxf}/C_{Df} **—** C_{fD} **=10,** $\omega = 1\times10^{-3}$, $\alpha = \lambda C_{Df} = 1\times10^{-3}$ **(fractured well in dual porosity system case — includes wellbore storage effects).**

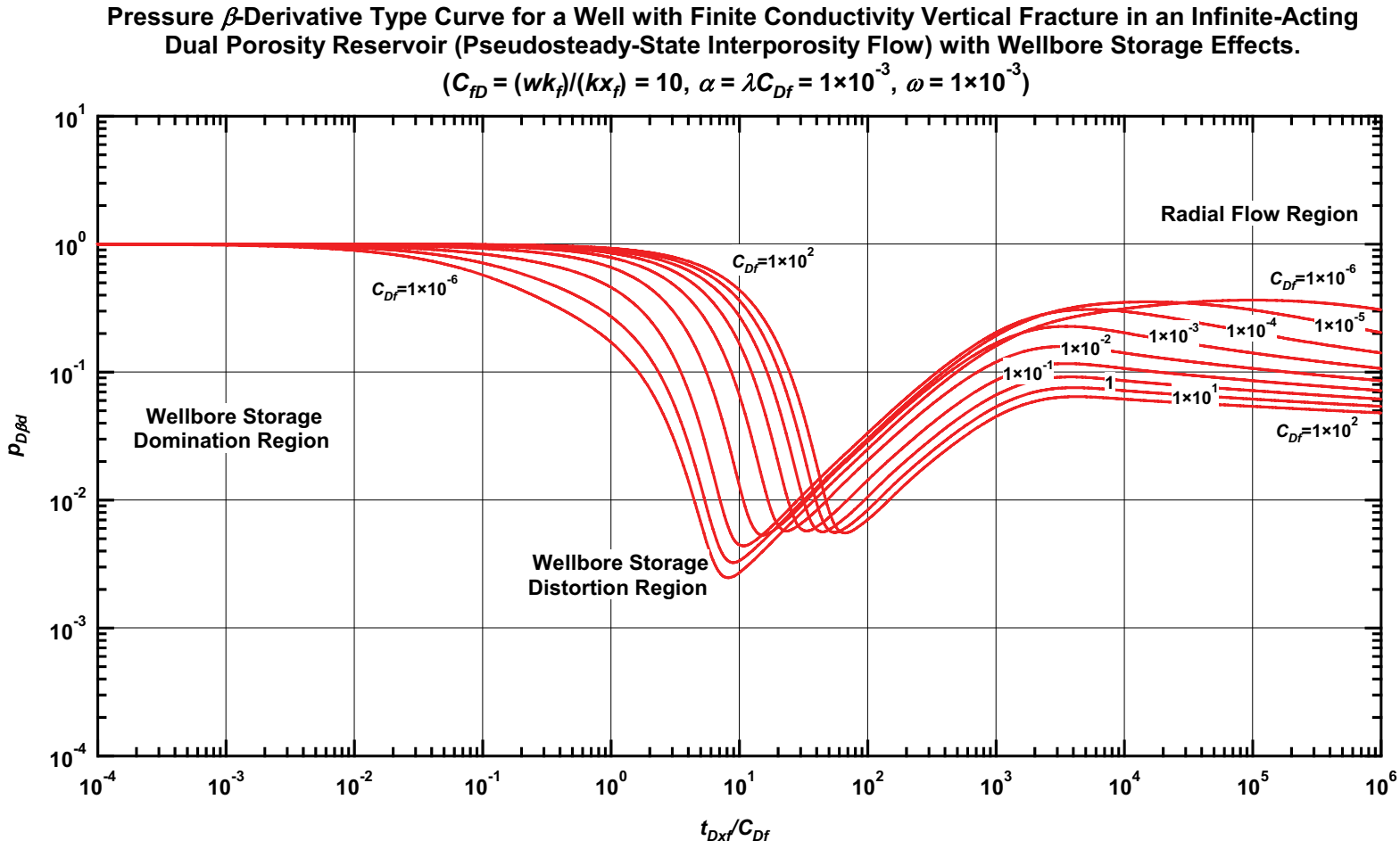

Figure D.51 — $p_{D\beta d}$ vs. t_{Dxf}/C_{Df} — C_{fD} =10, $\omega = 1\times10^{-3}$, $\alpha = \lambda C_{Df} = 1\times10^{-3}$ (fractured well in dual porosity system case — includes wellbore storage effects).

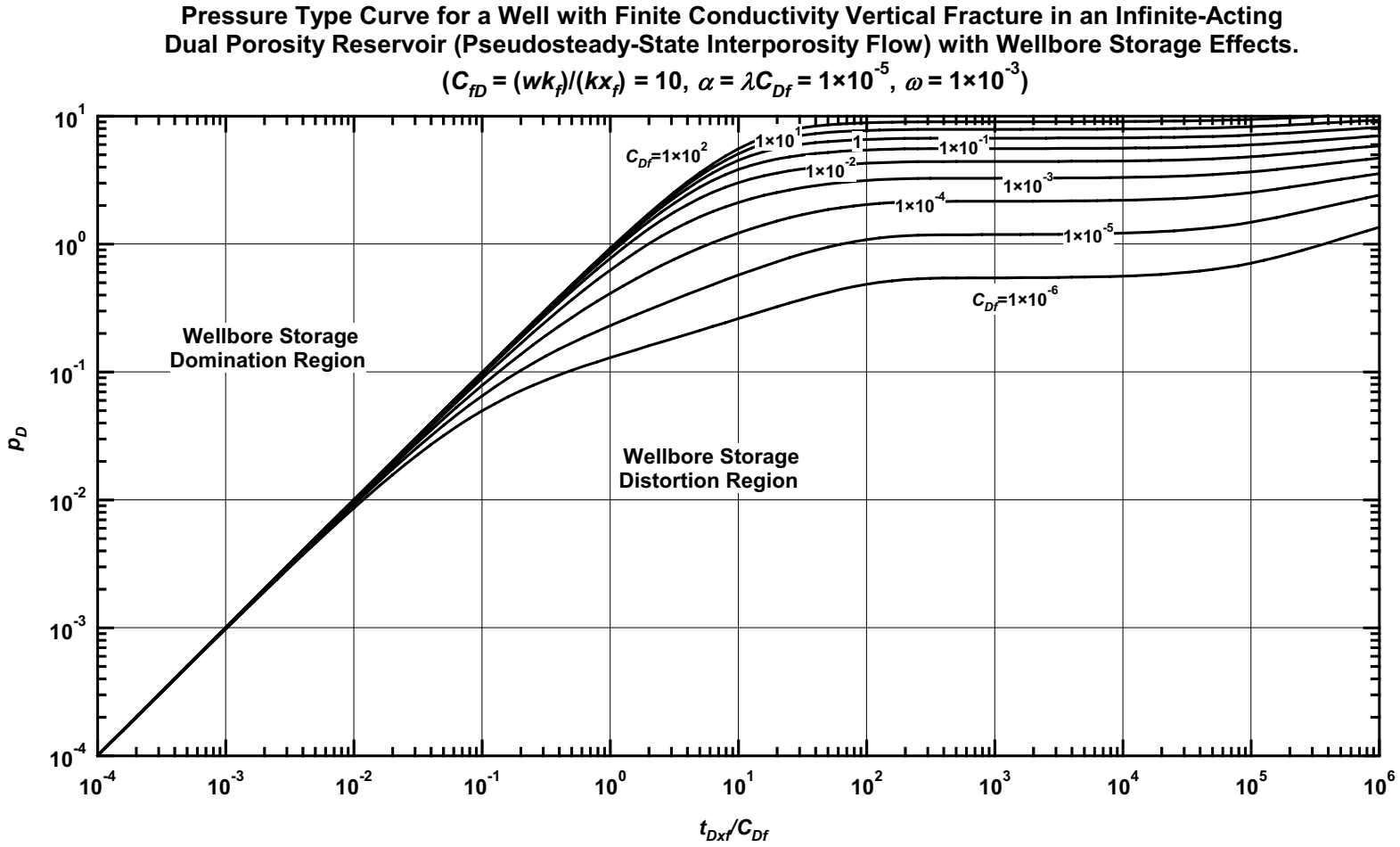

Figure D.52 — p_D **vs.** t_{Dxf}/C_{Df} **—** C_{fD} **=10,** $\omega = 1\times10^{-3}$, $\alpha = \lambda C_{Df} = 1\times10^{-5}$ **(fractured well in dual porosity system case — includes wellbore storage effects).**

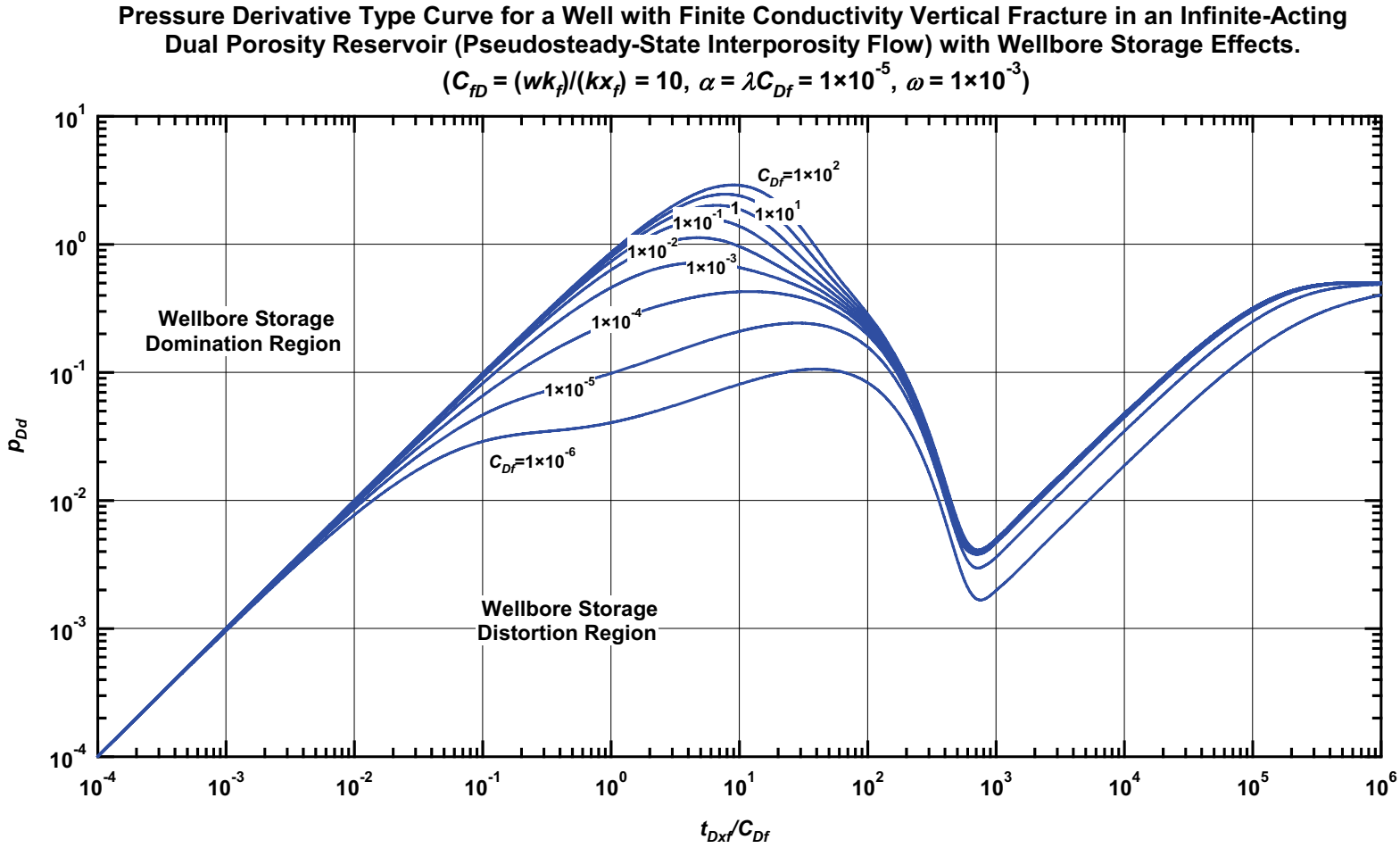

Figure D.53 — p_{Dd} **vs.** t_{Dxf}/C_{Df} **—** C_{fD} **=10,** $\omega = 1\times10^{-3}$, $\alpha = \lambda C_{Df} = 1\times10^{-5}$ **(fractured well in dual porosity system case — includes wellbore storage effects).**

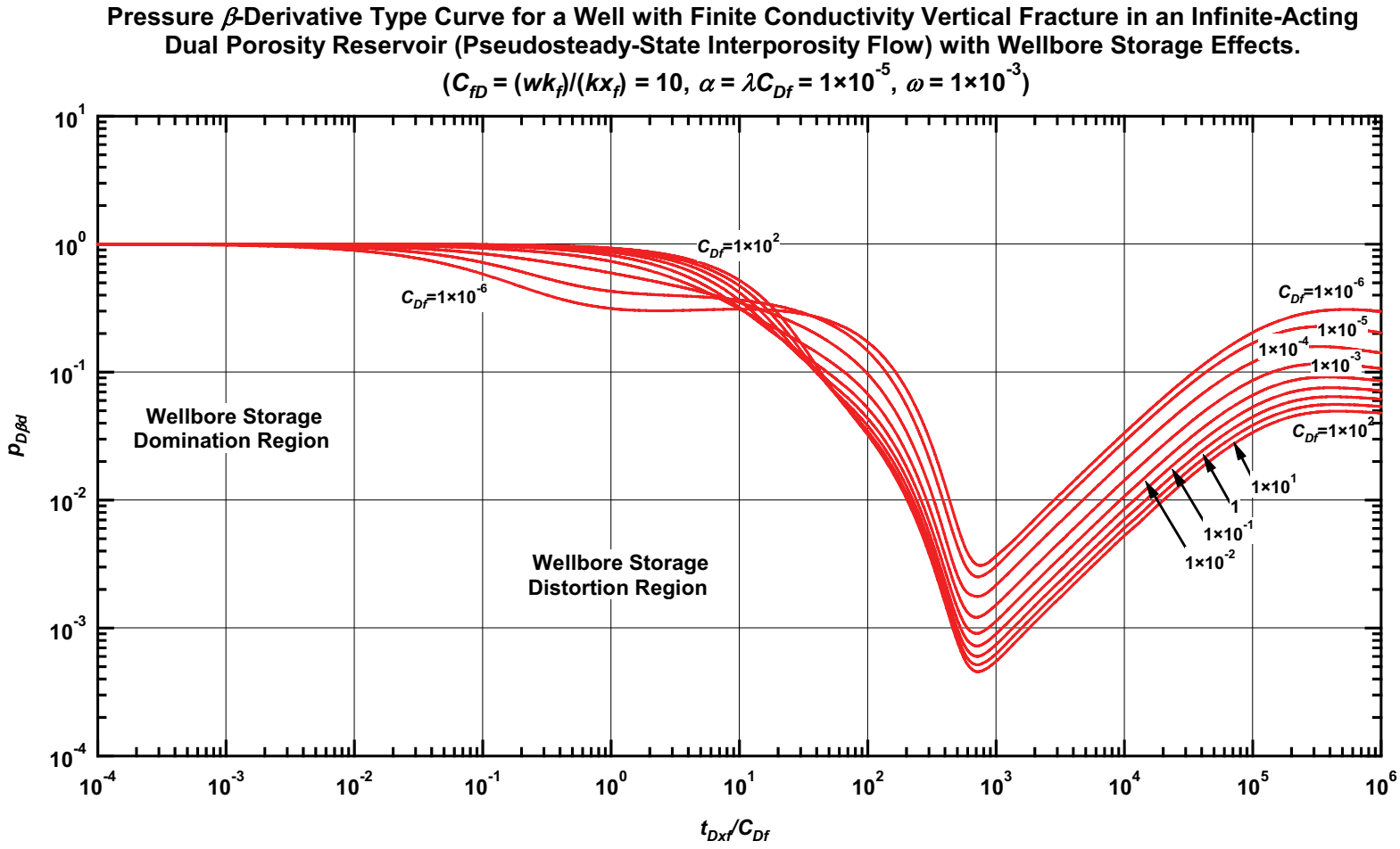

Figure D.54— $p_{D\beta d}$ vs. t_{Dxf}/C_{Df} — C_{fD} =10, $\omega = 1\times10^{-3}$, $\alpha = \lambda C_{Df} = 1\times10^{-5}$ (fractured well in dual porosity system case — includes wellbore storage effects).

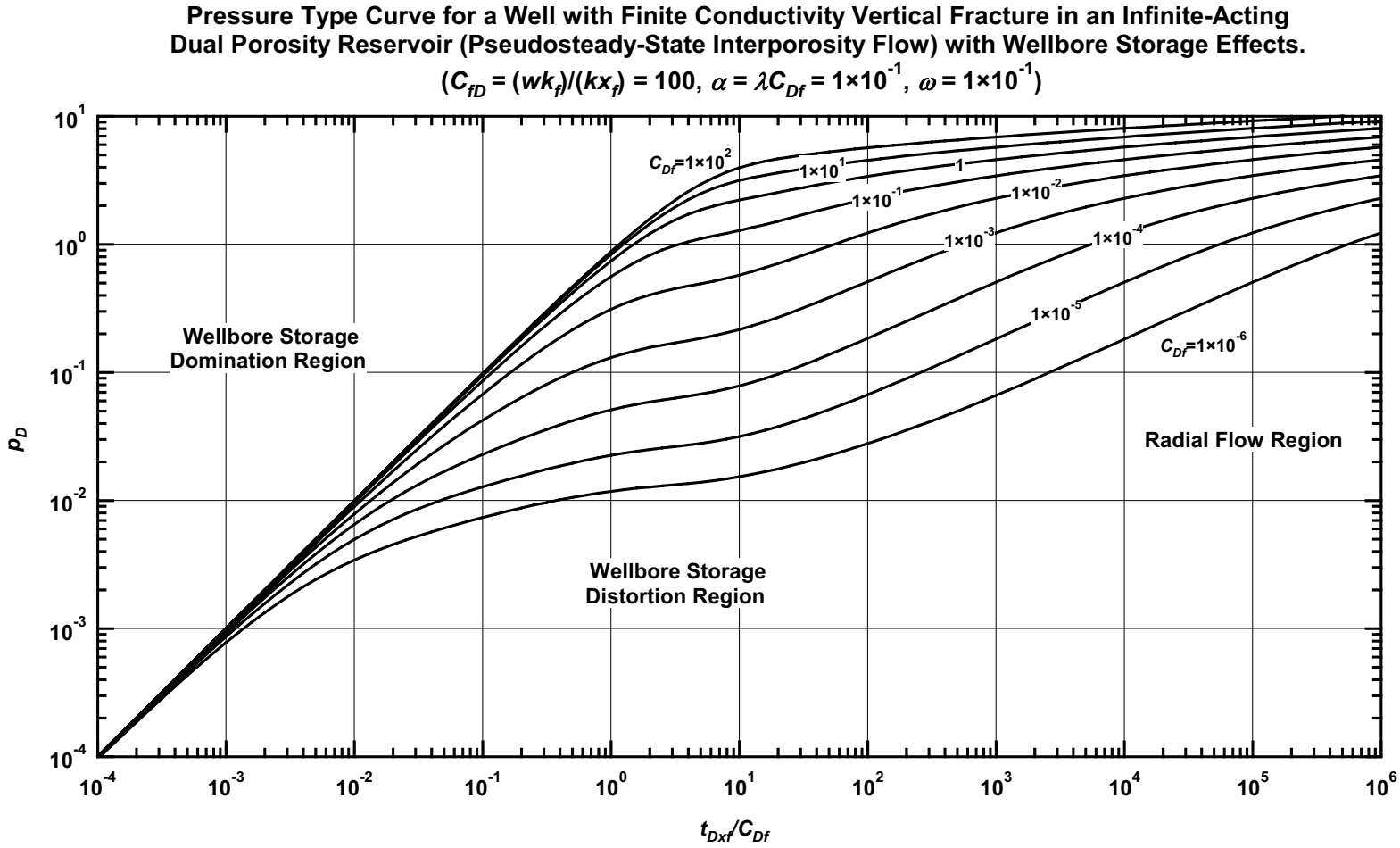

Figure D.55 — p_D **vs.** t_{Dxf}/C_{Df} **—** C_{fD} **=100,** $\omega = 1\times10^{-1}$, $\alpha = \lambda C_{Df} = 1\times10^{-1}$ **(fractured well in dual porosity system case — includes wellbore storage effects).**

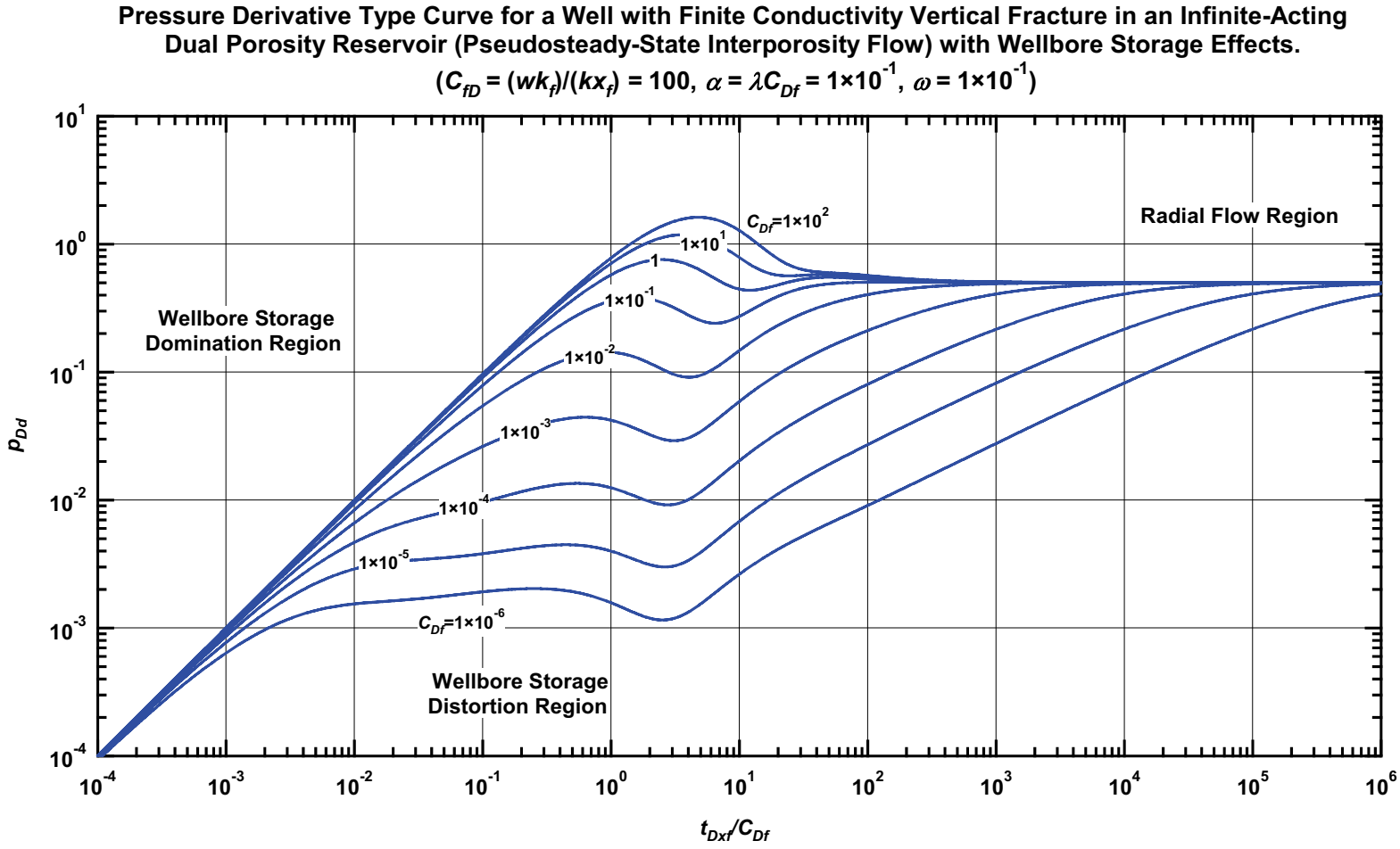

Figure D.56— p_{Dd} vs. t_{Dxf}/C_{Df} — C_{fD} =100, $\omega = 1\times10^{-1}$, $\alpha = \lambda C_{Df} = 1\times10^{-1}$ (fractured well in dual porosity system case — includes wellbore storage effects).

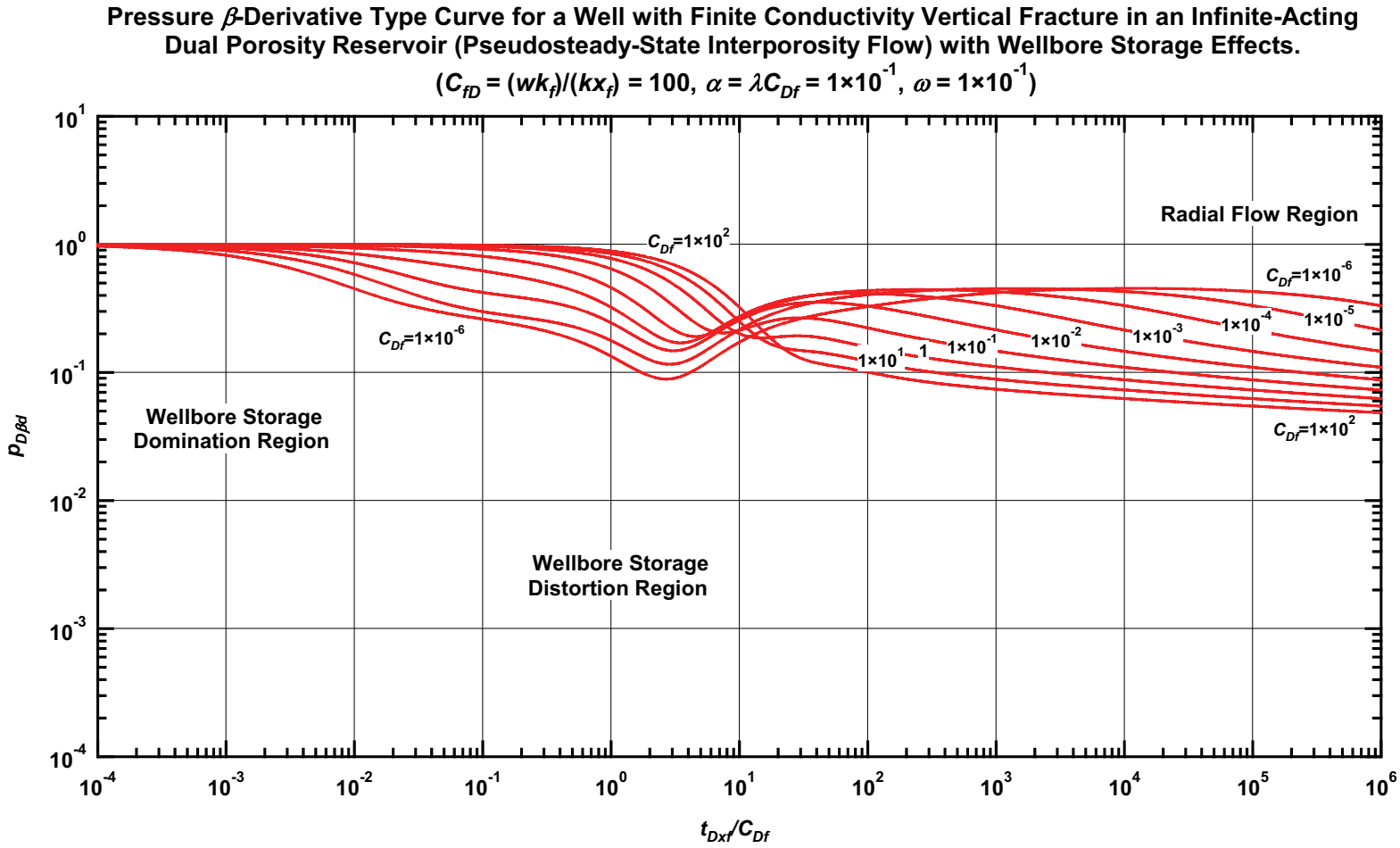

Figure D.57 — $p_{D\beta d}$ vs. t_{Dxf}/C_{Df} — C_{fD} =100, $\omega = 1\times10^{-1}$, $\alpha = \lambda C_{Df} = 1\times10^{-1}$ (fractured well in dual porosity system case — includes wellbore storage effects).

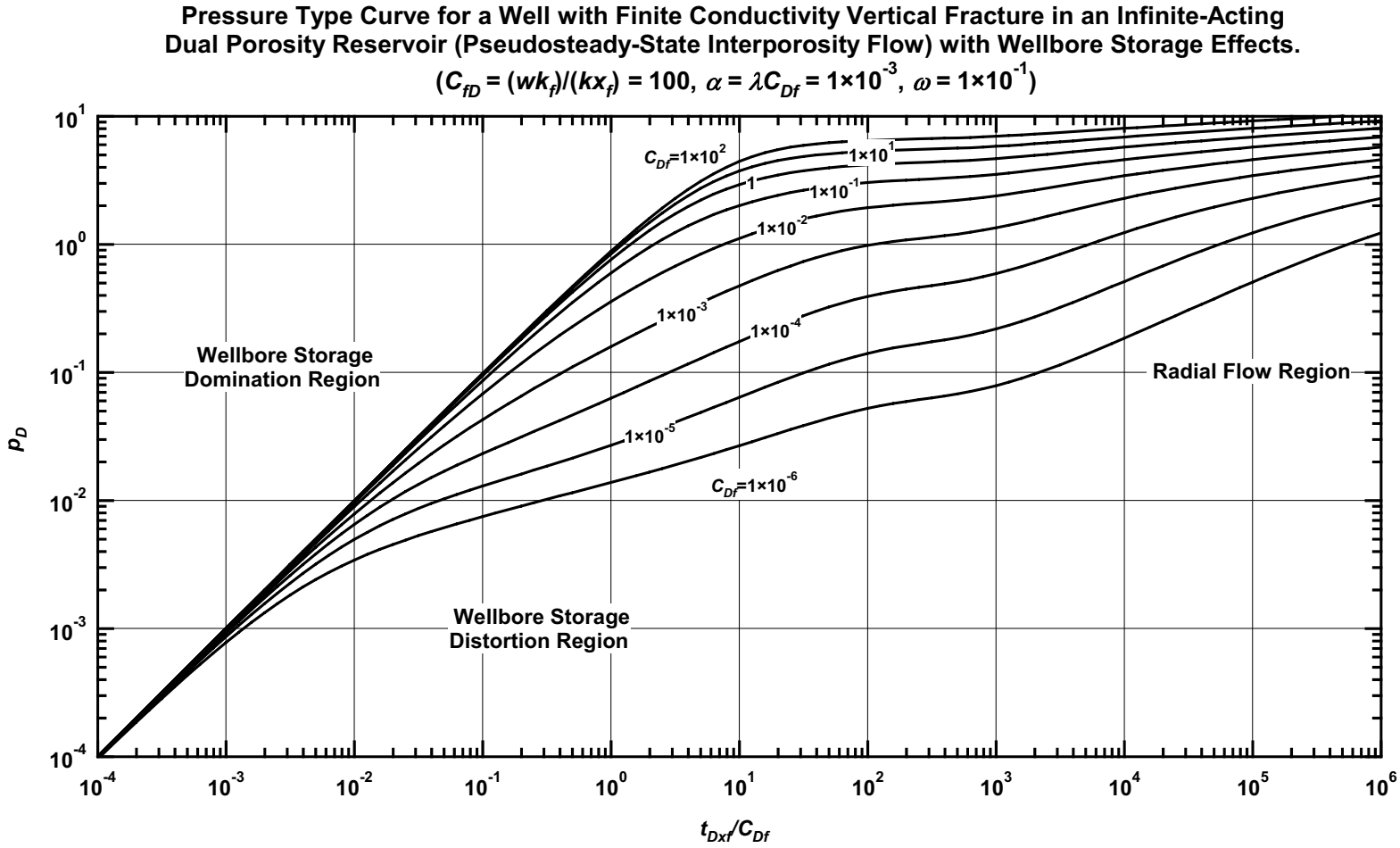

Figure D.58 — p_D **vs.** t_{Dxf}/C_{Df} **—** C_{fD} **=100,** $\omega = 1\times10^{-1}$, $\alpha = \lambda C_{Df} = 1\times10^{-3}$ **(fractured well in dual porosity system case — includes wellbore storage effects).**

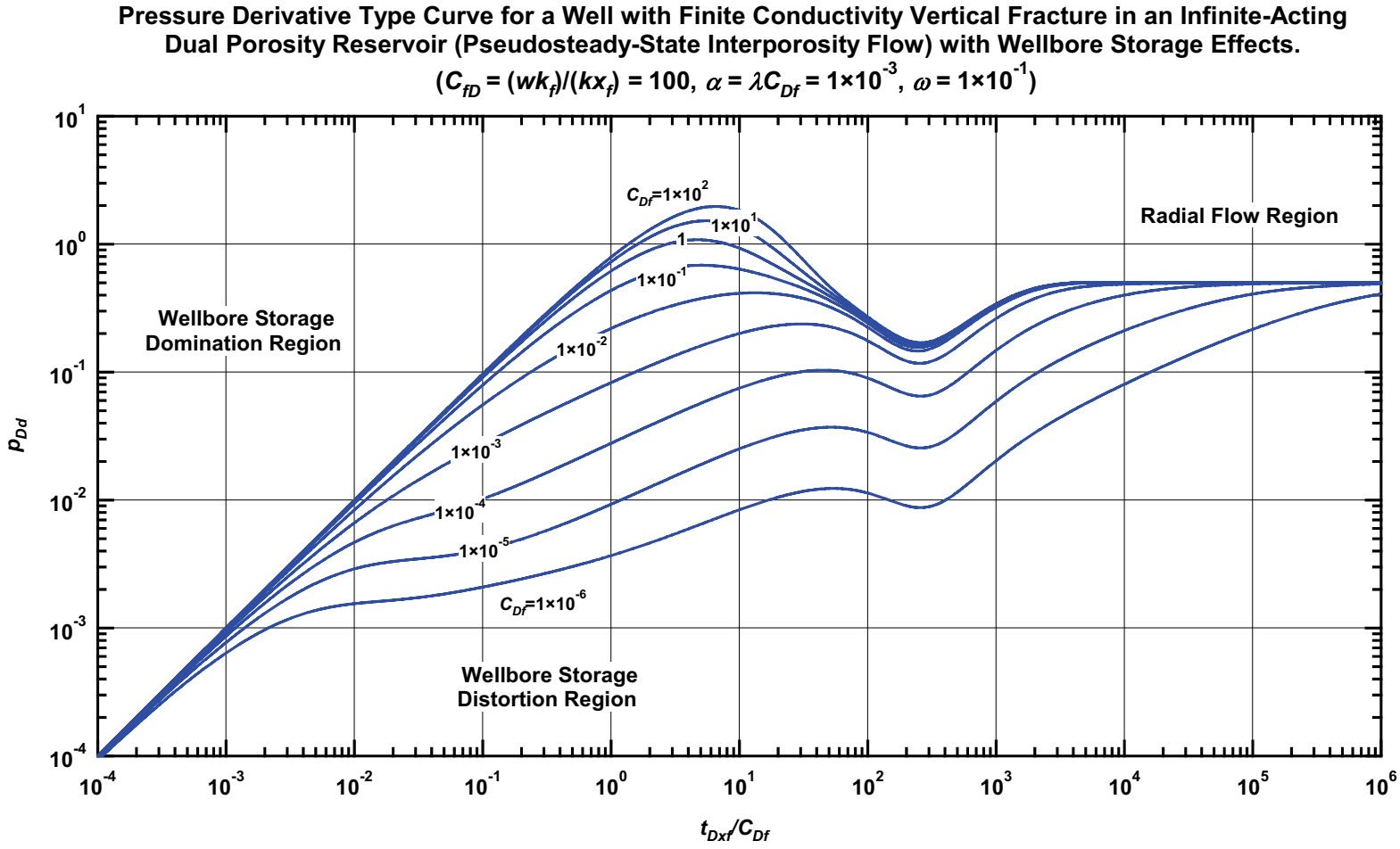

Figure D.59 — p_{Dd} vs. t_{Dxf}/C_{Df} — C_{fD} =100, $\omega = 1\times10^{-1}$, $\alpha = \lambda C_{Df} = 1\times10^{-3}$ (fractured well in dual porosity system case — includes wellbore storage effects).

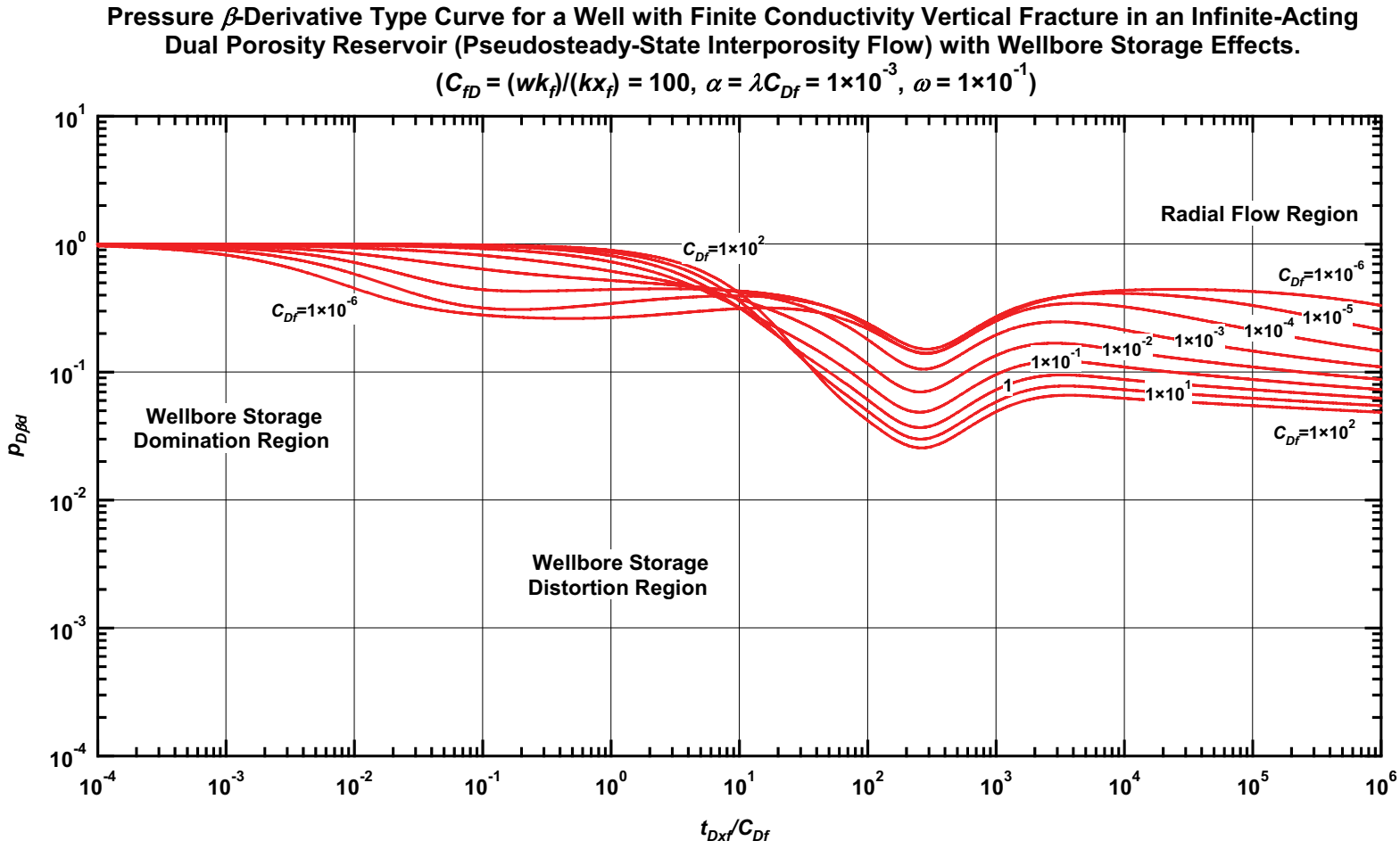

Figure D.60 — $p_{D\beta d}$ **vs.** t_{Dxf}/C_{Df} **—** C_{fD} **=100,** $\omega = 1\times10^{-1}$, $\alpha = \lambda C_{Df} = 1\times10^{-3}$ **(fractured well in dual porosity system case — includes wellbore storage effects).**

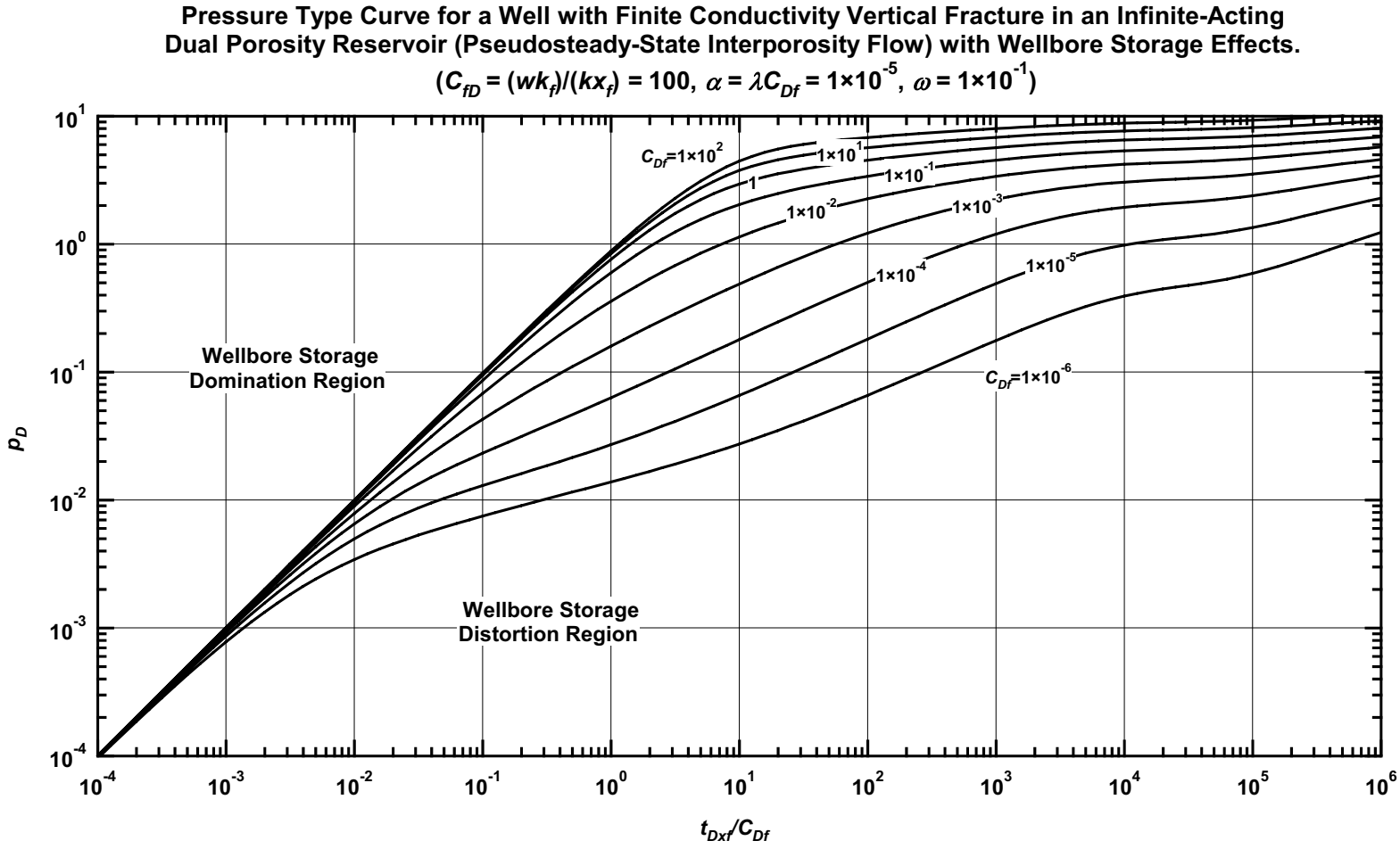

Figure D.61 — p_D vs. t_{Dxf}/C_{Df} — C_{fD} =100, $\omega = 1\times10^{-1}$, $\alpha = \lambda C_{Df} = 1\times10^{-5}$ (fractured well in dual porosity system case — includes wellbore storage effects).

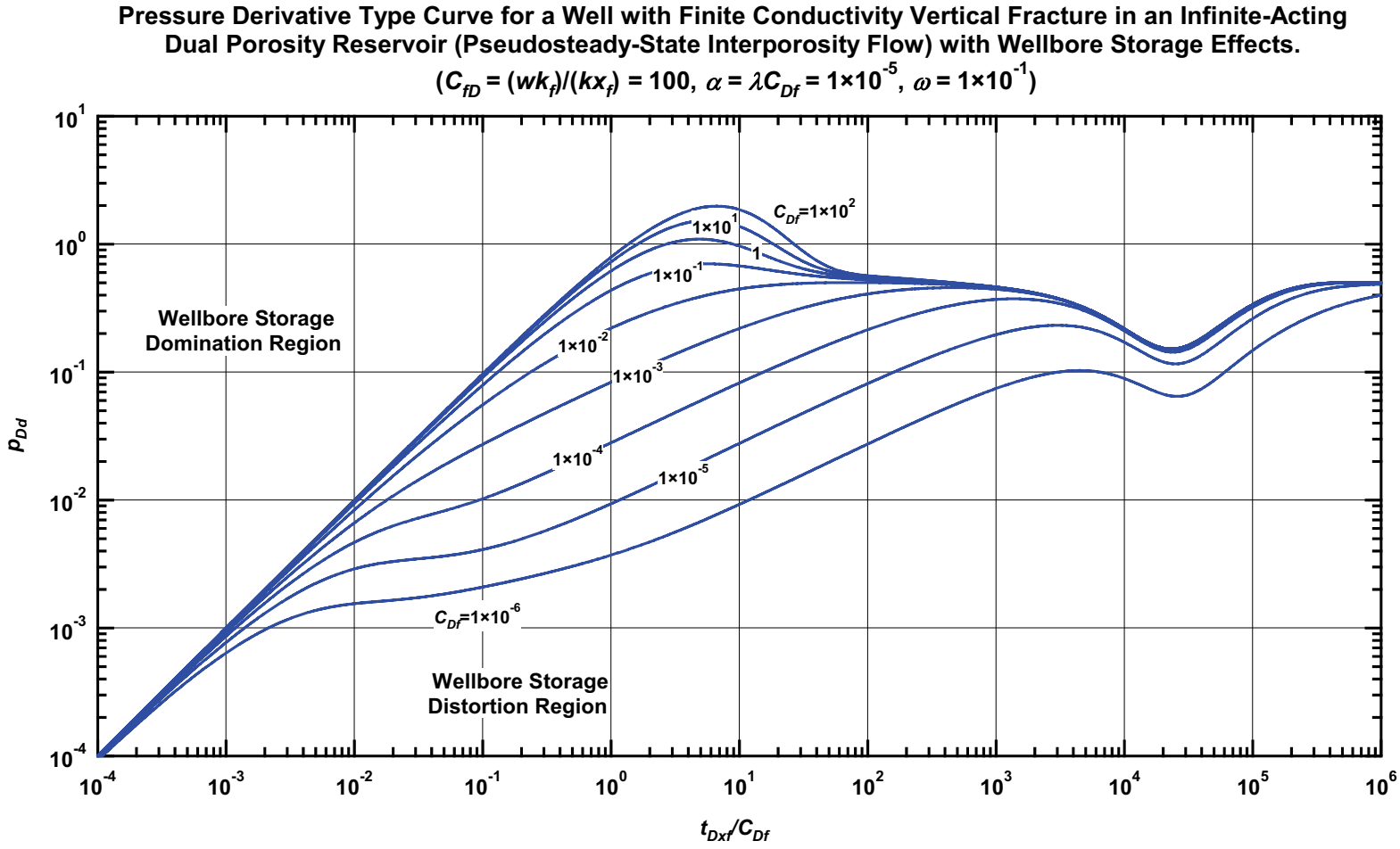

Figure D.62 — p_{Dd} vs. t_{Dxf}/C_{Df} — C_{fD} =100, $\omega = 1\times10^{-1}$, $\alpha = \lambda C_{Df} = 1\times10^{-5}$ (fractured well in dual porosity system case — includes wellbore storage effects).

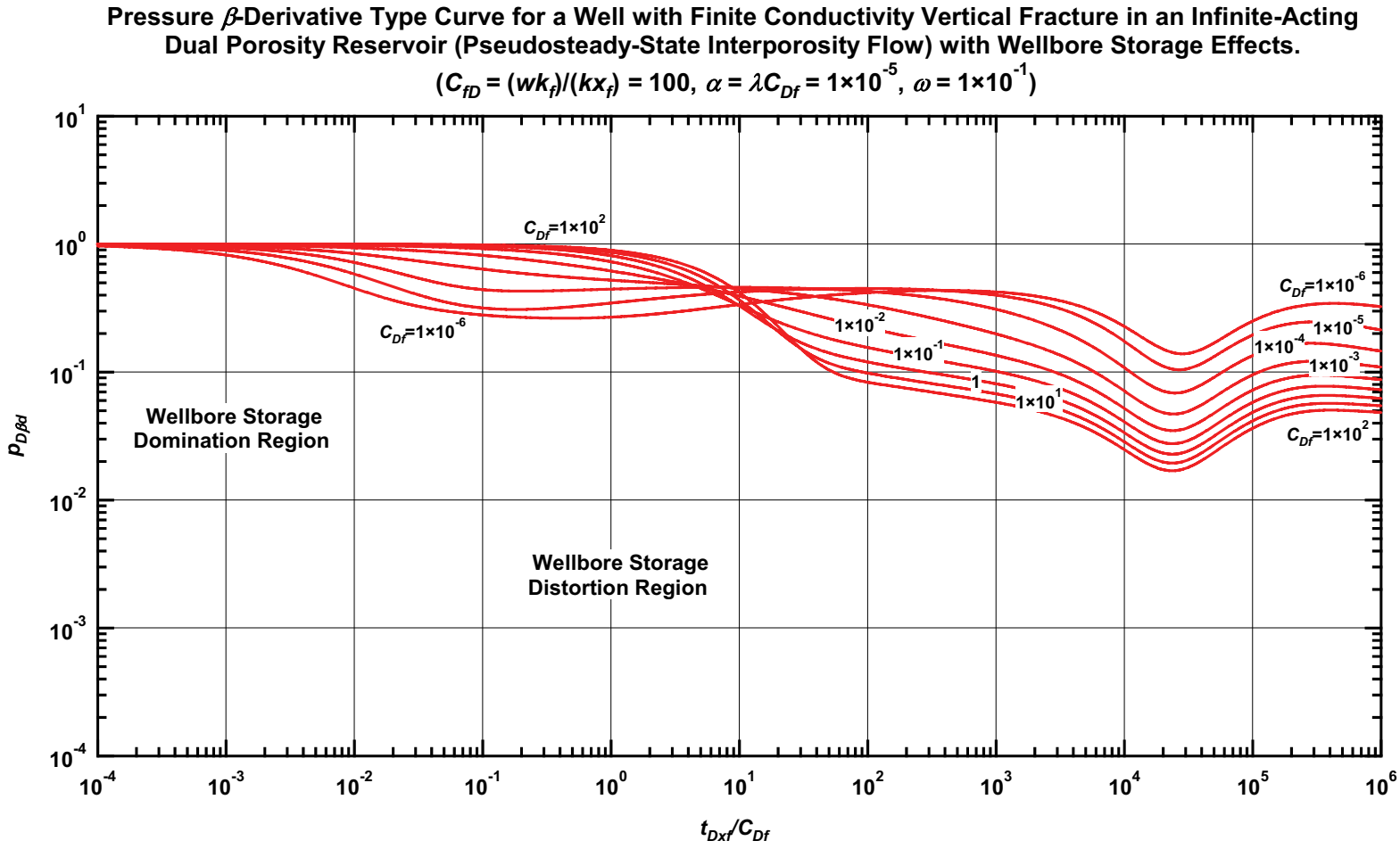

Figure D.63 — $p_{D\beta d}$ vs. t_{Dxf}/C_{Df} — C_{fD} =100, $\omega = 1\times10^{-1}$, $\alpha = \lambda C_{Df} = 1\times10^{-5}$ (fractured well in dual porosity system case — includes wellbore storage effects).

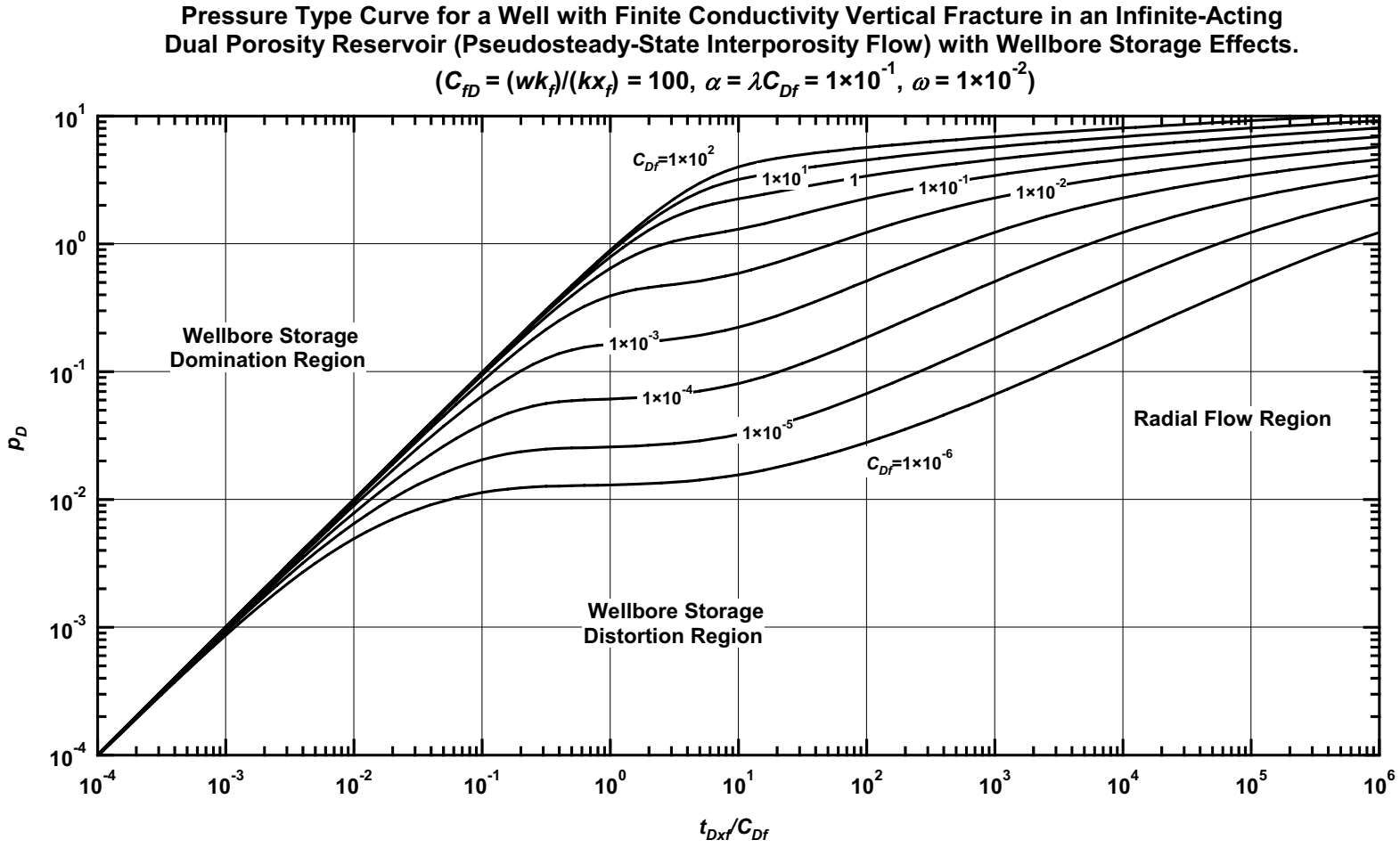

Figure D.64 — p_D **vs.** t_{Dxf}/C_{Df} **—** C_{fD} **=100,** $\omega = 1\times10^{-2}$, $\alpha = \lambda C_{Df} = 1\times10^{-1}$ **(fractured well in dual porosity system case — includes wellbore storage effects).**

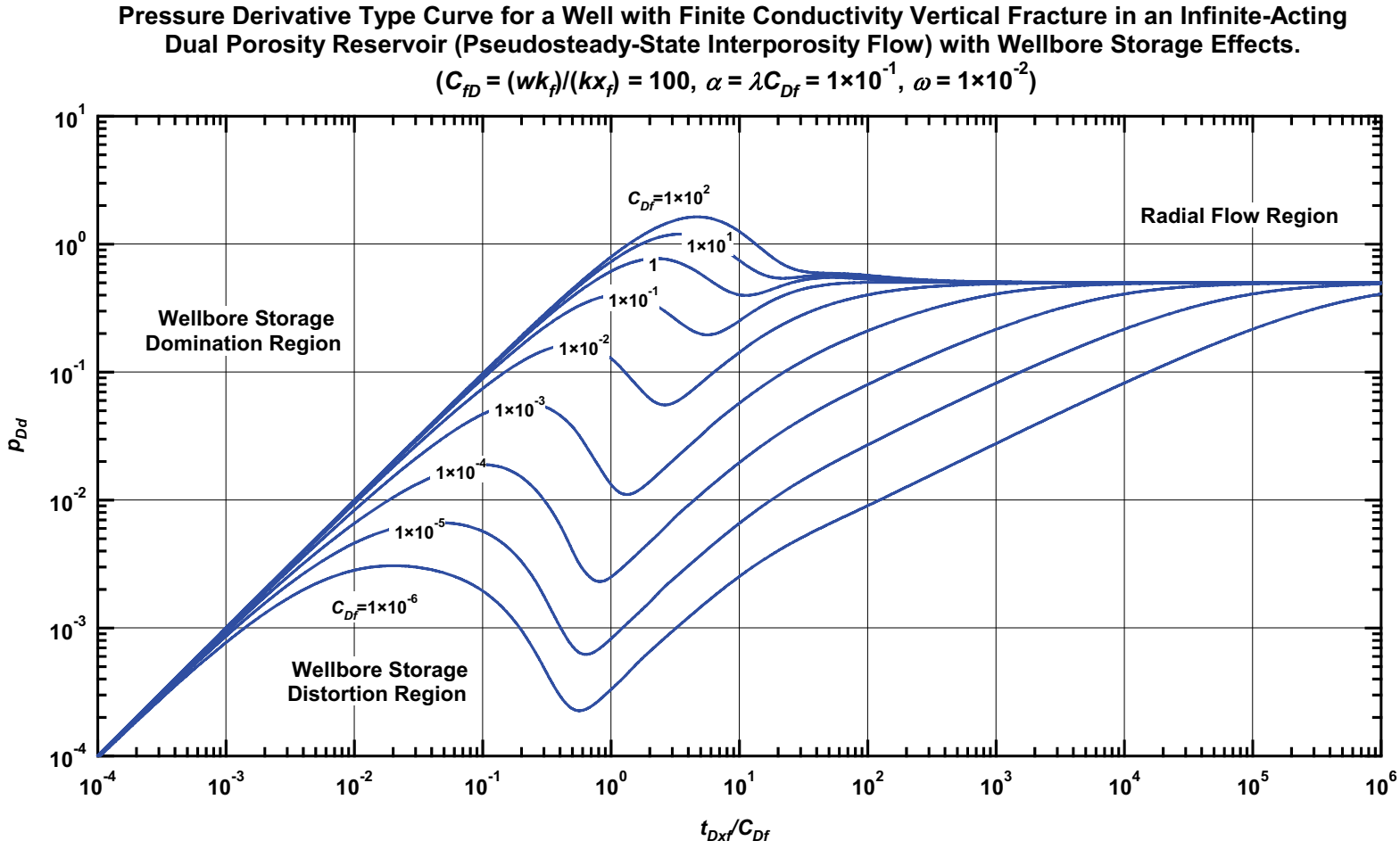

Figure D.65— p_{Dd} vs. t_{Dxf}/C_{Df} — C_{fD} =100, $\omega = 1\times10^{-2}$, $\alpha = \lambda C_{Df} = 1\times10^{-1}$ (fractured well in dual porosity system case — includes wellbore storage effects).

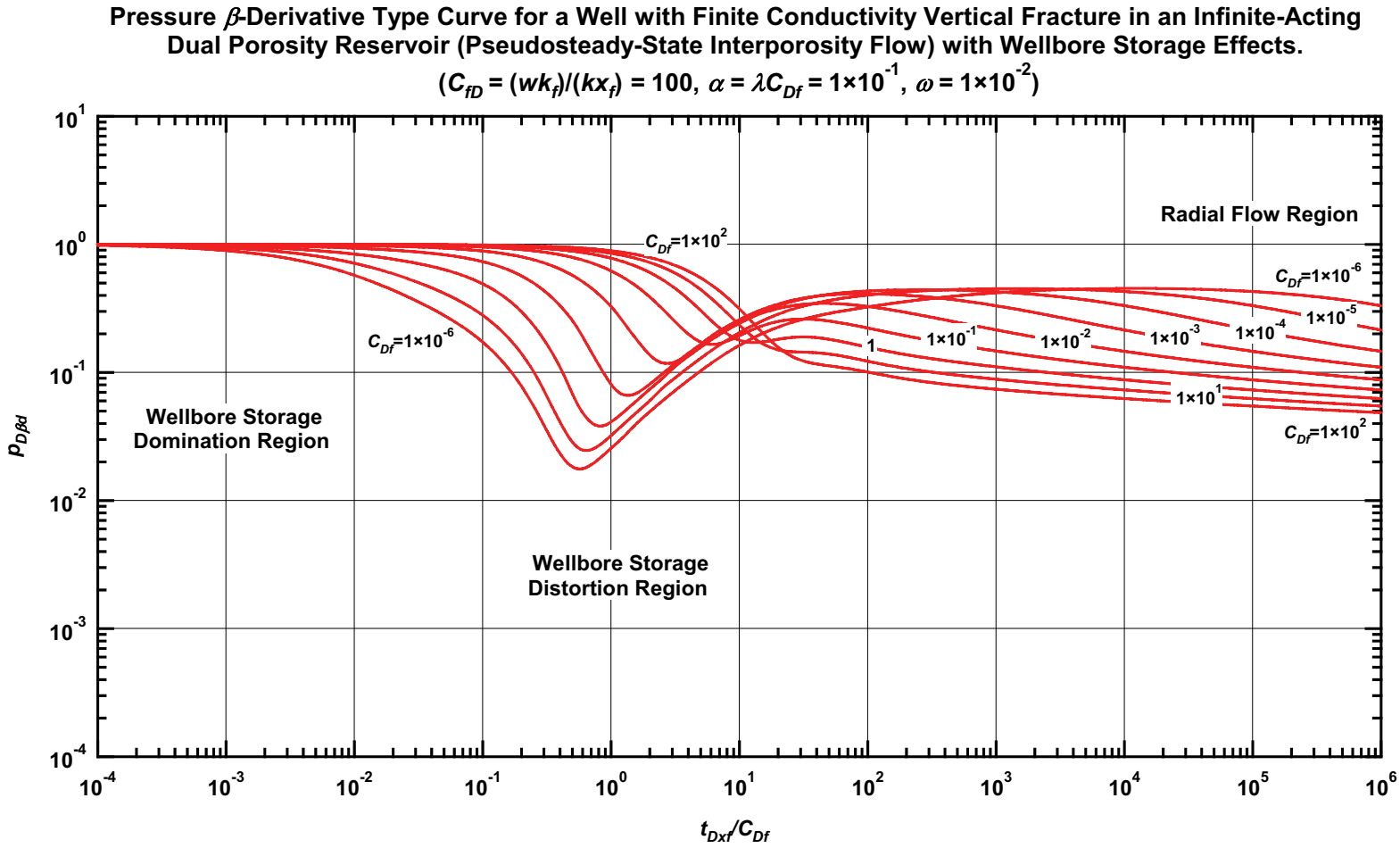

Figure D.66— $p_{D\beta d}$ vs. t_{Dxf}/C_{Df} — C_{fD} =100, $\omega = 1\times10^{-2}$, $\alpha = \lambda C_{Df} = 1\times10^{-1}$ (fractured well in dual porosity system case — includes wellbore storage effects).

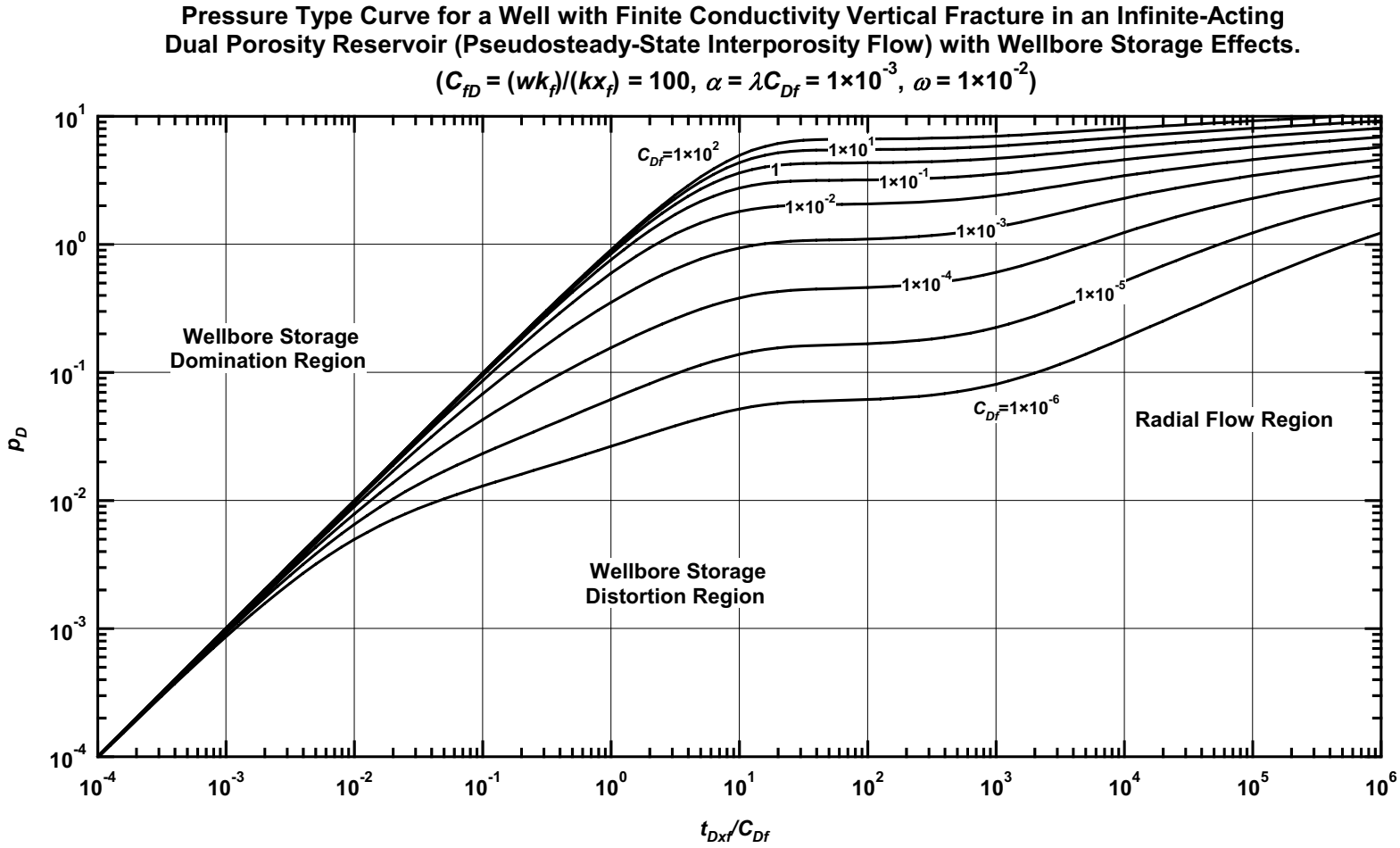

Figure D.67 — p_D vs. t_{Dxf}/C_{Df} — C_{fD} =100, $\omega = 1\times10^{-2}$, $\alpha = \lambda C_{Df} = 1\times10^{-3}$ (fractured well in dual porosity system case — includes wellbore storage effects).

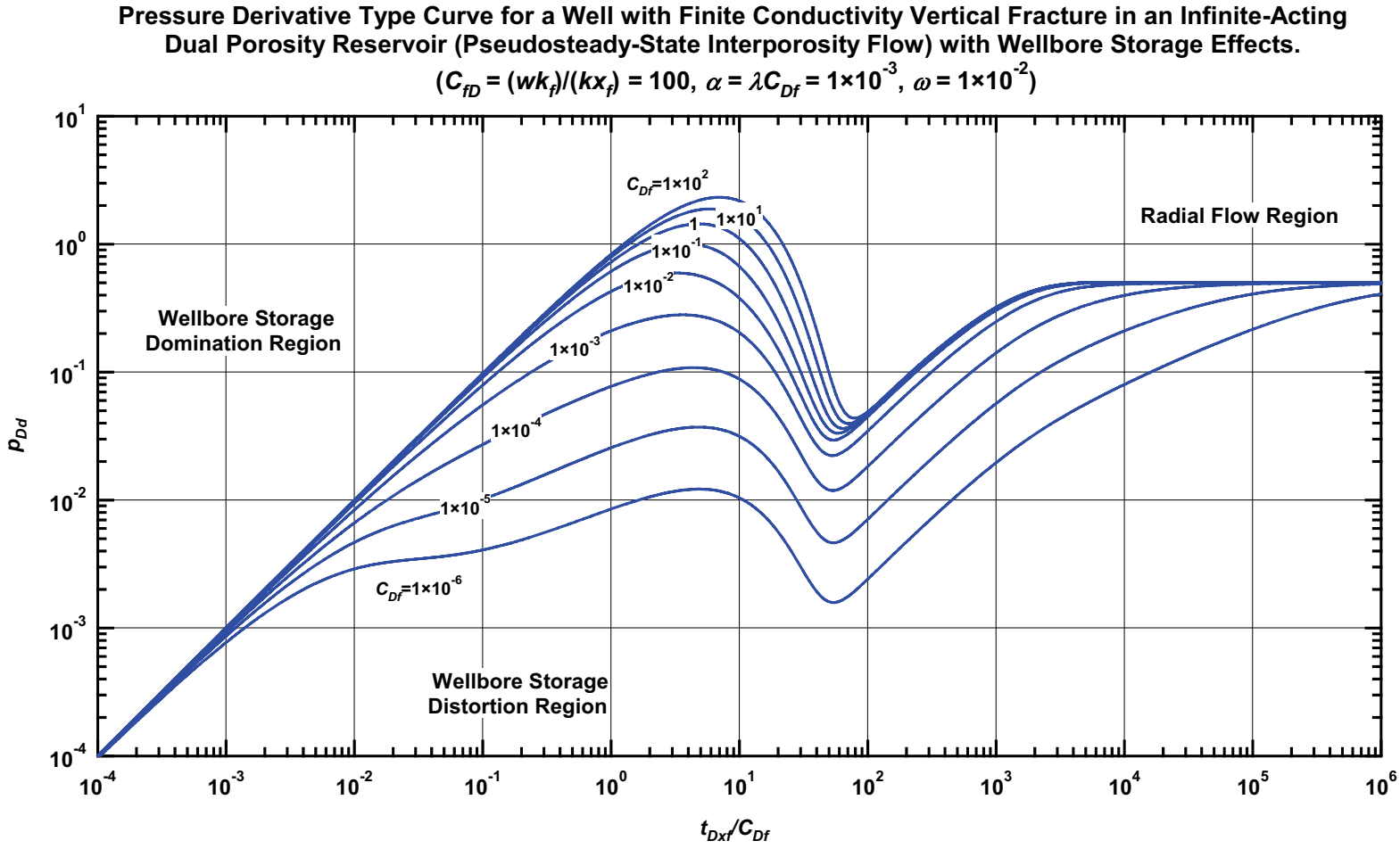

Figure D.68 — p_{Dd} **vs.** t_{Dxf}/C_{Df} **—** C_{fD} **=100,** $\omega = 1\times10^{-2}$, $\alpha = \lambda C_{Df} = 1\times10^{-3}$ **(fractured well in dual porosity system case — includes wellbore storage effects).**

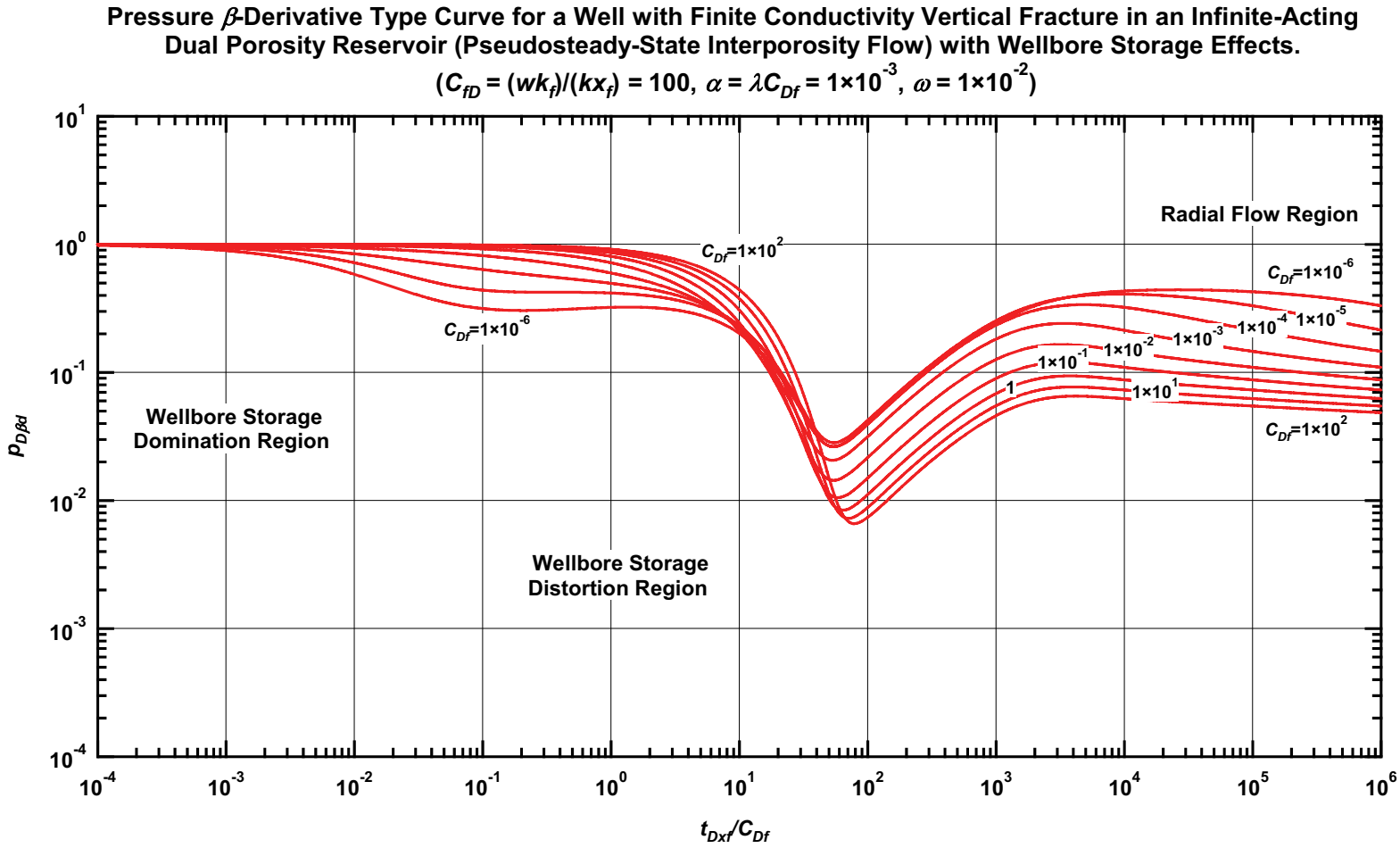

Figure D.69 — $p_{D\beta d}$ vs. t_{Dxf}/C_{Df} — C_{fD} =100, $\omega = 1\times10^{-2}$, $\alpha = \lambda C_{Df} = 1\times10^{-3}$ (fractured well in dual porosity system case — includes wellbore storage effects).

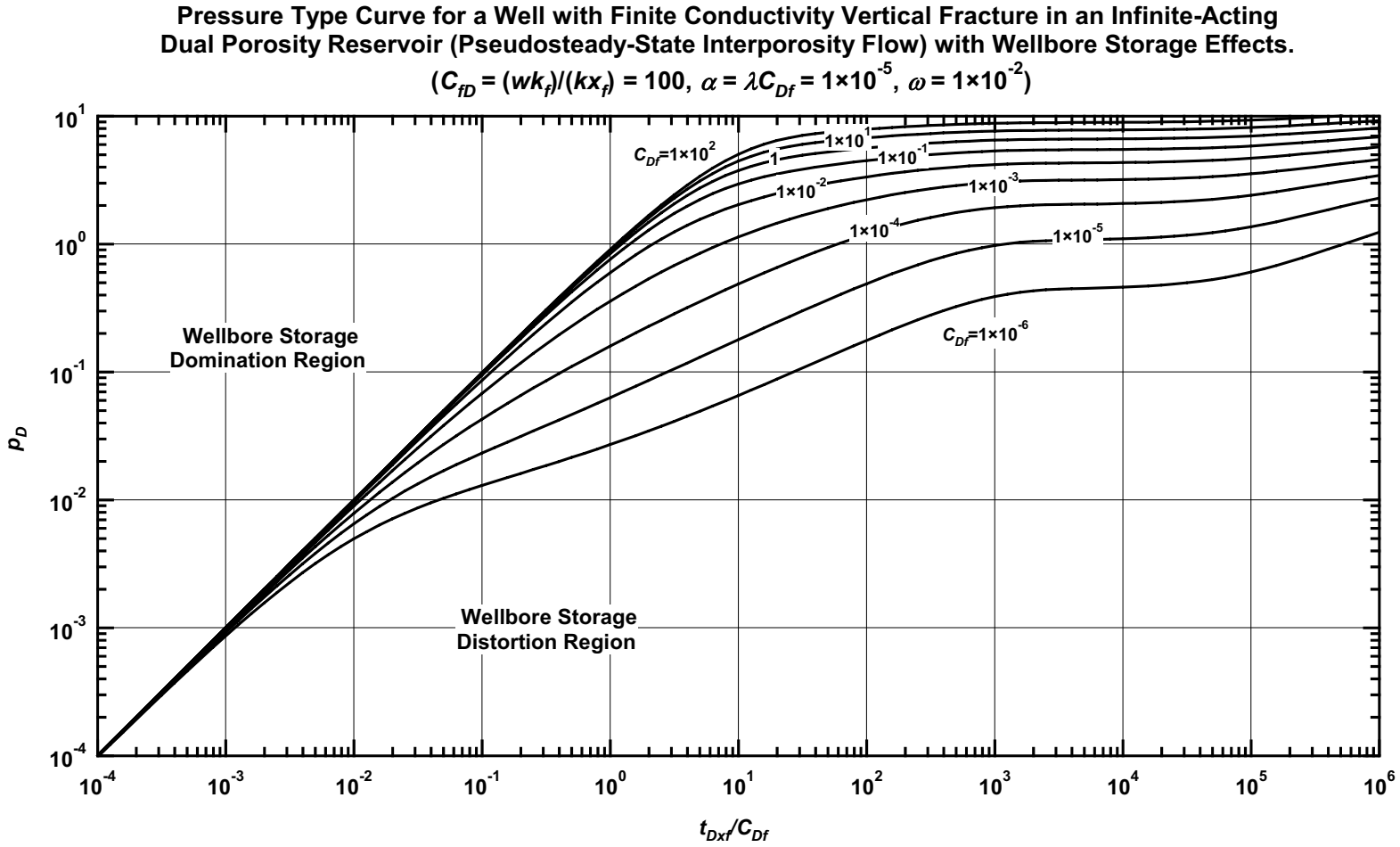

Figure D.70 — p_D vs. t_{Dxf}/C_{Df} — C_{fD} =100, $\omega = 1\times10^{-2}$, $\alpha = \lambda C_{Df} = 1\times10^{-5}$ (fractured well in dual porosity system case — includes wellbore storage effects).

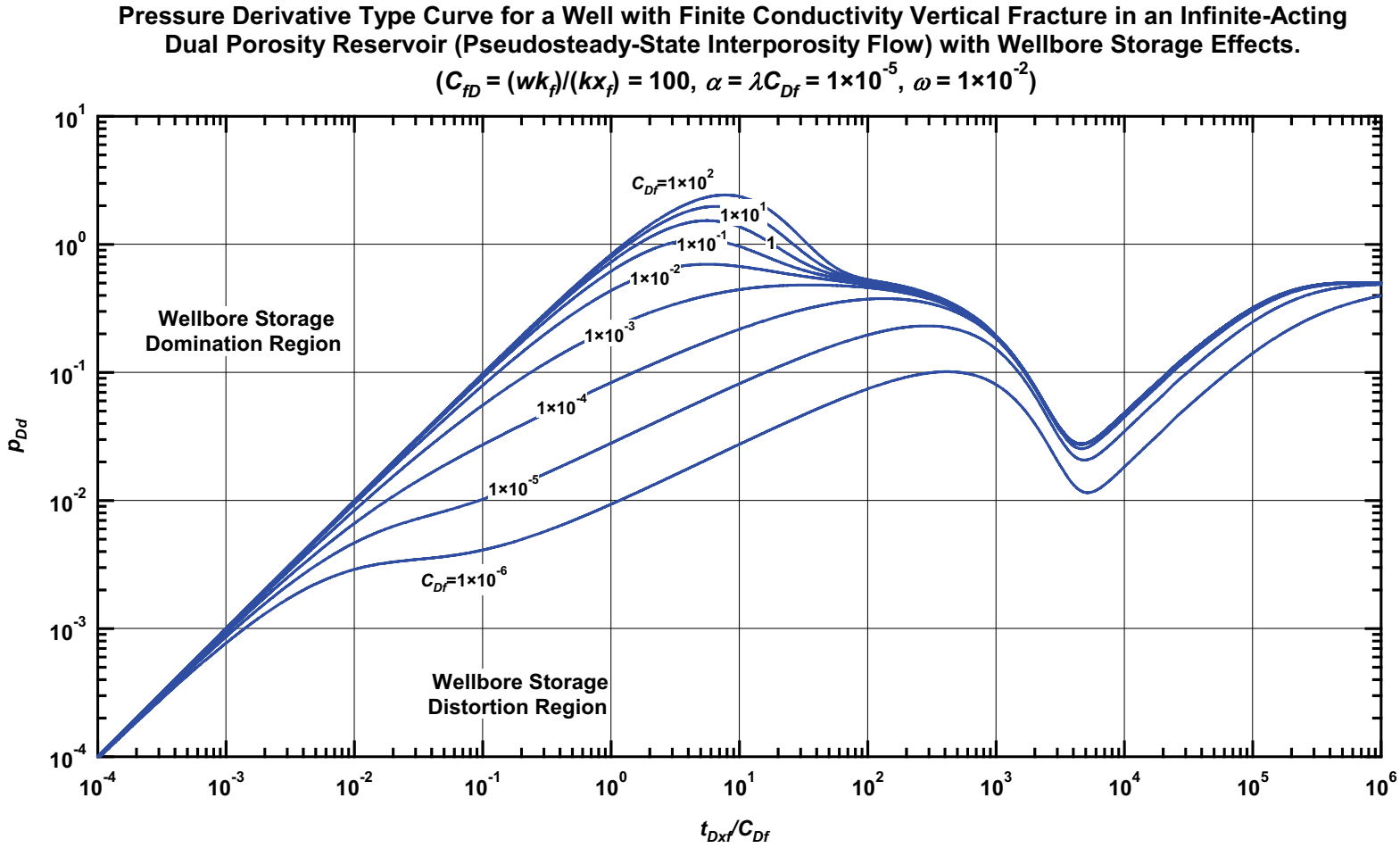

Figure D.71 — p_{Dd} **vs.** t_{Dxf}/C_{Df} **—** C_{fD} **=100,** $\omega = 1\times10^{-2}$, $\alpha = \lambda C_{Df} = 1\times10^{-5}$ **(fractured well in dual porosity system case — includes wellbore storage effects).**

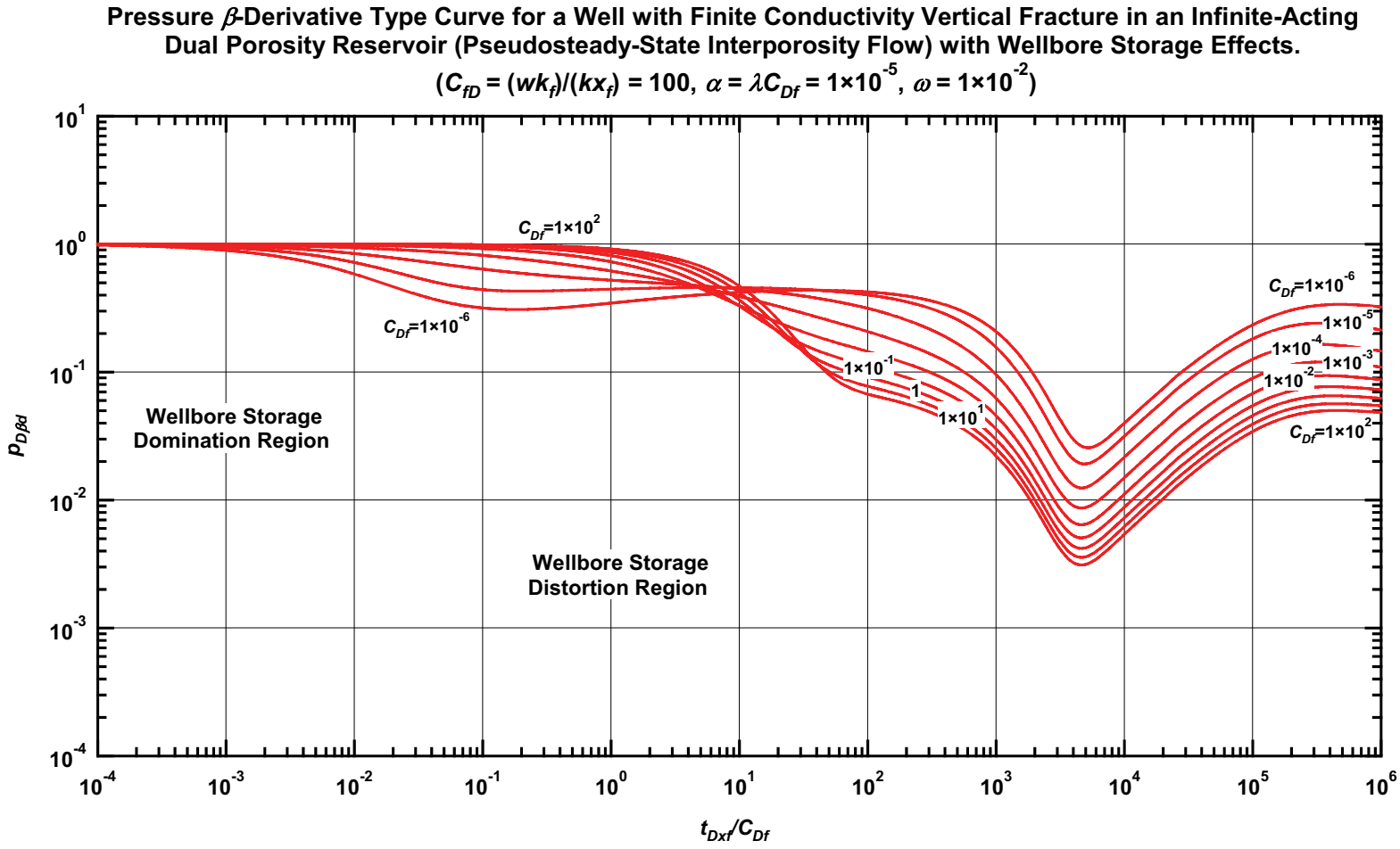

Figure D.72 — $p_{D\beta d}$ vs. t_{Dxf}/C_{Df} — C_{fD} =100, $\omega = 1\times10^{-2}$, $\alpha = \lambda C_{Df} = 1\times10^{-5}$ (fractured well in dual porosity system case — includes wellbore storage effects).

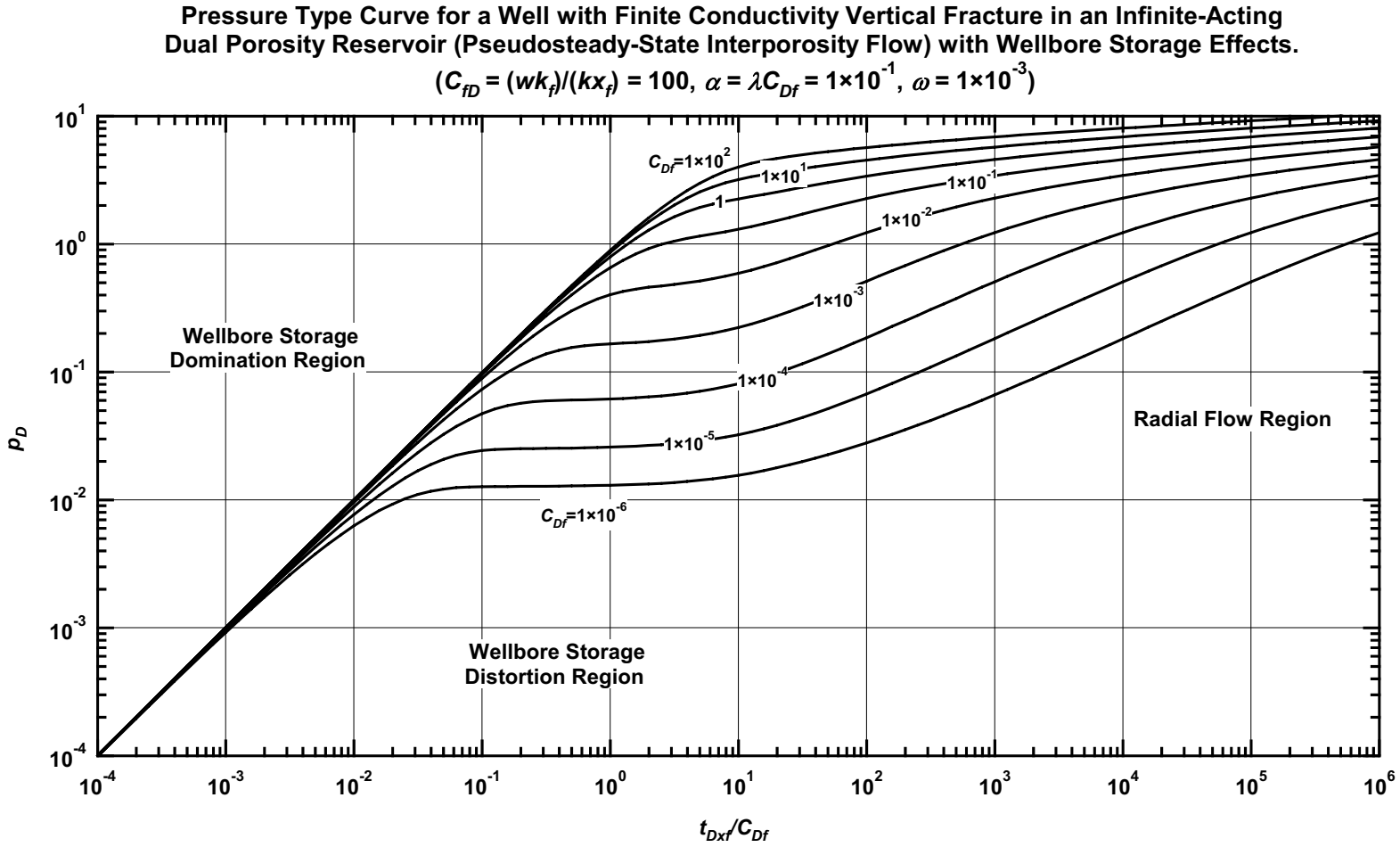

Figure D.73 — p_D **vs.** t_{Dxf}/C_{Df} **—** C_{fD} **=100,** $\omega = 1\times10^{-3}$, $\alpha = \lambda C_{Df} = 1\times10^{-1}$ **(fractured well in dual porosity system case — includes wellbore storage effects).**

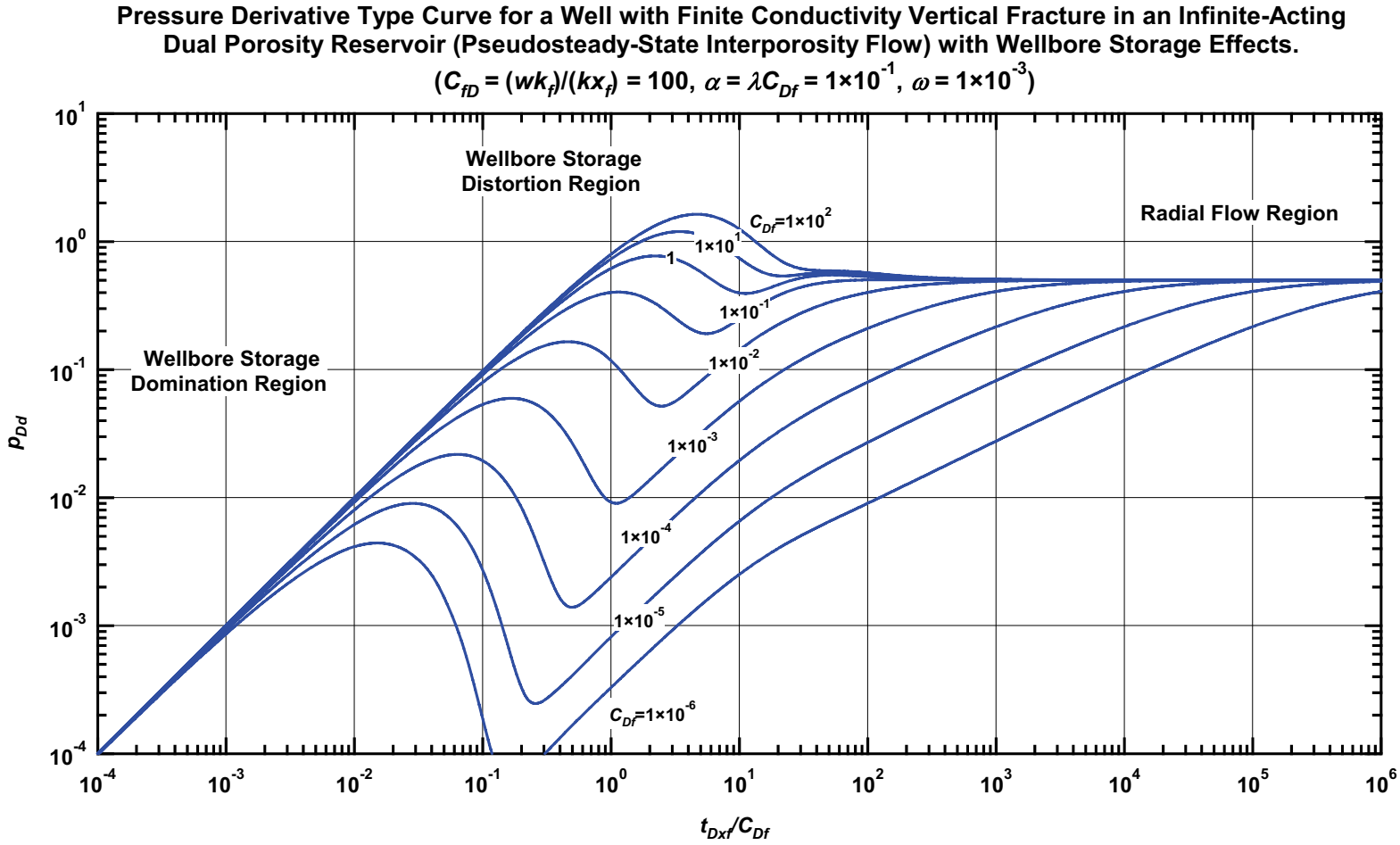

Figure D.74— p_{Dd} vs. t_{Dxf}/C_{Df} — C_{fD} =100, $\omega = 1\times10^{-3}$, $\alpha = \lambda C_{Df} = 1\times10^{-1}$ (fractured well in dual porosity system case — includes wellbore storage effects).

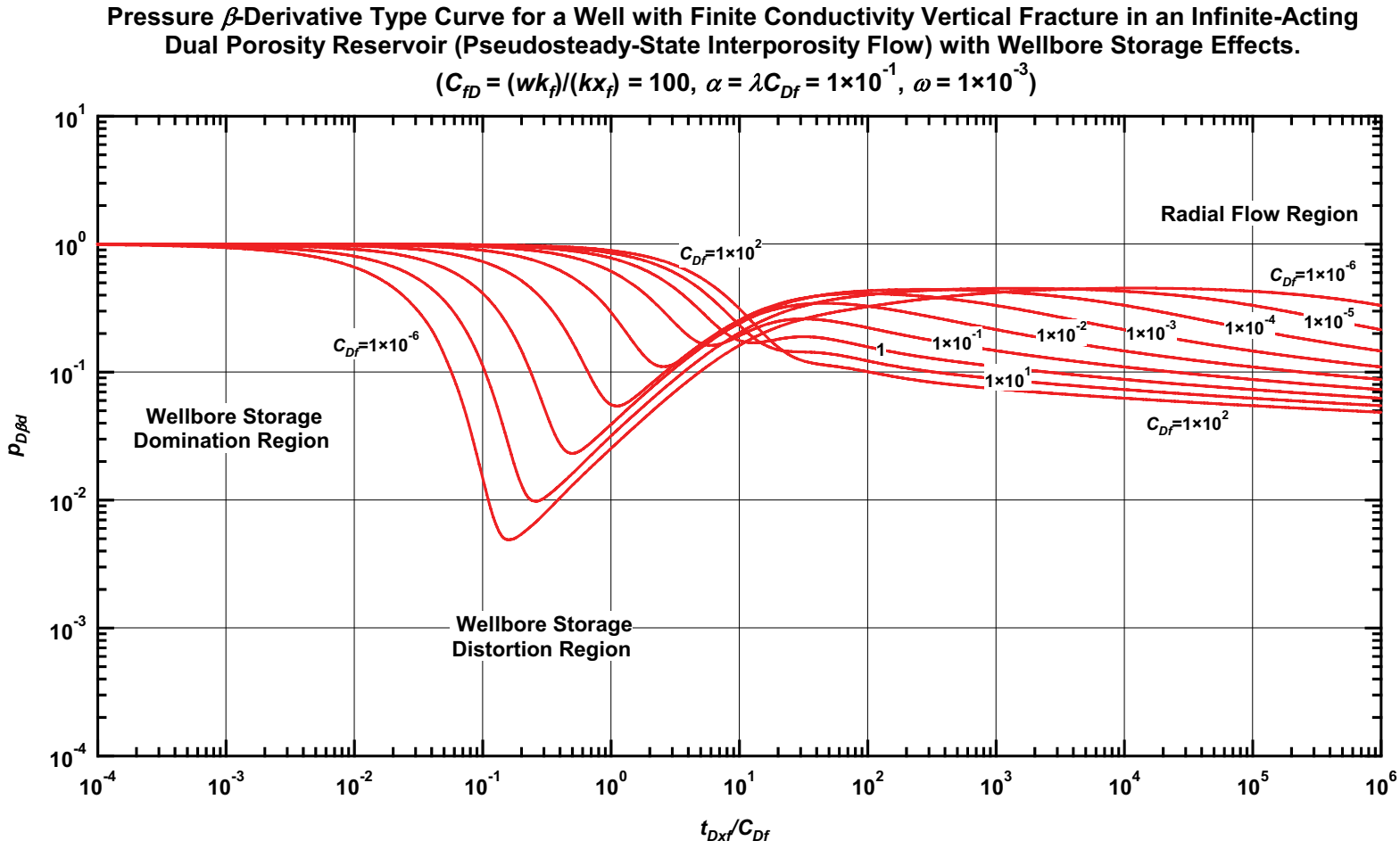

Figure D.75— $p_{D\beta d}$ vs. t_{Dxf}/C_{Df} — C_{fD} =100, $\omega = 1\times10^{-3}$, $\alpha = \lambda C_{Df} = 1\times10^{-1}$ (fractured well in dual porosity system case — includes wellbore storage effects).

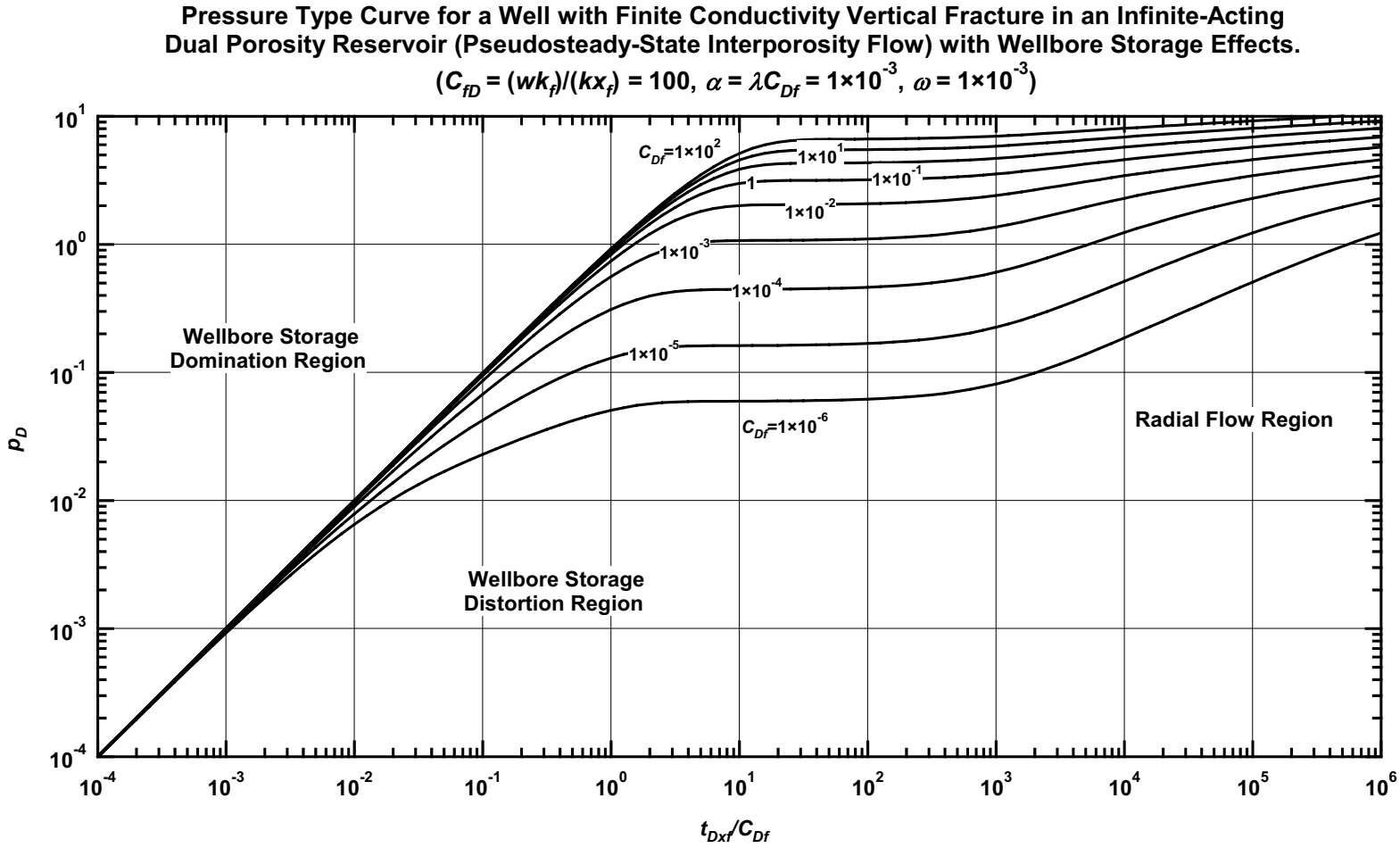

Figure D.76 — p_D vs. t_{Dxf}/C_{Df} — C_{fD} =100, $\omega = 1\times10^{-3}$, $\alpha = \lambda C_{Df} = 1\times10^{-3}$ (fractured well in dual porosity system case — includes wellbore storage effects).

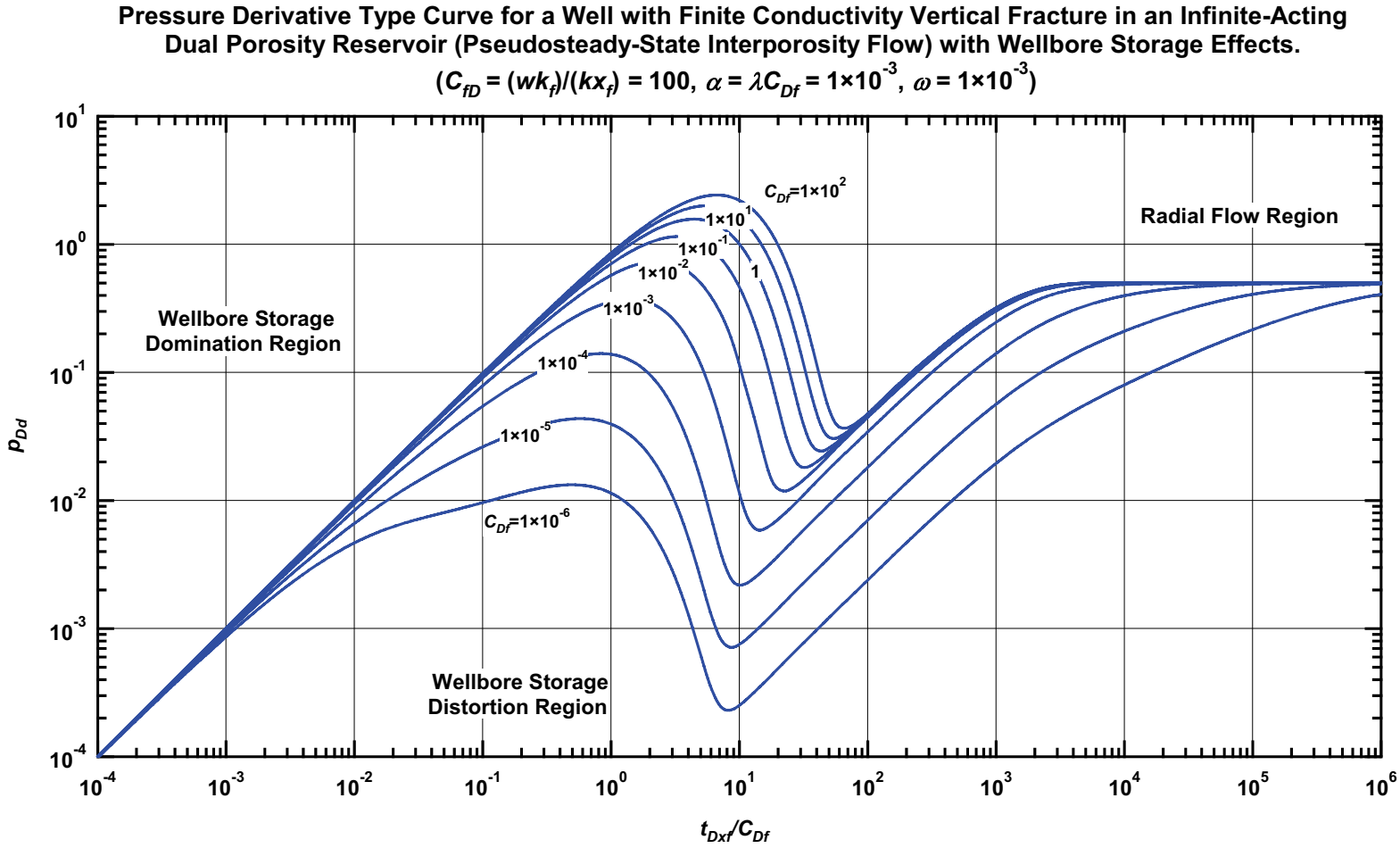

Figure D.77 — p_{Dd} vs. t_{Dxf}/C_{Df} — C_{fD} =100, $\omega = 1\times10^{-3}$, $\alpha = \lambda C_{Df} = 1\times10^{-3}$ (fractured well in dual porosity system case — includes wellbore storage effects).

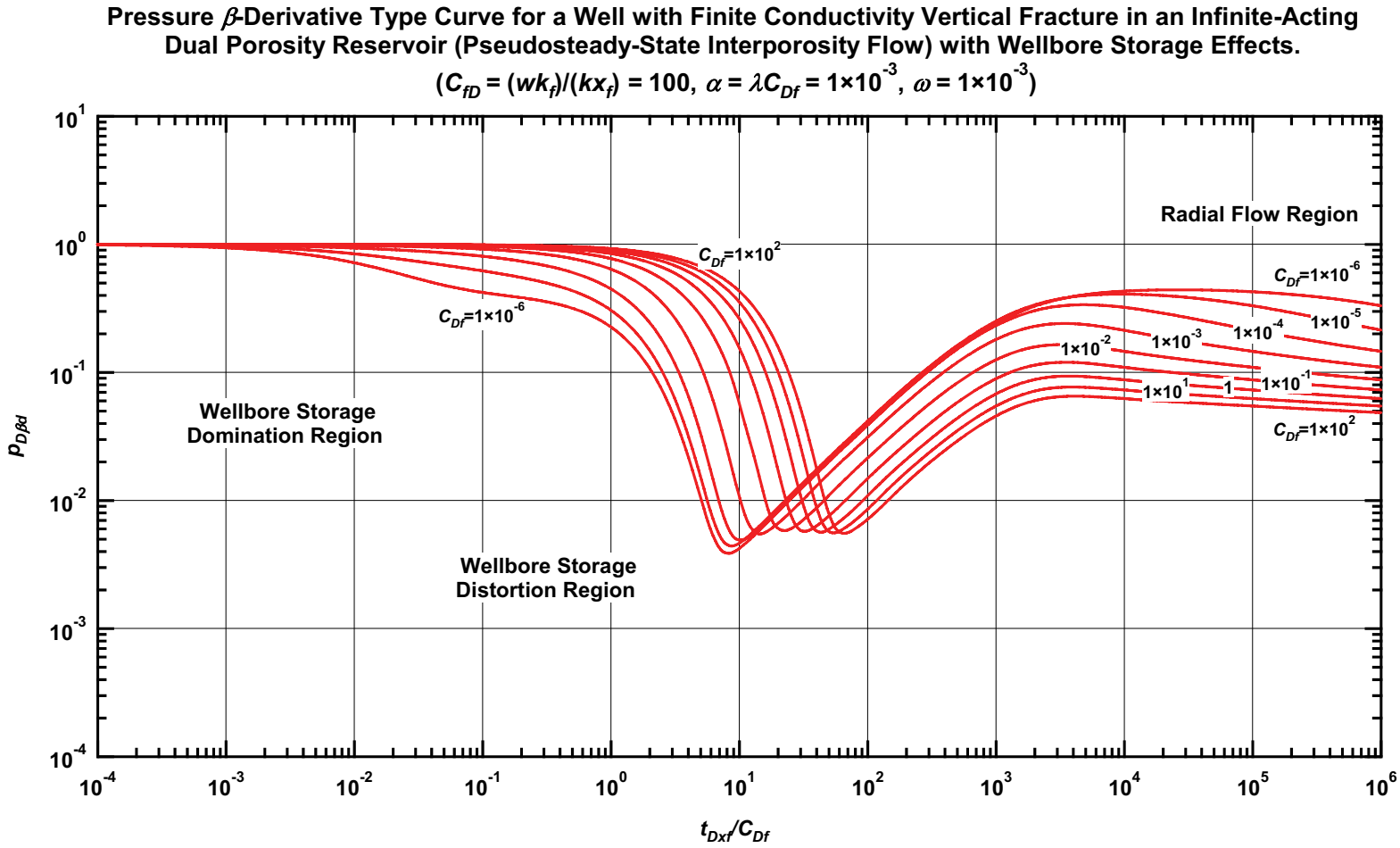

Figure D.78 — $p_{D\beta d}$ vs. t_{Dxf}/C_{Df} — C_{fD} =100, $\omega = 1\times10^{-3}$, $\alpha = \lambda C_{Df} = 1\times10^{-3}$ (fractured well in dual porosity system case — includes wellbore storage effects).

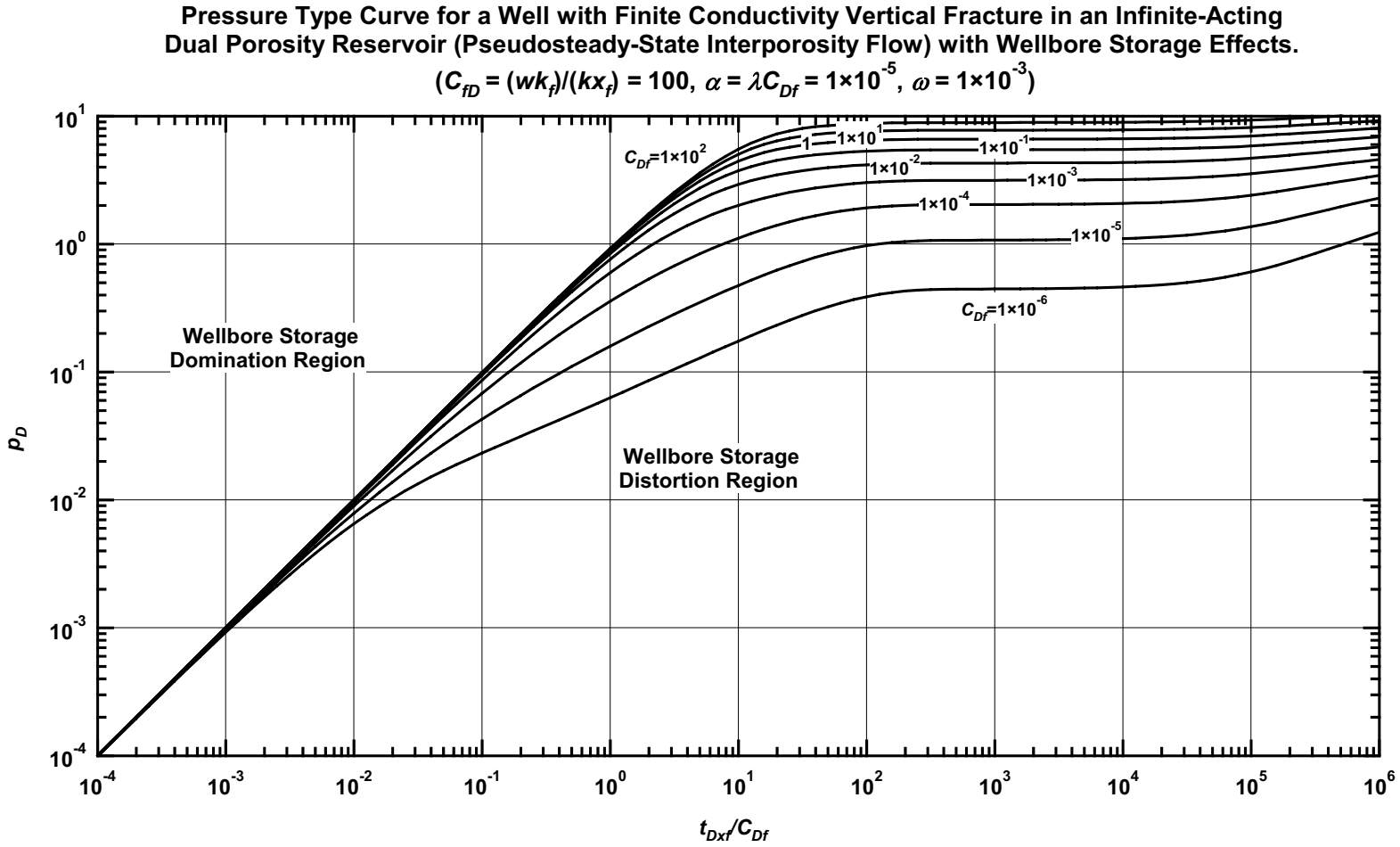

Figure D.79 — p_D **vs.** t_{Dxf}/C_{Df} **—** C_{fD} **=100,** $\omega = 1\times10^{-3}$, $\alpha = \lambda C_{Df} = 1\times10^{-5}$ **(fractured well in dual porosity system case — includes wellbore storage effects).**

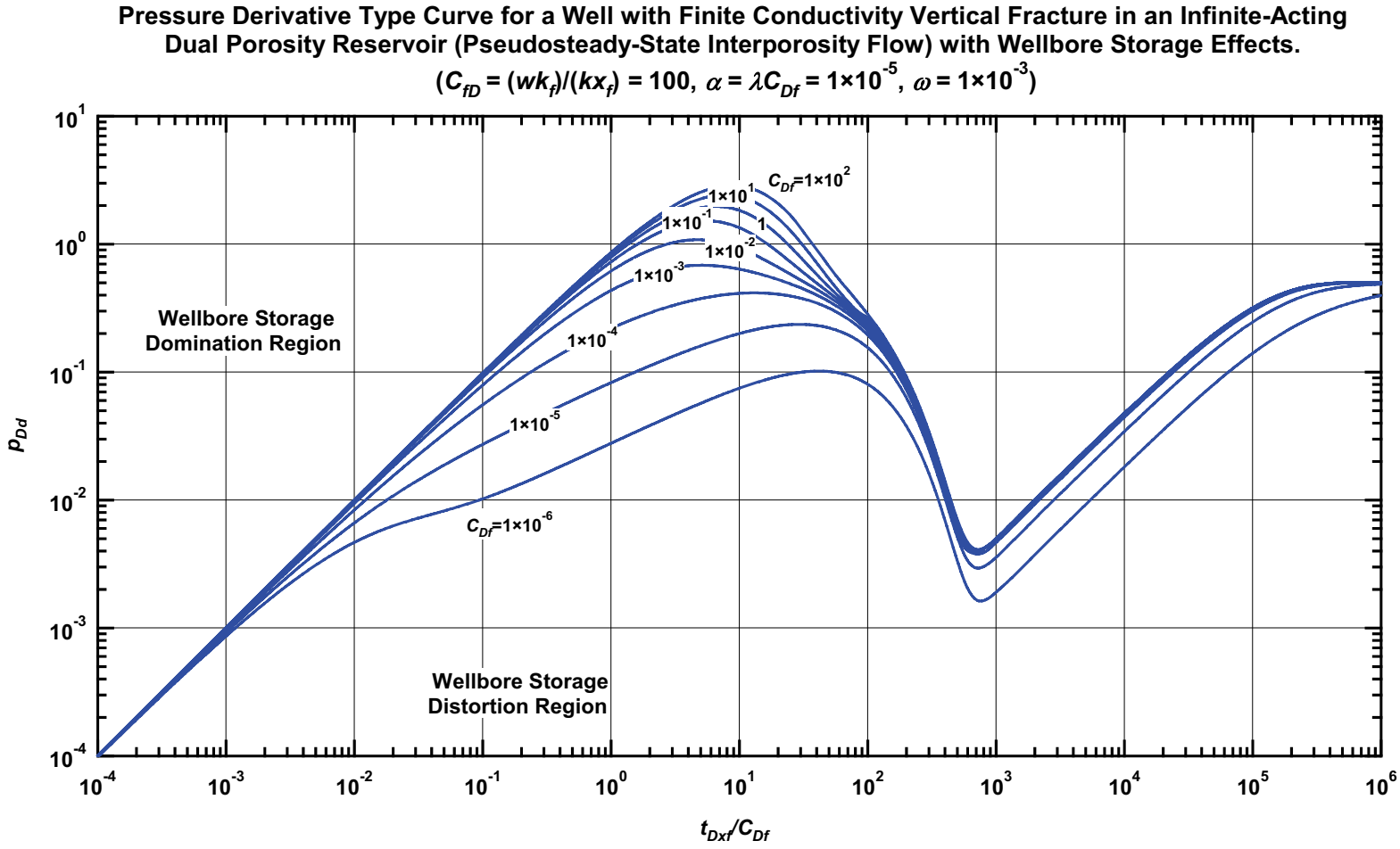

Figure D.80 — p_{Dd} vs. t_{Dxf}/C_{Df} — C_{fD} =100, $\omega = 1\times10^{-3}$, $\alpha = \lambda C_{Df} = 1\times10^{-5}$ (fractured well in dual porosity system case — includes wellbore storage effects).

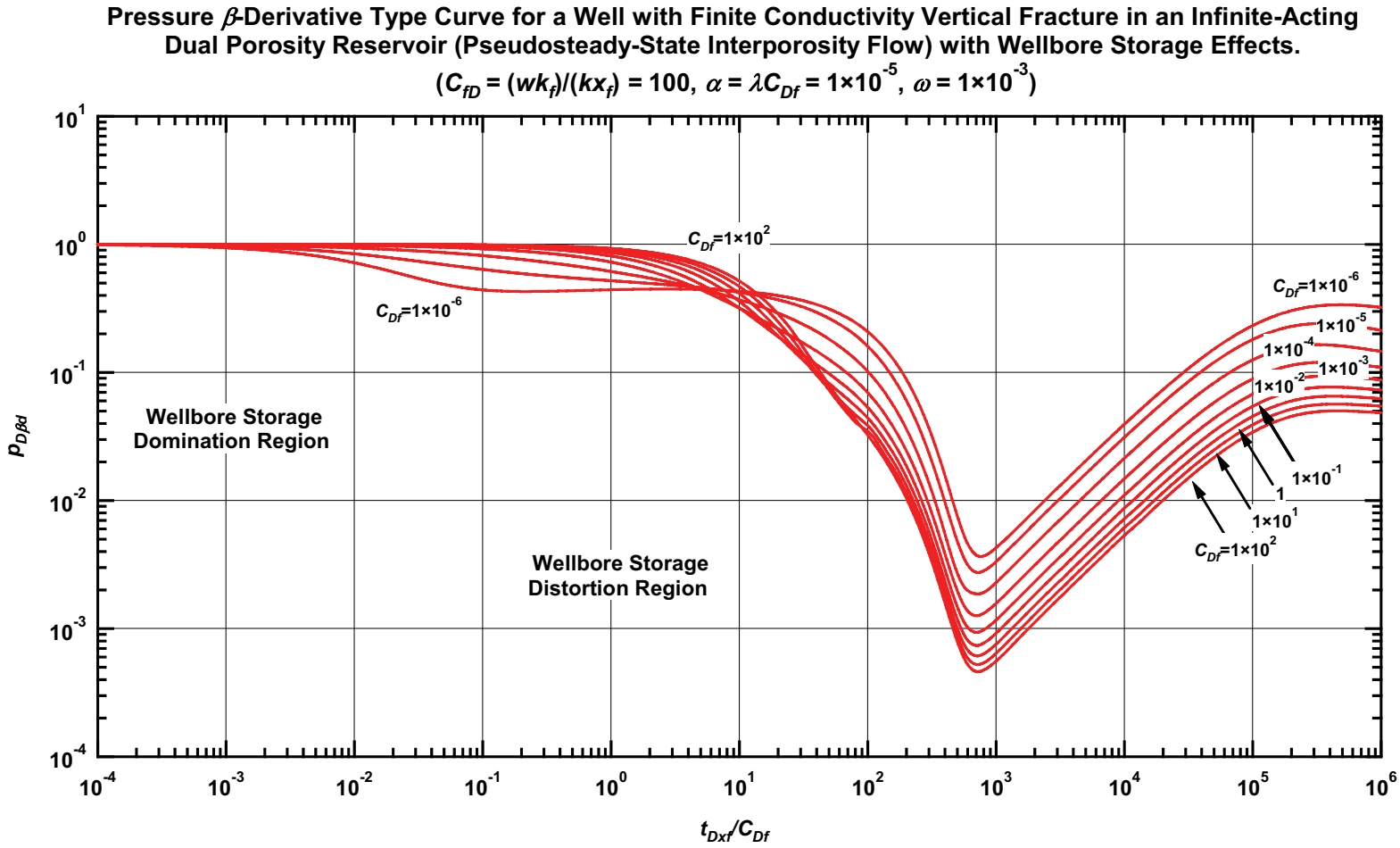

Figure D.81 — $p_{D\beta d}$ vs. t_{Dxf}/C_{Df} — C_{fD} =100, $\omega = 1\times10^{-3}$, $\alpha = \lambda C_{Df} = 1\times10^{-5}$ (fractured well in dual porosity system case — includes wellbore storage effects).

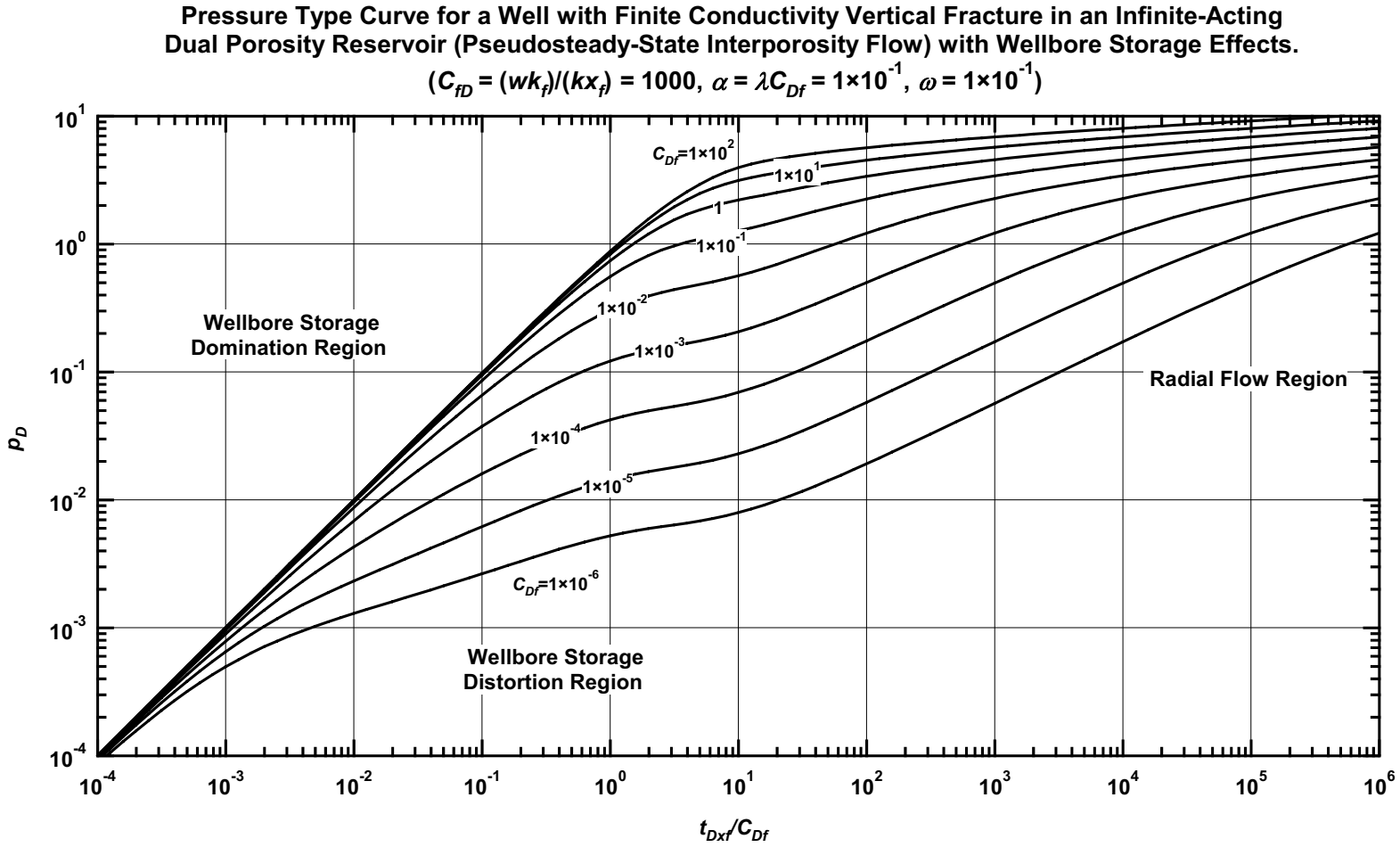

Figure D.82 — p_D **vs.** t_{Dxf}/C_{Df} **—** C_{fD} **=1000,** $\omega = 1\times10^{-1}$, $\alpha = \lambda C_{Df} = 1\times10^{-1}$ **(fractured well in dual porosity system case — includes wellbore storage effects).**

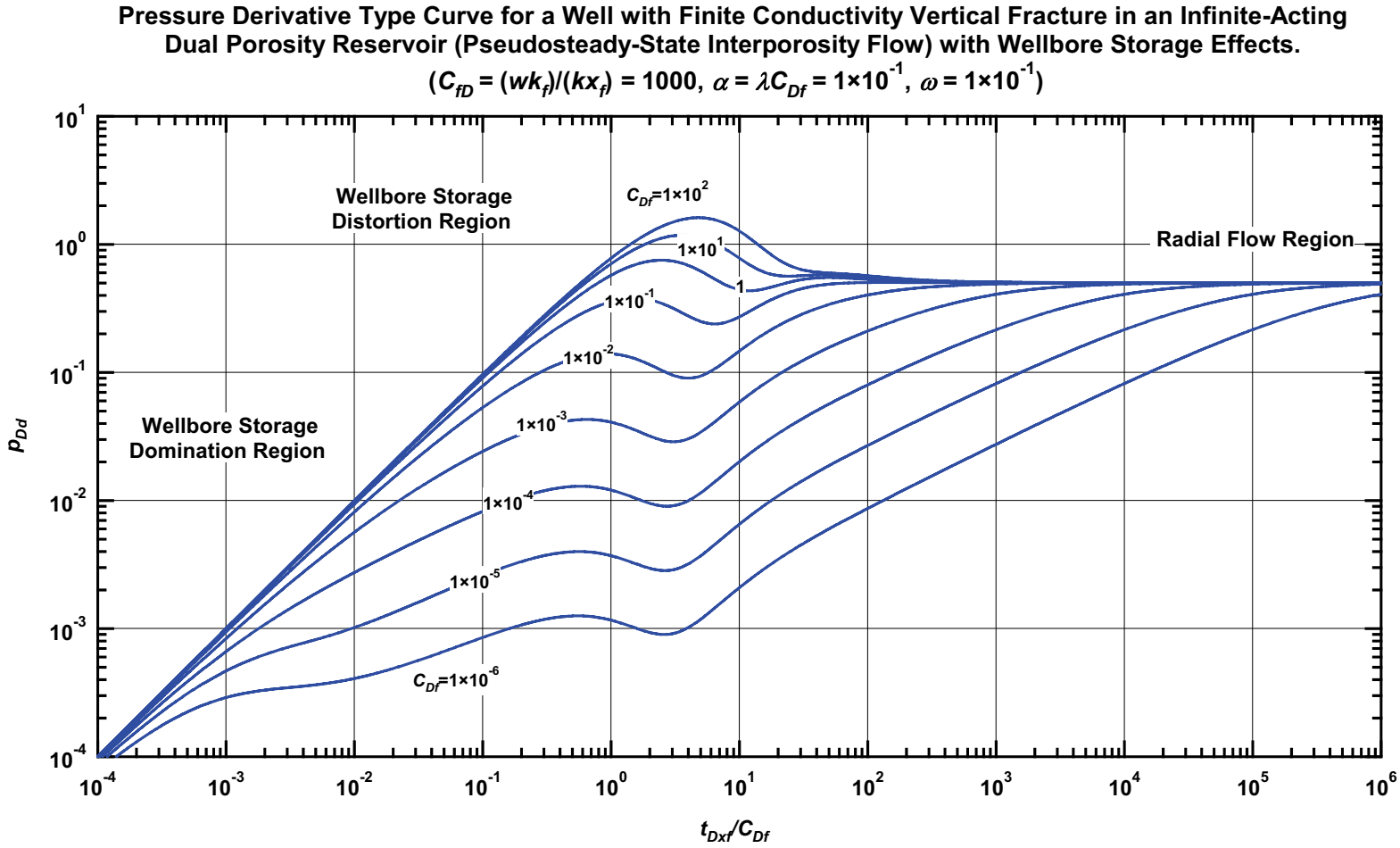

Figure D.83 — p_{Dd} vs. t_{Dxf}/C_{Df} — C_{fD} =1000, $\omega = 1\times10^{-1}$, $\alpha = \lambda C_{Df} = 1\times10^{-1}$ (fractured well in dual porosity system case — includes wellbore storage effects).

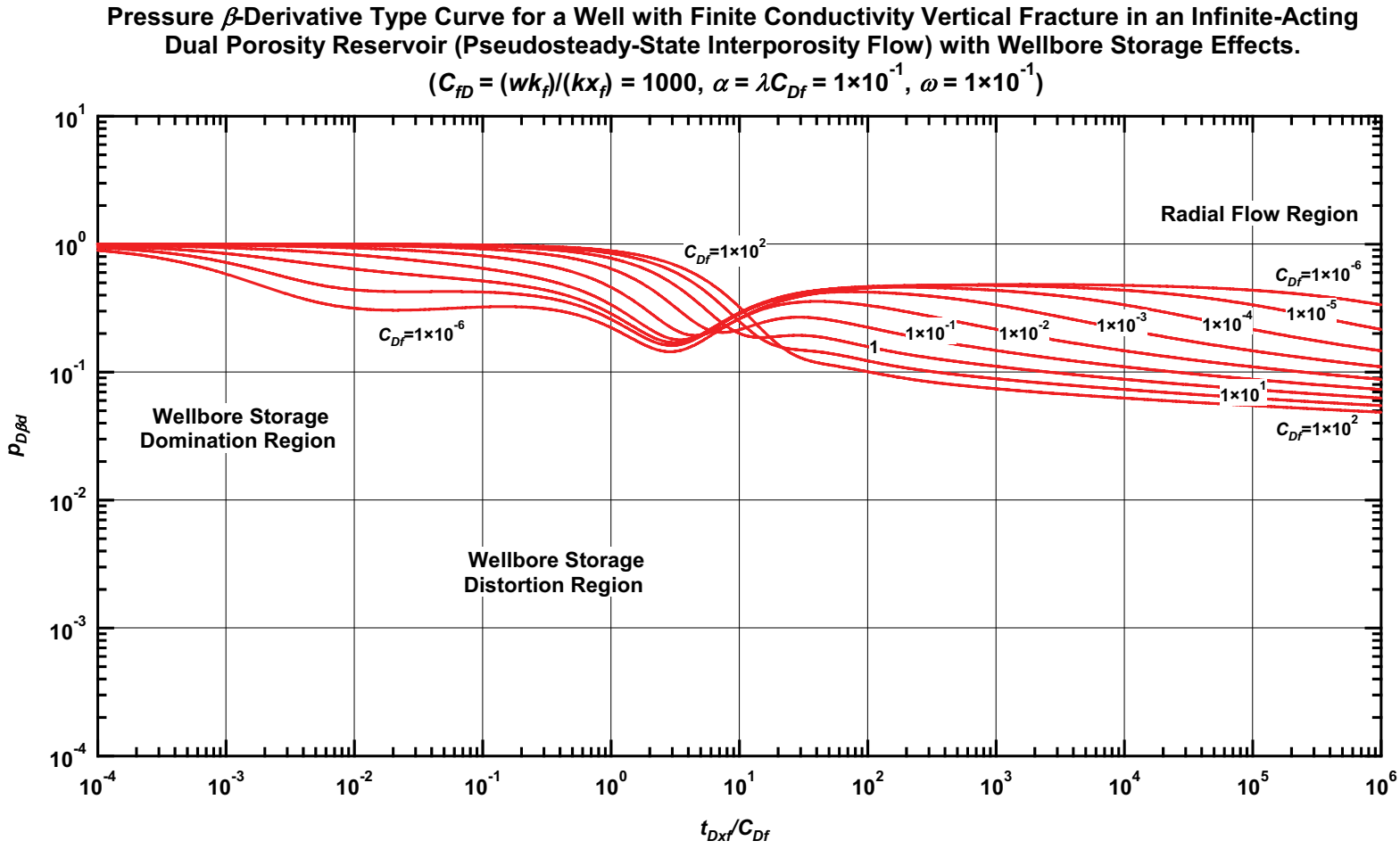

Figure D.84— $p_{D\beta d}$ vs. t_{Dxf}/C_{Df} — C_{fD} =1000, $\omega = 1\times10^{-1}$, $\alpha = \lambda C_{Df} = 1\times10^{-1}$ (fractured well in dual porosity system case — includes wellbore storage effects).

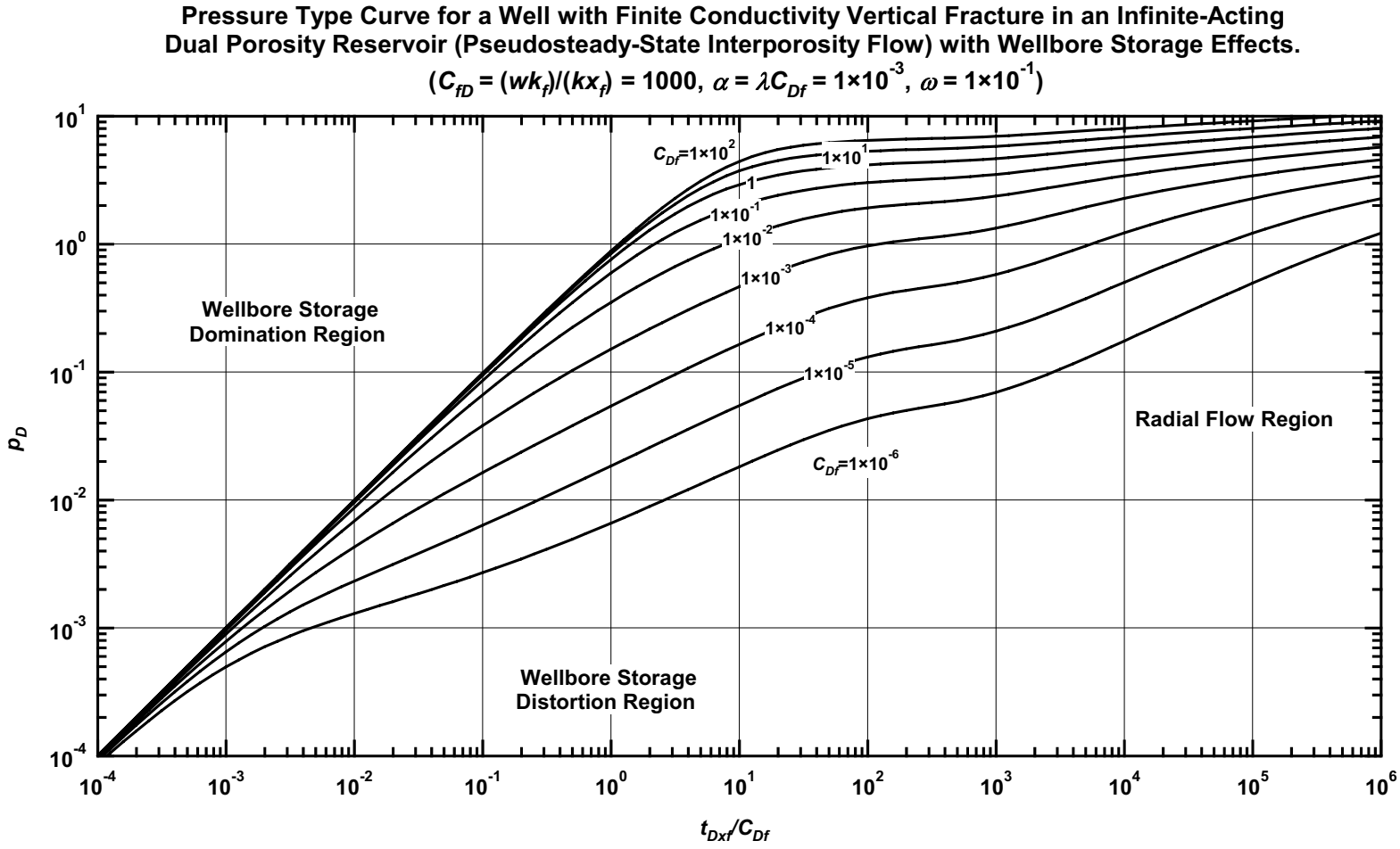

Figure D.85 — p_D vs. t_{Dxf}/C_{Df} — C_{fD} =1000, $\omega = 1\times10^{-1}$, $\alpha = \lambda C_{Df} = 1\times10^{-3}$ (fractured well in dual porosity system case — includes wellbore storage effects).

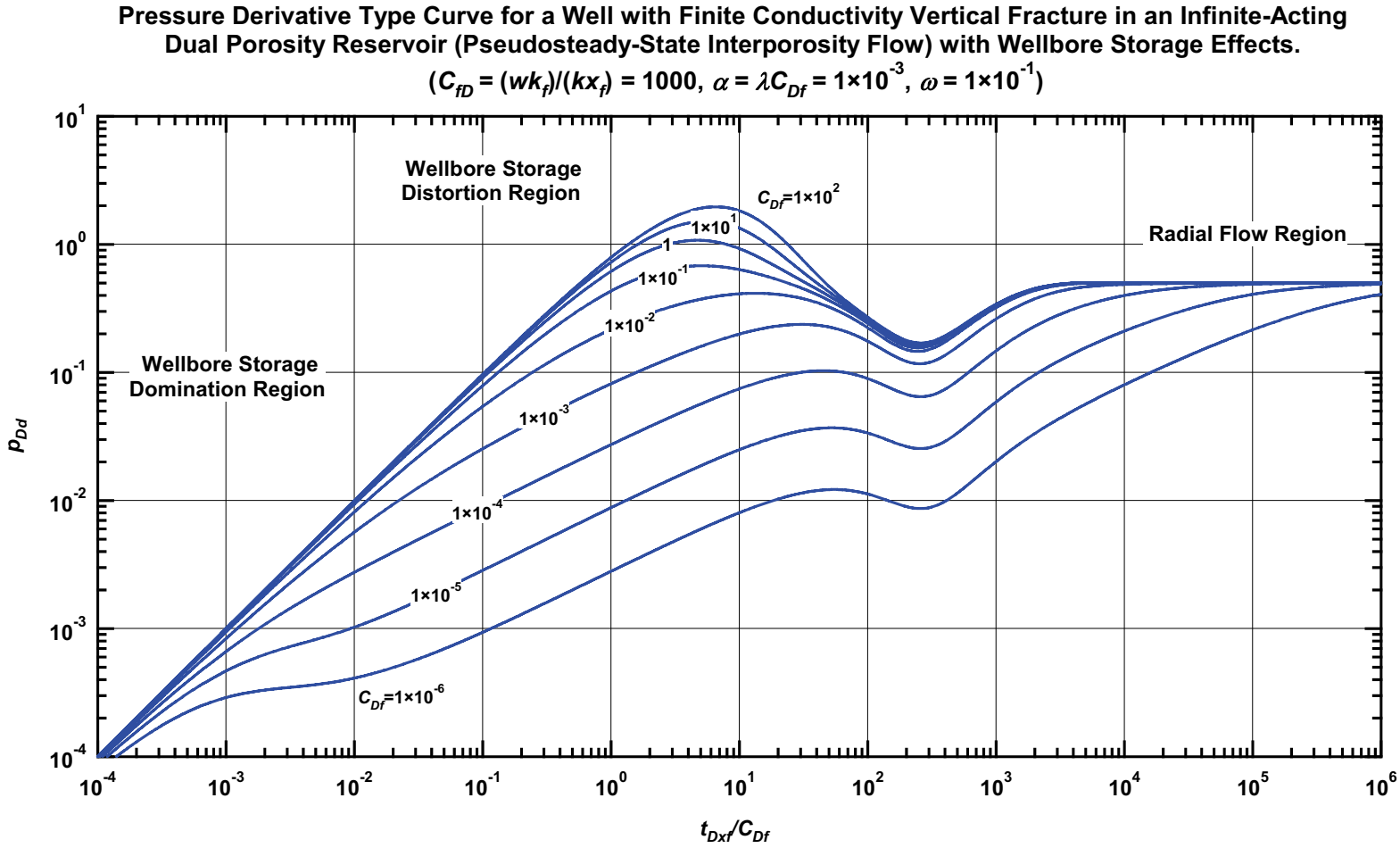

Figure D.86 — p_{Dd} vs. t_{Dxf}/C_{Df} — C_{fD} =1000, $\omega = 1\times10^{-1}$, $\alpha = \lambda C_{Df} = 1\times10^{-3}$ (fractured well in dual porosity system case — includes wellbore storage effects).

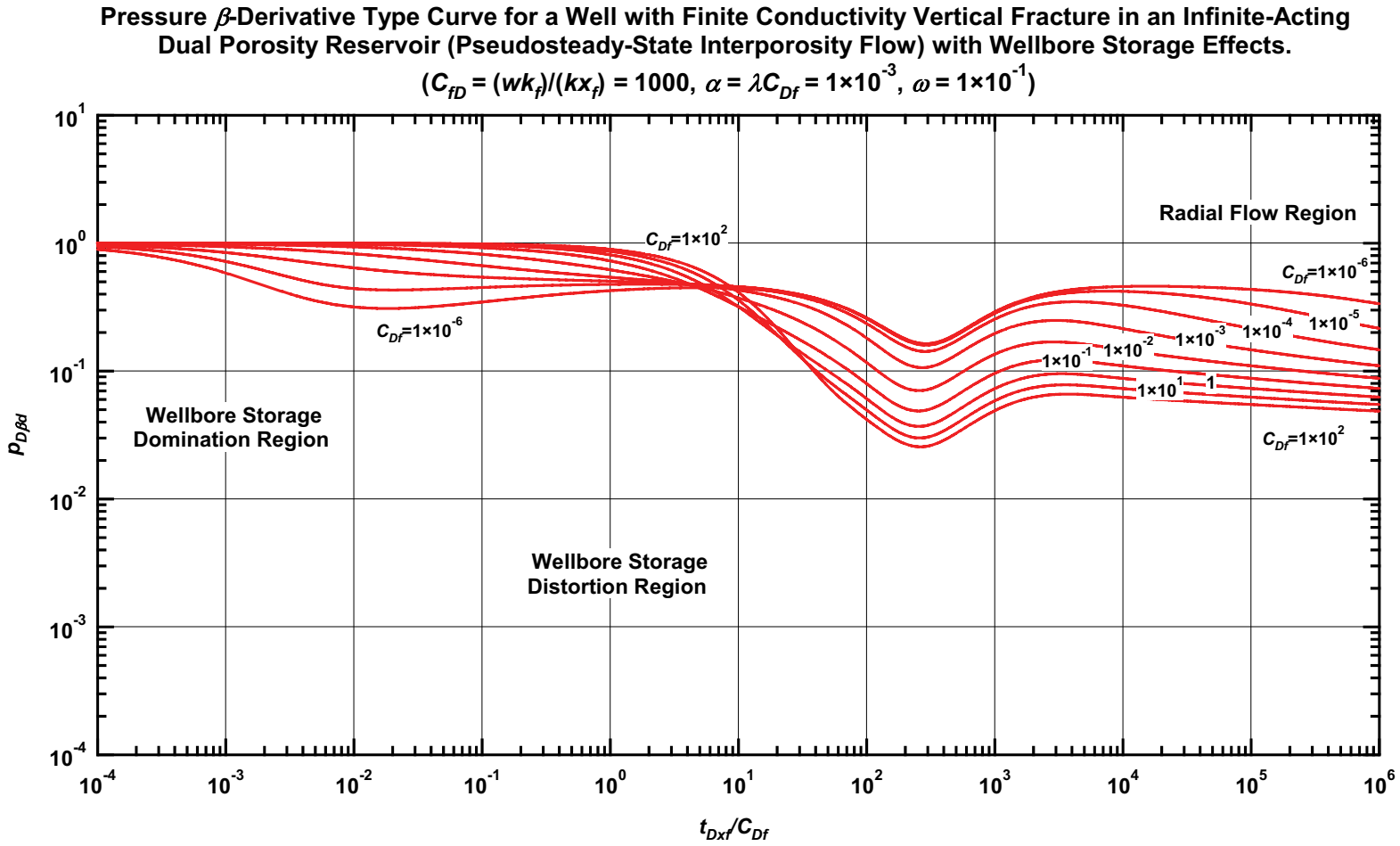

Figure D.87 — $p_{D\beta d}$ **vs.** t_{Dxf}/C_{Df} **—** C_{fD} **=1000,** $\omega = 1\times10^{-1}$, $\alpha = \lambda C_{Df} = 1\times10^{-3}$ **(fractured well in dual porosity system case — includes wellbore storage effects).**

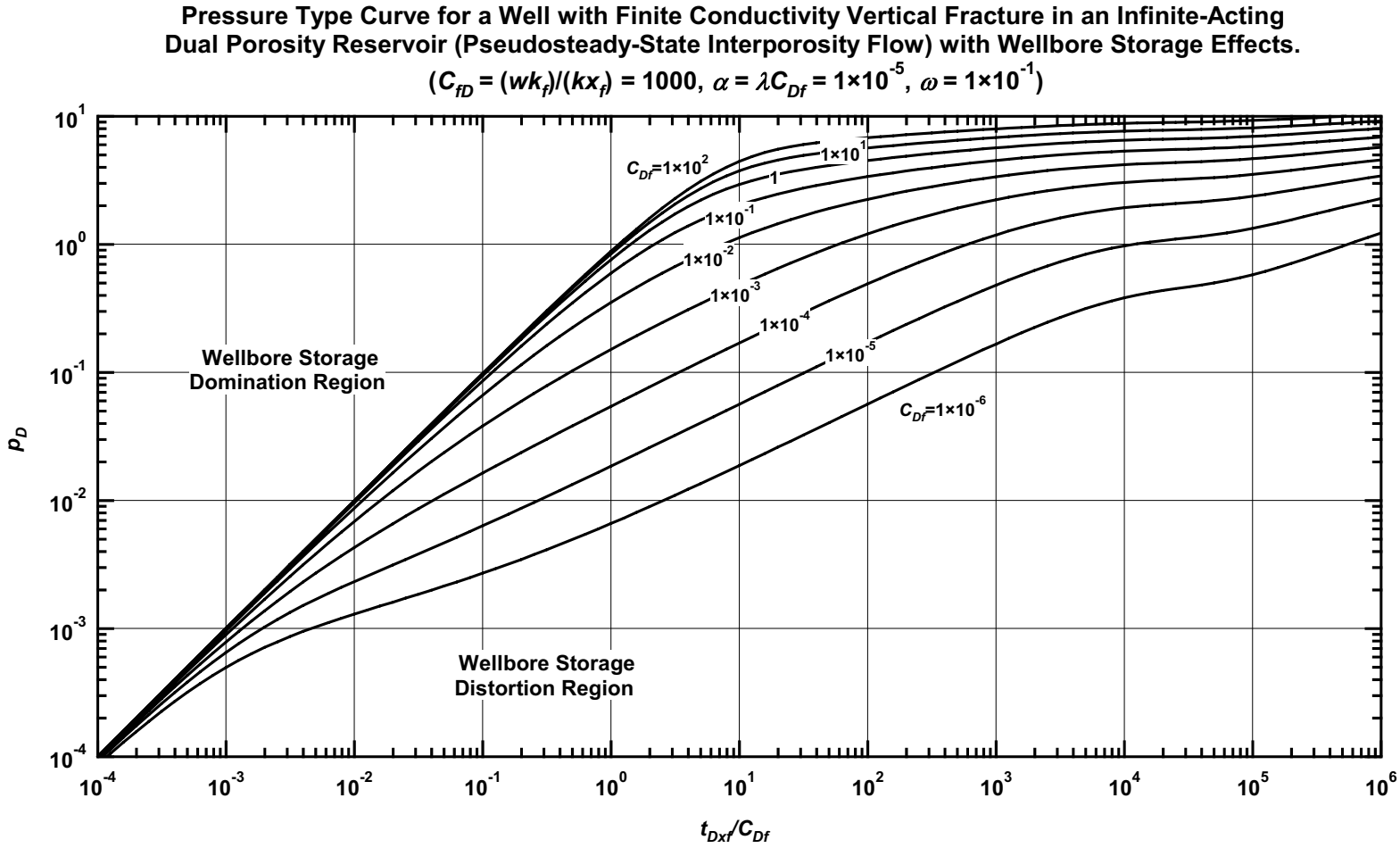

Figure D.88 — p_D vs. t_{Dxf}/C_{Df} — C_{fD} =1000, $\omega = 1\times10^{-1}$, $\alpha = \lambda C_{Df} = 1\times10^{-5}$ (fractured well in dual porosity system case — includes wellbore storage effects).

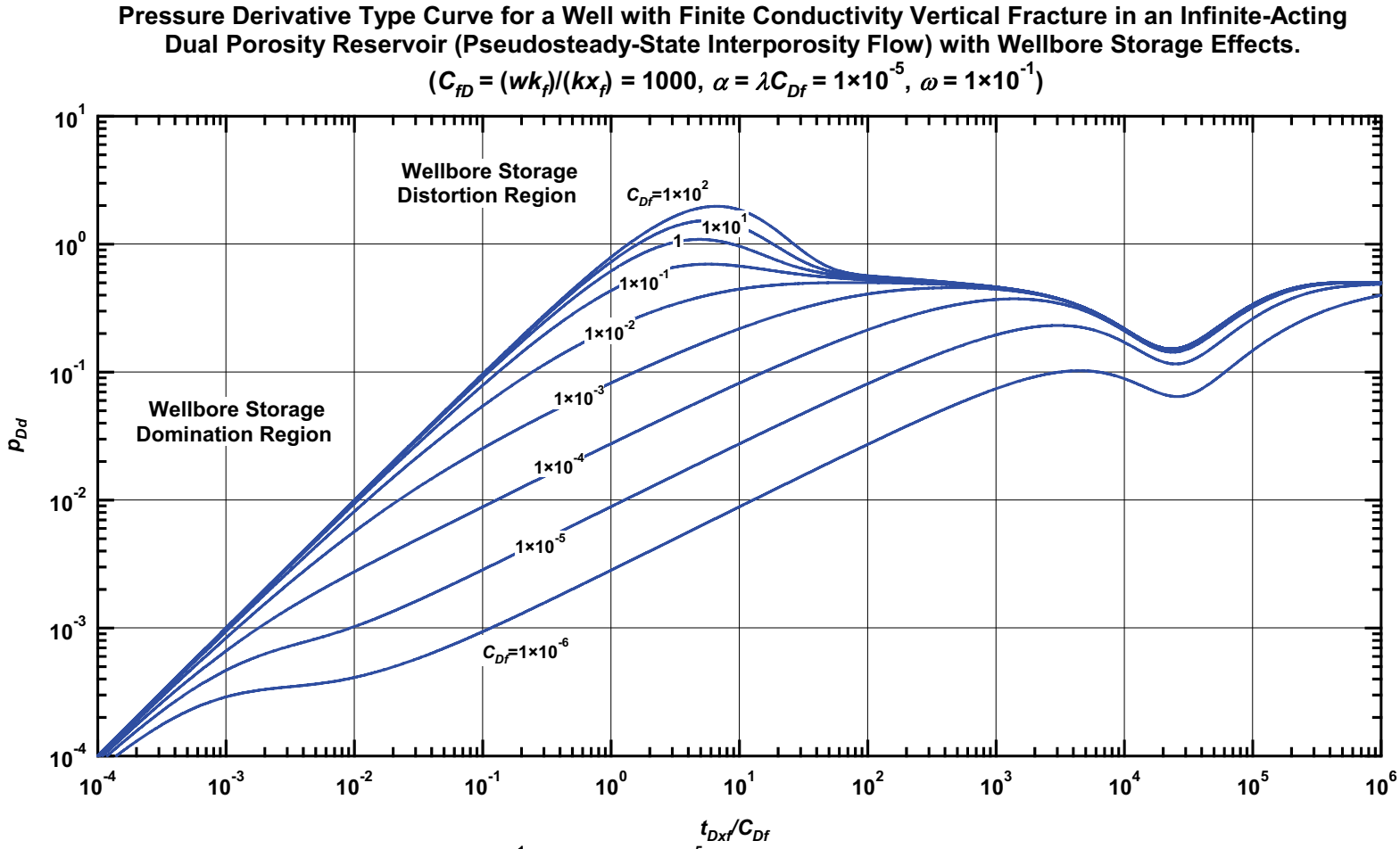

Figure D.89 — p_{Dd} vs. t_{Dxf}/C_{Df} — C_{fD} =1000, $\omega = 1\times10^{-1}$, $\alpha = \lambda C_{Df} = 1\times10^{-5}$ (fractured well in dual porosity system case — includes wellbore storage effects).

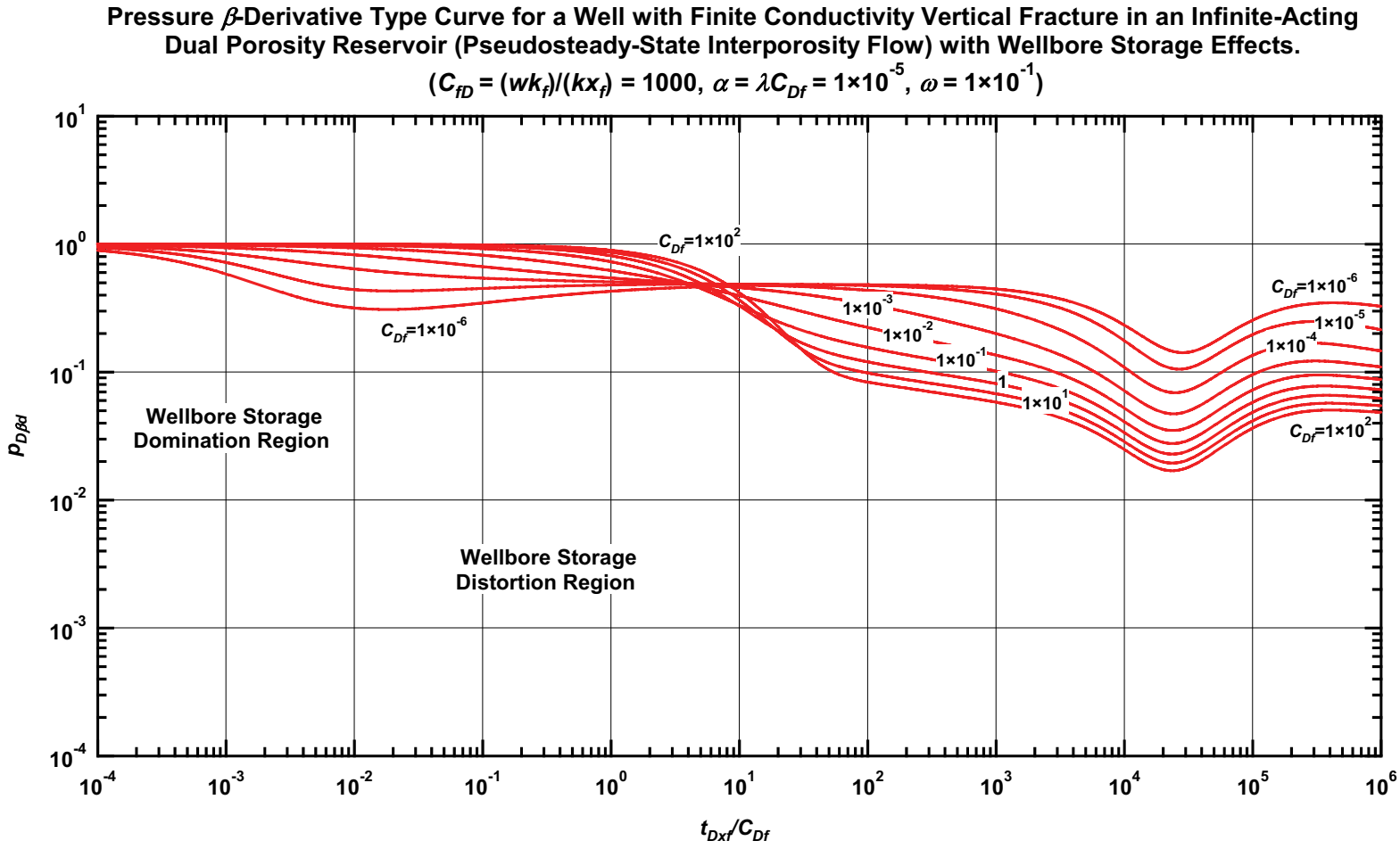

Figure D.90 — $p_{D\beta d}$ **vs.** t_{Dxf}/C_{Df} **—** C_{fD} **=1000,** $\omega = 1\times10^{-1}$, $\alpha = \lambda C_{Df} = 1\times10^{-5}$ **(fractured well in dual porosity system case — includes wellbore storage effects).**

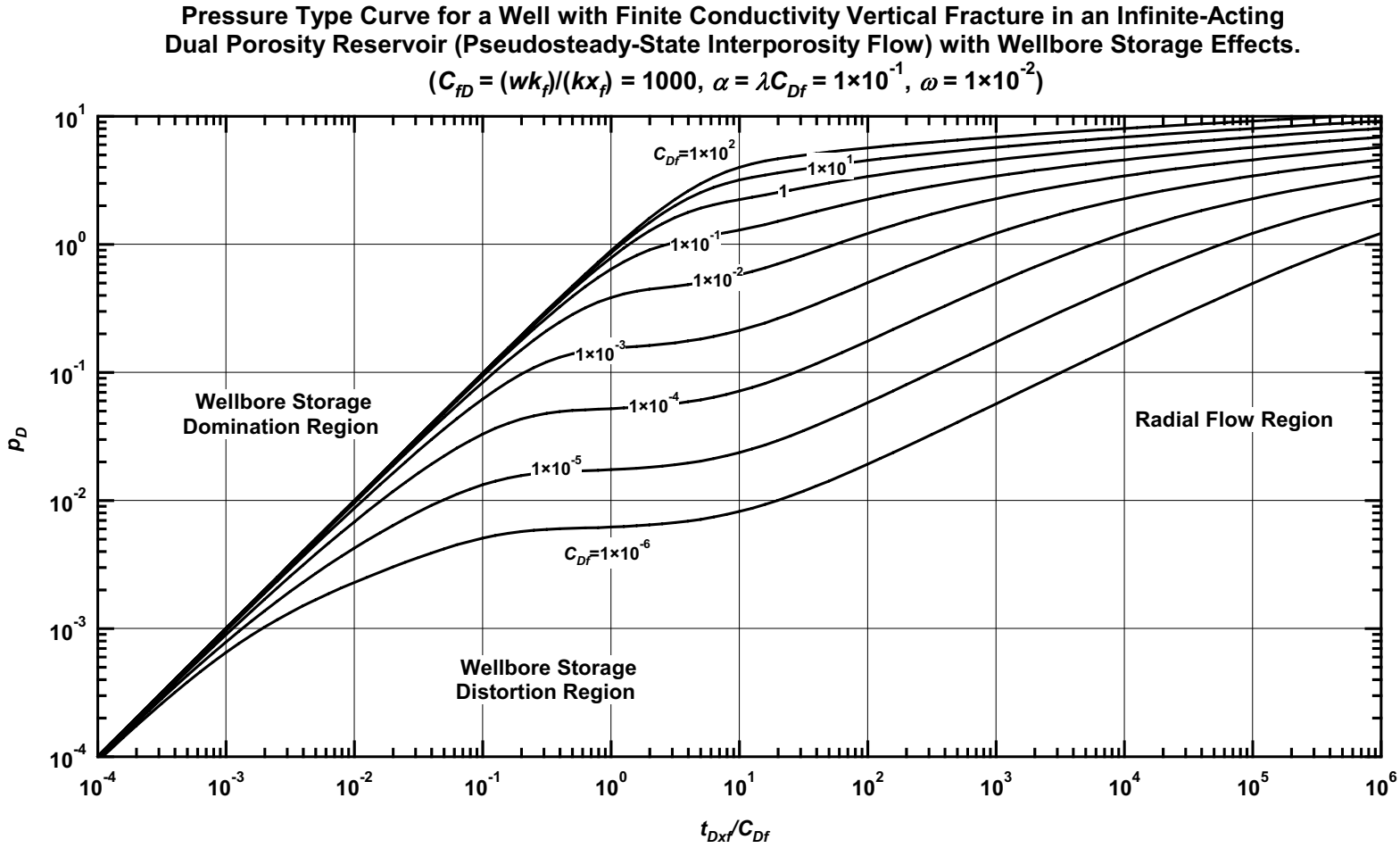

Figure D.91 — p_D vs. t_{Dxf}/C_{Df} — C_{fD} =1000, $\omega = 1\times10^{-2}$, $\alpha = \lambda C_{Df} = 1\times10^{-1}$ (fractured well in dual porosity system case — includes wellbore storage effects).

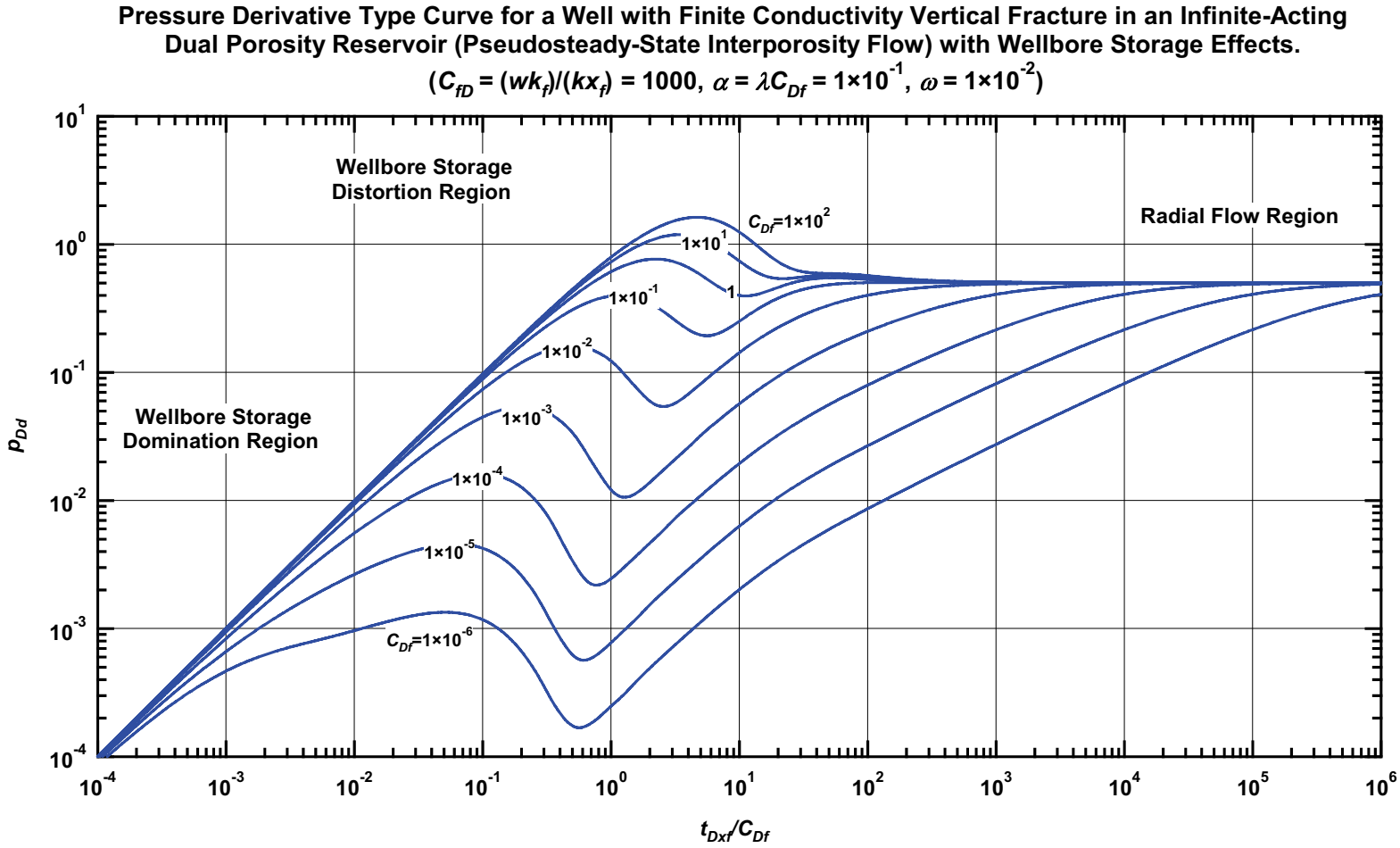

Figure D.92 — p_{Dd} **vs.** t_{Dxf}/C_{Df} **—** C_{fD} **=1000,** $\omega = 1\times10^{-2}$, $\alpha = \lambda C_{Df} = 1\times10^{-1}$ **(fractured well in dual porosity system case — includes wellbore storage effects).**

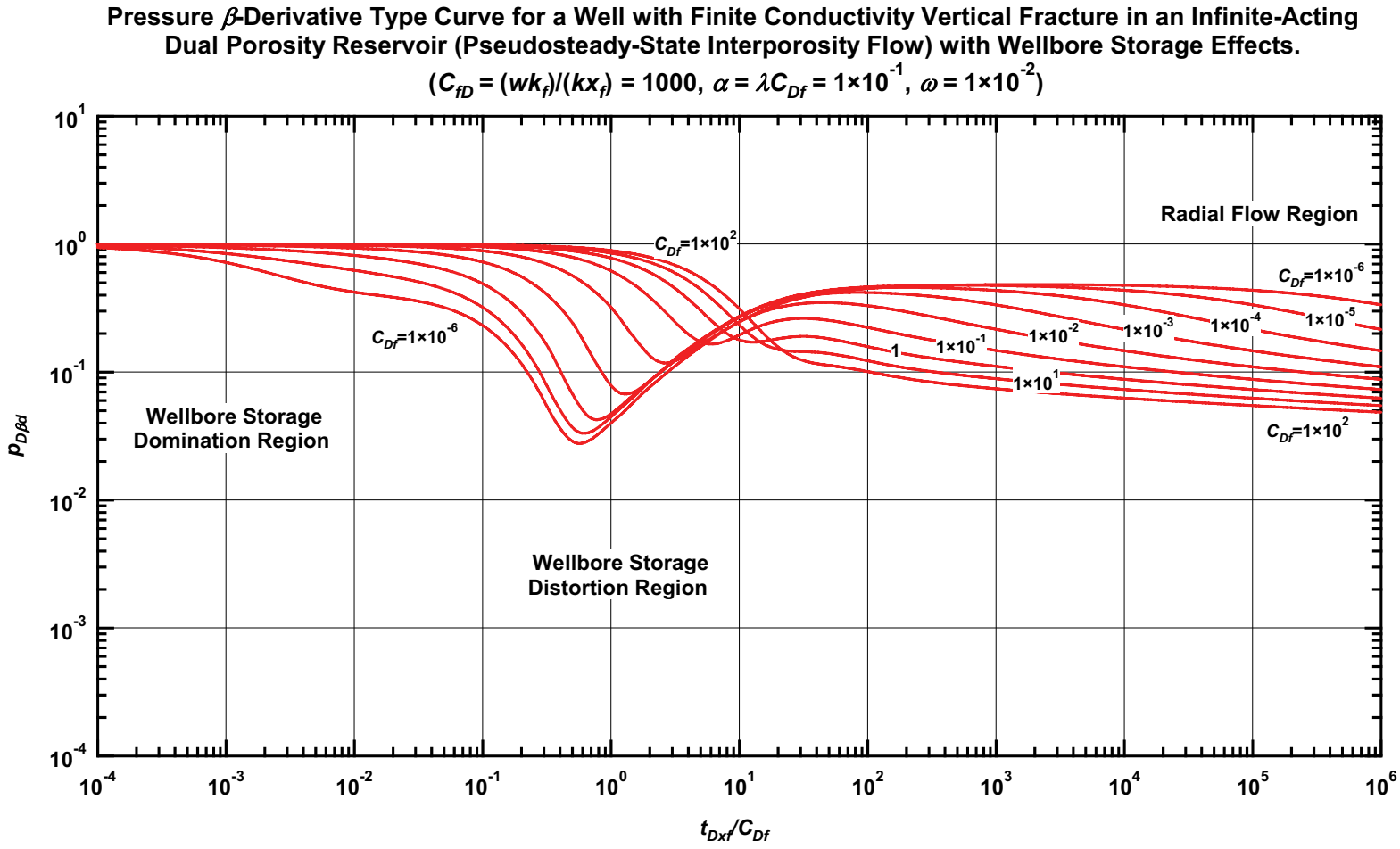

Figure D.93 — $p_{D\beta d}$ vs. t_{Dxf}/C_{Df} — C_{fD} =1000, $\omega = 1\times10^{-2}$, $\alpha = \lambda C_{Df} = 1\times10^{-1}$ (fractured well in dual porosity system case — includes wellbore storage effects).

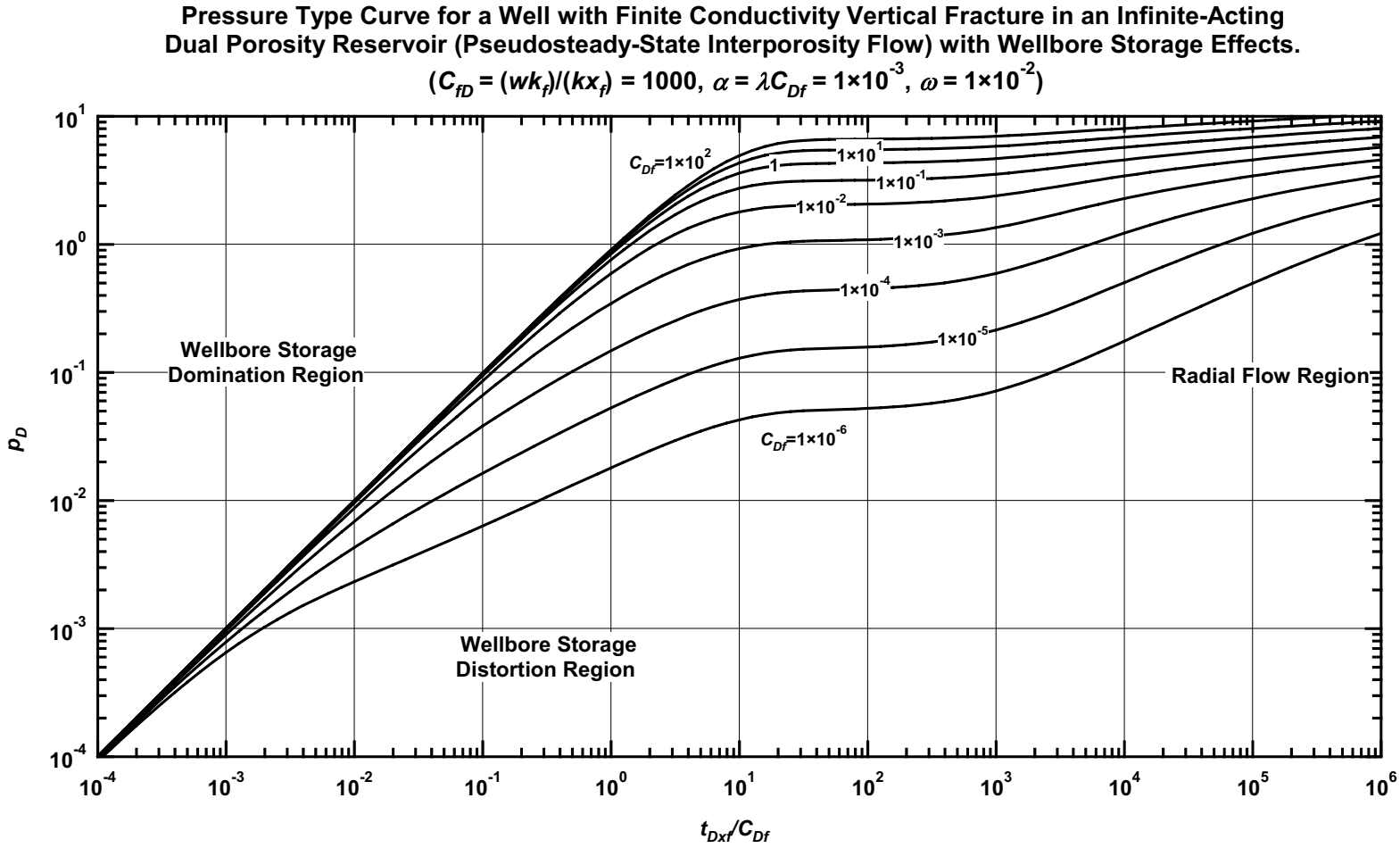

Figure D.94 — p_D **vs.** t_{Dxf}/C_{Df} **—** C_{fD} **=1000,** $\omega = 1\times10^{-2}$, $\alpha = \lambda C_{Df} = 1\times10^{-3}$ **(fractured well in dual porosity system case — includes wellbore storage effects).**

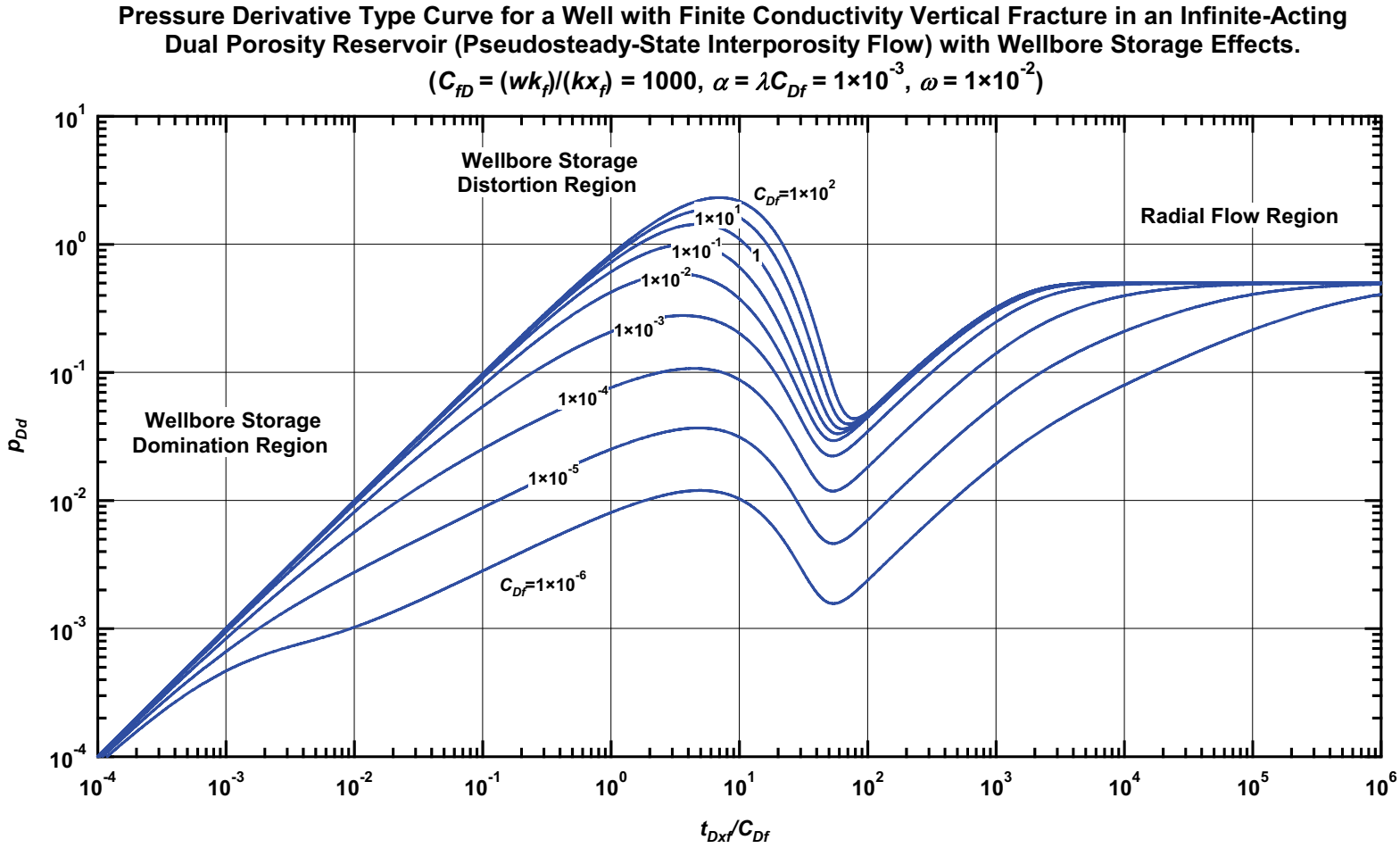

Figure D.95— p_{Dd} vs. t_{Dxf}/C_{Df} — C_{fD} =1000, $\omega = 1\times10^{-2}$, $\alpha = \lambda C_{Df} = 1\times10^{-3}$ (fractured well in dual porosity system case — includes wellbore storage effects).

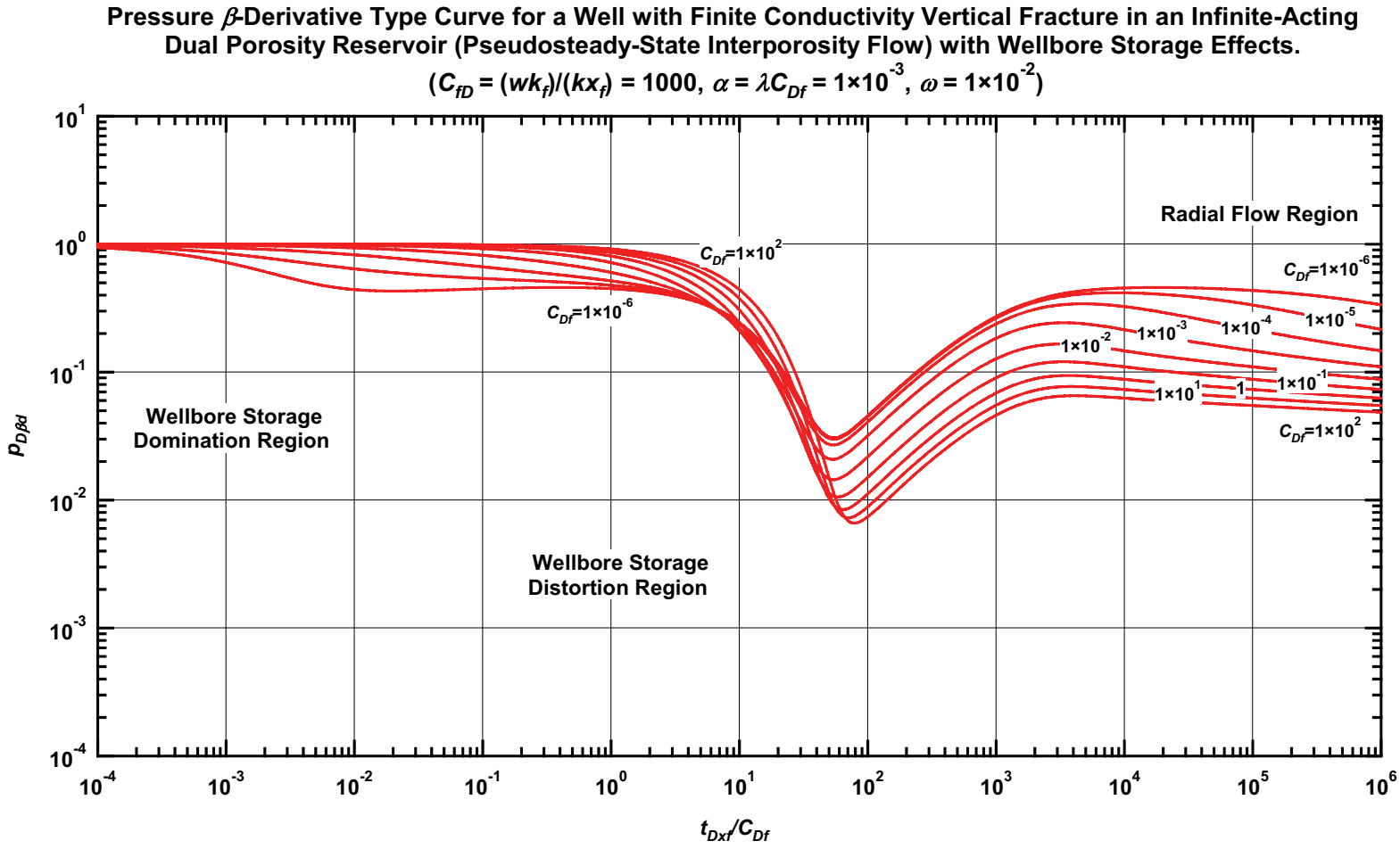

Figure D.96 — $p_{D\beta d}$ **vs.** t_{Dxf}/C_{Df} **—** C_{fD} **=1000,** $\omega = 1\times10^{-2}$, $\alpha = \lambda C_{Df} = 1\times10^{-3}$ **(fractured well in dual porosity system case — includes wellbore storage effects).**

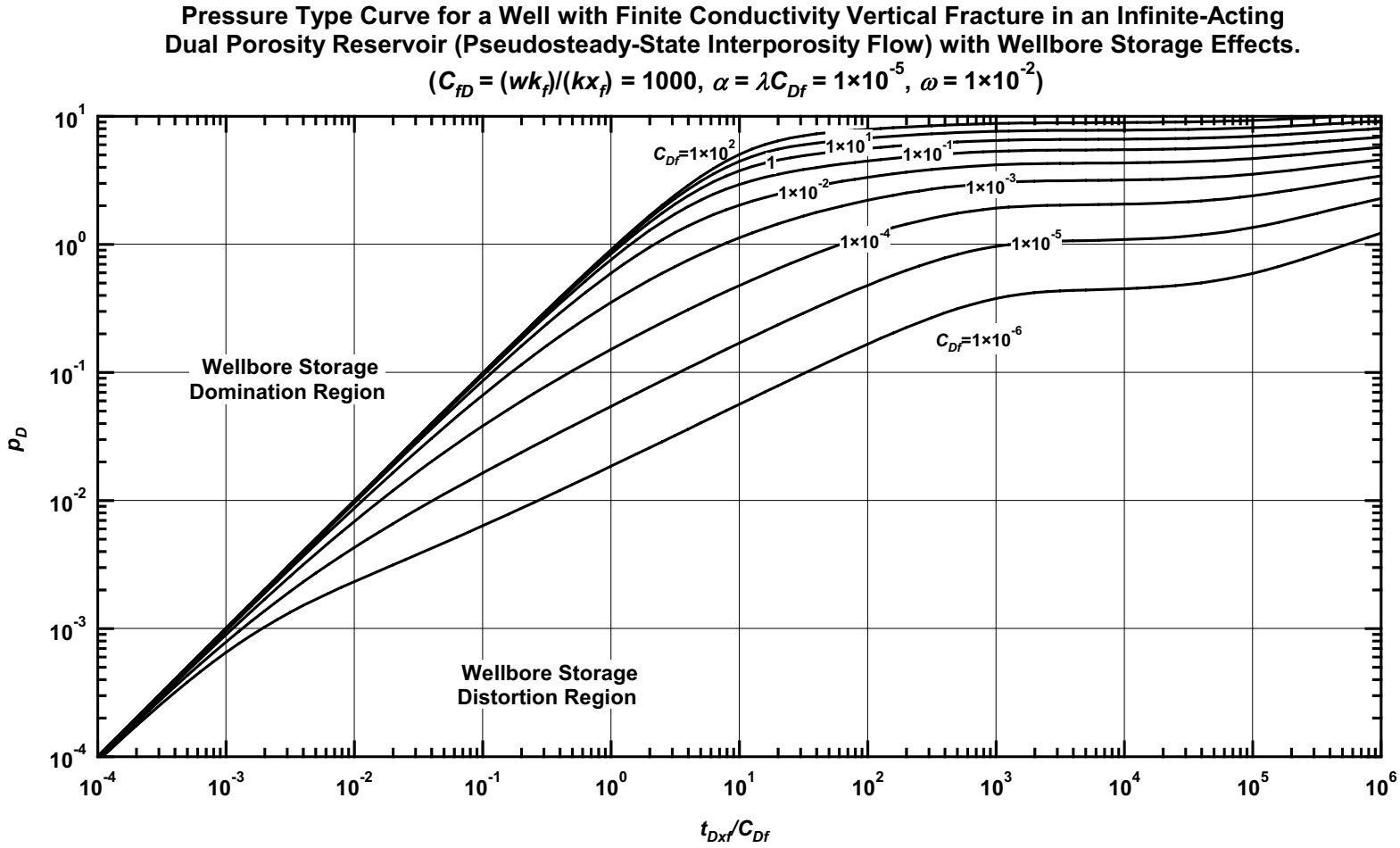

Figure D.97 — p_D vs. t_{Dxf}/C_{Df} — C_{fD} =1000, $\omega = 1\times10^{-2}$, $\alpha = \lambda C_{Df} = 1\times10^{-5}$ (fractured well in dual porosity system case — includes wellbore storage effects).

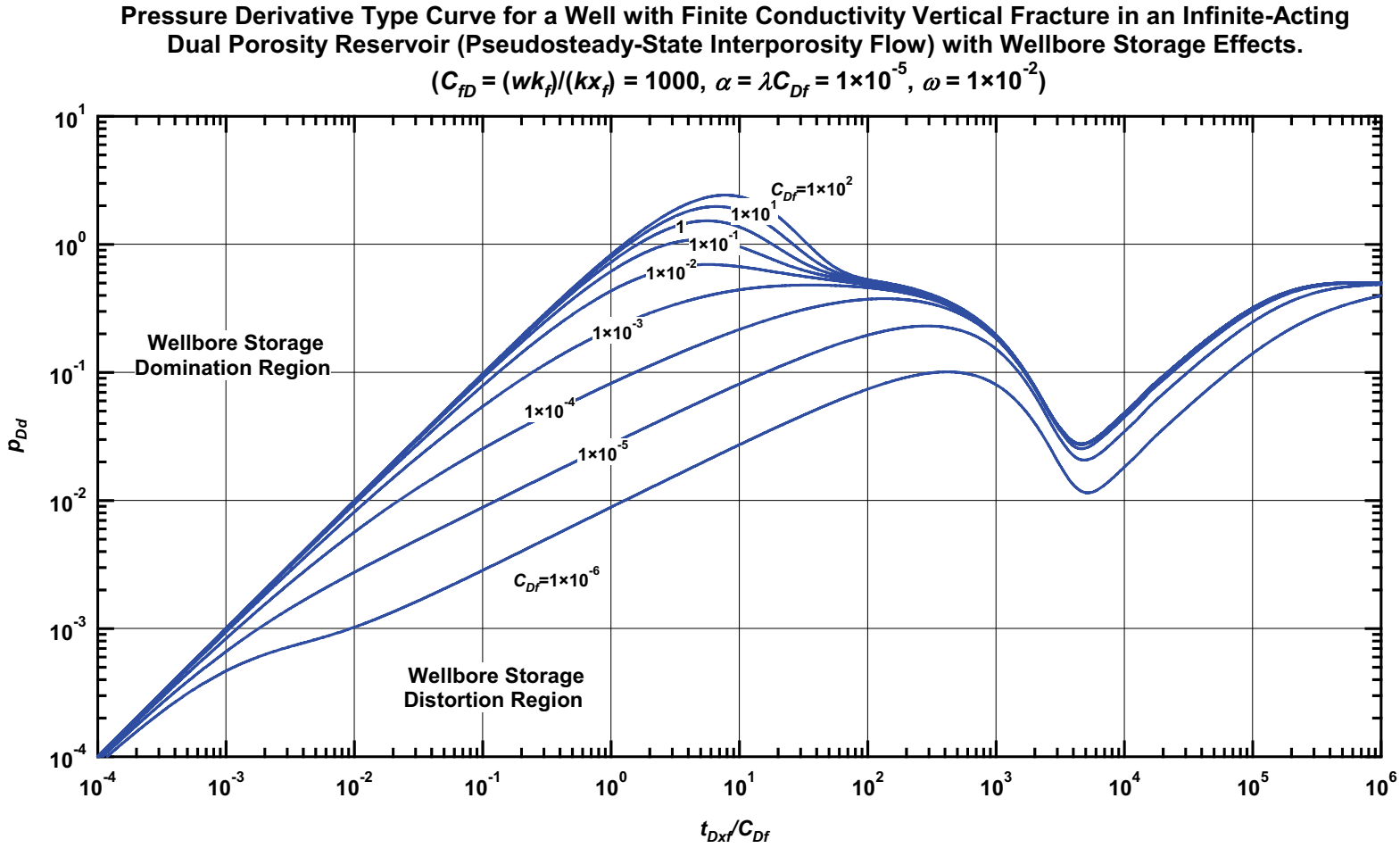

Figure D.98 — p_{Dd} **vs.** t_{Dxf}/C_{Df} **—** C_{fD} **=1000,** $\omega = 1\times10^{-2}$, $\alpha = \lambda C_{Df} = 1\times10^{-5}$ **(fractured well in dual porosity system case — includes wellbore storage effects).**

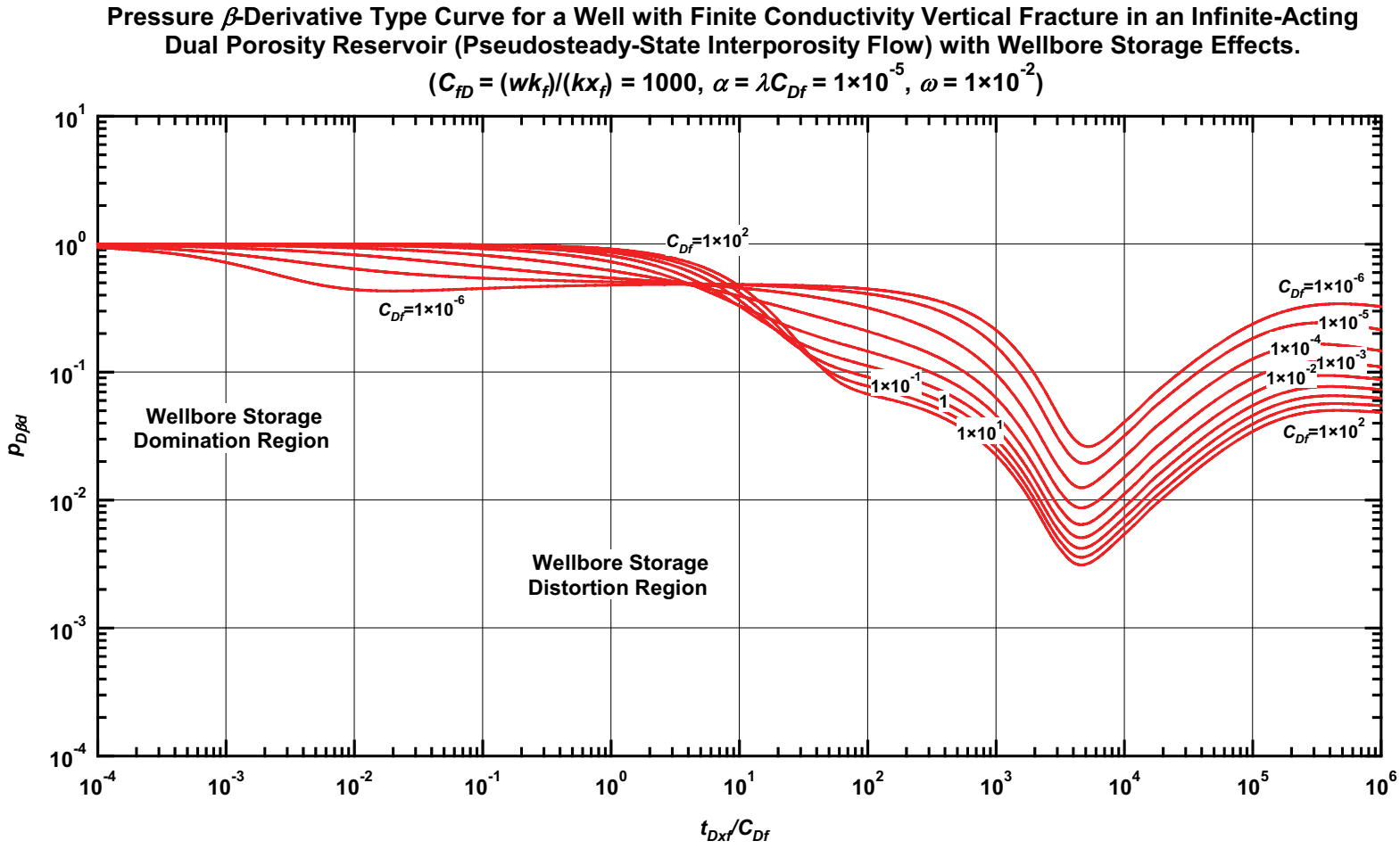

Figure D.99 — $p_{D\beta d}$ **vs.** t_{Dxf}/C_{Df} **—** C_{fD} **=1000,** $\omega = 1\times10^{-2}$, $\alpha = \lambda C_{Df} = 1\times10^{-5}$ **(fractured well in dual porosity system case — includes wellbore storage effects).**

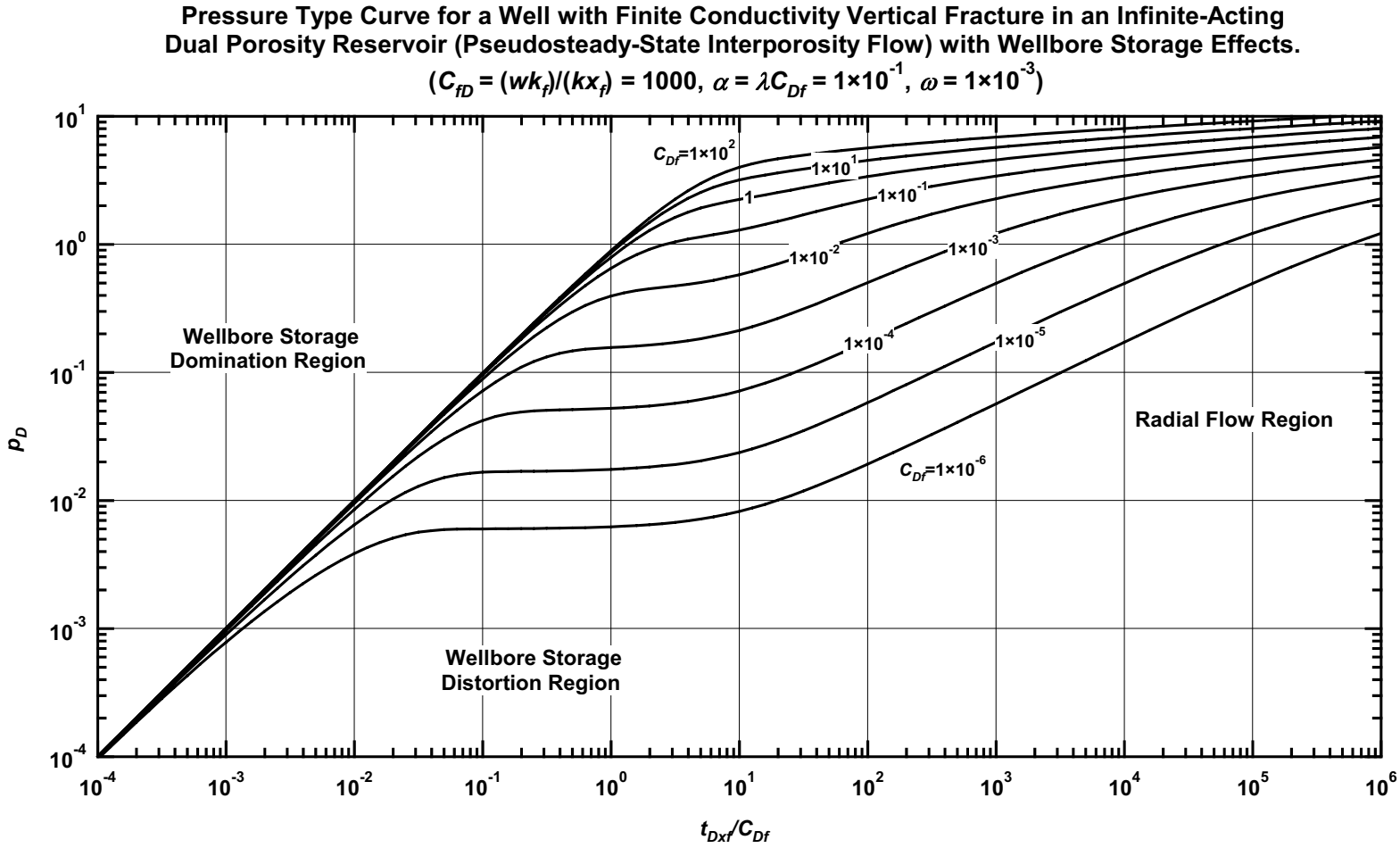

Figure D.100 — p_D vs. t_{Dxf}/C_{Df} — C_{fD} =1000, $\omega = 1\times10^{-3}$, $\alpha = \lambda C_{Df} = 1\times10^{-1}$ (fractured well in dual porosity system case — includes wellbore storage effects).

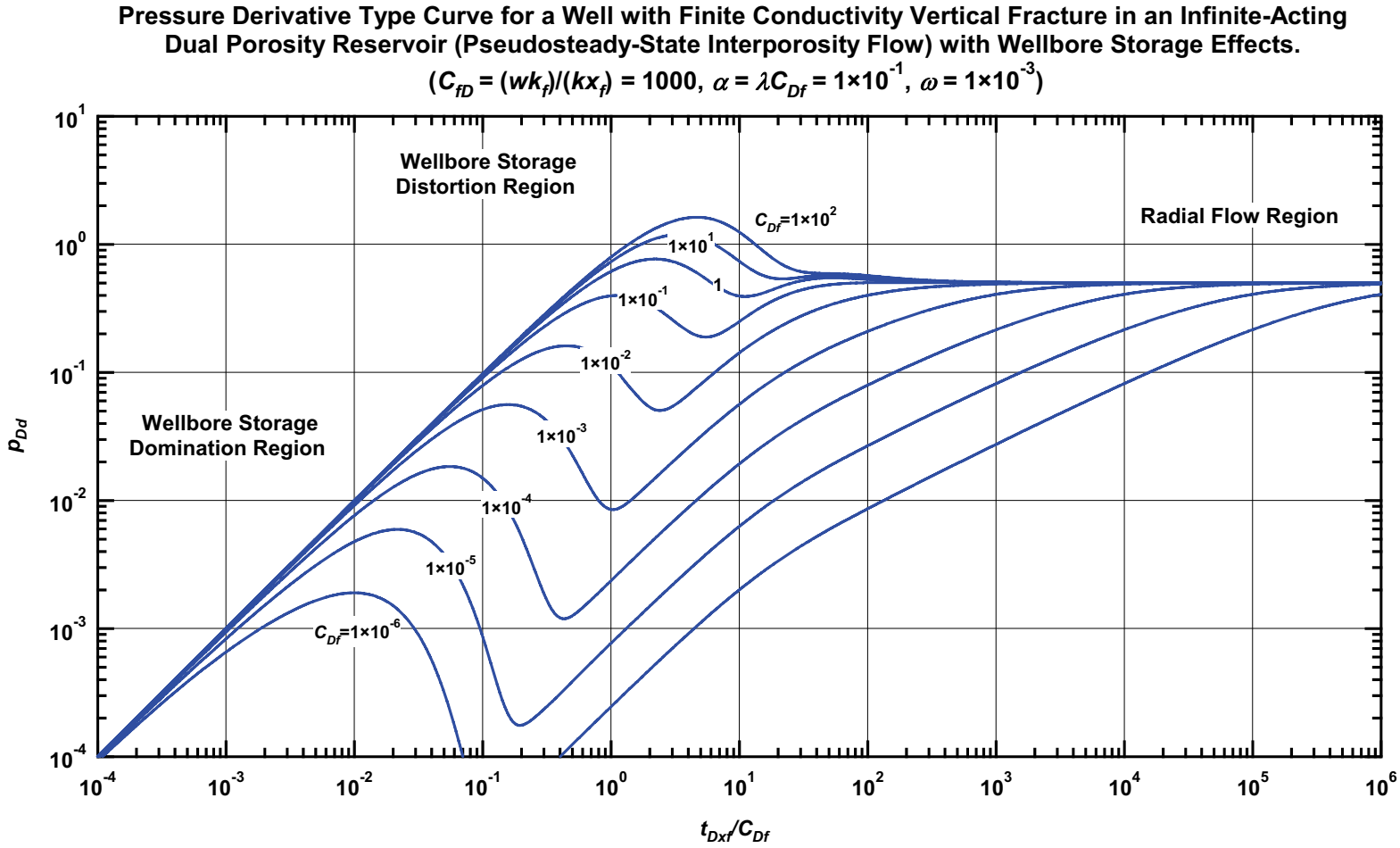

Figure D.101 — p_{Dd} vs. t_{Dxf}/C_{Df} — C_{fD} =1000, $\omega = 1\times10^{-3}$, $\alpha = \lambda C_{Df} = 1\times10^{-1}$ (fractured well in dual porosity system case — includes wellbore storage effects).

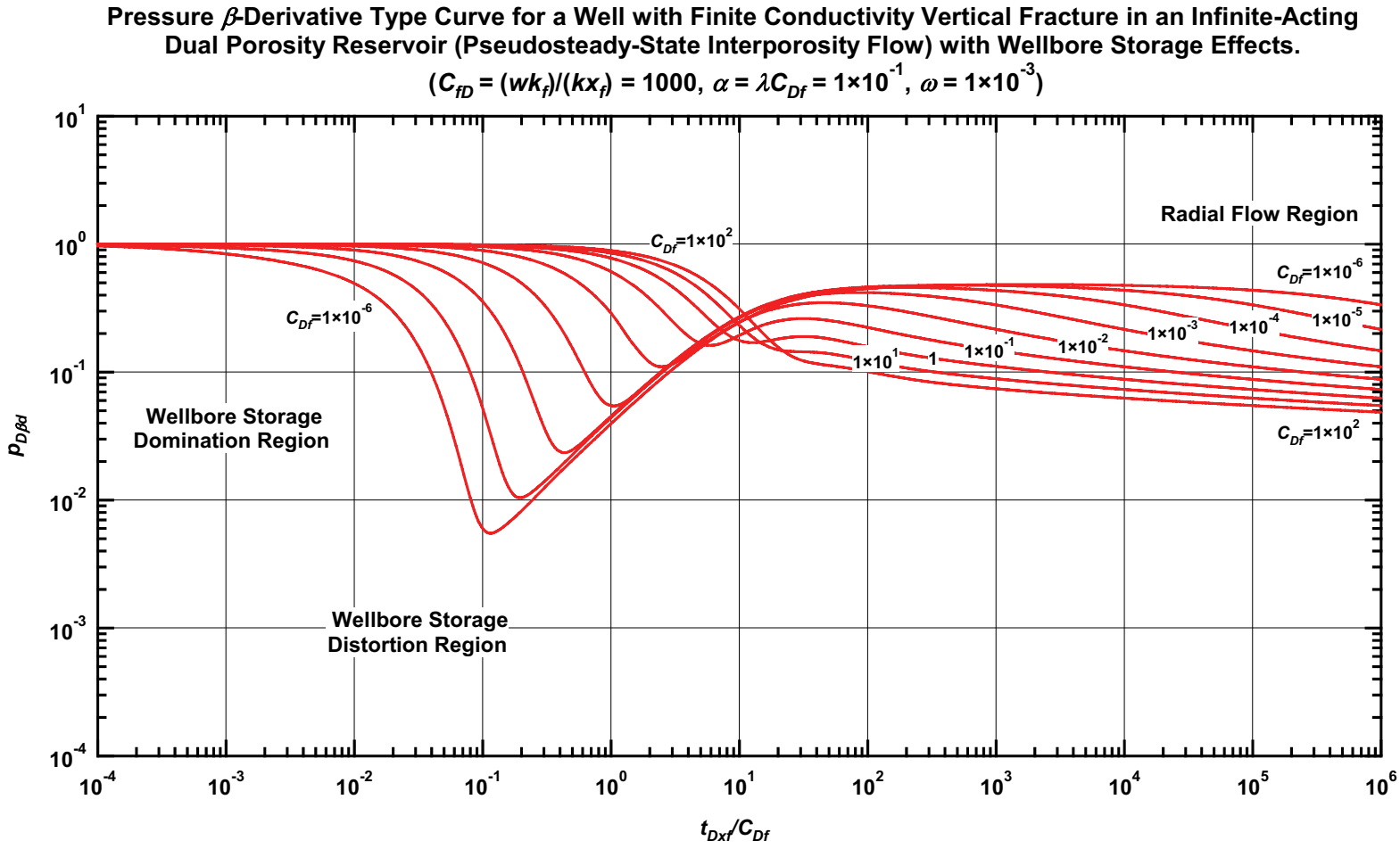

Figure D.102— $p_{D\beta d}$ vs. t_{Dxf}/C_{Df} — C_{fD} =1000, $\omega = 1\times10^{-3}$, $\alpha = \lambda C_{Df} = 1\times10^{-1}$ (fractured well in dual porosity system case — includes wellbore storage effects).

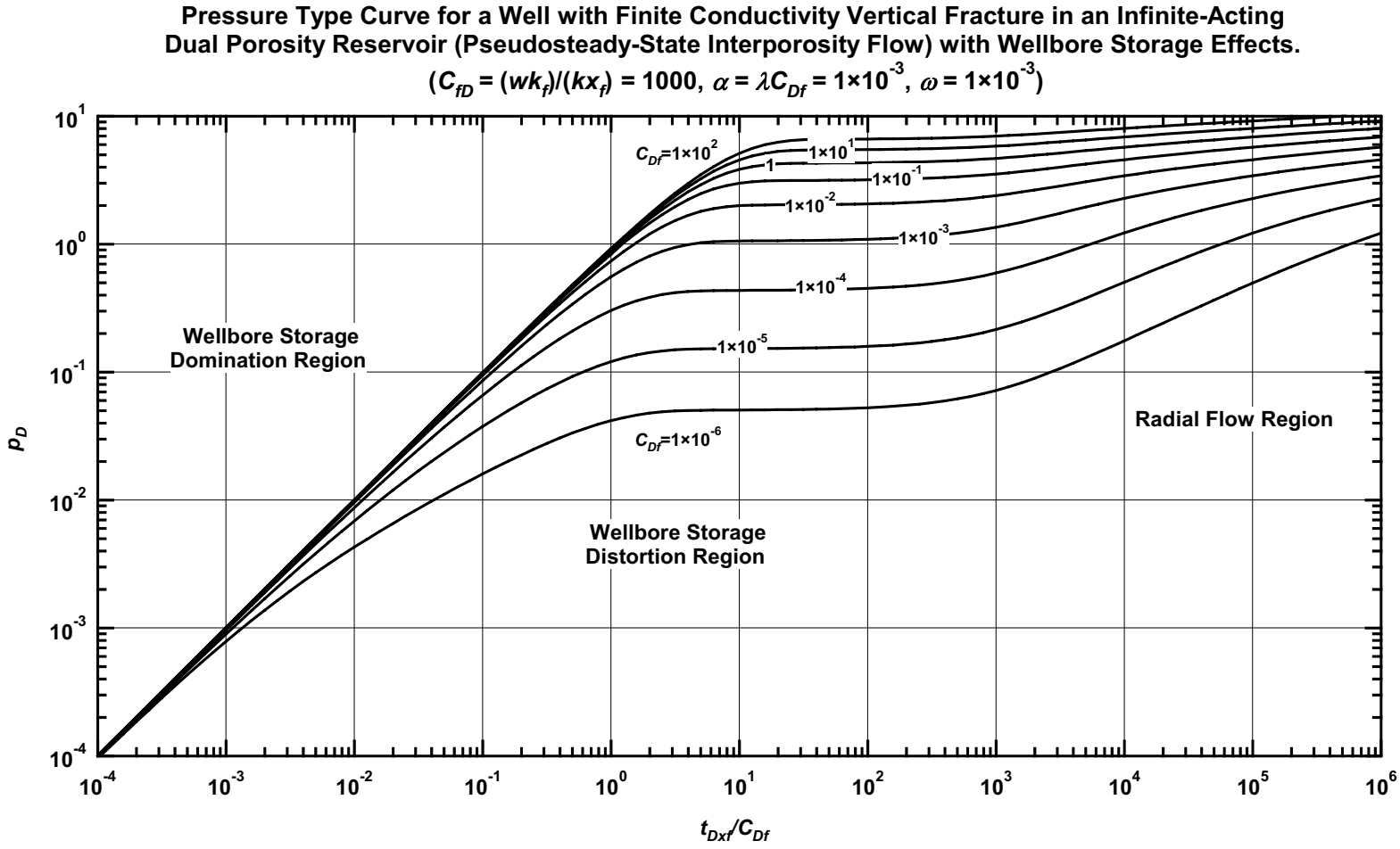

Figure D.103— p_D **vs.** t_{Dxf}/C_{Df} **—** C_{fD} **=1000,** $\omega = 1\times10^{-3}$, $\alpha = \lambda C_{Df} = 1\times10^{-3}$ **(fractured well in dual porosity system case — includes wellbore storage effects).**

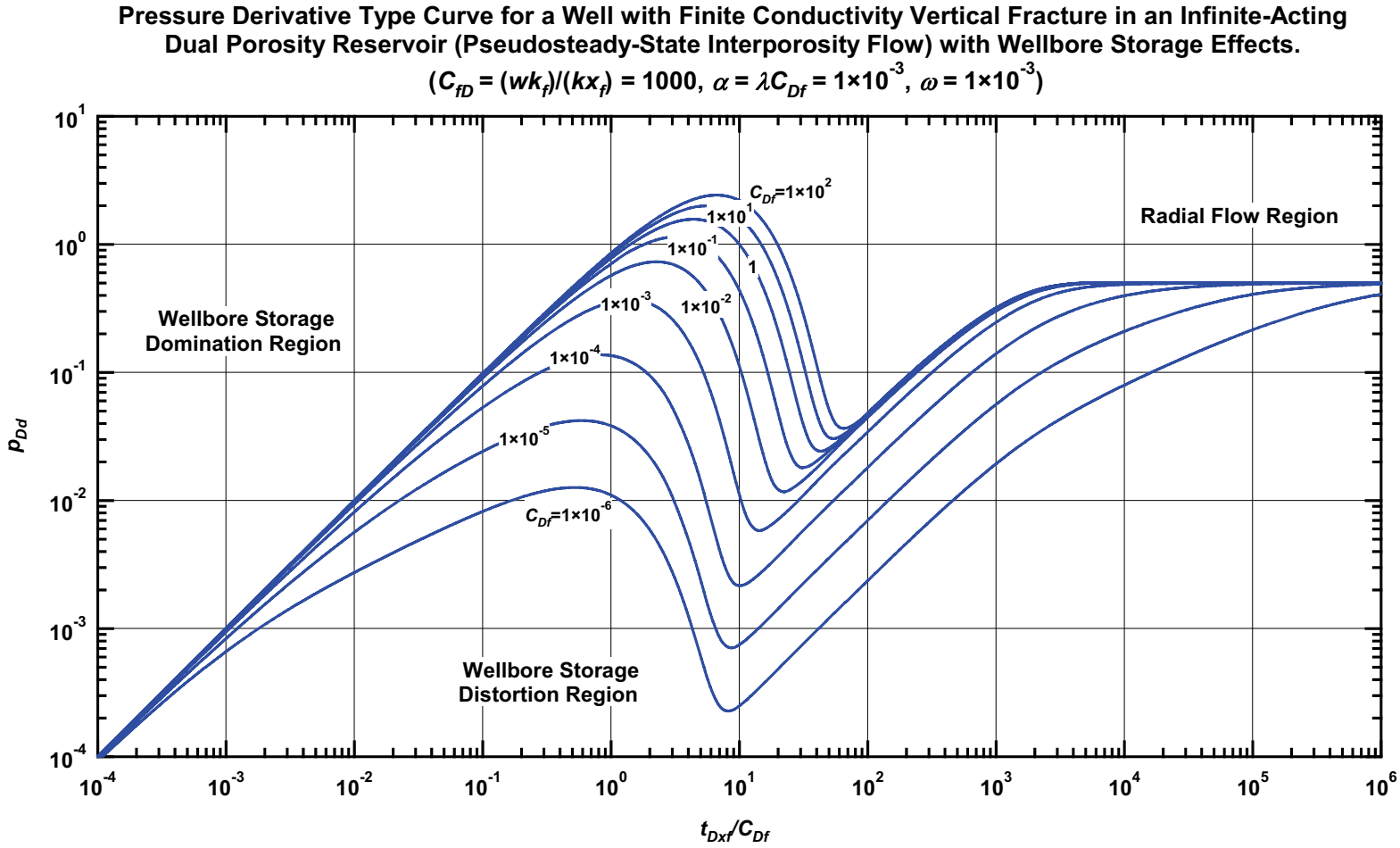

Figure D.104 — p_{Dd} **vs.** t_{Dxf}/C_{Df} **—** C_{fD} **=1000,** $\omega = 1\times10^{-3}$, $\alpha = \lambda C_{Df} = 1\times10^{-3}$ **(fractured well in dual porosity system case — includes wellbore storage effects).**

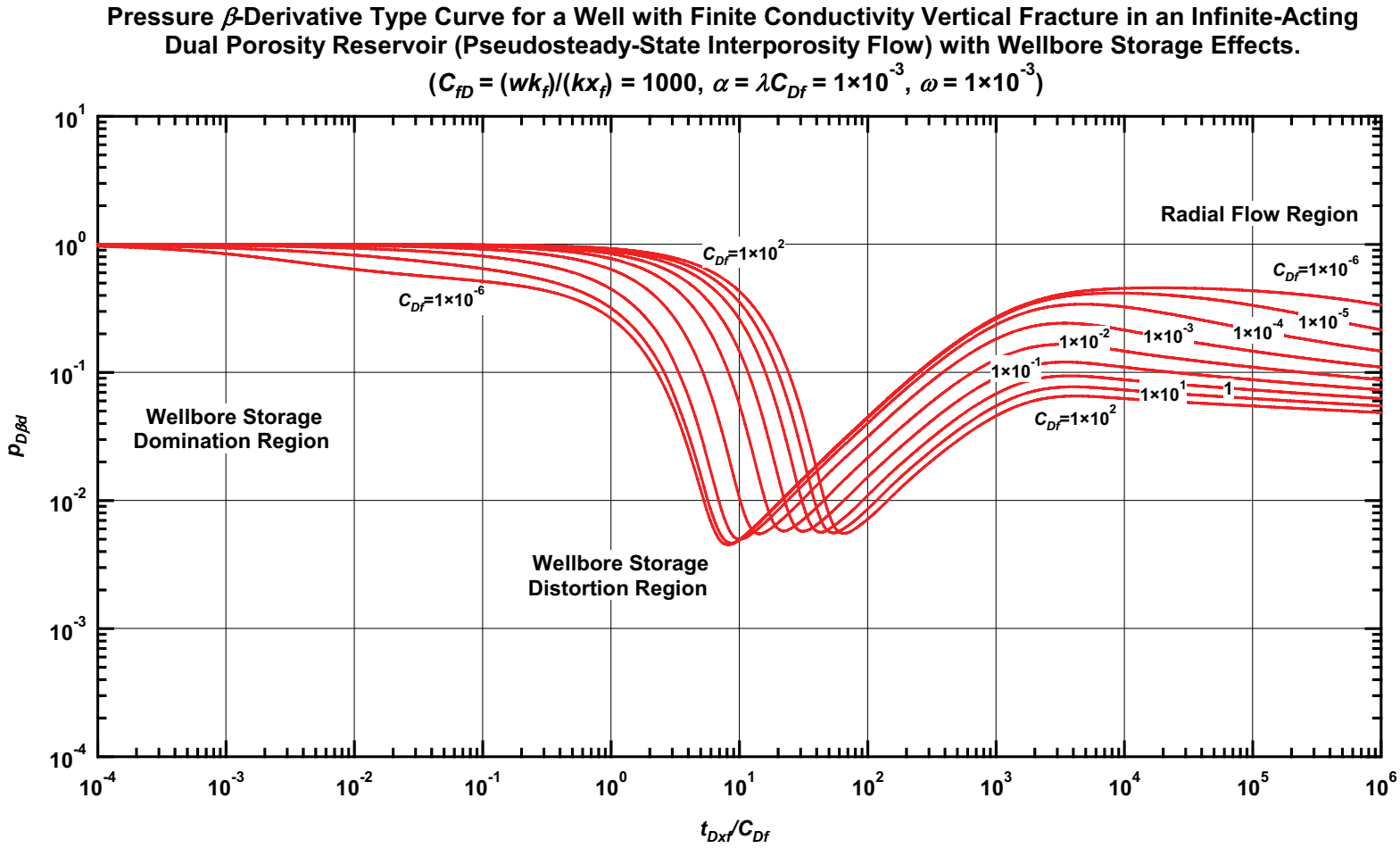

Figure D.105— $p_{D\beta d}$ vs. t_{Dxf}/C_{Df} — C_{fD} =1000, $\omega = 1\times10^{-3}$, $\alpha = \lambda C_{Df} = 1\times10^{-3}$ (fractured well in dual porosity system case — includes wellbore storage effects).

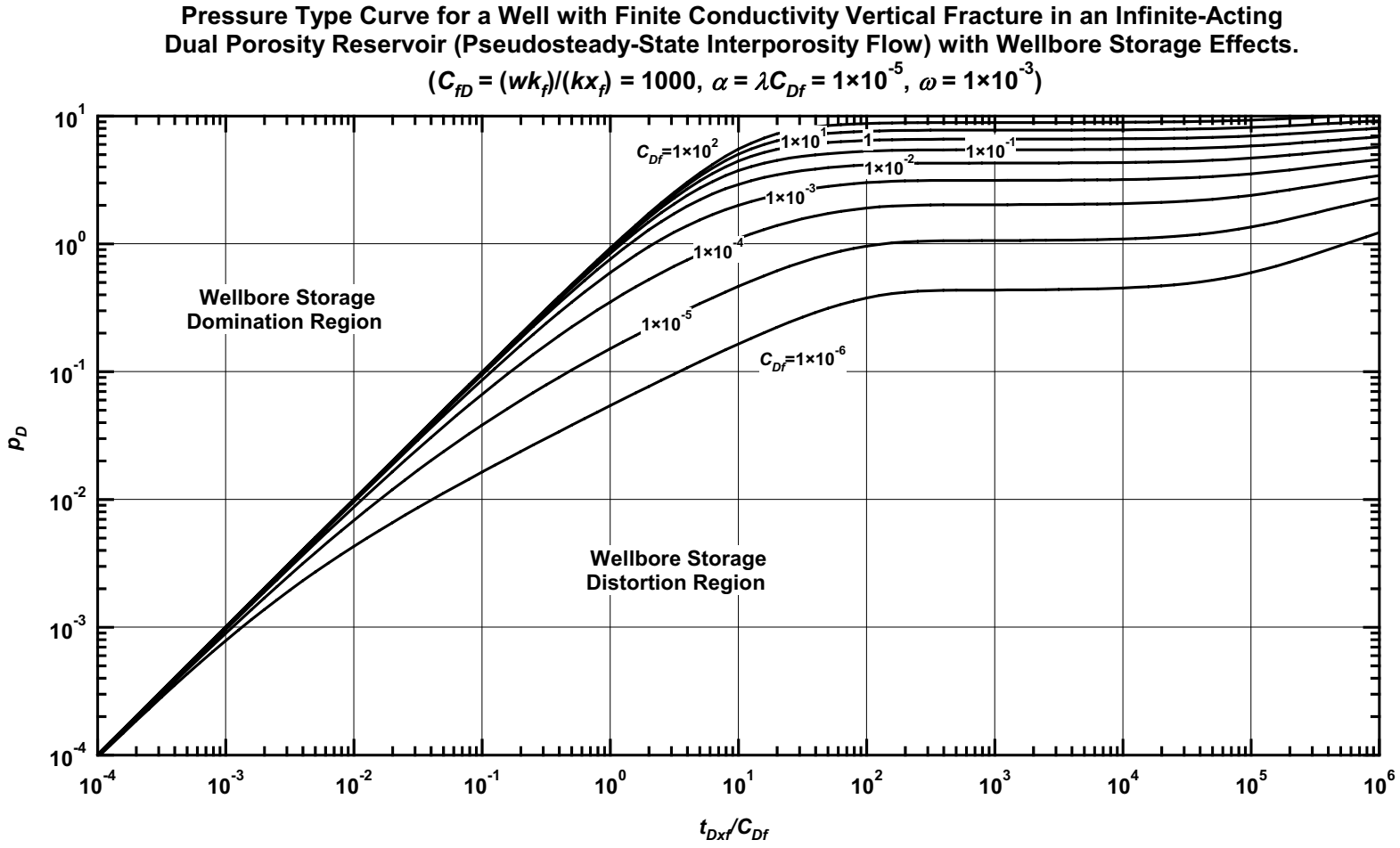

Figure D.106 — p_D vs. t_{Dxf}/C_{Df} — C_{fD} =1000, $\omega = 1\times10^{-3}$, $\alpha = \lambda C_{Df} = 1\times10^{-5}$ (fractured well in dual porosity system case — includes wellbore storage effects).

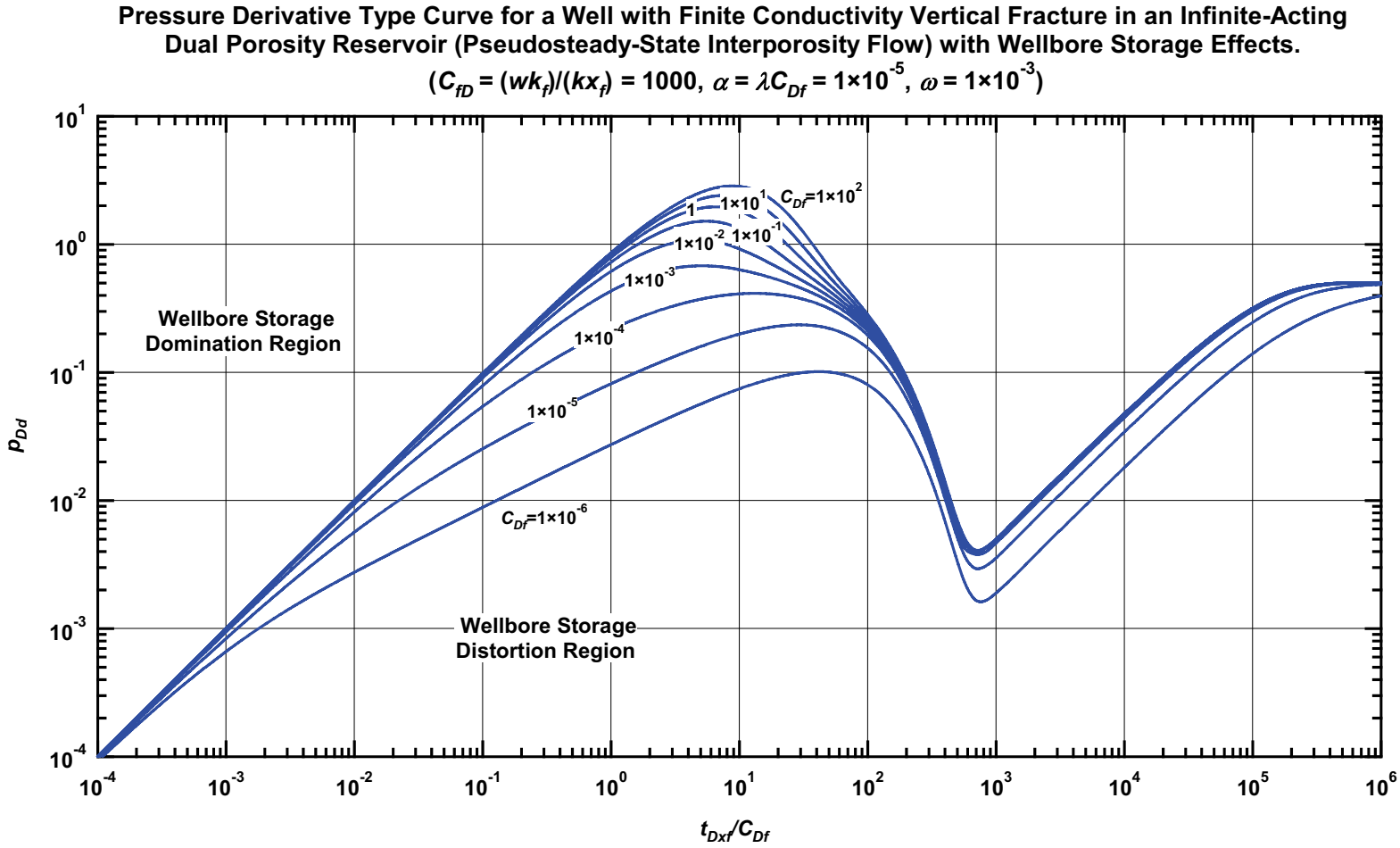

Figure D.107 — p_{Dd} **vs.** t_{Dxf}/C_{Df} **—** C_{fD} **=1000,** $\omega = 1\times10^{-3}$, $\alpha = \lambda C_{Df} = 1\times10^{-5}$ **(fractured well in dual porosity system case — includes wellbore storage effects).**

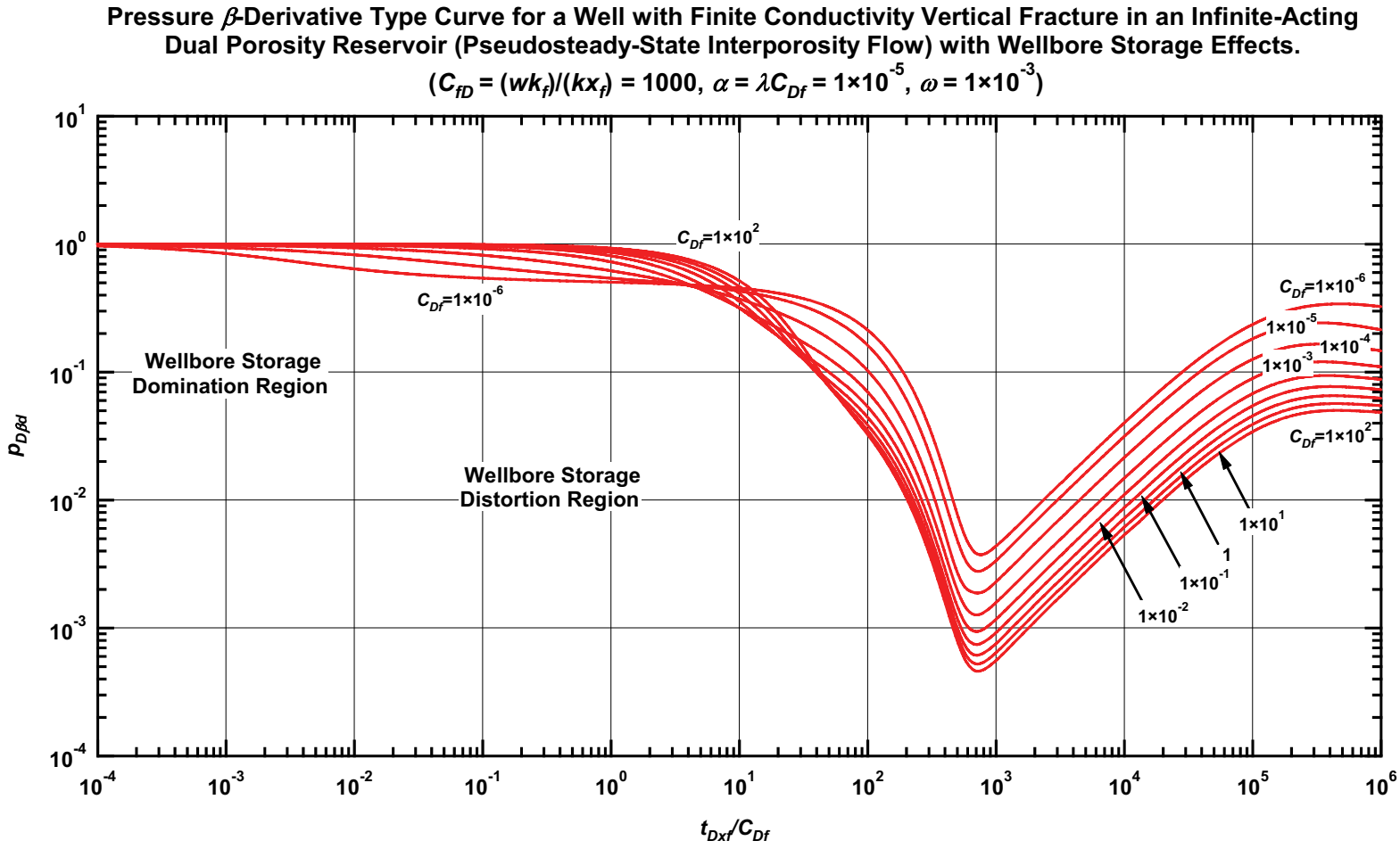

Figure D.108 — $p_{D\beta d}$ **vs.** t_{Dxf}/C_{Df} **—** C_{fD} **=1000,** $\omega = 1\times10^{-3}$, $\alpha = \lambda C_{Df} = 1\times10^{-5}$ **(fractured well in dual porosity system case — includes wellbore storage effects).**

APPENDIX E

CASE OF AN INFINITE CONDUCTIVITY HORIZONTAL WELL IN A HOMOGENEOUS, ISOTROPIC, AND INFINITE-ACTING RESERVOIR

In this appendix we provide pressure, pressure derivative, and β-derivative solutions (in dimensionless format, equations and type curves) for the case of horizontal well (infinite conductivity well) in a homogenous and isotropic reservoir system. For the purpose of generating graphical solutions (type curves) we varied the horizontal section length (L_D) from 0.1 to 100.

Table E-1 — Solutions for an infinite conductivity horizontal well in an infinite-acting, homogeneous (and isotropic) reservoir system.

Description	Relation
p_D	$p_D(t_{DL}) = \frac{\sqrt{\pi}}{4}\int_0^{t_{DL}} \left[\mathrm{erf}\left[\frac{0.866}{\sqrt{\tau}}\right] + \mathrm{erf}\left[\frac{0.134}{\sqrt{\tau}}\right]\right] \times \left[1 + 2\sum_{n=1}^{\infty} \exp(-n^2\pi^2 L_D^2 \tau)\cos n\pi z_D \cos n\pi z_{wD}\right] \frac{d\tau}{\sqrt{\tau}}$ (E.1.1)
	$p_D(t_{DL}) = \frac{1}{4L_D} \mathrm{E}_1\left[\frac{(z_D - z_{wD})^2 / L_D^2}{4t_D}\right]$ (early time approximation) (E.1.2)
	$p_D(t_{DL}) = \frac{1}{2}\left(\ln t_{DL} + 2.509843\right) + F$ (early time approximation) (E.1.3)
p_{Dd}	$p_{Dd}(t_{DL}) = \frac{\sqrt{\pi t_{DL}}}{4}\left[\mathrm{erf}\left[\frac{0.866}{\sqrt{t_{DL}}}\right] + \mathrm{erf}\left[\frac{0.134}{\sqrt{t_{DL}}}\right]\right] \times \left[1 + 2\sum_{n=1}^{\infty} \exp(-n^2\pi^2 L_D^2 t_{DL})\cos n\pi z_D \cos n\pi z_{wD}\right]$ (E.1.4)
	$p_{Dd}(t_{DL}) = \frac{1}{4L_D}\exp\left[-\frac{(z_D - z_{wD})^2 / L_D^2}{4t_{DL}}\right]$ (early time approximation) (E.1.5)
	$p_D(t_{DL}) = \frac{1}{2}$ (early time approximation) (E.1.6)

Table E-1 — Continue

$$p_{D\beta d}(t_{DL}) = \left[\sqrt{t_{DL}}\left[\operatorname{erf}\left[\frac{0.866}{\sqrt{t_{DL}}}\right]+\operatorname{erf}\left[\frac{0.134}{\sqrt{t_{DL}}}\right]\right] \times\left[1+2\sum_{n=1}^{\infty}\exp(-n^2\pi^2L_D^2t_{DL})\cos n\pi z_D\cos n\pi z_{wD}\right]\right]$$

$$p_{D\beta d}\ (=p_{Dd}/p_D) \qquad \times\left[\int_0^{t_{DL}}\left[\operatorname{erf}\left[\frac{0.866}{\sqrt{t_{DL}}}\right]+\operatorname{erf}\left[\frac{0.134}{\sqrt{t_{DL}}}\right]\right] \times\left[1+2\sum_{n=1}^{\infty}\exp(-n^2\pi^2L_D^2\tau)\cos n\pi z_D\cos n\pi z_{wD}\right]\frac{d\tau}{\sqrt{\tau}}\right]^{-1} \quad \text{(E.1.7)}$$

$$p_{D\beta d}(t_{DL}) = \exp\left[-\frac{(z_D-z_{wD})^2/L_D^2}{4t_{DL}}\right]\Bigg/\operatorname{E}_1\left[\frac{(z_D-z_{wD})^2/L_D^2}{4t_{DL}}\right]$$

(early time) (E.1.8)

$$p_{D\beta d}(t_{DL}) = \frac{1}{(\ln t_{DL}+2.509843)+F}$$

(late time) (E.1.9)

Definitions: (field units)

$$F = \sum_{n=1}^{\infty}\cos n\pi z_D\cos n\pi z_{wD}\int_{-1}^{+1}K_0[L_Dn\pi(0.732-\alpha)^2]\,d\alpha \quad \text{(E.1.10)}$$

$$t_{DL} = 2.637\times10^{-4}\frac{kt}{\phi c_t\mu(L/2)^2} \quad \text{(E.1.11)}$$

$$p_D = \frac{1}{141.2}\frac{kh}{qB\mu}(p_i-p_{wf}) \quad \text{(E.1.12)}$$

$$z_D = \frac{z}{h} \quad \text{(E.1.13)}$$

$$z_{wD} = z_D - r_{wzD} \quad \text{(E.1.14)}$$

$$r_{wD} = 2r_w/L \quad \text{(E.1.15)}$$

$$r_{wzD} = r_{wD}L_D \quad \text{(E.1.16)}$$

$$C_{DL} = \frac{0.8936C_s}{\phi hc_t(L/2)^2} \quad \text{(E.1.17)}$$

$$L_D = L/(2h) \quad \text{(E.1.18)}$$

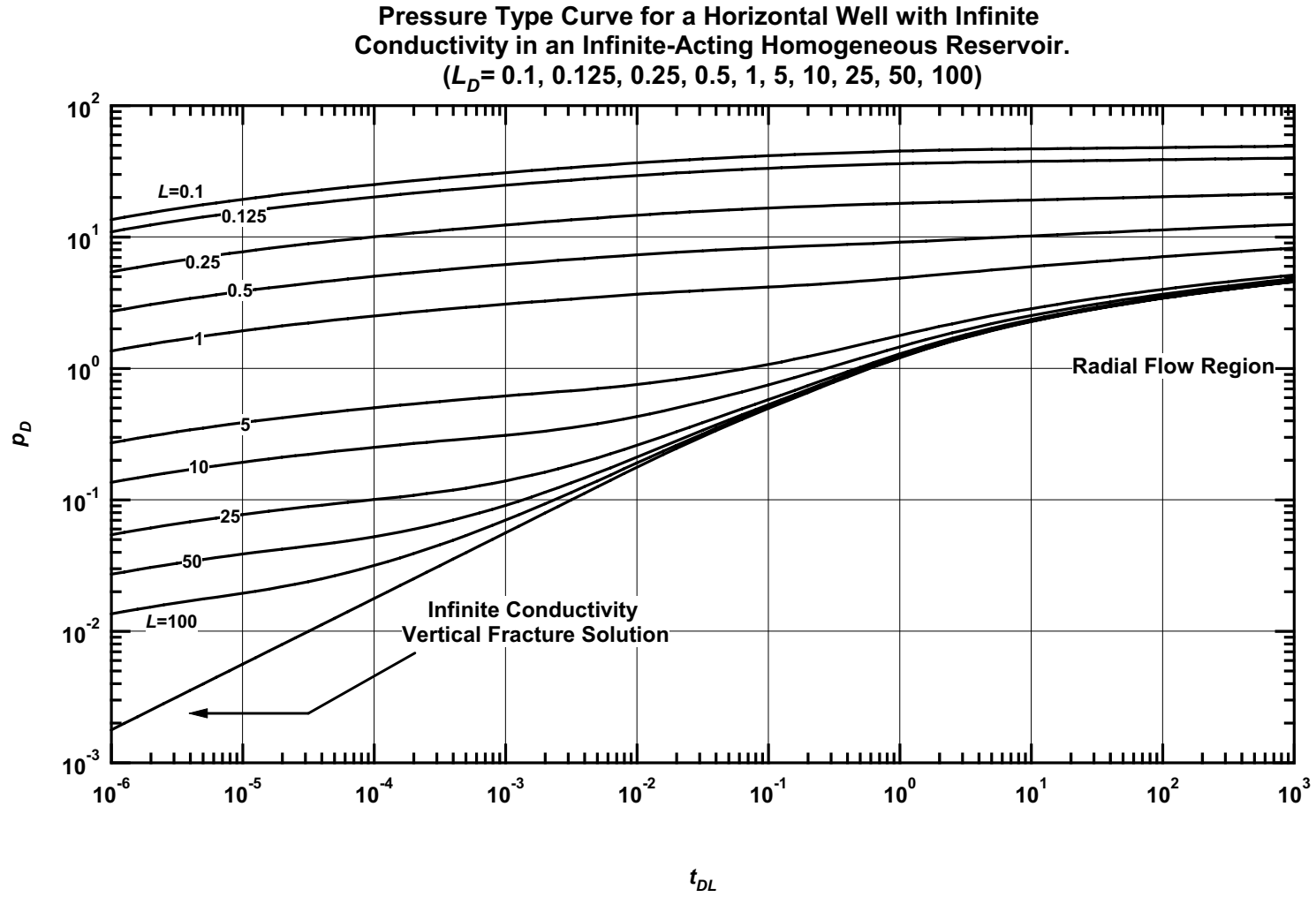

Figure E.1 — p_D vs. t_{DL} — solutions for an infinite conductivity horizontal well in an infinite-acting homogeneous reservoir— no wellbore storage or skin effects (various L_D values).

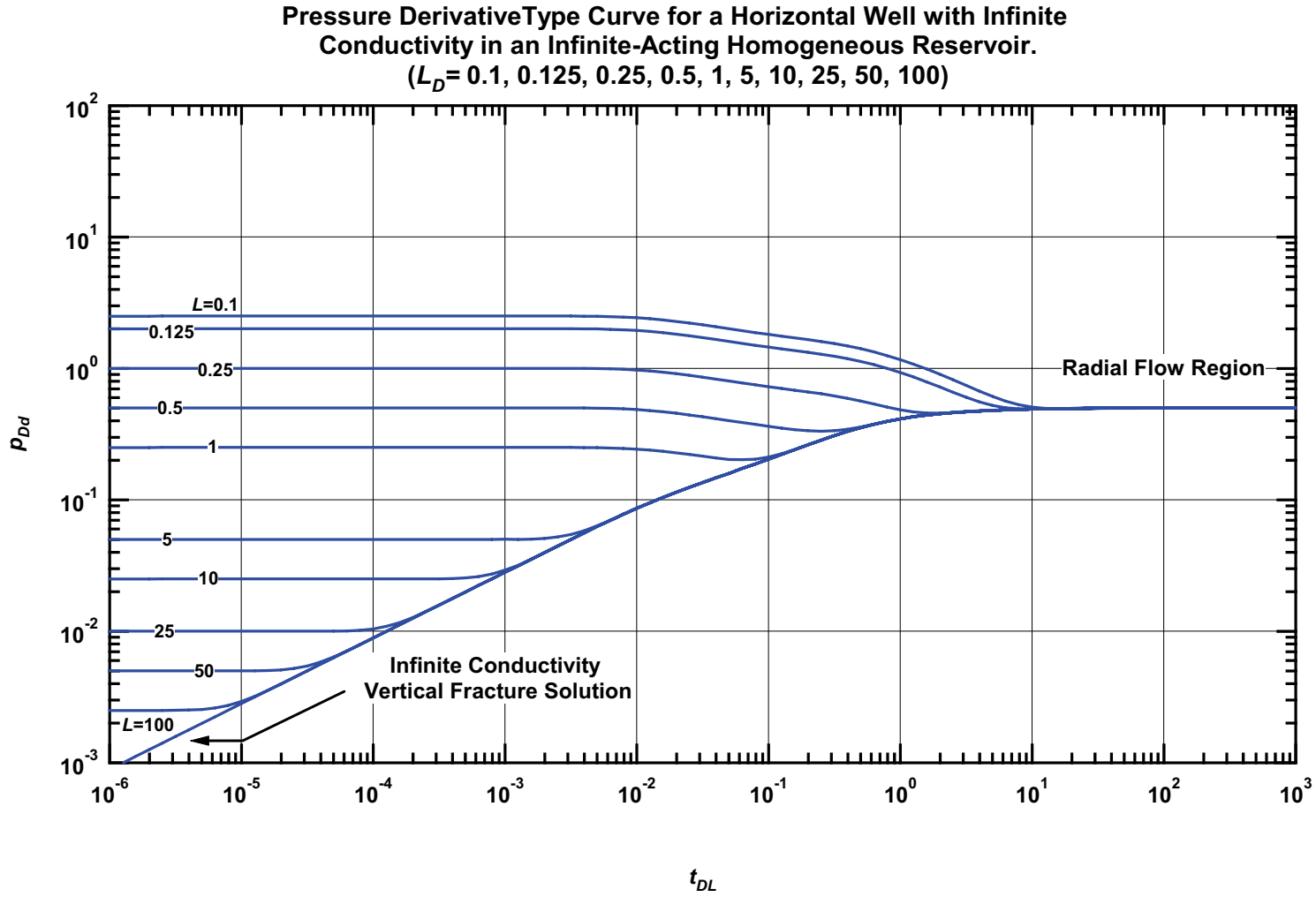

Figure E.2 — p_{Dd} vs. t_{DL} — solutions for an infinite conductivity horizontal well in an infinite-acting homogeneous reservoir— no wellbore storage or skin effects (various L_D values).

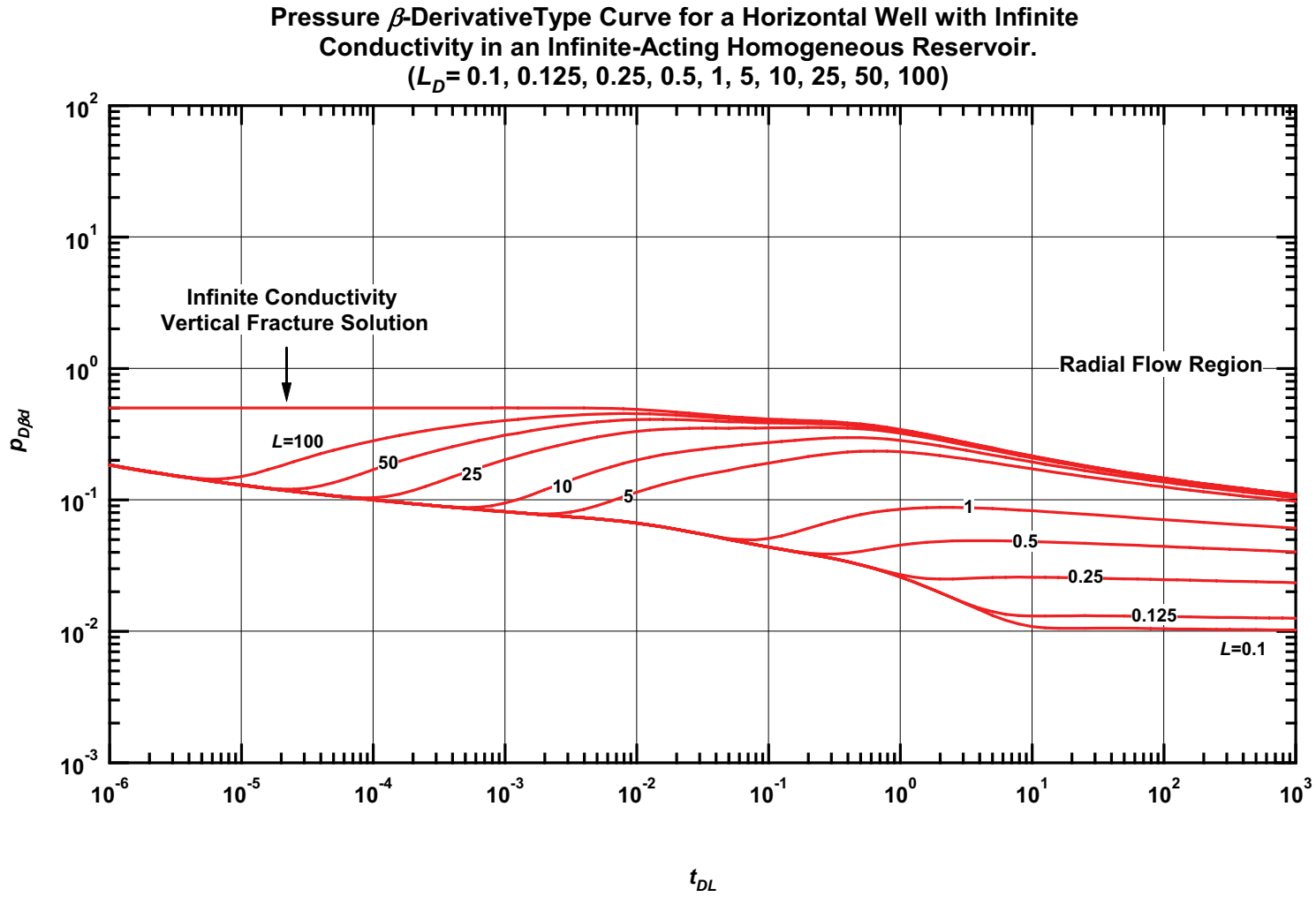

Figure E.3 — $p_{D\beta d}$ vs. t_{DL} — solutions for an infinite conductivity horizontal well in an infinite-acting homogeneous reservoir— no wellbore storage or skin effects (various L_D values).

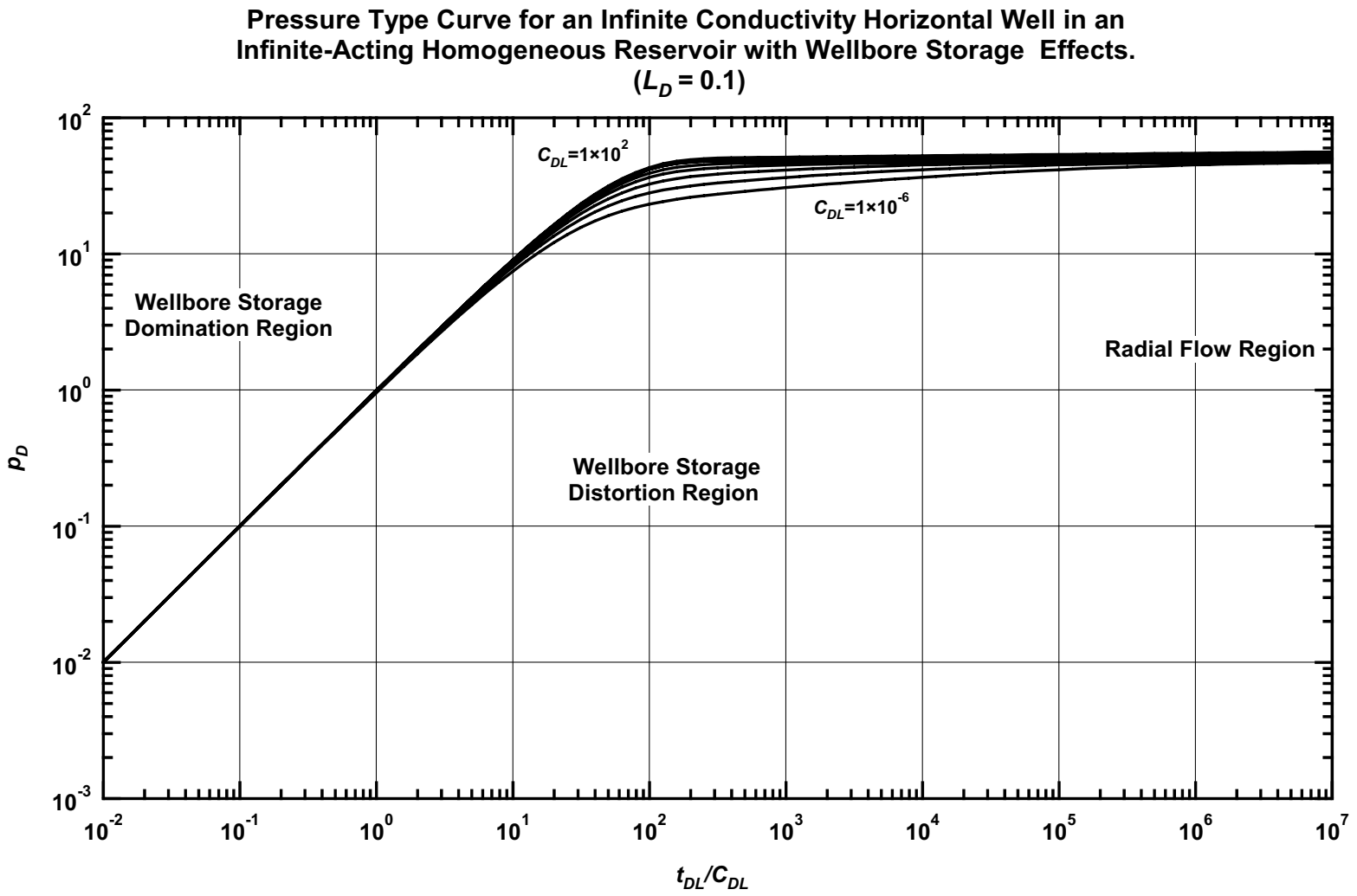

Figure E.4 — p_D vs. t_{DL}/C_{DL} — L_D=0.1 (horizontal well case — includes wellbore storage effects).

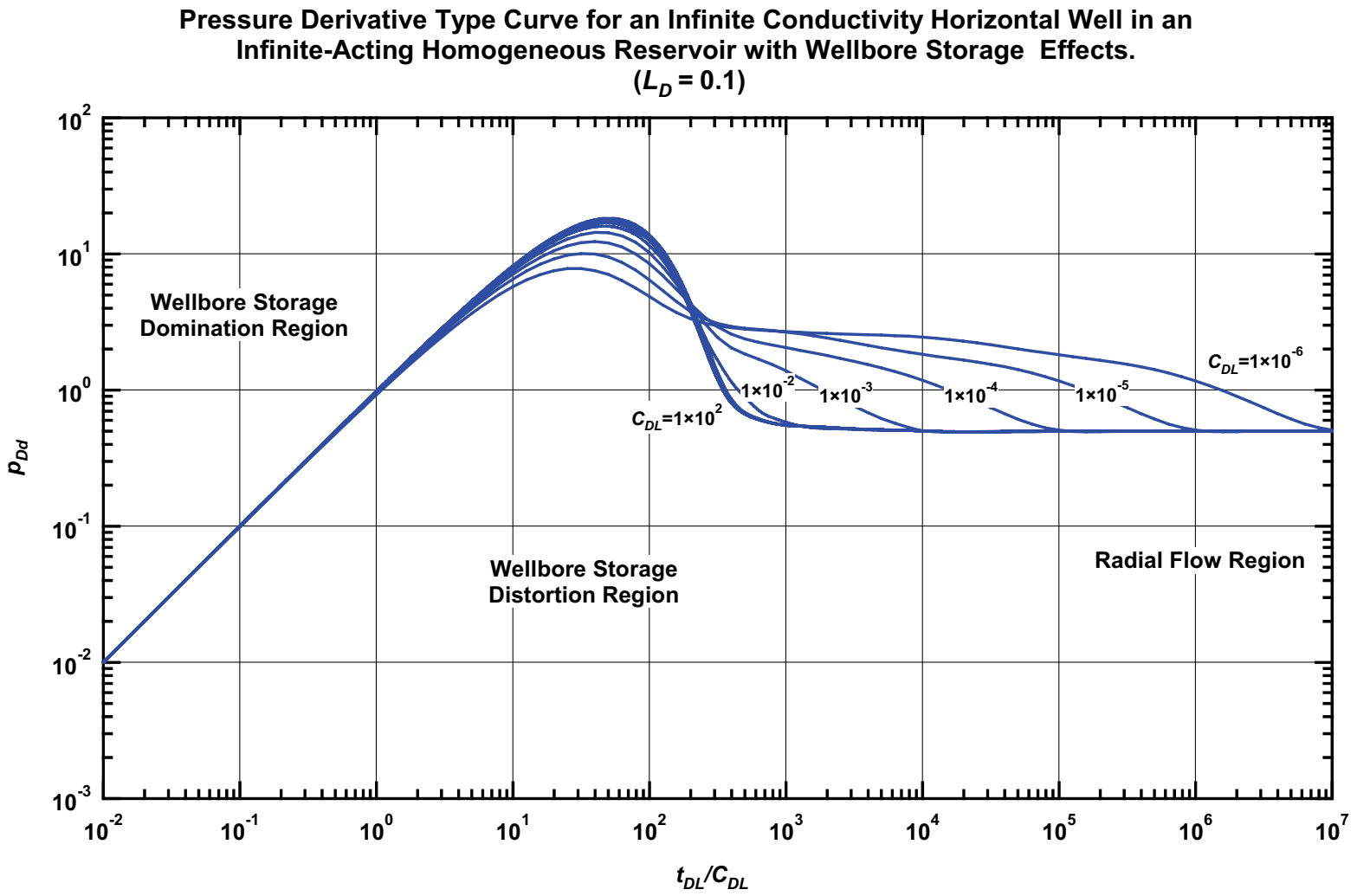

Figure E.5 — p_{Dd} vs. t_{DL}/C_{DL} — L_D=0.1 (horizontal well case — includes wellbore storage effects).

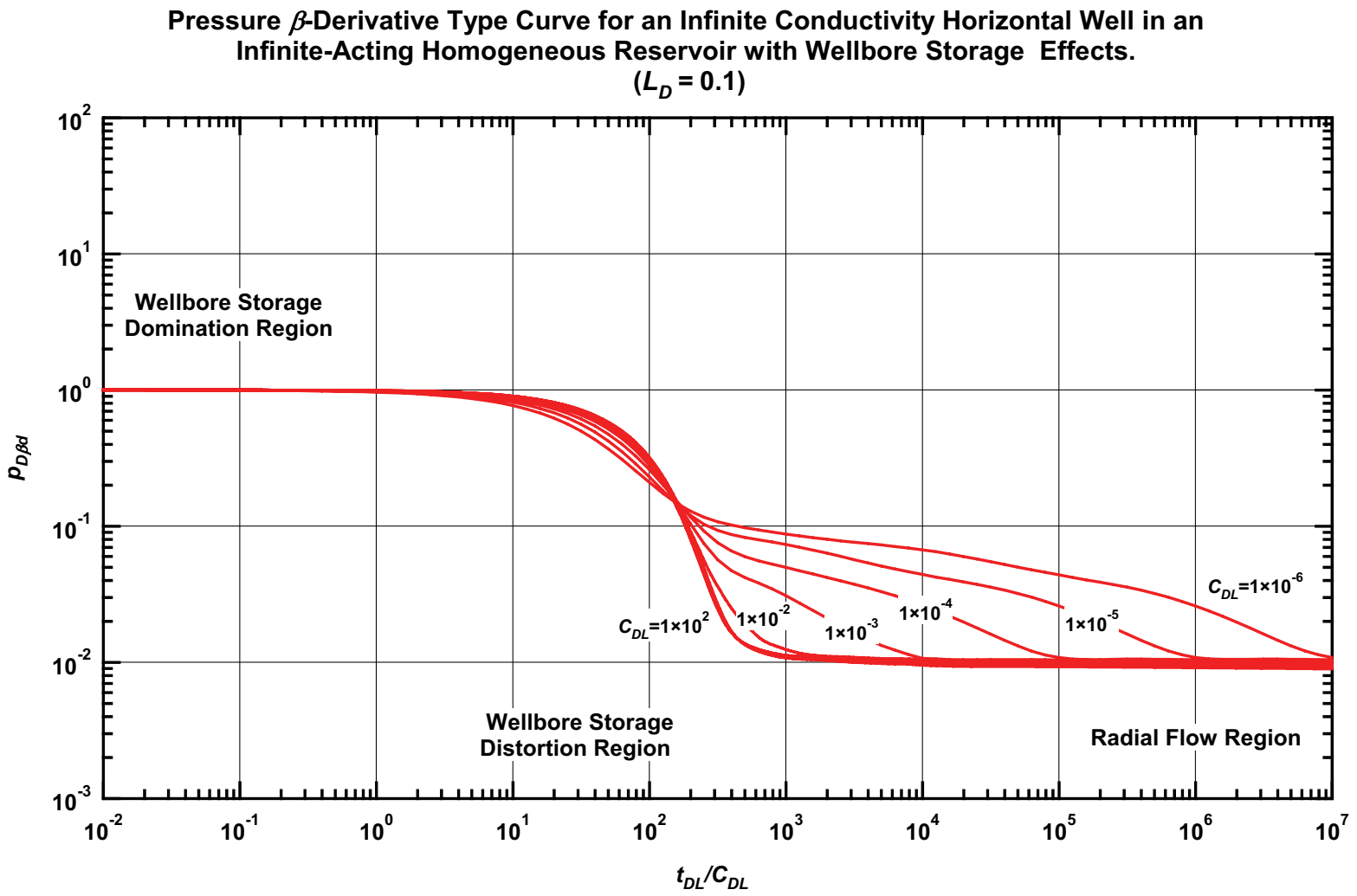

Figure E.6 — $p_{D\beta d}$ vs. t_{DL}/C_{DL} — L_D=0.1 (horizontal well case — includes wellbore storage effects).

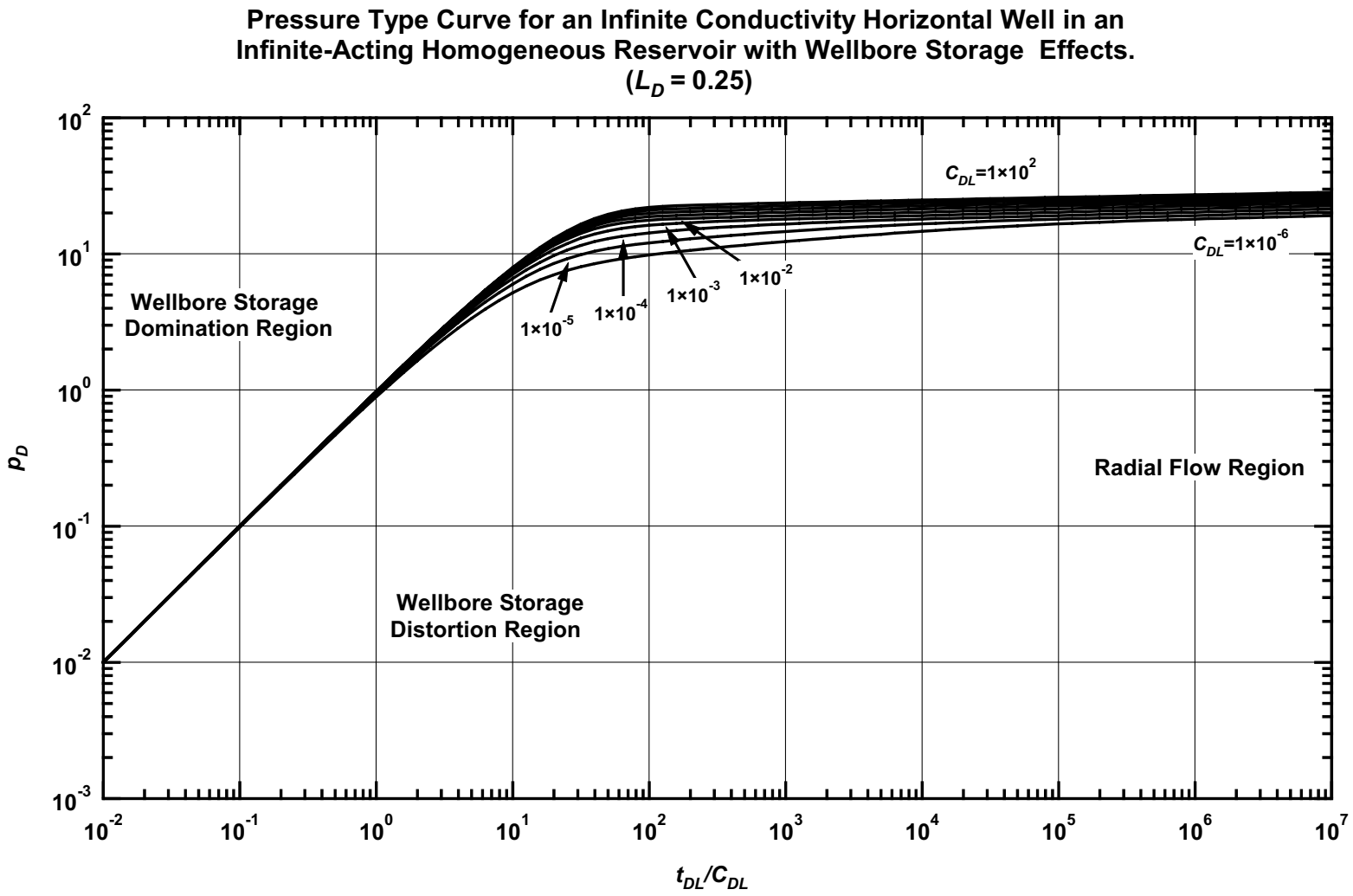

Figure E.7 — p_D vs. t_{DL}/C_{DL} — L_D=0.25 (horizontal well case — includes wellbore storage effects).

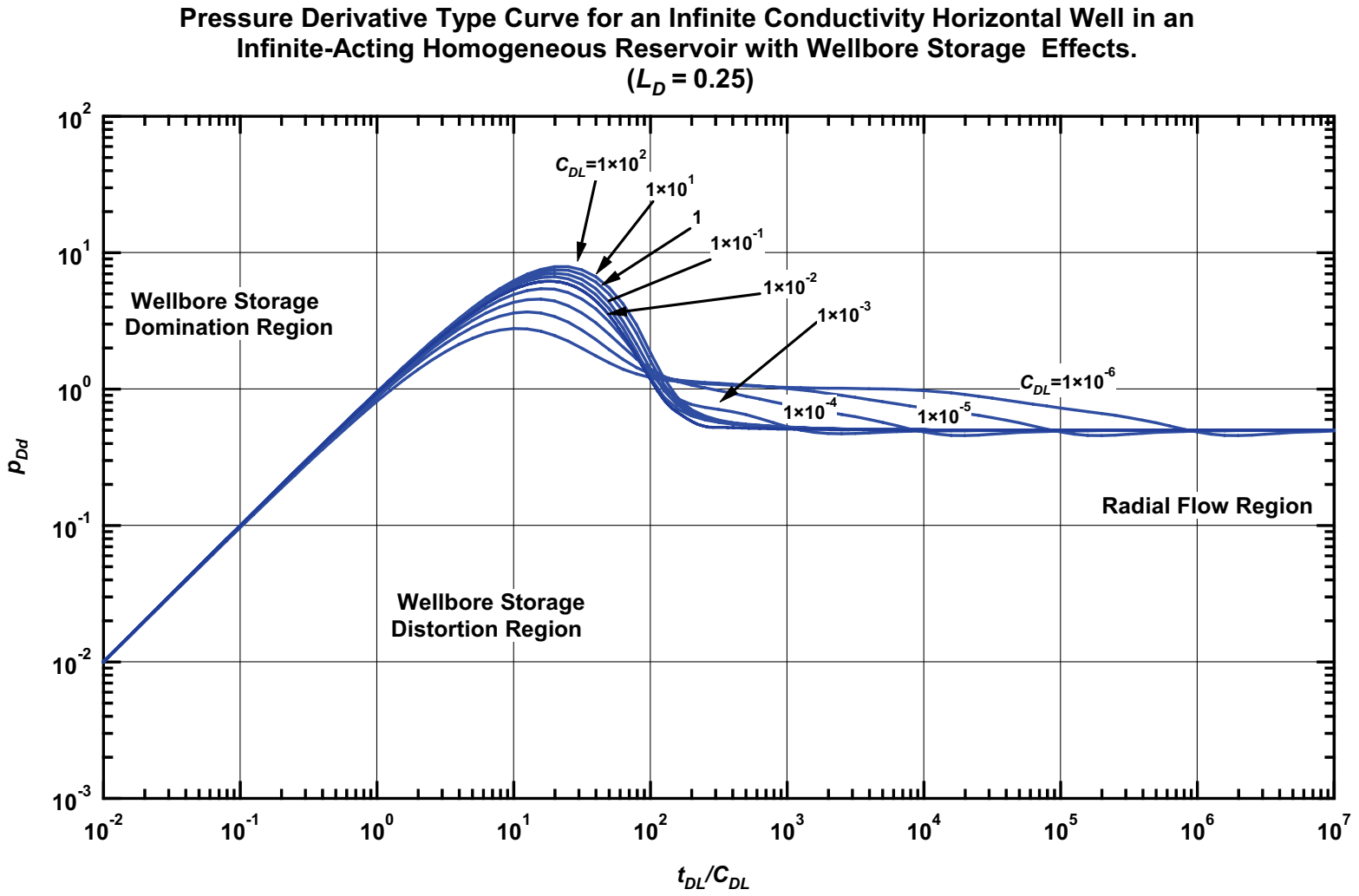

Figure E.8 — p_{Dd} vs. t_{DL}/C_{DL} — L_D=0.25 (horizontal well case — includes wellbore storage effects).

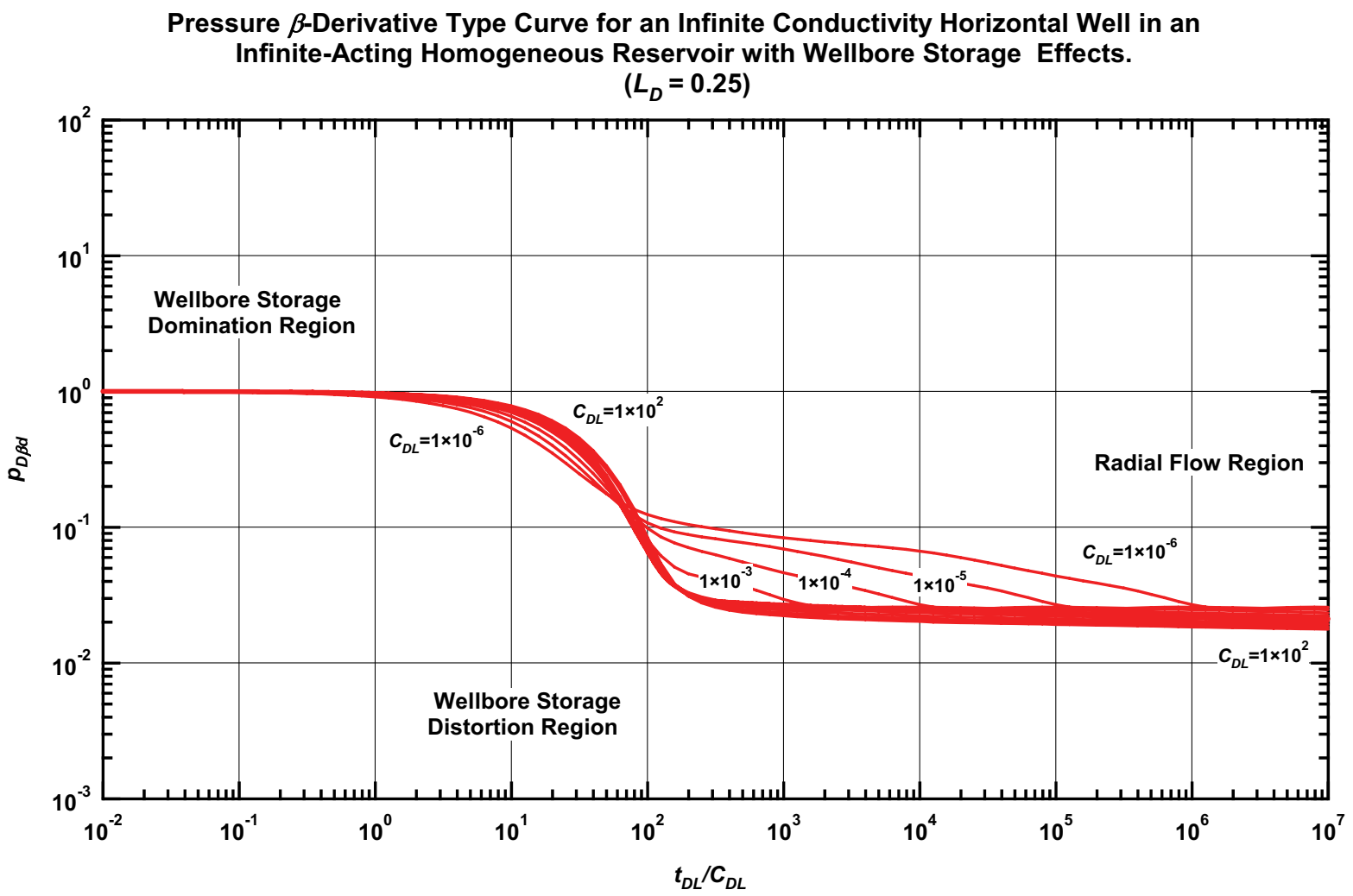

Figure E.9 — $p_{D\beta d}$ vs. t_{DL}/C_{DL} — L_D=0.25 (horizontal well case — includes wellbore storage effects).

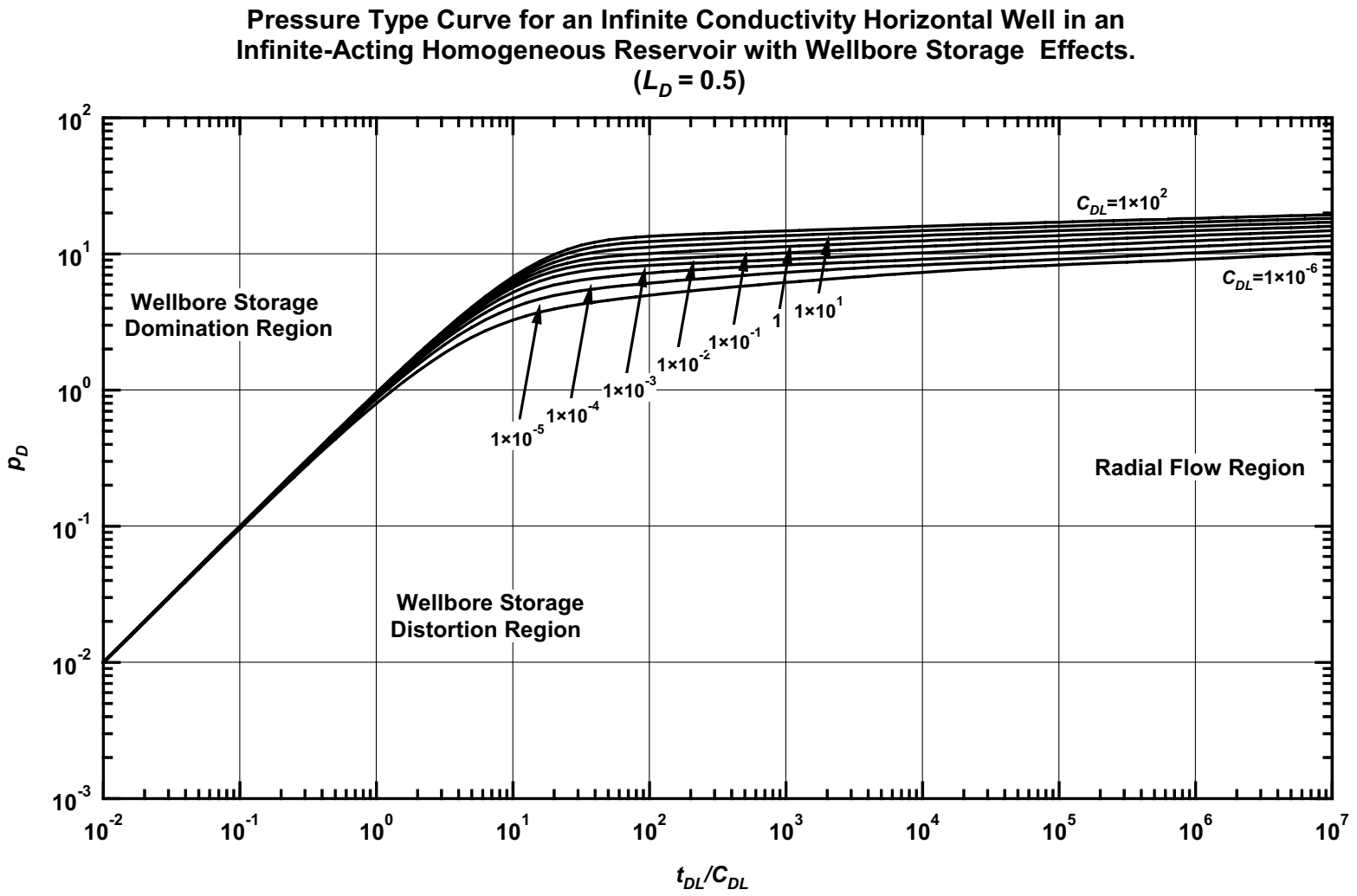

Figure E.10 — p_D vs. t_{DL}/C_{DL} — L_D=0.5 (horizontal well case — includes wellbore storage effects).

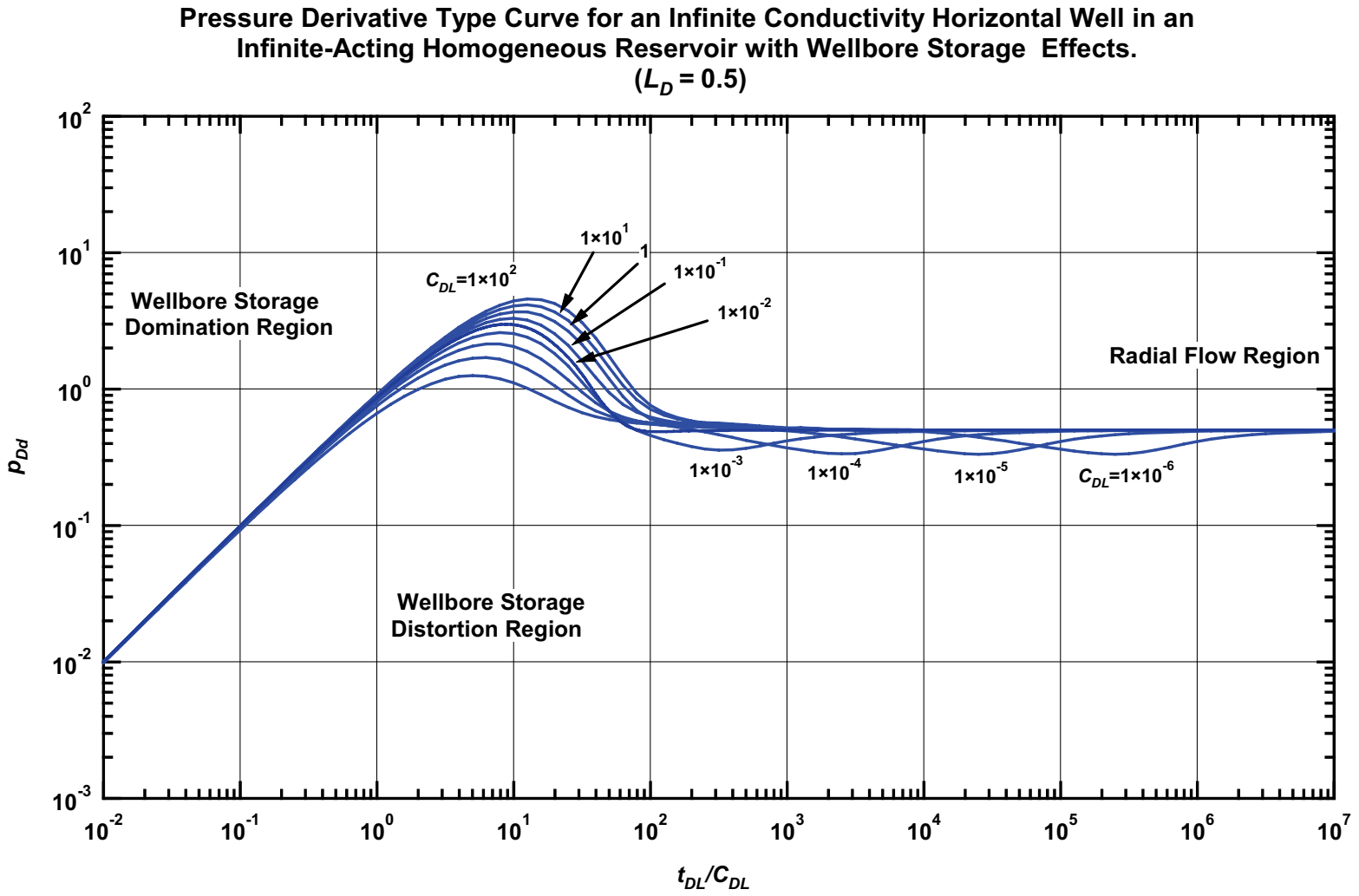

Figure E.11 — p_{Dd} vs. t_{DL}/C_{DL} — L_D=0.5 (horizontal well case — includes wellbore storage effects).

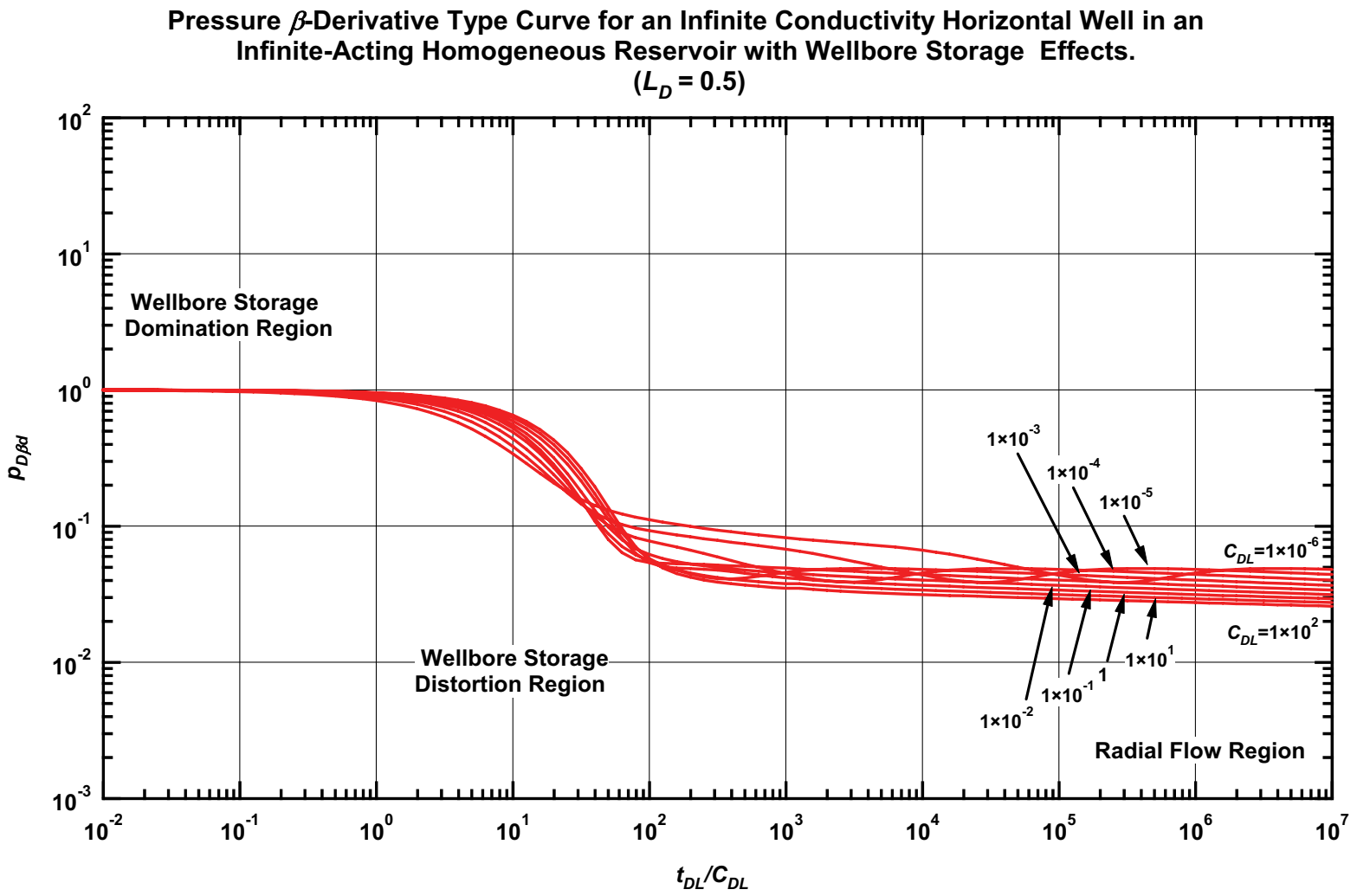

Figure E.12 — $p_{D\beta d}$ vs. t_{DL}/C_{DL} — L_D=0.5 (horizontal well case — includes wellbore storage effects).

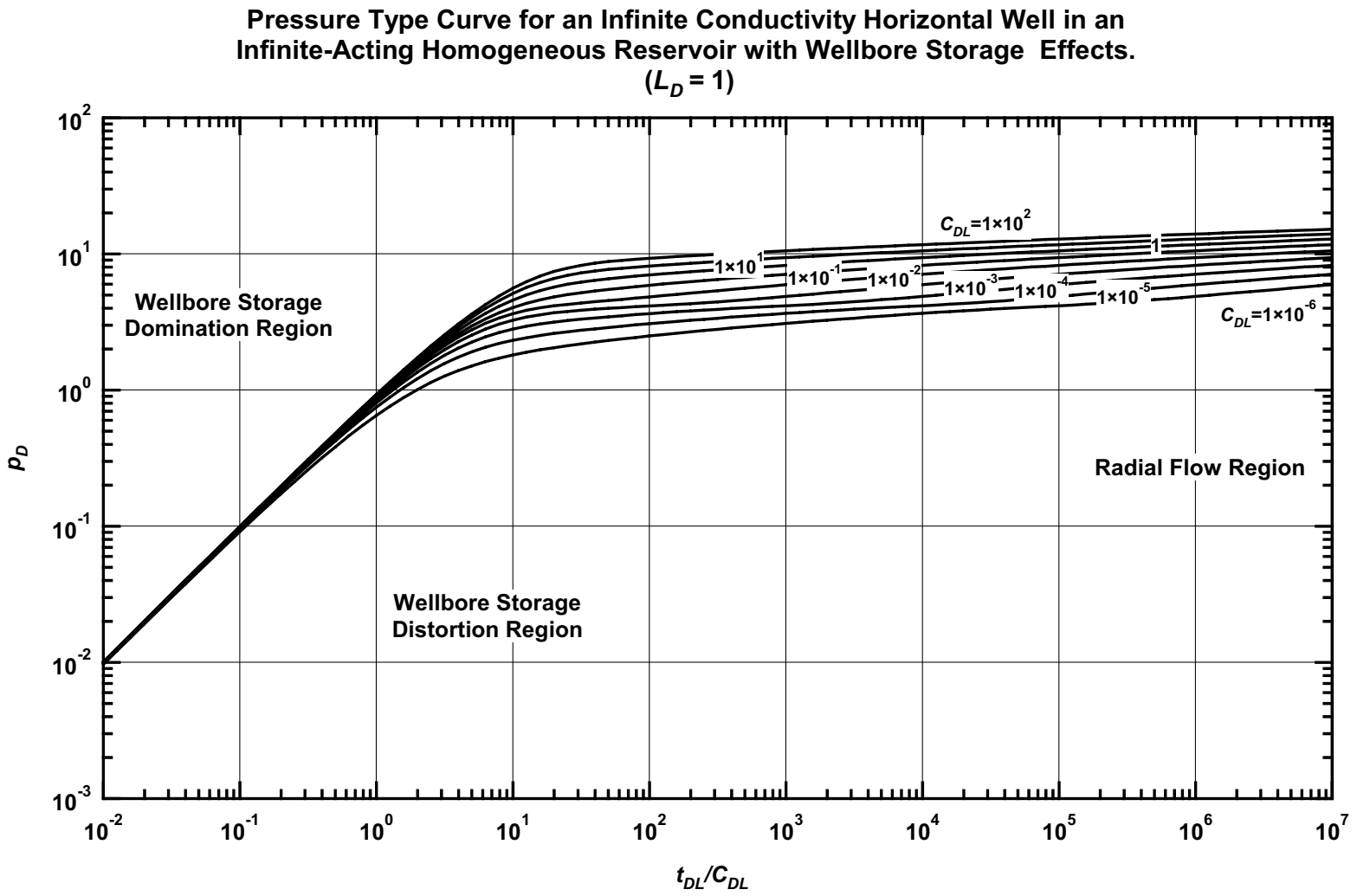

Figure E.13 — p_D vs. t_{DL}/C_{DL} — L_D=1 (horizontal well case — includes wellbore storage effects).

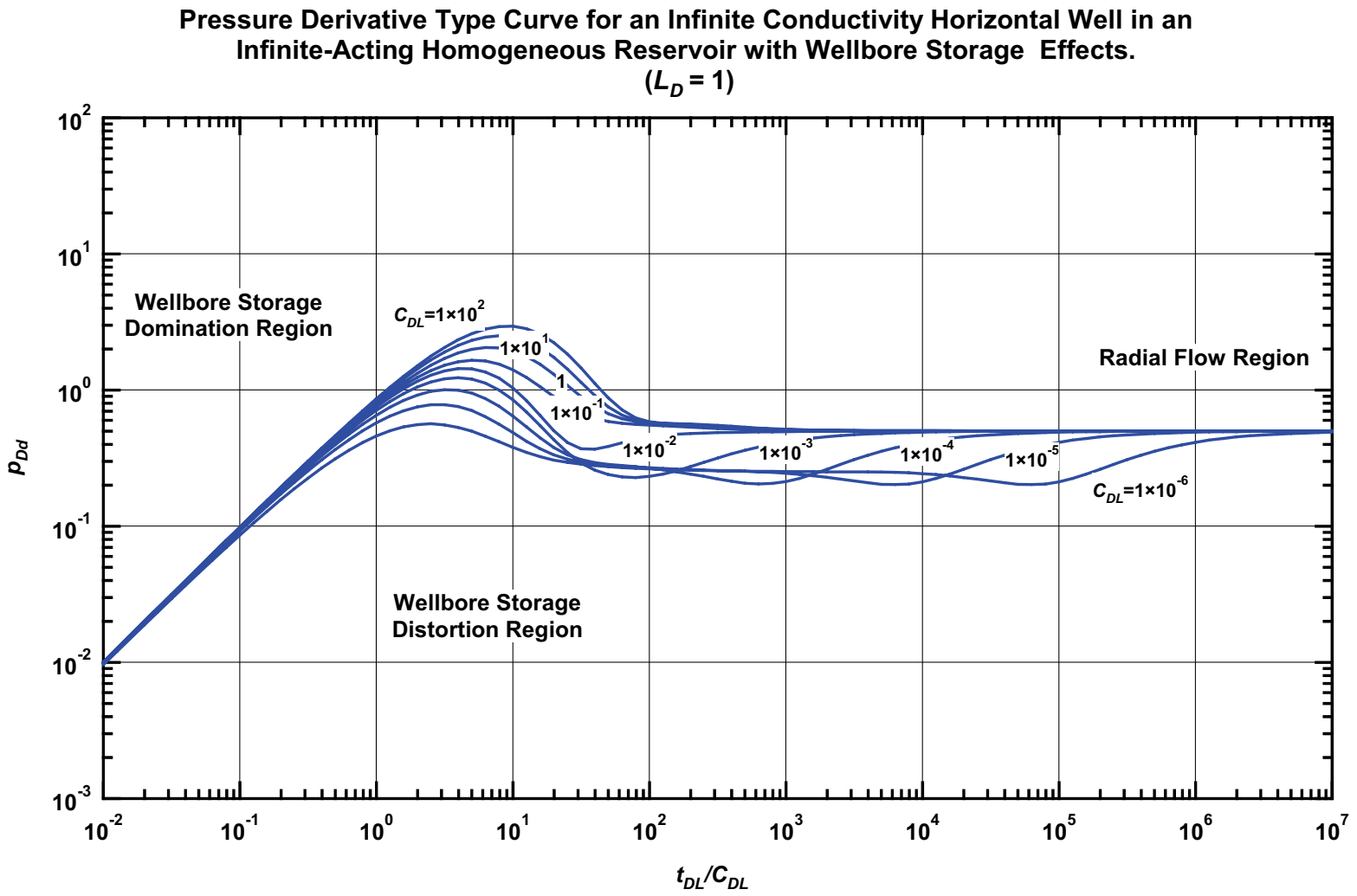

Figure E.14 — p_{Dd} vs. t_{DL}/C_{DL} — L_D=1 (horizontal well case — includes wellbore storage effects).

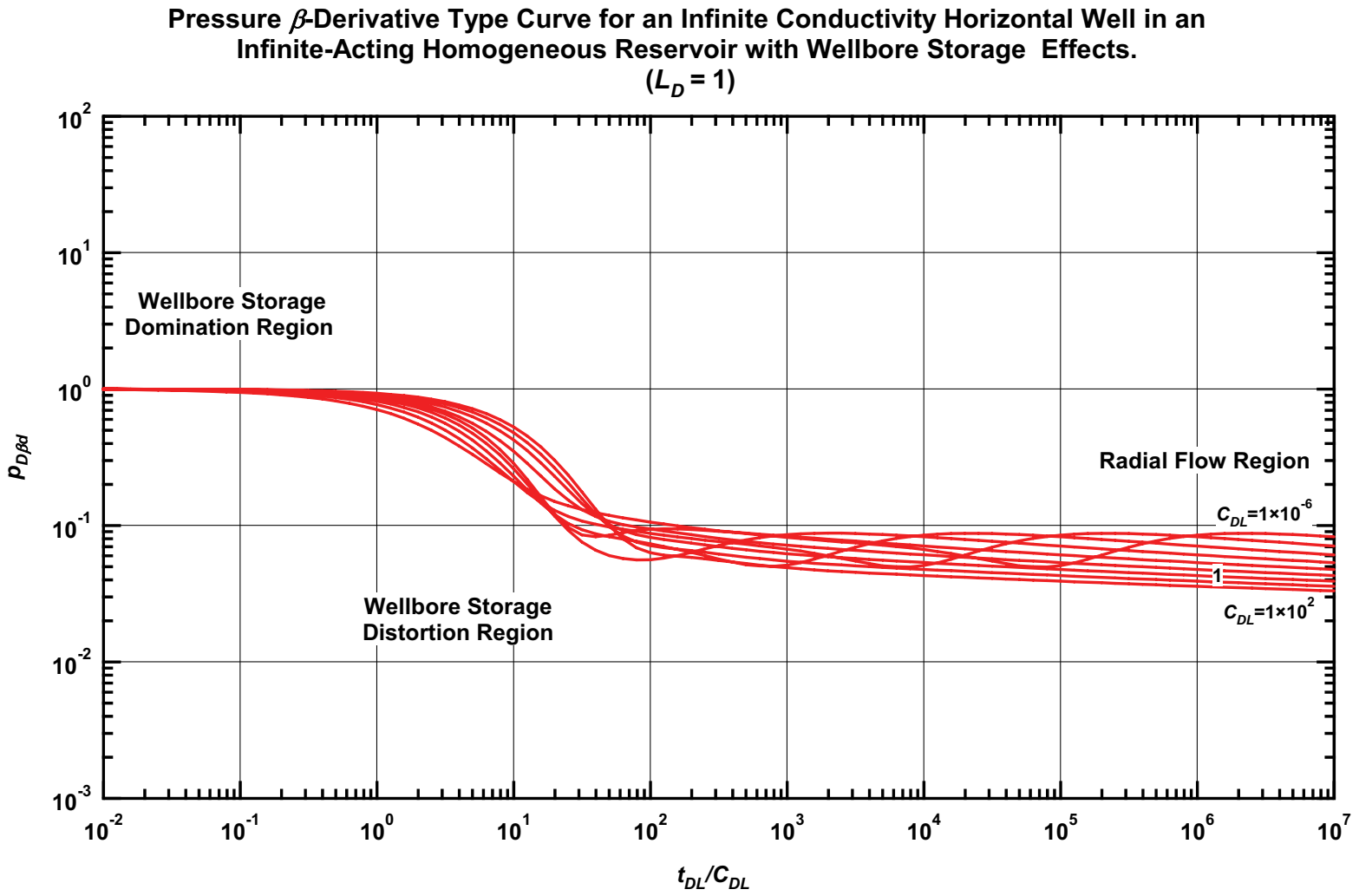

Figure E.15 — $p_{D\beta d}$ vs. t_{DL}/C_{DL} — L_D=1 (horizontal well case — includes wellbore storage effects).

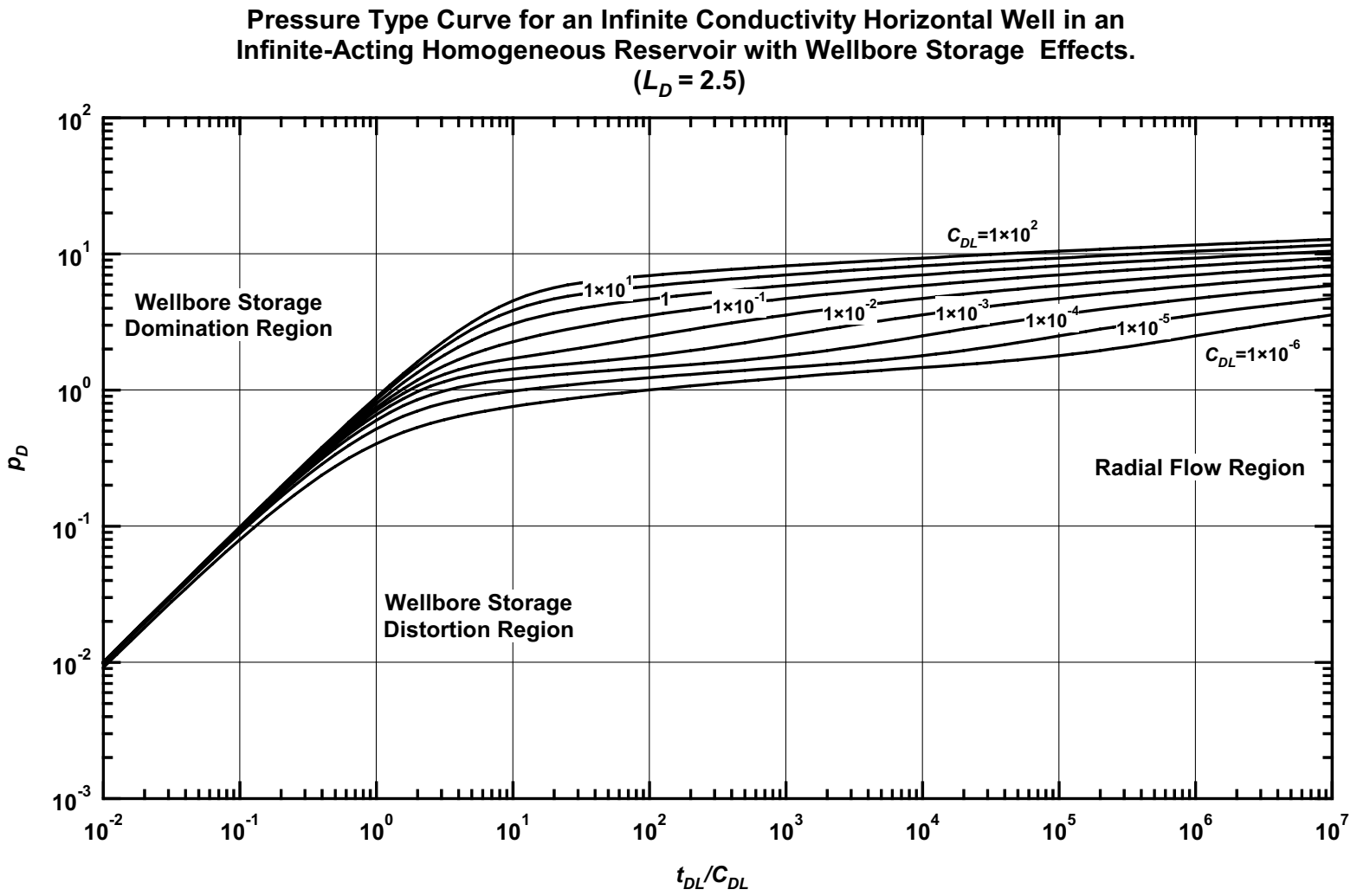

Figure E.16 — p_D vs. t_{DL}/C_{DL} — L_D=2.5 (horizontal well case — includes wellbore storage effects).

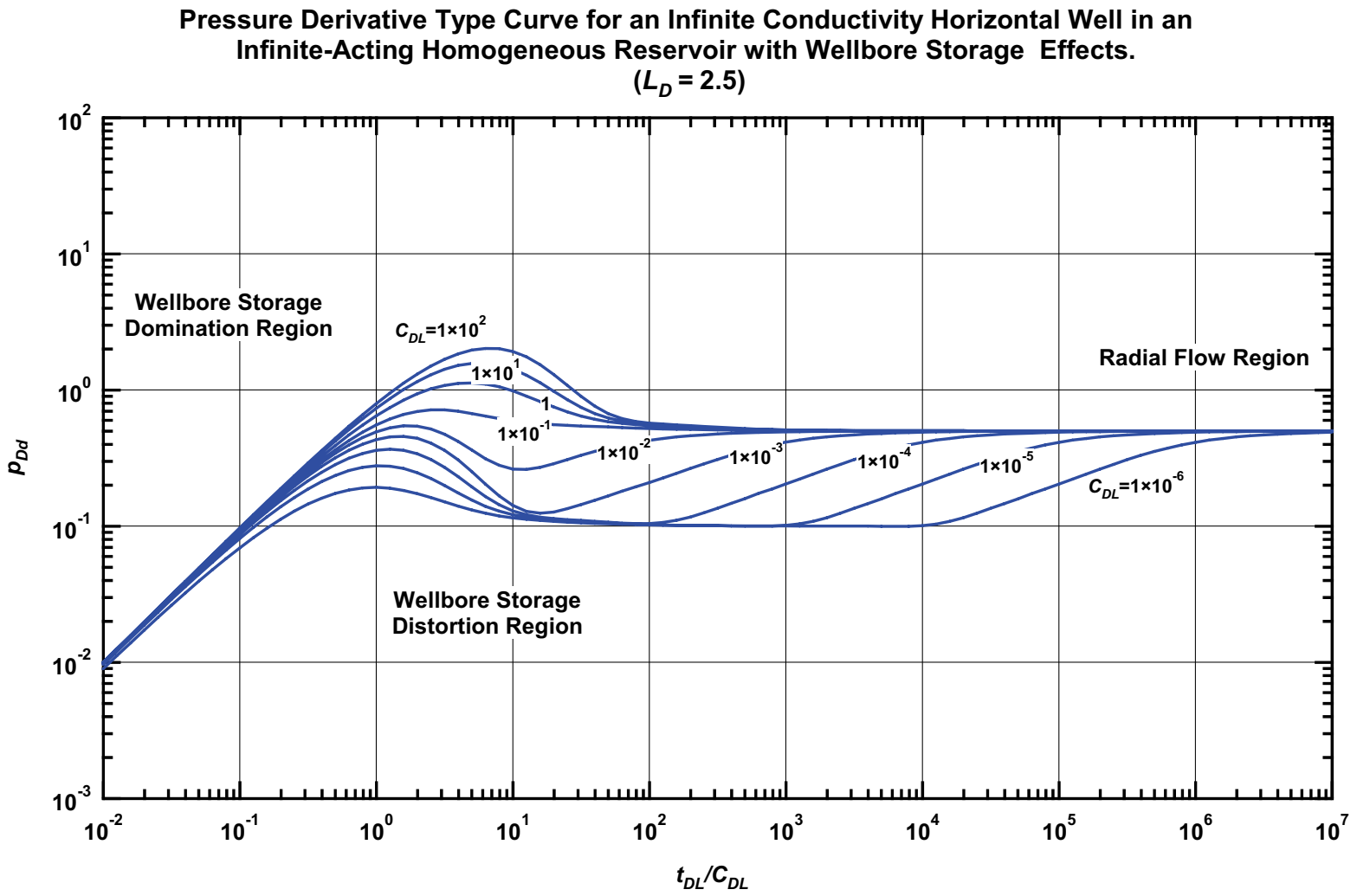

Figure E.17 — p_{Dd} vs. t_{DL}/C_{DL} — L_D=2.5 (horizontal well case — includes wellbore storage effects).

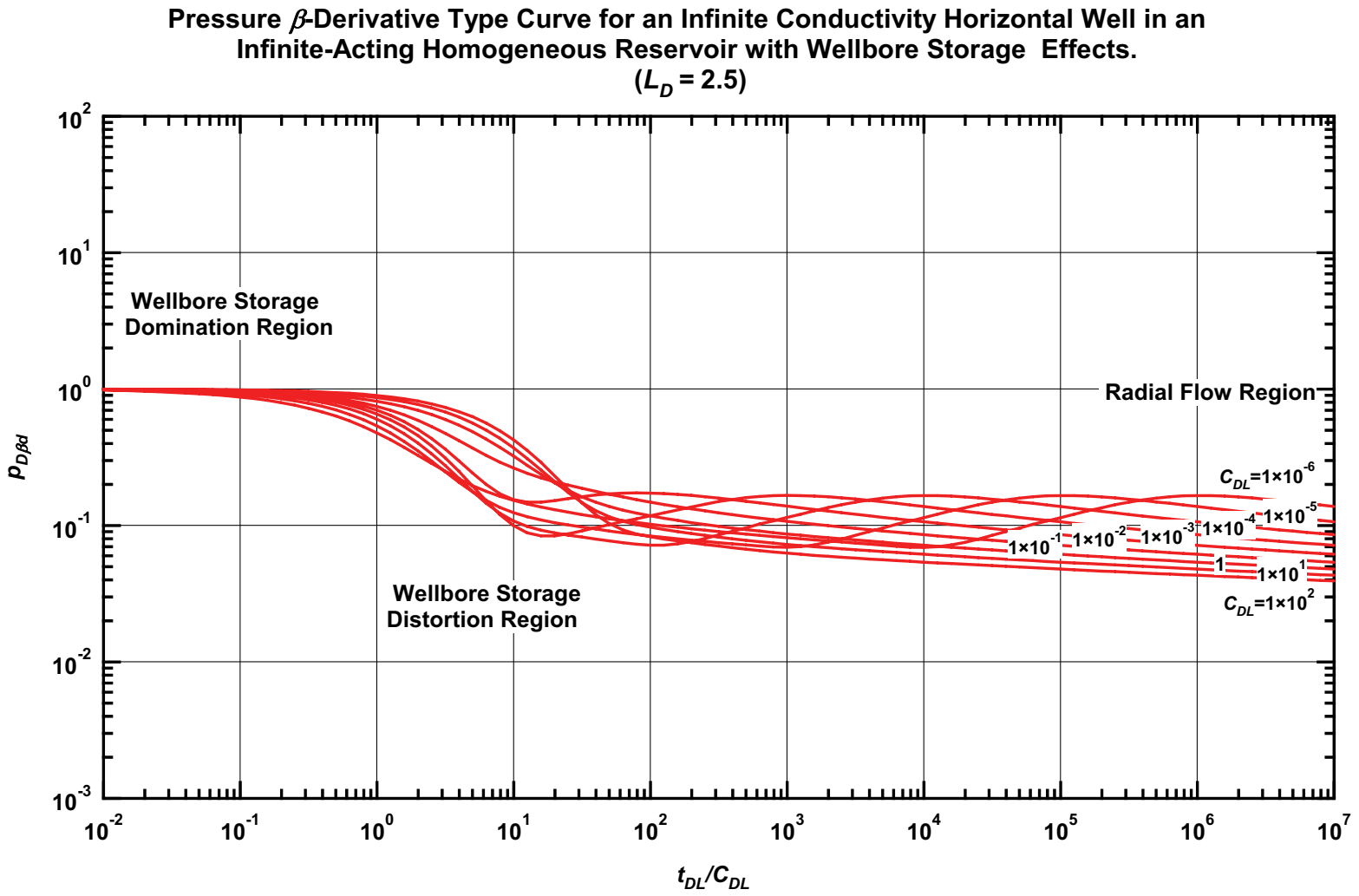

Figure E.18 — $p_{D\beta d}$ vs. t_{DL}/C_{DL} — L_D=2.5 (horizontal well case — includes wellbore storage effects).

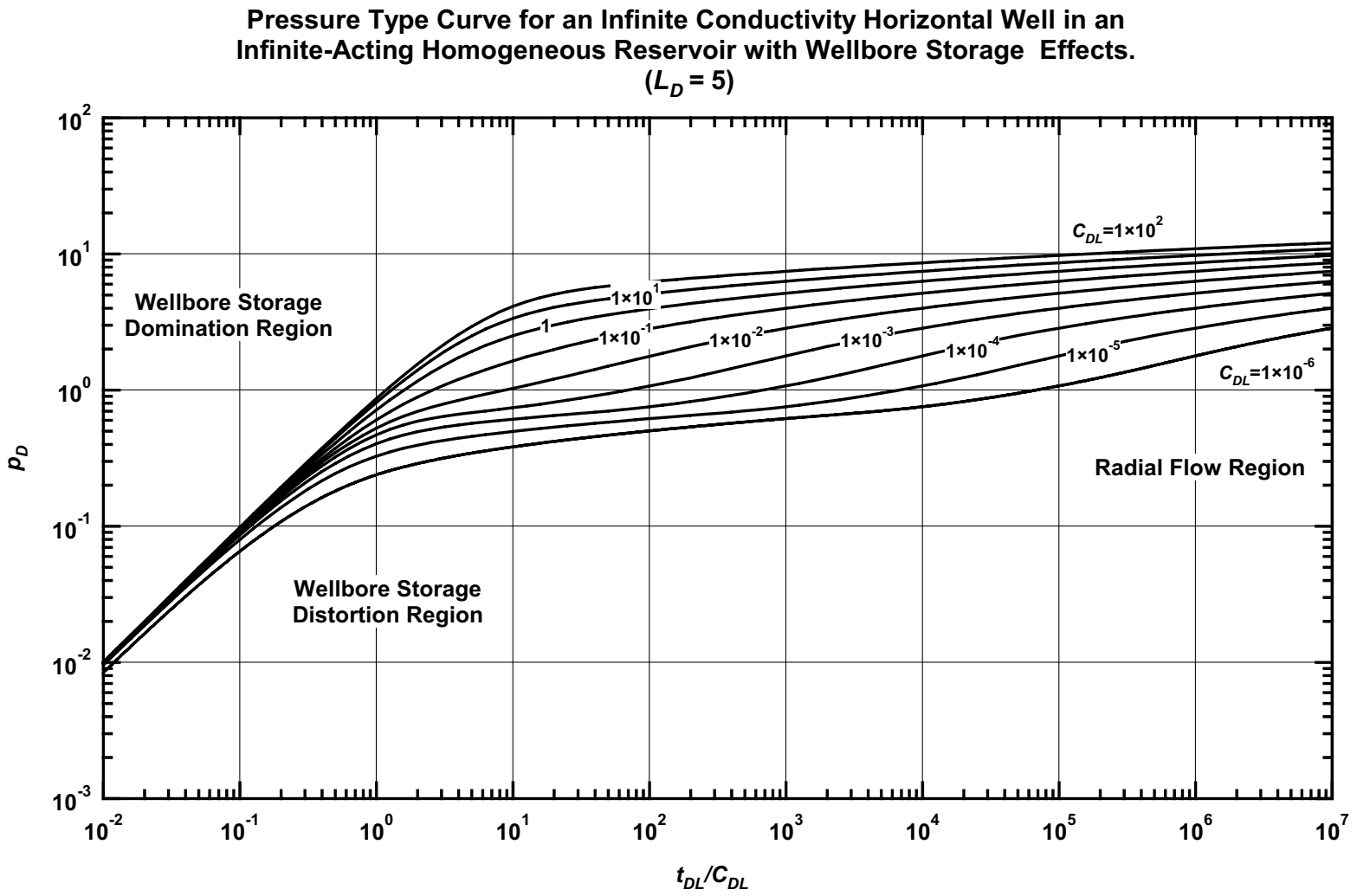

Figure E.19 — p_D vs. t_{DL}/C_{DL} — L_D=5 (horizontal well case — includes wellbore storage effects).

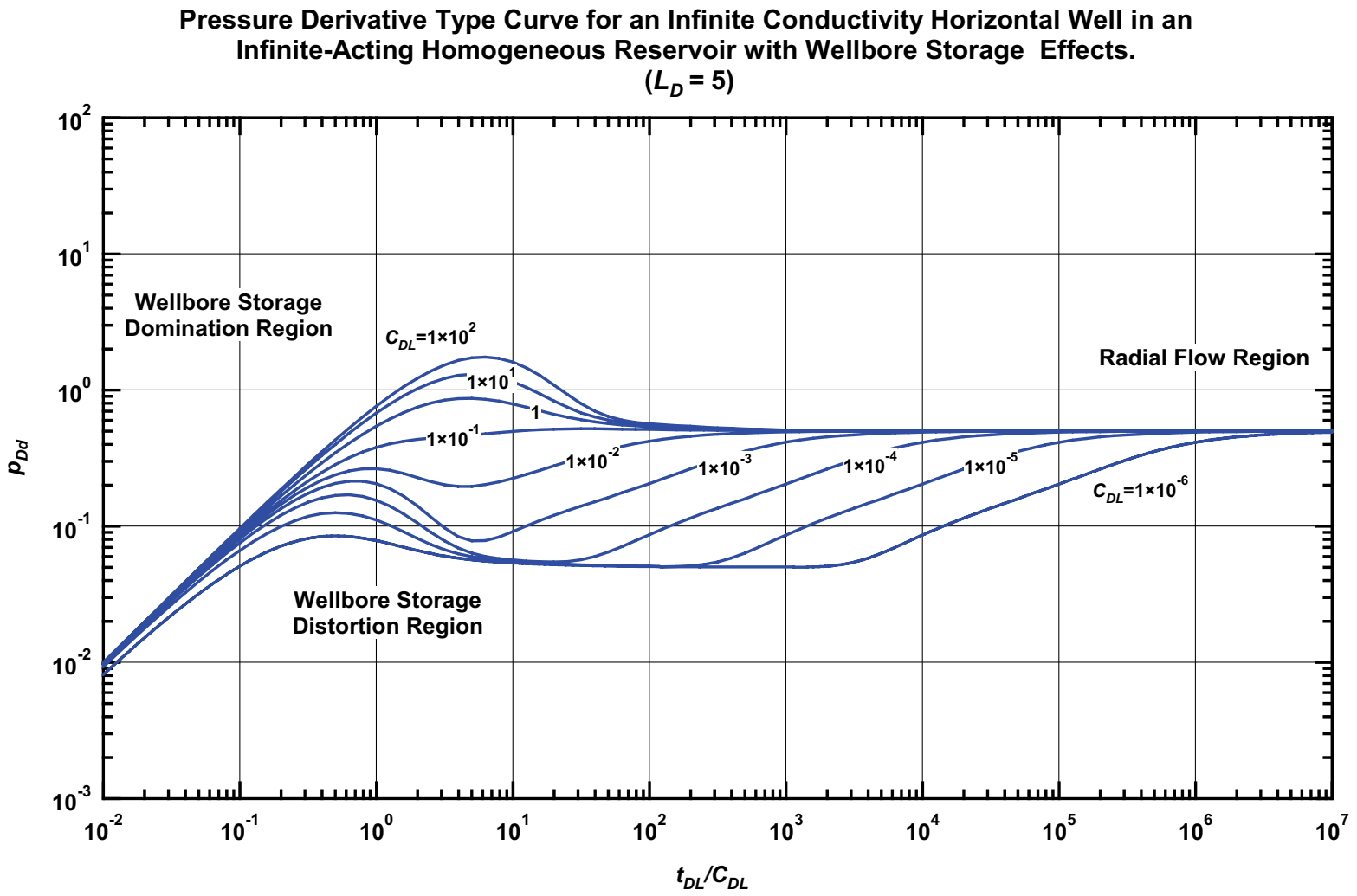

Figure E.20 — p_{Dd} vs. t_{DL}/C_{DL} — L_D=5 (horizontal well case — includes wellbore storage effects).

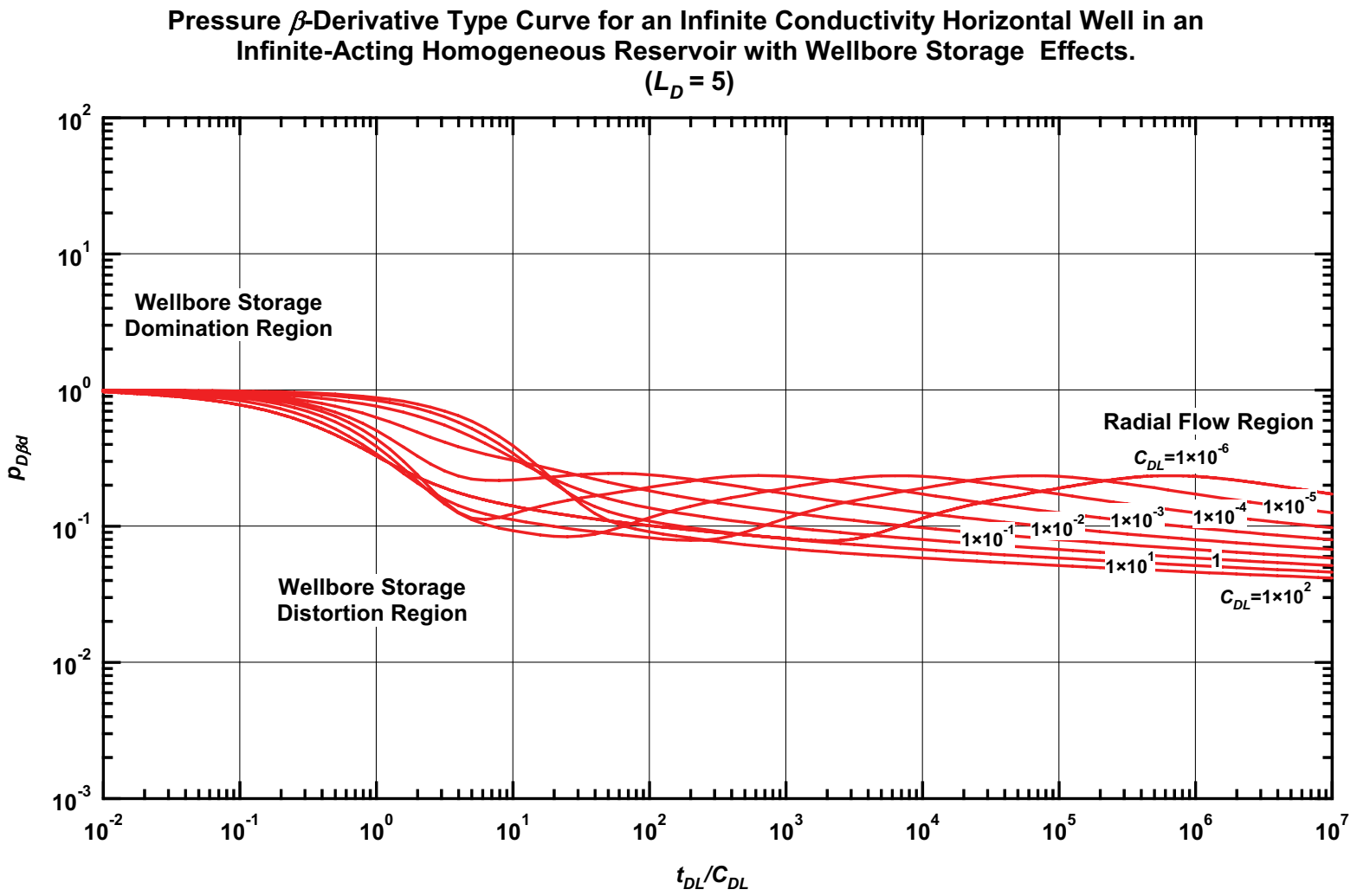

Figure E.21 — $p_{D\beta d}$ vs. t_{DL}/C_{DL} — L_D=5 (horizontal well case — includes wellbore storage effects).

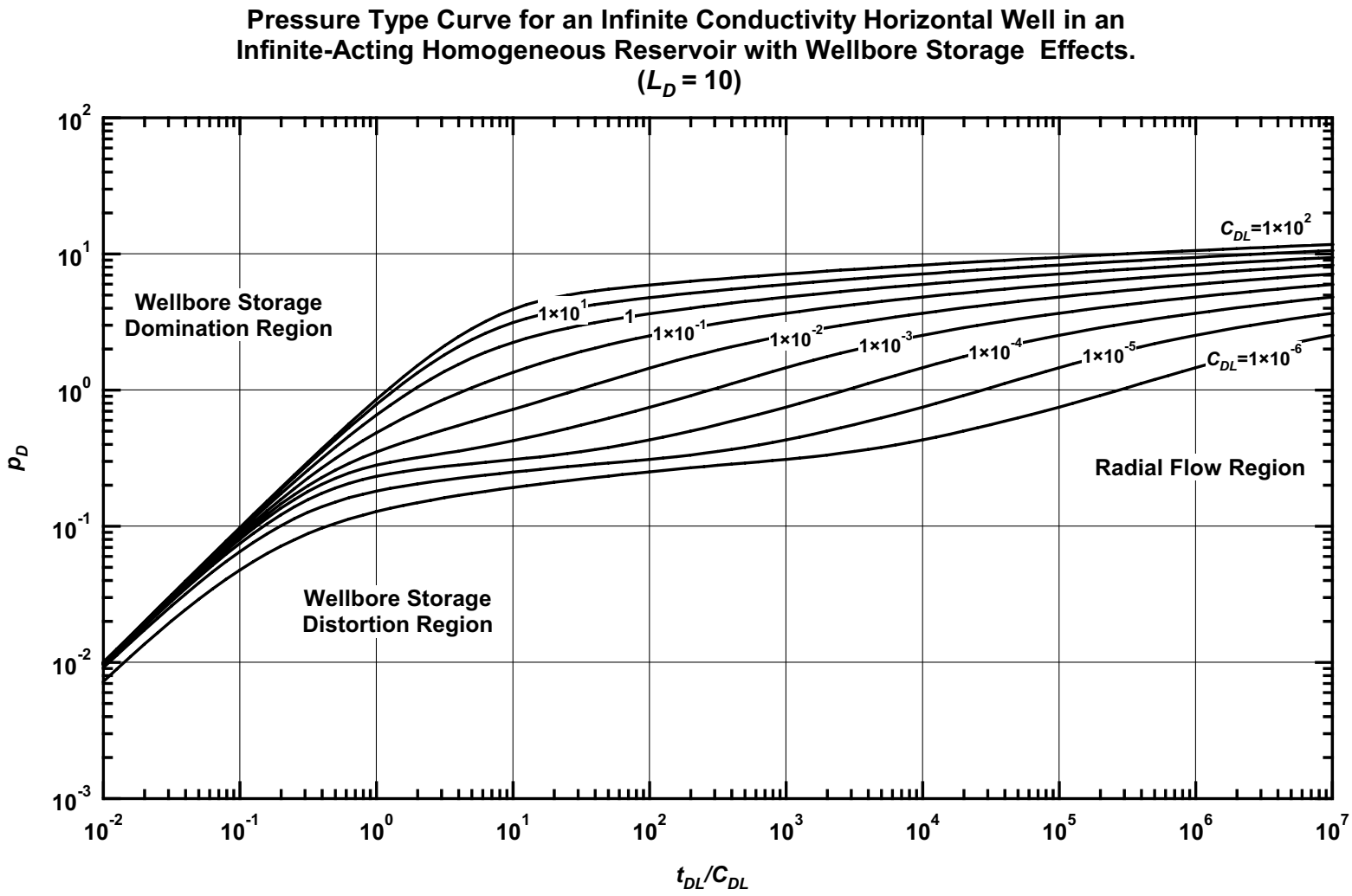

Figure E.22 — p_D vs. t_{DL}/C_{DL} — L_D=10 (horizontal well case — includes wellbore storage effects).

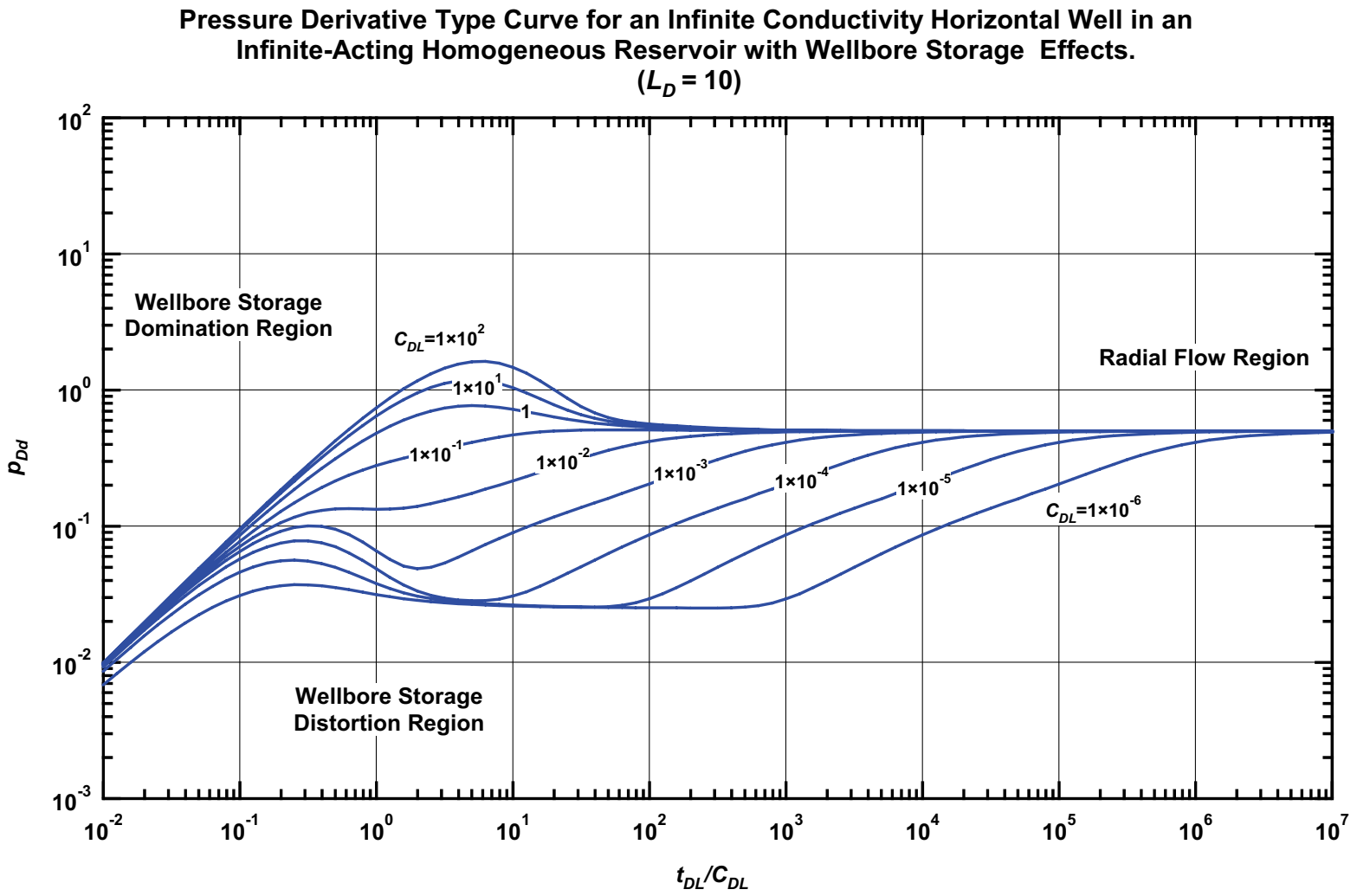

Figure E.23 — p_{Dd} vs. t_{DL}/C_{DL} — L_D=10 (horizontal well case — includes wellbore storage effects).

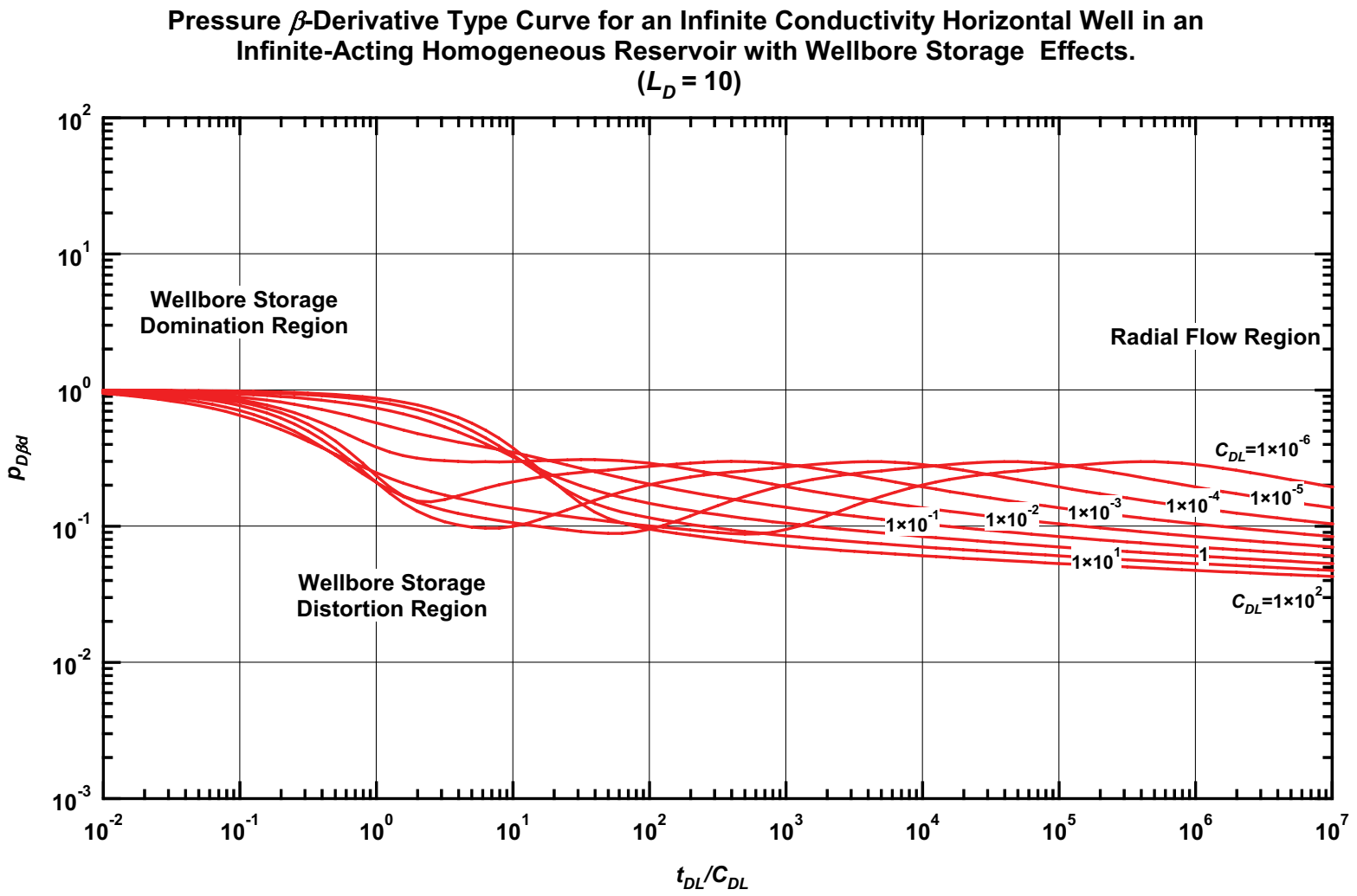

Figure E.24 — $p_{D\beta d}$ vs. t_{DL}/C_{DL} — L_D=10 (horizontal well case — includes wellbore storage effects).

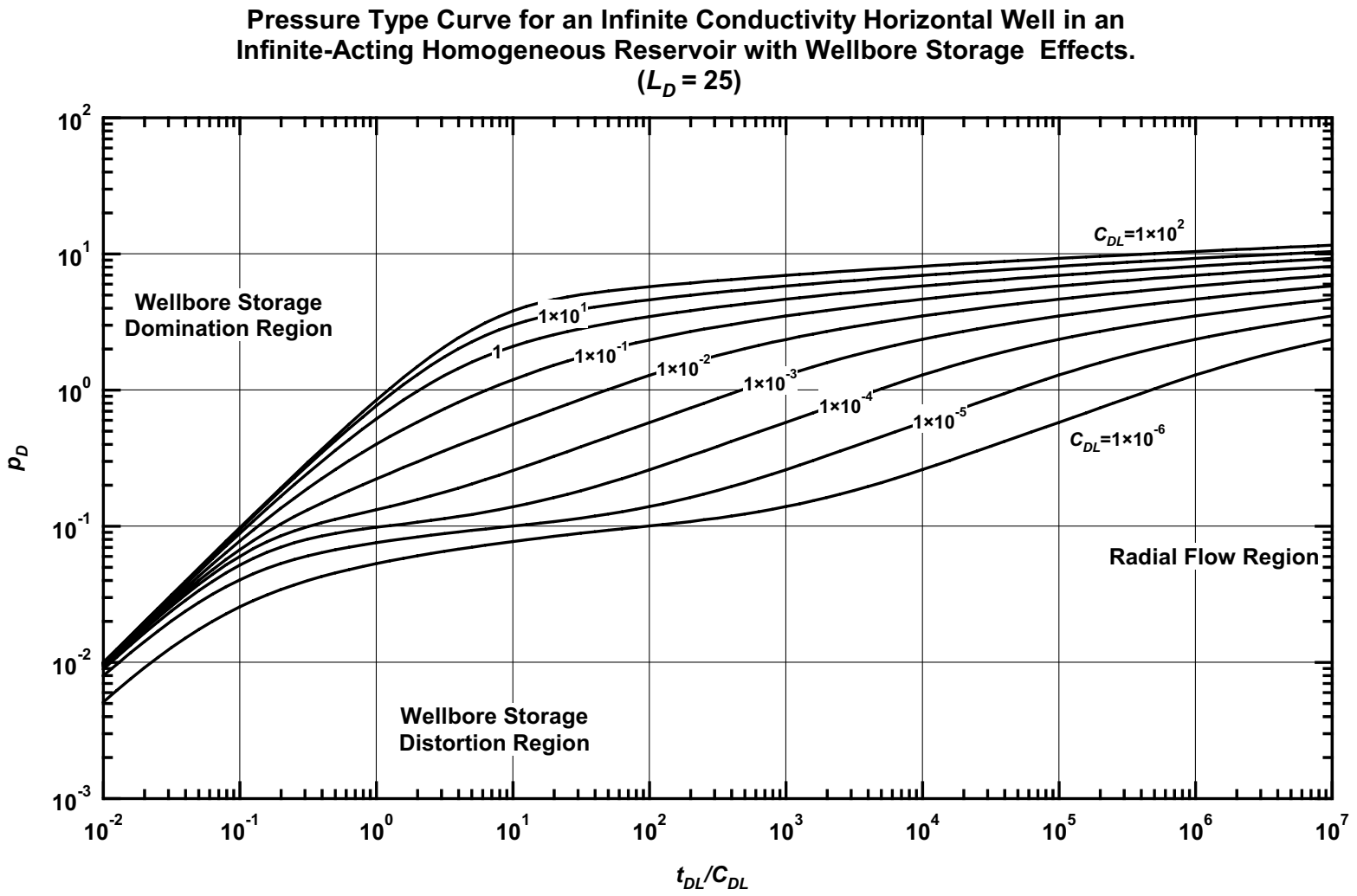

Figure E.25 — p_D vs. t_{DL}/C_{DL} — L_D=25 (horizontal well case — includes wellbore storage effects).

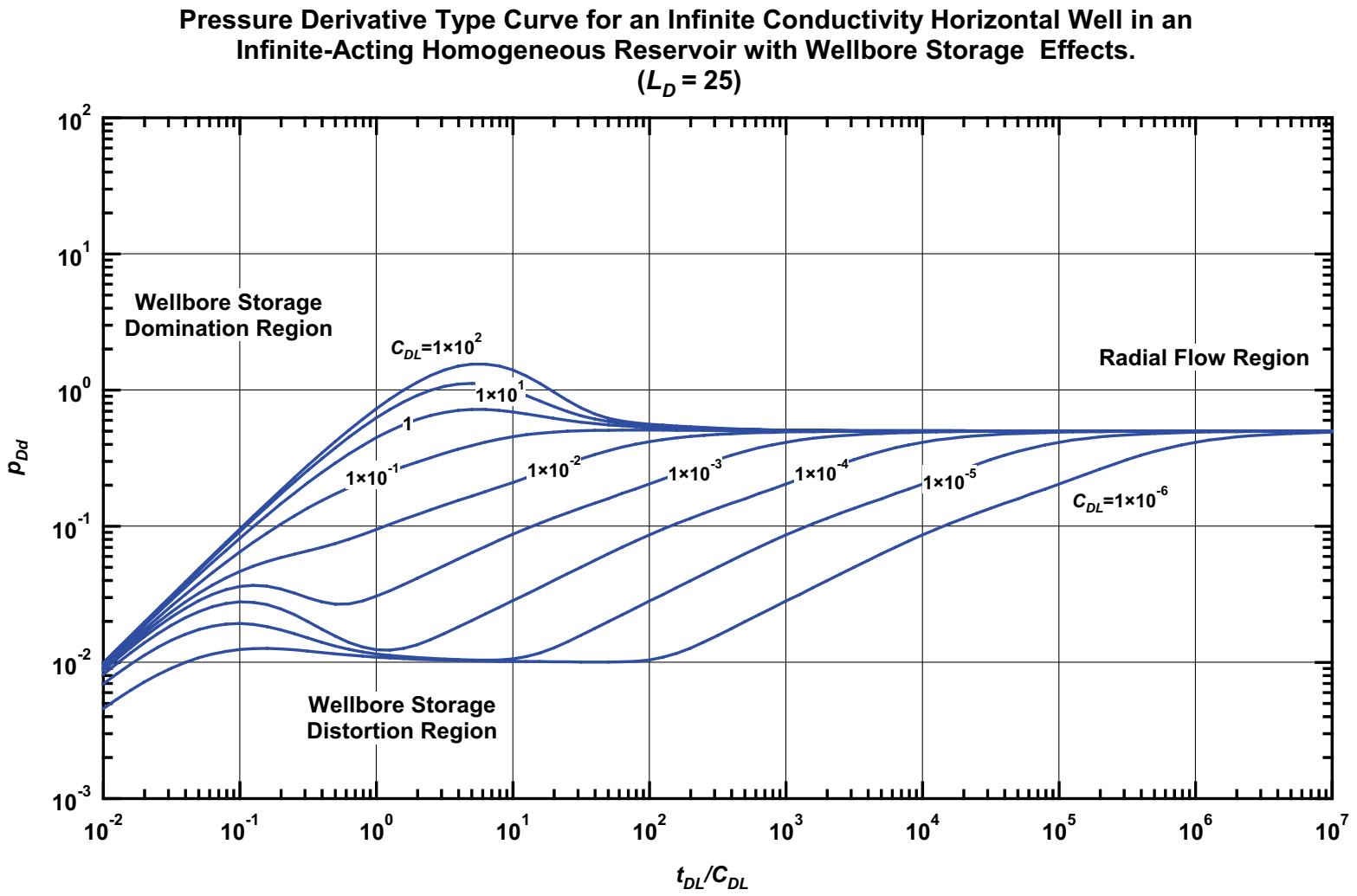

Figure E.26 — p_{Dd} vs. t_{DL}/C_{DL} — L_D=25 (horizontal well case — includes wellbore storage effects).

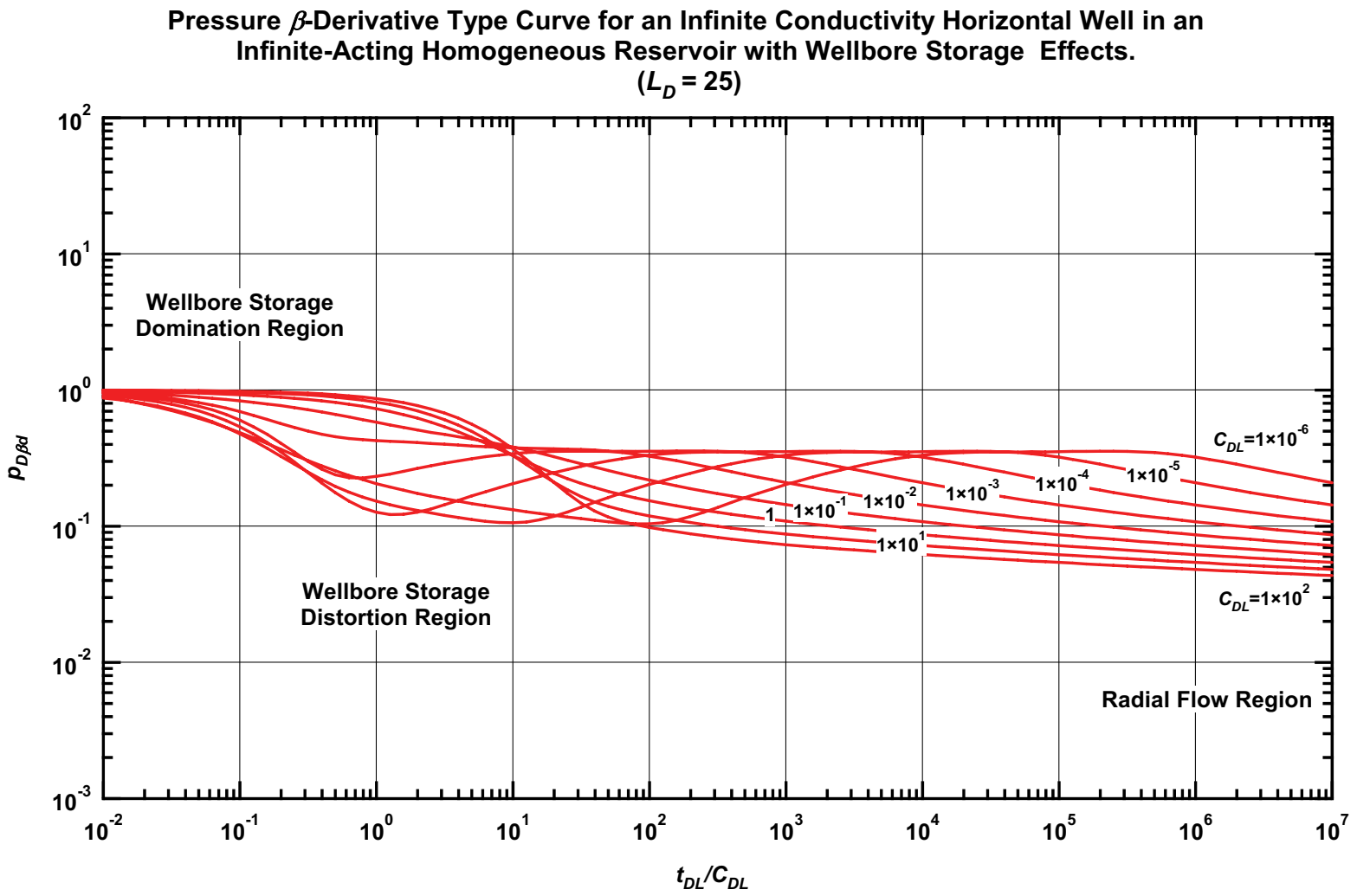

Figure E.27 — $p_{D\beta d}$ vs. t_{DL}/C_{DL} — L_D=25 (horizontal well case — includes wellbore storage effects).

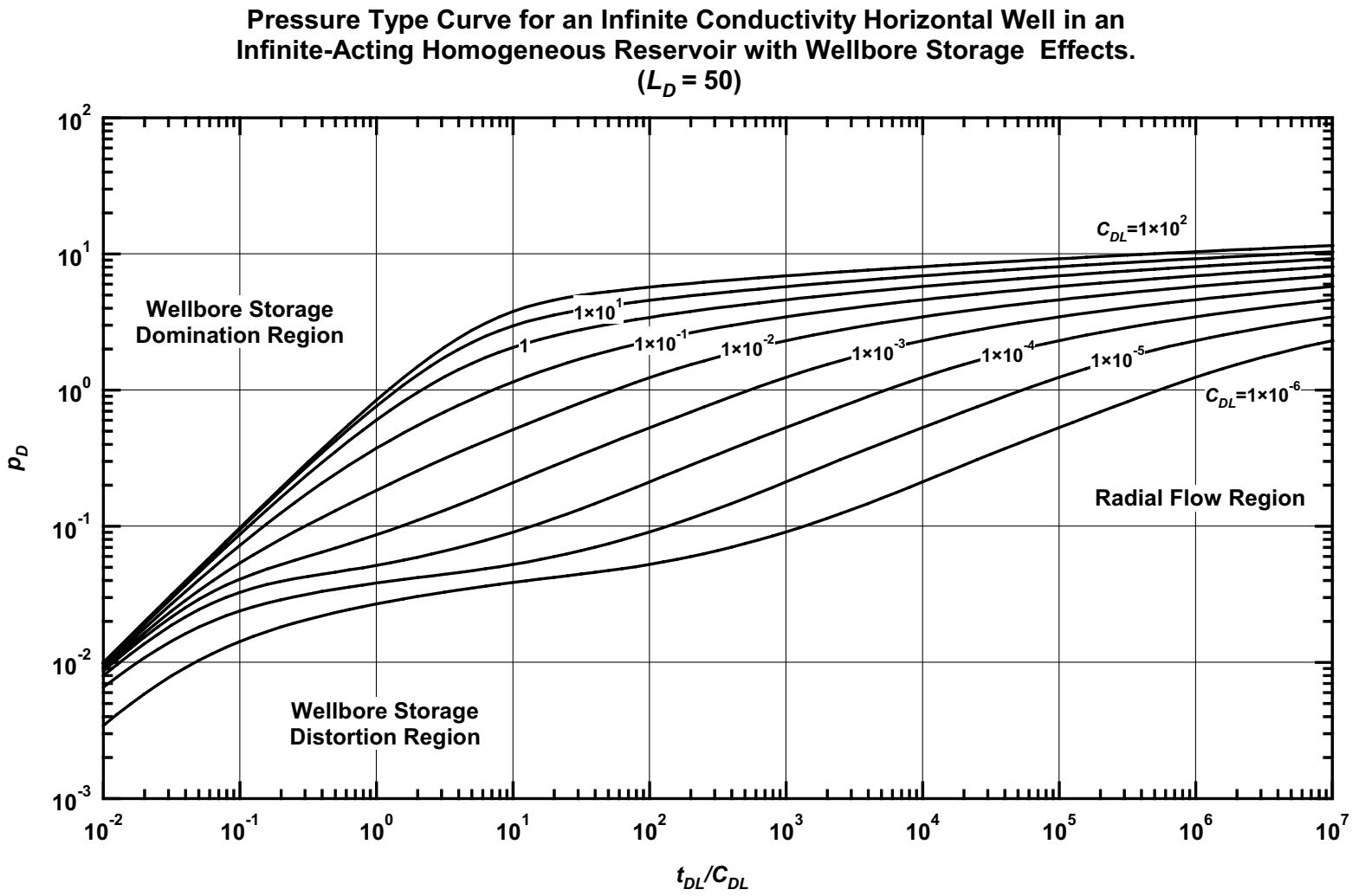

Figure E.28 — p_D vs. t_{DL}/C_{DL} — L_D=50 (horizontal well case — includes wellbore storage effects).

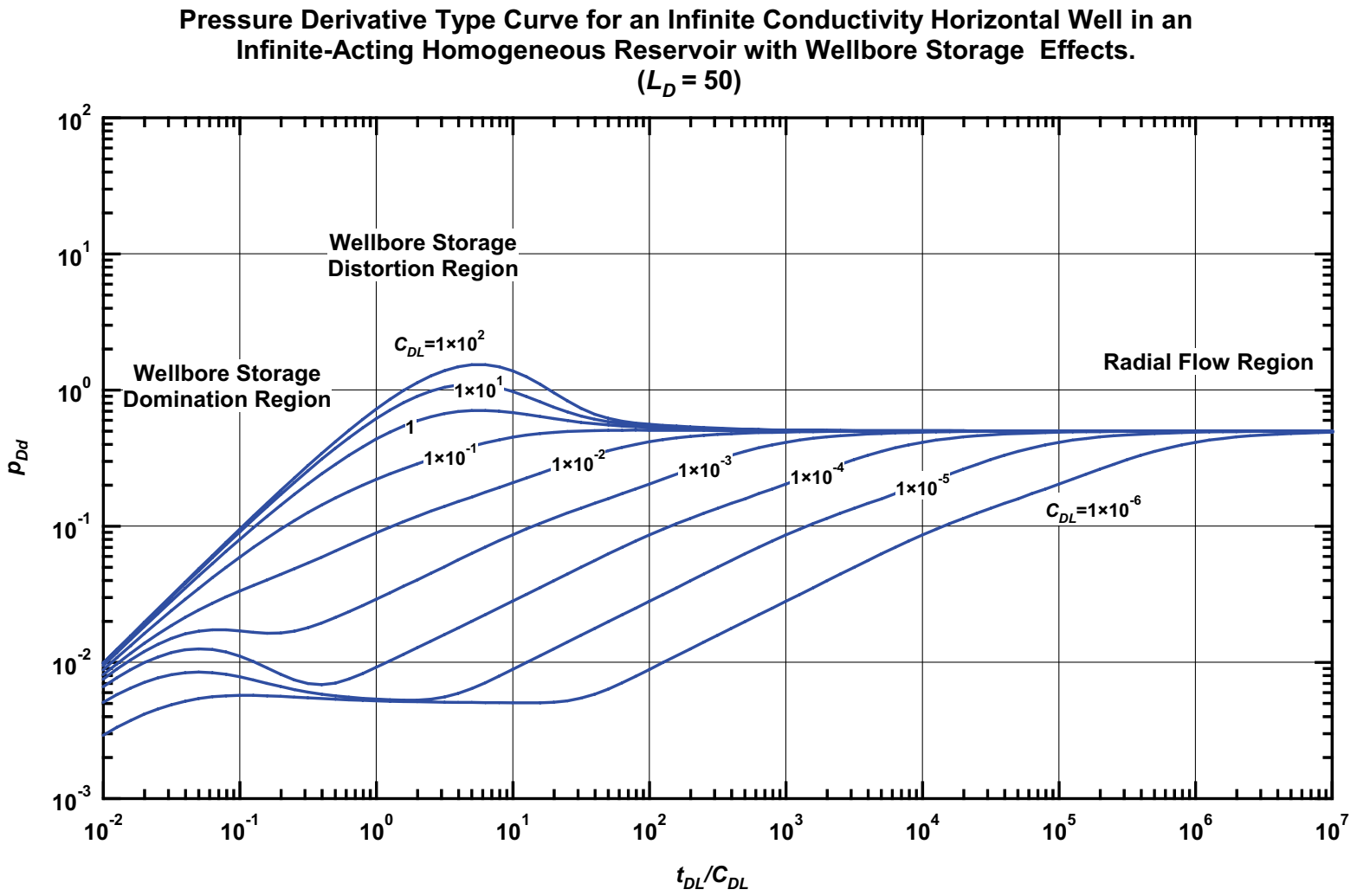

Figure E.29 — p_{Dd} vs. t_{DL}/C_{DL} — L_D=50 (horizontal well case — includes wellbore storage effects).

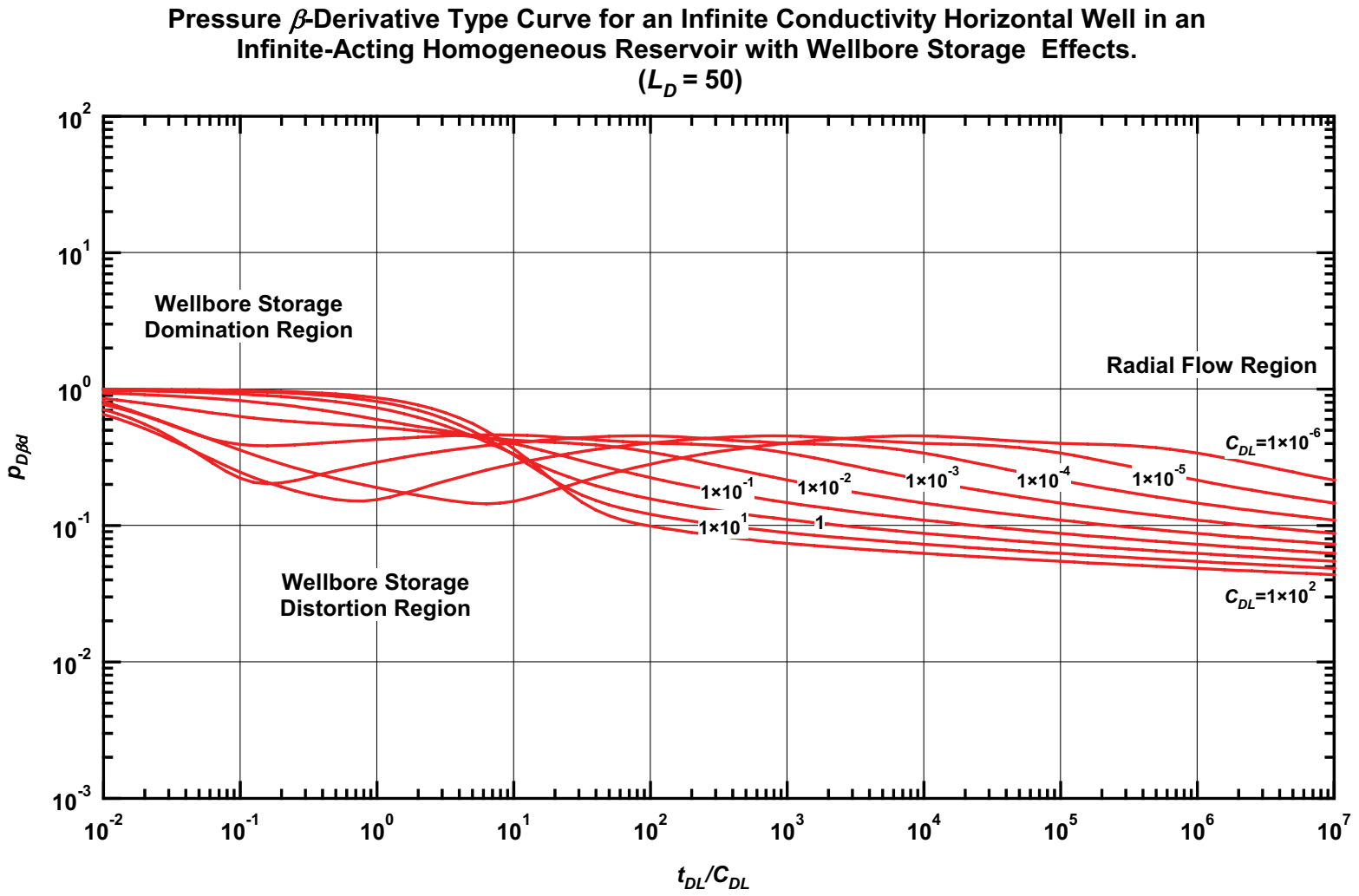

Figure E.30 — $p_{D\beta d}$ vs. t_{DL}/C_{DL} — L_D=50 (horizontal well case — includes wellbore storage effects).

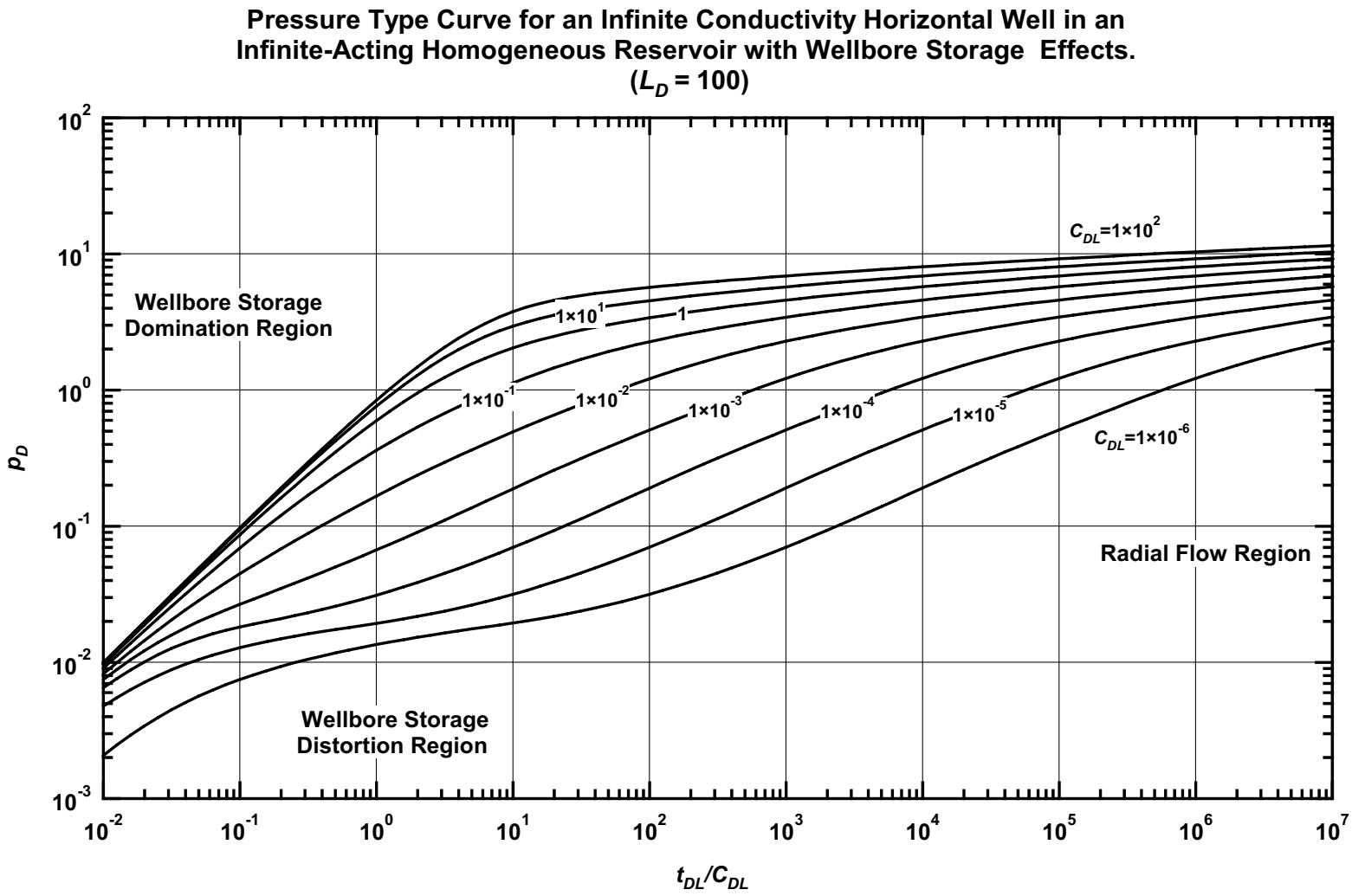

Figure E.31 — p_D vs. t_{DL}/C_{DL} — L_D=100 (horizontal well case — includes wellbore storage effects).

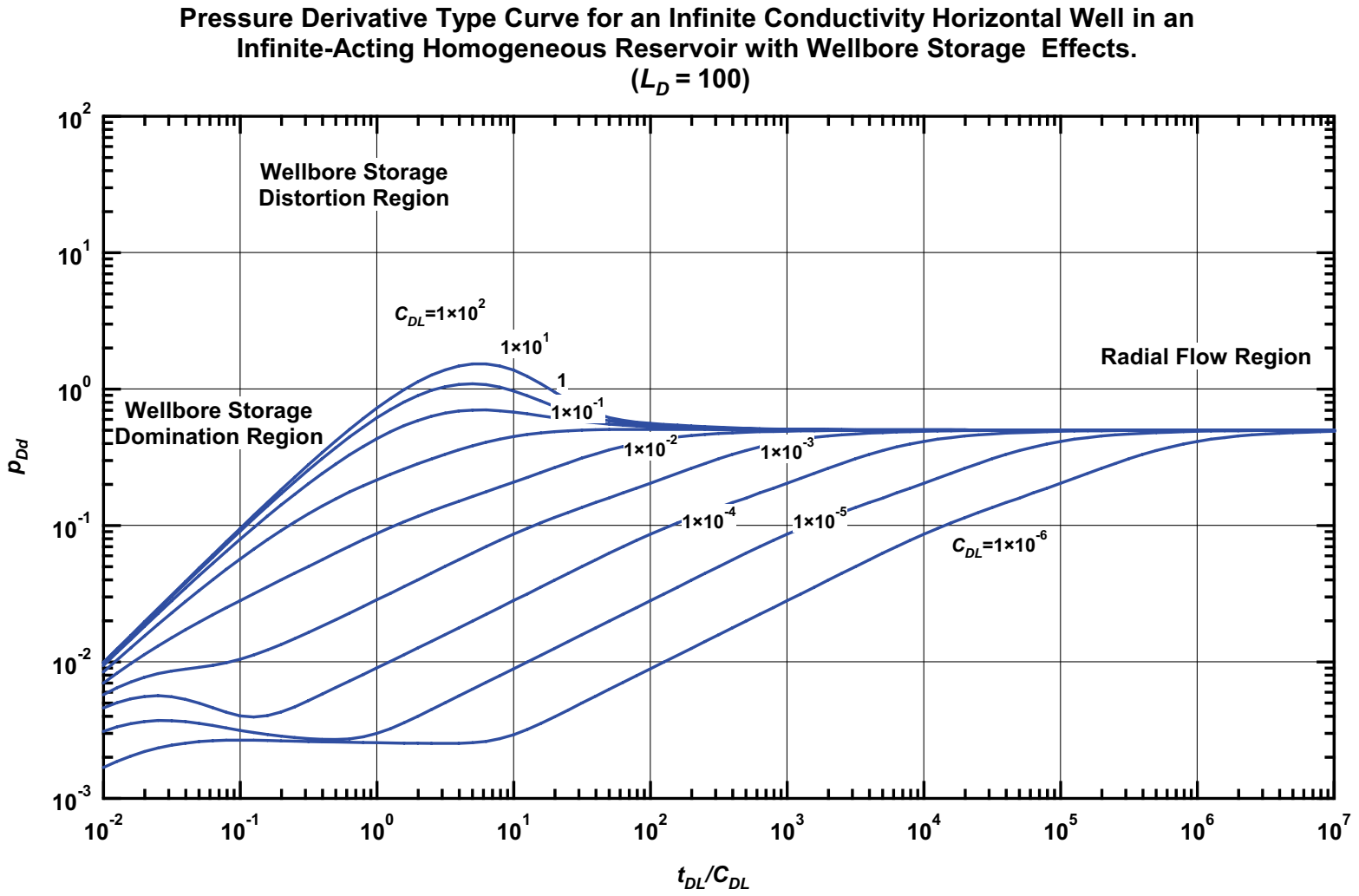

Figure E.32 — p_{Dd} vs. t_{DL}/C_{DL} — L_D=100 (horizontal well case — includes wellbore storage effects).

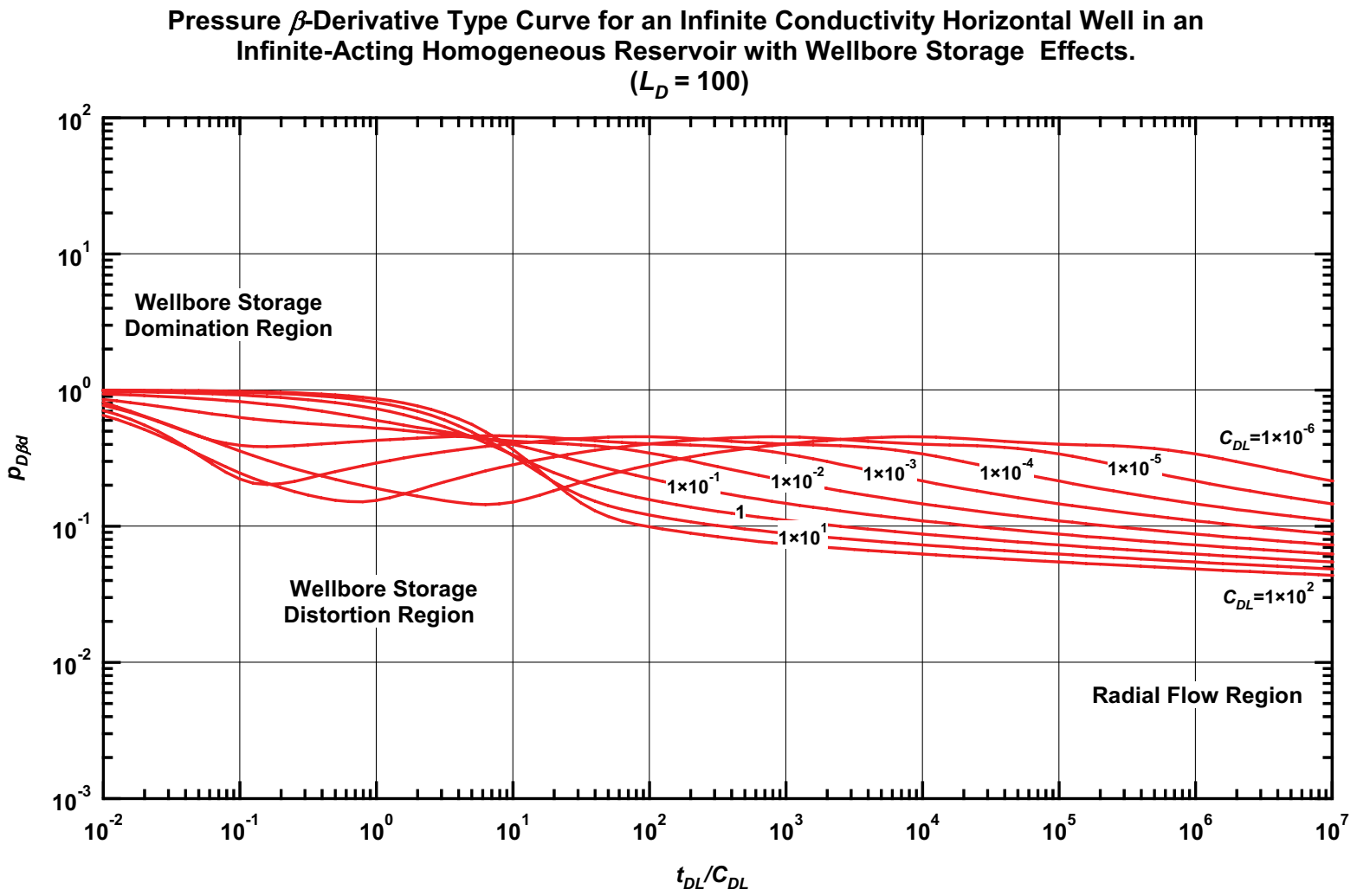

Figure E.33 — $p_{D\beta d}$ vs. t_{DL}/C_{DL} — L_D=100 (horizontal well case — includes wellbore storage effects).

VITA

Name:	Nima Hosseinpour-Zonoozi
E-mail Address:	nzonouzi@spemail.org
Education:	Texas A&M University, College Station, Texas, USA Master of Science Degree in Petroleum Engineering December 2006
	Petroleum University of Technology Bachelor of Science Degree in Petroleum Engineering September 2002
Affiliations:	Society of Petroleum Engineers